

# **Polymer Wear and Its Control**



ACS SYMPOSIUM SERIES **287**

# Polymer Wear and Its Control

**Lieng-Huang Lee, EDITOR**

*Xerox Corporation*

Developed from a symposium sponsored by  
the Division of Polymeric Materials Science and Engineering  
at the 187th Meeting  
of the American Chemical Society,  
St. Louis, Missouri,  
April 8–13, 1984

Publication Date: September 12, 1985 | doi: 10.1021/bk-1985-0287.fw001



American Chemical Society, Washington, D.C. 1985



### Library of Congress Cataloging in Publication Data

Polymer wear and its control.  
(ACS symposium series, ISSN 0097-6156; 287)

Bibliography: p.  
Includes index.

1. Polymers and polymerization—Congresses.
2. Mechanical wear—Congresses.

I. Lee, Lieng-Huang, 1924— II. American Chemical Society. Division of Polymeric Materials: Science and Engineering. III. American Chemical Society. Meeting (187th: 1984: St. Louis, Mo.) IV. Series.

QD380.P6537 1985 621.8'9 85-15755  
ISBN 0-8412-0932-4

Copyright © 1985

American Chemical Society

All Rights Reserved. The appearance of the code at the bottom of the first page of each chapter in this volume indicates the copyright owner's consent that reprographic copies of the chapter may be made for personal or internal use or for the personal or internal use of specific clients. This consent is given on the condition, however, that the copier pay the stated per copy fee through the Copyright Clearance Center, Inc., 27 Congress Street, Salem, MA 01970, for copying beyond that permitted by Sections 107 or 108 of the U.S. Copyright Law. This consent does not extend to copying or transmission by any means—graphic or electronic—for any other purpose, such as for general distribution, for advertising or promotional purposes, for creating a new collective work, for resale, or for information storage and retrieval systems. The copying fee for each chapter is indicated in the code at the bottom of the first page of the chapter.

The citation of trade names and/or names of manufacturers in this publication is not to be construed as an endorsement or as approval by ACS of the commercial products or services referenced herein; nor should the mere reference herein to any drawing, specification, chemical process, or other data be regarded as a license or as a conveyance of any right or permission, to the holder, reader, or any other person or corporation, to manufacture, reproduce, use, or sell any patented invention or copyrighted work that may in any way be related thereto. Registered names, trademarks, etc., used in this publication, even without specific indication thereof, are not to be considered unprotected by law.

PRINTED IN THE UNITED STATES OF AMERICA

American Chemical Society  
Library  
1155 16th St., N.W.  
Washington, D.C. 20036

# ACS Symposium Series

**M. Joan Comstock, *Series Editor***

## *Advisory Board*

**Robert Baker**  
U.S. Geological Survey

**Martin L. Gorbaty**  
Exxon Research and Engineering Co.

**Roland F. Hirsch**  
U.S. Department of Energy

**Herbert D. Kaesz**  
University of California—Los Angeles

**Rudolph J. Marcus**  
Office of Naval Research

**Vincent D. McGinniss**  
Battelle Columbus Laboratories

**Donald E. Moreland**  
USDA, Agricultural Research Service

**W. H. Norton**  
J. T. Baker Chemical Company

**Robert Ory**  
USDA, Southern Regional  
Research Center

**Geoffrey D. Parfitt**  
Carnegie-Mellon University

**James C. Randall**  
Phillips Petroleum Company

**Charles N. Satterfield**  
Massachusetts Institute of Technology

**W. D. Shults**  
Oak Ridge National Laboratory

**Charles S. Tuesday**  
General Motors Research Laboratory

**Douglas B. Walters**  
National Institute of  
Environmental Health

**C. Grant Willson**  
IBM Research Department

## FOREWORD

The ACS SYMPOSIUM SERIES was founded in 1974 to provide a medium for publishing symposia quickly in book form. The format of the Series parallels that of the continuing ADVANCES IN CHEMISTRY SERIES except that, in order to save time, the papers are not typeset but are reproduced as they are submitted by the authors in camera-ready form. Papers are reviewed under the supervision of the Editors with the assistance of the Series Advisory Board and are selected to maintain the integrity of the symposia; however, verbatim reproductions of previously published papers are not accepted. Both reviews and reports of research are acceptable, because symposia may embrace both types of presentation.

## PREFACE

**M**ANY HIGH STRENGTH POLYMERS have been developed in recent years. The dreams of all-composite airplanes as well as artificial hearts have become realities. Thus, it is almost a necessity for chemists to acquire tribological information about these new polymers or composites and, vice versa, for tribologists to seek chemical knowledge about these materials.

Thus, in the spring of 1984, an international symposium with the theme "Polymer Wear and Its Control" was held, and is the basis of this book. The purpose of the symposium was to seek better understanding about wear mechanisms of polymers and to develop new wear-resistant materials. Distinguished scientists and engineers were invited from West Germany, England, Japan, and the U.S.S.R. to present plenary lectures. Thirty-one papers were presented. The conference was very much appreciated by those who attended.

We are pleased to present, in this volume, 26 reviewed and revised chapters from the symposium in six parts: mechanisms of polymer wear; controls of polymer wear; tribological behaviors of polymers; wear of biomaterials and polymer composites; characterization and measurements of polymer wear; and degradation and wear of polymeric films and filaments.

Some authors chose to publish their papers elsewhere. The discussions during the meeting are printed at the ends of some of the papers. We hope that these proceedings will allow the research results to reach a much larger audience than we had in St. Louis.

I thank the session chairmen of the symposium—D. Dowson, D. H. Buckley, and N. S. Eiss, Jr.—and the authors of this volume for their valuable contributions.

Acknowledgments are made to the donors of the Petroleum Research Fund, administered by the American Chemical Society, to the Polymer Products Department of E. I. du Pont de Nemours & Company, and to Dow Corning Corporation for their financial assistance.

LIENG-HUANG LEE  
Webster Research Center  
Xerox Corporation  
Webster, NY 14580

January, 1985

# Contact Deformation and Static Friction of Polymers

## Influences of Viscoelasticity and Adhesion

Horst Czichos

Bundesanstalt für Materialprüfung, Federal Institute for Materials Research and Testing,  
Berlin-Dahlem, Federal Republic of Germany

In using a newly developed tribometer which allows the microscopic "in-situ" investigation of interfacial tribological processes through an optically transparent counterbody, contact deformation and static friction of thermoplastic polymers were studied. Examination of the contact deformation of polymers under load revealed that the contact deformation displacement is mainly influenced by the viscoelastic properties of the polymers. By measuring relaxed moduli and relaxation times the Hertzian theory of contacting bodies could be extended leading to a contact deformation formula which includes viscoelastic effects. For the onset of motion of polymer/polymer sliding pairs the static friction appears to be connected with interfacial adhesion. When data of the surface energy of the examined polymers were used, the experimentally determined friction values could be related to the adhesion energies of the different polymer/polymer sliding pairs.

All tribological processes, i.e. friction and wear processes of interacting materials start with two elementary steps:

- (i) The formation of the contact area under a given load.
- (ii) The initiation of relative motion between the contacting bodies by overcoming static friction.



The basis for the characterization of the contact behaviour of curved bodies is given by the well known classical Hertzian theory (1). Because this theory basically applies only to perfectly elastic materials with ideal smooth surfaces, some additional factors must be considered in discussing the contact behaviour of materials like polymers.

Johnson, Kendall and Roberts (2) extended the Hertzian theory taking into account the molecular attraction of interfacial adhesion between contacting bodies. Their analysis which has been experimentally confirmed for elastomer-glass contacts (2, 3, 4), shows that due to the existence of molecular attraction forces contact area and elastic displacement are larger than values deduced from the Hertzian theory. In addition, the influence of viscoelasticity on contact deformation has been studied, see e.g. (5 to 12). These theoretical analyses mainly concerning the contact between a rigid indenter and a viscoelastic half-space indicate also that contact area and contact displacements are larger for viscoelastic materials than for pure elastic materials and that a difference between loading and unloading is to be expected with viscoelastic materials (13).

In this paper (i) contact deformation and (ii) initial friction are studied experimentally and attempts are made to correlate the experimental results with bulk and surface properties of the polymers investigated.

#### EXPERIMENTAL

In the experimental investigations a ball-on-disc and a pin-on-disc configuration were used consisting of an optically transparent disc (glass or optically transparent polymer) and a polymer specimen. For the contact deformation investigations, compliance and contact size were measured by means of an inductive displacement transducer and an optical microscope connected with a TV set respectively. The accuracy of these measurements was better than  $+ 0.1 \mu\text{m}$  for the displacement measurements and better than  $\pm 1\%$  for the determination of the contact diameter. In Figure 1 the arrangement of the main parts of the test equipment is shown schematically. Figure 2 shows a photograph of the experimental apparatus. The test system operated under controlled conditions of ambient temperature ( $T = 23 \text{ }^\circ\text{C}$ ) and environmental atmospheric humidity (50% rel. humidity).

For the friction experiments with the help of a driving unit supported by an air bearing and a loading device, sliding motion and load could be applied. The normal force and the frictional force acting on the

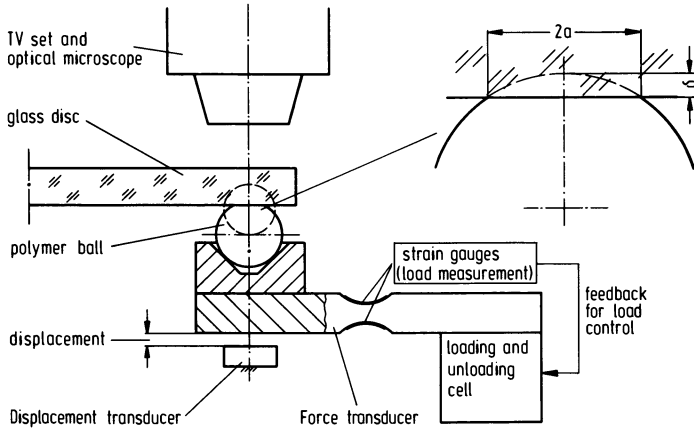


Figure 1. Schematic arrangement of experimental configuration.

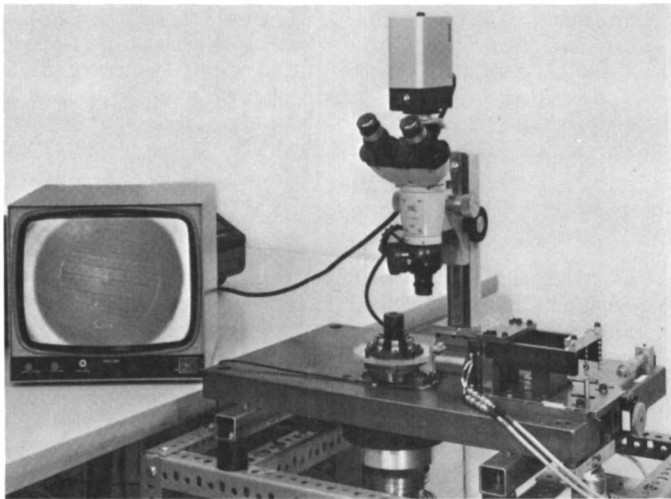


Figure 2. Photograph of the tribometer.

polymer specimen were detected by a two-component force transducer (14) and the signals of this force transducer were fed to an electronic divider which calculated directly the friction coefficient. Normal load, tangential frictional force, and friction coefficient were recorded on a three-channel recorder. A block diagram of this tribometer is given in Figure 3. Details of the experimental equipment, the materials studied, the preparation of the specimens and the performance of the tests are given elsewhere (15).

#### CONTACT DEFORMATION

The experiments were performed with the following polymers:

- Polyoxymethylene (POM)
- Polyamide 66 (PA 66)
- Polypropylene (PP)
- Polytetrafluoroethylene (PTFE)

All materials belong to the class of semi-crystalline thermoplastic polymers. Characteristic appearances of spherulitic microstructures of the polymers are shown in Figures 4 and 5 for the examples of POM and PA66.

The contact deformation of these thermoplastic polymers was studied experimentally by pressing polymeric balls (of 4 mm diameter) with continuously increasing load (0.6 N/s) against an optically smooth glass surface and measuring both contact deformation displacement and contact size under load as described above (see Figure 1). The polymer balls had a mean peak-to-valley roughness of  $R_p \approx 0.6 - 1.0 \mu\text{m}$  and a c.l.a. roughness of  $R_a \approx 0.2-0.3 \mu\text{m}$ .

Typical plots of the variation of contact diameter and displacement in compression for increasing and decreasing loads for one of the polymers investigated are shown in Figure 6 together with theoretical curves calculated with the well known Hertzian formulas:

$$a = \left[ \frac{3 R}{4 E'} F_N \right]^{1/3} \quad \delta = \left[ \frac{9}{16 E'^2 R} F_N \right]^{1/3} F_N^{2/3}$$

$$\text{where } \frac{1}{E'} = \frac{1 - \nu_1^2}{E_1} + \frac{1 - \nu_2^2}{E_2}$$

$\nu_{1, 2}$ : Poisson's ratio;  $E_{1, 2}$ : Elastic modulus;  
R: Ball radius

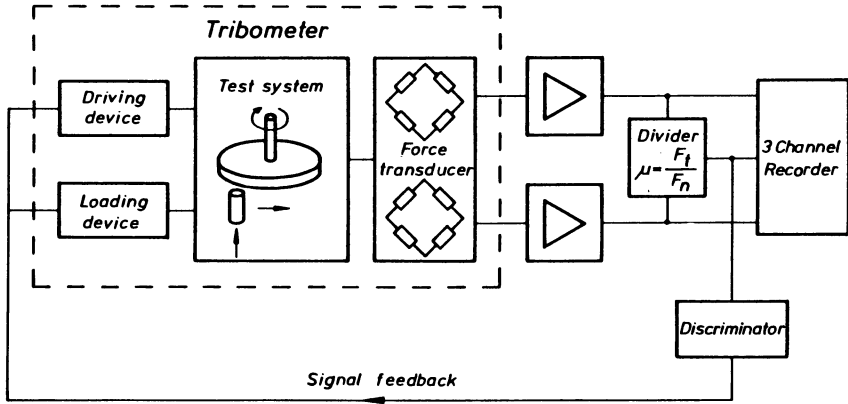


Figure 3. Block diagram of the tribometer.

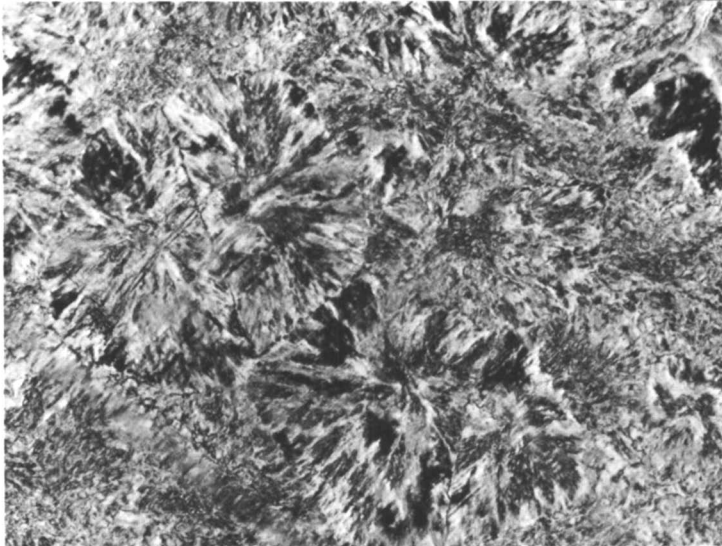


Figure 4. Microstructure of polyoxymethylene.

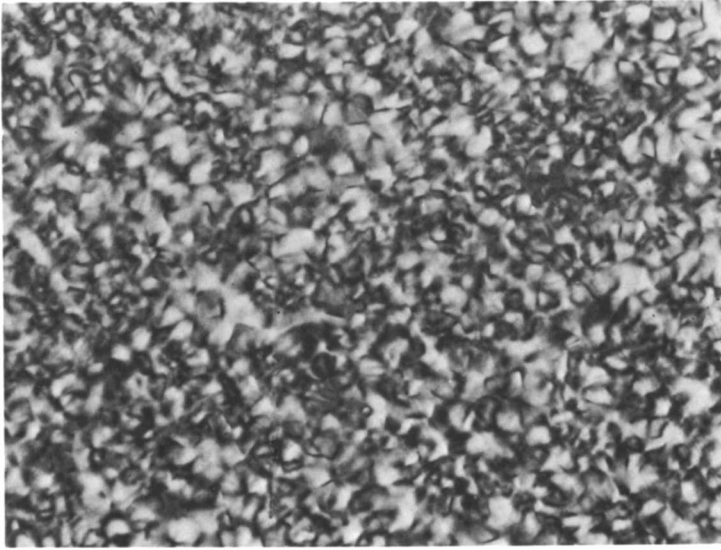


Figure 5. Microstructure of polyamide 66.

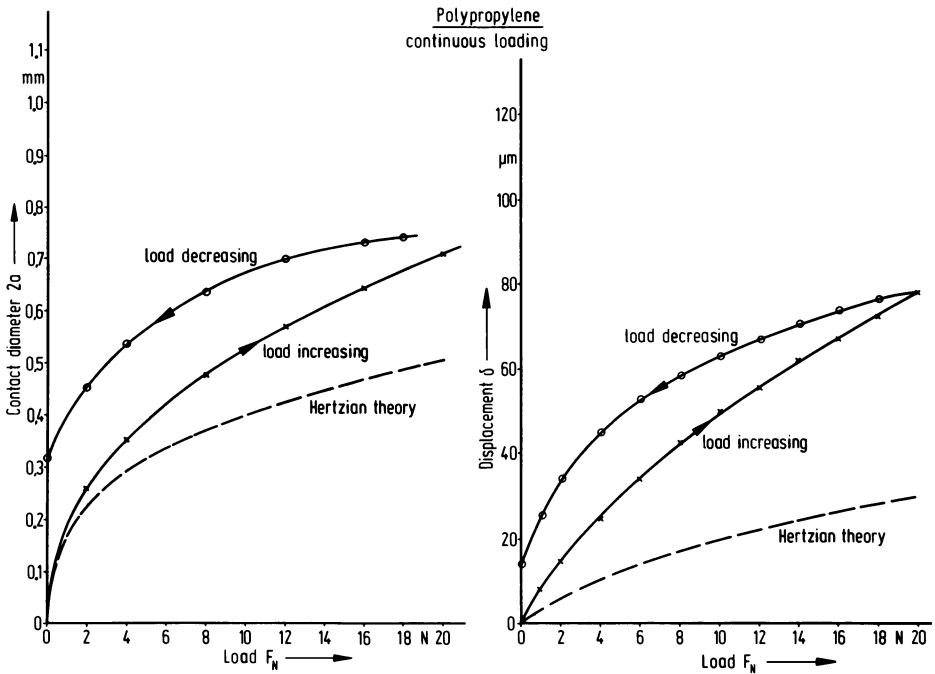


Figure 6. Contact diameter and contact deformation displacement curves.

In addition to the continuous loading and unloading procedure, a stepwise mode of loading was also applied. In Figure 7, contact deformation displacements for both continuous and stepwise loading are drawn for one of the polymers investigated. The plots of Figure 6 and the corresponding graphs for the other polymers studied indicate a residual deformation behaviour which may be discussed in connection with the elastoplastic hardness of the materials. In addition it is obvious that large differences between experimental contact deformation data and theoretical values calculated on the basis of the classical Hertzian theory exist so that besides the properties and operating variables of the Hertzian theory some other influencing factors must be considered.

Generally speaking, the following main phenomena may influence the contact deformation behaviour of polymers:

1. Elastic deformation processes
2. Viscoelastic deformation processes
3. Viscoplastic deformation processes
4. Strain hardening/softening effects
5. Interfacial adhesion

First, the possible influence of interfacial adhesion was studied by performing loading-unloading tests with unlubricated and lubricated specimens. If interfacial adhesion exerts a dominant influence on contact deformation behaviour, this influence should be significantly reduced by a lubricant. (For example, Johnson, Kendall and Roberts (2) found that if the contact of rubber spheres was immersed in a solution of sodium dodecyl sulfate, the influence of interfacial adhesion vanishes and the results of contact radius measurements agreed exactly with the Hertz' theory). From the results shown in Figure 8 it can be seen that the contact deformation behaviour is not significantly changed through a lubricant for the experimental conditions of this investigation. Although no comparative contact diameter measurements were performed, (because the lubricant permitted a clear microscopic distinction of the contact boundary) from the results of Figure 8, it is obvious that interfacial adhesion appears not to be a dominant influencing factor for the contact deformation displacement of the polymers studied.

#### A Model for the Contact Deformation of Polymers

In order to explain the experimentally observed contact deformation behaviour as shown in Figure 6, a simple rheological model which combines elastic, viscoelastic

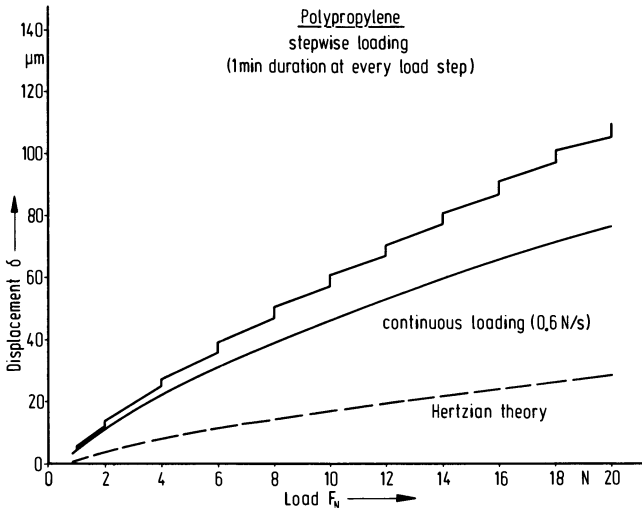


Figure 7. Displacement curves for continuous and stepwise loading.

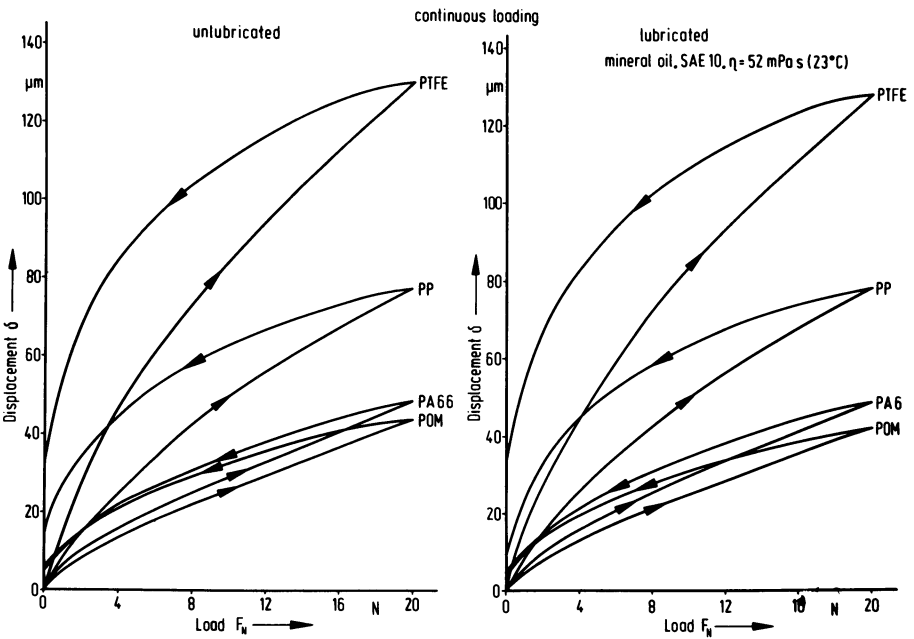


Figure 8. Displacement curves for unlubricated and lubricated polymer-glass contacts.

and viscoplastic influences is considered, see e.g. (16, 17), Figure 9. As illustrated in the upper part of Figure 9, with the help of a four-parameter or Burger model the deformation behaviour of polymers may be approximated through a combination of springs and dampers. The spring  $E_0$  characterizes the pure elastic state of the polymer. In addition, a time-dependent viscoelastic component described by the so-called Voigt-Kelvin configuration, i.e. the combination of spring  $E_r$  and damper  $\eta_r$  comes into action. Further, a viscoplastic flow component may exist, modelled by the damper of viscosity  $\eta_0$ .

Consider now a polymer under the instantaneous action of a constant uniaxial stress  $\sigma_0$ . Assuming that the deformation behaviour may be described by the model shown in Figure 9, we may hypothesize that the resulting deformation  $\epsilon_{total}$  is the sum of

- (i) elastic deformation  $\epsilon_{el}$  ( $E_0$ : elastic modulus)
- (ii) viscoplastic deformation  $\epsilon_v$  ( $\eta_0$ : "viscosity")
- (iii) viscoelastic deformation  $\epsilon_r$  ( $E_r$ : relaxed modulus)

These deformation components and their sum are plotted schematically in Figure 9. If the asymptote for the resulting  $\epsilon_{total}$ -curve is constructed, the relaxed modulus  $E_r$  may be determined from the intersection of this asymptote with the  $\epsilon$ -axis. In addition, the relaxation time  $\tau$  can be estimated as illustrated in Figure 9. Although the deformation model shown in Figure 9 is extremely simplified and neglects some important factors (e.g. the fact, that instead of a single relaxation time a complicated relaxation spectrum may be valid), the model may serve as a basis for the discussion of the contact deformation behaviour of polymers.

#### Discussion of the Experimentally Observed Contact Deformation Behaviour

In order to study the influence of viscoelasticity on the experimentally observed contact deformation behaviour, in analogy to the model illustrated in Figure 9 the displacements under given load as function of time were determined. A typical result for one of the polymers investigated is shown in Figure 10. These diagrams were determined for all four polymers and the relaxed moduli  $E_r$  of the polymers and their nominal relaxation times  $\tau$  were estimated in a similar manner as illustrated in Figure 9. The results compiled in Table I indicate that both relaxed moduli and relaxation times vary considerably within the range of the applied experimental conditions.



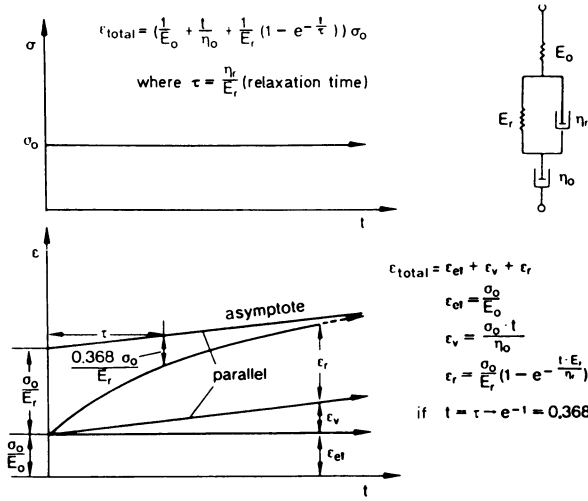


Figure 9. Four-parameter or Burger model for the deformation behaviour of polymers.

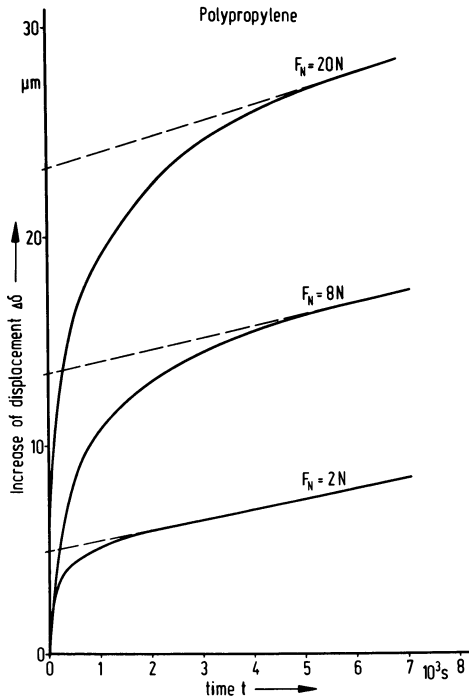


Figure 10. Variation of contact deformation displacement as function of time.

In addition to the study of viscoelasticity and the experimental determination of relaxed moduli and relaxation time, possible irreversible viscoplastic contact deformation effects were also studied. After a certain loading time, the load was totally released and the recovery of the polymers was measured. The results of Figure 11 show no viscoplastic effects for both PA66 and POM, a minor influence for PP but a clear effect of viscoplasticity for PTFE. (Note that the recovery curves of Figure 11 are governed by much higher relaxation times than those determined under an applied load and listed in Table I. This again indicates the dependence of relaxation times or relaxation spectra on operating conditions).

The results of Figure 11 indicate that the polymers studied were subject to different microstructural deformation mechanisms. In this connection it must be borne in mind that the maximum nominal deformation of POM and PA66 was only 1% whereas PP and PTFE were deformed up to 1.8% and 3.3% respectively. Therefore it may be assumed that for POM and PA66 only an instantaneously reversible deformation of the amorphous matrix of the spherulitic microstructure occurred (18) whereas for PP and PTFE some irreversible effects, like interlamellar shearing or re-orientation of the lamellae may have taken place.

With the determination of viscoplastic displacements from Figure 11 and the data of viscoelasticity compiled in Table I we are now in a position to derive on the basis of the model illustrated in Figure 9, a simple contact deformation formula if we assume that interfacial adhesion (see Figure 8) is negligible. As compiled in Figure 12, it is assumed that the total contact deformation displacement is the sum of an elastic, a viscoelastic and a viscoplastic deformation component. For the first component the Hertzian theory is assumed to be valid and for the second component in analogy to the model described in Figure 9, the elastic modulus  $E_0$  is replaced by a term which includes the relaxed modulus  $E_r$  and the relaxation time  $\tau$ . If the viscoplastic component can be neglected, the contact deformation formula, given in Figure 12, results.

It must be pointed out that the formula given in Figure 12 is extremely simplified because it has been derived in analogy to the model illustrated in Figure 9 under the assumptions of a linear superposition of deformation components and the action of an instantaneous constant load. Because of differences between these idealized assumptions and the actual experimental conditions (e.g. continuous loading instead of instantaneous loading) the formula should be considered only as a first rough approximation.

Table I. Material parameters of polymers

Polymer	Elastic modulus $E_0$ [N/mm <sup>2</sup> ]	Load $F_N$ [N]	Relaxed modulus $E_r$ / Elastic modulus $E_0$	Relaxation time $\tau$ [s]
POM	3200	2	0.56	$25 \pm 9$
		8	0.58	
		20	0.61	
PA 66	3000	2	0.54	$18 \pm 6$
		8	0.60	
		20	0.65	
PP	1600	2	0.13	$27 \pm 8$
		8	0.22	
		20	0.49	
PTFE	600	2	0.21	$52 \pm 15$
		8	0.41	
		20	0.57	

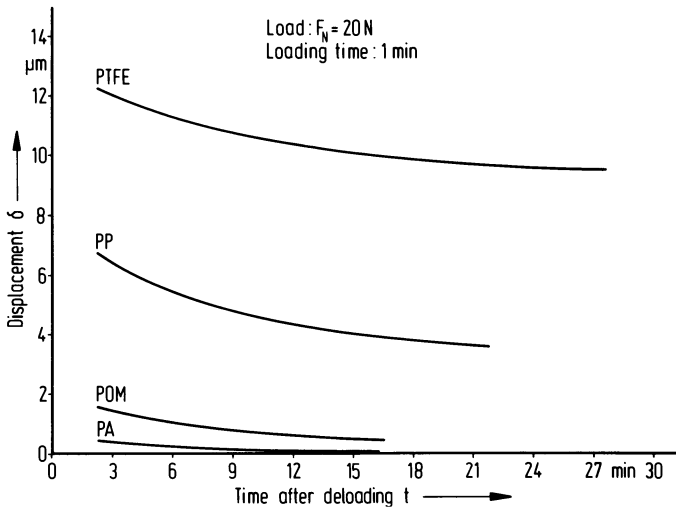


Figure 11. Recovery curves after contact deformation of polymers.

The simplified formula given in Figure 12 is valid only for the loading mode of contact deformation. For the unloading mode (i.e.  $F_N$  decreasing) further aspects must be considered. If after a certain loading time  $t^*$  the load  $F_N$  is lowered, the elastic component  $\delta_{el}$  instantaneously drops to the displacement connected with the lower load or stress level. For the viscoelastic component, however, the whole loading-unloading history must be taken into consideration: On the one hand, the viscoelastic component  $\delta_r$  reduces to the corresponding lower load or stress level in a delayed manner depending on the relaxation time. On the other hand, at the lower load or stress level the viscoelastic component increases again because of its dependence on time. In addition, a possibly remaining irreversible viscoplastic component must also be paid regard. Summing up all these components, a contact deformation formula for the unloading mode results which is also given in Figure 12. (It should be mentioned that for the sake of simplicity the same relaxation time  $\tau$  is assumed to be valid for both the loading and unloading mode. Theoretically, it should be distinguished between a "retardation time" for the loading mode and a "relaxation time" for the unloading mode.)

In Figures 13 to 16 the experimentally determined contact deformation displacement values together with curves calculated with the deformation formulas of Figure 12 and the Hertzian formula are plotted. In the displacement-load graphs for POM and PA66 only elastic and viscoelastic components were taken into consideration whereas for PP and PTFE also viscoplastic components (see Figure 11) were included. It can be seen that a reasonably good correlation between experimental data and theoretically determined curves results, so that the formulas compiled in Figure 12 may be used for the approximative estimation of the contact deformation behaviour of curved thermoplastic polymeric materials.

#### STATIC FRICTION

In addition to the investigations on contact deformation, the initial stage of friction has been studied (19). Whereas in recent years several investigations have been performed on polymer/metal sliding pairs (a comprehensive review was published recently by Briscoe (20) relatively little work has been done to study the tribological behaviour of polymers sliding against polymers. In the friction investigations a pin-on-disc configuration with the following polymers was used; the polymer pins were cut with a microtome in order to obtain a flat smooth polymer surface at the beginning of the tests:

Contact deformation = f (elasticity, viscoelasticity, viscoplasticity)

$$\delta_{total} = \delta_{el} + \delta_r + \delta_v$$

$\delta_{el}$  → Hertzian theory

$\delta_r$  → Hertzian theory with  $\frac{1}{E_0} \rightarrow \frac{(1 - e^{-t/\tau})}{E_r}$

where  $E_r$  : Relaxed modulus

$\tau$  : Relaxation time

If  $\delta_v = 0$ , for a ball-on-plate contact it follows

$$\delta_{total} = \left[ \frac{9}{16 E_0^2 R} \right]^{1/3} F_N^{2/3} + \left[ \frac{9(1 - e^{-t/\tau})^2}{16 E_r^2 R} \right]^{1/3} F_N^{2/3}$$

Unloading mode ( $t > t^*$ ;  $t^*$ : Loading time):

$$\delta_{total} (F_N < F_{Nmax}; t > t^*) = \delta_{el} (F_N) + \delta_r (F_N, t) + \delta_v (F_{Nmax}, t^*) + \left[ \delta_r (F_{Nmax}, t^*) - \delta_r (F_N, t^*) - \delta_v (F_{Nmax}, t^*) \right] e^{-\frac{(t-t^*)}{\tau}}$$

Figure 12. Simplified formulas for the contact deformation displacements of polymer balls.

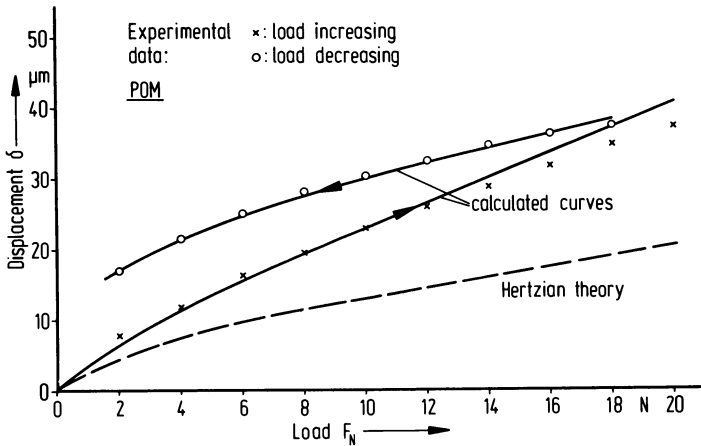


Figure 13. Experimentally determined contact deformation displacement and calculated curves for POM.

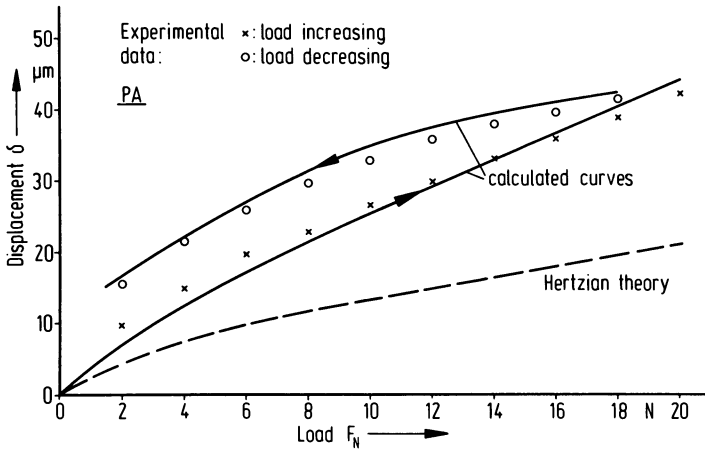


Figure 14. Experimentally determined contact deformation displacement and calculated curves for PA66.

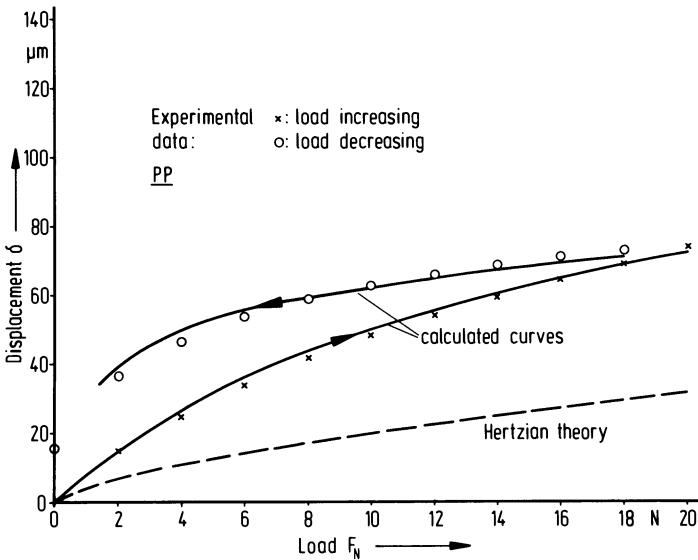


Figure 15. Experimentally determined contact deformation displacement and calculated curves for PP.

Pin materials: Polyoxymethylene (POM)  
 Polyamide 66 (PA66)  
 Polypropylene (PP)  
 Polytetrafluoroethylene (PTFE)

Disc materials: Acrylonitrile-styrene (ANS)  
 Polystyrene (PS)  
 Polymethyl methacrylate (PMMA)

The surface roughness data of the polymer pins were  $R_z \approx 1.3 \mu\text{m}$  and  $R_a \approx 0.2 \mu\text{m}$ . The tests were performed at very low sliding speeds in order to eliminate friction-induced thermal effects. The following experimental conditions were used: contact pressure  $p = 3.2 \text{ N/mm}^2$ ; sliding velocity  $v = 2.4 \times 10^{-7} \text{ m/s}$ ; ambient temperature  $T = 23 \text{ }^\circ\text{C}$ ; relative humidity 50%.

Figure 17 shows the friction coefficient as a function of sliding distance. A typical peak of static friction appears, which is followed by different levels of the friction coefficient for the different polymer-polymer combinations. Figure 18 shows values of the measured friction coefficient as a function of sliding distance for the same four polymer materials, used as pins, sliding in this case against the polymer PS. Figure 19 shows the friction data of the four polymeric materials sliding against PMMA. Optical investigations with the equipment, illustrated in Figure 2, revealed no detectable surface changes, which indicates that in all the combinations shown in Figures 17 to 19, sliding takes place at the original polymer-polymer interface.

In order to explain the frictional behaviour of the polymer-polymer pairs, a correlation was sought between the frictional behaviour and the relevant properties of the interacting polymers, like the adhesive forces acting between the contacting polymer surfaces. For this purpose the wellknown Dupr  equation was used as a starting point:

$$\Delta \gamma = \gamma_1 + \gamma_2 - \gamma_{12}$$

where  $\Delta \gamma$  is the work of adhesion,  $\gamma_1$  and  $\gamma_2$  are the surface free energies of bodies 1 and 2 and  $\gamma_{12}$  is the interfacial free energy between bodies 1 and 2.

For the values of the surface energies which must be inserted in the Dupr  equation, recent surface energy data for the polymers used in this study, which were determined by Erhard (21) could be used. Erhard determined experimentally the surface free energies of the polymers and computed the work of adhesion with the method of Owens and Wendt. Table II shows the data of the work of

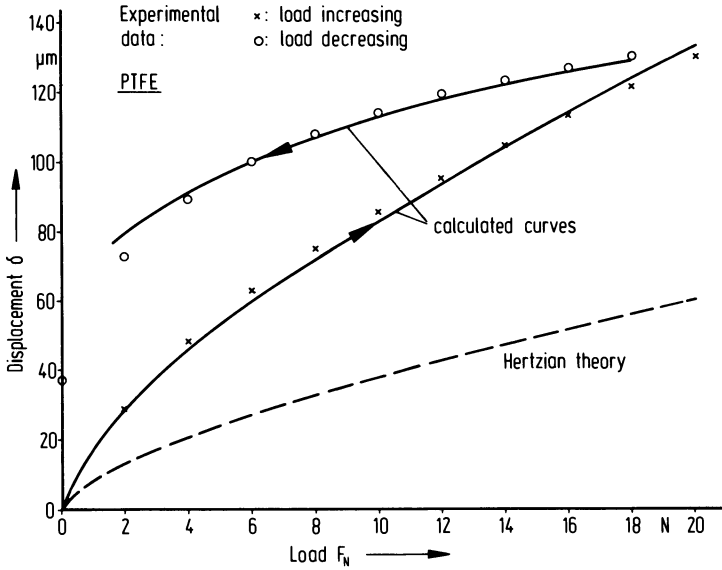


Figure 16. Experimentally determined contact deformation displacement and calculated curves for PTFE.

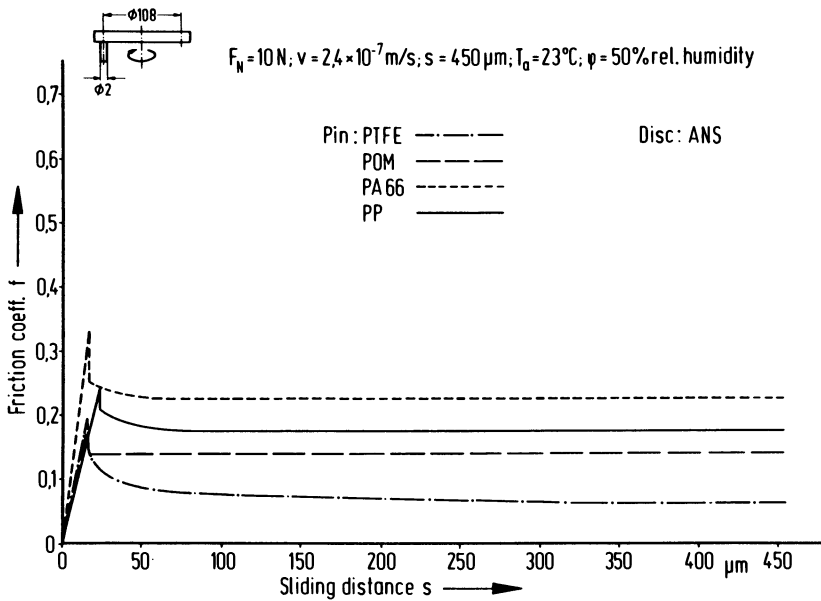


Figure 17. Friction of polymer/polymer pairs (PTFE, POM, PA66, PP against ANS).



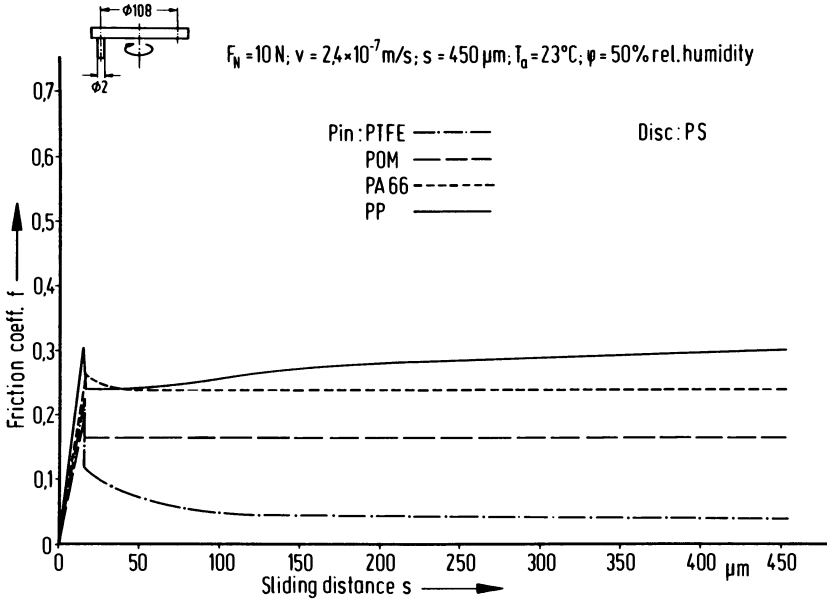


Figure 18. Friction of polymer/polymer pairs (PTFE, POM, PA66, PP against PS).

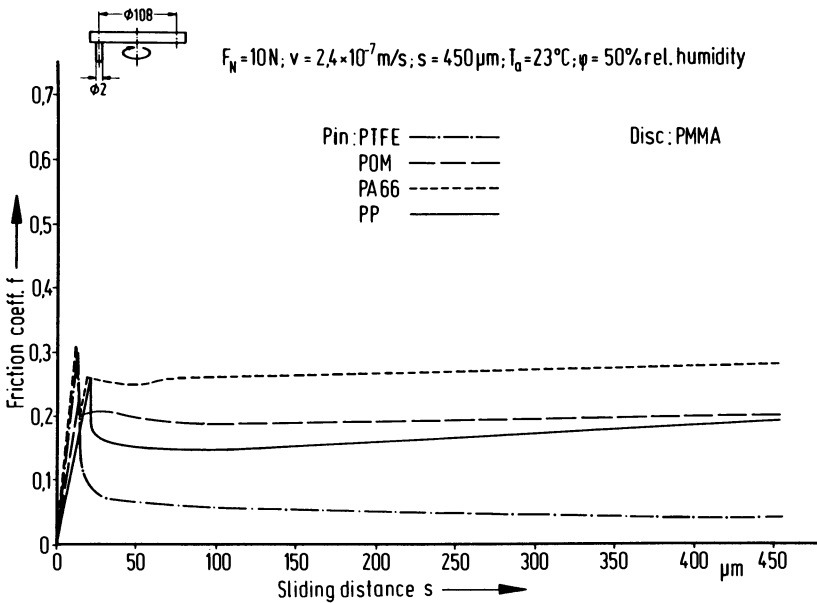


Figure 19. Friction of polymer/polymer pairs (PTFE, POM, PA66, PP against PMMA).

adhesion  $\Delta\gamma$ , computed by Erhard (21) and the experimentally determined frictional work,  $E_F$ . The frictional work,  $E_F$ , was determined by integrating the measured frictional forces plotted in Figures 17 to 19 over the sliding distance. The results are that the data for PTFE sliding against the three disc materials are lowest and the data for the PA66 pins, sliding against the three disc materials are generally highest. In Figure 20 the experimentally determined frictional work is plotted as a function of the calculated work of adhesion.

On a logarithmic scale the frictional work increases with the work of adhesion and the experimental data seem to be in a reasonably good correlation with the theoretically calculated values. (An exception perhaps may be the combination of PP sliding against PS). It appears that for the flat-to-flat conformal contact of the polymer combinations studied, the adhesion component at the interface may be the dominant factor governing the initial frictional behaviour of polymer-polymer sliding pairs. In contrast, in the case of the contact deformation displacement of ball-to-flat counterformal contacts discussed above no effect of adhesion was found as compared with the influence of the (bulk) viscoelastic properties of the materials. (This may be due to elastic relief forces which may burst adhesive junctions during the loading-unloading contact deformation cycles.)

## CONCLUSIONS

From the investigations of (i) contact deformation and (ii) initial static friction of thermoplastic polymers the following conclusions may be drawn:

- a) The contact deformation behaviour of counterformal polymer/glass contacts is considerably influenced by the (bulk) viscoelastic properties of the polymers.
- b) The contact deformation displacement for the unloading mode is considerably higher than for the loading mode.
- c) The contact deformation displacement in loading/unloading cycles can be estimated with a simplified extended Hertzian formula including relaxation characteristics of the polymers.
- d) The static friction at the onset of motion of conformal polymer/polymer sliding pairs is influenced mainly by interfacial adhesion.
- e) A correlation between experimentally measured frictional work and theoretically estimated work of adhesion was found.

Table II. Work of friction and adhesion of polymers

Pin	Disc	Frictional work $E_F$ [Nmm]	Work of adhesion $\Delta\gamma = \gamma_1 + \gamma_2 - \gamma_{12}$ [ $10^{-6}$ Nmm/mm <sup>2</sup> ]
PTFE	ANS	0.328	54.7
	PS	0.343	55.4
	PMMA	0.324	53.6
PP	ANS	0.795	73.0
	PS	1.215	75.3
	PMMA	0.730	73.0
POM	ANS	0.619	84.5
	PS	0.760	81.0
	PMMA	0.850	87.3
PA66	ANS	0.987	88.0
	PS	0.864	83.1
	PMMA	1.128	92.1

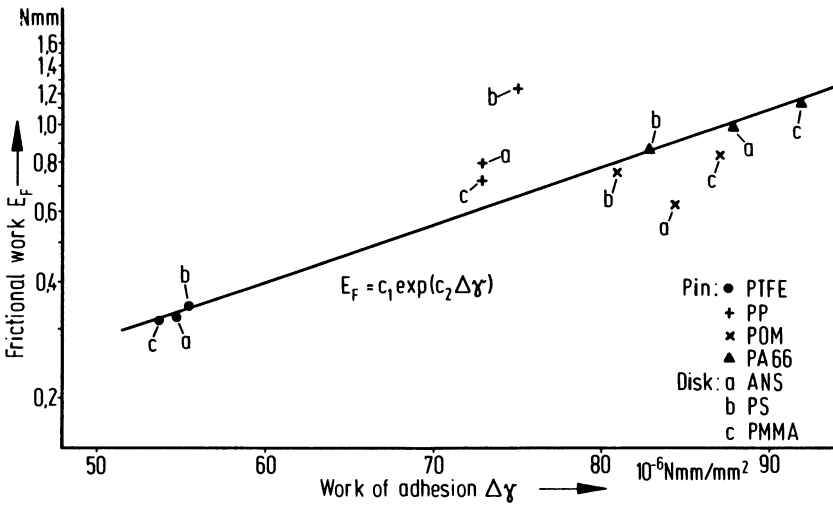


Figure 20. Correlation between frictional work and work of adhesion.

### Acknowledgments

I thank engineers Mr. N. Kelling and Mr. J. Schwenzien of BAM-Laboratory "Wear Protection, Tribometry and Tribophysics" for having skillfully performed the experiments, as well as Dr. P. Feinle for helpful discussions and Dipl.-Phys. H. Tischer of the BAM-Documentation Service on Tribology for providing background literature material. Financial support from the Deutsche Forschungsgemeinschaft (DFG) is gratefully acknowledged.

### Literature Cited

1. Gladwell, G. M. L. "Contact Problems in the Classical Theory of Elasticity", Sijthoff and Noordhoff, Alphen aan den Rijn, 1980.
2. Johnson, K. L.; Kendall, K.; Roberts, A. D. "Surface Energy and the Contact of Elastic Solids", Proc. R. Soc. London, Ser. A 324 (1971) 301.
3. Barquins, M.; Courtel, R. "Rubber Friction and the Rheology of Viscoelastic Contact", Wear 32 (1975) 133.
4. Barquins, M. "Adhesive Contact and Kinetics of Adherence between a Rigid Sphere and an Elastomeric Solid", Int. J. Adhesion and Adhesives 3 (1983) 71.
5. Lee, E. H.; Radok, J. R. M. "The Contact Problem for Viscoelastic Bodies", Trans. ASME (J. Appl. Mech.) 27 (1960) 438.
6. Ting, T. C. T. "The Contact Stresses between a Rigid Indenter and a Viscoelastic Half-Space", Trans. ASME (J. Appl. Mech.) 33 (1966) 845.
7. Comninou, M. "Contact between Viscoelastic Bodies", Trans. ASME (J. Appl. Mech.) 43 (1976) 630.
8. Kravchuk, A. S. "On the Problem for Linearly and Nonlinearly Elastic Bodies of Finite Dimensions", J. Appl. Math. Mech. 41 (1977) 320.
9. Chow, T. S. "Deformational Contact and Friction on Viscoelastic Substrates", Wear 51 (1978) 355.
10. Graham, G. A. C. "Viscoelastic Contact Problems with Friction", Int. J. Eng. Sci. 18 (1980) 191.
11. Sabin, G. C. W.; Graham, G. A. C. "The Normal Aging Viscoelastic Contact Problem", Int. J. Eng. Sci. 18 (1980) 751.
12. Aksel, N.; Buggisch, H. "On the Problem of Contact between a Rigid Ball and a Viscoelastic Half-Space" (in German), Z. Angew. Math. u. Mech. (ZAMM) 62 (1982) 101.
13. Johnson, K. L. "Adhesion at the Contact of Solids", in: "Theoretical and Applied Mechanics"; Koiter, W. T., Ed.; North Holland, Amsterdam, 1977; 133.
14. Mittmann, H.-U.; Czaika, N.; Czichos, H. "A New Device for Simultaneous Measurement of Friction Force, Normal Force and Friction Coefficient", Wear 31 (1975) 179.

15. Czichos, H.; Feinle, P. "Tribological Behaviour of Thermoplastic, Filled, and Glass-Fibre-Reinforced Polymers - Contact Deformation, Friction and Wear, Surface Investigations", BAM Research Report 83, July 1982, 105 p. (Bundesanstalt für Materialprüfung, Berlin-Dahlem) (in German).
16. Becker, G. W., Schreuer, E. "Deformation Mechanics and Relaxation Behaviour", in: "Structure and Physical Behaviour of Polymers" (in German); Nitsche, R. and Wolf, K. A., Eds.; Springer, Berlin/Göttingen/Heidelberg, 1962; 331 ff.
17. Ehrenstein, G. W. "Polymeric Materials" (in German); Hanser, München, 1978; 104 ff.
18. Höhn, W.; Jungnickel, B.-J. "Structure and Relaxation Behaviour of Compressed Polyoxymethylene" (in German), Colloid and Polym. Sci. **260** (1982) 1093.
19. Czichos, H. "Influence of Adhesive and Abrasive Mechanisms on the Tribological Behaviour of Thermoplastic Polymers", Wear **88** (1983) 27.
20. Briscoe, B.J. "Wear of Polymers: An Essay on Fundamental Aspects", Tribology Int. **14** (1981) 231.
21. Erhard, G. "Sliding Friction of Polymer-Polymer Pairs" (in German), Jahrbuch VDI-Ges. Werkstofftechnik (Düsseldorf), 1981; 7.

## DISCUSSION

Question by Professor S. Bahadur, Iowa State University: The viscoelastic effect in deformation reported by you is similar to what has been known for a long time in wood. As such the deformation values in loading and unloading are different. Have you given any consideration how these results could be factored into the adhesion theory of friction which has as one of its components the real area of contact?

Answer: The aim of the deformation experiments was to study the influences of possible viscoelastic and viscoplastic effects on the Hertzian contact behaviour of curved thermoplastic polymers. Because these experiments were performed only with normal loads we have not attempted to extend these results to sliding Hertzian contacts. In contrast, the static friction experiments reported in this paper were performed with flat polymer-polymer contacts (pin-on-disc configuration) in order to keep in these experiments the mechanical stress situation as simple as possible.

Question by Professor D. Dowson, University of Leeds: How was the lubricant applied in the deformation studies? Did the author observe any lubricant entrapment within the Hertzian contact zone in the normal approach process? Many authors have reported trapped pools of lubricant in

the centre of Hertzian contacts when elastic spheres are loaded against flat surfaces in the presence of liquids.

Answer: The lubricant was applied as a thin boundary film to the disc surface. An entrapment of lubricant was not visible in our in-situ microscopic observations of the contact zone.

Question by Dr. Briscoe, Imperial College, London: I feel that surface free energy is not a good parameter to correlate with surface friction. Surface free energy may be related to cohesive energy density. There is too much data which contradicts this, e.g. (1) static/dynamic friction, (2) spin effects, (3) temperature and velocity dependence of friction.

Answer: In considering the results of the friction experiments it must be borne in mind that only the initial static friction, with a sliding distance of less than 500  $\mu\text{m}$  and negligible influences of velocity and temperature was studied. Because the microscopic in-situ observations of the contact interface revealed that the initial sliding motion occurred at the actual interface (without indication of deformation or material transfer effects) it is hypothesized that initial static friction is the resistance to overcome interfacial adhesion as characterized by the Dupré equation.

Question by Dr. R.C. Cavestri, Copeland Corporation, Sidney, Ohio: Have you considered the effect of the density of the polymers and possible correlation with the scatter of pin-on-disc data?

Answer: The question of the influences of polymer densities was not considered in this paper but in another research report (see ref. (15) ).

Question by Dr. D.H. Buckley, NASA Lewis Research Center, Cleveland: Don't the moisture (50% rel. humidity) of your experimental environment alter the work of adhesion and should you expect therefore a correlation between friction and work of adhesion?

Answer: The influence of moisture adsorbed by the polymers may indeed have an influence on the work of adhesion. However, in this study only the ranking of data and not their absolute values is considered. It is possible that the effect of moisture is one possible reason for the experimentally observed scatter of data.

Question by Dr. Youti Kuo, Xerox Company: What is the role of shear in your experiments and analysis?

Answer: Because the deformation experiments were performed only with normal loads and the contact deformation

displacement perpendicular to the contact interface was experimentally measured, the role of shear was not studied explicitly.

RECEIVED January 23, 1985

## Fracture Energetics and Surface Energetics of Polymer Wear

Lieng-Huang Lee

Webster Research Center, Xerox Corporation, Webster, NY 14580

Polymer wear can take place in various modes, e.g., adhesive, abrasive, transfer, fatigue, and tribo-chemical. In reality, several mechanisms can also operate simultaneously. If impactation is involved, an impact wear can be the chief mechanism. The predominance of any one type of wear can be influenced by the form of polymers, e.g., thermoplastics, elastomers or composites.

This paper is to discuss polymer wear on the basis of energetics. For adhesive wear, surface energetics are the dominant factor. For example, the work of adhesion of the two counterfaces has been correlated with wear rate. For abrasive wear, fracture energetics can dictate the crack formation and the intensity of wear. Depending on the ductility of polymers, fracture energy  $G_C$  or  $J_C$  of the material can directly affect the wear. A severe tribo-chemical wear could involve the generation of energetic particles, e.g., free radicals, electrons, positive ions, etc. For polymer transfer, surface polarity has been shown to determine the direction of transfer. Fatigue wear under a cyclic load can involve fracture energy of the material. We found that for fatigue resistance, fracture energy is the most important property. Moreover, most wear mechanisms eventually lead to fatigue wear of polymers.

Since the first review on the effect of surface energetics on polymer friction and wear published in 1974,<sup>(1)</sup> many new works have appeared. Some of these papers<sup>(2-4)</sup> are on fracture mechanics. In this paper we shall review our current knowledge about both fracture energetics and surface energetics of polymer wear. First, we discuss wear mechanisms and then emphasize these two aspects related to each wear mechanism.



### Polymer Wear Mechanisms

Several mechanisms of polymer wear have been discussed in the literature:(5-7) adhesive wear, abrasive wear, fatigue wear, tribo-chemical wear, corrosive wear and impact wear. We shall limit this discussion to the four basic mechanisms shown in Figure 1. Neither corrosive(5) nor impact wear(8,9) are common, and we do not plan to discuss these in this paper.

**Adhesive Wear.** Adhesive wear(5) is the transfer of material from one counterface to the other as a result of the formation of an adhesive junction under a normal load. Adhesion is facilitated by close contact, plastic deformation, or frictional heating.(10) Upon further sliding, some of the junctions can rupture, and the polymer can be transferred to the counterface of a metal or another polymer.

For polymer-polymer sliding pairs,(11) adhesion appears to be the dominant mechanism of polymer friction. Adhesion can also take place at the polymer-metal interface provided that surface roughness is below a certain value.(12) For a smooth surface, it is difficult to differentiate fatigue from adhesive wear.(5)

The wear rate as expressed in wear volume  $V_w$  can be empirically obtained from the Archard's equation:(13)

$$V_w = k L \cdot d / H \quad (1)$$

where  $k$  = wear constant (a property of the counterbodies),  $L$  = normal load,  $H$  = hardness (by indentation) of the weaker material, and  $d$  = sliding distance. In this equation, hardness is the only material property. However, for polymers, hardness is difficult to define clearly because of creep and stress relaxation which can take place at different temperatures. In the following discussion, we shall include some of the other tribologically significant properties(7) listed in Table I.

Adhesion is strongly influenced by the interfacial properties, e.g., surface topography, surface energetics, interfacial shear strength, and surface adsorbed layer. Among them, surface energetics(1) are of prime importance for the following reasons: 1. the formation of an adhesive junction(11) is determined by the work of adhesion,  $W_a$ , and the work of plastic deformation,  $W_d$ ; 2. the cohesive fracture of the joints depends on the work of cohesion,  $W_c$ ; and 3. the direction of the transfer depends on the surface energies of counterfaces - generally from a low surface energy to a high surface energy.(14,15)

Since adhesive wear involves the fracture of junctions, not only surface energetics but fracture energetics(16,17) should be considered. The roles of fracture energy,  $G_c$  (or fracture toughness,  $K_{Ic}$ ), ductile fracture energy,  $J_c$ , and elastomeric fracture energy,  $T_c$ , will be discussed in the following section. For this reason, we need to identify the weaker polymer as brittle, ductile or elastomeric. For example, adhesive as well as fatigue wear involves mostly elastomers.

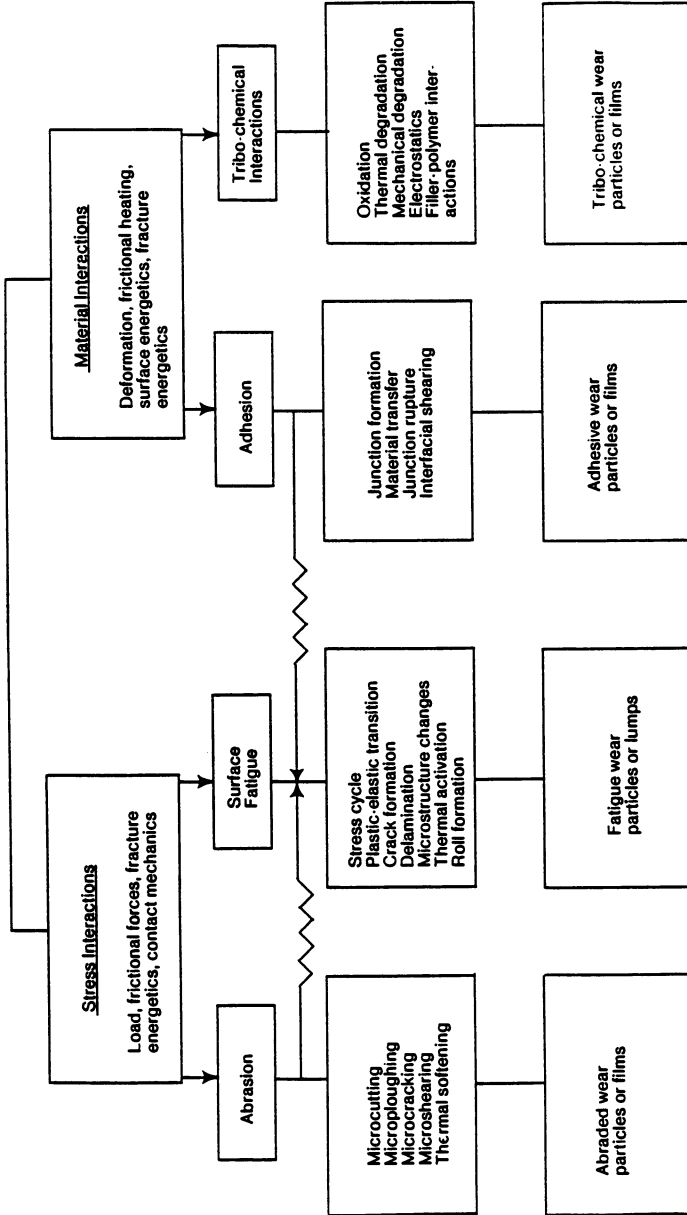


Figure 1. Tribological Interactions of Polymers

Table 1. Tribologically Significant Properties of Polymers

<u>Properties</u>	<u>Tribological Effects</u>
<u>Surface and Interface Properties</u>	
· Surface topography	- deformation, fatigue, abrasion, adhesion
· Surface energy	- adhesive wear, friction
· Interfacial shear strength	- friction, material transfer
· Adsorbed layers, surface films	· adhesion, friction, tribo-chemical effects
<u>Physical Properties</u>	
· Viscoelasticity	- deformation, friction, fatigue, abrasion
· Molecular weight and MW distribution	· surface energetics, fracture energy, fatigue, abrasive wear
· Glass (or melting) temperature	· friction, fatigue wear, abrasive wear, adhesive wear
· Cross-linking	- fatigue wear, deformation, friction, abrasive wear
· Cohesive energy density	- abrasive wear, deformation, friction, adhesive wear
· Thermal conductivity	· thermal effects, friction heating
<u>Mechanical Properties</u>	
· Elastic modulus	· deformation, fatigue, abrasive wear
· Yield pressure	· friction, deformation
· Hardness	· deformation, abrasive wear, fatigue, adhesive wear
· Shear strength	· deformation, friction, wear rate
· Fracture energy (or fracture toughness)	· asperity fracture, ploughing, abrasive wear, adhesive wear, fatigue
<u>Microstructure</u>	
· Crystal structure and orientation	· deformation, wear rate
· Second phase	· abrasive wear, wear rate
· Polyblend	- deformation, abrasion, fatigue, wear rate
· Reinforcing medium	· deformation, wear rate, abrasion
· Amorphous region	· deformation, abrasion, adhesion, ploughing, wear rate

**Abrasive Wear.** Abrasive wear(18) is common for brittle, ductile and elastomeric polymers. Abrasion is the wear by displacement of materials from surfaces in relative motion caused by the presence of hard protruberances or by the presence of hard particles either between the surfaces or embedded in one of them. As a result, microploughing, microshearing or microcutting can occur. Thus, fracture energetics and contact mechanics are involved in analyzing the wear results. We shall discuss briefly the wear rate with respect to different types of polymers.

**Brittle polymers.** A simple expression, similar to Archard's equation, has been used to determine the wear volume  $V_w$ (5):

$$V_w = k_1 L \cdot d \cdot \tan\theta / \pi H \quad (2)$$

where  $\theta$  = mean slopes of asperities (for a conical asperity, the friction force  $F = 2 \tan\theta / \pi$ ). In this equation, only one material property, hardness, is involved.

Ratner(19) found that there were three stages involved in the formation of a loose wear particle: 1) deformation of the surfaces to an area of contact determined by the hardness,  $H$ ; 2) relative motion opposed by a friction force  $F = \mu L$ ; and 3) rupture of the material at the junctions involving the work of rupture equal to the integral of the stress-strain relationship ( $\approx \sigma \cdot \epsilon$ ). Hence, the wear volume is

$$V_w = k_2 \mu \cdot d / H \cdot \sigma \cdot \epsilon \quad (3)$$

where  $\mu$  = friction coefficient,  $\sigma$  = breaking stress, and  $\epsilon$  = elongation at break. Noted that  $\sigma \cdot \epsilon$  is also a measure of toughness, which is the second material property to be considered. This should lead us to the discussion of fracture parameters involved in abrasion.

Fracture toughness,  $K_{IC}$ , has already been considered to be a variable in the fracture of metal.(2) Based on  $K_{IC}$ , the wear volume is measured as follows:

$$V_w = n^2 (P \cdot E \cdot L^{3/2} / K_{IC}^2 \cdot H^{3/2}) d \quad (4)$$

where  $n^2$  = work-hardening factor and  $P$  = yield strength. Since  $K_{IC}^2 = EG_{IC}$ (16), by setting  $n^2 = k_3$ , Eq. (4) becomes

$$V_w = k_3 (P \cdot L^{3/2} / G_{IC} \cdot H^{3/2}) d \quad (5)$$

where  $G_{IC}$  = fracture energy (mode I). Equation (5) indicates the direct involvement of a material property, fracture energy, in the abrasive wear. This equation was originally derived for metals and should be equally applicable to brittle polymers.

**Ductile polymers.** For ductile polymers, the linear elastic fracture mechanics do not apply. The introduction of the J-integral by Rice(20) has facilitated the application of ductile fracture mechanics for this polymer system.(17) Without detailed discussion, the ductile fracture energy  $J_{IC}$  is used instead of  $G_{IC}$  in Eq. (5):

$$V_w = k_4 (P \cdot L^{3/2} / J_{IC} \cdot H^{3/2}) d \quad (6)$$

The values of  $J_C$  for several polymers(17) are shown in Fig. 2. Note that  $J_C$  is always larger than  $G_C$  for most ductile polymers.

**Elastomers.** Ratner and Klitenik(21) obtained a wear rate equation for the abrasion of rubbers and their vulcanizates:

$$V_w = K_5 \mu(100-D)d/\sigma \quad (7)$$

where D is the percentage rebound resilience characterizing the hysteresis loss.

Champ, Southern and Thomas(22) found that the rate of wear ( $r_w$ ) was a function of the tear energy T:

$$r_w = BT^\alpha \quad (8)$$

where  $\alpha$  is an exponent which varies from 2 for natural rubber to 4 or more for noncrystallizing, unfilled rubbers, e.g., SBR, and B is a constant. Here, the tear energy, T is equivalent to G for brittle polymers.

**Fatigue wear.** Fatigue implies a mode of wear where nonapparent damage on the asperities is accumulated over a large number of loading and unloading cycles. As a result, apparent damage occurs in the formation and separation of wear particles from the surface of the weaker material. Fatigue wear is mild and generally appears in rolling. Under sliding conditions, fatigue wear can be found along with abrasive or adhesive wear.

The importance of fatigue wear was first recognized by Soviet scientists.(23) Some of extended fatigue wear equations were proposed by Kraghelsky and Nepomnyashchi,(24) and recently by Jain and Bahadur.(25,26) For our discussion, we use the simple relation based on Wohler's  $\sigma$ -N curve:(27)

$$N = (\sigma_0/\sigma)^b \quad (9)$$

where N is the number of cycles to failure,  $\sigma_0$  the static strength corresponding to a single application of stress to cause failure, and  $\sigma$  the applied cyclic stress. The exponent b is the fatigue resistance coefficient and is greater than 1. The b values for commonly known polymers are compiled in Table II.

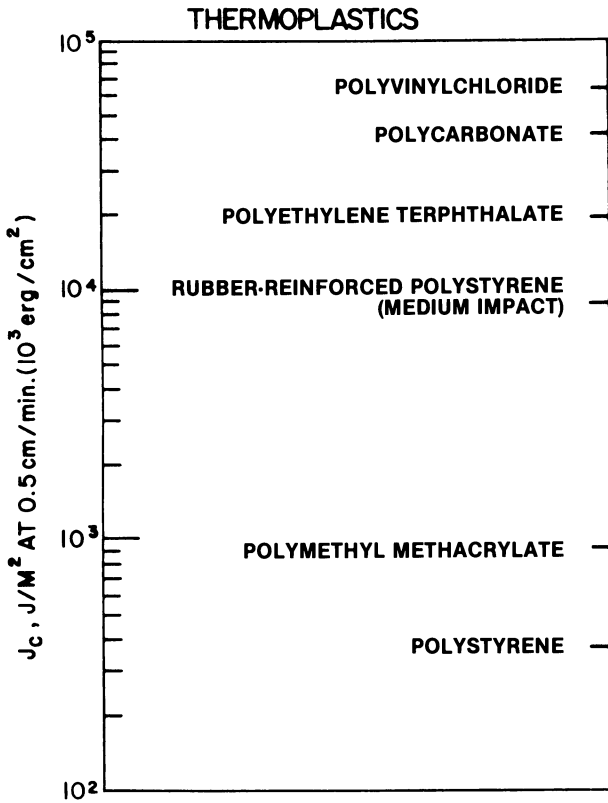


Figure 2 Ductile Fracture Energies,  $J_c$ , of Polymers

TABLE II. Fatigue Resistance Coefficients of Polymers

<u>Polymer</u>	<u>Fatigue Resistance Coefficient, b</u>	<u>Ref.</u>
Polymethyl methacrylate	(20.44)	26
	9.0	28
Acetal copolymer	7.7	28
Polyimides	7.3	29
Nylon 6,6	7.1	30
	4.7	28
High density polyethylene	4.51	26
Low density polyethylene	3.5	28
Polyvinyl chloride	3.15	26
Styrene-butadiene rubber (+ 5°C)	2.2	27
Styrene-butadiene rubber	1.9	27
Natural rubber	1.75	27
Sodium butadiene	1.4	27

Though fatigue wear generally takes place at the surface, it is somewhat affected by the fatigue properties of the bulk.(31) Fatigue involves crack formation and crack propagation (FCP), thus, it is a fracture process. For example, the crack growth rate per cycle,  $da/dN$ , has been related to  $\Delta K$  ( $K_{max} - K_{min}$ ) (Fig. 3):

$$da/dN = A\Delta K^m \quad (10)$$

where  $A$  and  $m$  are functions of materials, environment, frequency, temperature and stress ratio.  $K$  is the stress intensity factor.

The above relation has been further modified in the usual form of Paris Law(32) to include the material property, fracture toughness,  $K_C$ :

$$da/dN \sim (K/K_C)^m \quad (11)$$

The FCP rate is now inversely proportional to  $K_C$ . Thus, a polymer with high  $K_C$  should provide a long fatigue life during the wearing process.

Similar to Eq. (10), the crack growth rate per cycle(33) has also been expressed in terms of  $\Delta G$ :

$$da/dN = B_f \Delta G^q \quad (12)$$

where both  $B_f$  and  $q$  are constants. For ductile polymers, the growth rate has also been related to the J-integral(34):

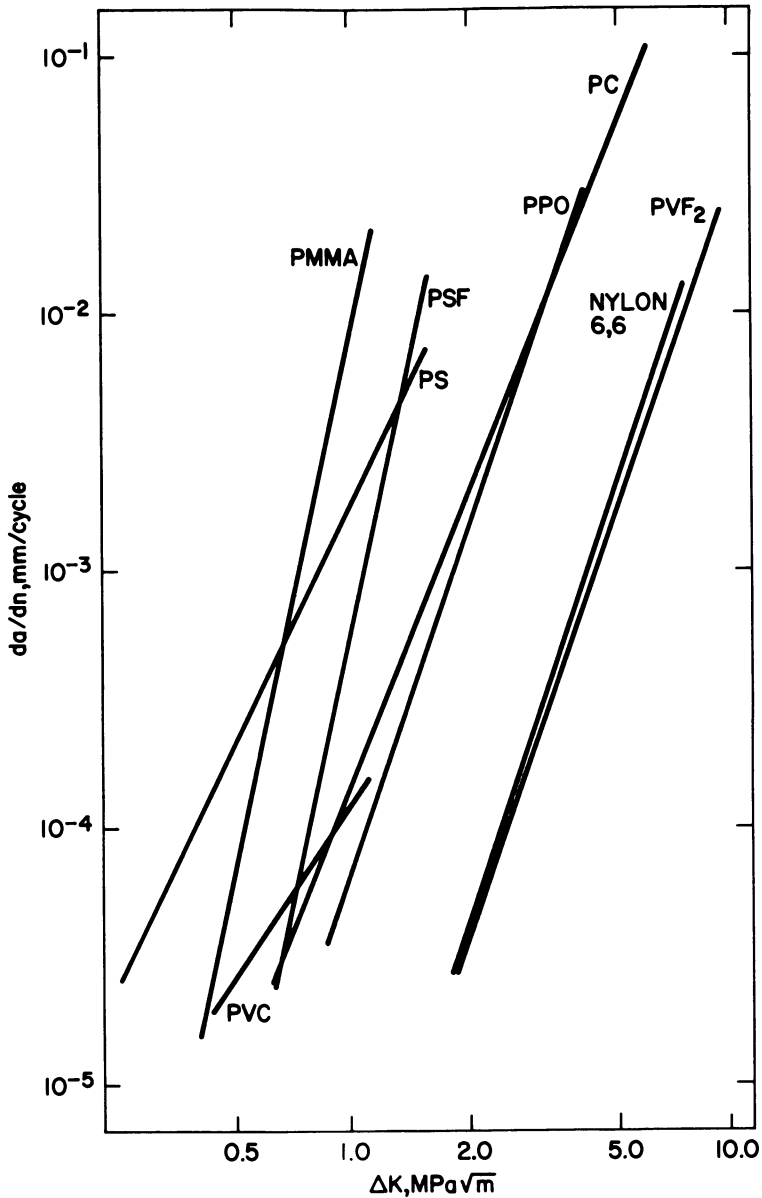


Figure 3. Fatigue Crack Propation Behavior of Polymers. (Reproduced with permission from Ref. 37. Copyright 1979, Plastics Rubber Institute.)



$$da/dN = B' \Delta J^n \quad (13)$$

An expression like Eq. (10) has been introduced for elastomers:

$$da/dN = A \Delta T^m \quad (14)$$

where  $T$  is the tear energy. Based on the Paris Law, we can further derive a similar relation as in Eq. (11):

$$(da/dN) \sim (T/T_C)^m \quad (15)$$

where  $T_C$  is the elastomeric fracture energy.

The importance of fracture energy in fatigue wear resistance is further implied by the work of Eiss and Potter,<sup>(29)</sup> as described in this volume. With the addition of polysiloxane elastomer to epoxide, the fracture energy, though not measured, should increase considerably. Their data show that the addition of 15% of the elastomer caused a decrease of the fatigue wear rate from 600 to 90  $\mu\text{m}^2/\text{kc}$ , while the elastic moduli decreased only slightly from 1.11 to 0.92 GPa. The increase in wear resistance appears to result also from the increase in fracture energy, instead of the decrease in modulus alone.

**Tribo-chemical Wear.** Besides the above three wear mechanisms, we should discuss tribo-chemical wear. Tribo-chemical wear<sup>(7)</sup> takes many forms. Some of these wears result from the interactions of the polymer with its environment, e.g., oxygen, ozone, heat (e.g., friction heat), surface contaminants, etc. The application of mechanical energy at the interface can also cause mechanochemical degradation<sup>(35)</sup> to generate free radicals which can further lead to cross-linking or other interactions. In the composites, polymer-filler interactions can also take place through mechanochemical mechanisms.

In brief, tribo-chemical wears are not easy to describe with a single expression. However, many of the tribo-chemical wears do transform into fatigue wear under multi-pass situations. Thus, the discussions about fatigue wear in the preceding section are still applicable to tribo-chemical wear under the fatigue mode.

Recent work by Dickinson on fracto-emission<sup>(36)</sup> indicates that ions, neutral particles, electrons and photons could be detected during the polymer fracture processes. The identification of these species during polymer wear may be of future research interests.

## Conclusions

Wear of polymers is a complete, system-dependent phenomenon which is influenced by a broad manifold of parameters. Fracture energetics and surface energetics are the most significant properties in determining various forms of polymer wear. For adhesive wear, surface energetics play a key role in junction formation and polymer transfer. A polymer of low surface energy tends to transfer to that of high surface energy. A wear-resistant material should be at least high in fracture energy. For abrasive resistance, a polymer needs to be hard and tough, while for fatigue resistance, toughness as determined by fracture energy appears the most important property.

LEGEND OF SYMBOLS  
(in metric units)

A	=	constant
a	=	crack growth length (cm)
B, B <sub>f</sub> , B'	=	constants
b	=	fatigue resistance coefficient
D	=	percentage rebound resilience (%)
d	=	sliding distance (cm)
E	=	elastic modulus (dyn-cm <sup>-2</sup> )
F	=	friction work (erg-cm <sup>-2</sup> )
G	=	crack release rate or crack extension force (erg-cm <sup>-2</sup> )
G <sub>c</sub>	=	fracture energy (erg-cm <sup>-2</sup> )
H	=	hardness
J	=	J-integral (erg-cm <sup>-2</sup> )
J <sub>c</sub>	=	ductile fracture energy (erg-cm <sup>-2</sup> )
K	=	stress intensity factor (dyn-cm <sup>-3/2</sup> )
K <sub>c</sub>	=	fracture toughness (dyn-cm <sup>-3/2</sup> )
k, k <sub>1</sub> , k <sub>2</sub> , k <sub>3</sub> , k <sub>4</sub> , k <sub>5</sub>	=	constants
L	=	load (erg-cm <sup>-2</sup> )
m, n	=	constants
N	=	cycle to failure
P	=	yield strength (dyn-cm <sup>-2</sup> )
q	=	constant
r <sub>w</sub>	=	wear rate
T	=	tear energy (erg-cm <sup>-2</sup> )
T <sub>c</sub>	=	elastometric fracture energy (erg-cm <sup>-2</sup> )
V <sub>w</sub>	=	wear volume (cm <sup>3</sup> )
W <sub>a</sub>	=	work of adhesion (erg-cm <sup>-2</sup> )
W <sub>c</sub>	=	work of cohesion (erg-cm <sup>-2</sup> )
W <sub>d</sub>	=	work of deformation (erg-cm <sup>-2</sup> )
a	=	constant
e	=	yield strain
s <sub>0</sub>	=	single application of failure stress (dyne-cm <sup>-2</sup> )
σ	=	applied cyclic stress, also breaking stress (dyne-cm <sup>-2</sup> )
μ	=	friction coefficient
θ	=	mean slopes of asperities

Literature Cited

1. Lee, L.H., "Advances in Polymer Friction and Wear," 5A, 31, Plenum, New York (1974).
2. Hornbogen, E., Wear, 33, 251 (1975).
3. Rosenfeld, A.R., Wear, 61, 125 (1980).
4. Rosenfeld, A.R., Wear, 72, 245 (1981).
5. Lancaster, J.K., in "Polymer Science," Jenkins, A.D., Editor, vol. 2, chapt. 4, North Holland, London (1972).
6. Briscoe, B.J.; Tabor, D., "Fundamental Tribology, Proceedings of International Conference," pp. 733-758, MIT Press, Cambridge, MA (1980).

7. Czichos, H., "Importance of Properties of Solids to Friction and Wear Behavior" in "Tribology in the 80," Proceedings of NASA Conference, Publication 2300, pp. 71-106, Washington, D.C. (1984).
8. Engel, P.A., "Impact Wear of Materials," Elsevier, Amsterdam (1978).
9. Ratner, S.B.; Styler, E.E., Wear, 73, 213, (1981).
10. Tanaka, K.; Uchiyama, Y. in "Advances in Polymer Friction and Wear," Lee, L.H., Editor, 50, p. 499, Plenum, New York (1974).
11. Czichos, H., Wear, 88, 27 (1983).
12. Eiss, Jr., N.S.; Bayraktaroglu, M.M., ASLE Transaction, 23, No. 3, 269 (1979).
13. Archard, J.F., J. Appl. Phys., 24, 981 (1953).
14. Sviridyonok, A.I., Bely, V.A., Smurugov, V.A.; Savkin, V.G., Wear, 25, 301 (1973).
15. Jain, V.K.; Bahadur, S., Wear, 46, 177 (1978).
16. Lee, L.H., in "Physical Aspects of Polymer Surfaces," Mittal, K.L., Editor, vol. 1, 523, Plenum, New York (1983).
17. Lee, L.H. in "Adhesive Joints - Formation Characteristics and Testing," Mittal, K.L., Editor, 739, Plenum, New York (1984).
18. Lancaster, J.K., Wear, 14, 223 (1969).
19. Ratner, S.B., Farberova, I.I., Radyukevich, O.V.; Lure, E.G., Soviet Plastics, 7, 37 (1964).
20. Rice, J.R., J. Appl. Mech., 35, 379 (1968).
21. Ratner, S.B.; Klitenik, G.S., Zav Lab., 25 (11), 1375 (1959).
22. Champ, D.H., Southern, E.; Thomas, A.G., in "Advances in Polymer Friction and Wear," Lee, L.H., Editor, 5A, 133, Plenum, New York (1974).
23. Bartenev, G.M.; Lavrentev, V.V., "Friction and Wear of Polymers," Lee, L.H.; Ludema, K.C., Editors, Translated from Russian into English by D.B. Payne, Elsevier, Amsterdam (1981).
24. Kraghelsky, I.V.; Nepomnyashchi, E.F., Wear, 8, 303 (1965).
25. Jain, V.K., Bahadur, S., Wear, 60, 237 (1980).
26. Jain, V.K.; Bahadur, S., Wear, 79, 241 (1982).
27. Reznikovskii, M.M. in "Abrasion in Rubber," James, D.T., Editor, pp. 119-126, McLaren & Sons, London (1967).
28. Lancaster, J.K., Plastics Polym., 41, (156), 297 (1973).
29. Eiss, Jr., N.S.; Potter III, J.R., this volume.
30. Bucknell, B., in "Polymer Science," Jenkins, A.D., Editor, vol. 1, chapt. 10, North Holland, Amsterdam (1972).
31. Hertzberg, R.W.; Manson, J.A., "Fatigue of Engineering Plastics," Academic Press, New York (1980).
32. Williams, J.G., J. Mater. Sci., 12, 2535 (1977).
33. Kinloch, A.J.; Young, R.J., "Fracture Behavior of Polymers," Applied Science Publishers, London and New York (1983).
34. Romanko, J., Liechti, K.M.; Knauss, W.G., "Adhesive Joints - Formations, Characteristics, and Testing," Mittal, K.L., Editor, 567, Plenum, New York (1984).
35. Barambolm, N.K., "Mechano-Chemistry of Polymers," MacLaren & Sons, London (1964).
36. Dickinson, J.T., in "Adhesive Chemistry - Developments and Trends," Lee, L.H., Editor, Plenum, New York (1984).

RECEIVED January 23, 1985

## Joint Role of Interfacial Forces and Viscoelastic Effects in Polymer Adhesion and Wear

Robert J. Good<sup>1</sup> and Fereydoun Shoraka<sup>2</sup>

<sup>1</sup>Department of Chemical Engineering, State University of New York-Buffalo, Buffalo, NY 14260

<sup>2</sup>Semiconductors Division, The Carborundum Company, Sanborn, NY 14132

A criterion is derived for predicting the presence or absence of strong adhesion in a polymer/solid system. It also predicts the mode of separation, and hence, in frictional situations, it predicts the wear of the polymer. The separation process is analyzed with the aid of a general model, which is developed by the following argument: "Craze matter", in a brittle, thermoplastic solid in which crazes have formed, consists of fibrils of oriented polymer. Fibrils are also observed at the separation front in the peeling separation of a pressure-sensitive adhesive. The difference between these two kinds of systems is chiefly a matter of time scales and of fibril size, and the nucleation of fibril formation. The main cause of dissipation of energy (and hence resistance to separation) in both cases is the deformation involved in pulling the fibrils. The role of interfacial forces is to anchor the bases of the fibrils to the substrate. If this anchoring is weak, the fibrils will detach before much energy is dissipated in drawing them. If the anchoring is stronger than the effective shear strength of the polymer, fibrils may be drawn until they reach a state where either (by strain-strengthening) they become stronger than the base attachment, or else they rupture. The model here proposed provides a unified theory of adhesion for systems ranging from hard, strong adhesives to pressure-sensitive tapes and to systems where "tack" is observed. It also provides a basis for a theory of adhesional wear of polymers.

A persistent puzzle in the theory of adhesion, for the past 30 years or more, has been the question of whether interfacial forces or viscoelastic effects control adhesion. The easy answer to this question is, both. But when this answer is accepted, the next question must be, What is their interaction? Can the interaction be expressed as a "universal" relationship? And how can a knowledge of viscoelas-

tic and interfacial properties be used jointly, to predict the behavior of adhering systems?

The principal hindrance to the understanding of the interaction has been the lack of a suitable model for polymer deformation at and near an interface, during a separation process. Workers in the field of adhesion have been aware of polymer crazing, as a process that is highly relevant to the problem of adhesive strength, for a number of years. A paper on crazing was given at a Gordon Conference on Adhesion, by R. Kambour, and the material was subsequently published (1). But up to the present, the craze concept has not been successfully applied to adhesion problems.

In 1983, an important review volume on crazing was published (2); and a number of other relevant reviews on polymer fracture (3) and assemblages of papers on adhesion (4-6) have been published recently. These and other developments enable us, now, to propose a theory of the separation process that will make it possible to predict and correlate experimental results, e.g., as to when strong or weak adhesion of a polymer to a hard, strong solid will occur.

This theory is also applicable to polymer wear. Indeed, the theory that we will present could be considered to cover the "wear" aspect of adhesion and the adhesional aspect of wear, simultaneously. See the recent reviews by Briscoe, for earlier discussions of the adhesional aspects of polymer wear (7,8). We will discuss wear explicitly, after developing the general theory.

## Theory

### Review of Some Important Facts about Polymer Failure, and Crazing.

We may consider two extremes in regard to heat effects in the failure of a bulk polymer: (1) adiabatic systems and (2) isothermal systems. And we may consider two qualitative extremes with regard to polymer hardness and strength: the polymer may be (a) hard and brittle, or (b) soft and tough. Some examples of the four combinations of these extremes are:

(1a) A hard, strong, brittle polymer such as PMMA or PS, loaded to failure in simple tension. The failure front propagates across the specimen at a speed that may range from 10 to 100 m/sec (2b). (The theoretical limit is 1/3 the speed of sound, or about 700 m/sec.) The local temperature rise (9) may approach the  $T_g$  of the polymer, or temperatures up to 200° above it (10,11).

(2a) With a brittle polymer under sub-critical tensile loading normal to a pre-existing crack, a slow propagation regime may persist, with propagation at a speed as slow as  $10^{-8}$  m/sec. At such slow speeds, the process should be isothermal.

(1b) A pressure-sensitive tape with adhesive, say, 75  $\mu\text{m}$  thick, folded back upon itself into a T peeling configuration. When peeled at speeds faster than about 0.015 m/sec., a temperature rise is detectable; and at a rate of 0.15 m/sec., a rise as large as 10° has been observed (12). It was found that the peeling force was a linear function of the temperature rise.

(2b) When the T-peel sample just described was pulled at less than 0.005 m/sec., the temperature rise was less than 0.1°C.

Phenomena such as these can be expected in the case of any polymer adhering to a rigid solid, when separation occurs.

When a crack propagates through a brittle polymer, the crack is "led" by a craze. Since the void space of a craze is bridged by fibrils, it is believed that the energy required for propagating a crack is dissipated in the pulling of those fibrils (1), and in the release of elastic energy when stretched fibrils rupture and retract as the actual separation front passes (13). The initial formation of fibrils, as a craze tip advances, is now believed to occur, most commonly, by the local flow mechanism of the Taylor meniscus instability (14-16), although microcavitation (17) may also be involved. This question is reviewed in Ref. (2a). The thickening of a craze may occur by two mechanisms (2a,18): either elongation at constant mass of a fibril (Kramer refers to this as a creep mechanism) or by an increase in the mass of the material that constitutes a fibril, by drawing from the bulk polymer outside the craze (surface drawing mechanism). The deformation may undergo a transition from surface drawing to constant-mass extension, as the craze approaches its limiting thickness. The behavior in regard to the thickening mechanism varies with the environment (e.g., presence or absence of a craze-promoting liquid) and with polymer composition and properties such as molecular weight, chain entanglement, etc.

Full details of the final rupture of fibrils are not available at present; and the mechanism probably varies considerably, from one system to another. See section 7 of Ref. (2a). Electron micrographs of fracture surfaces have been interpreted as showing the final separation front progressing by discontinuous jumps, particularly during fatigue experiments (19) and also in experiments with continuous loading (20,21). The jumps appear to occur both along a central surface within a craze, and with lateral jumping from one side of the craze to the other.

In principle, the rupture of a fibril may occur by at least two or three mechanisms, which are not always clearly separable. One is the end point of the drawing (creep) mechanism at constant mass of polymer in the fibril. A condition of local necking down could develop, leading to failure (22). See Fig. 1. This would be more likely to exist with low than with high MW polymers. Alternatively, and particularly with high MW polymers, chain scission might occur. Or an event might occur as an immediate sequel to an increase in local resistance to surface drawing. The resistance could increase on account of local structural fluctuations within the bulk polymer, e.g., of density of chain entanglements. The surface drawing mechanism would be replaced by elongation at constant mass; and the local fluctuations could lead to an enhancement of sensitivity to rupture by one of the mechanisms just mentioned.

The release of elastic energy stored in the fibrils themselves, when they rupture, must be mentioned in developing a model of the separation process for adhering systems. Retraction of fibrils after rupture can be observed visually, in the peeling of a pressure-sensitive tape (11,23). See Figure 2. Döll (2b) reports for PMMA, that the stored elastic energy,  $U_0$ , is as large as 30 to 40% of the total fracture energy,  $\mathcal{G}$ , and he estimates that the elastic fibril elongation is by 200 to 400%, in slow fracture. This may be taken to indicate that, in slow crack growth, the rupture mechanism is predominantly by chain scission rather than necking down. At the transition from slow to fast fracture, Döll estimates that "In PMMA,

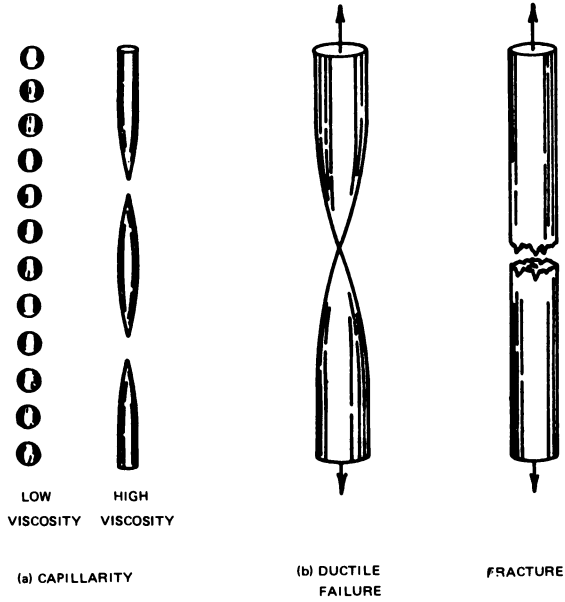


Figure 1. Mechanisms of instability of filaments that are being uniaxially stretched. (Reproduced with permission from Ref. 20. Copyright 1979 John Wiley & Sons, Inc.)

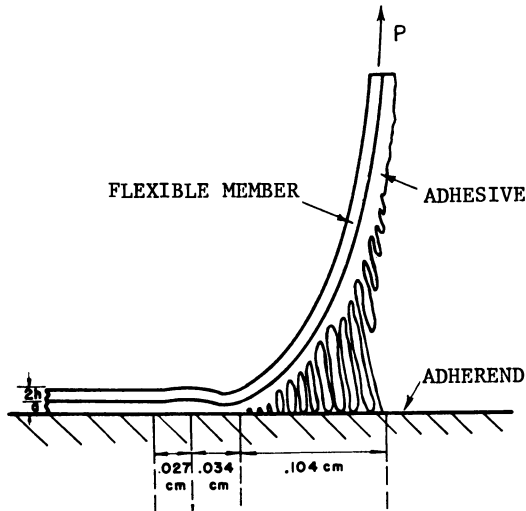


Figure 2. Fibrillar structure in peeling a pressure-sensitive tape. Note the retraction of fibrils that have separated from the solid. (Reproduced with permission from Ref. 21. Copyright 1969 John Wiley & Sons, Inc.)

nearly 60% of the strain energy release rate is directly converted into heat."

In the adiabatic case, with rapid advance of the failure front, the local temperature rise may lead to heating polymer fibrils to a range where their shear and extensional viscosity are so severely reduced that necking-down and rupture will quickly ensue. This means that there is a much greater probability that fibril rupture occurs by plastic necking down rather than chain scission, in a fast crack than in a slow one.

The length of a craze, leading a slowly-advancing crack in PMMA, is in the range of 30 to 50  $\mu\text{m}$  (2b). The length of a craze leading a rapidly-advancing crack is difficult to measure; but it is not likely to differ from the slowly-advancing case by more than an order of magnitude. If the crack is advancing at, say, 100 m/sec. (2a), the "deformation zone" (between the undisturbed polymer and the ruptured, rear edge of the craze) will pass a point in space in less than 1  $\mu\text{sec}$ . This is many orders of magnitude shorter a time than the relaxation time of a polymer such as PMMA or PS at room temperature. So the formation of craze fibrils in a craze leading a fast-moving crack can occur only if there is local heating, to reduce the relaxation time.

As mentioned above, in the peeling separation of a pressure-sensitive tape, a temperature rise of 1 to 10°C is observed, with drive rates that are very modest compared to the rate of advance of a freely propagating crack in a brittle polymer. This temperature rise lowers the relaxation time, even though the polymer may be 10 to 50° above its  $T_g$  already. With a "hot melt adhesive" polymer, the  $T_g$  may be in the range of about 40 to 80°C. Such an adhesive may exhibit extremely "tough" mechanical behavior, no doubt because it resembles the pressure-sensitive tape case, described above, more than the brittle polymer case.

Adhering and Wearing Systems: The Fibril/Craze Model. We may apply the concepts just described, to an adhering system, either for a thermoplastic polymer adhering to another solid, or for the case where two solids are glued together by a thermoplastic polymer. This requires that we postulate a fracture front progressing either at some distance from the polymer-solid interface, or else at the interface itself. The former corresponds to "cohesive failure" of the polymer, and need not concern us, as it has already been discussed by the senior author (24).

Brittle separation of an adhering system, under loading perpendicular to the interface, normally occurs in a crack-opening mode. The force requirement for separation, in a mode in which rigid facing surfaces remain exactly parallel, would be enormous (25). Brittle separation at an interface, in the absence of a dissipation mechanism resembling the mechanism that controls bulk fracture, would occur at a much lower level of force. So it will be necessary to postulate a dissipation mechanism, such as an interfacial craze, for those cases in which a polymer that has a high  $T_g$  does not separate easily from a hard solid.

We will also apply the concepts discussed above, to systems in which the polymer is not brittle, e.g., the peeling of pressure-sensitive tapes. For such polymer-solid systems, when separation



occurs at or near the interface, fibrils can often be observed with the naked eye or at low magnification. These fibrils are similar to those that bridge crazes. See Figure 2. A major difference is geometric: they are several orders of magnitude larger in diameter and in length. The formation of these fibrils is probably initiated by the Taylor instability mechanism, in most cases. The adhesive formulation is commonly chosen (empirically) so that, in peeling from a rigid solid, the bases detach from the solid leaving no apparent residue. It is possible, however, to use formulations with which, in peeling, the fibrils rupture and an easily-detectable residue is left on the solid. Connelly, *et al.* (26) and Gupta (27) have recently analyzed the force required for peeling, in terms of the tensile properties of the fibrous material shown in Figure 2.

This brings us to a crucial question about the separation process in an adhering system: whether or not polymeric material is deposited on the solid. It is in answering that question that we can achieve an understanding of, and make predictions about, the strength of adhesion and the occurrence of polymer wear. (We will discuss just why this is a crucial question, below.)

In the separation of an adhering system at or near an interface, in terms of a craze mechanism, there will be four differences from separation within a bulk polymer. One is, that interfacial voids (or proto-voids) may exist. These can act as cavitation nuclei; and interfacial craze formation, starting from such nuclei, would be orders of magnitude more rapid than crazing by homogeneous nucleation. Such cavitation could also be more rapid than the processes that occur in the Taylor instability mechanism, particularly if it should happen that the voids at the interface formed a two-dimensional continuum. Patches of low-energy matter in the solid surface can also be loci of void initiation, even if no voids are present before loading.

A second difference is that, if interfacial voids are not present, and if a Taylor instability mechanism initiates the craze formation at the interface, then the columns that initially form can terminate either at the substrate, as column bases, or in a region of polymer that is, in effect, a thin, continuous layer of matter. In the latter case, we would have a near-interfacial craze.

Third, if any effectively bare areas of substrate appear, the stress on adjoining areas (the column bases) will increase; and as the columns are stretched into fibrils, the areas of the bases of the fibrils will decrease. Then, it will be a matter of comparison of two force terms: the strength of the interface, and the force requirement for drawing fibrils, by whatever mechanism. This comparison will determine whether detachment or fibril rupture (or further surface drawing) will occur.

Fourth, even in the absence of interfacial void areas or patches of lower-energy matter on the solid, small-scale stress concentrations under load can arise by reason of ridges, peaks, and other topographical features of the solid. These will lead to the triaxial stress that can cause cavitation, and hence initiate crazing. Ridges and peaks will, of course, be accompanied by valleys; and the stress across the polymer-solid interface will be locally reduced below the average, in such depressions. Hence, enhanced attachment of bases of fibrils to the solid at valleys will be quite possible.

Separation within a bulk polymer and separation at or near an interface will, however, have one feature in common. Consider what occurs after a fibril has been formed and has been drawn to the maximum elongation it can achieve without rupture. A final rupture process in, say, the middle of a fibril, is confined to a segment whose length is not more than a few times its diameter. Since the length-to-diameter ratio for a typical fibril is greater than  $10^3$ , the mass that is involved in the final rupture must be less than  $10^{-2}$  of the fibril mass. So the energy requirement for the final rupture will be one or two orders of magnitude less than the energy required to draw the fibril and orient the polymer chains in it. (Cf. the well-known fact that  $\mathcal{G}$ , the energy dissipated per unit increase in crack area, for a polymer such as polystyrene or PMMA, is two or more orders of magnitude larger than the value estimated from the breaking of covalent bonds.) The energy requirement to rupture a fibril near its center will bear the same relation to the energy required to draw the fibril without breaking, for crazes in the bulk, as for crazes at or near an interface — and also for the fibrils that are drawn in the peeling of a pressure-sensitive tape.

Analysis of the Separation Process. We may eliminate from consideration, here, the case of separation wholly in one bulk phase or the other, far from the interface, and also the case in which the forces across the interface are many orders of magnitude weaker than the inter-chain forces within either phase. (These cases are irrelevant to the analysis.) We can approximate what happens by means of a detailed, branching scenario, as follows, for a polymer on a rigid solid.

(1) Transition from the intact system to a system in which either (a) at, or (b) very near, the interface, either the cavitation mechanism or the Argon "Taylor instability" mechanism has functioned, and voids have formed. Other than void formation, there has been little polymer deformation.

(2a) If (1a), the interfacial voids may (i) grow without limit, under small stress and small displacement of the driving system, without craze formation, until interfacial detachment is complete. Then the practical strength of adhesion is "weak". Or (ii) the void growth may slow down and stop, leaving many isolated patches of intact interface, which then become the bases of columns that are the precursors of fibrils.

(2b) If (1b), and the cavitation mechanism is operative, the matter between the voids becomes reorganized, under minor tensile deformation, into columns; see above. If the Argon mechanism is operative, the columns exist without further reorganization.

(3) If the applied force on a column is greater than the effective shear strength of the polymer, then the columns are drawn into fibrils. See Figure 3. This may occur (as already noted with regard to crazes in bulk polymer) either at constant fibril mass, or by a "surface drawing" mechanism, pulling matter out of the bulk at the polymer side of the craze (2a). Again, elastic stretching of the fibrils may also take place (2b). If the process is slow, it is isothermal; if rapid, adiabatic. The applied force acts with an appreciable displacement, and hence does considerable deformational work.

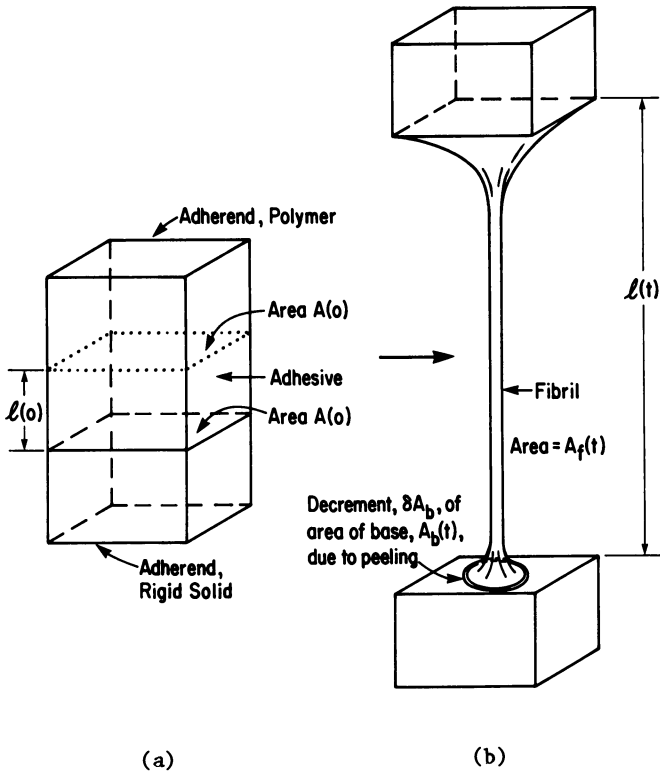


Figure 3. Drawing out of a fibril that has its base attached to a solid.

(a) If, as in (1b), a continuous layer of polymer covers the substrate, surface drawing can occur and molecules can be pulled out of that layer, thinning it, and possibly causing the formation (nucleation) of patches of bare substrate — in which case, the situation is as in (2a) (ii).

(b) If, however, bare patches do not develop, then no true interfacial separation can occur. Instead, drawing of fibrils continues until rupture occurs, as with crazes in bulk polymer. At the end of a separation process with fibril rupture, polymer will be found on the surface of the solid.

(4) Starting from a condition in which fibrils are attached to the substrate at discrete bases, and are being elongated under tension, there are two possibilities:

(a) The fibril base areas will shrink, by a radial inward peeling mode of separation. Once this starts, the perimeter of the base decreases, and so does the force that opposes this deformation. The local system becomes unstable, and detachment ensues. Note that the initial stage of this process involves a linear displacement of at most, very few atom diameters. So even if the force required per unit interfacial area is large, the work,  $\Delta G^a \Delta A_b$ , will be extremely small. (Here,  $A_b$  is the base area of the fibril.) It is, then, fully justified to call this a differential process, and to write,  $\Delta G^a dA_b$ .

(b) Alternatively, fibril drawing will continue until rupture occurs.

For each branch point, it is possible to set up an inequality that expresses the criterion for one fork or the other. The most important branch point of the scenario is the one involving the high-energy step, of fibril-drawing; and so we will write down the inequalities that pertain to stages 3 and 4 only.

Figure 3 shows, schematically, the pulling of a fibril. The initial state is an idealized one in which the polymer material, and the block of substrate, have been detached from the surrounding matter, so that we can examine stages 3 and 4 of the scenario. If  $\Delta G^a$  is the free energy of adhesion (i.e., "anchoring" the column base or foot to the solid) and  $\sigma_y$  is the yield strength of the polymer, then the condition for drawing a fibril by extension, at constant mass, vs. that for interfacial peeling, is:

$$\Delta G^a dA_b < \sigma_y A_f dl: \text{ Interfacial peeling at fibril base.} \quad (1a)$$

$$\Delta G^a dA_b > \sigma_y A_f dl: \text{ Yielding of polymer;} \quad (1b)$$

fibrils drawn, uniformly or  
with necking.

Here,  $A_b$  is the base area at time  $t$ ; at the time when fibril drawing may be said to start, we may take  $A_b = A_b(0)$ .  $A_f(t)$  is the area of a fibril at time  $t$ . Of course, all fibrils will not have the same initial areas  $A_b(0)$  and  $A_f(0)$ .

We have already mentioned that craze thickening (without rupture) may occur by one or both of two mechanisms. That discussion, above, may be taken over intact, for the case of interfacial crazes. The rheological analysis of the surface drawing mechanism is not available, so we cannot include it in the present analysis; if it

plays a part in the real process, we must let the constant-mass process stand as surrogate for it, and, likewise, for the process of rupture by chain scission. See Figure 3. We will discuss this approximation, below.

There are two reasons why interfacial peeling of a fibril base should not be confused with interfacial peeling on a macroscopic scale. First, macroscopic separation involves the drawing-out of fibrils; and so we must define the "microscopic" scale as being the dimensional magnitude in which there are not any yet-smaller fibrils formed. We must avoid the "big fleas have little fleas . . ." infinite regress, of course.

Second, macroscopic peeling separation occurs along a linear front, with a constant force requirement, on the average. But the microscopic separation of a fibril base will proceed radially inward, with a steadily decreasing force requirement per unit distance of motion normal to the solid. And as the base peels, the base volume decreases and fibril volume increases as polymer passes from base into fibril.

If the radius,  $r$ , of the base decreases by  $dr$ , the area  $A_b$  decreases by  $dA = 2\pi r dr$ . Hence as separation proceeds,  $dA_b/dr$  decreases. Also,  $\sigma_y$  is likely to increase, if the local temperature is constant; this commonly occurs in the drawing of fibres for textile applications. In addition, elastic energy will be stored in the fibril; see above. So, if the system starts out conforming to the inequality, (1b), (i.e., no base peeling) the right side will increase, as the extension,  $l$ , increases. The result may be a switch to the inequality (1a), and, as already noted, the start of base peeling, and the complete interfacial detachment of the fibril at its base. We will examine the inequalities, (1a) and (1b), below, with numerical examples.

The argument just made assumes, implicitly, a model in which the substrate is molecularly flat. Appropriate revision to account for roughness effects can be made, which will be relevant when the substrate microtopography is known. The mathematical methods that have been employed to treat the contact angle of a liquid on a rough surface (28) may be employed. For example, we may define  $\underline{a}$  as actual area of interface and  $\underline{A}$  as actual area projected on a plane parallel to the envelope of the surface. The roughness ratio,  $\rho$ , is

$$\rho \equiv \frac{\underline{a}}{\underline{A}} = \frac{da}{dA} \geq 1$$

For separation that faithfully follows the true interface, the criteria (1a) and (1b) will become

$$\rho \Delta G^a dA_b < \sigma_y A_f dl: \text{ Interfacial peeling} \quad (3a)$$

$$\rho \Delta G^a dA_b > \sigma_y A_f dl: \text{ Yielding of polymer} \quad (3b)$$

(The comparison of the inequalities, (1a) and (1b) vs. (3a) and (3b) explains quantitatively why adhesion to a roughened surface is generally stronger than to a smooth surface, provided molecular contact has been made over the whole microscopic area.)

Finally, at time  $t$ , after a fibril has been fully drawn, its

cross section is  $A_f(t)$  and its ultimate tensile strength (true stress) is  $\sigma_{uf}$ . The separation criterion for a flat surface is:

$$\Delta G^a dA_b < \sigma_{uf} A_f(t) dl: \text{ Interfacial separation before } \quad (4a)$$

fibril rupture

$$\Delta G^a dA_b > \sigma_{uf} A_f(t) dl: \text{ Fibril ruptures } \quad (4b)$$

See above, section on Adhering and Wearing Systems, regarding the small magnitude of the energy requirement in the step that corresponds to (4b).

It is clear that if the criterion (1a) or (3a) holds for interfacial separation before fibril drawing (whether on account of  $\Delta G^a$  being small or  $\sigma_y$  being large) then there will not be a large dissipation of energy,  $\mathcal{E}$ , per unit advance of the macroscopic separation front, and there will be very little work for the applied force to do. So the force required to open up an interfacial crack, in brittle separation, will be small:

$$\sigma_u \approx 0 \quad (5a)$$

where  $\sigma_u$  is the ultimate strength of the system as a whole.

If, however, the criterion (1b) or (3b) holds, then the system can be treated by Griffith-Irwin (29,30) crack theory, as extended by Good (24) to interfacial separation. That treatment yields the expression,

$$\sigma_u = k \sqrt{\frac{E^* \mathcal{E}}{\lambda}} \quad (5b)$$

where  $k$  is a geometric coefficient near unity, and  $\lambda$  is length of the preexisting crack.  $E^*$  is the effective elastic modulus of the system; it is obtained from the Young's moduli of the adherends and the adhesive, weighted in proportion to their contribution (transmission) of energy from the strain field to the crack tip as failure starts. Compare Good's earlier analysis (24) of the criteria for "adhesive" vs. "cohesive" separation. Both interfacial separation without further fibril elongation and fibril rupture without further elongation other than the rupture, require only very small displacements, and hence, the dissipation of very little energy. Thus, it is the plastic deformation in drawing fibrils, before rupture or interfacial separation, that provides the large dissipation of energy that accounts for appreciable resistance to separation.

In the adiabatic case, local heating of the fibrils during drawing will have a profound influence on the inequalities, (1) and (3). The yield strength term,  $\sigma_y$ , in these inequalities may decrease rapidly, particularly if the rate of elongation is large, as will be the case with a rapidly-moving separation front. This decrease in  $\sigma_y$  (which opposes the strain-strengthening mentioned above) will have the effect that, if (1b) holds initially, it will continue to hold throughout the process. Interfacial separation will not occur; and the effective adhesion will be "strong".

The analysis given above, leading to the inequalities (1), (3)

and (4), is independent of whether the energy that is required comes (as in brittle separation) from the elastic strain field, or directly from the external drive mechanism. The force per unit width, for peeling a pressure-sensitive tape (the case in which the elastic strain energy of the backing tape is negligible), will then be

$$P = \frac{G}{\gamma} \text{ if interfacial forces are strong relative to force required to draw fibres.} \quad (6a)$$

$$\approx 0 \text{ if interfacial forces are weak.} \quad (6b)$$

Discussion. The transition between conditions (1a) and (1b), as a function of variables in the system, will be abrupt. This will be true because of the trends that have already been mentioned: the strain-strengthening of the fibrils, and the decrease in base area of fibril base/substrate contact, as deformation proceeds.

The fact of this abrupt transition leads to an answer to a question that has not been formally addressed in the literature on adhesion up to the present. In ordinary parlance, "adhesion" is often spoken of as a property that is present or absent, without qualification. In systems of stiff adherends, for which the separation process resembles fracture, it is not common to speak of "weak adhesion" other than as essentially zero strength. While it is possible to attain strength that is intermediate between the tensile strength of the weaker of two adherends, and nearly zero strength, it is not always particularly easy to do so. The question, Why is this so? has the following answer: If the interfacial strength at the fibril bases is great enough that base-detachment does not occur, then it is most probable that a relatively large dissipation of work, in fibril drawing and craze thickening, will occur. The required force for separation will be large. But if the effective interfacial strength at the fibril base drops below the initial yield strength of the fibres, then the fibrils will not be drawn; and the force requirement will be small. It is only if there is a very close balance of strengths (i.e., of the interface, vs. yield strength of the polymer) that there may be initially some polymer drawing, followed by weakening due to local heating on other causes, such that an intermediate amount of work will be required, to propagate a separation front.

It was mentioned, above, that the question of whether or not polymeric material remained on the solid after separation, was crucial. We can now see why this is so. In the absence of a weak boundary layer, the transfer of polymeric material of a hard, strong polymer will occur under conditions that resemble the bulk fracture of that polymer, i.e., craze/crack propagation; and the requirement of energy dissipation will be similar. So the effective strength of the two-phase system will be approximately the same as that of the bulk polymer — which was assumed to be weaker than the (rigid) solid. On the other hand, separation without leaving a detectable polymer residue will commonly occur without appreciable drawing of craze fibrils, and so the requirement of energy dissipation will be small.

For pressure-sensitive adhesives, it is possible to have a continuous gradation of peeling force, over a wide range, depending on

the rate of peeling and on the thickness and other properties of the adhesive layer (31). The variation as a function of thickness is related to the volume of adhesive in which deformation occurs, per unit distance of advance of unit width of separation front. The gradation, as a function of rate of peeling, has been shown (12) to be directly related to the local temperature rise. When the peeling rate is sufficiently slow, the deformation process is one of isothermal, macroscopic creep; and if the adhesive layer is thick enough, separation at a low level of peeling force may occur, entirely in the adhesive phase.

Application to Adhesion. We can now make some order-of-magnitude calculations, to illustrate the theory. It will quickly become evident that the numerical results will depend on factors that are, at present, poorly known — e.g., the temperature dependence of the yield strength of the fibrils, and the shape of the base region of the fibrils; see Figure 3b. Since the exact configuration of the base region is not known, either theoretically or experimentally, it is justified to assume (provisionally) an arbitrary shape such as a 45° cone with base radius,  $r_b$ , and height,  $h$ , which merges into a fibril that has a constant radius,  $r_f$ . We may employ Eq. (1), in the form of an equality, as the demarcation between "clean" interfacial separation of the base from the solid, and intracraze rupture. In the model process, the volume of the fibril plus that of the base cone is constant; i.e., there is no further surface drawing from the polymer on the other side of the craze.

Assume, first, that base peeling occurs, i.e., inequality (1a) is obeyed. The cone base shrinks; and either the cone height increases as the cone angle decreases, or polymer from the base region becomes part of the fibril, with the cone angle remaining constant. For ease of calculation, we will assume that the latter occurs. Then the cone height decreases, but the fibril length increases. The net contribution of the change in cone height to the change in fibre length depends on  $(r_f/r_b)^2$ . If  $r_f \leq 0.2 r_b$ , this term affects the fibre length by less than 4%; in view of the crudeness of the model, this correction can be neglected. We may also make the approximation, that the plastic work dissipated in the base, as polymer passes into the fibril, can be neglected; then the first term in Inequality (1) becomes,

$$\Delta G^a dA_b = \Delta G^a \times 2\pi r_b dr_b \quad (7)$$

Using the condition,  $V_{\text{fibre}} + V_{\text{cone base}} = \text{constant}$ , we obtain

$$dr_b = \frac{r_f^2}{r_b^2} d\ell \quad (8)$$

$$\Delta G^a dA_b = \Delta G^a \cdot \left( \frac{2\pi r_f^2 d\ell}{r_b} \right) \quad (9)$$

Next, assume that the base does not peel, but the fibril elongates by  $d\ell$ . Since the fibre cross section area is  $\pi r_f^2$ , we may set the right



side of Inequality (1) equal to  $\sigma_y \pi r_f^2 d\ell$ . At the demarcation between base peeling and fibre yielding, we may equate the right side of (7) to  $\sigma_y \pi r_f^2 d\ell$ , and simplify the result; we obtain, for the case of  $\rho = 1$ ,

$$\frac{2\Delta G^a}{\sigma_y r_b} = 1 \quad (10)$$

We may call the left side of Eq. (10),  $\Omega$ , the parameter that controls the separation process,

$$\Omega \equiv \frac{2\Delta G^a}{\sigma_y r_b} \quad (11)$$

and set up inequalities in the form:

$$\Omega > 1, \text{ fibril drawing and rupture} \quad (12a)$$

$$\Omega < 1, \text{ fibril base detachment} \quad (12b)$$

If the condition, (12b), develops before appreciable work has been done in fibril drawing and craze thickening, the observed adhesive strength will be low.

For a more general definition of the demarcating parameter, we may write

$$\Omega \equiv \frac{\alpha \rho \Delta G^a}{\sigma_y r_b} \quad (13)$$

where  $\alpha$  is a constant, of the order of 2, and  $\rho$  is now included explicitly in the definition. This parameter will be used in the expressions, 12a and 12b. The evaluation of  $\alpha$  must await a further analysis of the fibre base-separation and elongation processes; the number, 2, will be used provisionally.

We may now make some quantitative estimates, using plausible numbers for the physical and mechanical properties that are involved. For a fibril drawn from the adhesive of a pressure-sensitive tape, we may assume an order of magnitude for  $r_f$ , of about 0.01 mm, and  $r_b \approx 5 r_f$ , i.e. about 0.05 mm. We assume the substrate to be hard, strong and smooth, and that "physical" forces act across the interface, so that  $\Delta G^a$  will be of the order of  $100 \text{ ergs/cm}^2 = 0.10 \text{ J/m}^2$ . The shear strength of the polymer, for a practical rate of elongation, may be about  $1.0 \times 10^6 \text{ N/m}^2$  (32) or about 140 psi. Then  $2\Delta G^a / \sigma_y r_b \approx 0.004$ . Since  $0.004 \ll 1$ , this computation predicts clean interfacial separation. And such separation is commonly observed, with well-formulated pressure-sensitive tapes.

The yield strength,  $\sigma_y$ , generally increases with rate of pulling, at constant temperature; so this prediction remains unchanged if the rate is increased. But if the rate of displacement is decreased into the "creep" range,  $\sigma_y$  may become small enough that the inequality is reversed. Then the prediction will be that fibrils will rupture, and adhesive polymer will be left on the substrate; and indeed, this transition in separation mode is sometimes observed.

The same prediction, i.e. fibril rupture, will be made if the yield strength of the polymer is low, as with a "tacky" film, or "fly-paper", at ordinary rates of separation. See below, in the discussion of hard, strong adhering systems, for other factors that may reverse the inequality.

Next, we may make an estimate with respect to brittle separation by a craze mechanism. We can assume a fibril radius of the order of  $0.1 \mu\text{m}$  (2a), and base radius about to  $0.5 \mu\text{m}$ . Again, we will assume  $\Delta G^a$  to be  $0.1 \text{ J/m}^2$ . The value chosen for  $\sigma_y$  will be quite speculative. Takaki & Bogue (33) report  $2 \times 10^6 \text{ N/m}^2$  for the stress at break, of polystyrene (high molecular weight) at  $160^\circ$ . This temperature is near the value observed (9) in PS fracture. (The value of  $\sigma_y$  reported ranged over about an order of magnitude, with molecular weight and MW distribution, and with temperature.) This leads to a value of 0.2 for  $\Omega$ . This means a prediction of interfacial separation; but 0.2 is close enough to 1 that the prediction is not a strong one. If  $\sigma_y$  is larger (as would be expected if the local maximum temperature in the advancing craze/crack is lower than  $160^\circ$ )  $\Omega$  will be smaller than this estimate, and the prediction of interfacial separation will be strengthened.

Then we may estimate the effect of roughness. A value of  $\rho$  equal to 3 is reasonable, for a "high" value. This would yield a value of 0.6 for the left side of the inequality and an equivocal prediction.

Finally, we can estimate the effect of covalent or other strong bonds across the interface, for a smooth interface. Instead of  $100 \text{ ergs/cm}^2$  (a magnitude appropriate to "physical" forces across the interface), let us use  $4000 \text{ ergs/cm}^2$ , corresponding to intermolecular energies between about 160 and  $280 \text{ kJ/gm mole}$ , depending on bond density, or  $4 \text{ J/m}^2$ , for  $\Delta G^a$ . Now the inequality is reversed, and  $2\Delta G^a/\sigma_y r_b = 8$ . So the prediction will be, that fibril rupture will occur and that the effective "strength of adhesion" will be large; but this prediction will not be dogmatic. If, in addition, we multiply by a roughness factor, 3, we obtain  $2\rho\Delta G^a/\sigma_y r_b = 24$ , which indicates a fairly definite prediction of fibril rupture, and strong adhesion. Thus, the presence of covalent bonds across an interface with a rough solid is likely to make the difference between strong and weak adhesion; and this is in accord with observations.

As already noted, these numerical estimates are sensitive to the assumptions, e.g., the shape of the fibril base, and the values of  $\Delta G^a$  and  $\sigma_y$  for a fibril. These are speculative properties, at present. Moreover, the (as yet, un-analyzed) flow field for the deformation indicated at the top of Figure 3b, i.e., for surface drawing, will be an important, and often a controlling, influence on the process.

However, the results of the calculations, above, are highly suggestive. The trends predicted are in qualitative agreement with common observations, e.g., that practical adhesion is stronger with moderately roughened surfaces, and when covalent bonding is possible. And, in particular, we have indicated an answer to a practical question, as to why there are systems in which a hard, brittle polymer may act as if the strength of adhesion to a solid were far less than the cohesive (fracture) strength of the polymer.

An interesting application of these results is, to show why it

has been possible, in transmission electron microscopy, to find polymers that could be used in the replica technique. The requirement for such a polymer is, first, that the free energy of adhesion for the substrates involved should be in the range found when the interfacial forces are "physical". Second, the yield strength of fibres drawn from the polymer should be large. Third, the polymer should not exhibit a serious propensity for crazing; and if crazing does occur, the diameter of the fibrils (and hence of fibril bases) should be small.

We may now identify some of the nonlinear viscoelastic parameters that (as mentioned at the start of this paper) are critical to adhesion. The most important property is the yield strength,  $\sigma_y$ . After that, there is the property of elongational strengthening, i.e., the increase of force with rate of pulling on the end of a rod or fibre of the polymer; and also the temperature coefficient of  $\sigma_y$ .

The property of shear-thinning will also be involved. If this property comes into play during craze thickening, which is where the major dissipation of energy occurs, its importance will be very great. There is a place, in this regard, for future studies of the rheology of fibre "surface drawing", in a configuration that corresponds to the top of Figure 3b. This will be essential for the development of a criterion demarcating surface drawing from fibril elongation at constant mass.

The fluctuation in polymer properties is, no doubt, of high importance in adhesion. A fibril less than  $0.1 \mu\text{m}$  in diameter contains few enough chains that low MW chains, if concentrated in a single fibre, would seriously weaken it relative to its neighbors. Early rupture of a fibril would place an excess load on the neighbors, which could lead to their failure either by rupture or by base detachment. Hence the theory predicts that the width of distribution of MW will have a major influence on adhesive strength. Entanglements, and other fluctuations in local properties, will also have a strong influence.

Application to Adhesional Wear. For adhesional wear, as opposed to adhesion itself, the property or process that is of direct interest is the rupture of interfacial crazes and the transfer of polymeric material, rather than the force or energy requirement. It is clear that the inequalities, (1b), (3b) and (4b) are the criteria that predict the occurrence of polymer wear. In terms of molecular properties, small values of the yield strength, and a rapid decrease in  $\sigma_y$  with temperature, should lead to the occurrence of polymer wear, and to the transfer of polymer to the solid. Large values of  $\sigma_y$  and small values of  $d\sigma_y/dT$  will be conducive to the absence of wear.

Small values of the free energy of adhesion,  $\Delta G^a$ , for the polymer on the solid, and low levels of roughness, will be conducive to low wear; and high wear will be the consequence of large values of  $\Delta G^a$  and of  $\rho$ .

These conclusions are not surprising. A novel point, however, is the important adhesional role of roughness of the solid in wear, in addition to its obvious role in plowing wear. Another point is the source of the local heating which leads to enhanced wear: the work that is done in drawing the craze fibrils of the polymer. Extensional viscosity is an important rheological property that

controls this heating; so we may suggest that a study of extensional viscosity should be on the agenda as part of the general research program on polymer wear.

The theory that we have developed does not demand that all fibrils and their bases be the same size, or that their mechanical properties be identical. Chain entanglement is a statistical property, and (as already noted) the number of chains per fibril is small enough that serious fluctuations in local properties are to be expected. Even if, in a particular case, the vast majority of fibrils detach cleanly and without leaving any polymer on the solid, a small fraction of the fibrils may rupture, in an experiment of "adhesive" separation. Likewise in a frictional experiment: even when, at the majority of points of adhesional attachment, detachment occurs without appreciable fibril drawing, there may be fibril-drawing and rupture at a few sites; and consequently, wear will occur.

### Summary

The joint role of interfacial forces and viscoelastic properties may be described in two ways: First, the role of strong interfacial force,  $\sigma_i$ , is to anchor the "bases" of fibrils to the substrate. When this occurs, and when  $\Delta G^a$  and  $\sigma_i$  are large enough, considerable work will be dissipated in the viscoelastic process that constitutes fibril formation, before fibril rupture. That is to say, Equations (1b) or (3b) constitute the necessary condition for high strength. This may be considered a local "all-or-nothing" criterion. There will be a critical level of interfacial force,  $\sigma_{ic}$ , and of free energy of adhesion,  $\Delta G_c^a$ , that is characteristic with respect to a particular set of viscoelastic and crazing properties of a particular adhesive or adhering phase, such that high practical adhesion will be achieved.

Second, the role of the viscoelastic deformation properties is to provide a mechanism by which a useful fraction of the (enormous) theoretical interfacial force can be exploited in joint strength.

Third, numerical calculations based on the inequalities that we have proposed lead to qualitative predictions of the transfer of matter, and of general strength in adhering systems, that are in agreement with observations. The trends of these practical properties, with variation in fundamental properties such as polymer yield strength and free energy of adhesion, are in excellent agreement with observed results.

We may make a tentative estimate of the bounds of reliability of the inequalities, (12a and b), taking account of the uncertainties in the model, such as the ratio of fibril base area to cross section, the shape of the fibril base, the variation of tensile strength with strain rate and with temperature, the local temperatures achieved in the fibrils during separation, and the structure of the flow field at the upper and lower ends of a fibril. It seems intuitively reasonable to set the following rough bounds of prediction:

$$\frac{2\rho\Delta G^a}{\sigma_y r_b} > 10: \quad \text{fibril drawing and rupture}$$

$$0.1 < \frac{2\rho\Delta G^a}{\sigma_y r_b} < 10: \text{ predictions equivocal}$$

$$\frac{2\rho\Delta G^a}{\sigma_y r_b} < 0.1: \text{ fibril base detachment}$$

Fourth, the criterion that we have derived does not override other well-known criteria, such as that the presence of weak boundary layer material is a sufficient, though not a necessary, condition for poor adhesion. Indeed, our theory may be regarded as showing just when boundary-layer material will qualify as "weak", in a particular system.

Finally, it is clear that the generalizations that we have given are broadly valid for brittle adhesives, for tough adhesives, and for systems containing a pressure-sensitive adhesive in a peeling geometry, and for systems in which the property that is of interest is "tack".

#### Acknowledgments

The authors thank Professor R. K. Gupta and Dr. R. P. Kambour for discussion of the manuscript.

#### Literature Cited

1. Kambour, R. Macromol.Rev. 1973, 7, 1.
2. Kausch, H.H., Ed. "Crazing in Polymers"; Advan. Polymer Sci. 52/53; Springer, 1983.
  - (a) Kramer, E.J. "Microscopic Fundamentals of Crazing"; p. 1.
  - (b) Döll, W. "Optical Interference Measurements and Fracture Mechanics Analysis of Crack Tip Zones"; p. 105.
  - (c) Dettenmaier, M. "Intrinsic Crazes in Polycarbonate: Phenomenology and Molecular Interpretation of a New Phenomenon"; p. 57.
3. Andrews, E.H. (a) "Fracture in Polymers"; Oliver & Boyd: London, 1968; (b) "Developments in Polymer Fracture"; Applied Science Publishers, Ltd.: London, 1979.
4. Lee, L.H., Ed. "Adhesion & Adsorption of Polymers"; Plenum: New York, 1980; Vols. 1 and 2.
5. Mittal, K.L., Ed. "Physicochemical Aspects of Polymer Surfaces"; Plenum: New York, 1981; Vols. 1 and 2.
6. Mittal, K.L., Ed. "Adhesion Aspects of Polymeric Coatings"; Plenum: New York, 1983.
7. Briscoe, B.J. Phil. Mag. A, 1981, 43, 511-27.
8. Briscoe, B.J. "Adhesion"; Barking: England, 1981, Vol. 5, pp. 49-80.
9. Gruntfest, I.J. In "Fracture of Solids"; Drucker, D.C. and Gilman, J.J., Eds.; Interscience: New York, 1963.
10. Fox, P.G.; Fuller, K.N.J. Nature, Physics 1971, 234, 13.
11. Fuller, K.N.G.; Fox, P.G.; Field, J.E. Proc. Roy. Soc. London, A341, 1975, p. 537.
12. Good, R.J. In "Aspects of Adhesion"; Alner, D.J., Ed.; Univ. of London Press, 1971; Vol. 6, p. 24.

13. Döll, W. Ref. 2b, p. 136.
14. Argon, A.S.; Salama, M. *Materials Sci. & Eng.* 1976, 23, 219.
15. Argon, A.S.; Hanoosh, J.G. *Phil. Mag.* 1977, 36, 1195.
16. Argon, A.S.; Salama, M. *Phil. Mag.* 1977, 36, 1217.
17. Beahan, P.; Bevis, M.; Hull, D. *J. Materials Sci.* 1972, 8, 162.
18. Kramer, E.J. Ref. 2a, pp. 13-14.
19. Döll, W. Ref. 2b, pp. 117-9.
20. Irani, J. Ph.D. Thesis, State Univ. of New York, Buffalo, 1979.
21. Murray J.; Hull, D. *Polymer* 1969, 10, 451.
22. Ide, Y.; White, J.L. *J. Appl. Polymer Sci.* 1976, 20, 2511.
23. Kaelble, D.H. "The Physical Chemistry of Adhesion"; Interscience: New York, 1971; p. 423; *Trans. Soc. Rheol.* 1965, 9, 135.
24. Good, R.J. *J. Adhesion* 1972, 4, 133.
25. Good, R.J. In "Treatise on Adhesion and Adhesives"; Patrick, R.L., Ed.; Marcel Dekker: New York, 1967, Vol. I, p. 9.
26. Connelly, R.W.; Parsons, W.F.; Pearson, G.H. *J. Rheol.* 1981, 25, 315.
27. Gupta, R.K. *J. Rheol.* 1983, 27, 171.
28. Good, R.J. *J. Am. Chem. Soc.* 1953, 74, 5041.
29. Griffith, A.A. *Phil. Trans. Roy. Soc. London*, 1920, 221, 163.
30. Irwin, G.R. In "Fracturing of Metals" (Am. Soc. Metals, 1947); *Trans. Am. Soc. Metals* 1948, 40, 147.
31. Gardon, J.L. In "Treatise on Adhesion & Adhesives"; Patrick, R.L., Ed.; Marcel Dekker: New York, 1967, Vol. I, p. 269.
32. Ferry, J.D. "Viscoelastic Properties of Polymers" Wiley: New York, 1961.
33. Takaki, T.; Bogue, D.C. *J. Appl. Polymer Sci.* 1975, 19, 419.

RECEIVED January 23, 1985

## Fatigue Wear of Polymers

N. S. Eiss, Jr.<sup>1</sup> and J. R. Potter III<sup>2</sup>

<sup>1</sup>Virginia Polytechnic Institute and State University, Blacksburg, VA 24061

<sup>2</sup>Teledyne Allvac, Monroe, NC 28110

Wear of polycarbonate, polyvinyl chloride, ultra-high molecular weight polyethylene, siloxane modified epoxies, and polyimides was studied in experiments in which a steel ball bearing was slid repeatedly on a polymer surface. Over a certain range of loads for a given polymer, a range of cycles of polymer disk rotation was observed before a wear track initiated. Because of the absence of wear prior to wear track initiation, the predominant wear mode was assumed to be fatigue. The number of cycles to initiate wear was negatively correlated with the ratio of the tensile stress in the contact to the tensile yield strength. After wear initiated the wear rates for epoxies and polyimides correlate positively with elastic modulus. Correlations of wear rates with load generally did not agree with fatigue models.

The wear of polymers is general believed to be caused by one or more of the following mechanisms: adhesive transfer, abrasive cutting, and fatigue. When the polymer slides on very smooth hard surfaces wear occurs primarily by adhesive transfer. On rough surfaces with sharply pointed asperities abrasive cutting is the predominant wear mode. For more gently rounded asperities which do not cause stresses in the polymer large enough to cause cutting many stress cycles (repeated traversals) are required to produce wear particles. This last mode is called fatigue wear and is believed to be a significant contributor to the steady-state wear of polymers.

In the model most commonly used for fatigue wear of polymers, the wear rate is assumed proportional to the volume of a wear particle divided by the number of stress cycles  $N$  necessary to produce the wear particle. The number of cycles  $N$  is given by

$$N = (S_0/S)^t \quad (1)$$

where  $S_0$  is the stress for failure in one load cycle,  $S$  is the applied stress, and  $t$  is an empirically determined constant (1). Investigators have made various assumptions to express the fatigue

wear rate in terms of the load, surface topography, and the elastic properties of the contacting materials. These assumptions include defining the area of contact by using the bearing area curve (1), a Gaussian distribution of asperity heights (2), and a Hertzian elastic contact of a sphere on a plane (3). Wear particles have been assumed to be flattened spheres with a volume proportional to the contact area radius squared (2) or equiaxed of dimensions proportional to the contact radius (3).

Experimental verification of the fatigue wear model has largely been based on the determination of the exponent  $t$  from log-log plots of steady-state wear rate versus load (3), radius of curvature of asperities (4), and modulus of elasticity (5). The values of  $t$  found for various polymers range from 4 to 10, which resulted in the wear rate being proportional to the load to a power greater than one. Since both the abrasive and adhesive wear models predict proportionality between wear rate and load, investigators concluded that fatigue wear was the predominant mechanism. A positive correlation has also been found between the values of  $t$  determined from wear experiments and those determined in conventional fatigue tests (6).

The most comprehensive fatigue wear model (2) proposed in the literature was used to predict wear rates to within 30 percent or less of the experimentally measured values (7). The exponent  $t$  was determined from notched cylindrical specimens in reverse bending. The number of contacts and the areas were determined from surface profiles of the polymer and the counterface after steady-state wear was attained. The wear data was obtained from a polymer pin sliding on a rotating cylinder.

When polymers slide on machined metal surfaces, it is quite possible that steady-state wear involves a combination of abrasive, fatigue, and adhesive wear mechanisms. To study fatigue wear, it would be desirable to minimize the contributions of the abrasive and adhesive wear modes. In this paper, the following polymers: polycarbonate, polyvinyl chloride, ultra-high molecular weight polyethylene, siloxane modified epoxies, and polyimides are tested in experiments in which the fatigue wear mode is predominant.

### Experimental

The experiment chosen to emphasize the fatigue wear mechanism was a 52100 steel ball 3.18 mm dia. loaded against a rotating polymer disk (8). The load was adjusted so that stresses in the polymer were not high enough to cause wear and the formation of a wear track when sliding was started. Under these conditions, the polymer disk could rotate from a few to several thousand cycles with no detectable wear of the polymer. A profile meter was used to detect the cross-sectional area of the wear track once it had formed. During the period of no detectable wear, there was no abrasive wear and any removal of polymer by adhesive transfer to the ball must have been below that amount which could be detected by the profile meter. Thus, the experimental conditions favored the fatigue mode of wear.

Two sets of experiments were performed. In the first set, three polymers with very different mechanical properties were chosen to determine their response to this experiment. Polycarbonate PC, rigid polyvinyl chloride PVC, and ultra-high molecular weight polyethylene UHMWPE, were loaded with 10, 8.5, and 7.2 N and tested at 0.04 m/s sliding speed. In these tests, the friction force was continuously



monitored and the number of cycles required before the wear track initiated was noted. The experiments were terminated shortly after the initiation of the wear track, thus no wear measurements were made (9).

In the second set of experiments, two polymer systems were tested. One system consisted of cast epoxies which were toughened by the incorporation of chemically bound siloxanes (5). The friction and wear were measured as functions of the percentage of the siloxane PSX in the epoxy, the percentage of the siloxane which had a polytrifluoropropyl group TFP, and the normal load (10, 5 and 2 N).

The other system consisted of three aromatic polyimides (see (10) in this volume for structures) which differed only by the linking groups CH<sub>2</sub>, O, and CO. The polyimides were cast on stainless steel substrates and cured to yield films 50 μm thick. The friction and wear were measured as functions of the linking group and the normal load (10 and 5 N). The sliding speed was 0.63 m/s for the second set of experiments and all experiments were run in laboratory air, typically 22°C and 40 percent relative humidity.

### Results

The first set of experiments was characterized by a period of no wear and relatively low friction, followed by an increase in friction as the wear track initiated. The number of cycles of disk rotation required to initiate the wear track and the coefficient of friction before and after wear track initiation are summarized in Table I.

Table I. Wear Track Initiation Data

Polymer	Cycles to Initiate Load		Coefficient of Friction Load			
	10 N	7.2 N	10 N		7.2 N	
			Before	After	Before	After
PC	23±33*	60**	.33	.48	.32	.51
PVC	250±65	343±402	.15	.29	.17	.31
UHMWPE	No Initiation in 435 cycles		.13		.08	

\* 95 percent confidence limits

\*\* one test

The maximum tensile stresses for a sphere sliding on a plane with friction is given by (2,11).

$$S = \frac{3P}{2\pi a} \left\{ f(4 + \nu)\pi/8 + (1 - 2\nu)/3 \right\} \quad (2)$$

where

S = stress

P = load

a = radius of contact based on Hertzian elastic contact

f = friction coefficient

ν = Poisson's ratio

These stresses are given in Table II with the tensile yield strength for the polymers. A comparison of the data in Tables I and

II shows that the number of cycles to initiate the wear track is inversely related to the ratio of the tensile stress to yield strength.

Table II. Mechanical Properties and Tensile Stresses

Polymer	Elastic Modulus (GPa)	Poisson's Ratio	Yield Strength (MPa)	Tensile Stress (MPa)	
				10 N	7.2 N
PC	2.38	0.40	62	116 (1.9)*	101 (1.6)
PVC	3.84	0.42	60	79 (1.3)	79 (1.3)
UHMWPE	1.10	0.46	24	29 (1.2)	17 (0.7)

\* Ratio of tensile stress to yield strength

The second set of experiments was also characterized by a period of no wear with low friction followed by wear track initiation and an increase in the friction. In these experiments the tests were continued and measurements of the wear track were made every 2000 cycles up to 16 kc of disk rotation. After the first 2000 to 4000 cycles the wear rate was constant and the wear rates were calculated using a linear regression on the wear vs. number of cycles data.

The wear rates for the siloxane modified epoxies are given in Table III as a function of the normal load. Also contained in Table III is the value of  $b$  as obtained by linear regression of the equation

$$\text{Log(Wear Rate)} = \text{Log}(k) + b \text{Log(Load)} \quad (3)$$

It should be noted that transformed data were not linear for the epoxy without the modifier (0 PSX, 0 TFP) and for the 10 PSX, 0 TFP composition. For these, the rate of increase of the wear rate with load decreased at the higher loads. The highest wear rates were recorded for the compositions with the highest elastic moduli.

Table III. Wear Rates for Siloxane Modified Epoxies

Composition %PSX	%TFP*	Elastic Modulus, GPa	Wear Rate $\mu\text{m}^2/\text{kc}$			$b$ , Load Exponent <sup>+</sup>
			2N	5N	10N	
0	0	1.11	312	671	802	.60
5	0	1.01	227	479	956	.89
10	0	0.97	281	531	544	.42
15	0	0.92	0	0	266	--
5	20	1.14	222	458	906	.87
10	20	0.88	0	0	0**	--
15	20	0.88	0	0	0**	--
10	30	--	121	172	235	.41

\* Percentage of the PSX containing the trifluoropropyl group

\*\* No Measureable wear after 30 kc.

<sup>+</sup> Wear Rate =  $K(\text{Load})^b$

The wear rates and the cycles to initiation for the polyimides are given in Table IV. The wear rates correlated positively with the elastic moduli. However, the effect of load on the cycles to initiate varied with the linking group with the oxygen linkage showing no change while the CH<sub>2</sub> linking group almost quadrupled its initiation time when the load was doubled.

Table IV. Wear Rates for Polyimides

Polyimide Linking Group	Elastic Modulus (GPA)	Load 5 N		Load 10 N
		Wear Rate ( $\mu\text{m}^2/\text{kc}$ )	Cycles to Initiate	Cycles to Initiate
CH <sub>2</sub>	1.19	171	269	1060
O	0.97	56	557	442
CO	1.24	168	115	--

NOTE: See Ref. (10) for confidence limits.

### Discussion

The ball-on-polymer disk experiment had the following characteristics which indicate that the polymer was subjected primarily to fatigue wear. Under the appropriate loads, the polymer did not begin to wear until it has been subjected to a certain number of stress cycles. No wear was detected by a profile meter during this initiation period. Thus, if any wear occurred during this period by abrasive and adhesive mechanisms, the alteration of the polymer topography must have been below the sensitivity of the surface profile meter. In addition, any wear which occurred during this initiation period was insignificant compared to the wear which occurred when the wear was initiated and a measurable wear track was formed.

The ball-on-polymer disk experiment has a well defined geometry for which contact stresses including the effects of friction can be calculated (See Table II). Thus, the results can provide a direct means for evaluating the empirical constants  $S_0$  and  $t$  in Equation 1 where  $N$  would be the number of cycles to initiate the wear track. As noted in Table I and in Ref. (10) there was considerable variation in the number of cycles to initiate wear for replicate experiments. Thus, evaluation of the constants in Equation 1 would require many replications so that confidence limits could be reduced to magnitudes which would permit significant differences to be measured for changes in the normal loads.

The data in Tables I and II show that a decrease in the ratio of the tensile stress to tensile yield strength for PC caused an increase in the number of cycles to initiate wear. For PVC a decrease in normal load was accompanied by an increase in the coefficient of friction. Hence, the stress-to-strength ratio did not change and there was no significant change in the number of cycles to initiate wear. Both these relationships are consistent with Equation 1.

A comparison of the cycles-to-initiate wear and the ratio of the tensile stress to the yield strength for the three polymers also indicates that as the ratio decreased the number of cycles to initi-

ate wear increased. A similar relationship was found between the ratio of the shear stress to shear strength and the number of cycles to produce wear on the order of the original surface finish (12). These data then became the basis for the Zero Wear Model (13).

When the wear track initiated, several significant changes occurred. The geometry of the contact changed from a sphere on a flat to a sphere in a cylindrical groove. Measurements of the groove geometry indicated that the groove had a larger radius than the ball. When the sphere is loaded against the polymer wear groove, the groove and ball must have the same radius. Because the normal stresses are highest at the center of the groove and zero at the edges, when the sphere is removed from the groove the elastic recovery in the center is greater than at the edges. Hence, the groove radius is larger than the radius of the ball which formed the groove. As a result of the change in contact geometry, the real area of contact as calculated by the Hertzian equations increased. The increase for the polyimides, for example, was 16 to 50 percent (14).

The friction coefficient rose when the wear tracks initiated. For example, the coefficient of friction for the polyimides increased from 200 to 300 percent, which is much greater than can be accounted for by the increase in real area of contact. Most of this increase is attributed to the deformation losses accompanying the formation of wear particles and their transport out of the contact region (10).

Prior to the formation of the wear groove, stresses were calculated assuming a smooth sphere and a smooth polymer surface. The validity of these assumptions in the context of a study of fatigue wear can only be judged when the size of the domains in which the fatigue failure occurs is known. In the absence of this knowledge, the topographies of the ball and polymer were compared before and after the track initiation assuming that both were smooth initially. After the wear track formed, the worn surface became rougher (10). The consequence of the increased roughness is to superimpose a stress which varies according to the roughness topography on the semi-elliptical stress distribution of the ideally smooth contacting surfaces.

The wear particles will be generated where the stresses are highest. Initially this will occur in the center of the contact. Thereafter, the wear particles will be generated from the portion of the contact where the highest stresses exist. In view of the stress variation caused by surface roughness which exists throughout the contact region, the significance of stresses calculated based on smooth geometry is questionable. In addition, it is also not clear how to include the increased friction forces into the stress calculations if some of the friction force is caused by deformation of wear particles residing in the wear track. Consequently, the relationship between the wear which occurred and the model expressed by Equation 1 becomes much more tenuous.

However, the following trends in the wear data were noted. The wear rates of the siloxane modified epoxies and the polyimides were positively correlated with the elastic moduli. In Equation 2, the stress is proportional to  $a^{-2}$ , and  $a$  is proportional to  $E^{-(1/3)}$ . Hence, stress is proportional to  $E^{2/3}$ . Thus, the data indicate that within a specific polymer system, the wear rate is positively correlated with the magnitude of the maximum stresses in the surface.

For the polyimides, at the 5 N load, the wear rates were negatively correlated with the cycles to initiate wear. This result is consistent with the fatigue wear model which states that the wear rate is inversely proportional to the number of cycles to fatigue failure. Comparing the cycles to initiate at the 5 and 10 N load, it is noted that cycles to initiate significantly increase for the 10 N load for the CH<sub>2</sub> linkage while the cycles to initiate for the oxygen linkage is not significantly changed. These results are not consistent with the fatigue model.

The wear rate-load data for the modified epoxies have load exponents less than one. Several fatigue models for wear predict that the exponent should be greater than one (3). Explanation for this discrepancy will require a much better understanding of the fatigue wear process than is presently known.

### Conclusions

For a certain range of loads between a ball and a specific polymer, a range of cycles to initiate a wear track will result. During these cycles no polymer wear can be detected using a surface profile meter. Thus, the significant wear mode is fatigue. The experiment has the potential for evaluating the constants  $S_0$  and  $t$  in Equation 1, because the stress equations for a ball on a flat with friction have been solved. However, because of the random nature of fatigue, many replicates will be required to obtain statistically significant results.

The ratio of the calculated maximum tensile stress to the tensile yield strength was negatively correlated with the cycles to initiate wear which is in agreement with Equation 1. For three very different polymers, PC, PVC, and UHMWPE it was found that the ratio of stress to strength also was negatively correlated with the cycles to initiate wear. However, the limited number of experiments would preclude any generalization of this finding.

For the siloxane modified epoxies and the polyimides, the wear rates correlated positively with the elastic moduli, which is also in agreement with the fatigue model. However, the wear rate-load relationship predicted by fatigue models was not corroborated by the data. Likewise, the effect of load on the cycles to initiate for the polyimides was not consistent with the fatigue model.

### Acknowledgments

The first set of experiments involving PC, PVC, and UHMWPE and the polyimide experiments were supported by a contract from the U.S. Army Research Office, Research Triangle Park, North Carolina. The epoxy experiments were supported by a contract from the Office of Naval Research, Arlington, Virginia.

### Literature Cited

1. Kraghelsky, I. V.; Nepomnyashchi, E. F., *Wear*, 1965, 303-319.
2. Jain, V. K.; Bahadur, S., *Wear*, 1980, 60, 237-248.
3. Lancaster, J. K., *J. Lub. Tech., Trans. ASME*, 1975, 97, 187-194.
4. Hollander, A. E.; Lancaster, J. K., *Wear*, 1973, 25, 155-170.

5. Hu, T. Y.; Eiss, N. S., Jr.; Yorkgittis, E. M.; Wilkes, G. L.; Tran, C.; Yilgor, I.; McGrath, J. E., Proc. ACS Div. Poly. Mat. Sci. and Eng., 1983, 49, 508-512.
6. Lancaster, J. K., Plastics and Polymers, 1973, 41, 297-305.
7. Jain, V. K.; Bahadur, S., Wear, 1982, 79, 241-253.
8. Eiss, N. S., Jr.; Milloy, S. C., In Wear of Materials 1983, Ludema, K. C., Ed. ASME, New York, NY, 1983, 650-656.
9. Potter, J. R., III, Master of Science Thesis, Virginia Polytechnic Institute and State University, Blacksburg, VA, August 1983.
10. Jones, J. W.; Eiss, N. S., Jr., this volume.
11. Hamilton, G. M.; Goodman, L. E., Jl. Appl. Mech., Trans. ASME, 1966, 33, 371-376.
12. Bayer, R. G.; Clinton, W. C.; Nelson, C. W.; Schumacher, R. A., Wear, 1962, 5, 378-391.
13. Bayer, R. G.; Shalkey, A. T.; Wayson, A. R., Mach. Des., Jan. 9, 1969, 142-151.
14. Jones, J. W., Master of Science Thesis, Virginia Polytechnic Institute and State University, Blacksburg, VA, May 1983.

### Discussion

Question: Dr. B. Briscoe, Imperial College, London, England

I can see that you have good evidence for fatigue failure. Have you considered environmental changes as a means of inducing premature failure? Lancaster and Evans thought they had data which indicated that this was the case. Are thermal effects a problem in this work?

Answer:

The only environmental effects studied were in the experiments with PC, PVC, and UHMWPE. In these tests, four liquids were applied to the polymeric surface; water, water plus three percent trisodium phosphate, methanol, and mineral oil. These liquids reduced friction forces compared to dry sliding and prevented the initiation of the wear track.

In 2000 cycles of sliding between wear track measurements, temperatures rose only 10 to 15°C. Unless the polymers had significant morphological and property changes at temperatures from 22 to 37°C, thermal effects were not significant in these tests.

Question: Dr. H. Czichos, Federal Institute for Materials Research and Testing, Berlin, West Germany

Have you also studied the appearance of the steel balls? Did you find some damage, like scratches or polymer transfer?

Answer:

If the steel balls were used for several tests, then a wear scar formed on the ball. Consequently, the steel ball was changed after each test to preserve the original surface topography.

RECEIVED January 23, 1985

## A Fatigue-Abrasive Wear Mechanism for Polymeric Surfaces

T. S. Chow

Webster Research Center, Xerox Corporation, Webster, NY 14580

A model based on a fatigue-abrasive wear mechanism has been developed for calculating the wear of polymeric surfaces due to its interaction with small particles and a foam roller. The wear is related to the contact deformation and fatigue resistance which are determined and expressed in terms of material, geometrical and process parameters. The material parameters are the modulus, yield strength and hardness of particles and polymers, the frictional coefficient, the foam modulus and the fatigue behavior of polymers. The geometrical and process parameters are the normal load, particle size, foam roll radius, surface velocity of foam roller and surface coverage of particles. The analysis and calculation reveal the weak dependence of the foam modulus on wear which benefits the investigation of the direct interaction between the small particles and polymeric surface and the understanding of its wear mechanism.

A model is presented which describes the wear of polymeric surfaces in contact with small particles and a foam roll. Wear is defined as the progressive loss of material from the surface as a consequence of relative motion. Two primary wear mechanisms can be identified when particles travel on a surface while under compression of a foam roll. These are abrasive wear which is caused by the micro-cutting and longitudinal scratching by particles between the polymeric surface and foam and fatigue wear resulting from the accumulated damage caused by cyclic stressing and deformation similar to the mechanical fatigue.

Other mechanisms, such as adhesive wear and corrosive wear, are considered to be less important in this problem and are not explicitly included in the analysis. The wear is related to the contact stress, deformation, surface coverage of particle and fatigue resistance, each of which is determined and expressed in terms of the material,

geometric and process parameters. The material parameters include the compression modulus, hardness, and fatigue resistance of the polymer; the compression modulus, yield strength, and frictional coefficient for the particle; and the compression modulus for the foam. The process parameters considered are the load, particle size, foam roll radius, velocities of the foam roller and surface and the number of cycles. Analysis and calculation are carried out to investigate the functional behavior of these variables and served as the basis understanding the physics of the interaction wear.

### Theory

When small particles move on a polymeric surface while being compressed by a rotating foam roll (see Figure 1), the surface is subjected to cyclic stresses. The accumulated damage of the surface due to abrasion by particles initiates cracks which propagate incrementally and eventually lead to a fracture of the surface layer. Although a great deal of research is ongoing in the area of friction and wear (1-4), the wear problem is much too complex to treat completely rigorously. The pressure distribution inside the contact zone, the distribution of particles on the surface and the particle size distribution are not considered. Corresponding mean values are applied. Contributions from the micro-cutting and surface roughness to the shear stresses on the surface are combined with the frictional coefficient. A new parameter called the effective frictional coefficient ( $\mu$ ) is defined.

When the strain (or stress) level is insufficient to generate crazes, the fatigue life is evaluated as a function of strain ( $\epsilon$ ), resulting in the conventional S-N curve of the form (5)

$$2N = (\epsilon / \epsilon_0)^\beta, \text{ for } \epsilon > \epsilon_{cr} \quad (1)$$

where N is the number of cycles to failure,  $\beta$  is the coefficient of fatigue resistance,  $\epsilon_0$  is proportional to the failure strain in tensile tests and  $\epsilon_{cr}$  is the critical strain below which fatigue does not occur. Parameters  $\epsilon_{cr}$ ,  $\epsilon_0$  and  $\beta$  are determined from the S-N curve. The fatigue resistance  $\beta$  is an intrinsic property which characterizes the material resistance to repeated loading,  $\epsilon_0$  is a stronger function of molecular weight than is  $\beta$  at room temperature (5). For polycarbonate (6), we have  $\beta = 3.6$ ,  $\epsilon_0 = 0.435$  and  $\epsilon_{cr} = 0.0085$ .

Continuing with the concept of fatigue-abrasive wear mechanism, the volume of material removed from a surface,  $V_{wear}$ , by a particle is defined as

$$V_{wear} = V_{def}/N \quad (2)$$

where  $V_{def}$  is the deformed volume of surface caused by traveling particle. Eliminating N from Eqs. (1) and (2), the thickness of the surface being worn away,  $\Delta h$ , by particles with surface coverage,  $\phi$ , is

$$\Delta h = 2 \phi (V_{def} / \pi R_3^2) (\epsilon / \epsilon_0)^\beta, \text{ for } \epsilon > \epsilon_{cr} \quad (3)$$



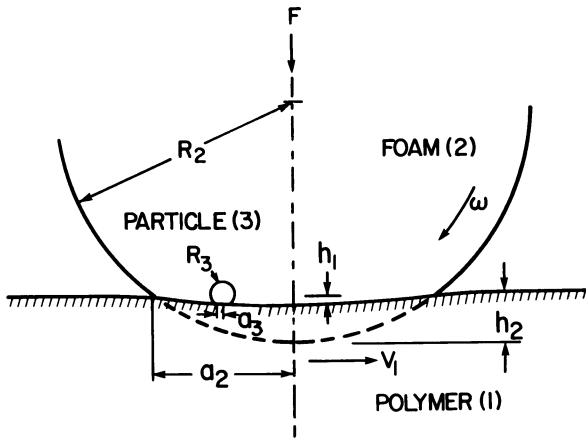


Figure 1. Contact geometry.

where  $R_3$  is the average particle radius. The wear,  $\Delta h$ , is zero for  $\epsilon < \epsilon_{GR}$  which rarely happens in any practical range of application. In equation (3), the contact strain,  $\epsilon$ , has to be determined by analyzing load transfers from the foam  $\rightarrow$  particle  $\rightarrow$  surface and the elastic and/or plastic deformations inside the contact zones. In the end result, both  $\epsilon$  and  $V_{def}$  are derived in terms of material and process parameters.

### Determination of Wear

When particles move on a surface while under a rotating and compressed foam roll, the surface is subjected to normal ( $\sigma$ ) and shear ( $\tau$ ) stresses. The total contact stress can be determined from a strain energy relationship.

$$\sigma_{total}^2 / 2E'_1 = \sigma^2 / 2E'_1 + \tau^2 / 2G_1 \quad (4)$$

where  $E' = E / (1 - \nu^2)$  and subscript 1 identifies the polymeric substrate.  $E$  is Young's modulus,  $G$  is the shear modulus and  $\nu$  is Poisson's ratio.  $E'$  may be treated as the compression modulus. In the case of isotropic materials,  $E'/G = 2/1(1 - \nu) = 3$  for common polymers with  $\nu = 1/3$ . Eq. (4) reduces to the familiar von Mises yield criterion under plastic yield conditions(7), and serves to describe the local strain energy. A simplifying assumption is that  $\sigma = \bar{p}_3$  and  $\tau = \mu \bar{p}_3$  in the contact zone. Thus Eq. (4) becomes

$$\epsilon = \sigma_{total} / E'_1 = (1 + 3\mu^2)^{1/2} \bar{p}_3 E'_1 \quad (5)$$

where  $\bar{p}_3$  is the mean pressure between the particle and substrate and  $\mu$  is defined as the effective friction coefficient. Three main factors contribute to the friction generated between unlubricated particles and surface in relative motion. The first factor is the abrasion and microcutting, the second factor is the adhesion which is a pure surface contribution and the third is described as deformation which is a bulk term. It is difficult to predict  $\mu$  but it is known that  $\mu > 1$  for abrasive wear.

The mean pressure  $\bar{p}_3$  can be related to the mean pressure  $\bar{p}_2$  between the foam roll and substrate(8)

$$\bar{p}_3 = \alpha (R_3/a_3)^2 \bar{p}_2 = [4E'_1 E'_3 / 3 \pi (E'_1 + E'_3)]^{2/3} (\alpha \bar{p}_2)^{1/3} \quad (6)$$

where  $E'_3$  is the compression modulus of the particle and  $\alpha$  characterizes the interaction of particles. For large values of  $\phi$ ,  $\alpha \sim 1/\phi$ . Introducing the subscript 2 to identify the foam rolls, the mean pressure ( $\bar{p}_2$ ), foam semi-contact length ( $a_2$ ), foam radius ( $R_2$ ), compression modulus ( $E'_2$ ) and the load per unit length ( $F$ ) applied to foam roller can be related by Hertz's equation.

When particles move in the gap between the foam and substrate under compression, the abrasive particles deform the surface and the volume of deformation is obtained by a geometrical consideration,

$$V_{def} = \lambda h_1 a_3 / 3 \quad (7)$$

where  $h_1$  is the depth of surface penetration,  $a_3 = (2R_3 h_1)^{1/2}$  is the

particle contact radius and  $\ell$  is the distance traveled by particles in the compression mode after C number of operating cycles (not to be confused with number of cycles N to fatigue failure). Since  $E'_1 \gg E'_2$ , the particle can be assumed to have the same velocity as the foam  $v_2^2 = R_2 \omega$ , we obtain

$$\ell = C(v_2 + v_1)t = C(v_2 + v_1) a_2 / v_2 \quad (8)$$

where  $v_1$  is the surface velocity and t is the time.

During plastic deformation, the penetration depth for a spherical contact is inverse proportional to the material hardness  $(H)(2,3)$ . In the present situation

$$h_1/h_3 = H_3/H_1 \quad (9)$$

where the subscripts 1 and 3 are for the substrate and particle, respectively. Since the abrasive particles are assumed to be softer than polymeric substrates, the normal load (P) is equal to  $A_r H_3(2)$  and the real area of contact  $A = 2\pi R_3 h_3$ . The normal load at which the plastic deformation of a compressed particle takes place is related to the particle yield stress ( $Y_3$ ) by

$$P = \pi R_3^2 Y_3 \quad (10)$$

Thus

$$h_3 = R_3 Y_3 / 2H_3 \quad (11)$$

Eqs. (9) and (11) lead to the surface penetration expression for substrates

$$h_1 = R_3 Y_3 / 2H_1 \quad (12)$$

Substituting Eqs. (8) and (12) into Eq. (7), the result is

$$v_{def} = C(1 + v_1/v_2) a_2 R_3^2 (Y_3/H_1)^{1.5} / 6 \quad (13)$$

Combining Eqs. (3), (5), (6) and (13), the thickness of a polymeric surface being worn away is given by

$$\Delta h = C \phi a_2 (1 + v_1/v_2) (Y_3/H_1)^{1.5} [ (1 + 3\mu^2)^{1/2} / \bar{p}_3 / \epsilon_0 E'_1 ]^\beta / 3\pi \quad (14)$$

with

$$\bar{p}_3 = [ 4E'_1 E'_3 / \pi(E'_1 + E'_3) ] ( \alpha F / 2a_2 )^{1/3}$$

and

$$a_2 = 2(FR_2 / \pi E'_2)^{1/2}$$

### Discussion

Consider the wear of a polycarbonate surface. The material and process parameters involved in the calculation are tabulated in Table I unless otherwise specified. Figure 2 reveals that the compression

Table I.  
Material and Process Parameters

	Modulus ( $10^5$ psi)	Yield Stress ( $10^3$ psi)	Others
Polycarbonate(1)	4.0	$H_1 = 20$	$V_1 = 10$ in/sec
Foam(2)	$5 \times 10^{-5}$	---	$R_2 = 0.94$ in. $\omega = 500$ rpm
Particle (3)	1	2.65	9.5
	2	2.65	7.0
	3	2.10	7.0
	4	0.75	5.0

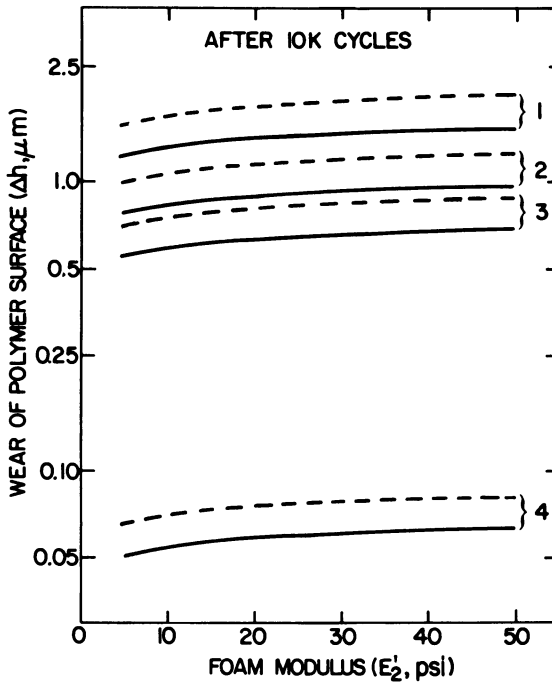


Figure 2. Wear as a function of foam modulus and particle properties. —  $F=0.205$  lb/in.; ---  $F=0.256$  lb/in. The numbers represent the particles defined in Table I.

modulus of foam has very little effect on the wear of polymeric surface, on the other hand the properties of particle have a very strong effect. This is mainly due to the high ratio  $p_3/p_2 \sim 0(10^3)$  and  $p_2 \sim 0(1 \text{ psi})$ . The weak dependence of the compression modulus of the foam roll on wear benefits the investigation of the direct interaction between the small particles and polymeric surface. During the wear measurement, the compression modulus of a given foam can increase in time with an increase of trapped particles which has little influence on wear. We found that the calculated curves in Figure 2 compare reasonably well with the measured wear range(9) from 0.7 to 1.4  $\mu\text{m}/10\text{K}$  cycles for type 1-3 particles.

Figure 3 illustrates how the wear varies with the hardness and modulus of polymer substrate. Figure 4 shows that the wear increases drastically with an increase of the effective frictional coefficient ( $\mu$ ) between the particle and polymeric surface. As was mentioned earlier, the friction  $\mu$  depends not only on the bulk and surface properties of materials in contact but also on such parameters as contact geometry and surface roughness. The direct determination of  $\mu$  from the first principle has yet to be established. The present model can be used to estimate its value from experiment. When a surface becomes smoother and harder, the effective frictional coefficient usually decreases and so does the wear.

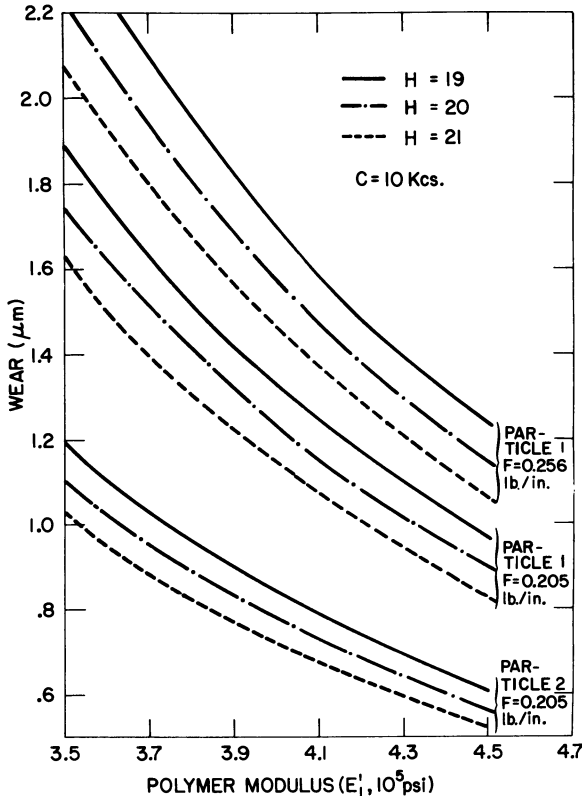


Figure 3. Wear versus the modulus and hardness of polymeric substrates.

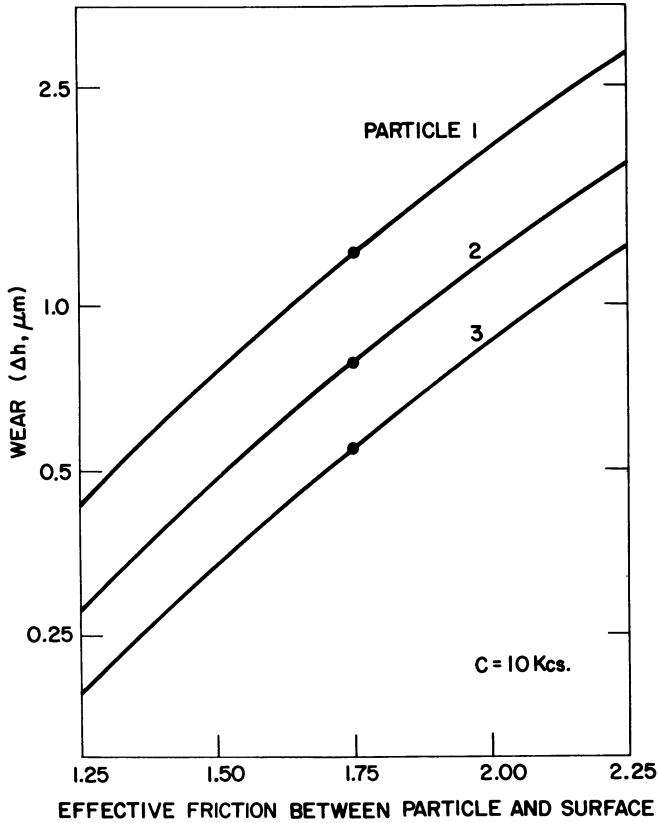


Figure 4. Wear versus the effective frictional coefficient.

#### Literature Cited

1. Moore, D.F. "Principles and Applications of Tribology", Pergamon Press, 1975.
2. Bowden, F.P.; Tabor, D "Friction and Lubrication of Solids", Clarendon Press, Oxford (1964).
3. Kragelsky, I.V.; Dobychin, M.N.; Komalov, V.S. "Friction and Wear", Pergamon Press, 1982.
4. Chow, T.S. *Wear* 1978 51, 355.
5. Sauer, J.A.; Foden, E; Morrow, D.R. *Polym. Engr. Sci.* 1977 17, 246.
6. Rabinowitz, S; Beardmore, P. *J. Mater, Sci.* 1974 9, 81.
7. Ward, I.M. "Mechanical Properties of Solid Polymers", Wiley, N.Y., 1971.
8. Landau, L.D.; Lifshitz, E.M. "Theory of Elasticity", Addison-Wesley, Reading, Mass. 1957.
9. Penwell, R.C.; Chow, T.S. unpublished data.

RECEIVED January 23, 1985

## Various Approaches in Controlling the Wear of Polymers

Lieng-Huang Lee

Webster Research Center, Xerox Corporation, Webster, NY 14580

Several basic mechanisms of polymer wear have recently been discussed with respect to fracture energetics and surface energetics (1). For each wear mechanism, we found necessary measures which can be taken to control the wear. In general, the wear can be achieved by: 1. controlling or designing bulk properties, e.g., molecular weight, molecular weight distribution, entanglement density, microstructure, liquid crystalline structure, etc.; 2. modifying the surface by plasma techniques, photopolymerization, silicone, etc.; 3. particulate or fibrous reinforcement; and 4. interpenetrating network (IPN). Each approach will be illustrated with existing or probable examples.

In comparison with metals, most conventional polymers are low in wear resistance. For wear control, we need to understand various wear mechanisms for each polymer system (1). As discussed in a previous paper, for adhesive wear, surface energetics can determine the extent of surface wear. Thus, a low surface energy is preferred to minimize the surface attrition. In addition, a harder polymer is desired to lower the wear rate. For abrasive wear, fracture energetics become important; a harder and tougher material should be more wear resistant.

Most wear modes tend to lead to fatigue wear upon cyclic stress. For fatigue wear, fracture energetics appear to be the dominant factors, thus a tough polymer should be more resistant to wear and tear. A universally wear-resistant material is hard to come by. If such a material exists, presumably it should be low in surface energy and high in toughness and hardness. For example, a hard and tough polymer can be surface modified with a low surface energy polymer, such as polytetrafluoroethylene. As a result, this material may be wear resistant to adhesive, abrasive and fatigue interactions.

Since, in reality, wear control is not as simple as it is generalized, we shall discuss some of the approaches in this paper:

1. Structural design,
2. Surface modifications,
3. Particulate or fibrous reinforcement, and
4. Interpenetrating network.

Indeed, not all of these approaches have been investigated for polymer wear control. A brief discussion of each of these concepts may lead to new opportunities in technological breakthroughs.

### Structural Design

In theory, through a proper design of physical structure, a polymer can be made more wear resistant to some aspects of tribological interactions. There are at least four structural design features that deserve considerations:

- o Molecular weight and molecular weight distribution,
- o Backbone structure,
- o Microstructure, and
- o Liquid crystalline structure.

### Molecular Weight and Molecular Weight Distribution

The first design feature has been known for many years. Molecular weight can affect mechanical and rheological properties of polymers (2). The introduction of ultrahigh molecular weight polyethylene (UHMWPE) is a demonstration of wear control for a conventional polymer. Interestingly, molecular weight also influences surface energetics (3) and fracture energetics of polymers (4). A high molecular weight polymer results in high fracture energy  $G_c$  (5). Moreover, molecular weight and its distribution also effect crazing, tensile properties, and impact resistance (6). These properties, in turn, control wear resistance of a polymer.

Entanglement of chains is necessary to support external stresses. A high entanglement density (7) is generally desired. Basically, the entanglement density increases with the number-average molecular weight and the quotient of the length to the molecular weight of the repeating unit (empirically found to be related to the critical entanglement molecular weight,  $M_c$ ).

### Backbone Structure

The second design feature is the backbone structure of the main chain. The backbone can be flexible, semirigid, or rigid. Rigid backbone generally results in high modulus or high hardness or both. Based on this concept, many high strength polymers have been commercially produced in recent years. Besides polycarbonate and polysulfone, new polymers include polyethersulfone (PES), polyimides (PI), polyamide-imide (PAI), polyphenylene sulfide (PPS), and polyether ether ketone (PEEK). Tribological properties of these polymers have been reported by Tanaka, et al. (8,9). In general, these polymers are rather wear resistant at normal operating temperatures. However, wear resistance drastically decreases at very high temperatures.

A highly rigid backbone is not necessarily the most desirable. A certain degree of flexibility can enhance wear resistance. For



example, Jones and Eiss (10) deliberately varied the flexibility of the backbone of polyimide (Fig. 1) and found that, indeed, wear resistance in the fatigue mode significantly increases.

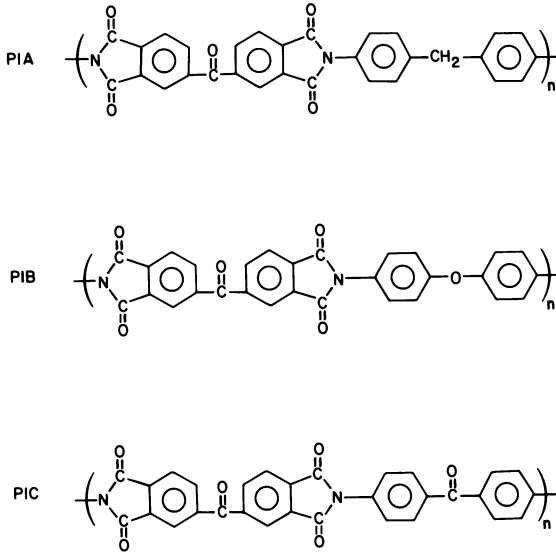


Figure 1. Polyimides with designed backbone flexibility (After Jones, J.W.; Eiss, Jr., N.S., Ref. (10)).

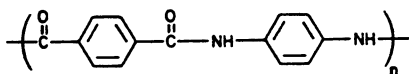
### Microstructure

The third design feature is the polymer microstructure. Morphology of polymer can influence wear resistance of polymers. For example, in a semicrystalline polymer, both amorphous and crystalline phases coexist. The amorphous phase has been shown by Tanaka (8) to be weaker than the crystalline phase, thus the former wears faster than the latter. In addition to the difference in phases, the size of the spherulites and the molecular profile can also influence the wear rates. Thus, a control of the morphology through crystallization can improve the wear resistance of a polymer such as polytetrafluoroethylene (11).

### Liquid Crystalline Structure

The fourth design feature is the formation of a liquid crystalline structure. During the last fifteen years, liquid crystalline polymers (LCP) have become one of the most exciting polymer families synthesized by chemists. Recently, the syntheses of LCPs were reviewed by Griffin (12). Interesting physical properties of liquid crystalline polyesters were described by Huynh-ba and Cluff (13). To the interest of tribologists, some of LCPs are rather wear resistant.

The first LCP reaching industrial significance is duPont Kevlar<sup>R</sup> aramide, p-phenylenephthalamide (PPD-T) (14) with the following rigid backbone structure:



Kevlar is a lyotropic liquid crystal which can be obtained from a sulfuric acid solution when the concentration reaches a critical value, e.g., 10%. However, this polymer like other LCPs is also anisotropic and its mechanical properties is directional, but less so in fibers than in the extruded plaques. The fiber properties in Table I are compared with other organic fibers and steel (15). On an equal weight basis, Kevlar has a strength several times that of steel. Perhaps, Kevlar is the first polymer at least comparable to metals.

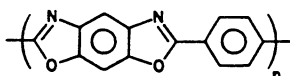
Table I. Comparison of Properties for Various Fiber Types

Fiber Type	Young's Modulus (GN m <sup>-2</sup> )	U.T.S. (GN m <sup>-2</sup> )	Breaking Strain (%)	Specific Gravity
Kevlar-49	144	3.06	2.3	1.45
Polyester (high tenacity)	18.5	1.4	20	1.2
Nylon 66 (high tenacity)	12.5	1.0	17	1.2
E-glass	70	1.8	3	2.5
Carbon type I	400	1.9	0.5	2.0
Carbon type II	200	2.6	1.0	1.7
Steel	200	0.6-0.8	16.0	7.8

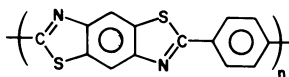
Source: Ref. 15.

Because of its high strength, Kevlar has been used in tires, bullet-proof vests, and in composites for aerospace and marine applications. With its high abrasion resistance, Kevlar has been used for the rugged wear essential for friction materials (16), e.g., heavy-duty truck brake blocks, railroad brakes, automotive disc brakes, rear drum linings, clutch facings and gasket sheets.

Among lyotropic LCPs, there are at least two rod-like polymers with excellent thermal and mechanical properties. These two polymers are poly(p-phenylenebenzobisoxazole) (PBO)



and poly (p-phenylenebenzobisthiazole) (PBT) (17).



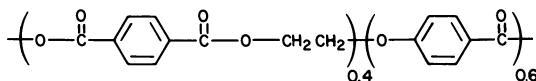
PBT is soluble in exotic solvents, such as methanesulfonic acid (MSA) and chlorosulfonic acid (CSA), in which it forms a nematic mesophase at a concentration of  $\sim 10\%$  with a molecular weight of 13,000  $\sim$  16,000. This polymer is especially attractive for aerospace applications because of its high thermal stability. Composite films have been made from PBT (18). So far, processing of this polymer is still a problem.

Since the discovery of Kevlar, scientists world-wide have attempted to synthesize many thermotropic LCPs that the liquid crystalline state can be formed in a melt instead of in a solution as lyotropic LCPs. Generally, two kinds of thermotropic LCPs can be prepared depending on the position of mesogens (19):

- o Comb-like LCPs - mesogens on the side-chain, and
- o Semi-flexible linear LCPs - mesogens on the main chain.

The first type is not as strong as the second type. Today, there are many second type LCPs containing stable liquid crystal phases in the range between 100 $^{\circ}$ -400 $^{\circ}$ C. For ease of processing, it is necessary to lower the melting point either by modifying the rigid backbone through copolymerization or by building flexible spacers between aromatic chains.

The modification through copolymerization is illustrated with polyethyleneterephthalate (PET) modified with p-hydroxybenzoic acid (PHB). The melt viscosity reaches a minimum as the PHB content becomes 60 mol % (20).



The properties of the extruded copolymer are also anisotropic (Table II) (21).

Table II. Mechanical Properties of PET-PHB Copolymer (40:60)

Property	Parallel to flow	Perpendicular to flow
Ultimate tensile strength (MPa)	107	28.4
Tensile elongation (%)	8	10
Flexural modulus (GPa)	11.8	1.67
Notched Izod impact strength (Jm)	317.8	31.4
Coefficient of linear thermal expansion (10 $^{-5}$ / $^{\circ}$ C)	0.0	4.5

Source: Ref. 21.

It appears that the application of extruded LCPs as wear resistant materials may be limited by their anisotropy.

### Surface Modifications

Besides the design of the bulk structure, polymer surfaces can also be modified by various means to achieve low friction or low wear or both. Early work on the fluorination of polymer surfaces (22), or the polymerization of tetrafluoroethylene on the surface (23), or the formation of poly (p-xylylene),  $(-\text{CH}_2-\text{C}_6\text{H}_4-\text{CH}_2-)_n$  (24), are examples of modifications of polymer or metallic surfaces.

Surface modification techniques vary (25). We shall only discuss three relevant methods:

- o Plasma treatment,
- o Surface photopolymerization, and
- o Silicone modifications.

Among them, plasma treatment (26) and plasma polymerization (27) appear to be the most widely investigated. Recently, Yasuda (28) reviews the status of both of two methods with respect to wear control applications.

### Plasma Treatment

A plasma is a gaseous state consisting of atoms, molecules, ions, metastables (and related excited states), and electrons such that in the same system negative charges equal positive charges. The plasmas used for surface polymerization or treatment are relatively "cool" in comparison to those "hot" plasmas employed by physicists.

The advantages of the plasma treatment (26) are that it is: 1. applicable to both batch and continuous processes, 2. low in initial capital investment, 3. suitable for a wide range of systems, and 4. experimental conditions are controllable. However, there are at least two disadvantages: 1. the treatment is unable to produce films to a specific formula and 2. it is prone to produce thick films, either brittle and/or discolored.

In the past ten years, there have been at least 200 monomers or monomer-like compounds which have been claimed to be polymerized by plasma. However, most of them have not been properly characterized. With the advent of new surface analytical techniques, e.g., ESCA (or XPS) (29), the structures of some plasma-polymerized products have been elucidated. For example, by the ESCA technique, some polymers have been shown to be vertically homogeneous on the surface (26).

Through plasma treatment, grafting of monomers can also take place on the polymer surface. For example, monomers, e.g., tetrafluoroethylene or hexafluoroethane, can be grafted onto wool or polypropylene fibers (26). This type of grafting can improve such tribological properties as low friction.

Polymer surfaces can also be treated by plasmas, e.g., inert gases or oxygen. The inert gas plasma treatment may involve direct energy transfer besides the commonly known, radiative energy-transfer process, which takes place during cross-linking. In

general, the cross-linked surface is more wear resistant than the non-cross-linked surface.

A new application of plasma is to convert an organic surface into a ceramic surface. In recent years, there has been much interest in producing glassy (or amorphous) material of high thermal stability and/or unusual technological significance. For example, the plasma-polymerized, organosilazane thin films derived from hexamethylcyclotrisilazane (30) can be pyrolytically converted into a glassy material which adheres strongly to the metal surface. This new material has a high content of siliconoxynitride (amorphous) which is rather wear and corrosion resistant.

### Surface Photopolymerization

Besides plasma techniques, surface photopolymerization (25,31) is another versatile method for modifying a polymer or a metal surface with a thin coating (<500Å). The process involves polymerizable or nonpolymerizable compounds. Under UV radiation, tetrafluoroethylene and many vinyl monomers can be polymerized. Other compounds including imides, anhydrides, saturated hydrocarbons, and ketones can all be used for the in vacuo deposition process.

Silicone-containing compounds, e.g., vinyltriethoxysilane, divinyltetramethyldisiloxane and cyanoethyl triethoxysilane (31) have also been photopolymerized at elevated temperatures. These coatings may be wear resistant.

### Silicone Modifications

In addition to the surface photopolymerization of silicones, some broader approaches in modifying the surface with silicone have yielded low friction and/or low wear surface for polymers (32). For example, the abrasion-resistant coatings based on a silicone-silica hybrid (33) have provided a scratch- and mar-resistant finish for polycarbonate as well as metals. The chemistry involved is discussed by Vincent, Kimball and Boundy (34). The coating consists of polysiloxane and silane-modified submicron silica particles, microscopically dispersed in the solution. The coating is then cured at elevated temperatures. Currently, this type of abrasion resistant coating is marketed in the U.S. by Dow Corning and General Electric Company.

### Particulate or Fibrous Reinforcement

The third well-known technique enhancing wear resistance of polymers is particulate or fibrous reinforcement to form composites. In the case of particulate materials, elastomers have been used to increase fracture energies  $G_C$  of the brittle matrices. For example, polyimides and epoxy resins are brittle materials with low fracture energies (35). With rubber reinforcement, fracture energies can be increased several orders of magnitude (36). Generally, as fracture energy increases, fatigue resistance also increases (1).

In the case of fiber-reinforcement, polymers, e.g., polyimides can be made more wear resistant. However, the wear resistance should be treated as a system approach. In one system, a material

may be wear resistant to a certain counterbody, but not to the other. For example, Sutor (37) shows that graphite-PI composites containing solid lubricant additives wear less on steel surfaces than on silicon nitride surfaces.

Besides graphite, carbon and glass fibers, organic fibers, e.g., Kevlar, have also been used to reinforce thermosetting resins, e.g., epoxy resin (38). One of the newest developments is fiber-reinforced thermoplastics, e.g., carbon fiber-reinforced polyether ether ketone (PEEK) (38). These materials are rather tough as demonstrated in the interlaminar toughness values (Table III). The values for the thermoplastic composites can be five to ten times higher than those of thermoset type (39).

Table III. Interlaminar Toughness of Composites

Composite	Interlaminar Toughness
(Based on unidirectional carbon-fiber) (in-lb/sq. in)	
Epoxy (thermoset)	0.6 - 0.8
Polysulfone	3.7
Polyphenylene sulfide (PPS)	7.8
Polyether ether ketone	8.0

(Source: Phillips Petroleum)

#### Interpenetrating Networks (IPN)

The fourth design feature is interpenetrating networks (IPN), which could improve wear resistance of polymers. There are two kinds of IPN's: thermosetting and thermoplastics. IPNs are mixtures of two or more distinct polymer phases that cannot be separated physically (40). On a molecular scale of 10 Å or less, most IPNs are heterogeneous with phase domains rich in one or more of the polymer components. Generally, a monomer is polymerized within a cross-linked network to form a thermosetting IPN. In some cases, the resulting network is very tough.

Recently, the thermoplastic IPNs have been developed to involve non-cross-linked networks (41). The first type of non-cross-linked networks are polymers which are capable of flowing at high temperatures, yet resemble (or behave as) cross-linked polymers at room temperature. For example, the thermoplastic elastomers (42) are triblock copolymers, having an elastomeric center capped with glassy end blocks. Above the glass temperature,  $T_g$ , the end-blocks would flow together with the elastomeric center. However, at room temperature, the center is rubbery, while the glassy end-blocks resemble physical cross-links. The second type is the ionomers forming noncovalent cross-links (43). The third type can be a semicrystalline polymer giving rise to some physical cross-links.

Any combination of the above two types of polymer can form thermoplastic IPNs in which some degree of dual-phase continuity is attained. Some of the thermoplastic IPNs have been claimed to be tough materials (44, 45). Though tribological properties of these new materials have not been investigated, they should be of

interest in producing wear-resistant polymers. Thus, IPNs may be another new family for further research.

### Conclusions

In this paper, we have summarized various approaches to controlling the wear of polymers. Several methods appear to be promising: 1. structural design, 2. surface modifications, 3. particulate or fibrous reinforcement and 4. interpenetration networks.

For structural design, the availability of high strength polymers and liquid crystalline polymers in recent years opens up new opportunities in competing with metals as wear resistant materials. Certainly, there are still more tribological studies needed to be done in establishing low wear polymers for each tribological system.

Surface modifications with plasmas have specific applications for systems requiring special protections, e.g., low surface energy or low wear resistance. Surface photopolymerization has yet to prove its value. The protection of a polymer surface with abrasion-resistant, silicone-silica hybrid material has demonstrated some utilities for polycarbonate or other optical materials.

The formation of composites by reinforcing polymers with particulate or fibrous polymeric or inorganic materials has been accepted as a general means in improving the wear resistance of polymers. One of the interesting developments is reinforced thermoplastics, such as carbon fiber-PEEK. The uses of LCPs, e.g., Kevlar, PBT, as reinforcing media for amorphous matrices are also of significant interest.

The concepts of the interpenetrating networks are indeed intriguing. IPNs have been made in both thermosetting and thermoplastic systems. Some tough materials have been developed based on these concepts. However, there has not been careful characterization work to establish the existence of IPNs and tribological work to demonstrate the wear resistance of some of the IPNs.

In brief, with the advent of polymer technology, more polymers today can be made wear resistant by various approaches discussed in this paper.

### Literature Cited

1. Lee, L.H. Editor "Polymer Wear and Its Control," ACS Symposium Series, American Chemical Society, Washington, D.C. (1985).
2. Nunes, R.W., J.R. Martin; J.F. Johnson, Polym. Eng. and Sci., 22, No. 4, 205, (1982).
3. LeGrand, D.G.; Gaines, Jr., G.L. J. Colloid Interface Sci., 31, 162 (1969).
4. Berry, J.P., in "Fracture Processes in Polymeric Solids," Rosen, B., Editor, p. 213, Wiley, New York, (1964).
5. Lee, L.H., in "Physicochemical Aspects of Polymer Surfaces," Mittal, K.L., Editor, Vol. 1, 523, Plenum, New York (1983).
6. Margolies, A.F., S.P.E.J., 27, 44 (1971).
7. Bersted, B.H., J. Appli. Polym. Sci., 24, 37 (1979).
8. Tanaka, K., "Tribology in the 80's" Vol. I., 253 NASA Lewis Research Center, Cleveland, Ohio (1984).
9. Tanaka, K., in Ref. 1.

10. Jones, J.W.; Eiss, Jr., N.S., in Ref. 1.
11. Tanaka, K., Uchiyama, Y., in "Advances in Polymer Friction and Wear," Lee, L.H., Editor, Vol. 2, 499, Plenum, New York (1974).
12. Griffin, L.C., in "Liquid Crystalline Polymers," Editor, Blumstein, A. Plenum, New York, to be published in 1985.
13. Huynh-Ba, G.; Cliff, E.F., in "Liquid Crystalline Polymers," Editor, A. Blumstein, A., Plenum, New York to be published in 1985.
14. Carter, G.B.; Schenk, V.T.J., Phys. Bull., 24, 716 (1973).
15. Bunsell, A.R., J. Mat. Sci., 10, 1300 (1975).
16. duPont Company Bulletin, "Modern Plastics Encyclopedia," 1981-1982.
17. Wolfe, J.F., Loo, B.H.; Arnold, F.E., Macromolecules, 14, 915 (1981).
18. Husman, G., Helminiak, T., Adams, W., Wiff, D.; Benner, C., "Resins for Aerospace," May, C., Editor, ACS Symposium Series, p. 203, American Chemical Society, Washington, D.C. (1980).
19. Ringsdorf, H.; Schneller, A., Brit. Polym. J., 13, 43, (1981).
20. Jackson, Jr., W.J.; Kuhfuss, H.F., J. Polym. Sci., Poly. Chem., 14 2043 (1976).
21. Menges, G.; Hahn, G., Modern Plastics, 58, 56, Oct. 1981.
22. Lagow, R.J., Margrave, J.L., Shimp, L.A., Lam, D.K.; Baddour, R.F., in "Advances in Polymer Friction and Wear," Vol. 1, 355, Plenum, New York (1974).
23. O'Kane, D.F.; Rice, D.W., J. Macromole. Sci. - Chem., A10, 567 (1976).
24. Szwarc, M., Polym. Eng. and Sci., 16, 473 (1976).
25. Tazuke, S., Polym. - Plast. Technol. Eng., 14, 107 (1980).
26. Clark, D.T., Dilks, A.; Shuttleworth, D., in "Polymer Surfaces," Clark, D.T., Feast, W.J., Editors, p. 185, Wiley, New York (1978).
27. Yasuda, H.; Hsu, T., J. Polym. Sci., Poly. Chem., 15, 81 (1977).
28. Yasuda, H., in Ref. 1.
29. Clark, D.T. in "Advances in Polymer Friction and Wear," Lee, L.H., Editor, Vol. 1, p. 241, Plenum, New York (1974).
30. Wrobel, A.M.; Kryszewski, M., in "Plasma Polymerization," ACS Symposium Series No. 108, p. 237, American Chemical Society, Washington, D.C. (1979).
31. Wright, A.N., in "Polymer Surfaces," Clark, D.T.; Feast, W.J., Editors, p. 155, Wiley, New York (1978).
32. Clark, P.J. in "Polymer Surfaces," Clark, D.J.; Feast, W.J., p. 235, Wiley, New York (1978).
33. Clark, H.A., U.S. Patent 3,986,997 (2976).
34. Vincent, H.L., Kimball, D.J.; Boundy, R.R., in Ref. 1.
35. Ting, R.Y.; Cottington, R.L., Adhesives Age, 24, 35, June 1981.
36. Bascom, W.D., Cottington, R.L.; Timmons, C.O., Appl. Polym. Sym., 32, 165 (1977).
37. Sutor, P., in Ref. 1.
38. Mai, Y.W.; Castino, F., J. Mat. Sci., 19, 1638 (1984).
39. Goldsworthy, W.B., Plastics World, 56, Aug. 1984.
40. Frisch, H.L., Frisch, K.C.; Klempner, D., CHEMTECH, 189, Mar. 1977.
41. Sperling, H.L., Modern Plastics, 58, 74, Oct. 1981.



42. Holden, G.; Mikovich, R. (Assigned to Shell Oil Company) U.S. Patent 3,265,765 (1966).
43. Rees, R.W. (Assigned to duPont deNemours and Company), U.S. Patent 3,264,272 (1966), and 3,404,134 (1968).
44. Skinner, E., Emcott, M.; Jevne, A., (Assigned to General Mills Chemicals), U.S. Patent 4,128,600 (1978).
45. Sperling, L.H., Manson, J.A.; Devia-Manjarres, U.S. Patent 4,254,002 (1981).

RECEIVED January 23, 1985

# Modification of Polymer Surfaces by Plasma Treatment and Plasma Polymerization

H. K. Yasuda

Department of Chemical Engineering and Graduate Center for Materials Research,  
University of Missouri-Rolla, Rolla, MO 65401

Plasma (partially ionized gas) can be utilized to alter the surface characteristics of polymers by (1) exposing a surface of polymer to non-polymer-forming plasma (e.g.,  $O_2$ ,  $N_2$ ,  $H_2O$ , Ar, He, etc.) or by (2) depositing very thin layer of plasma polymer on a surface of polymer. Both processes can produce significant changes on the surface properties of polymers and can contribute to the improvement of wear resistance of polymers, since many changes which can be related to the wear resistance of polymers generally start to take place at the polymer surface. Fundamental aspects of plasma treatment of polymers and plasma polymerization are reviewed.

It is only recently that the users of polymers have become aware of their wear resistance, and these users are even less aware of this characteristic in plasma polymers, because it is only very recently that the true advantages of plasma polymers have been recognized and utilized in a practical manner. Consequently, plasma polymers that are used to improve the wear resistance of other polymers has not been explored sufficiently for the results to be discussed effectively. However, some basic characteristics of plasma polymers have been revealed by recent studies, which indicate the significant role that plasma polymers can play in increasing the wear resistance of other polymers. Because of this and in spite of a lack of information directly relevant to the wear characteristics of polymers, the author has agreed to present herein an overview of plasma polymerization and plasma polymers with regard to the latter's potential for improved wear resistance of other polymers.

It is important to recognize that plasma polymers are ideal "interface polymers" rather than "bulk polymers" and that the wear of polymeric materials often begins at the interface of the polymer-surrounding medium. Therefore, it is advisable to examine first the characteristics of these ideal "interface polymers" and to seek uses for them that are most appropriate.

### Plasma Polymerization and Plasma Polymers

The formation of polymeric materials in the plasma state of organic vapor(s) (partially ionized state) is referred to as plasma polymerization, and the resultant materials are plasma polymers. Because the most practical way to create low temperature plasma is to employ an electric glow discharge, the terms glow discharge polymerization and glow discharge polymers are often used synonymously for plasma polymerization and plasma polymers.

Although the term polymer is used, a material formed by plasma polymerization is not a polymer in the strict sense of the definition (1). In order to understand the real advantages of plasma polymers, it is necessary to recognize the characteristics that set them apart from other conventional polymers.

System Dependent Phenomena. Perhaps the most important aspect of plasma polymers is that their method of formation, plasma polymerization, is highly system dependent. For example, a monomer will not yield a well defined polymer, but a variety of polymers can be formed from a monomer depending on how plasma polymerization is used. This is definitely different from conventional polymerization. For instance, styrene can be polymerized by many different polymerization techniques, but the products can always be identified as polystyrene. This is because the polymerizations are essentially molecular processes, and, consequently, the chemical structure of the monomer is retained within the resulting polymer in a very predictable manner.

In plasma polymerization, the chemical structure of a monomer is generally not retained in the polymer unless a special effort is made to do so. If conventional polymerization is viewed as a molecular process, plasma polymerization has components of atomic processes whose contributions depend on the conditions of plasma polymerization.

Because of the contribution of atomic polymerization, the plasma polymer of styrene in its most practical and useful form is distinctly different from polystyrene. This is exactly why plasma polymers can be used to improve the wear resistance of other polymers. If the plasma polymerization of styrene did produce a conventional polystyrene, one could not expect any improvement in the wear resistance of polystyrene by using plasma polymerization. Because the plasma polymer of styrene is not polystyrene, the deposition of the plasma polymer of styrene on the surface of polystyrene can produce a remarkable improvement.

Because of the system dependent aspect of plasma polymerization, there is no material that can be adequately described as the plasma polymer of a particular monomer, e.g., the plasma polymer of styrene, the plasma polymer of tetrafluoroethylene, and so on. The factors that influence the system dependent aspect of plasma polymerization are operational parameters, such as flow rate, discharge power, system pressure, and substrate temperature, and the design factors of the reactor, such as its size and shape, mode of electric discharge, and location of the substrate.

A typical example of the system dependent aspect of plasma polymerization can be seen in the data that are derived from the

effect of different substrate temperatures in a reactor that is operated under identical conditions of plasma polymerization (2). Figure 1 depicts the ESCA C1s spectra of the plasma polymer of perfluoro-2-butyl tetrahydrofuran (PFBTHF) deposited onto substrates at different temperatures under two sets of plasma polymerization conditions. The temperature dependence in both cases was observed under identical conditions. As can be seen in Figure 1, the chemical structure of the plasma polymer of PFBTHF depends on both the substrate temperature and the conditions of plasma polymerization. The quantitative changes of the ESCA C1s peaks as a function of substrate temperature are shown in Table I. It is clear that the substrate temperature alone, under otherwise identical conditions, can cause significant changes in the chemical structure of plasma polymers.

Table I. Change of ESCA C1s Peaks of Plasma Polymers of PFBTHF Due to the Change of Substrate Temperature and of W/FM

W/FM (J/kg)x10 <sup>-7</sup>	Substrate Temp. (°C)	Percent peak area of component peaks*				
		#1	#2	#3	#4	#5
0.65	75	16.0	21.1	19.4	26.6	17.0
	50	16.5	26.8	18.5	22.9	15.2
	25	17.3	27.2	19.5	22.7	13.3
	0	18.5	27.8	14.9	22.1	16.7
	-25	19.1	30.9	16.8	21.4	11.8
11.6	75	14.9	18.1	18.8	19.3	28.9
	50	15.0	18.8	18.3	20.0	28.1
	25	16.6	20.0	17.7	18.8	27.2
	0	16.7	20.2	17.5	19.4	26.2
	-25	17.8	21.0	17.8	18.8	24.6
	-49.5	18.0	21.2	17.1	19.8	24.0
* Peak		Approx. peak position (eV)		Approx. peak width (eV)		
#1	-CF <sub>3</sub>	295		2.0		
#2	-CF <sub>2</sub> -	293		1.9		
#3	-C-F	291		2.3		
#4	-C-CF*	288		2.3		
#5	>C-H and -C-C-	286		2.8		

**Networks of Short Segments and Branches.** Plasma polymers in useful forms consist of highly crosslinked and branched networks. There is no long chain segment in a plasma polymer, and it can be generally considered that no longer segment than C<sub>5</sub> or C<sub>6</sub> exists between the crosslinks and/or branching in the network. Unlike most crosslinked polymer networks, even these short segments are not chemically uniform, consequently the material is completely amorphous.

Because of this extremely tight network, the behavior of plasma polymers is significantly different from conventional polymers.

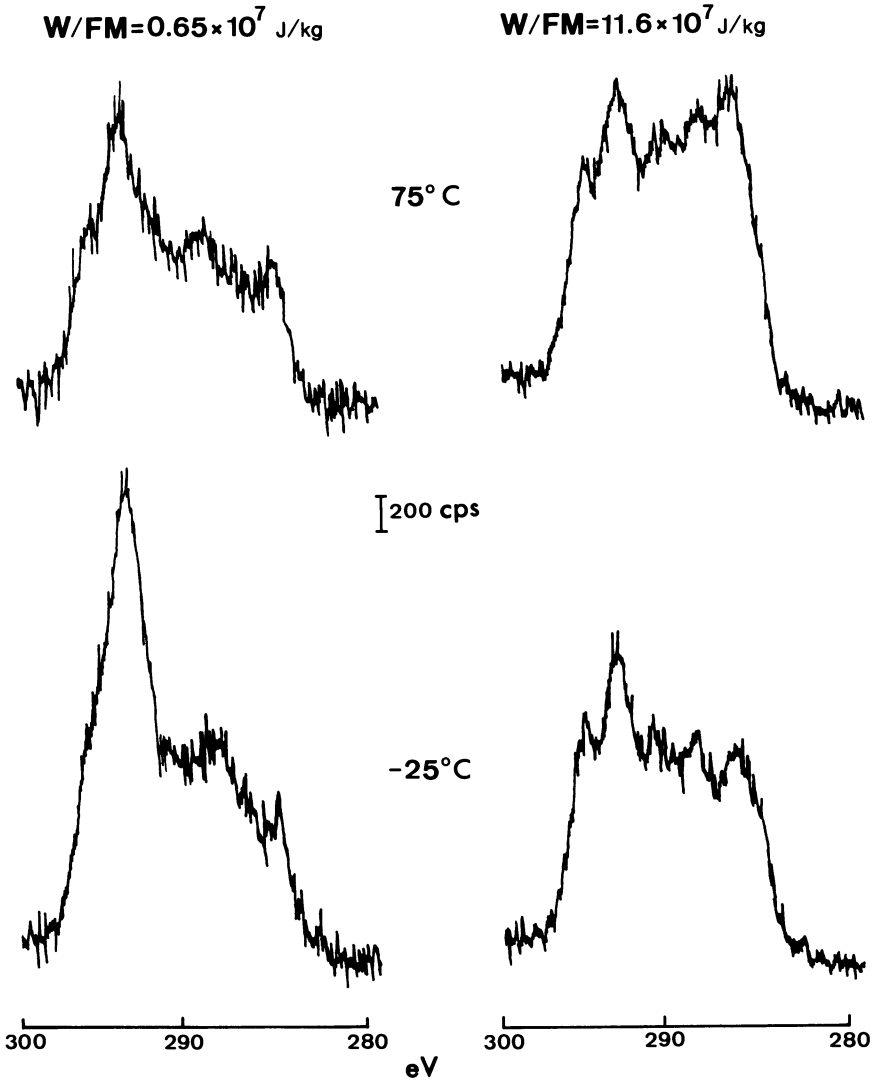


Figure 1. ESCA C1s spectra of plasma polymers of PFBTHF obtained at different (W/FM) and substrate temperatures.

This difference may be seen in the different permeability characteristics of conventional polymers and plasma polymers to water vapor and oxygen.

The permeability of gases and vapors in a flawless polymer matrix is well established by the solution-diffusion principle in which permeability,  $P$ , is given by the product of solubility,  $s$ , and the diffusivity,  $D$ , i.e.,  $P = sD$ .

In conventional polymers, their chemical nature influences both the molecular interaction of the polymers and the molecular interaction of the polymers and water. The former situation largely determines diffusivity, and the latter influences solubility. For example, the polarity of polymers will increase the interaction between polymers and decrease the diffusivity, whereas a water-polymer interaction increases with an increase in the polarity of polymers and leads to an increase in solubility. These situations may be seen in the schematic representations of  $S$ ,  $D$ , and  $P$  in Figure 2 as functions of cohesive energy density.

In gas permeability, the gas-polymer interaction is relatively small, and its dependence on the polarity of polymers may be negligible. In such cases,  $P$  is largely determined by the magnitude of  $D$ . Consequently, the molecular architecture to reduce the value of  $D$  will produce a good barrier material for gases. On the other hand, in the case of water vapor, which has high polarity and a stronger interaction (in orders of magnitude) with polymers than with permanent gases, the increase of solubility cannot be neglected. As a result, as shown in Figure 2, the  $P$  for water vapor passes the minimum, which indicates the low limit of water vapor permeability obtainable by conventional polymers. This relationship, which is shown schematically in Figure 2, is indeed seen in actual polymers. In Table II, the permeability values (3) of oxygen and water are compared. The polymers are arranged in the order of increasing cohesive energy density (starting with the lowest at the top). The values for the permeability of oxygen decrease monotonously with increasing C.E.D., whereas the permeability of water passes the minimum and increases with further increase of C.E.D. Thus, the ratio of  $P(\text{H}_2\text{O})/P(\text{O}_2)$  reaches  $10^6$  for highly polar polymers, such as polyacrylonitrile.

Table II. Oxygen Permeability and Water Vapor Permeability of Polymers

Polymer	$P_{\text{O}_2} \times 10^{10}$	$P_{\text{H}_2\text{O}} \times 10^{10}$
Poly(dimethylsiloxane)	605	43,000
Natural Rubber	23.3	2,290
Polyethylene, $d = 0.914$	2.88	90
Poly(trifluorochloroethylene)	0.025	0.29
Poly(vinylidene chloride)	0.0053	0.50
Poly(acrylonitrile)	0.0002	300
Plasma Polymer of $\text{CH}_4$		0.0076
Sputtered Cu Layer		0.0026

Data at near  $25^\circ\text{C}$ ,  $P$  in  $\text{cm}^3(\text{STP}) \cdot \text{cm}/\text{cm}^2 \cdot \text{sec} \cdot \text{cmHg}$ .

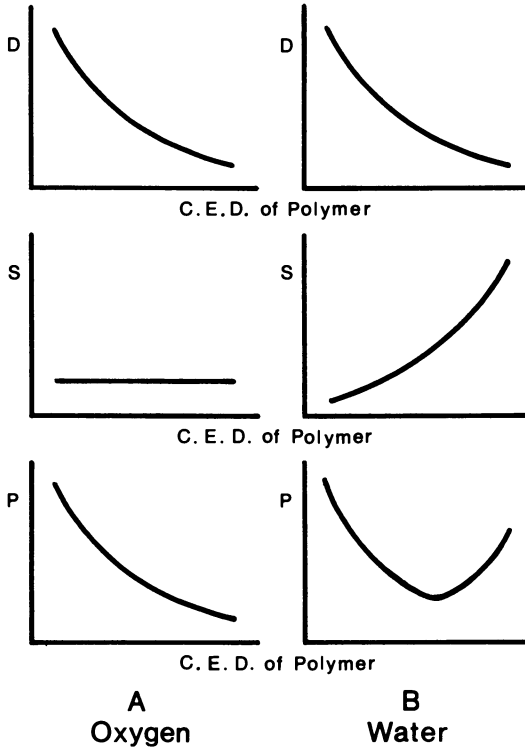


Figure 2. Dependence of diffusion constant,  $D$ , solubility constant,  $S$ , and permeability constant,  $P$ , of oxygen and water on the cohesive energy density of polymer.

The implication of this relationship is that there is a limiting value of  $P$  for water, and it is extremely difficult to make a polymer that has a significantly lower water vapor permeability in its molecular architecture as long as conventional polymers are employed.

The significance of plasma polymers in this respect is that a different principle applies in governing the magnitude of  $D$  and  $S$ , consequently the limiting case observed with conventional polymers does not apply to plasma polymers. A value of the water vapor permeability of a plasma polymer is also included in Table II.

Because of significantly lower levels of solubility, permeation through a plasma polymer is often not governed by a truly solution-diffusion principle. Many plasma polymers show characteristics in between solution-diffusion type polymers and molecular sieves. This difference in permeation mechanisms might be utilized favorably in applications of plasma polymers.

### Some Advantageous Features of Plasma Polymers

The surface characteristics of polymers can be modified by depositing an ultrathin layer of plasma polymer, i.e., an ultrathin coating that is developed by plasma polymerization. Although the objective of such a coating is similar to that of a conventional coating, the effects are significantly different from what one can achieve by using conventional processes. Some of these advantageous features are brought into focus by the following important aspects of plasma polymerization and plasma polymers.

Adhesion of Plasma Polymers to Substrate Polymers. Because of the unique polymerization/deposition mechanisms of plasma polymers, the adhesion of plasma polymers to substrate polymers is generally strong. The growth mechanism of plasma polymerization may be explained by the bicyclic rapid step-growth mechanisms shown schematically in Figure 3. In the figure, the reactive species are represented by free radicals; however, any other reactive species can contribute to each step. Step (1) and step (4) are essentially the same as adding reactive species to a monomer, but the kinetic chain length in a vacuum is extremely short, and in a practical sense, these reactions can be considered as step-wise reactions. Cycle 1 consists of reactions of monovalent reactive species, and cycle 2 is based on divalent reactive species. Step (3) is essentially a cross-cycle reaction from cycle 2 to cycle 1. Cycle 1 requires reexcitation, whereas cycle 2 is self-perpetuating as long as divalent reactive species exist. Any of the species involved will collide with the substrate's surface, but not all of them will remain on the surface, depending on the kinetic energy of the impinging species. The sticking coefficient may be defined in terms of the number of particles that remain on the surface divided by the total number of impinging particles. The deposition occurs when an impinging particle fails to leave the surface either through the loss of kinetic energy or the formation of a chemical bond. Thus, a plasma polymer layer is often chemically bonded to the substrate polymer, and in such cases it is impossible to remove it without destroying either the film or the substrate.



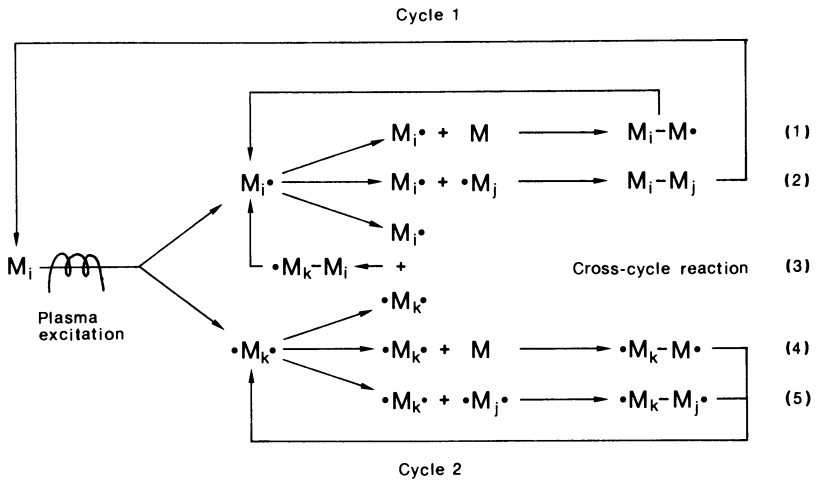


Figure 3. Schematic representation of bicyclic step-growth mechanism of plasma polymerization.

Barrier Characteristics of Plasma Polymers. As indicated by the water vapor permeabilities of plasma polymers, an extremely tight network sets up a barrier against many molecules larger than gases and water vapor. The significance of such a barrier is that total blockage against the penetration of small molecules into the bulk of the substrate polymer can be achieved by a layer thinner than 500Å. Such a barrier is illustrated by the data derived from the permeation of dye through a film of plasma polymer coated Nylon 6 (4). The experimental arrangement is as follows: a plasma polymer of methane approximately 250Å thick is applied to one surface of a film of Nylon 6 (0.05 mm thick), a dye is allowed to permeate the film, and the rate of permeation is measured. The dyes used for the study are shown in Table III, and the permeability data are shown in Table IV. The apparent permeability, Pa, is calculated from the

Table III. Types and Molecular Structures of Dyes Used for Permeability Study

Dyestuff		Molecular weight	Maximum wave length (nm)	
Acid dyes	Solar orange R	364	495	
	Acid blue black 10B	616	600	
	Brilliant scarlet 3R	604	518	
	Solar light orange GX	452	480	
	Tartragine NS conc	534	429	
	Disperse dye	Celliton fast yellow 5R	316	390

Table IV. Permeabilities of Dyes Through Nylon 6 Film With and Without 250Å Thick Layer of Plasma Polymer of Methane

DYE			FILM		Pa (mm <sup>2</sup> /sec)x10 <sup>12</sup>	
Type	Name	M	Methane Plasma	W/FM (J/kg)x10 <sup>-10</sup>	From Coated Side	From Uncoated Side
Acid Dye	Solar Orange R	366	uncoated		161	161
			coated	0.076	0.34	5.08
	Acid Blue	616	uncoated		5.69	5.69
	Black 10B		coated	0.076	0	1.71
	Brilliant	604	uncoated		37.4	37.4
	Scarlet 3R		coated	0.074	0	8.31
	Solar Light	454	uncoated		111	111
	Orange GX		coated	0.10	0	4.73
	Tartragine	537	uncoated		83.2	83.2
Disperse Dye	NS Conc		coated	0.10	0	7.89
	Celliton Fast	316	uncoated		1.82	1.82
	Yellow 5R		coated	0.076	0.82	1.65

permeation rate, with the thickness of the coating being neglected in the calculation. It is interesting to note that there is a considerable directionality in the permeability of the coated film to the different dyes. For instance, the film is impermeable to the larger acid dyes from the coated side, but is permeable to them from the uncoated side, even though significant reductions in permeability is observed in both cases. Thus, a very thin layer of plasma polymer can prevent small molecules from penetrating most of the polymers, and as a result a remarkable solvent resistance is often imparted to them by such a coating.

Inperturbable Surface Characteristics of Plasma Polymers. The surfaces of polymer solids are decidedly different from those of more rigid materials, such as metals and ceramics. Polymer molecules have much greater freedom for rearrangement within the bulk phase of the polymer or at its surface, but they may orient themselves differently at the surface than within the bulk phase. Accordingly, the surface properties of a polymer solid may not be the same as the properties within the solid. Phenomena related to this aspect of polymers were recognized in the early 1960's by investigators who were engaged in studies of the hydrogels of methacrylates (crosslinked networks of hydrophilic methacrylate polymers) (5). The surfaces of hydrophilic gels, which contain as much as 98% water, exhibit surprisingly pronounced hydrophobic characteristics. The contact angle of water on the surface of a hydrogel is very high, even though one would be expected, because of the water content of the hydrogel, that the water would spread on the surface.

Some data, which seem to support the concept of differential orientation of molecules at the surface of a polymer, have appeared in the literature. As early as 1938, Langmuir stated that the wettability of a surface involves only short range forces and depends primarily on the nature and arrangement of the atoms that form the actual surface and not upon the characteristics of the underlying molecular layers (6). Through the deposition of films of stearic acid or its barium salt on solid surfaces, he discovered that under special circumstances the surface layer may undergo an almost instantaneous reversal of orientation and thus bring about a change in the surface's physical and chemical properties; complexation (anchoring) of reactive groups was found to prevent such a change.

Thomas and co-workers demonstrated by ESCA that sodium and sulfonic groups of ion-exchange resin made of crosslinked sodium polystyrene sulfonate are not exposed to the resin-air interface but are buried in the bulk of the resin in the dry state (7).

Ratner and Hoffman (8) reported that in their experiments ESCA did not reveal as many hydrophilic groups on the surface of a grafted polymer (a hydrophilic polymer grafted onto a hydrophobic substrate polymer) as was expected from the grafting yield. They also suggested that a considerable number of grafted polymer molecules could be buried in the bulk phase depending on the condition of the grafted polymers after treatment.

Sung and Hu (9) showed that the Auger spectrum of a segmented urethane-siloxane polymer (Avcothane) is quite different for that of

the air-dried surface and the bottom surface in contact with the casting mold. They also stated that the surface of a polymer is very different from its bulk.

These observations can be attributed to the high mobility of macromolecules and to their capability of rearranging their orientation at an interface according to a change in the surrounding phase, such as water or air. This concept can also be applied to the slow change of the surface properties of some polymers. It is well known that flaming, corona, and glow discharge treatments increase the wettability of hydrophobic polymers, such as polyethylene and polypropylene. These processes are widely used to increase the wettability of adhesives for better bonding and of ink for improved printability. Although ESCA studies clearly indicate an increase in the number of carbon-oxygen bonds after plasma treatment (10-12), the improvement in the wettability of a polymer is often attributed to the increased roughness of its surface occasioned by such treatment (13,14). On the other hand, it is known that the wettability introduced by these processes decays with time after the treatment. The cause of the decay had been generally attributed to the contamination of the surfaces, but it has become clear that the slow burying of hydrophilic functional groups in the polymer matrix is largely responsible for the decay.

It has been demonstrated that a tight network of a plasma polymer can prevent the loss of hydrophilic nature through the rotational burying of hydrophilic moieties into the bulk phase of a polymer (15).

A similar phenomenon also occurs at the hydrophobic surface when the surface is kept in water for a prolonged period of time (16). This phenomenon as well as the prevention of it by application of a plasma polymer layer may be seen in the following examples.

First, the surface of a conventional polymer, such as poly(ethylene terephthalate), can be converted to a highly hydrophobic water repellent surface by treating its surface with a plasma of perfluorosaturated hydrocarbons, such as  $C_2F_6$ . This process occurs as an exchange reaction by eliminating  $HF$  (H coming from the polymer surface) and proceeds more or less in a self-extinguishing manner. In other words, it is very difficult to polymerize such saturated perfluorohydrocarbons in the absence of H, and what one obtains is the implantation of F containing moieties on the surface but not the deposition of a plasma polymer of the perfluorocompound. ESCA C1s peak of the surface reveals the presence of a high concentration of  $CF_3$ , and the contact angle of water is around  $97^\circ$ . When this sample is immersed in water, the contribution of the C1s peak, occasioned by carbon without F, starts to increase with immersion time as shown in Figure 4. After 120 min immersion in water, the contact angle of the water drops to around  $72^\circ$  indicating the loss of water repellency as a result of the rotational rearrangement of moieties at the surface.

When a similar treatment is employed after a thin layer of plasma polymer of methane (600Å thick) is applied onto a PET film surface, the corresponding results are shown in Figure 5. Because of the less amount of H available at the surface, the relative contribution of  $CF_3$  is less than in the case in which  $C_2F_6$  plasma

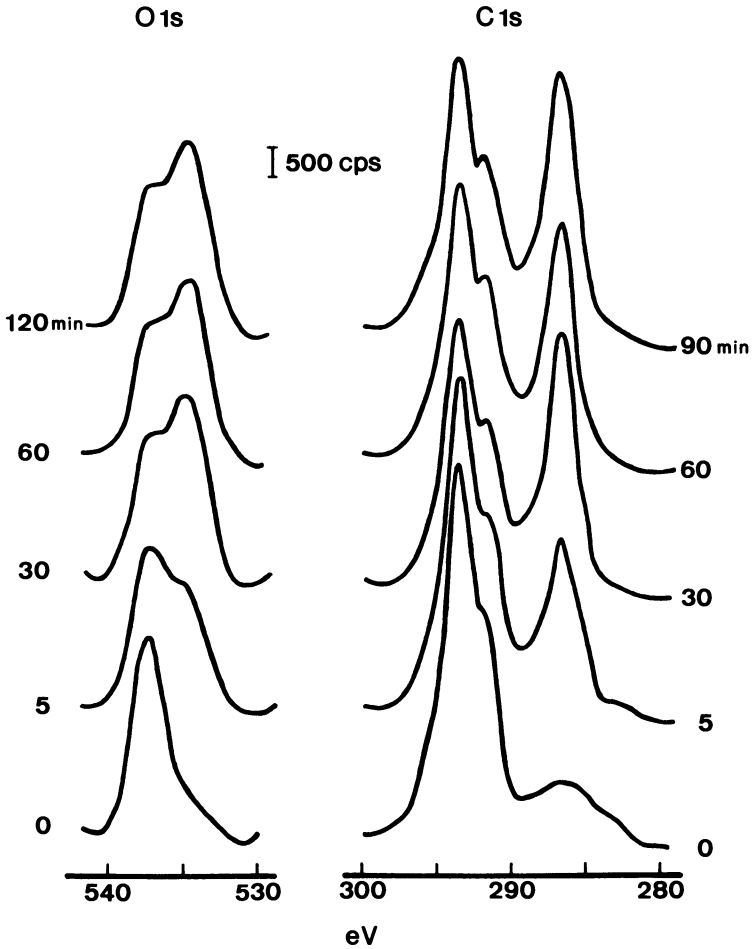


Figure 4. Change of ESCA O1s and C1s peaks of PET film treated with  $C_2F_6$  plasma as immersion time in water.

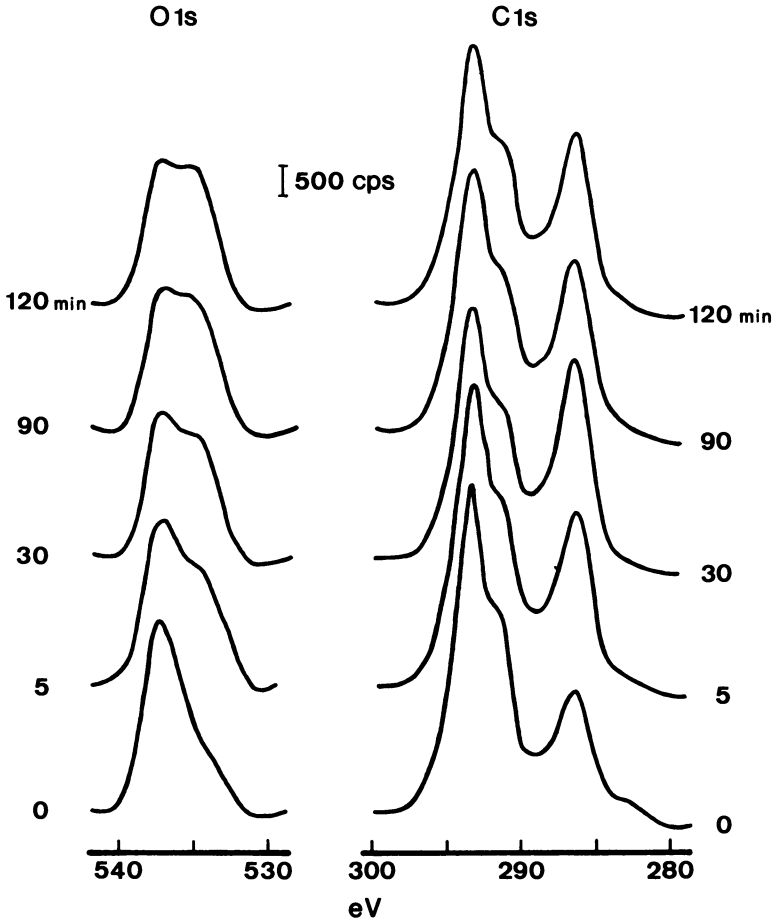


Figure 5. Change of ESCA O1s and C1s peaks of PET film with 300Å thick layer of plasma polymer of methane which is subsequently treated with C<sub>2</sub>F<sub>6</sub> plasma.

treatment is applied directly to the PET surface. However, the effect of water immersion is less pronounced, i.e., the increase of Cls peak at 285 eV is not as pronounced as in the previous case. After 120 min immersion in water, the contact angle of water remains at around 90°, indicating the more persistent water repellent characteristic of the surface.

The characteristics described in the above examples may be expressed as "unperturbable surface characteristics" brought about by the extremely tight network of plasma polymers. Such rearrangement of surface configuration occurs repeatedly according to the change of the surrounding environment in the actual use of polymers. Phenomena related to such rearrangement may not be easily understood in the concept of wear resistance; however, such a failure of expected performance should also be taken into consideration in the broader meaning when dealing with the wear of polymers.

In view of fact that most time-dependent failures, such as the fatigue of polymers, initiate at the surface, more precisely at the interface of the polymer and the surrounding medium, it is to be expected that the application of plasma polymers will contribute to the improvement of the wear characteristics of polymers at least in certain cases.

#### Literature Cited

1. H. Yasuda, "Contemporary Topics in Polymer Science," 3, edited by M. Shen, 103 Plenum Publication Corp., New York (1979).
2. H. Yasuda ; C. R. Wang, paper submitted to J. Polym. Sci., Polym. Chem. Ed. (1984).
3. H. Yasuda ; V. Stannett, "Permeability" in Polymer Handbook, 2nd Ed., edited by J. Brandrup ; E. H. Immergut, John Wiley, New York (1975).
4. T. Yasuda, A. K. Sharma ; H. Yasuda, Organ. Coatings and Applied Polymer Science Proceedings, 47, (1982) 454.
5. F. J. Holley ; M. F. Refojo, J. Biomed. Matls. Res., 9, (1975) 315.
6. I. Langmuir, Science, 87, (1938) 493.
7. R. Thomas ; R. Trifilet, Macromolecules, 12, (1979) 1197.
8. B. D. Ratner, P. K. Weathersby, A. S. Hoffman, M. A. Kelly ; L. H. Scharpen, J. Appl. Polym. Sci., 22, (1978) 643.
9. C. S. P. Sung and C. B. Hu, J. Biomed. Matls. Res., 13, (1979) 45.
10. H. Yasuda, H. C. Marsh, S. Brandt ; C. N. Reilley, J. Polym. Sci., Polym. Chem. Ed., 15, (1977) 991.
11. D. T. Clark ; A. Dilks, "Characterization of Metal and Polymer Surfaces," edited by L. H. Lee, Academic Press, Inc., New York, Vol. 2, (1977) p. 101.
12. J. M. Burkstrand, J. Vac. Sci. Technol., 15(2), (1978) 223.
13. A. M. Wrobel, M. Kryszewski, W. Rakowski, M. Okoniewski ; Z. Kubacki, Polymer, 19, (1978) 908.
14. R. H. Hansen, J. V. Pascale, T. De Benedictis ; P. M. Rentzepis, J. Polym. Sci., Part A, 3, (1965) 2205.
15. H. Yasuda, A. K. Sharma ; T. Yasuda, J. Polym. Sci., Polym. Phys. Ed., 19, (1981) 1285.
16. T. Yasuda ; H. Yasuda, paper to be published.

## Effect of Temperature on the Friction and Wear of Some Heat-Resistant Polymers

Kyuichiro Tanaka and Yoshinori Yamada

Faculty of Engineering, Kanazawa University, Kanazawa 920, Japan

Friction and wear of polyimide, polyamide-imide, polyether ether ketone, polyphenylene sulfide (filled with glass fibers) and polyether sulphone sliding against a smooth steel disk were studied at various disk temperatures. A friction experiment in which a steel sphere was slid on flat polymer plates was also carried out at various temperatures. Friction of the heat resistant polymers generally varied markedly with the temperature. Polyimide, polyamide-imide and polyether ether ketone exhibited relatively low friction at the temperatures above 200 °C in their wear process. Polyimide and polyamide-imide showed wear peak at given temperatures; this appeared to be due to chemical reaction in the polymer chains during sliding at high temperatures. Polyether ether ketone, polyphenylene sulfide and polyether sulphone exhibited little variation in wear rates with temperature up to a certain temperature. A thick transferred polymer layer was generally produced at high temperatures, decreasing the friction and wear of polymers.

It is well known that the generation of heat at sliding contact of polymers can produce local decomposition, hence limiting the usefulness of polymers in a sliding application. Some of the heat resistant polymers developed in relatively recent years are expected to be useful under severe slide conditions. Friction and wear of polyimide which does not flow at high temperatures have been studied by a few authors (1,2,3). Some of the results obtained indicate that variations of friction and wear of polyimide with temperature and sliding speed are relatively large. Buckley (1) reported that polyimide produced a transferred film on the countersurface which then decreased friction. Matsubara et al. (2) found that polyimide exhibited the peak of wear at a certain sliding speed as sliding speed was increased and at a certain temperature as the temperature was increased. They



attributed this wear peak to a chemical reaction during the wear process. In addition to polyimide, there are some heat resistant polymers such as polyamide-imide, polyether ether ketone, polyphenylene sulfide and polyether sulphone. At present, however, there exist few studies on friction and wear of heat resistant polymers other than polyimide. Thus, it is important to investigate the friction and wear of these heat resistant polymers. The purpose of this work is to study the effect of temperature on the friction and wear of some typical heat resistant polymers and the mechanisms of wear of these polymers.

### Experimental

Procedures for Studying the Fundamental Frictional Properties of the Polymers. To study the fundamental frictional properties of the heat resistant polymers, a steel sphere of 2.38 mm in radius was slid on flat polymer plates at a low speed of 0.25 mm/s under various loads ranging from 1 N to 8 N and at various temperatures up to 300 °C, and the frictional force was measured. The temperature of the specimen polymer surface was controlled by thermocouple and electric heater. A steel ball for ball bearing use was used as the sphere in the experiments. The polymer surfaces were abraded with a 1000-grade abrasive cloth and cleaned with ethyl alcohol.

Wear-Testing Apparatus and Experimental Procedures. To study the effect of temperature on the wear behavior of specimen polymers, the pin-on-disk type wear testing apparatus used in our previous work (4) was employed and the frictional force and wear depth of the flat ended polymer pins 3 mm in diameter were measured at a sliding speed of 0.1 m/s under a load of 10 N and at various experimentally possible disk temperatures up to 300 °C. The disk was made of stainless steel (SUS 304) and heated by an electric heater mounted under the disk. The surface roughness of the frictional surface of the disk was about 0.02  $\mu\text{m}$  c.l.a. The diameter of the frictional track on the disk was 7 cm. The specimen pin was initially rubbed against 1000-grade Emery paper placed on the disk. This pre-rubbing was useful for allowing uniform contact between the specimen surface and the disk. After the pre-rubbing the specimen and disk surfaces were cleaned by rubbing with a soft cloth soaked in ethyl alcohol. All experiments in this work were carried out in ambient air of 60  $\pm$ 10 % R.H. and room temperature of 23  $\pm$ 4 °C.

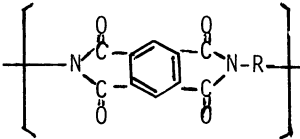
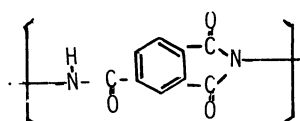
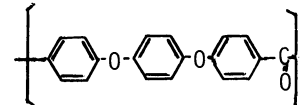
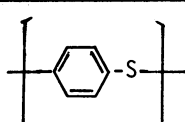
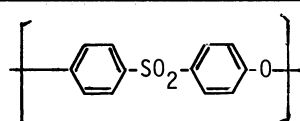
Polymer Specimens. The materials used in this work were polyimide (PI), polyamide-imide (PAI), polyether-ether-ketone (PEEK), polyphenylene sulfide (PPS) and polyether sulphone (PES). The chemical formulas and physical properties of the specimen polymers are summarized in Table I. The specimen polymers, except PPS, were unfilled while the PPS specimen was filled with glass fiber of 40 wt. %. PAI and PES are amorphous polymer with considerably high glass temperature  $T_g$ . The polymers, except PI, can flow at high temperatures and allow the use of injection molding.

### Experimental Results and Discussion

#### Sliding of a Steel Sphere on Flat Plates of Specimen Polymers.

Figures 1 (a) and (b) show variations in the coefficients of friction

Table I. Polymer specimens - Chemical formula and some properties.

Chemical type (Abbr.)	Chemical formula	Melting point °C	Glass temp. °C	Heat distor- tion temp. °C	Tensile strength kg/cm <sup>2</sup>
"Tradename"					
polyimide ( PI ) "Vespel-SP1"		>900			740 (23°C)
polyamide- imide ( PAI ) "Torlon"		—	ca.280	274	1900 (23°C)
polyether ether ketone ( PEEK )		334	143	135- 160	910 (23°C)
polyphenylene sulfide ( PPS ) "Ryton R-4": (PPS+G.F. 40%)		275	94	260	1504
polyether sulphone ( PES ) "Viktrex"		—	225	203	860 (23°C)

of various specimen polymers with load at temperatures of 23°C and 150 °C. The coefficient of friction generally decreases with the increase in load  $W$  and is proportional to  $W^{-n}$ . Although the index  $n$  is generally very small, its value is dependent upon the type of polymer and the temperature. The small value of the index  $n$  indicates that the contact between the steel sphere and specimen polymers is approximately plastic under the experimental condition. Figure 2 shows the relationship between coefficients of friction at a load of 8 N in various polymers and temperatures. PI and PES show relatively high friction at all temperatures while PAI and PEEK exhibit considerably low friction at temperatures up to 150°C with the friction increasing rapidly with temperature in the higher temperature range. The high friction at higher temperatures for PEEK and PAI may be due to a large increase of the deformation component of friction at higher temperatures. The width  $d$  of frictional tracks at a load of 8 N was measured and the temperature dependence of the contact pressures at sliding contact was obtained, assuming that the real area of sliding contact is  $\pi d^2/4$ . Since the contact may be assumed to be approximately plastic, the contact pressure at a load of 8 N is approximately equal to the yield pressure of polymers. Figure 3 shows the temperature dependence of the yield pressures of various polymers. The yield pressure of PI is generally lower than that of PAI, and PEEK exhibits relatively higher yield pressure at temperatures up to about 200 °C. Although PPS specimen indicates high yield pressure at low temperatures, its yield pressure decreases markedly with increasing temperature. This suggests that unfilled PPS shows very low yield pressure at higher temperatures. Assuming that the frictional force is only due to the shearing of the adhesive junction at the sliding contact, the shear strength  $s$  was obtained from the frictional force and the area of contact at a load of 8 N. Figure 4 shows the temperature dependence of shear strengths of various polymers. It is seen that the shear strength of PI is similar to that of PPS, and also PEEK has a shear strength similar to that of PAI. PI and PPS have much higher shear strengths than PEEK and PAI at temperatures up to 150 C. It is also noted that the shear strength of PES is relatively high and is little dependent upon temperature. Although the shear strengths of PEEK and PAI increase with increasing temperature at temperatures above about 150 °C, this must be due to the large contribution of the deformation component to friction at higher temperatures. Therefore, it is reasonable to consider that Figure 4 does not show true shear strength at higher temperatures while it shows approximate shear strength at lower temperatures.

Variations in Coefficient of Friction and Wear Depth of Various Polymers Rubbed Against Steel Disk with Sliding Distance. Figures 5 (a),(b),(c),(d) and (e) show variations in the coefficient of friction  $\mu$  and wear depth  $h$  with the sliding distance in the wear processes of PI, PAI, PEEK, PPS and PES, respectively. With all specimen polymers, the steady states of friction and wear appear following the initial transient states. The wear rates of various polymers generally decrease gradually in the initial transient wear state, and the wear rates in the steady state are much lower than those in the initial transient state. However, the steady state of higher wear rates appears following the initial state of lower wear at 150°C in the

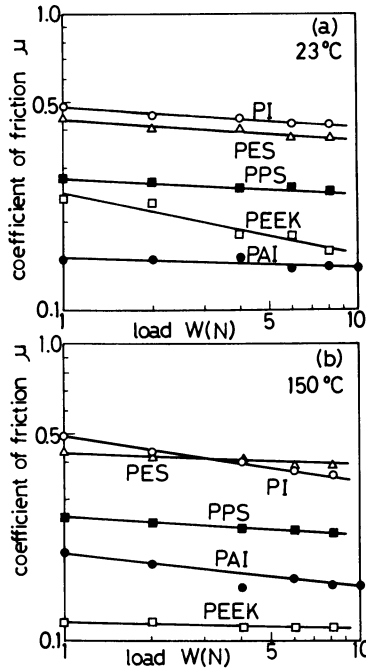


Figure 1. Variations of the coefficients of friction in the sliding of steel sphere on various polymers with load. (a) 23°C, (b) 150°C.

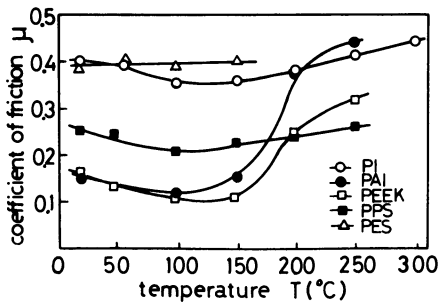


Figure 2. Relation between the coefficients of friction in the sliding of steel sphere on various polymers and temperature. (load, 8 N)

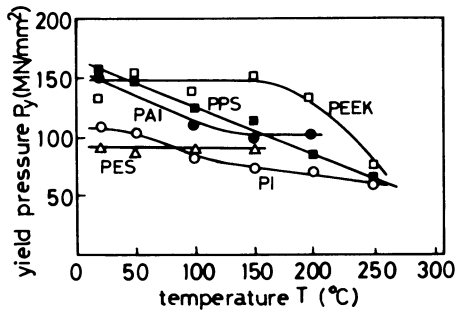


Figure 3. Variations of yield pressures of various polymers with temperature.

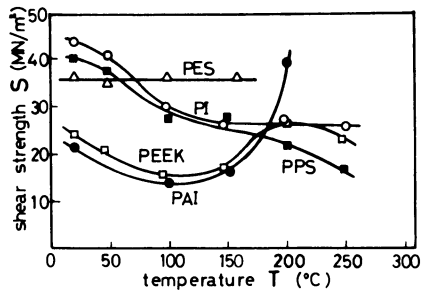


Figure 4. Variations of shear strengths of various polymers with temperature.

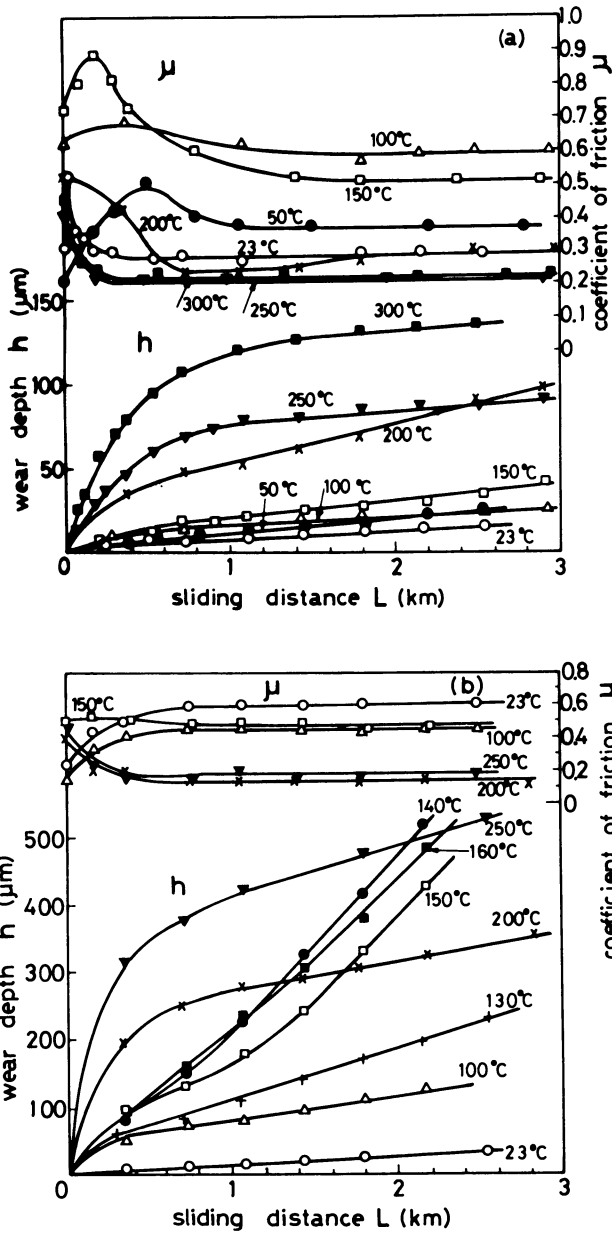


Figure 5 a and b. Variations in the coefficient of friction  $\mu$  and the wear depth  $h$  at various disk temperatures with the sliding distance  $L$ . (a) PI, (b) PAI.

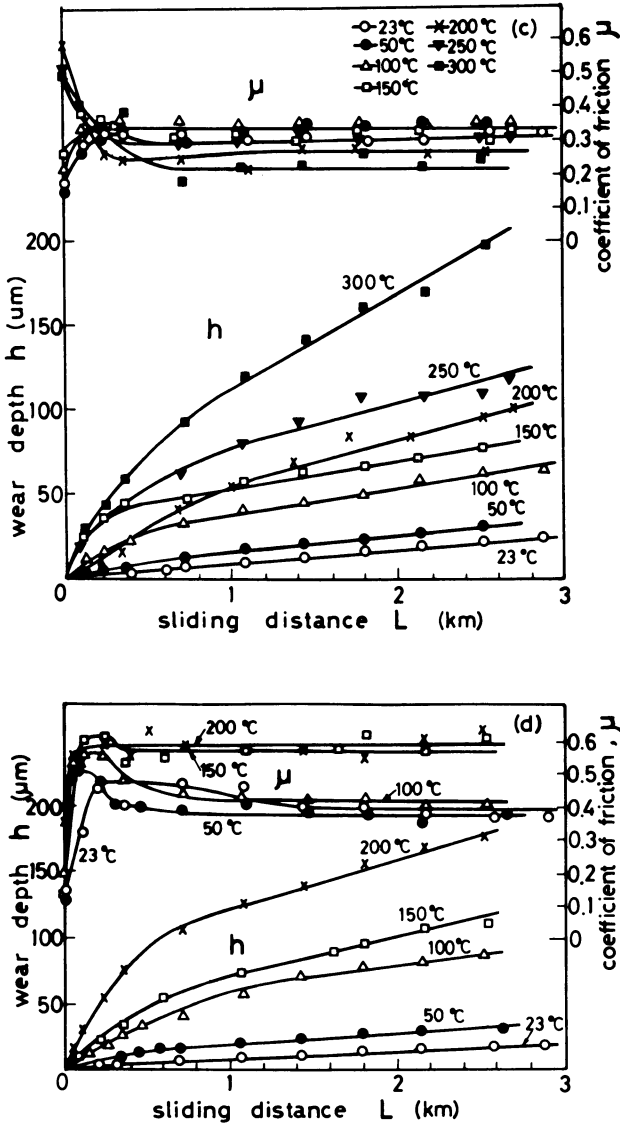


Figure 5 c and d. Variations in the coefficient of friction  $\mu$  and the wear depth  $h$  at various disk temperatures with the sliding distance  $L$ . (c) PEEK, (d) PPS.

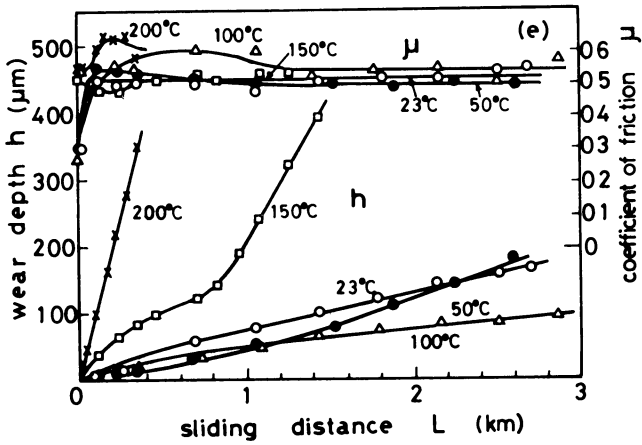


Figure 5e. Variations in the coefficient of friction  $\mu$  and the wear depth  $h$  at various disk temperatures with the sliding distance  $L$ , PES.



case of PES. On the other hand, two steady states of wear appear at some temperatures in the case of PAI and the wear rate in the second steady state is considerably higher than that in the first steady state. It is noted that the wear depth at the sliding distance which the steady state of wear begins to occur generally increases with disk temperature.

The variation of friction in the initial transient state with the sliding distance is somewhat complicated. With PI, the initial friction is much higher than the steady-state friction and friction decreases with increasing distance at disk temperatures above 200 °C, while at lower temperatures friction increases initially and reaches a maximum at a certain sliding distance in the transient state of friction. In the cases of PAI and PEEK, the friction is generally low at the start of rubbing and increases with distance at lower temperatures, while initial friction is generally high and the friction decreases initially with increasing distance at high temperatures. On the other hand, the initial friction of PPS is lower than the steady-state friction and reaches a maximum in the initial transient state of friction at any temperature. PES shows lower initial friction than steady-state friction at lower temperatures.

#### Microscopic Examinations of the Frictional Surfaces. (1) Polymer pin surfaces.

Before discussion of the variation of friction and wear of polymers with disk temperature, it will be useful to describe the results of microscopic examinations made on the frictional surfaces after wear tests. The microscopic examinations were made using an optical microscope and, in some cases, the scanning and transmission electron microscopes (SEM and TEM). Figure 6 shows TEM micrographs of the worn surfaces of PI pins rubbed at three different temperatures. Figures 6 (b) and (c) indicate that the flow of PI is severe on the frictional surface at 200 and 300 °C; this severe flow is probably due to thermal softening at high temperatures. In fact, the temperature dependence of the yield pressure of PI suggests that the yield pressures at 200 and 300 °C are considerably small. Figure 7 shows SEM micrographs of the worn surfaces of PEEK rubbed at four different temperatures. The surface at temperatures below 150 °C is very smooth compared with that at 200 and 300 °C, and the surface feature of PEEK rubbed at 300 °C indicates severe surface softening. The temperature dependence of yield pressure also suggests that severe thermal softening occurs at 300 °C. Figure 8 shows SEM micrographs of the worn surfaces of PPS at 20 and 200 °C. It was observed that the glass fibers at the worn surface of PPS rubbed at lower temperatures were generally covered with thin PPS polymer film, as seen in Fig. 8 (a), while no PPS polymer film existed on the worn surface of glass fibers at high temperatures, as seen in Figure 8 (b). Figure 8 (b) suggests that the contact load is supported mainly by the glass fibers and severe wear of PPS matrix polymer surrounding the glass fibers occurs during rubbing at high temperatures. Figure 9 shows SEM micrographs of the worn surfaces of PES rubbed at 100 and 200 °C. Considerable thermal softening of PES frictional surface occurred at high temperature such as 200 °C, while it was mild at 100 °C.

(2) Frictional tracks on disks. Figure 10 shows TEM micrographs of the frictional tracks rubbed against PI at 100, 200 and 300 °C. The scratches produced on the surface finish of the disk are seen in the cases of 100 and 200 °C, suggesting that the transferred film is

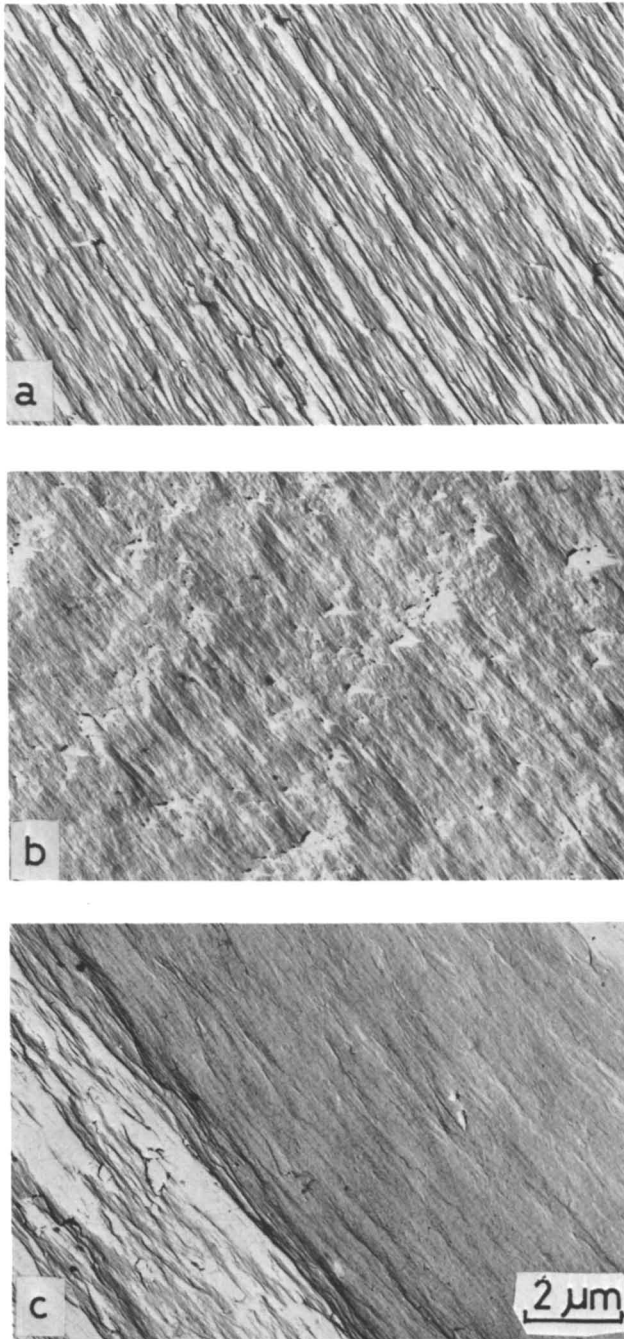


Figure 6. TEM micrographs of worn surfaces of PI rubbed at various temperatures. (a) 100°C, (b) 200°C, (c) 300°C.

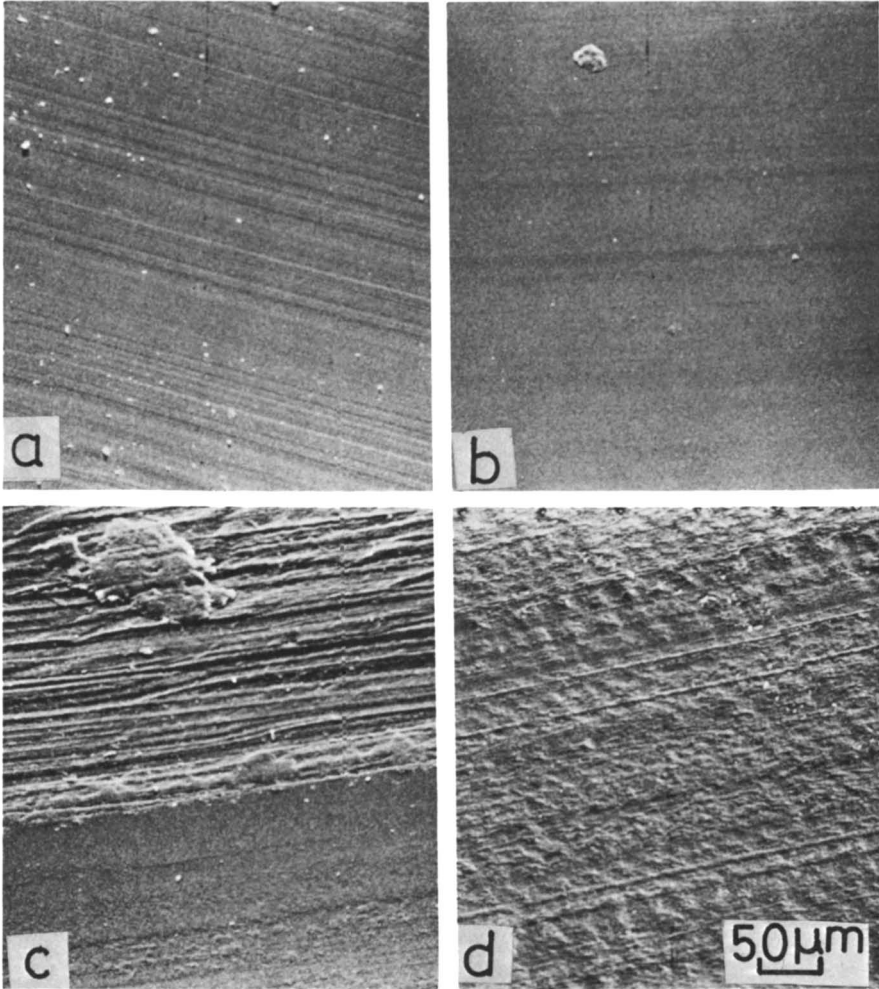


Figure 7. SEM micrographs of worn surfaces of PEEK rubbed at various temperatures. (a) 23 °C, (b) 150 °C, (c) 200 °C, (d) 300 °C.

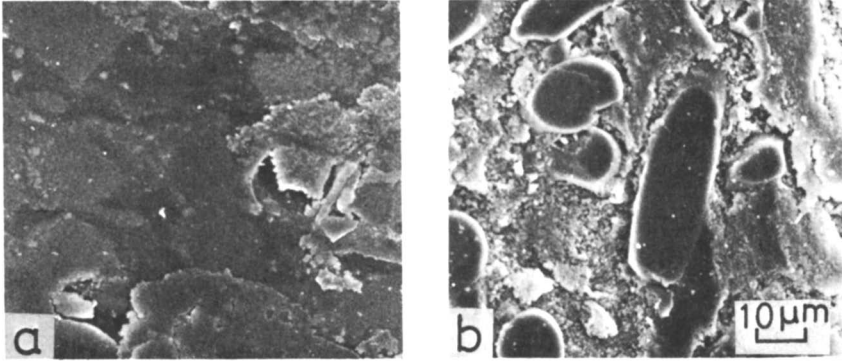


Figure 8. SEM micrographs of worn surfaces of PPS rubbed at different temperatures. (a) 23°C. (b) 200°C.

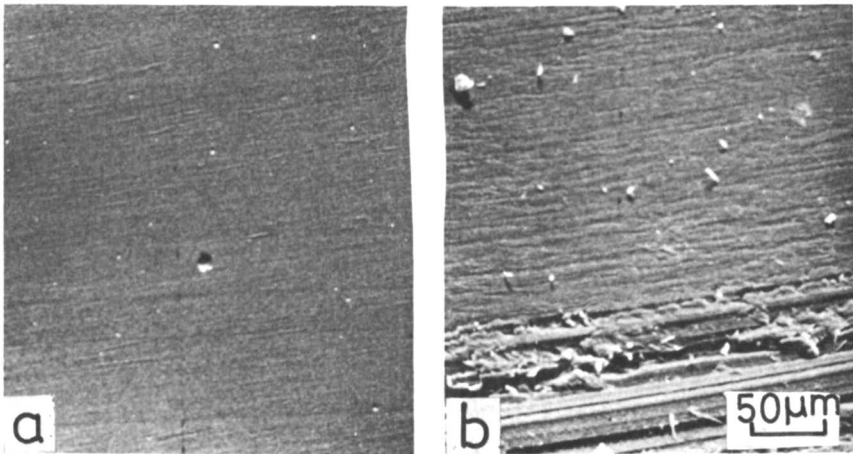


Figure 9. SEM micrographs of worn surfaces of PES rubbed at different temperatures. (a) 100°C, (b) 200°C.

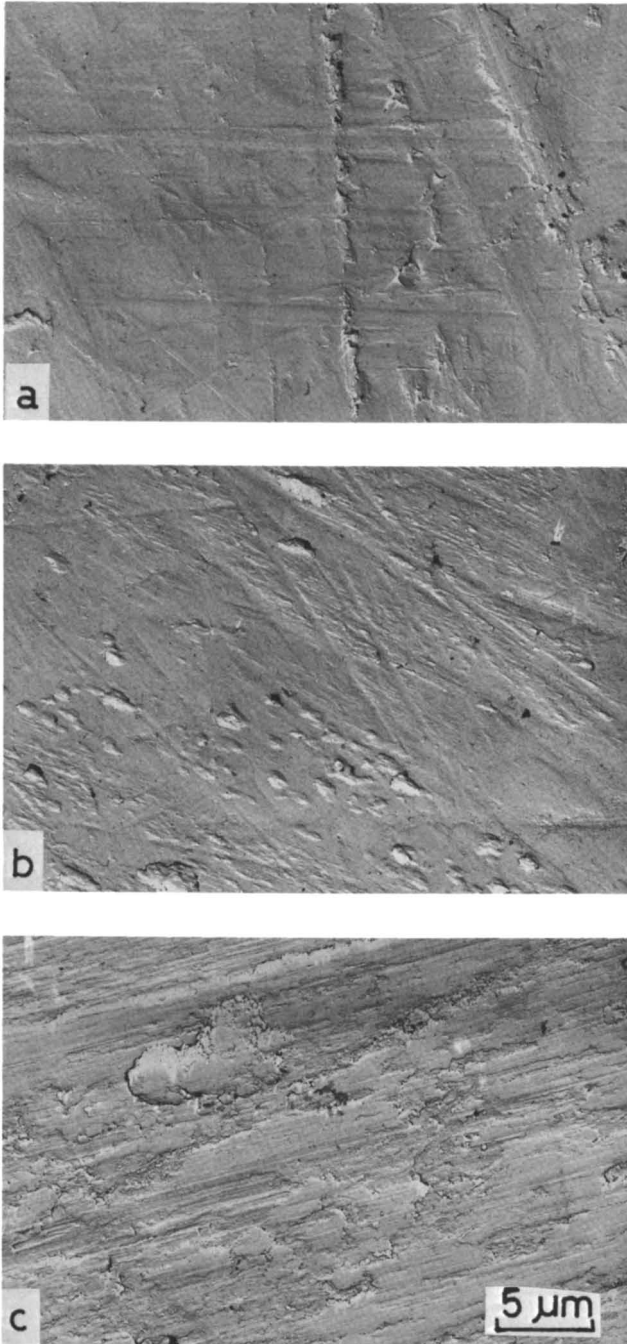


Figure 10. TEM micrographs of disk surfaces rubbed against PI at various temperatures. (a) 100°C, (b) 200 °C, (c) 300°C

relatively thin at these temperatures. On the other hand, a thick transferred PI layer is produced on the track at 300°C. The micrograph at 300 °C indicates lumps as well as film transfer on the countersurface at very high temperature. Figure 11 shows optical micrographs of the frictional tracks rubbed against PI at 150, 250 and 300 °C. Very thick transferred layer is produced at 250°C and 300 °C while transferred material is much smaller at 150°C. From Figures 10 and 11, it is concluded that PI produces a very thick transferred layer when temperature exceeds 200 °C. Figure 12 shows optical micrographs of frictional tracks rubbed against PAI at four different temperatures. It is noted that transferred material is very small at 150 °C as well as 23°C while that at 100 °C is as thick as that seen at 200 °C. The small transfer at 150 °C suggests that a change in wear mechanism of PAI occurs at temperatures between 100 °C and 200 °C. Figure 13 shows optical micrographs of frictional tracks of PEEK. Transfer of PEEK increases with temperature. However, the transferred material at 200 °C seems to be smaller compared with PAI of the same temperature.

Figure 14 shows optical micrographs of frictional tracks on PPS specimen at four different temperatures. The transferred material of the PPS specimen also increases with temperature and there is very much of it at 100 °C as well as at 200 °C. There appear to be many short glass fibers in the transferred layer at high temperature. Figure 15 shows optical micrographs of frictional tracks made by PES at four different temperatures. The transferred material of PES also increases with temperature and a considerably thicker transferred layer is produced at high temperatures than at low temperatures.

Summarizing these microscopic examinations, transfer of heat resistant polymers onto the countersurface generally increases with temperature and much transferred material is produced when thermal softening of the polymer surface becomes severe. However, the amount of transferred material did not always increase with thermal softening of polymer frictional surface in the cases of PI and PAI. Although thermal softening of PI frictional surface at 200 °C was clearly observed in electron microscopy, electron microscopic examination of the frictional track rubbed at 200 °C indicated a relatively small amount of transferred material. On the other hand, transfer at 150°C was considerably less than that at 100 and 200 °C in the case of PAI.

Friction of Polymer Pins Sliding Against Steel Disk. Figures 16(a) and (b) show variations of the coefficients of friction of various polymers with disk temperature in the steady state of friction and at the initial stage of sliding, respectively. It may be assumed that friction in the steady state corresponds approximately to the friction between the polymers and their transferred layer while the initial friction indicates that between the polymers and steel disk. Except for PPS, the initial friction is considerably lower than steady-state friction in temperature ranges below a certain critical temperature which depends upon the type of polymer. The critical temperature is approximately 60, 140, 150 and 150°C, for PI, PAI, PEEK and PES, respectively. For PPS, the coefficient of initial friction is about 0.3 less than that of steady-state friction at any temperature. This is probably due to the effect of the glass fibers in the specimen.

The differences between the coefficients of initial and steady-state friction at temperatures below the critical temperature are

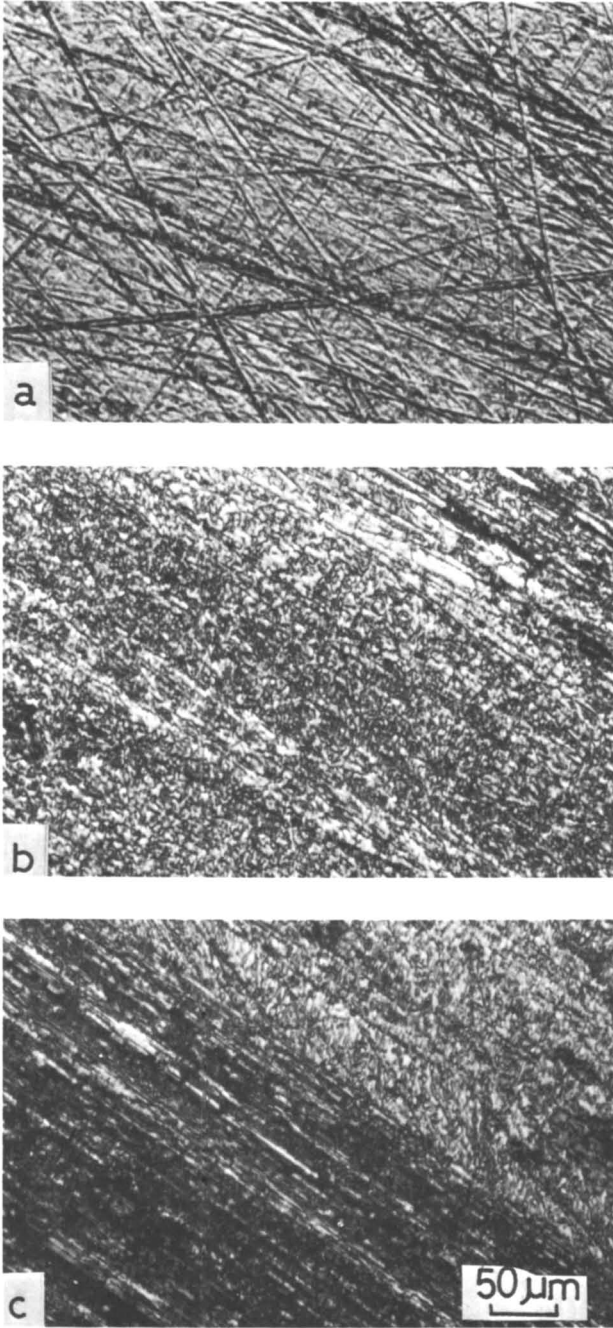


Figure 11. Optical micrographs of disk surfaces rubbed against PI at various temperatures. (a) 150°C, (b) 250°C, (c) 300°C.

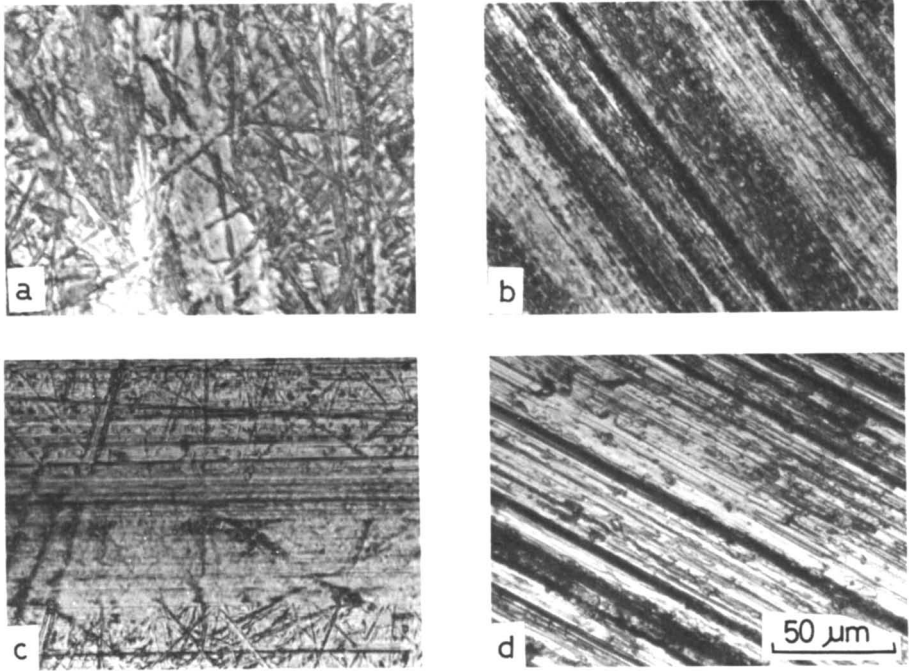


Figure 12. Optical micrographs of disk surfaces rubbed against PAI at various temperatures. (a) 23°C, (b) 100°C, (c) 150°C, (d) 200°C.



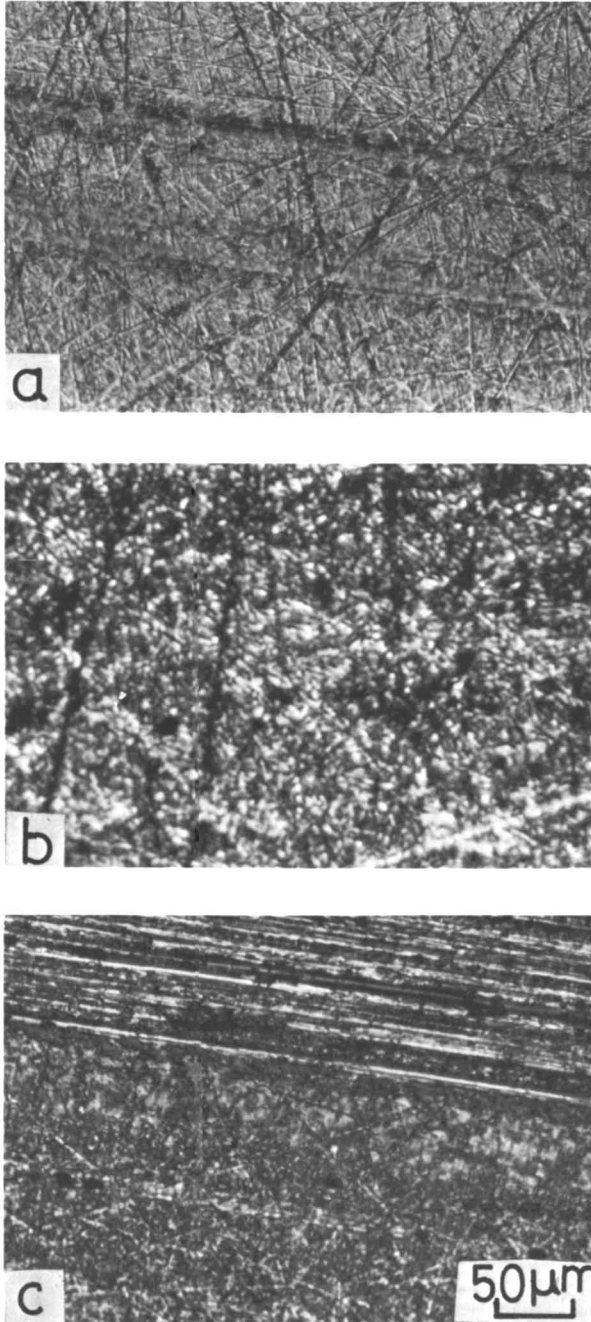


Figure 13. Optical micrographs of disk surfaces rubbed against PEEK at various temperatures. (a) 23°C, (b) 150°C, (c) 200°C.

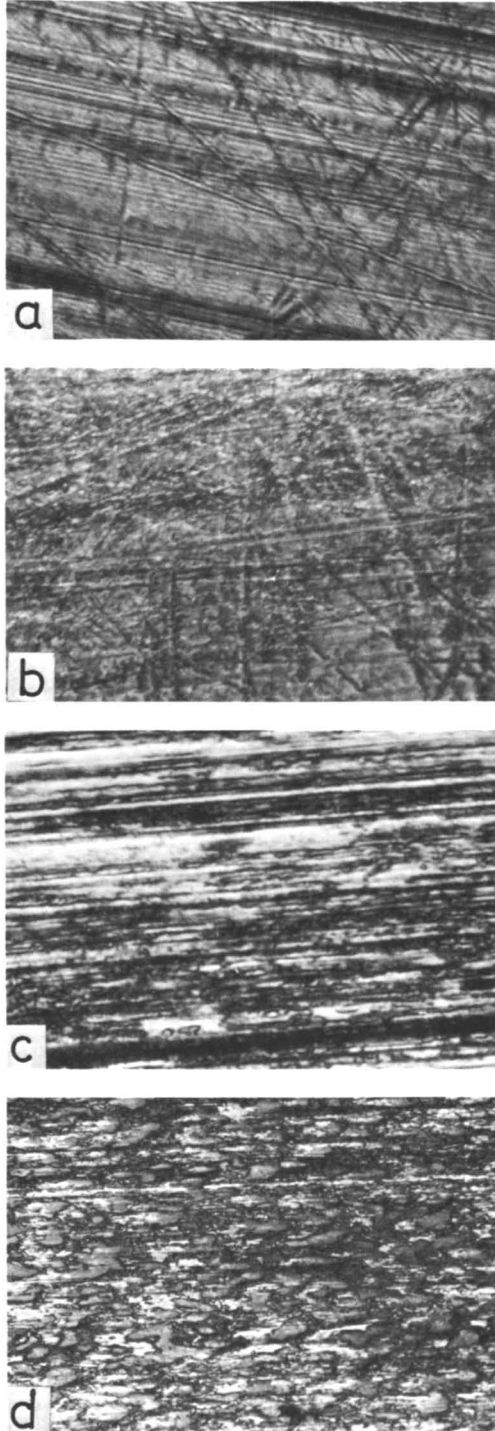


Figure 14. Optical micrographs of disk surfaces rubbed against PPS at various temperatures. (a) 23°C, (b) 50°C, (c) 100°C, (d) 200°C.

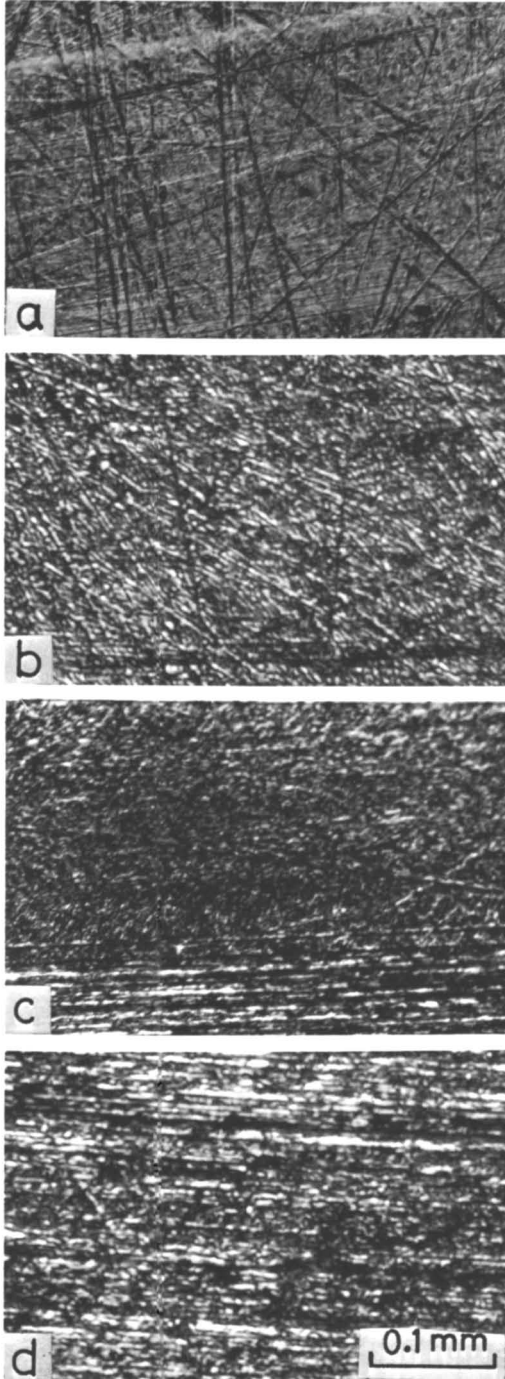


Figure 15. Optical micrographs of disk surfaces rubbed against PES at various temperatures. (a) 50°C, (b) 100°C, (c) 150°C, (d) 200°C.

approximately 0.35, 0.2 and 0.25 in the cases of PAI, PEEK and PES, respectively. For PI, the critical temperature is very low and the coefficient of initial friction is smaller by about 0.1 or less than that of steady-state friction.

The steady-state friction is generally much lower than the initial friction at temperatures above the critical temperature, although PES exhibits a steady-state friction similar to its initial friction at high temperatures. Therefore it is concluded that the transferred layer of polymer generally leads to a large decrease of friction of a similar polymer sliding against the layer at temperatures above the critical temperature. However, PES exhibits considerably high steady-state friction over a wide temperature range from 20°C to 200°C, and its steady-state friction is only slightly dependent upon the temperature. PI shows the peak of initial and steady-state friction at about 150°C and its steady-state friction is very low at temperatures above 250°C. Furthermore, the steady-state friction of PAI at temperatures above 200°C is as small as that of PI at 200°C and 300°C. In addition, PEEK exhibits relatively low steady-state friction over a wide temperature range from 20°C to 300°C.

A large increase in initial friction generally occurs suddenly when the temperature exceeds a certain transition temperature, which is dependent upon the type of polymer. This must be related to the thermal softening of polymers seen in Figure 3. However, the finding in this figure is not always applicable to the contact between the surface asperities of disk and polymer pin specimens because a steel sphere with a much larger radius than the disk surface asperities was used in the case of Figure 3. Thus, the transition temperature for Figure 16(b) is probably more sensitive to the thermal softening than the temperature dependence of the yield pressure as seen in Figure 3. Approximate transition temperatures are 70, 120, 170, 170 and 130°C for PI, PAI, PEEK, PPS and PES, respectively. According to Archard's multiple contact theory (5), it may be assumed that friction of a flat polymer surface sliding against a steel disk decreases with increasing countersurface roughness when the contact deformation is elastic. In addition, the contact deformation between polymer pin specimen and steel disk may be elastic or approximately elastic in this work. Therefore, Archard's theory may be applicable to the experimental results shown in Figure 16(b). The initial low friction at low temperature seems to be due to the surface roughness of the disk and friction increases with the amount of transferred material produced as the result of the increase of sliding distance, because the transfer apparently decreases the surface roughness of disk and the real area of contact increases. This seems to explain the fact that the initial friction is lower than the steady-state friction at low temperatures. On the other hand, the real area of contact corresponding to the initial friction increases with temperature, and this must become very large when the thermal softening of the polymer becomes very severe at temperatures above the transition temperature. The disk surface asperities penetrates the polymer surface more deeply at such high temperatures. Therefore, the increase of initial contact area and of penetration of disk surface asperities causes very high initial friction at temperatures above the transition temperature. However, the thickness of the transferred polymer layer increases with sliding distance and the sliding of the polymer begins to occur on the thick and softened transferred polymer layer at high temperatures, resulting in lower steady-state friction.

Wear of Polymer Pins Sliding Against Steel Disk. Figures 17 (a) and (b) show the variations of specific wear rates obtained in the steady states of wear for various polymers with disk temperature. PI and PAI exhibit wear peak at about 200 °C and 150 °C, respectively, with the peak of PAI being notably high. On the other hand, the wear rate **begins** to increase rapidly with temperature above a certain critical temperature in the cases of PEEK, PPS and PES. The higher the melting point, the higher the critical temperature. The low critical temperature of PES must be due to the fact that PES is an amorphous polymer whose glass temperature is much lower than the melting points of PES and PEEK. The wear rate is slightly dependent upon the temperature in the range below the critical temperature in the cases of PEEK, PPS and PES. PI generally shows a much lower wear rate than the other polymers. PAI shows a much higher wear rate than PPS and PEEK over a wide temperature range. It is also seen that the amorphous polymer PES exhibits a much higher wear rate than the crystalline polymers PEEK and PPS, while the low wear of PPS is probably due mainly to the glass fiber. In addition, the results shown in Figure 17 indicate that the specific wear rates at room temperature for the heat resistant polymers are generally higher than those for nylon and polyacetal.

For PPS and PES, the transient temperature at which the initial friction suddenly increases is very similar to the temperature at which the rapid increase of specific wear rate begins to occur. This suggests that the severe thermal softening of polymers causes a rapid increase of wear rate with temperature. However, such rapid increase of wear rate corresponding to the transient temperature of initial friction does not occur in the cases of PI, PAI and PEEK, and the thick transferred layer in these polymers seems to strongly suppress the increase of wear rate at high temperatures. Microscopic examinations of frictional surfaces indicate that the wear of heat resistant polymers is due mainly to the transfer of polymers. However, the rapid increase of wear rate at high temperatures for PES, PPS and PEEK may be due to an outflow of the severely softened polymers from the pin surface layers, as seen in the case of the thick molten polymer layer produced on the pins of some crystalline polymers rubbing against glass disk (6).

With PI and PAI, the color of wear debris varied with increasing temperature and became very dark at temperatures higher than a certain temperature near the wear peak. This suggests that the wear peaks of PI and PAI are due to thermal decomposition of the polymer molecules. Furthermore, it was observed that the wear peak of PI shifted to a lower temperature when rubbed at higher sliding speed, as shown in Figure 18. The frictional heat generated at sliding contact is greater at higher sliding speeds, and this increases the temperature at sliding contact. Therefore, the shift of wear peak with the sliding speed also suggests that the wear peak is due to a chemical reaction at high temperature in the cases of PI and PAI. For the syntheses of PI and PAI, we may assume the chemical reactions shown in Figure 19. When some unreacted portion shown in Figure 19 (a) remains after the synthesis, the imide bond formation may occur during sliding at high temperatures and water vapor may be generated at the frictional surface. Furthermore, the COOH group existing in

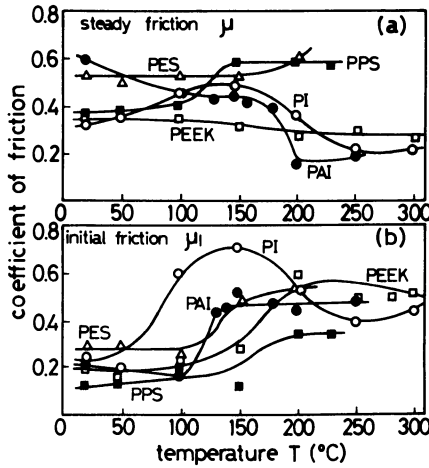


Figure 16. Variations in the coefficients of friction of various polymers with disk temperature. (a) Friction in the steady state, (b) Friction at the initial stage.

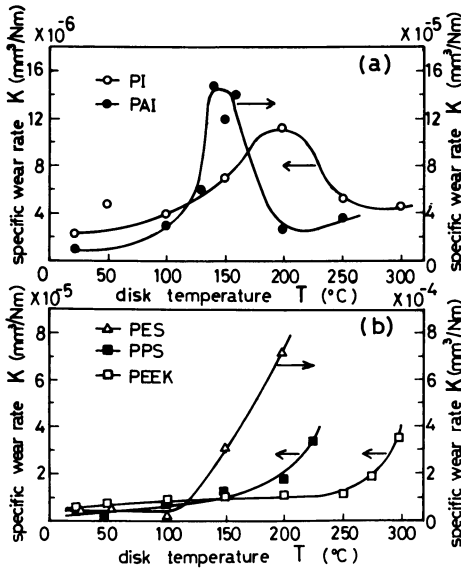


Figure 17. Variations of the specific wear rates with disk temperature in the steady states of wear of various polymers. The arrows show the scales of specific wear rate at left or right side.

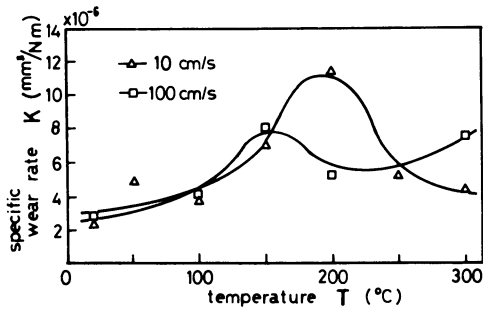


Figure 18. Variation of the wear peak of PI with sliding speed.

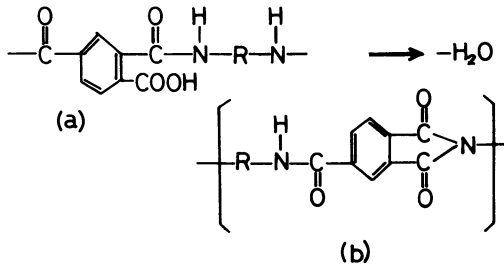


Figure 19. An assumed reaction of imide bond formation in the synthetic processes of PI and PAI

the unreacted part of the polymer chains may decompose easily upon high temperature sliding and generate CO<sub>2</sub> gas, and the main polymer chain may easily break. Generation of water vapor and CO<sub>2</sub> at the frictional surface probably acts to suppress the production of transferred polymer layer. Indeed, the transfer at a temperature corresponding to the wear peak was very small, as seen in Figures 10 (b) and 12(c) for PI and PAI, respectively. Therefore, the wear peaks seen in PI and PAI seem to be due to the unreacted portion of the polymer chains. The decrease of wear rate with increasing temperature in the range above the wear peak temperature may be due to the wear suppressive action of the thick transferred polymer layer at high temperatures.

### Conclusions

Temperature dependence of friction and wear of some heat resistant polymers was studied. Except the one filled with glass fibers of 40 wt. %, PPS, the specimen polymers were unfilled.

The main conclusions obtained from this investigation are as follows:

- (1) Friction of heat resistant polymers generally varies markedly with temperature.
- (2) PI, PAI and PEEK exhibit relatively low friction at temperatures above 200 °C in their wear processes. This is due to the thick transferred polymer layer produced during sliding. The friction of PES is generally high at any temperature.
- (3) PI exhibits friction peak at about 150 °C in its wear process.
- (4) PI and PAI exhibit wear peak at a certain temperature and the peak of PAI is very high. The wear peak seems to be due to the chemical reaction during sliding at high temperatures in the unreacted portion of the polymer chains.
- (5) PI exhibits lower wear rate than the other heat resistant polymers over a wide temperature range, while the wear rate of PAI is higher by a factor of about 10 compared with that of PI.
- (6) PEEK shows a low specific wear rate of 10<sup>-5</sup> mm<sup>3</sup>/Nm or less and relatively low friction in the temperature range from 20 °C to 250 °C.
- (7) The wear rates of PEEK, PPS and PES are slightly dependent upon the temperature up to certain critical temperature and begin to increase rapidly with temperature above the critical temperature, which is higher for polymers with high melting point or glass temperature.

### Acknowledgment

We wish to express our thanks to Mr. S. Ueda for his assistance.

### Literature Cited

1. Buckley, D. H. NASA TN., 1966, D-3261, 1.
2. Matsubara, K.; Watanabe, M.; Karasawa, M. Junkatsu 1969, 14, 43. (in Japanese)
3. Giltrow, J. P. Tribology 1973, 6, 253.



4. Tanaka, K. ; Uchiyama, Y. ; Toyooka, S. Wear 1973, 23, 153.
5. Archard, J. F. Proc. Roy. Soc., London, 1957, A243, 190.
6. Tanaka, K. ; Uchiyama, Y. In " Advances in Polymer Friction and Wear", vol.5B, Lee, L. H., Ed.; Plenum Pub. Corp., New York 1974 ; p. 499.

RECEIVED January 23, 1985

## Polysiloxane-Silica Hybrid Resins as Abrasion-Resistant Coatings for Plastic Substrates

H. L. Vincent, D. J. Kimball, and R. R. Boundy

Dow Corning Corporation, Midland, MI 48601

A coating prepared by the hydrolysis of an alkyltrialkoxysilane in the presence of an acidic silica sol exhibits a number of new and interesting features. It is soluble in an alcohol-water solution, can be readily applied to transparent plastic articles, and cured at temperatures below the  $T_g$  of the plastic to form a clear, hard, chemical and abrasion resistant coating. The cured film consists of small silica particles chemically bonded within a silicone resin matrix.

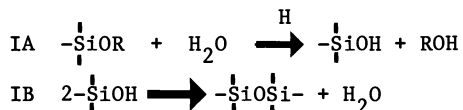
The use of transparent plastic materials in place of glass is becoming more widespread in applications such as transportation, (e.g., automotive sunroofs) glazing for trains, buses and aircraft, windows in public buildings, safety enclosures in high risk areas and eyeglass lenses. While polymers such as the acrylics and polycarbonates can be readily formed into the desired shapes, are more resistant to breakage than glass and weight less, their resistance to abrasion and chemical attack is relatively low. This lack of surface hardness and abrasion resistance has in the past severely restricted the use of these transparent polymeric materials.

Abrasion resistant coatings such as polysilicic acid fluorinated copolymer compositions (1) did find limited commercial use as abrasion resistant coatings. However, in 1976, H. A. Clark, (2,3) described a new type of coating that provided the combination of adequate shelf life, ease of application, low temperature cure and excellent resistance to abrasion and chemical attack. These novel coatings are based on the hydrolysis of alkyltrialkoxysilanes in the presence of an acidic colloidal silica. The term "colloidal silica" refers to stable dispersions or sols of discrete particles of amorphous silica. Both inorganic and organic coatings have been prepared using colloidal silica as a component of the coating (4). This new family of polysiloxane/silica resins is considered unique

because it forms an extremely hard, clear protective coating comprised of very small silica particles chemically bonded within a silicone resin matrix. This paper describes H. A. Clark's pioneering work on these abrasion resistant coatings. It also contains additional information on film formation, cured film properties and concludes that the exceptional performance is due to a tightly crosslinked structure in which the colloidal silica particles act as a part of the crosslinking system.

### SYNTHESIS

Small samples of these hybrid resins can be prepared by simply mixing the alkoxy silane and aqueous silica sol using the water present in the sols as the hydrolysis medium. We have found that maintaining the pH on the acid side results in an adequate hydrolysis rate (IA) without an accompanying acceleration of silanol condensation (IB) that could result in the formation of highly crosslinked resin and gel particles.



While many acids can be used, (5), acetic acid has been found to be very effective at promoting the hydrolysis reaction while minimizing the silanol self-condensation reaction and thus producing more of the desirable silanol endblocked monoalkylpolysiloxane resin.

Synthesis Example. Methyltrimethoxysilane (50.0 grams) was acidified with glacial acetic acid (1.0 gram). An aqueous dispersion of a commercial colloidal silica (66.7 grams) having a pH of 9.8 and containing 50% weight silica of 13-14 millimicrons particle size was added to the acidified silane to form a methanol-water dispersion of silica and monomethylpolysiloxane particle condensate. The silica to methylpolysiloxane ratio was 60/40 (weight). After diluting to 22.5 weight % with isopropanol, the pH was adjusted to 5.35 with acetic acid.

### CATALYSIS

Control of the spontaneous condensation of the silanols formed during and after the hydrolysis reaction is very important. If too many silanols condense during hydrolysis, the shelf life will be very short and gel formation will readily occur. Therefore, the hydrolysis of the alkoxy silane is carried out under mild conditions and the resulting partial condensate is diluted with water soluble solvents to a lower solids level. The resin is cured by further silanol condensation which can occur with heat alone. This, however, is a relatively slow process that requires cure temperatures above the glass transition temperature ( $T_g$ ) of the plastic substrate. While many catalysts can be used, including acids,

bases, and organic compounds of metals, it has been found that small amounts of the salts of weak organic acids and strong bases provide the desired balance of shelf life and cure rate. Such catalysts include sodium acetate, potassium acetate, and the acetate salts of quaternary ammonium compounds.

### COATING

The substrate must be clean and free from particulate matter. Adhesion to acrylic plastics is normally excellent. We have found that the combination of isopropanol and acetic acid will gently attack and swell a polymethylmethacrylate (PMMA) surface and is more aggressive as the molecular weight of the PMMA is decreased. Excellent adhesion to polycarbonate can be obtained by heating the polycarbonate for two hours at 125°C before the coating is applied.

The plastic articles can be coated using conventional dip, flow or spray techniques. However, in order to achieve optimum film formation and performance, controls on the temperature, relative humidity and cleanliness of the environment during solvent removal are necessary. The coatings contain fast evaporating solvents such as methanol, isopropanol and n-butanol and the solvent mixture can further contain 10-15 weight percent water. The solvent removal must be sufficiently slow enough, especially at greater than 50% relative humidity so that the coating surface is not cooled below the dew point of the surrounding atmosphere. This would result in the formation of water droplets known as lacquer blush. High air speeds across the surface of the article can also induce this film blushing. Benard cells (6) can also be formed by a vortex flow being created by the fast evaporating solvent in the wet film. Humidity changes can drastically alter evaporation rates and the solvent balance of water/solvent mixtures. High humidity prolongs drying time by slowing down the rate of water evaporation from the solvent blend (7). Film formation at about 25°C and less than 50% relative humidity eliminates these kinds of film defects.

### CURE CONDITIONS

It is necessary to thermally cure the coated plastic in order to achieve full crosslinking of the air dried film. The degree of crosslinking affects not only the abrasion resistance of coating, but also the adhesion and the long term performance under environmental conditions. The temperature and time of cure is also dictated by the thermal stability and properties of the plastic substrate. The following table lists recommended cures for various plastics.

TABLE I - RECOMMENDED CURE PROFILE

<u>PLASTIC</u>	<u>TEMPERATURE</u>	<u>TIME (hours)</u>
polycarbonate	125°C	4
acrylics	75-95°C	4-8

SURFACE PROPERTIES OF COATED PLASTICS

Transparent plastic glazing is often subjected to wiping and cleaning and the maintenance of optical quality is important. One of the best known methods of measuring such abrasion or wear by a Taber abraser and to evaluate the degree of wear by determining the percentage of light that is diffused by the abraded specimen (8), (9). The results of comparing coated and uncoated acrylic and polycarbonate to plate glass using this test are shown in Table II. The resistance of glazing materials to common chemicals, solvents and cleaning agents is also important. A twenty-four hour spot test in which 1 ml of the reagent was placed upon the surface of the coated plastic and covered with a watch glass was used to measure chemical resistance. After the exposure period, the spot was wiped clean and examined immediately for signs of degradation. The chemicals listed in Table III had no effect upon the surface of the cured polysiloxane/silica coating.

TABLE II

## ABRASION RESISTANCE

<u>SUBSTRATE</u>	<u>DELTA % HAZE</u>
Plate Glass	0.5%
Uncoated Acrylic	20%
Coated Acrylic	2.5%
Uncoated Polycarbonate	40%
Coated Polycarbonate	1.7%

Test Method: Taber Abraser, 500 cycles, 500 gram load, CS-10F wheels

TABLE III

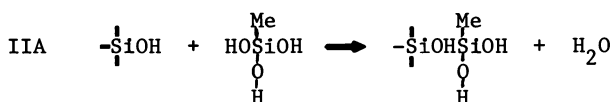
## CHEMICAL RESISTANCE

The following chemicals had no effect upon the surface of coated acrylic or polycarbonate plastics when tested for 24 hours, ASTM D1308, spot test, covered.

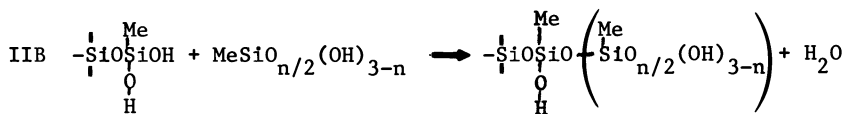
Windex Glass Cleaner	Ammonia (A&P sudsy brand)
Formula 409 Household Cleaner	Kerosene
Gasoline-Regular Grade	Methanol
SAE-30 Motor Oil	Toluene
VM&P Naphtha	Lighter fluid - Ronsonal
Isopropanol	Sodium hydroxide 10%
Butyl Ether of Ethylene Glycol	Sulfuric acid - 90%

DISCUSSION

Unlike conventional silicone resins, the monomethylpolysiloxane silica hybrid resins exhibit excellent resistance to abrasion and chemical attack. It is fairly well established that silane coupling agents form metal-oxygen-silicon bonds with metal surfaces (11). The silanol groups on the freshly hydrolyzed methyltrimethoxysilane are essentially the same as the silanols on neutral silane coupling agents. Therefore the surface of the silica sol particles can react with the monomethylsilane triol (IIA).



As the resin film undergoes cure, these monomethyl reactive sites on the silica surface can crosslink with the polysiloxanes contained in the surrounding media (IIB).



Microphotographs show that the silica particles are not agglomerated as they pass from the initial aqueous sol through the hydrolysis with methyltrimethoxy silane to the cured film stage. Torsional braid analysis studies of cured 50/50 weight %  $\text{MeSiO}_{3/2}/\text{SiO}_2$  resin films show very little loss of modulus up to  $300^\circ\text{C}$  (12). The modulus of conventional silicone resins would be reduced by 50-70% over this temperature span. The abrasion resistance is increased as the silica level is increased (Table IV).

TABLE IV

<u>SAMPLE NO.</u>	<u>SUBSTRATE</u>	$\text{MeSiO}_{3/2}:\text{SiO}_2$	<u>DELTA % HAZE</u>
1	PMMA	100/0	4.2
2	PMMA	90/10	3.0
3	PMMA	80/20	1.4
4	PMMA	70/30	0.6
5	PMMA	60/40	1.5
6	PMMA	50/50	0.6

The observations, coupled with the cured films excellent solvent resistance, indicates a tightly crosslinked structure free from the plasticizing effects of low molecular weight polysiloxanes and in which the colloidal silica particles act as part of the crosslinking system.

#### Acknowledgments

We would like to thank Harold A. Clark for his pioneering effort on this new class of silicone resins, for his continual optimism and the ideas received after his retirement.

#### Literature Cited

1. Engelhardt, E. H.; U.S. Patent 3,390,203 (1968).
2. Clark, H. A.; U.S. Patent 3,986,997 (1976).
3. Clark, H. A.; U.S. Patent 4,027,073, (1977).
4. Iler, R. K.; "The Chemistry of Silica", Wiley-Interscience, 312 (1979).
5. Noll, W.; "Chemistry and Technology of Silicones", Academic Press (1968).
6. Patton, T. C.; Paint Flow and Pigment Dispersion, Wiley Interscience, 593, (1979).
7. Rocklin, A. L.; Journal of Coatings Technology, 50, No. 646, 46, (1978).
8. ASTM D1044, Resistance of Transparent Plastic Materials to Abrasion.
9. Haluska, L. A.; Wear Testing of Abrasion - Resistant Coated Plastics, Special Technical Publication 769, American Society for Testing and Material, (1982).
10. ASTM D1308, Effect of Household Chemicals on Clear and Pigmented Organic Finishes.
11. Plueddemann, E. P.; "Silane Coupling Agents", Plenum Press, 114, 120, (1982).
12. Baney, R.; Unpublished data.

RECEIVED January 23, 1985

## Effect of Chemical Structure on the Friction and Wear of Polyimide Thin Films

J. W. Jones<sup>1</sup> and N. S. Eiss, Jr.<sup>2</sup>

<sup>1</sup>Harris Corporation, Melbourne, FL 32901

<sup>2</sup>Department of Mechanical Engineering, Virginia Polytechnic Institute and State University, Blacksburg, VA 24061

The friction and wear behavior of three thin polyimide films of known chemical structure was tested. An attempt was made to correlate differences in chemical structure, primarily the presence of flexible linkages and highly polar side groups, to differences in tribological properties. The wear test results showed lowest wear for the polyimide with the flexible oxygen linkage. The wear mechanism was deduced to be fatigue since wear did not occur immediately and a positive correlation was noted between wear rate and elastic modulus. The friction results showed highest friction for the polyimide with the highest density of polar side groups.

Polyimides are long chain molecules which have recurring imide groups as an integral part of their main chain. High thermal stability is especially characteristic of aromatic polyimides, which are derived from aromatic diamines.

The major portion of research on the friction and wear of polyimides has been done by R. L. Fusaro. In tests performed on polyimide thin films, (25 $\mu$ m thick), using a pin-on-disk apparatus, Fusaro found that polyimides fall into two groups according to friction and wear properties. Group I polyimides, generally have lower friction and higher wear than group II polyimides. The wear of both groups, according to Fusaro, occurs by an adhesive wear mechanism, with larger wear particles being formed by group I polyimides (1). Fusaro's results suggested that a linear non-crosslinked polyimide will have a higher wear rate than a polyimide characterized by some crosslinking. Other tribological information suggested by Fusaro is that the polyimide thin films undergo linear wear rates, and have an order of magnitude longer wear lives in inert atmospheres (2). Fusaro has also noted that polyimides undergo a transition from high friction, high wear to low friction, low wear as the temperature is increased above about 40°C. No correlation between this transition and a molecular relaxation was



found (3,4). However, in the discussion of (4) Ludema noted that this lack of correlation between friction transition and molecular relaxations may be due to the different strain rates in the tests.

Fusaro compared the tribological properties at 25°C of seven polyimide films bonded to type 301 stainless steel. Brittle fracture and spalling occurred in all films in less than 1000 cycles of sliding. Of the seven polyimides tested in this study, Fusaro provided chemical structures for two of them, PIC-6 and PIC-7. PIC-6 had oxygen groups linking some of its aromatic rings while PIC-7 had a high density of carbonyl groups. The PIC-7 polyimide underwent much worse spalling and wore away much quicker than the PIC-6 polyimide. This could be predicted from the chemical structures since the PIC-6 backbone contains the flexible oxygen carbon links and consequently should have lower elastic modulus than the more rigid PIC-7 structure (5).

In much of the previous research on the tribological properties of polyimides, the chemical structure was proprietary. Consequently, generalizations about structure-property relationships have been hindered. In this research friction and wear testing on three polyimides of known chemical structure is presented. The relative tribological performance of each polyimide is related to its chemical structure.

#### EXPERIMENTAL PROGRAM

Polyamic acids were polymerized from dianhydride and diamines which differed by only a linking group. The polyamic acids were dissolved in N,N-dimethylacetamide (DMAC) at a concentration of 15 per cent weight of acid per volume of solvent. The solutions were spread onto AISI 410 stainless steel substrates, 1.26 $\mu$ m R<sub>a</sub> roughness, and allowed to air dry for 24 hours. The films were cured by heating successively at 70°C, 140°C, and 200°C for one hour each to produce films with a thickness of approximately 50 $\mu$ m. The structures of the resulting polyimides which were arbitrarily named PIA, PIB, and PIC are shown in Fig. 1.

The mechanical properties of the polyimide film were measured in tension tests. To do this polyimide films were cast and cured on glass substrates. The films were removed and tensile test specimens were stamped from the films using a die. The specimens were then pulled to fracture at a cross-head speed of 10 mm/min. The mechanical properties obtained from the load-elongation curves are given in Table I.

All friction and wear testing was performed using a pin-on-disk machine (6). A 3.175 mm diameter AISI 52100 steel ball was loaded, using a pneumatic device, against the polyimide film which was rotated at a rate to give a sliding velocity of 0.628 m/s. The ball was commercially lapped to a surface roughness of 0.01  $\mu$ m R<sub>a</sub>. In all tests, the ambient temperature was 22°C and the relative humidity was 40 per cent.

Friction forces caused a deflection, measured by a proximity transducer, of a cantilever beam to which the ball was attached. The friction force was measured continuously throughout the experiment. The wear of the polyimide film was measured by stopping

Table I Film Mechanical Properties

95 per cent confidence range is given in parenthesis

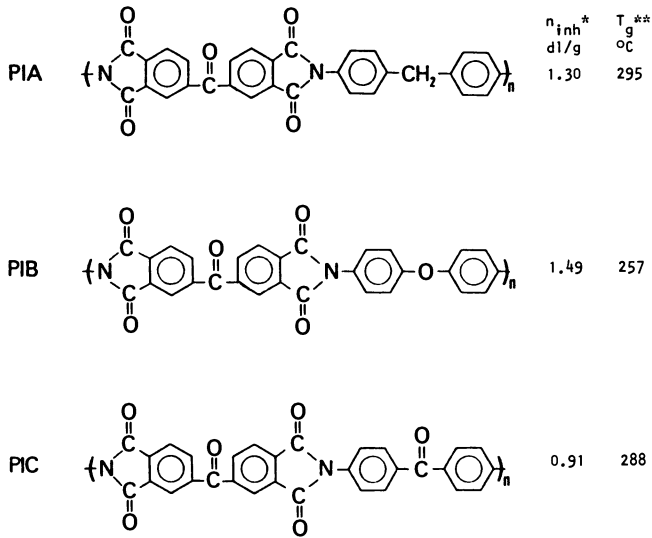
	Ultimate Tensile Strength (MPa)	Elongation to Break (per cent)	Energy to Rupture Parameter (MPa)	Modulus of Elasticity (GPa)
PIA	113.4 (97.3-129.5)	9.2 (6.8-11.5)	10.425 (7.542-13.309)	1.194 (.986-1.401)
PIB	86.0 (80.4-91.5)	8.7 (6.9-10.4)	7.492 (5.684-9.299)	.974 (.902-1.046)
PIC	102.9 (87.7-118.0)	6.5 (5.3-7.7)	6.843 (4.548-9.138)	1.239 (1.079-1.399)

the tests at intervals of 2000 cycles and taking four surface profiles of the track cross section using a stylus profile meter. The wear was quantified by taking the average of four cross-sectional areas. The wear rates were obtained by using a linear regression on the average cross section area versus number of cycles. The wear values at 2000 cycles were not used in the regression because they did not represent steady state conditions. Preliminary tests were run at normal loads from 2 to 10 N. As a result of these tests a normal load of 5 N was selected to measure the wear rates. Friction data were obtained at both 5 and 10 N normal load. During the preliminary tests scanning electron micrographs were taken of wear tracks formed after 50 kc of sliding with a normal load of 3 N.

### RESULTS

The friction and wear tests were characterized by an initial period during which the friction coefficient was less than 0.1 and no wear was observed. This initial period terminated with an abrupt rise in the friction coefficient for PIA and PIC (Figure 2) followed by a gradual increase over the duration of the test (Figure 3). PIB underwent a more gradual friction transition than PIA and PIC. The friction coefficients at 2 kc and 16 kc are listed in Table II.

The initiation of the wear track occurred simultaneously with the abrupt rise in the friction. The wear rate decreased from its initial value to a steady state value in less than 4 kc after initiation (see Figure 4). The steady state wear rates, expressed in square micrometers of track cross section area per kilocycle of sliding, are given in Table III.



\* Inherent viscosity in deciliters per gram of polyamic at 25°C.

\*\* Glass transition temperature of polyimide film dried through 200°C for one hour, thermal mechanical analysis at heating rate of 5°C/min.

Figure 1. Chemical Structure and Properties of Polyimides

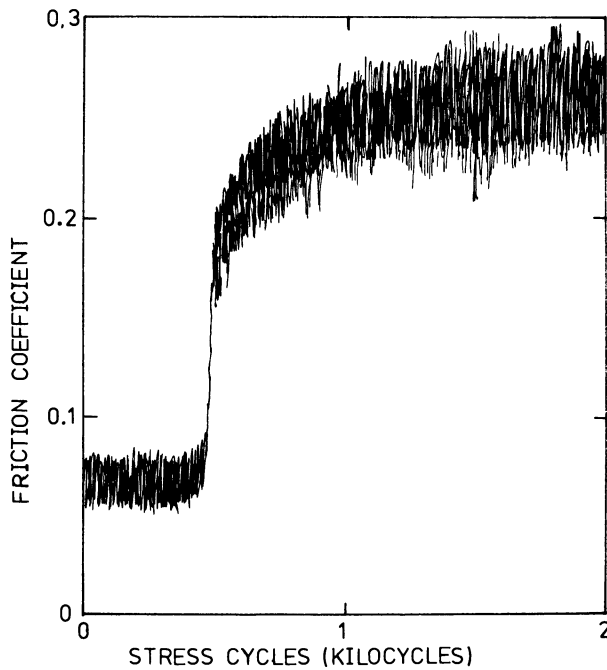


Figure 2. Friction Coefficient During Wear Track Initiation

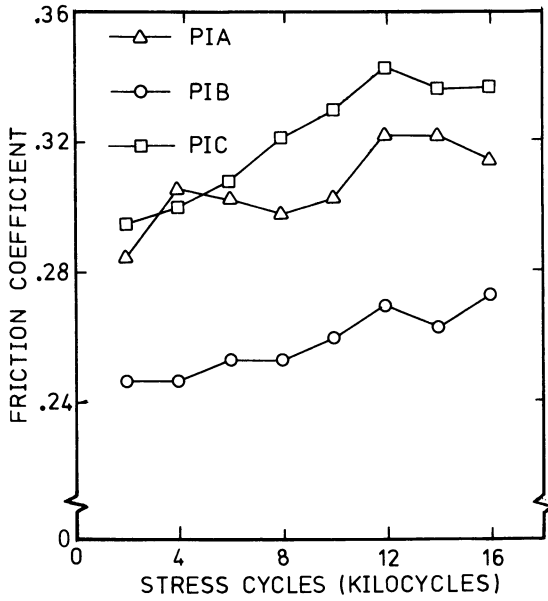


Figure 3. Effect of Structure on Friction Coefficient

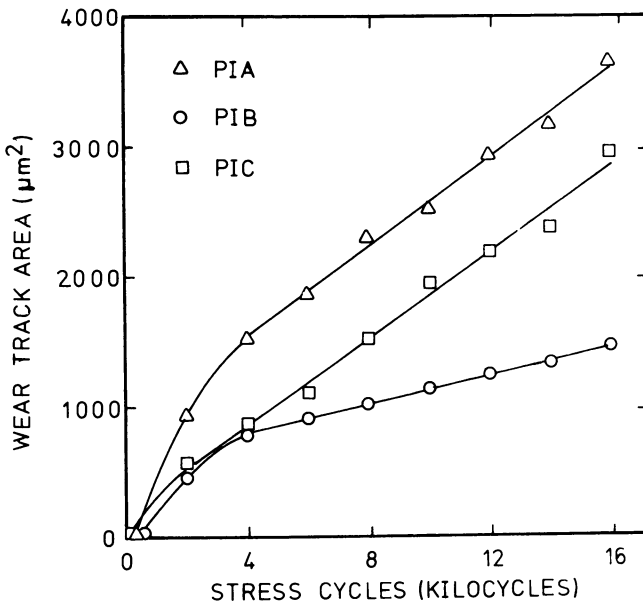


Figure 4. Effect of Structure of Polyimides on Wear, 5 N Load, 0.63 m/s sliding speed

Table II Effect of Structure on Friction Coefficient

5 N Normal Load				
	$\mu_{2000}$	95% Confidence Range	$\mu_{16000}$	95% Confidence Range
PIA	0.26	0.24-0.29	0.32	0.30-0.33
PIB	0.23	0.21-0.26	0.27	0.26-0.29
PIC	0.29	0.28-0.31	0.34	0.31-0.36

10 N Normal Load		
	$\mu_{2000}$	95% Confidence Range
PIA	0.19	0.17-0.21
PIB	0.23	0.19-0.26
PIC	0.27	0.26-0.28

The number of cycles required to initiate a wear track was affected both by the polyimide type and the normal load as shown in Table III. The 95 per cent level confidence range was a measure of the large variability in the initiation periods; the only statistically significant differences were that PIC initiated sooner than PIB at 5 N load and that PIA at 5 N load initiated earlier than at the 10 N load.

Table III Wear Rates and Incubation Periods

Polyimide	Load 5 N		Load 10 N
	Wear Rate ( $\mu\text{m}^2/\text{kc}$ )	Incubation period (cycles)	Incubation period (cycles)
PIA	171 (159-183)	269 (90-448)	1060 (490-1630)
PIB	56 (54-58)	557 (355-759)	442 (221-662)
PIC	168 (150-186)	115 (6-224)	-- --

95 per cent confidence range is given in parenthesis.

Scanning electron micrographs were made of the wear tracks to illustrate possible differences in the nature of the wear among the polyimides. The polyimide films which were examined were run for 50 kc at a sliding speed of 0.63 meters per second under a load of 3 N. The wear track of PIC, Figure 5, shows grooves formed by

plastic deformation and by tearing. Platelet particles are either wear particles embedded in the wear track by the sliding action or incipient wear particles similar to those predicted by the delamination theory of wear. Evidence of tearing wear was not detected in the wear tracks of PIA and PIB (Figures 6 and 7). Both PIA and PIB exhibited finer wear debris than PIC.

## DISCUSSION

Polyimide Wear. A unique feature of the results was the initial period during which no measurable wear occurred. This feature occurred because the contact stresses were below the magnitude required to generate wear particles when sliding commenced. Hence, multiple stress cycles were required to cause wear particles to form: This phenomenon is called fatigue wear.

Another explanation for the initial period of no wear is that the polyimide and ball surfaces were contaminated by a film. This film caused low friction and surface stresses below that required for immediate wear particle generation. The initial period is the time during which the film is worn away resulting in an increase in adhesion, increase in surface stress, and subsequent wear particle formation. Obviously, both fatigue and contaminant film removal could be operative during the initiation period. Experiments with carefully controlled environments and surface cleaning procedures would be necessary to discriminate between these two explanations.

After the wear particles were generated and a groove was worn in the polyimide, a period of steady state wear occurred. The steady state wear rates did not correlate with the energy to rupture and correlated positively with the ultimate tensile strengths and the elastic moduli of the polyimides (see Tables I and II). The lack of correlation with the rupture energy suggests that the predominant wear mechanism is not abrasive wear because a positive correlation has been found between wear rate and the inverse of the rupture energy for abrasive wear (7). Because the fracture energy was not measured, it is not known how this property would correlate with the wear rates.

Adhesive wear is caused by the adhesive bonds at the interface being strong enough to cause cohesion failure in the polyimide and transfer to the steel ball. Thus, the lower strength polyimides should fail more readily and have higher wear rates. However, in these tests, the higher strength polyimides had higher wear rates. Hence, the adhesive wear is not the predominant mechanism.

The positive correlation of wear rates with elastic moduli  $E$  of the polyimides is consistent with the fatigue model for wear (8). The reason for this correlation is that the surface stresses which are calculated using the Hertzian contact equations are proportional to  $E^{2/3}$ . Higher stresses lead to high wear rates because less stress cycles are required to cause a fatigue failure and produce a wear particle.

The experimental results suggest that, for these polyimides, the most flexible system had the lowest wear rate. Of the three polyimides tested, PIB should have the most flexible chain, as indicated by the glass transition temperature, because of the presence of the oxygen linking group. Chain rigidity is approximated

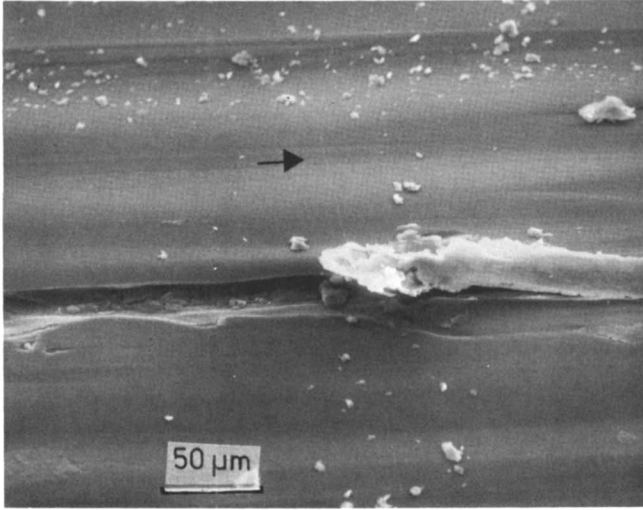


Figure 5. PIC Wear Track, 50000 cycles at 0.63 m/s, 3 N Load

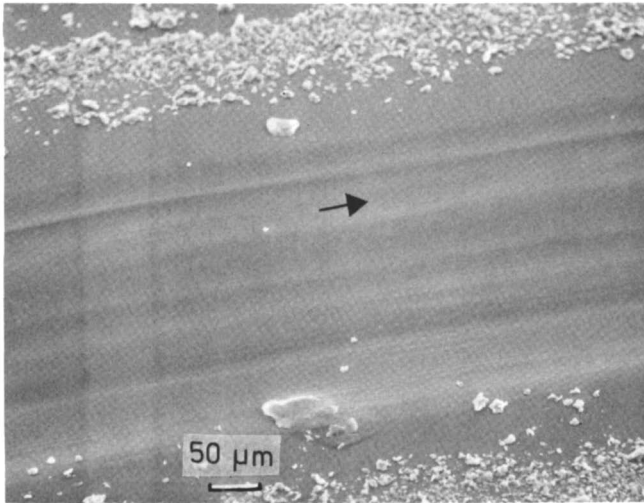


Figure 6. PIA Wear Track, 50000 cycles at 0.63 m/s, 3 N Load

by the glass transition temperature since chains with less internal mobility inhibit the glass transition by storing thermal energy through steric hindrance (9). The oxygen linking group allows a great deal of chain movement and can have a marked effect on the bulk rigidity of a polyimide. For example a certain aromatic polyimide which contains the linking group A shown in Figure 8 has an elongation to failure of 2 per cent, while the same polyimide with the more flexible linking group B has an elongation to failure of 80 per cent. The same polyimide with the even more flexible group C has a elongation to failure of 120 per cent (10). Correspondingly, PIB, the polyimide polymerized from the diamine with the flexible oxygen linkage, had the lowest wear rate.

Of the two remaining polyimides, PIC would have the less flexible chains due to its greater density of double bonds and highly polar carbonyl groups. The chain is stabilized by a double bond because the pi orbital bond restricts the movement of neighboring atoms and hence increases chain rigidity. A high density of polar groups increases chain rigidity due to the repulsion of like charges. Despite this, the glass transition temperature of PIA is slightly higher than that of PIC. This is probably due to PIA's higher molecular weight and correspondingly longer average chain length as indicated by the significantly larger inherent viscosity. If one accepts glass transition temperature as a measure of chain rigidity, then there is a good correlation between chain rigidity and wear rate.

In addition to their effect on chain flexibility, highly polar side groups may have a direct effect on wear rate. In crystalline and semi-crystalline systems, the presence of highly polar side groups would tend to lower wear by inducing a higher degree of crystallinity, thereby inhibiting crack propagation. In crystalline polymers, crack propagation involves the breaking of primary bonds because the polymer chains cannot reorient to allow slippage (11). For predominantly amorphous systems, the increased tendency toward some degree of crystallinity has much less effect on crack propagation, since cracks may easily propagate through the amorphous regions. Therefore, for the primarily amorphous polyimides tested, the wear inhibiting effects of polarity-induced crystallinity are greatly diminished since wear properties are dominated by the amorphous regions.

Highly polar side groups could conceivably lead to increased interaction and adhesion to the contacting metal or transferred film. Increased adhesion would lead to higher tractive stresses and correspondingly higher wear rates. The S.E.M. photographs support this hypothesis since PIC, with the highly polar carbonyl group, was the only polyimide to exhibit signs of tearing.

The effect of the structure on chain regularity may also play some role in determining wear. Of the three polyimides, PIC would have the most regular chain because the PIC diamines, containing carbonyl linkages, are more similar to the common dianhydride than the PIA and PIB diamines are. A structural unit that would tend to increase regularity would tend to produce a less elastic, more rigid polymer (12). It is hypothesized that, for fatigue wear, this change in properties would lead to a higher wear rate. However, like the polarity effect, increased regularity is believed to



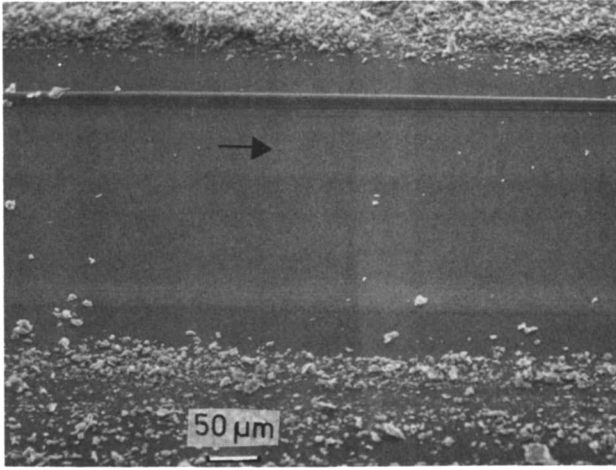


Figure 7. PIB Wear Track, 50000 cycles at 0.63 m/s, 3 N Load

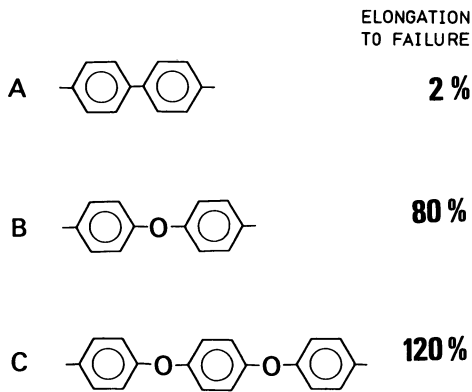


Figure 8. Effect of Flexible Oxygen Linkage on Rigidity

play a much smaller role in determining wear for amorphous polymers relative to crystalline polymers.

Though not directly related to structure, the chain length, as approximated by molecular weight, may have affected the wear rates of the polyimides. Longer polymer chains in high molecular weight materials lead to higher mechanical properties and tend to decrease wear since they more likely require primary bond breakage for crack propagation (11). Possibly molecular weight did play a significant role in determining wear performance as suggested by the decreased wear rate for PIB, the polyimide with the highest molecular weight. However, molecular weight was obviously not the dominant factor as evidenced by the similar wear performance of PIA and PIC despite the relatively large difference in their molecular weights.

Fusaro tested two condensation type polyimides whose tribological performance may have been affected by some of the previously mentioned factors. Fusaro's PIC-7, analogous to PIC, had a high density of highly polar carbonyl groups, while his PIC-6 had a number of oxygen linkages making it analogous to PIB. In tests conducted at 25°C, Fusaro observed a wear rate for PIC-7 three times higher than that of PIC-6 (4).

Polyimide friction. The friction of polymers consists of an adhesion component and a deformation component. The adhesion component arises from the shearing of adhered junctions and is usually modeled as the product of the real area of contact and the shear strength of the polymer. The deformation component arises from the frictional work required to balance the energy dissipated in plastic deformation. Some investigators have developed friction models in which the adhesive bonds at the junctions increase the amount of plastic deformation over that which would exist in the absence of these bonds (13).

In these experiments two factors could contribute to the increase in friction observed when the wear track initiated 1) an increase in real area of contact, and 2) an increase in ploughing by polyimide wear particles. When the wear track initiated the geometry of the contact changed from a sphere-on-flat to a sphere-on-concave cylinder. The Hertzian contact equations were used to calculate an increase of real area of contact of 15 to 30 per cent for the ball in the wear groove. This increase in area could account for a portion of the friction increase either by increasing the area sheared during sliding or by increasing deformation losses. However, this increase is insufficient to account for the 300 to 400 per cent increase in friction when the track formed.

The scanning electron micrographs and profiles of the wear track indicated that grooves were formed in some of the wear tracks. The tracks which were grooved also had higher coefficients of friction than smooth tracks. The grooves are most likely formed by polyimide wear particles trapped between the sphere and the wear track; the wear particles ploughed grooves in the wear track thus increasing the friction forces. This ploughing action is assumed to be the major cause of the increase in friction.

There was an interaction between the polymer structure and the normal load and their effect on the friction coefficient as shown in Table II. At a load of 5 N the friction coefficient of PIB was

significantly less than that of PIC but no significant difference could be found between either PIB and PIA or PIA and PIC. At the 10 N load, the friction coefficient of PIC was significantly greater than that of PIA and PIB while there was no significant difference between PIA and PIB. Polarity may explain the higher friction for PIC. Belyi (14) found that extremely high friction resulted when rubbing highly polar polymers such as polymethylmethacrylate and polycapromide. He attributed the high friction directly to the polar nature of the polymers. As noted above, PIC, with the highly polar carbonyl group, is the most polar of the three polyimides and was the only polyimide to show signs of severe tearing in the wear tracks.

### CONCLUSIONS

The wear results were characterized by an initial period of no wear followed by catastrophic initiation of the wear track. This initiation was distinguished by a sharp increase in friction coefficient and a wear rate which was higher than the subsequent steady state wear. Fatigue wear is proposed as the predominant wear mechanism because of the multiple stress cycles required to initiate wear and because of the positive correlation between the wear rates and the elastic moduli of the polyimides.

A correlation between chain flexibility and wear rate was noted. The more flexible the chain, as approximated by the glass transition temperature, the lower the wear rate. S.E.M. photographs and pitted wear tracks suggested that the presence of highly polar side groups led to higher wear for PIC. Molecular weight, or chain length, was not a dominant wear determining factor. The importance of the deformation component of friction is suggested by the correlation of wear track roughness to high friction. Increased wear track roughness and increased polyimide polarity contributed to PIC having the highest coefficient of friction.

### Acknowledgments

This research was supported by a grant from the U.S. Army Research Office, Research Triangle Park, North Carolina under the mentorship of E. Saibel.

### Literature Cited

1. Fusaro, R. L., ASLE Trans., 1982, 25, 465-477.
2. Fusaro, R. L., NASA-TN-D-6914, 1972.
3. Fusaro, R. L., NASA-TN-D-7954, 1975.
4. Fusaro, R. L., Trans. ASLE, 1977, 20, 1-14.
5. Fusaro, R. L., NASA-TM-81413, 1980.
6. Eiss, N. S., Jr.; Milloy, S. C. In Wear of Materials 1983, Ludema, K. C., Ed. ASME, New York, NY, 1983, pp. 650-656.
7. Warren, J. H.; Eiss, N. S., Jr., Jl. Lub. Tech., 1978, 100, 92-97.
8. Eiss, N. S., Jr.; Potter, J. R., III, this volume.
9. Rosen, S. L., Fundamental Principles of Polymeric Materials, John Wiley & Sons, New York, 1982.

10. Koton, M. M., RAE-LIB-TRANS-1499, N71-19631, Oct. 1970.
11. Sauer, J. A.; Foden, E.; Morrow, D. R., Pol. Eng. Sci., 1977, 17, 246.
12. Prokopchuk, N. R.; Baklagina, Y; Korzhavin, L; Sidorovich, A; Koton, M., Pol. Eng. Sci. USSR, 1977, 19, 1297-1304.
14. Johnson, K. L., In Friction and Traction, Dowson, D., Taylor, C. M.; Godet, M; Berthe, D., Ed., Westbury House, Guildford, England, 1981, pp. 3-12.
15. Belyi, V.; Savkin, V; Sviridyonok, A., In Advances in Polymer Friction and Wear, Lee, L. H., Ed., Plenum Press, New York, 1974, pp. 759-764.

### DISCUSSION

Question: Anderson, T. G., Amoco Chemicals Corp., Naperville, Ill.

Were the polyimide films checked for inherent viscosity (molecular weight) changes after annealing? Our experience is that this type of polymer is sensitive to heat history.

Answer: No

Question: Bahadur, S., Iowa State University, Ames, Iowa

1. In your presentations you have been considering the gross area of contact. Are you implying that fatigue occurs due to the reversal of stresses in this gross contact region? Should the reversal of stress not be considered for fatigue in the microasperity contact regions.

2. Since you are considering fatigue, should you not consider in the interpretation of your wear data the effect of coefficient of friction with the normal load?

Answer:

1. The geometry of a sphere on a flat with normal and tangential loads generates a stress distribution in the polymer which is maximum on the centerline of the wear track. An element of polymer in the center of the track experiences alternating compressive and tensile stresses each time the slider passes. Consequently, wear particles will be formed from the center of the tracks first. As material is removed from the track center, the other portions of the track must support the load so that the maximum stress now shifts to other elements in the polymer wear track. Thus, wear particles are produced from microasperity sized regions and would have dimensions much smaller than the gross contact area.

2. The effect of friction must be considered in determining the variable stress which any element of polymer experiences because it is the friction force which gives rise to a tensile stress on the surface. The tensile stress is necessary to propagate cracks which, eventually lead to polymer wear particle formation.

Question: Schmidt, M., Brewer Science Inc., Rolla, MO

Does placement of the hinge in the polyimide structure affect wear resistance?

**Answer:**

This has not been studied.

**Question:** Briscoe, B., Imperial College, London, England

1. Do you consider that your trends in friction may be due to topographical changes?
2. Are the temperature rises significant during your test and could they be important?

**Answer:**

1. When the wear track forms, there are grooves within the wear tracks which are caused by ploughing of the wear track by wear debris trapped by the slider. The increase in deformation during ploughing results in the increase in friction. In this sense the friction is related to the change in topography.

2. The tests were stopped every 2000 cycles to measure the wear track cross-sectional area. The temperature of the steel ball was measured by a thermocouple contacting the ball surface. During 2000 cycles the temperature rose 5 to 10°C. As there are no significant thermal transformations in the range of room temperature 22°C to 32°C, no significance was attached to this temperature rise.

RECEIVED January 23, 1985

## Wear of Poly(tetrafluoroethylene)

### A Maverick or Not

B. J. Briscoe

Department of Chemical Engineering, Imperial College, London SW7 2BY, England

The wear characteristics of polytetrafluoroethylene (PTFE) have been widely studied; it is an important commercial polymer. This special attention has sometimes created a thesis that this polymer has very unusual or special wear characteristics when compared with the response of other polymers. This review compares the wear behaviour of PTFE with that of a range of polymers and examines the basis of this belief. The experimental evidence indicates that it is only in the area of transfer wear that a major contrast in characteristics is seen. Even in this restricted wear mode the differences are arguably ones of extent and not kind.

The wear processes observed in polytetrafluoroethylene, PTFE, share many features which are common to other thermoplastics. When the polymer is slid over relatively smooth rigid counterfaces it forms thin transferred layers on its counterface under isothermal contact conditions even at room temperature. The generic class of polyethylenes behave in a similar, although generally less extensive manner. The rates of transfer wear, as the overall process is termed, are comparatively high but may be effectively reduced by the inclusion of hard secondary phases into the polymer matrix. Such an expedient is widely adopted to some extent in almost all commercial polymeric bearings on some occasions. As the scale of the roughness of the counterface is increased, transfer wear is replaced by abrasive wear. The hard asperities on the counterface now cut into the softer polymer and microchips or fine filaments are removed from the polymer surface. Hard filler phases are usually ineffective in suppressing this mode of wear although filler particles may modify the surface topography of the counterface. Again this is commonly observed with thermoplastics.

In both these regimes of wear, high rates of power dissipation in the contact first lead to surface and then subsurface thermal softening. These thermal effects generally limit the maximum PV (pressure-velocity) product of polymeric contacts. Furthermore,

fluid lubrication or boundary lubrication of PTFE is normally ineffective. The specific frictional work of the dry contact is low and hence fluid or weak boundary layers offer no great advantages and what is more these layers will often undermine the tenacity of the adhesion of transfer layers to the counterface with the result that the rate of wear is increased. There are similarities in the response of other "cold" or isothermal transferring of polymers.

These things are well known and numerous specific papers and review articles emphasise these points from various viewpoints (1-9). In summary, the tribology of PTFE, although somewhat unusual in some respects, is not exceptionally different from that of other organic polymers, particularly low temperature (gross softening below ca. 350°C) thermoplastics. The review will focus on the way in which PTFE differs from other polymers bearing in mind that these differences are not really ones of kind but of extent. Three topics will be discussed: abrasive wear, transfer wear and lubricated wear.

### Abrasive Wear of PTFE

There are two ways of approaching abrasion. The now classical single pass abrasion experiment which involves sliding the polymer over a rough surface and measuring the mass loss provides a useful correlation with material and topographical properties. Invariably, this experiment does not reveal the microscopic nature of the wear process although the study of the form of the free debris and debris adhered on the counterface offers a useful indication of the deformation processes involved. An alternative approach is to study the effects produced by "isolated stress concentrations"; a method used successfully by Schallamach in his early studies with elastomers (10, 11). Schallamach used sharp needles or spheres to deform the rubber under the combined action of a normal load and a frictional force. A comparison of the response produced in PTFE using both experiments will be briefly reviewed.

### Isolated stress concentration: scratch hardness

Various geometries may be used to provide model asperity deformations; Tabor (12,13) has reviewed these in several definitive papers mainly in the context of metals. Currently we favour the use of cones as they are a relatively simple geometry to fabricate. Figure 1 is a sketch adopted from Archard (14). If we neglect the volume of material displaced out of the plane of the polymer surface, two very simple expressions for the friction,  $f$ , and "wear",  $W_v$ , may be obtained (8,9). The "wear" is not the volume removed but the volume displaced; the product of the cross section area of the groove,  $A$ , and its length,  $l$ , (Figure 1)

$$f = \frac{2W}{\pi} \tan \theta' \quad (1)$$

$$\text{and} \quad A l = W_v = \frac{2W}{\pi \rho_0} l \tan \theta' \quad (2)$$

$\theta'$  is the cutting angle formed by the cone and  $\rho_0$  is a flow stress.

After the cone has passed over the polymer surface the width,  $w$ , of the groove remains largely unchanged (say 10% reduction), but invariably there is a significant relaxation of the strain in the direction of the normal load (Figure 1) (12,15). The experiment can therefore be carried out conveniently by measuring,  $w$ , and hence  $A$  can be computed. Figure 2 shows data for such an experiment with PTFE and polymethylmethacrylate, PMMA; the ordinate is the  $A/W$ , where  $W$  is the normal load ( $1N$ ) (15). The sliding velocity is fixed at  $4.2 \times 10^{-5}$  m/s. The interesting feature is the close similarity of the two data sets, and the fact that equation (2) is a good approximation. The normal indentation hardness of PMMA and PTFE are typically in the ratio of ten for cones in the range of,  $\theta$ , semi-apical angle between  $80^\circ$  and  $25^\circ$ . A similar ratio is seen in the scratch hardness in this range. Lubricating both contacts produces a reduction in  $A/W$  of comparable amounts as would be expected from the decrease in the interfacial traction (16). Lubricating sliding contacts of this type generally produces a reduction in penetration in contrast to the lubrication effects seen in normal hardness studies where lubrication promotes penetration (12,16). Finally, it is also noted that the form of load and sliding velocity variations seen in these type of data follow, to a first order, the relationship given by equation (2) but where  $\rho_0$  is a time-dependent variable.

In a scratch hardness experiment of this sort, it is possible to make a subjective assessment of the nature of the deformation in terms of the relative contribution of ploughing or ironing and cutting or chip formation. There seems to be a critical value of  $\theta'$  above which ploughing is replaced by cutting. The magnitude of  $\theta'$  is a function of many variables including the depth of penetration and the state of lubrication (16,18). Typical values of  $\theta'$  for PMMA and PTFE are respectively  $45^\circ$  and  $90^\circ$  as judged from electron micrographs. Actually, the real picture is more complex as the geometry of the damaged surfaces are rather different. PTFE shows extensive plastic flow and fibrillation whereas in PMMA there is often evidence of crack formation, Figure 3 (15). Bethune (19) and Lamy (17) have shown similar results.

As an expediency we have compared PTFE and PMMA but a more comprehensive comparison with other polymers leads to a similar conclusion. The general behaviour of PTFE is comparable in kind to that seen with other polymers. Perhaps the only unusual feature is the marked evidence of surface fibrillation.

This conclusion would lead us to suppose that the abrasion characteristics of PTFE would also be rather similar to that found with other polymers. This is found to be the case.

#### Abrasion by multiple asperity contacts

The study of single asperity interactions does not directly resolve a number of the important questions which arise when we attempt to understand abrasive wear. The critical cutting angle for material removal often exceeds the realistic slopes of asperities, and in any event it is useful to question whether material can be removed by multiple interactions which involve grooving. There is good circumstantial evidence to suggest that this is an important feature of abrasion processes, and it is an important factor in particle erosion



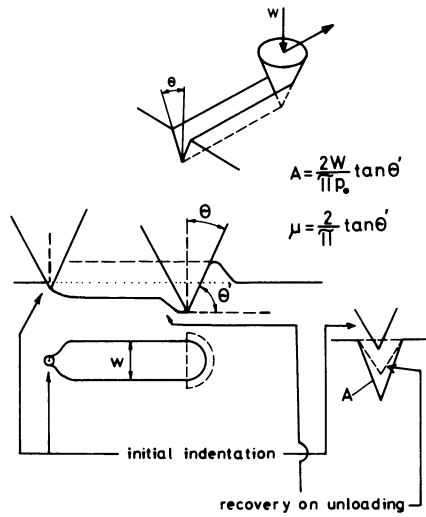


Figure 1. (a) A rigid cone of semi-apical angle  $\theta$  cutting through a soft plane. (b) Various sections of Figure 1(a) to indicate the initial and final deformations. The track width is  $w$  and the cone produces a cutting angle  $\theta'$ .

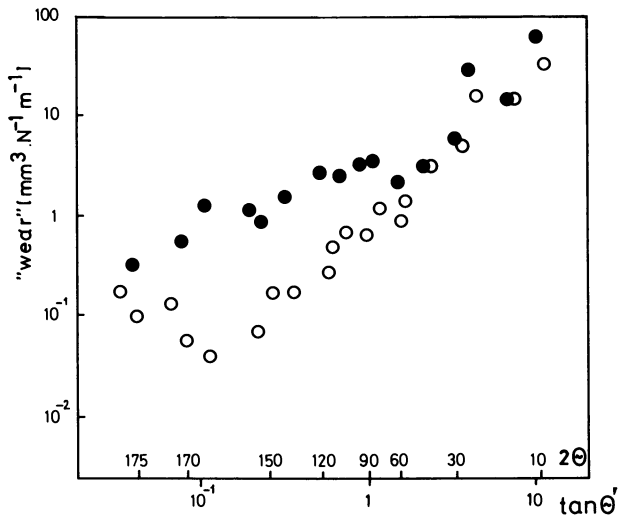


Figure 2. "Wear" as a function of  $\theta$  and  $\tan \theta'$  for the experiment shown in Figure 1. Load 1N; sliding velocity ca.  $4 \times 10^{-5} \text{ ms}^{-1}$ ; no lubrication; temperature ca.  $20^\circ\text{C}$ . The wear is calculated from,  $w$ , the scratch width. Open symbols PMMA and closed symbols PTFE. These cutting angles are functions of load, velocity and the state of lubrication.

(18,22). Apart from this question there must be concern about the modification of the surface topography by loose debris. In addition, there are important details to be considered regarding the stress distributions over the numerous asperity contacts.

If we take an uncritical view and build on the scratch hardness model assuming that the volume displaced,  $A$ , in some way defines the wear rate of the whole assembly of asperities we produce a relationship for the abrasive wear per unit distance (8,23):

$$Z = \frac{KW}{\rho_0} \tan\theta' \quad (3)$$

Kragehlskii (24) and others have applied this argument to ductile metals.  $\theta'$  is now some average slope or cutting angle and the  $K$  parameter expresses the probability of forming a loose wear particle in a single deformation. Invariably,  $K$  is small and hence we suppose that multiple encounters are required to loosen debris; alternatively we have a fatigue process operating. Lancaster (24,25) and others (26,27) have examined the variables  $\theta'$  and  $W$  in single pass abrasion; the model is a reasonable account of their data. Of more interest is the significance of  $K$  as proposed by Ratner (28,29). The Russian school considered that  $K$  was related to the inverse of the toughness measured in tension in a unit deformation. This approach does not exclude the idea of a fatigue process but clearly the role of multiple deformations is not stressed. It is usual to write the Ratner relationship (sometimes called the Ratner-Lancaster relationship) as

$$Z = K' \frac{f}{\rho_0 \sigma_y \epsilon_y} \quad (4)$$

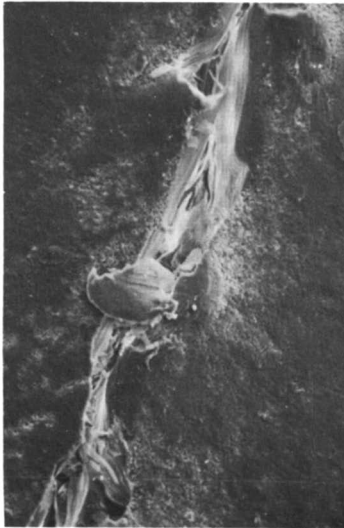
by comparing (1) and (3).  $K'$  now contains the fatigue parameter which specifies the probability of particle detachment.  $\sigma_y$  and  $\epsilon_y$  are respectively the stress and strain at tensile rupture as measured<sup>y</sup> in a macroscopic sample. The product of  $\sigma_y \epsilon_y$  is approximately equal to  $\int_0^{\epsilon_y} \sigma d\epsilon$ .

The inadequacy of referencing a bulk rupture parameter,  $\int_0^{\epsilon_y} \sigma d\epsilon$ , to an interfacial deformation is obvious; the structure, chemistry, quasi-hydrostatic stresses, temperatures and rates of strain are certainly not comparable in the two cases. A well quoted example of the quality of the Ratner-Lancaster relationship is shown in Figure 4. The wear of PTFE fits into the overall trend. The wear debris in the case of PTFE is normally highly fibrillar in structure however. The glassy polymers, such as PMMA, form powders of more regular aspect ratio with less evidence of extensive plastic flow. Figure 5 shows the pronounced fibrillar formations produced by a PTFE pin when it is slid over an optical diffraction grating.

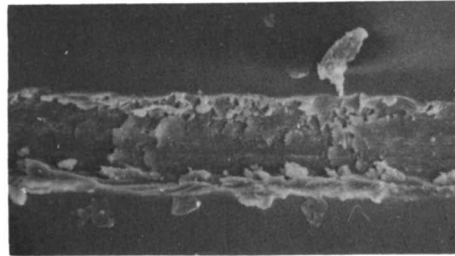
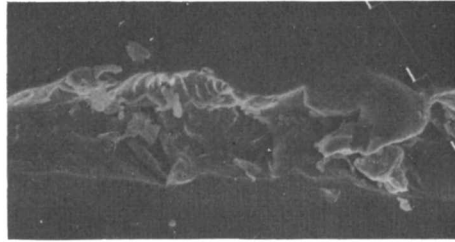
The value of the correlation between toughness and abrasive wear may be taken further with PTFE. PTFE is unusual in the fact that gamma irradiation in vacuum does not appear to lead to extensive chain cross-linking but does produce appreciable chain scission (30). The details are not clear but significant increases in density (and hence possible crystallinity) are observed as the dose level is increased. Of more significance in the present context is the marked

15 cone angle  
mag. x 200

POLYCARB



PTFE



PMMA

Figure 3. Surface damage produced by a truncated 15° cone under a load of 1N. Evidence of fibrillation is seen in PTFE along with extensive plastic flow. The surfaces of PMMA and polycarbonate PC show that significant brittle fracture occurs.

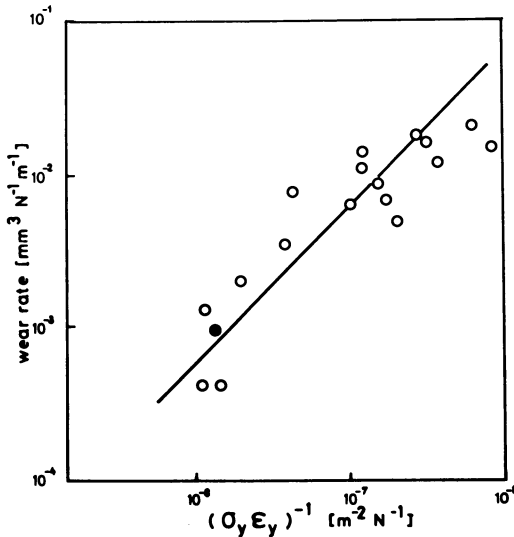


Figure 4. A Ratner-Lancaster plot for eighteen nominally pure and commercially available polymers. Data obtained in a "single-pass" over a rough steel surface of σ 12. μm. The data for a PTFE is shown as a closed symbol.

reduction in toughness. The data shown in Figure 6 are plotted according to a modified form of equation (4) (30):

$$Z = \frac{K' f}{\sigma_y 2 \epsilon_y} \quad (5)$$

where  $\rho$  is assumed to be proportional to  $\sigma_y$ . Actually  $\rho$  will exceed  $\sigma_y$  because of the quasi-hydrostatic environment in normal approach. The data in Figure 6, neglecting the virgin PTFE, follow  $Z \propto (\sigma_y 2 \epsilon_y)^{-n}$  where  $n$  is ca. 0.25. The wear is a slower function of the increase of the toughness than expected. Also the virgin polymer wears more rapidly than the trend indicated by the radiation damaged specimens. There may be several reasons for this result but in view of the crude nature of this model it is not prudent to draw firm conclusions. It is however noted that the size of the average wear debris particles decreases very significantly as the gamma dose increases. This effect does not explain, in itself, the observation that as the dose level increases the wear is less than expected on the basis of toughness measurements but it may be a contributory factor. The important point is that the toughness as measured in a unit deformation may not be the important macroscopic variable. A parameter based on fatigue strength may be more relevant. There are indications that this is the case with elastomers although early work found reasonable correlations with macroscopic toughness (31).

Several authors have demonstrated a close correlation between the value of the toughness measured in a single deformation and the fatigue crack propagation (FCP) rates measured in cyclic loading at lower stresses; Hertzberg and Manson have produced a useful summary of this area (32). The FCP rates,  $R_f$ , may be expressed by the Paris equation which contains two material parameters,  $A$  and  $m$ ;

$$R_f = A \Delta K^m$$

$\Delta K$  is related to the stress variation generated at the crack tip during the load cycle. The parameter  $m$  covers a wide range and indeed may be a function of  $\Delta K$ . The value for PMMA is about six; for poly(vinylidene fluoride), PVDF, it is less, about 0.3. For a fixed value of  $R_f'$  the quantity  $\Delta K$  may be computed and compared with the toughness,  $K_C$ . It is found that for a wide range of polymers  $\Delta K'/K_C \approx 0.5$  where  $\Delta K'$  is  $\Delta K$  for the fixed value of  $R_f'$ . If we consider that the rate of wear is proportional to  $R_f'$  (this is the basis of the Champ, Southon and Thomas (31) analysis) then a number of interesting analyses may be explored. For example if the fatigue toughness of PTFE is comparable with PVDF, i.e.  $m \approx 0.3$ ; then we could tentatively explain the  $\gamma$ -irradiated PTFE data given in the above terms of a cyclic fatigue process;  $R_f \propto (\text{toughness})^m$ .

In summary, at present we may conclude that while fatigue-based correlations are conceptually more acceptable, correlations based on toughness measured in tensile tests generally follow the correct trend. As far as PTFE is concerned there are no very special features, save for the unusually large aspect ratios found in the abrasive wear debris.

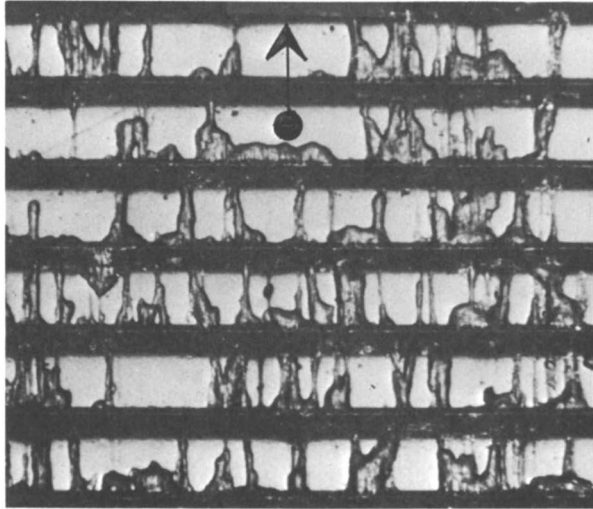


Figure 5. An optical image of the transfer of filaments formed on an optical grating (312 lines per inch) after 28 traversals over its surface by a PTFE pin under a normal load of 20N. The grating is of steel.

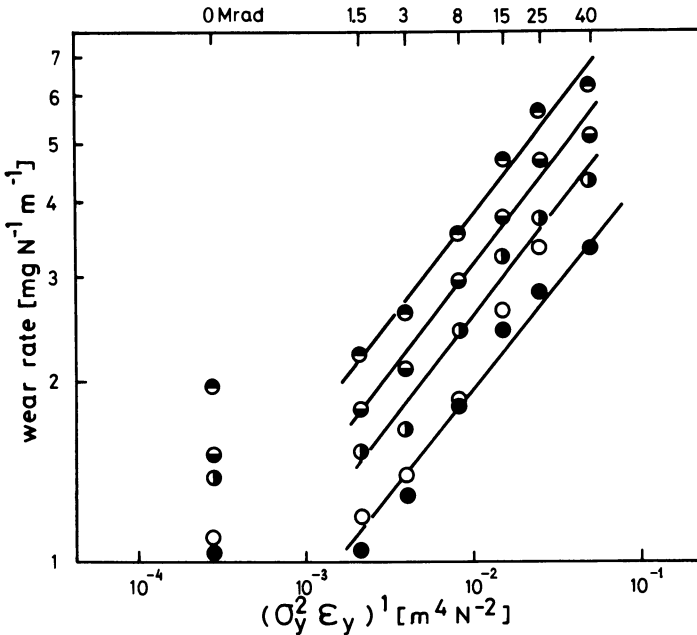


Figure 6. Abrasive wear of  $\gamma$ -irradiated PTFE plotted against  $\gamma$ -dosage and the quantity  $(\sigma^2 \epsilon_y)^{-1}$ . Mechanical properties measured at  $\dot{\epsilon} \sim 10^{-2} \text{ s}^{-1}$ . Load  $Y 4.7 \text{ N}$ ; sliding velocity  $4 \times 10^{-4} \text{ ms}^{-1}$ ; "single-pass" abrasion over abrasive papers of  $\sigma$  values  $\bullet$ ,  $6.2 \mu\text{m}$ ;  $\circ$ ,  $6.7 \mu\text{m}$ ;  $\ominus$ ,  $9.5 \mu\text{m}$ ;  $\odot$ ,  $11.3 \mu\text{m}$ ,  $\oplus$ ,  $15.8 \mu\text{m}$ .

The transfer wear modes in PTFE

If PTFE has anomalous wear characteristics, it is in the area of what is now described as transfer or adhesive wear. Much has been written on this topic and opinions do not really differ on the important features of this process (34-43). Before discussing PTFE in particular it is useful to briefly review two general aspects of transfer wear processes; the transition between abrasive and transfer modes and the categories of transfer wear.

The transition between abrasive and transfer modes

The idea of a transition from a transfer process to an abrasion process is really a question of semantics. In a transfer process it is adhesive forces which transmit the stresses which ultimately remove surface layers from the polymer matrix. The adhesive forces are sufficiently strong at the sliding interface to cause cohesive failure of the polymer near the interface and the polymer is transferred onto the counterface. Simple models of abrasion like the ones reviewed above do not regard surface forces as a contributing factor although we will return to this point later in the context of lubrication. The deformation work in abrasion is transmitted to the surface by rigid geometric asperity engagements. The soft material may form free chips although this is unlikely with machined counterfaces whose asperity slopes are normally less than  $20^\circ$ . More likely it is a fatigue process which involves the ploughing and hence repeated deformation of the polymer surface. In practice, of course, adhesive forces or interfacial friction will be involved. A further complication arises when the wear debris begins to modify the topography of the counterface; this is the case even during what is termed "single-pass" abrasion.

There are currently no clear answers to the relative importance of abrasion and transfer as the scale of the surface roughness is reduced. The problem does however have some potentially important practical consequences; this involves the observation that there is often an optimum surface roughness for minimum wear (41-43). Figure 7 is an example for a polar graphite filled PTFE (43). An optimum surface roughness of ca.  $0.25 \mu\text{m c.l.a.}$  is evident. Similar results have been noted with ultra high molecular weight polyethylene (UHMPE). It is tempting to ascribe this point to the transition region between transfer and abrasion; a reason why the transfer wear might decrease with the scale surface topography up to  $0.25 \mu\text{m c.l.a.}$  is discussed later. Above  $0.25 \mu\text{m c.l.a.}$  abrasion predominates and the severity of the abrasion increases rapidly as the c.l.a. roughness,  $\sigma$ , is increased. In none of these studies was a careful study of surface topography carried out. There are few studies where this has been done; a notable exception is the work of Lancaster and Hollander (47). They measured both  $\sigma$  and  $R_b$  the mean asperity radius and hence computed a mean value of  $\theta'$ , the average slope. They then found good correlations between single-pass abrasive wear, and the ratio  $\sigma/R_b$  which is related to  $\tan \theta'$ . ( $\tan \theta' = (\sigma/2R_b)^{1/2}$ .) Clearly the trend in Figure 7 may be due to changes in  $R_b$ . Eiss has recently looked specifically at the influence of  $R_b$  in the wear of branched polyethylenes and polyvinyl chloride (48); it is an important variable.

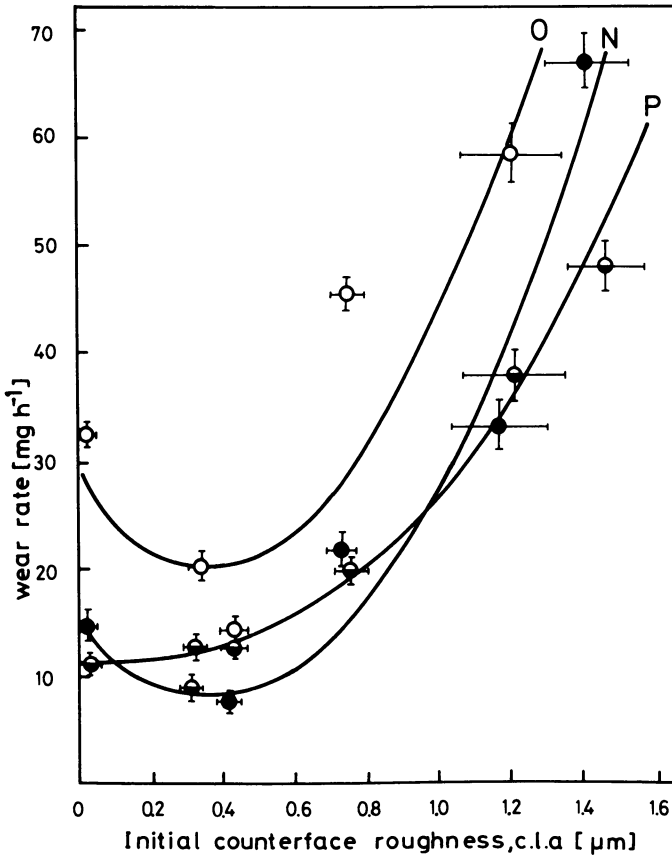


Figure 7. Wear rate as a function of initial counterface roughness for a series of carbon filled PTFE composites running in air against a steel counterface. The fillers are present at 10% by weight and the carbons differ in particle size, aspect ratio and surface chemistry. Little change in counterface topography is noted during the course of this experiment; these carbons are not particularly abrasive towards steel. The evidence of a minimum in wear is not strong but it is consistent with other work. In this experiment there is a detectable inverse trend in the friction; the lower the wear the higher is the friction. The symbols refer to carbons of different particle size and aspect ratio. Open symbol is for a graphite high aspect ratio sheet. The fully closed symbol is for a particle of lower aspect ratio. Both particles were prepared from a nuclear grade graphite,  $\theta$  (46).

### Transfer modes; general classification

Under a given set of contact conditions organic polymers divide into two types in respect of their transfer behaviour; some form transferred films and others do not. In the case of PTFE we often observe a type of transfer which we may call predominantly isothermal or cold, "whole" transfer. There is some frictional heating and chain scission but these effects are not large when compared with some other polymers. PMMA, for example, shows no detectable transfer below its glass transition temperature although there may be transfer of low molecular weight species which have segregated on the free surface. At high sliding speeds surface melting occurs and transfer films are formed from the melt (49) with some chain scission (41,50). This is hot, total transfer. On the other hand, a highly cross-linked system, such as a rubber or resin, only forms extensive transfer films via extensive chemical degradation at the interface during high speed sliding. This is degraded transfer. There is no transfer when isothermal conditions are maintained although surface "bloom" may be transferred.

PTFE is therefore amongst a class of polymers which exhibits cold, total transfer. It is the wear which arises from this type of transfer which is usually described as transfer wear. As we shall see the behaviour of PTFE is not unique but it is unusual in its extent.

### Transfer wear

The part that the transfer process plays in the overall wear process has been reviewed elsewhere (8,9). The basic elements can be identified broadly as follows:

- (i) the nature and magnitude of the adhesive forces which provide surface transitions;
- (ii) the position of the locus of junction failure and the morphology and thickness of the transfer layer;
- (iii) the magnitude of the adhesion of the transfer film to the substrate and the means by which it is detached from the substrate;
- (iv) and finally the details of the processes whereby the film is displaced from the contact.

Significant rates of transfer are observed when the initial interfacial adhesion is sufficient to develop cohesive failures in the polymer under the action of the transmitted shear stresses. If this transferred layer is weakly attached to the substrate, it is detached by the same tractions. Providing the geometry of the system allows, this material is displaced from the contact. More film is transferred to the substrate and a high equilibrium wear rate results; typically in a polymer pin-on-disc configuration about 10 nm of polymer is removed from the pin during each cycle over the face of the disc. In confined or conforming contacts with



unfilled polymer the wear is less simply because the debris cannot escape and back transfer occurs. A rationale, which explains much of transfer wear behaviour, is that the polymer does not readily transfer on to its own transfer film. If the transfer film is adhered strongly to the substrate or cannot escape, the wear is reduced, often by large factors.

These general comments apply to some extent to all cold, "whole" transfer wear processes. PTFE is unusual in that it transfer very readily in this type of process; more so than any other known polymer. Further, the transfer films have particularly poor adhesion to most substrates and also have extremely high degrees of orientation. Some chain scission can be detected (38,42,50). They are also uncommonly thin; sometimes no more than 10 nm in thickness (some workers believe they may be of the order of one molecular-chain cross section diameter in thickness, ca. 0.8 nm).

The facility shown by PTFE to form highly oriented and thin transfer films is not unique to this polymer. Linear polyethylenes and possibly polyoxymethylene behave in a similar fashion although not with the same efficiency. The tendency to form highly oriented films can be readily detected in the spin sensitivity of the wear rate (see companion paper by Dr. T. Stolarski and the present author). The wear rates of these smooth molecular profile polymers (PTFE and linear polythenes) decreases with real and apparent load axis spin. At the same time the friction increases. The same trends are not seen with branched polyethylenes, which form rather poorly oriented transferred layers and PMMA which does not transfer layers. This experiment underlines the important process of interface reorientation and shear softening which occurs in smooth molecular profile polymers. The imposition of spin about the load axis disrupts this process and as a result the frictional work increases and the wear rate decreases. The change in the frictional work can be explained quite simply in qualitative terms. Why the transfer wear should decrease cannot be easily explained. However, there is a general observation which seems to be true for many PTFE and other polymeric contacts wearing by the cold transfer process; the higher the friction the lower is the wear. Figure 7 may be recalled in this context. Other exponents indicate that when the friction is high the wear is less. The inference that has been drawn is that the higher friction promotes a stronger adhesive function at the transfer film-substrate interface (51). We should also note here that PTFE has a rather low friction when slid on smooth counterfaces.

It is now worth summarising the characteristics of PTFE in the transfer wear mode. The basic process resembles that seen in other transferring polymers; many rather ill-defined and diffuse steps are involved. PTFE is unusual insofar as it transfers very efficiently to clean surfaces and its transfer films do not adhere strongly. The fact that the frictional work is rather low as a result of interfacial reordering may be important here. The low friction also ensures a wider operating range of quasi-isothermal or cold transfer. The special highly oriented transfer film character is also shared with linear polythenes although these materials do not transfer so readily. For the polythenes it appears that the higher the molecular weight the less pronounced is

the transfer. The relative importance of molecular weight and morphology in governing the case of PTFE transfer has been examined by several authors as have the extents of chain scission and crystallinity change produced in the wear debris. High crystallinity and high molecular weight seem to inhibit transfer or at least transfer wear (50). Figure 8 shows the influence of gamma radiation on the transfer wear of PTFE (30). No cross-linking occurs but there is a significant increase in density and hence probably crystallinity. The rate of wear is reduced to levels comparable with those obtained with good filler packages for doses in excess of 20 M Rad. At this point the crystallinity is calculated as ca. 80% from density measurements; the virgin polymer has a crystallinity of ca.60%. Eiss and Hu found similar trends although they also detect the expected trend with increasing molecular weight (50).

In loose terms, the presence of ordered units or long range affine connections suppresses the necessary chain mobility required to generate oriented polymer surfaces and hence the formation of thin oriented transfer films by rupture at the oriented surface-bulk isotropic polymer interface. The solid particles included in PTFE to reduce transfer wear may act in the same way (41).

A discussion of the wear of PTFE would not be complete without some reference to PTFE composites. This has been a popular field of study simply because without fillers the wear of PTFE is normally unacceptable. A good filler will reduce transfer wear rates by up to three orders of magnitude. Various mechanisms have been proposed and the subject has been reviewed by the present author (8,9) and others (2,52). The simplest idea is that fillers wear less than the polymer when exposed at the interface. They may also suppress transfer and improve transfer film adhesion. A good deal of effort of high quality has been put into the search for chemically induced adhesion promotion at the transferred film-substrate interface but the evidence is equivocal (53,54). Chemical changes are detected but their precise contribution to the adhesion is uncertain in commercial applications. PTFE is a remarkably stable polymer to chemical attack even at sliding interfaces.

To conclude this section we may state that, with respect to transfer wear, PTFE is not entirely unique. Even its special transfer behaviour is seen elsewhere. It is really a matter of the extent not the kind of its character which is remarkable.

#### Lubrication of PTFE

There is more interest in the effect of marginal lubrication or spurious contamination than in full or intentional lubrication. The very indifferent performance of PTFE in the original human hip joint replacements emphasises the problem faced with PTFE and even some of its composites. Providing that a full fluid film is maintained there is no serious problem. However, if direct contact between the polymer and the counterface occurs a transfer film is deposited. The fluid naturally undermines the adhesion of this film to the substrate and also facilitates debris removal from the contact; an accelerated wear may then ensue. Figure 9 is the data from Lancaster which clearly exemplifies this point (55). Certain fillers may improve matters but in general it is not a good practice to use

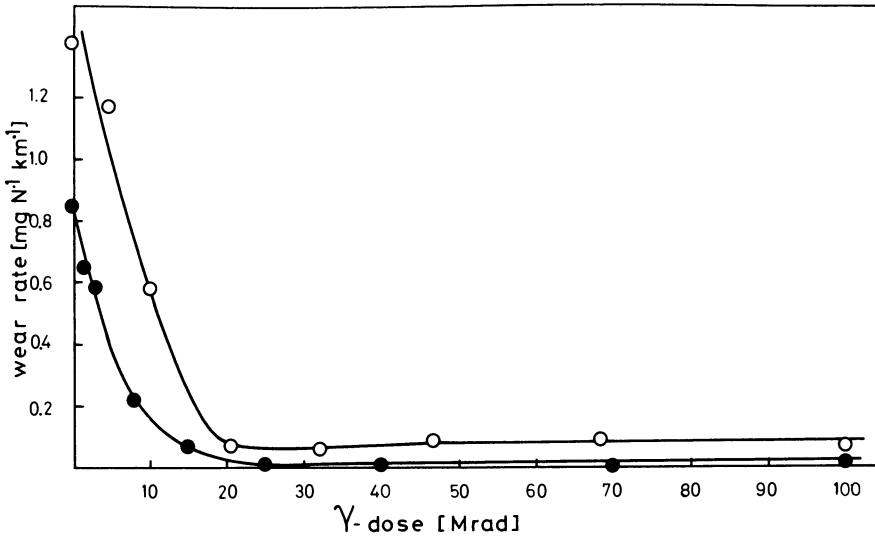


Figure 8. Wear rate of  $\gamma$ -irradiated PTFE as a function of  $\gamma$ -dose. Counterface mild steel,  $\sigma = 0.4 \mu\text{m}$ ; closed symbols gamma damage in vacuum; open symbols gamma damage in air. In both cases the transfer wear reaches a minimum at about 20 M Rad. In the case of gamma treatment in air significant oxidation of the sample, particularly the surface, is found to occur.

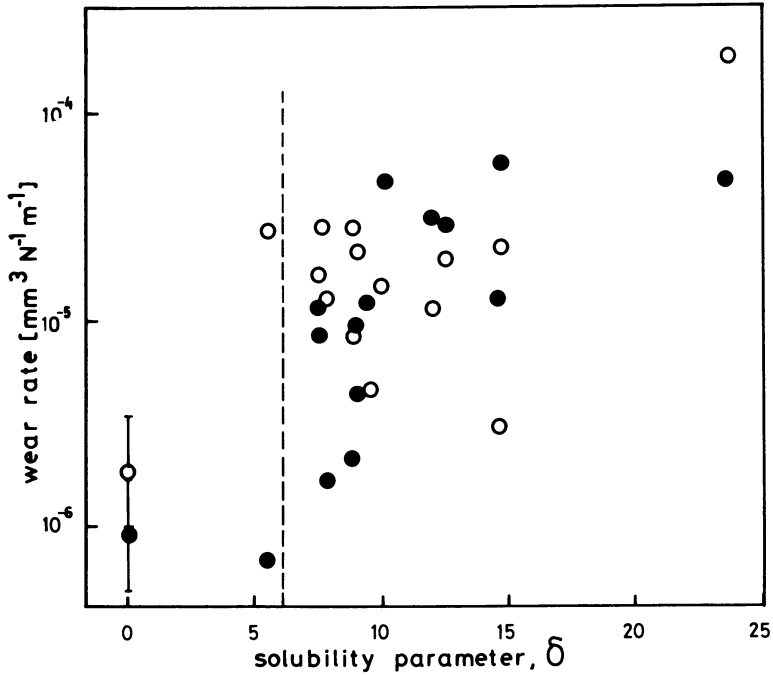


Figure 9. Transfer wear rates in "lubricants" of two PTFE composites (●, PTFE-polyimide and ○, PTFE-25% w.w. I carbon fibre) as a function of the solubility parameter,  $\delta$ , of the lubricating media. The wear of the dry contacts is shown at  $\delta = 0$  and the calculated value of  $\delta$  for PTFE is ca. 6.0. The solubility parameter is defined as the square root of the cohesive energy density and is therefore nearly proportional to the square root of the surface tension,  $\gamma$ , of the fluid. The trend for the wear to increase with  $\gamma$  and  $\delta$  is apparent. In the dry contact secure transfer films are formed but they are not evident in lubricated contacts. It is reasonable to suppose that as  $\gamma$  increases the wetting of the steel counterface improves and hence the transfer films are more readily displaced. Data adapted from Lancaster and Evans.

PTFE in this way. There are also numerous commercial examples of where small amounts of even condensable vapours may accelerate wear by presumably destabilising the formation of good and securely attached transferred layers. Figure 10 is an illustration which also shows that in composites the environmental sensitivity of the wear may be conveyed by the filler; in this case carbon (56).

As PTFE so readily forms transferred layers, this type of gross "lubrication" failure is an acute problem. In many applications it has to be accepted as a low dry friction is required when full fluid film lubrication is lost. This is sometimes the case at the ends of the stroke in a reciprocating contact.

We have made no direct reference to the role played by the uniquely low surface free energy of PTFE in its wear behaviour. This point is discussed briefly in the conclusion to this paper where the significance of surface free energy as a primary variable is argued to be of no great consequence. A more useful notion is the low cohesive energy density of the polymer and the low surface free energy is just a manifestation of the low cohesive energy density. Having made this point it is worth stating that the low surface free energy of the polymer does inhibit extensive wetting by fluid media and there are tentative examples where this poor wetting phenomenon seems to play a part in promoting starved fluid lubrication (57, 58). Poor wetting interferes with the generation of effective fluid entry in the entry region.

### Conclusions

If the PTFE's have special character it is the way in which they easily reoriented their surfaces under the action of interfacial shear stresses. This produces fibrillation in abrasion against rough surfaces and extensive thin oriented film transfer on smoother counterfaces. These things are a surprise in such a high molecular weight polymer which contains both lamella and spherulites. The amorphous regions are well above their glass transition temperature but generally the contact operates at a temperature at least 200°C below its crystalline temperature. There are two relaxation temperatures near ambient but these are unlikely to be of great significance in the overall picture. Our best view is that because PTFE is a very weak van der Waals solid of low cohesive energy density, as demonstrated by its uniquely low surface free energy, the chain-chain interactions are not strong in the matrix. It is its high molecular weight (large entropy per chain) which keeps the material in the solid state. Actually PTFE's do not normally melt in the general sense. The fact that the chains are so smooth enables them to pack efficiently to form a coherent solid. The same smooth molecular topography also facilitates molecular slip and hence the relative displacement of molecules and molecular domains required for surface reorientation even at low temperatures. The consequences on the type and rate of wear and magnitude of the sliding friction for PTFE need not be repeated. It is a moot point as to whether these things make the PTFE's a maverick polymer or not. There is however a value in regarding the wear characteristics of PTFE as being generally similar to that of other polymers and very similar to certain linear polyethylenes. Here, the differences are ones of extent not kind.

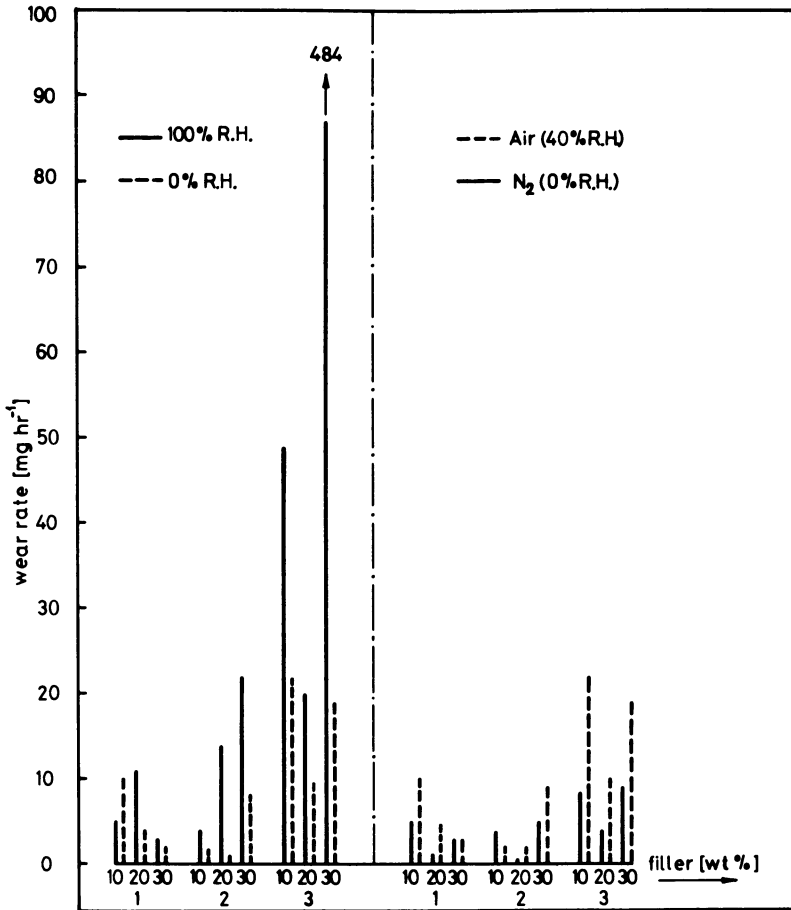


Figure 10. The influence of environment on the wear of three carbon filled PTFE composites. (a) the effect of relative humidity in air, (b) the effect of oxygen (as air) compared with nitrogen at a nominal zero humidity. The three carbons are: 1. a nuclear graphite; 2. the same nuclear graphite milled in a polar fluid; and 3. an agglomerated flake graphite formed from nuclear graphite by milling in a hydrocarbon. The main mode of wear is by a transfer process. The details of the changes produced by the environment are not resolved but it appears that a significant part of the environmental sensitivity is due to changes induced at the filler-counterface interface. For example, the filler particles are wearing more rapidly in an oxygen environment, presumably by the process of oxidation (54).

### Acknowledgments

I am grateful to Professor D. Tabor, Dr. T. Stolarski, Dr. J. Lancaster and Mr. Paul Evans for useful discussions which have helped in the formulation of the ideas expressed in this paper.

### Literature Cited

1. Steijn, R.P., American Soc. for Metals, 9-12 May 1967.
2. Evans, D.G.; Lancaster, J.K., "The Wear of Polymers" in "Materials Science and Technology, Wear", Ed. Scott, D., Vol.13, Academic Press, New York, 36-140, 1979.
3. Barteney, G.M.; Laurentev, V.V., "Polymer Friction and Wear", trans. Payne, D.B., ed. Lee, L.H., Chemistry Publisher, Leningrad, 1972, Eng.Ed., Elsevier, The Netherlands, 1981.
4. Bely, V.A. et al., "Friction and Wear in Polymer-based Materials", trans. Granville-; Jackson, P., Pergamon Press, 1982.
5. Lee, L.H. ed., "Advances in Polymer Friction and Wear", Vol.5A, 5B. Plenum Press, New York, 1974.
6. Dowson, D., Godet, M.; Taylor, C.M., ed. "The Wear of Non-Metallic Materials", Mechanical Engineering Publications Ltd., 1978.
7. Ludema, K.C., Glaeser, W.A., Rhee, S.K., et al. ed., "Wear of Materials", various editions 1977, 1979, 1981, Am.Soc.Mech. Engrs.
8. Briscoe, B.J.; Tabor, D., "Friction and Wear of Polymers", Ch. I, "Polymer Surfaces" ed. Clark, D.T. and Feast, W.J., Wiley, New York, 1978.  
"The Sliding Wear of Polymers" in "Fundamentals of Tribology" ed. Suh, N.P. and Saka, N., MIT Press, Cambridge, Mass., 1980.
9. Briscoe, B.J., Tribology International, 231-242, August 1981 and "Tribology of Polymers" in "Physicochemical Aspects of Polymer Surfaces" ed. Mittal, K.L., Plenum Press, New York, 1981.
10. Schallamach, A., J.Polymer Sci., 9 (5) 1952, 385.
11. Schallamach, A., Wear, 1, 1958, 384.
12. Tabor, D., "The Hardness of Metals", Oxford University Press, 1951.
13. Tabor, D., "Indentation Hardness and its Measurement; Some Cautionary Comments". Private Communication.
14. Archard, J.F., "Wear" in Interdisciplinary Approach to Friction and Wear, ed. Ku, P.M., NASA. SP-181 Washington DC, 1968.
15. Briscoe, B.J., Evan, P.D.; Lancaster, J.K., J.Mat.Sci., in press.
16. Johnson, K.L., "Aspects of Friction", in "Friction and Trac-tion", ed. Dowson, D. et al., Westburg House, London 1981.
17. Lamy, B., Tribology International, 17 (1), 1984, 35.
18. Tabor, D., "Wear - A Critical Synoptic View" in "Wear of Materials 1977", ed. W.A. Glaeser et al., American Society of Mechanical Engineers, 1977.
19. Bethune, B. J.Mat.Sci., 11, (1976), 199.
20. Hutchings, I.M., Winter, R.E.; Field, J.E., Proc.Roy.Soc., A348, 1976, 379.

21. Ahman, L. ; Oberg, A., "Wear of Materials", 1983, Am.Soc. Mech.Engrs.
22. Tilly, G.P., Wear, 23, 1973, 87.
23. Kragehlskii, I.V., "Friction and Wear", Butterworth, London, 1965.
24. Lancaster, J.K., "Abrasion and Wear of Polymers" in "Encyclopedia of Polymer Science and Engineering", Vol. I, John Wiley & Sons, 1985.
25. Lancaster, J.K., Proc.Inst.Mech.Engrs.Lub. and Wear Group, 190, 1964.
26. Ratner, S.B.; Farberova, I.I. in "Abrasion of Rubbers", ed. James, D.I., McLaren & Sons, London, 1967, 23, 297.
27. Warren, J.H.; Eiss, N.S. in "Wear of Materials 1977", ed. Glaeser et al, American Society of Mechanical Engineers, 1977, 494.
28. Ratner, S.N., Farberova, I.I., Radyukeuich, O.V.; Lure, E.G., Soviet Plastics, 7, 1964, 37.
29. Lancaster, J.K., Plastics and Polymers, 41, 1973, 297.
30. Briscoe, B.J.; Ni, Z., "Wear of Materials 1983", ed. Ludema, K.C., American Society of Mechanical Engineers, 1983, 643.
31. Champ, D.H., Southern, E., Thomas, A.G. in "Advances in Polymer Friction and Wear", Polymer Science and Technology 5A, ed. Lee, L.H., Plenum Press, New York, 1974, 133.
32. Hertzberg, R.W. and Manson, J.A., "Fatigue of Engineering Plastics", Academic Press, New York, 1980.
33. Briscoe, B.J., Phil.Mag., 43A, (3), 1981, 511.
34. Pooley, C.M.; Tabor, D., Proc.Roy.Soc. A329, 1972, 251.
35. Sviridyonok, A.I., Belyi, V.A., Smurugov, V.A.; Saukin, V.G., Wear, 25, 1973, 301.
36. Bowers, R.C.; Zisman, W.A., Eng.Chem.Prod.Res.Develop., 13, 1974, 115.
37. Jain, V.K.; Bahadur, S. in "Wear of Non-Metallic Materials", ed. Dowson, D. et al., Mechanical Engineering Publications Ltd, London 1978.
38. Bonfield, W., Edwards, B.C. ;Markham, A.J., Wear, 37, 1973, 153.
39. Tanaka, K.; Uchiyama, Y. in "Wear of Materials 1977", ed. Glaeser, W. et al., American Society of Mechanical Engineers, New York, 1977, 499.
40. Kar, M.K.; Bahadur, S. in "Wear of Materials 1977", ed. Glaeser et al, American Society of Mechanical Engineers, New York, 1977, 501.
41. Arkles, B.C.; Schireson, M.J., Wear, 39, 1976, 177.
42. Czichos, H. in "Wear of Non-Metallic Materials", Mechanical Engineering Publication Ltd., ed. Dowson, D. et al, London, 1978, 285.
43. Tanaka, K. in "Wear of Materials 1981", ed. Rhee, S.K. et al., American Society of Mechanical Engineering, New York, 1981,98.
44. Eiss, N.; Bayraktaroglu, H.M., Trans.Amer.Soc. of Lubri.Eng., 23, (3), 1980, 269.
45. Dowson, D., Challen, J.M., Holmes, K.; Atkinson, J.R. in "Wear of Non-Metallic Materials", Mechanical Engineering Publications Ltd., London, 1978, 99.



46. Briscoe, B.J.; Steward, M.D., in "Materials Performance and Conversation", Inst.Mech.Engrs. Publication, London 1978.
47. Lancaster, J.K.; Hollander, D.E., Wear, 25, 1973, 1955.
48. Eiss, N.S.; Milloy, S.C. in "Wear of Materials 1983", ed. K.C. Ludema, American Society of Mechanical Engineers, New York, 1983, 650.
49. Tanaka, K.; Uchiyama, Y. in "Advances in Polymer Friction and Wear", 5B, ed. Lee, L.H., Plenum Press, New York, 1974, 499.
50. Hu, T.-Y. ;Eiss, N.S. in "Wear of Materials 1983", ed. K.C. Ludema, American Society of Mechanical Engineers, New York, 1983, 636.
51. Briscoe, B.J. in "Adhesion 5", ed. Allen, K., Applied Science Publishers, London, 1981.
52. Czichos, H., "Systems Approach to Tribology", Elsevier, The Netherlands, 1979.
53. Pocock, G.; Cadman, P., Wear, 37, 1976, 129.
54. Pepper, S.V., J. Applied Phys. 45(7), 1976, 2949.
55. Lancaster, J.K. Private Communication.
56. Briscoe, B.J., Steward, M.D.; Groszeck, A., Wear, 42, 1977, 99.
57. Lewis, R.B., American Society of Automotive Engineers, Inc., Nation. Combined Fuels and Lubrication and Transportation Meetings, Houston, Texas, 1969.
58. Briscoe, B.J., Stolarski, T.A. ; Davis, G., Tribology International, 17, 1984, 121.

RECEIVED January 23, 1985

## **Influence of Counterface Topography on the Wear of Ultra High Molecular Weight Polyethylene Under Wet or Dry Conditions**

**D. Dowson<sup>1</sup>, M. M. El-Hady Diab<sup>2</sup>, B. J. Gillis<sup>3</sup>, and J. R. Atkinson<sup>4</sup>**

<sup>1</sup>Department of Mechanical Engineering, Institute of Tribology, The University of Leeds, Leeds LS2 9JT, United Kingdom

<sup>2</sup>285 A. Ramsis Street, Cairo, Egypt

<sup>3</sup>Adelaide Brighton Cement Ltd., Birkenhead, South Australia

<sup>4</sup>Department of Metallurgy, The University of Leeds, Leeds LS2 9JT, United Kingdom

It has been noted earlier that there is an optimum counterface topography which produces a minimum rate of wear of ultra-high molecular weight polyethylene when sliding takes place against stainless steel under dry conditions. Further experiments have shown that in the presence of water, the wear rate of the polymer decreases steadily as the counterface roughness is decreased. Furthermore, the curved 'dry' and linear 'wet' characteristics intersect, thus indicating that the presence of water increases or decreases the wear indicating that the presence of water increases or decreases the wear rate compared with dry conditions, depending upon whether or not the surface roughness exceeds, or is less than, a critical value.

It is shown that the transfer film of polyethylene on the steel counterface plays a crucial role in determining the observed wear rates. The results of an investigation of the role of various features of counterface topography upon the wear of polyethylene are also recorded. The influence of different machining processes upon wear was minimized by producing a large number of finely lapped surfaces, following careful grinding, and then 'back-lapping', or roughening, the test specimens to produce a range of similar surface topographies, but different roughnesses. The experiments were all carried out on similar linear, reciprocating friction and wear machines under comparable conditions.

In general the wear rates of relatively soft materials sliding against hard counterfaces decrease as the surface quality of the counterface is improved. However, Buckley(1) observed that ultra-high-molecular weight polyethylene (UHMWPE) exhibited a minimum wear rate when sliding against a ground steel  $0.37 \mu\text{m}$  (rms) counterface. Swikert and Johnson(2) reported a similar result from hip joint simulator studies in which cobalt-chromium alloy balls were prepared by a liquid honing method, but the optimum roughness was about  $0.11 \mu\text{m}$  (rms).

Dowson et al.(3) evaluated the wear rate of UHMWPE sliding against surgical grade austenitic stainless steel under dry conditions in a six-station reciprocating linear wear testing machine. A programme of thirty tests revealed a minimum wear rate at a counterface roughness of about  $0.03 \mu\text{m}$  Ra, but it was also noted that the optimum roughness coincided, approximately, with a transition from grinding to lapping in the procedures adopted for counterface preparation. It therefore became necessary to explore in more detail the role of surface topography upon the wear of UHMWPE under dry conditions and to determine whether the observation of a minimum wear factor was related to counterface manufacturing processes or some inherent feature of the wear mechanism.

In the present paper we report the results of two further extensive studies of dry wear tests of UHMWPE on stainless steel by Gillis(4) and Diab(5) together with a range of results by Diab(5) for interfaces submerged in distilled water.

#### Apparatus, Test Specimens and Experimental Procedure

Experiments were carried out on a six-station reciprocating pin-on-plate machine of the type shown in Figure 1. The mean sliding speed was  $0.25 \text{ m/s}$  and loads ranging from  $42.5\text{N}$  to  $100\text{N}$  were applied to the polyethylene wear pins. The basically cylindrical UHMWPE wear pins of diameter  $9.5\text{mm}$  and length  $9.5\text{mm}$  had a truncated conical form as shown in Figure 2 and the initial, circular, wear face had a diameter of  $3\text{mm}$ .

The flat plate counterfaces were machined from surgical grade stainless steel EN58J. All plates were cut, rough ground and then fine ground parallel to the sliding direction adopted in the wear tests, until a surface finish of  $0.1 \mu\text{m}$  Ra had been attained. A chalked alumina wheel was used in the fine grinding process. The plates were then lapped on Logitech lapping machines using brass plates until a surface finish of about  $0.025 \mu\text{m}$  Ra had been achieved and all the initial grinding marks had been removed. A nylon lapping cloth on steel plates and various grades of carborundum and diamond pastes were used to prepare the final surfaces with a random surface texture and various roughnesses. The plates were then cleaned ultrasonically in isopropyl alcohol before surface topography evaluation and immediately prior to wear testing.

The counterface topography was analysed on a Rank Taylor Hobson Talysurf instrument linked to a VAX computer. Surface profiles were analysed at intervals of  $1.554 \mu\text{m}$  over a traverse length of  $3.8 \text{ mm}$  to give some 2445 data points. All the height readings were input as positive numbers relative to an arbitrary datum. They were then

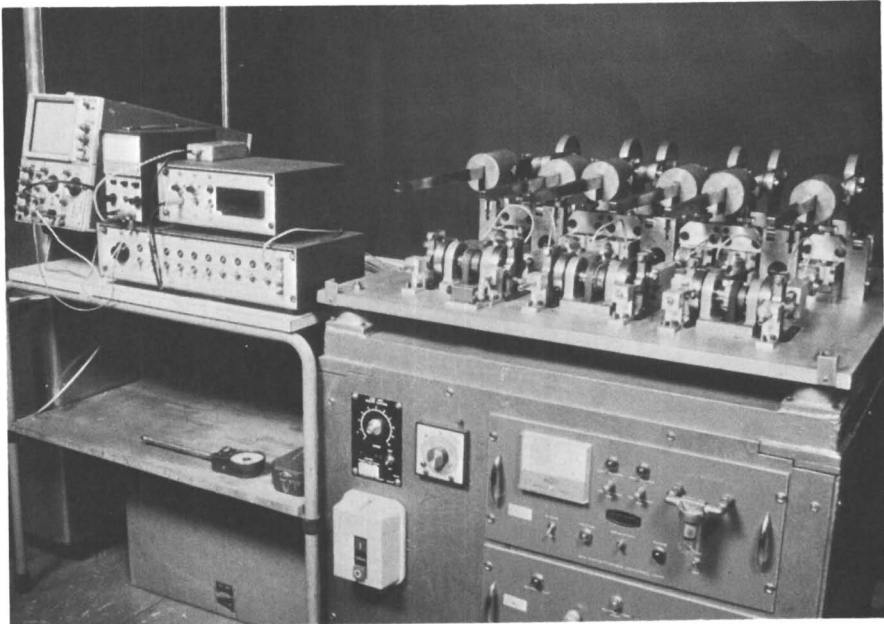
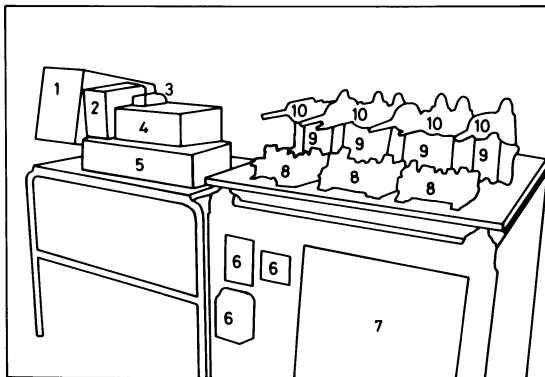


Figure 1(a) Six Head Linear Reciprocating Wear Machine - photograph



KEY TO FIG. 1

- 1 Cathode Ray Oscilloscope
- 2 Power Pack
- 3 Filter
- 4 Microstrain Recorder
- 5 Multi-channel Switching Unit
- 6 Speed and Control Units
- 7 Air Conditioning Unit
- 8 Drive Mechanisms 1-6  
(from right to left)
- 9 Test Heads 1-6  
(from right to left)
- 10 Cantilever Loading Weights 1-6  
(from right to left)

Figure 1(b) Six Head Linear Reciprocating Wear Machine - Key

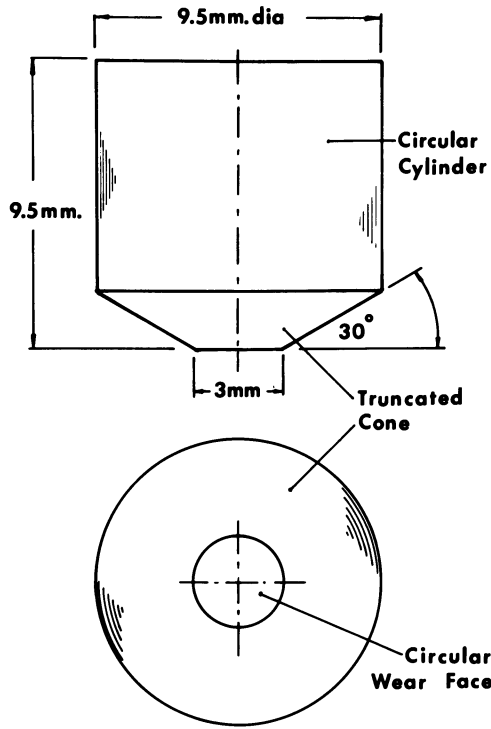


Figure 2 Geometry of Polymeric Wear Pin

re-interpreted as heights with respect to a least squares datum line. The computer program calculated (r.m.s.) and (Ra) values but also revealed the statistical distribution of ordinates, peaks, valleys, radii of curvature of peaks and valleys and profile slopes. For each distribution the program also calculated the values of the mean and standard deviations and the maximum and minimum limits of the distribution. Auto-correlation functions and bearing area curves were also generated. At the end of some wear tests Talysurf traces across the counterface wear track were recorded to reveal the general nature and extent of the polymeric transfer film.

Each test specimen was subjected to a constant load and a fixed cycle of reciprocating motion. Long term wear tests were performed with the total sliding distance in each case extending to several hundred km. The material removed by wear was monitored by periodic measurements of the weight of the UHMWPE wear pins on a Mettler microbalance with a sensitivity of 1 g. Density measurements enabled volume loss (V) against sliding distance (X) relationships to be established at each load (P) and wear factors (k) were then determined from the relationship,

$$k = \frac{V}{PX} \text{ (mm}^3\text{/Nm)}$$

### Results

Statistical analysis of the counterfaces employed by both Gillis(4) and Diab(5) revealed meaningful relationships between (Ra) and other significant features of the counterface topography. These relationships are illustrated graphically for the counterfaces used in the 'dry' experiments by Gillis(4) in Figure 3 and for those used in 'wet' experiments by Diab(5) in Figure 4. The relationships detected enabled the wear data to be recorded as a function of any preferred feature of surface topography. The measurements of features of lapped counterface topography recorded by Gillis(4) can be summarized by the following relationships, where each symbol associated with the statistical distribution of some feature of the surface topography represents the standard deviation of that distribution. Since the analysis was based upon all the data points provided by the digital output from the Talysurf, all the peaks and valleys were incorporated in the derivation of standard deviations, whether they existed above or below the computed mean line for the profile.

$$Ra = 0.82 (\sigma)^{1.07}; Ra = 0.85 (P)^{0.96}; Ra = 0.8(V)^{1.05};$$

$$Ra = 10.4 (\tan\theta)^{1.1}$$

where,  $\sigma$  = Profile height ( $\mu\text{m}$ ); V = Valley depth ( $\mu\text{m}$ );  
 P = Peak height ( $\mu\text{m}$ );  $\theta$  = Mean absolute slope of profile;  
 and Ra = Centre line average roughness ( $\mu\text{m}$ )

The wear factors (k) recorded in a large number of experiments carried out under 'dry' conditions are shown as a function of counterface roughness (Ra) in Figure 5. Some 36 dry tests were carried out by Gillis(4), half of the counterfaces being produced by grinding and the other half by the grinding and lapping procedures

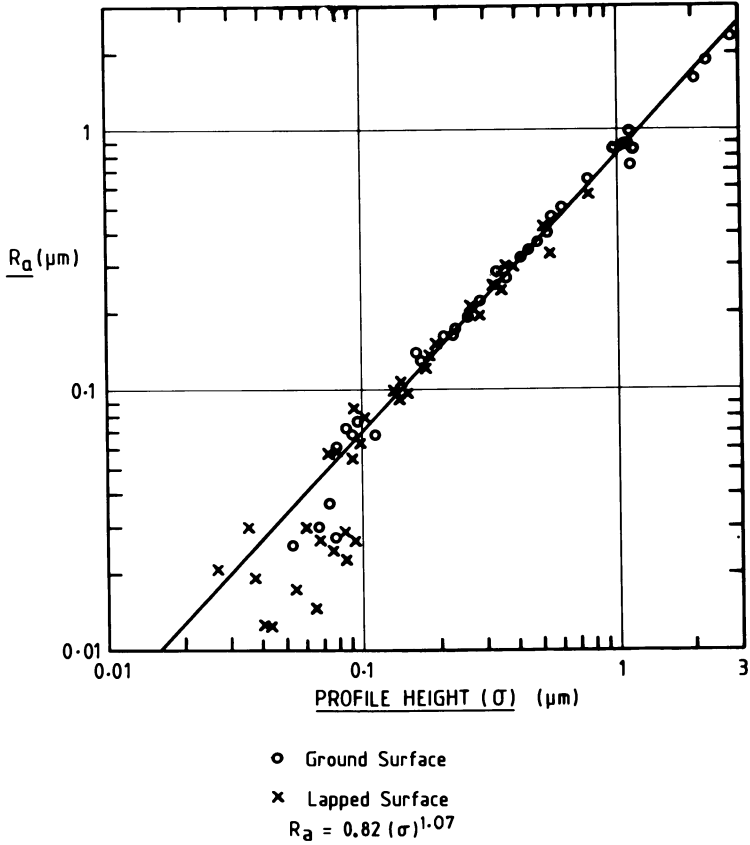
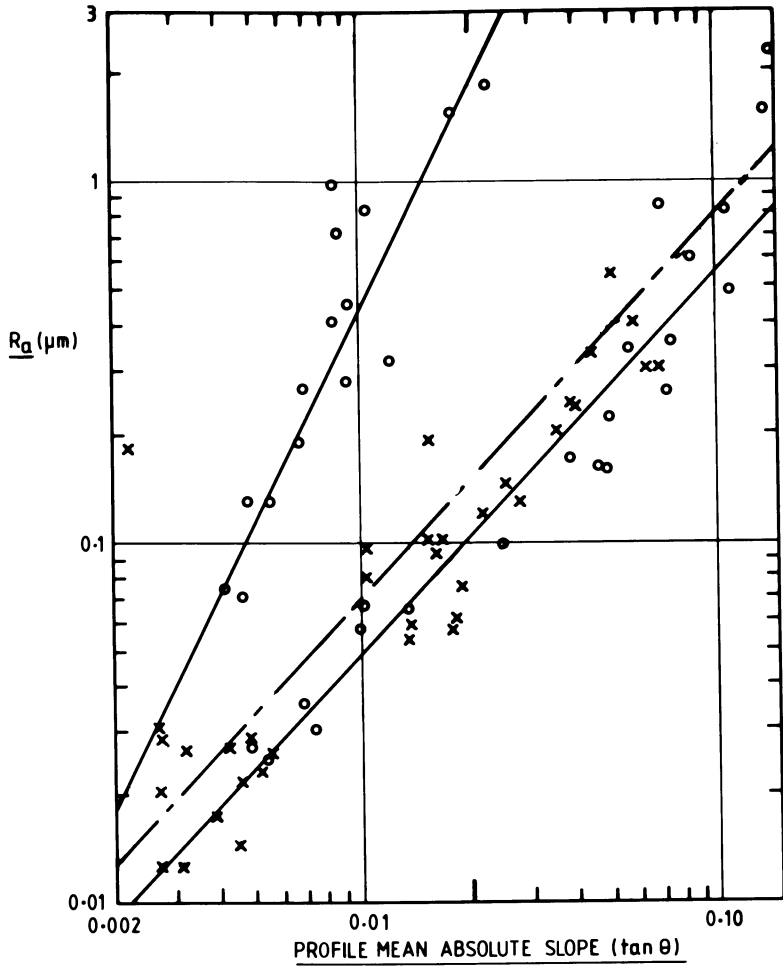


Figure 3(a) Relationship Between ( $R_a$ ) And Profile Height ( $\sigma$ ) (After Gillis)



—○ Ground Specimens. Parallel to Sliding Direction  $R_a = 4444(\tan \theta)^2$   
 Perpendicular to Sliding Direction  $R_a = 7.03(\tan \theta)^{1.1}$   
 - - - x Lapped Specimens  $R_a = 104(\tan \theta)^{1.1}$

Figure 3(b) Relationship Between ( $R_a$ ) And The Profile Mean Absolute Slope ( $\tan \theta$ ) For Ground And Lapped Surfaces (After Gillis)



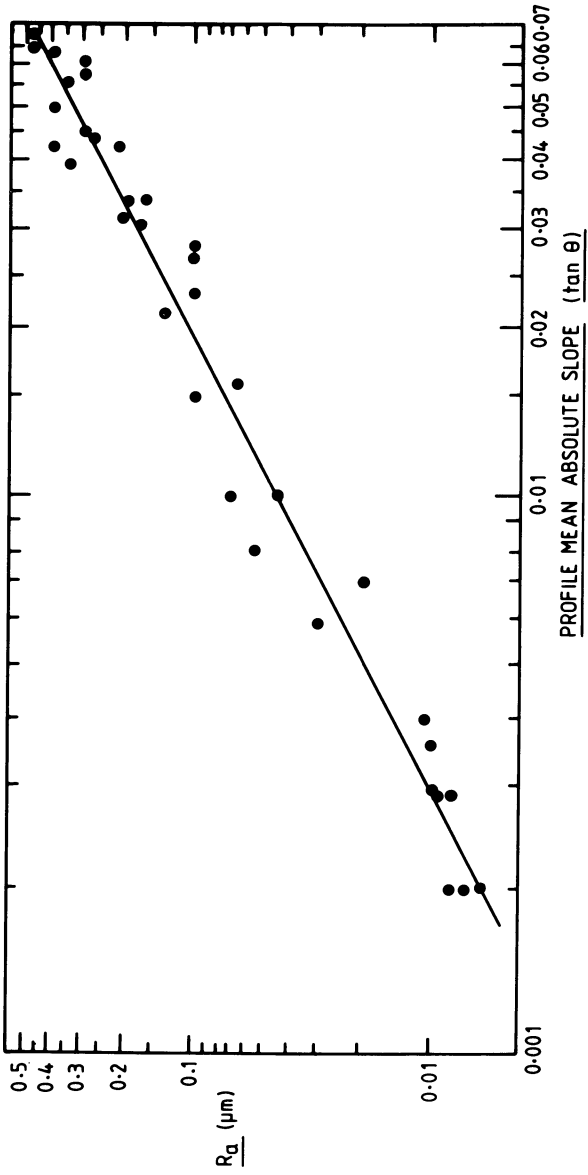


Figure 4(a) Relationship Between  $R_a$  And Profile Mean Absolute Slope  $(\tan \theta)$ . Lapped Surfaces.

$$R_a = 13.92(\tan \theta)^{1.237} \mu\text{m (After Diab)}$$

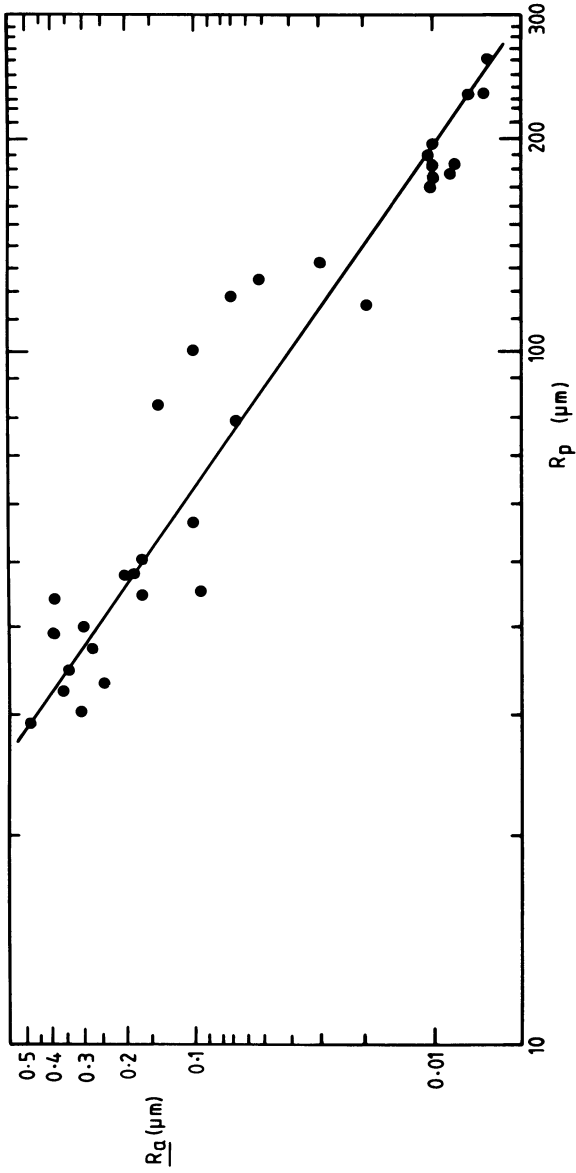


Figure 4(b) Relationship Between ( $R_a$ ) And Average Radius Of Curvature of Asperity Peaks ( $R_p$ ) (After Diab)

$$R_a = 4 \times 10^{-10} / R_p)^2 \mu\text{m}$$

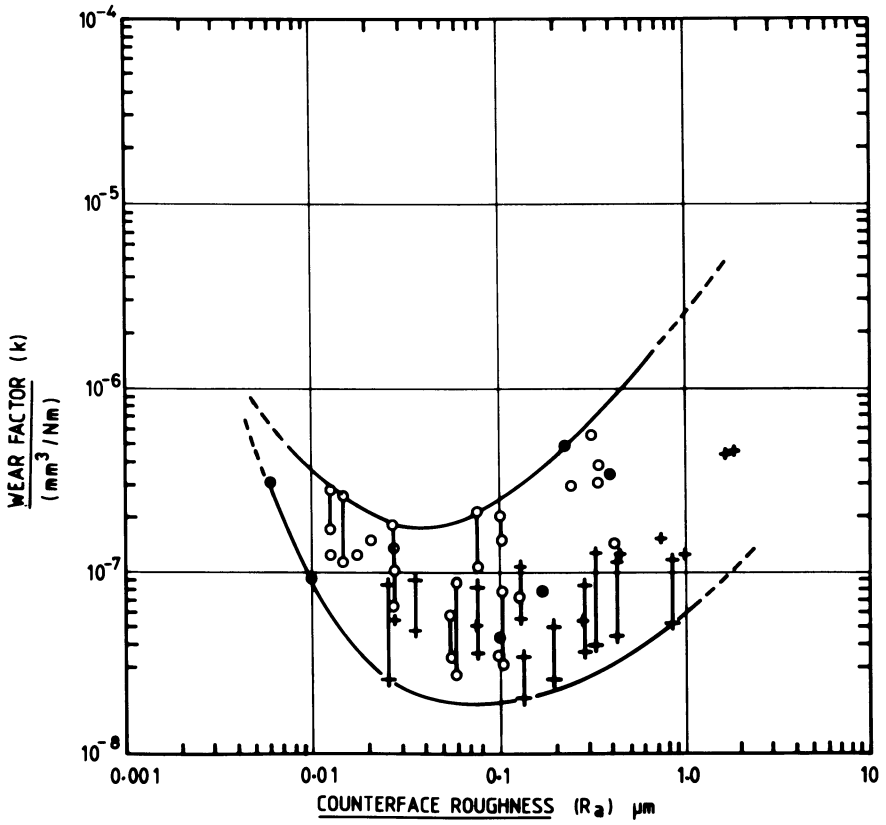


Figure 5 Wear Factor ( $k$ ) As A Function Of Counterface Roughness ( $R_a$ ) Under Dry Conditions

outlined earlier. Diab(5) found that six further dry tests revealed a similar relationship with (Ra) to that observed by Gillis(4) and these additional results are also recorded in Figure 5. Diab(5) also completed twenty-two tests in distilled water on counterfaces having a wide range of surface roughness and the results are recorded in Figure 6.

The relationship between the wear factor (k) and the counterface roughness (Ra) under wet conditions depicted in Figure 6 is linear, corresponding to

$$k = 4.0 \times 10^{-5} (Ra)^{1.2}$$

Lines representing the wear rates (k) as functions of surface roughness (Ra) under both 'dry' and 'wet conditions are shown together in Figure 7. Gillis(4) also examined the profiles of the polymer transfer films deposited on the steel counterfaces under dry conditions and typical records of Talysurf traces are shown in Figure 8. The two upper traces show Talysurf profiles from the transfer film for a ground counterface having an initial roughness (Ra) of 0.08  $\mu\text{m}$  parallel to the sliding direction.

The two lower traces show similar profiles for a transfer film developed on a lapped counterface having an initial roughness (Ra) of 0.02  $\mu\text{m}$  parallel to the sliding direction. It can be seen that the transfer film on the much smoother lapped counterface is considerably thicker than that on the initially rougher ground surface. The films were by no means uniform, but a very substantial increase in thickness was evident on counterfaces having  $Ra < 0.1 \mu\text{m}$ , compared with the films on rougher counterfaces, as shown in Figure 9.

### Discussion

There has been considerable discussion about the most appropriate feature of counterface topography to be employed in the representation of wear factors for polymers. However, it is evident from Figures 3 and 4 that there is a firm relationship between (Ra) and other principal features of counterfaces prepared by consistent manufacturing processes. It may, therefore, be adequate to represent the wear factors as functions of (Ra) until more complete theoretical relationships are established for the polymer wear process.

The experiments reveal that under wet conditions  $k \propto (Ra)^{1.2}$  and since it has also been shown that, over the range of surface roughnesses considered  $Ra \propto (\tan\theta)^{1.1}$  (Gillis (4)) or  $Ra \propto (\tan\theta)^{1.24}$  (Diab (5)), it seems probable that if the mean slope of the counterface surface asperities plays an important role in the wear process, it will have a significant effect upon (k).

The earlier suggestion by Dowson et al.(3) that for the dry wear of UHMWPE against stainless steel there was an optimum initial surface finish corresponding to a minimum wear factor, has been confirmed by further detailed and extensive studies by Gillis(4) and Diab(3). These experiments indicate that the optimum (Ra) is slightly less than 0.1  $\mu\text{m}$  and in the range 0.05 to 0.1  $\mu\text{m}$ .

The 'dry' wear factors are, in fact, remarkably steady over a wide range of counterface roughnesses extending over about two orders of magnitude, as shown in Figure 5.

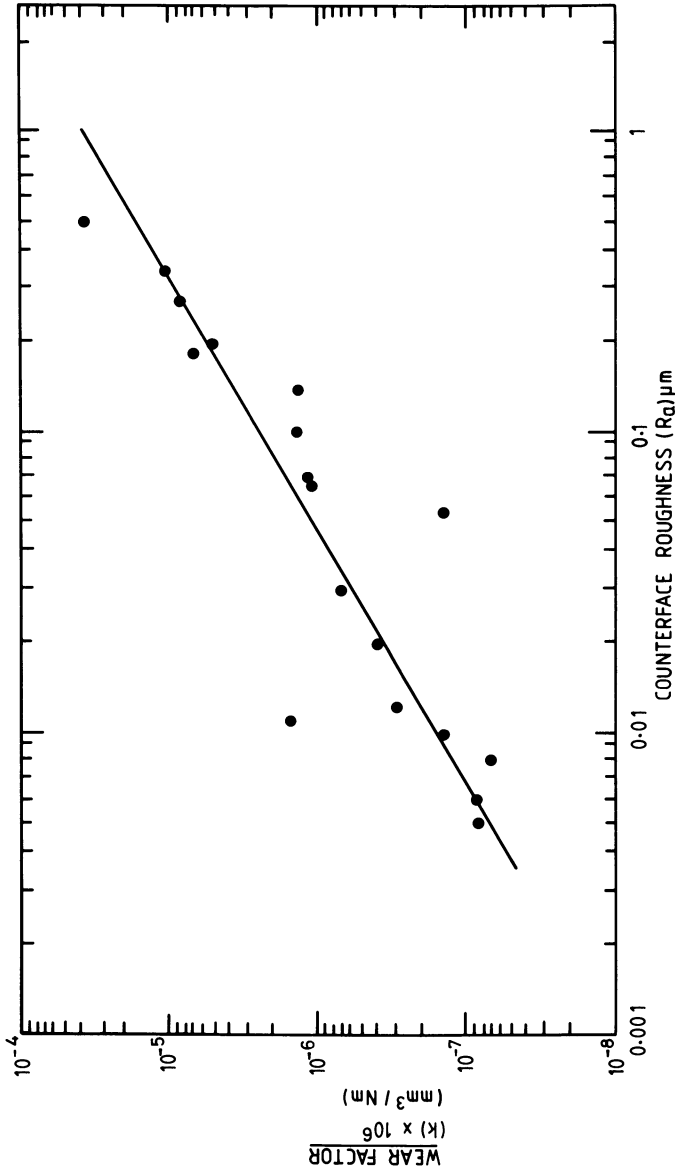


**Figure 6** Wear Factor (k) As A Function Of Counterface Roughness (Ra) Under Wet Conditions  
 $(k = 4.0 \times 10^{-5} (Ra)^{1.2} \text{ mm}^3 / \text{Nm})$

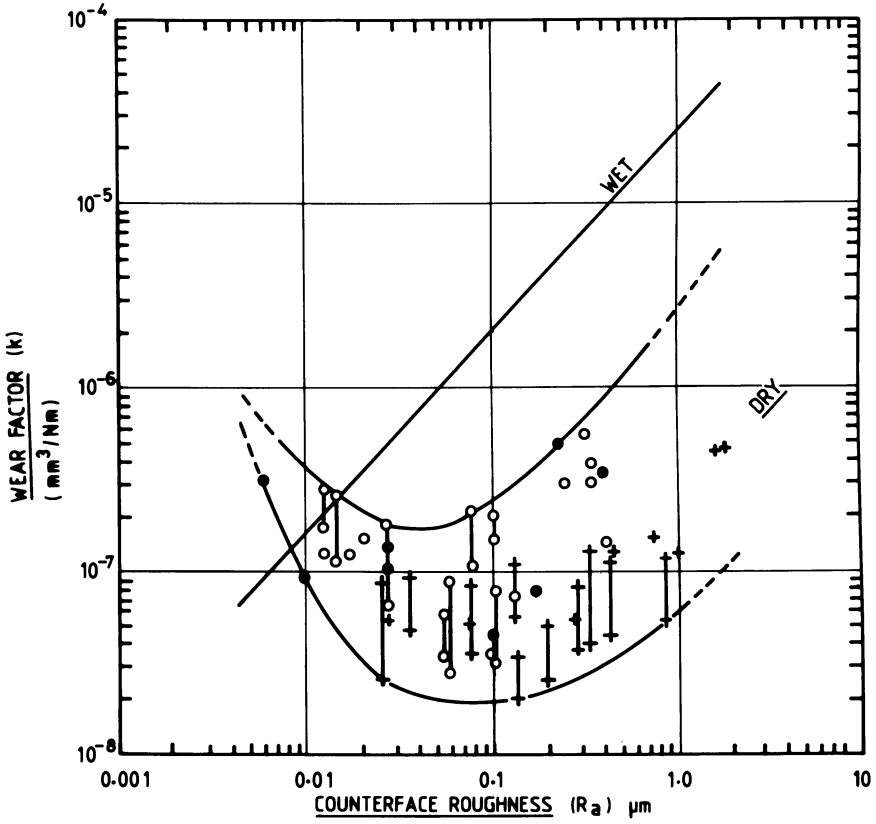


Figure 7 Wear Factor (k) As Functions Of Counterface Roughness (Ra)

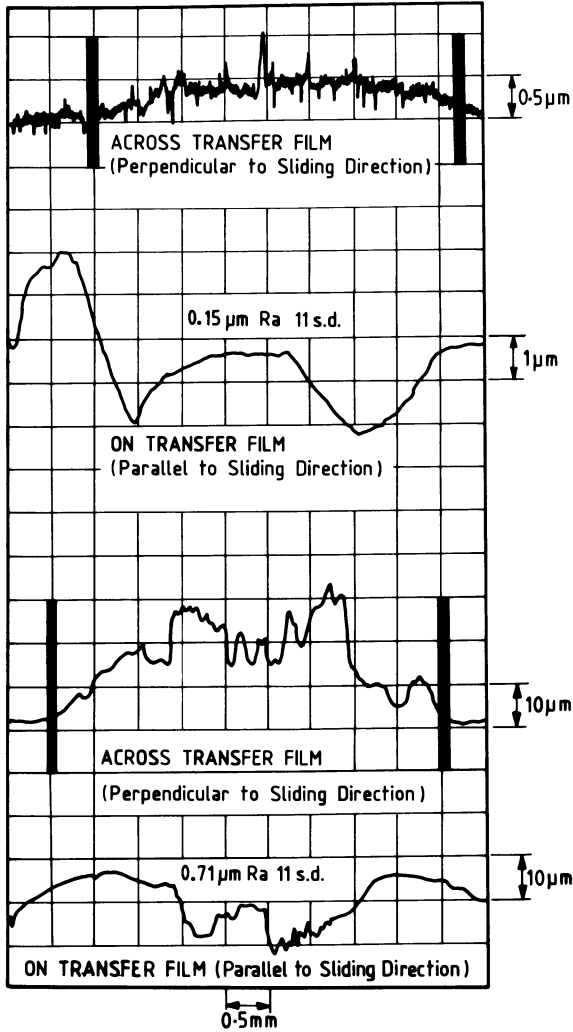


Figure 8 Profiles Of Ultra-High-Molecular Weight Polyethylene Transfer Films On Stainless Steel Counterfaces Recorded After Dry Wear Tests

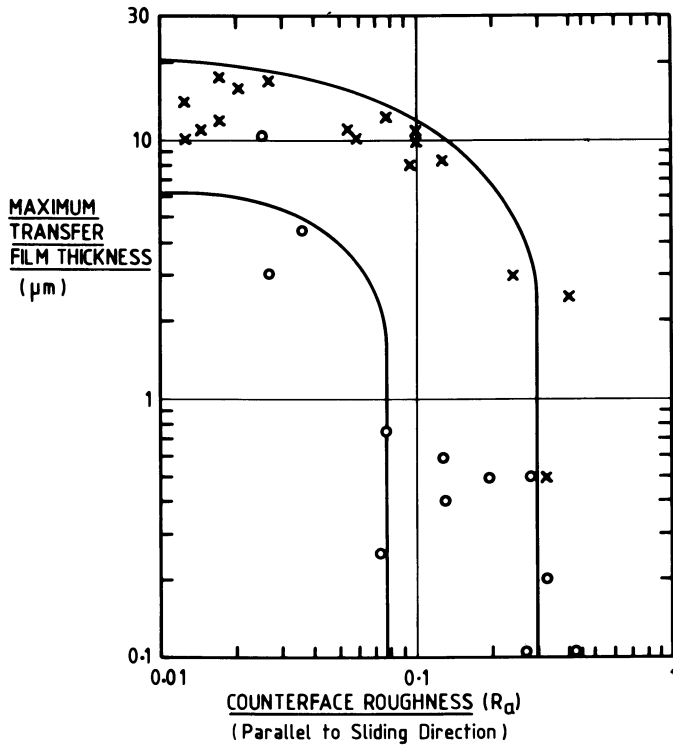


Figure 9

Variation Of Maximum (UHMWPE) Transfer Film Thickness With Original (EN58J Stainless Steel) Counterface Roughness ( $R_a$ )



The presence of distilled water largely inhibits transfer film formation and this results in a much more pronounced effect of counterface roughness upon the wear factors (Figure 6). For counterface roughnesses in excess of about  $0.01 \mu\text{m}$  the 'wet' wear factors exceed the 'dry' wear factor, with the differences being as large as one order of magnitude, on the rougher counterfaces.

On very smooth counterfaces, as  $(R_a)$  progressively decreases, the 'dry' wear factors rise whilst the 'wet' factors fall. This causes a complete reversal of the characteristics observed on rough surfaces since the 'dry' wear now exceeds the 'wet' wear. In broad terms the wear factors on very smooth counterfaces ( $R_a < 0.01 \mu\text{m}$ ) are little affected by the change from a 'dry' to a 'wet' environment.

The distinctive characteristics observed for the wear factors as functions of counterface roughness and the intersection of the traces at a value of  $(R_a)$  of about  $0.01 \mu\text{m}$  provides an explanation of the contradictory views which are held about the influence of environment on the wear of UHMWPE. It is now clearly evident that comparisons must be related to the counterface roughness.

It is interesting to note that very thick transfer films were established on smooth counterfaces (Figures 8 and 9). Such films are typically  $10 \mu\text{m}$  thick and clearly submerge the details of the initial counterface profile, rather like snow drifts on the initial land topography. In this case the bulk polymer will slide on relatively thick transfer films and it will then be the interfacial conditions between the two polymeric features which dictate the wear process, rather than the details of the buried metallic counterface.

It is particularly interesting to note that the transfer film thickness builds up as the counterface becomes smoother and that it exceeds the counterface roughness at a value of  $(R_a)$  of about  $0.1 \mu\text{m}$ , which is close to the optimum surface roughness observed for dry conditions. It is suggested that it is the polymeric transfer film, and particularly its thickness relative to the surface roughness of the counterface, that is responsible for the observed minimum wear factor under dry conditions.

### Conclusions

A comprehensive study of the influence of counterface topography upon the wear rate of ultra high molecular weight polyethylene is reported. The combined results from experiments carried out under 'dry' (atmospheric) or 'wet' (distilled water) environments enabled the following conclusions to be drawn.

1. There are simple relationships between  $(R_a)$  and principal features of counterface topography for the ground and lapped specimens studied. This means that it is acceptable to consider the influence of some simple and readily measured feature of counterface topography like  $(R_a)$  upon wear, since the role of other topographic features can then be deduced.
2. Under 'dry' conditions the influence of counterface topography upon the wear factor is relatively small over a very wide range of  $(R_a)$ .

3. The existence of an optimum (Ra) of the counterface for a minimum wear factor has been confirmed and found to be in the range 0.05 to 0.1  $\mu\text{m}$  (Ra).
4. Under 'wet' conditions the long term wear factors (k) decrease steadily as the quality of the counterface improves. It has been found that the wear factor is given, to a good approximation, by,

$$k = 4 \times 10^{-5} (\text{Ra})^{1.2}$$

5. It appears from the study of 'wet' wear factors and the separate studies of features of counterface topography that changes in the slope of the counterface asperities ( $\tan\theta$ ) will have a significant influence upon the wear factor (k).
6. The 'wet' and 'dry' wear factors intersect at a surface roughness (Ra) of about 0.01  $\mu\text{m}$ .
7. On very smooth countersurfaces, (Ra < 0.01  $\mu\text{m}$ ), the 'dry' wear factor exceeds the 'wet' wear factor, whereas the reverse is true on rougher counterfaces (Ra > 0.01  $\mu\text{m}$ ).
8. On relatively rough surfaces (Ra > 0.1  $\mu\text{m}$ ) the 'wet' wear factor exceeds the 'dry' wear factor by at least one order of magnitude.

#### Literature Cited

1. Buckley, D.H., "Advances in Polymer Friction and Wear", ed. Lee, L.H. Plenum Press, N.Y., 601-603, (1974).
2. Swikert, M.A.; Johnson, R.L., NASA TN D-8174, (1976).
3. Dowson, D.; Challen, J.M.; Holmes, K.; Atkinson, J.R., Proceedings 3rd Leeds-Lyon Symposium on Tribology, 'The Wear of Non-Metallic Materials', 99-102, 1977.
4. Gillis, B.J.; Ph.D. Thesis, Department of Mechanical Engineering, The University of Leeds, 1978.
5. El-Hady Diab, M.M.; Ph.D. Thesis, Department of Mechanical Engineering, the University of Leeds, 1981.

RECEIVED January 23, 1985

# Theory of Rubber Abrasion by a Line Contact

S. W. Zhang<sup>1</sup>

Department of Mechanical Engineering and Applied Mechanics, The University of Michigan,  
Ann Arbor, MI 48109

On the basis of the investigation of rubber abrasion by small-scale tearing on a line contact, a theory has been presented. According to the physical processes of rubber abrasion and its mathematic description proposed, a general process of rubber abrasion can be described by using a simple wear curve. A wear equation obtained describes the basic correlation among the material property, running condition and wear characteristic. It is pointed out that the number of revolution to transform the wear state from unsteady to steady can be considered as a criterion of rubber abrasion. An approximate relationship between the state criterion and tensile rupture ratio has been obtained. These theoretical results agree qualitatively with experimental observation.

Rubber abrasion is an extremely complex process. Recently, a simplified test method has been developed, by choosing a line contact (in practice a razor blade) as the abrading apparatus (1). A number of experimental studies about this mode of wear have been carried out (1-4). Champ, Southern, and Thomas proposed a simple theory relating the rubber abrasion in steady state to the crack growth property of rubber (1,2). However, a complete explanation of the formation and development of the abrasion pattern has not yet been given. In this paper, a theory concerning the mechanism of rubber abrasion is presented. It is supported by some experimental observation in different stages of abrasion. These experimental results were obtained for several elastomers, using a blade abrader as described by Southern and Thomas (2) and a scanning electron microscope (5,6).

## Physical Processes of Rubber Abrasion

As a blade moves relative to the rubber surface, under the action of a normal force, abrasive wear of rubber occurs. According to some of the experimental observations and theoretical analyses, the processes of dry (particulate) abrasive wear might be considered to be

<sup>1</sup>Current address: Department of Mechanical Engineering, East China Petroleum Institute, Dongying, Shangdong, China

comprised of the following periodically repeating processes.

- (a) The blade deforms and tears the rubber surface under the action of the normal force and the frictional force. Consequently, crack growth appears and a torn tongue of rubber forms (Figure 1, a).
- (b) As the blade moves, the tongue of rubber is bent backwards; therefore, a part of the rubber surface is protected from the scraping action of blade at the rear. This process is similar to using a needle or a small hemisphere of 1 mm in diameter to scratch the rubber surface, as described by Schallamach (7-9).
- (c) Under the tension caused by the frictional force, the tip of tongue is ruptured. Then, the remaining part of the tongue is released (Figure 1, b).

(d) Along with the gradual crack growth and the rupture of the tongue tip, ridges are formed, leading to a sawtooth profile on the rubber surface. Such a photograph can be found in Reference 2. As seen, the abrasion processes of rubber are involved not only the crack growth via mechanical fatigue, but also the rupture of tongue tip resulting from tensile stress. Moreover, the latter is the proximate cause of the loss of material.

#### Mathematic Description of the Processes of Rubber Abrasion

A physical model of rubber abrasion in unsteady state and the corresponding processes of tongue ruptured are shown in Figures 2 and 3 respectively. As seen from Figure 3,

$$\tan\theta = \frac{\Delta y_1}{\Delta x_1} = \frac{\Delta y_2}{\Delta x_1 + \Delta x_2} = \dots = \frac{\Delta y_i}{\sum \Delta x_i}, \quad (1)$$

then

$$\Delta y_i = \sum \Delta x_i \tan\theta \quad (i = 1, 2, \dots) \quad (2)$$

For a given material and constant frictional force, the angle  $\theta$  can be considered as a constant approximately. Thus,

$$\Delta y_i \propto \sum \Delta x_i \quad (3)$$

However, in light of the physical processes stated above, the thickness of tongue is unchangeable once steady state has been reached. At this point, assuming that  $N$  represents the number of revolutions to attain steady state, the rupture thickness of tongue can be deduced from Figure 2:

$$\Delta y_N \cong N \cdot r \sin\theta \quad (4)$$

Apparently, the magnitude of the rupture thickness of tongue has a maximum which is given by

$$\Delta y_{\max} = \bar{F}/\sigma_b \quad (5)$$

In order to describe the process of the rupture of tongue tip precisely, a technical term, tensile rupture ratio, is introduced and defined as a ratio of the rupture length of the tongue tip to the original length of the tongue (Figure 2). Thus,

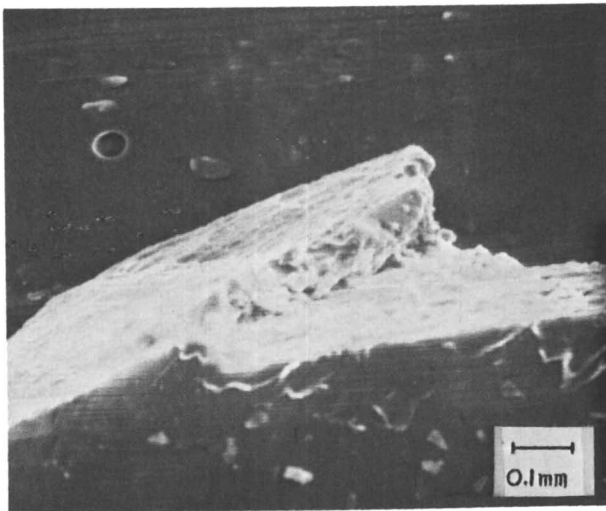
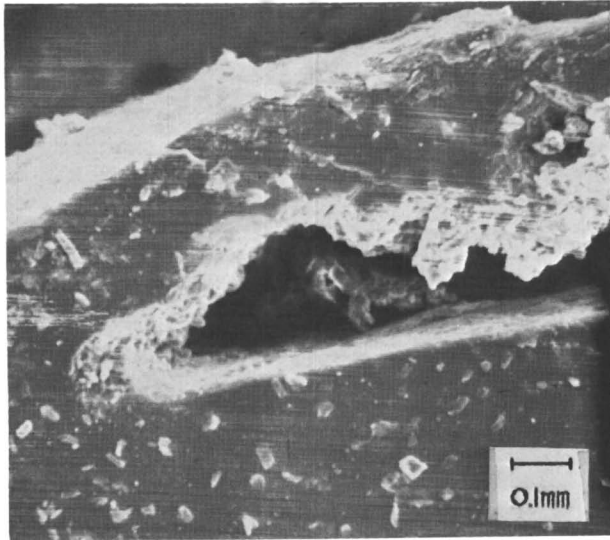


Figure 1. Formation of ridge from filled NBR,  $W = 1.5 \text{kJ/m}^2$  (100x): (top) tongue formed; (bottom) tongue ruptured.

$$\xi_K = \Delta x_i / l_i \tag{6}$$

As seen from Equations (3), (5) and (6), the tensile rupture ratio can be roughly considered to be directly proportional to the frictional force and inversely proportional to the tensile strength:

$$\xi_K \propto \bar{F} / \sigma_b \tag{7}$$

Therefore, it is supposed to be a constant for a given material and constant frictional force. Under the circumstances,  $\Delta x_i$  is directly in proportion to  $l_i$ ; the length  $l_i$ , which mainly results from crack growth, increases with the number of passes of the blade only. Moreover, the crack growth per revolution (pass),  $r$ , is nearly a constant. Hence, the processes of rupture of the tongue tip can be described as follows:

Since,

$$l_i = ir - \sum_{i=1}^{i-1} \Delta x_i, \quad \Delta x_0 = 0,$$

then, after the 1st pass ( $i = 1$ ),

$$\Delta x_1 = l_1 \xi_K = r \xi_K,$$

after the 2nd pass ( $i = 2$ ),

$$\Delta x_2 = l_2 \xi_K = (2r - \Delta x_1) \xi_K = 2r \xi_K - r \xi_K^2,$$

.....

after the  $i$ th pass ( $i = i$ ),

$$\begin{aligned} \Delta x_i &= l_i \xi_K = [ir - (\Delta x_1 + \dots + \Delta x_{i-1})] \xi_K \\ &= ir \xi_K - [(i-1) + \frac{(i-1)(i-2)}{2!}] r \xi_K^2 \\ &\quad + [\frac{(i-1)(i-2)}{2!} + \frac{(i-1)(i-2)(i-3)}{3!}] r \xi_K^3 - \dots \end{aligned} \tag{8}$$

Thus,

$$\Delta x_i = \phi(i) \quad (i = 1, 2, 3, \dots) \tag{9}$$

According to the analysis above, the sum of rupture length of a tongue after  $N$  revolutions will be given by

$$\begin{aligned} \sum_{i=1}^N \Delta x_i &= Nr \xi_K \left\{ \frac{1}{2} (N+1) - \left[ \frac{(N-1)}{2!} + \frac{(N-1)(N-2)}{3!} \right] \xi_K \right. \\ &\quad \left. + \left[ \frac{(N-1)(N-2)}{3!} + \frac{(N-1)(N-2)(N-3)}{4!} \right] \xi_K^2 - \dots \right\} \\ &= Nr \xi_K f_o(N, \xi_K), \end{aligned} \tag{10}$$

$$f_o(N, \xi_K) = \frac{1}{2}(N+1) - \left[ \frac{(N-1)}{2!} + \frac{(N-1)(N-2)}{3!} \right] \xi_K$$

$$+ \left[ \frac{(N-1)(N-2)}{3!} + \frac{(N-1)(N-2)(N-3)}{4!} \right] \epsilon_K^2 - \dots \tag{11}$$

As for the sum of the volume loss of a tongue after N revolutions, as seen by Figure 3, it can be determined by

$$V_N = \frac{1}{2} \Delta y_N h \sum_{i=1}^N \Delta x_i = \frac{1}{2} N r \epsilon_K f_o(N, \epsilon_K) \Delta y_N h \tag{12}$$

Wear Curve: Description of General Process of Rubber Abrasion

From the physical processes of rubber abrasion and its mathematic description, it can be deduced that a general process of rubber abrasion might be regarded as consisting of three stages and expressed correspondingly in terms of a wear curve (Figure 4):

1. first stage ( $t = 0-t_1$ ), unsteady state (wear in)

$$\Delta x_i < r = \text{const} \tag{13}$$

$\Delta x_i, \Delta y_i$  and A are increased gradually.

2. second stage ( $t = t_1-t_2$ ), steady state (normal wear)

$$\Delta x_i = r = \text{const} \tag{14, a}$$

$$\Delta y_i = \Delta y_N \leq \Delta y_{\text{max}} = \text{const} \tag{14, b}$$

$$A = \text{const}$$

3. third stage ( $t > t_2$ ), damage (accident wear)

$$\Delta x_i = r \neq \text{const}$$

$\Delta x_i, \Delta y_i, r$  and A are increased steeply.

The figure of this theoretical wear curve is coincident with that one of an experimental curve of the abrasion process (Figure 5).

Wear Equations

In general, the ridges are uniformly distributed on the whole cylindrical surface of the testing rubber wheel (2). In the early (unsteady) stage of rubber abrasion, according to the experimental observation(5) and the physical processes stated above, the spacing of ridges is approximately equal to the crack growth taking place during the development of wear. Thus, we have

$$S_i \cong ir \tag{15}$$

Hence, an equation for the amount of wear per revolution from 0 to N revolutions (i.e.,  $i = N$ ) can be derived as follows

$$A = \frac{2\pi R}{S} \cdot \frac{V_N}{N} = 2\pi R h \tag{m/rev} \tag{16}$$

where,

$$\bar{S} = \sum_{i=1}^N S_i / N \cong S_N / 2 \tag{17}$$

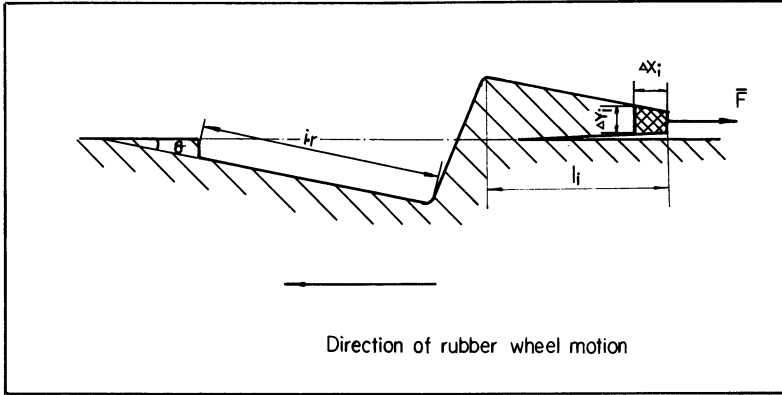


Figure 2. Physical model of rubber abrasion

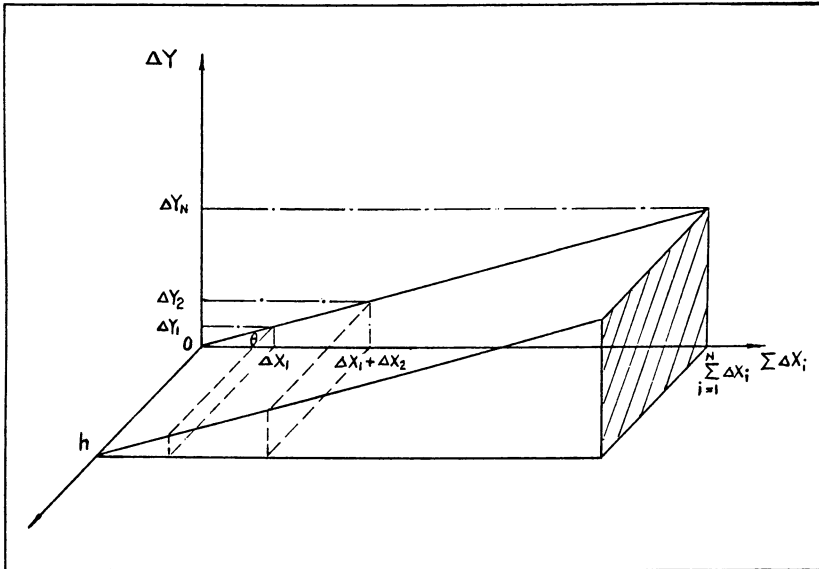


Figure 3. Rupture process of a tongue



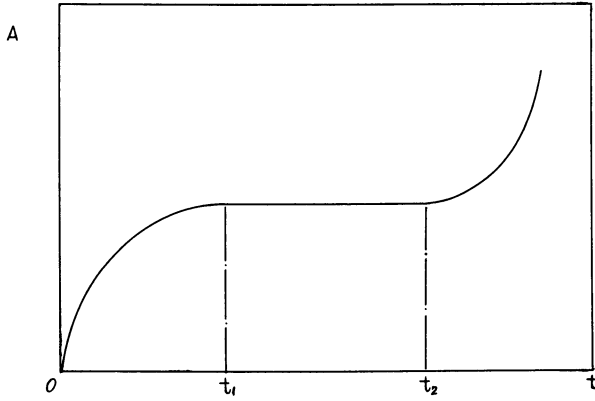


Figure 4. Theoretical wear curve.

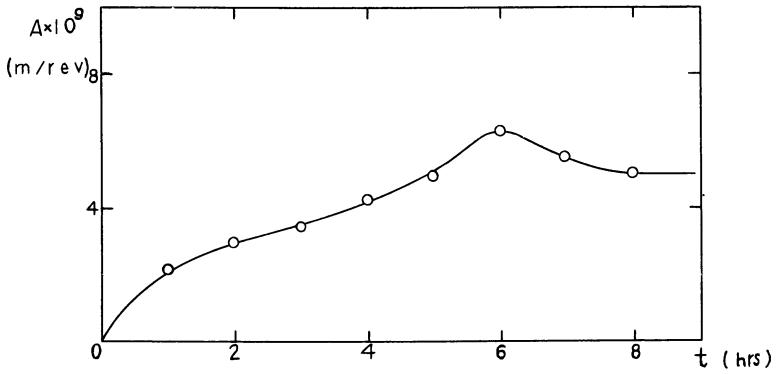


Figure 5. Experimental wear curve of filled NBR ( $W = 0.62 \text{kJ/m}^2$ ).

As seen,

$$S_N = Nr \quad (18)$$

Thus,

$$\bar{S} \approx Nr/2 \quad (19)$$

Inserting Equations (12), (19), and (4) into Equation (16), we have

$$A = r \sin \theta \mathcal{E}_K f_o(N, \mathcal{E}_K) \quad (\text{m/rev}) \quad (20)$$

According to Reference 2, the crack growth per revolution,  $r$ , is given approximately by

$$r \approx B(2\bar{F})^\alpha \quad (21)$$

Then

$$A = B(2\bar{F})^\alpha \sin \theta \mathcal{E}_K f_o(N, \mathcal{E}_K) \quad (\text{m/rev}) \quad (22)$$

This is the wear equation of rubber abrasion in unsteady state. Assuming that the steady state has been reached when the number of revolution is equal to  $N$ , on the basis of Equations (14, a) and (14, b), the sum of volume loss of a tongue after another  $N$  revolutions, i.e., from  $N$  to  $2N$  revolutions, can be calculated by

$$V_N = Nr \Delta y_N h \quad (23)$$

As for the equation of steady-state rate of wear, it is about the same as Equation (16):

$$A = \frac{2\pi R}{S} \cdot \frac{V}{N} / 2\pi R h \quad (\text{m/rev}) \quad (24)$$

However, in this equation, the spacing of ridges is  $S$  instead of  $\bar{S}$  as it is considered to be unchanged only if the frictional force is kept constant. Obviously, in this case,  $S = S_N$ . Inserting Equations (18), (23), (4), and (21) into the equation above, the wear equation of rubber abrasion in steady state is given by

$$A = B(2\bar{F})^\alpha \sin \theta \quad (\text{m/rev}) \quad (25)$$

This equation is identical to that obtained by Southern and Thomas (2).

Comparing Equation (22) with Equation (25), as will be readily seen, the term,  $\mathcal{E}_K f_o(N, \mathcal{E}_K)$ , is the characteristic of rubber abrasion in unsteady state. It can be termed characteristic function of unsteady state, denoted  $\eta(N, \mathcal{E}_K)$ . Thus,

$$\eta(N, \mathcal{E}_K) = \mathcal{E}_K f_o(N, \mathcal{E}_K) \quad (26)$$

Inserting this function into Equation (22) gives

$$A = \eta(N, \mathcal{E}_K) B (2\bar{F})^\alpha \sin\theta \quad (\text{m/rev}) \quad (27)$$

Making a comparison between Equations (25) and (27), it is known that the value of characteristic function is always less than unity and approaches unity as a limit in the unsteady-state process of wear according to the theoretical wear curve (Figure 4) and the experimental results (4,5) (Figure 6). Apparently, it is a mark to transfer unsteady state into steady state that  $\eta(N, \mathcal{E}_K) = 1$ .

As seen from the wear Equations (25) and (27), in either cases, the wear rate is mainly dependent on the frictional force. This conclusion is in accordance with the results of a number of experimental studies (1-6) (Figures 6 and 7); moreover, Southern and Thomas pointed out that the exponent  $\alpha$  is equal to 2 at least for the steady-state rate of wear (2). As for the unsteady-state rate of wear, it increases as abrasion proceeds. This result is consistent with the experimental observation (Figure 8) (5).

After a steady state has been reached and the pattern has been fully developed, the scale of the abrasion pattern appears to be approximately proportional to the friction force for a given temperature, as described by Southern and Thomas (2), then

$$S = c\bar{F} \quad (28)$$

Inserting Equations (23), (28), (5), and (21) into Equation (24) the modification of the steady-state wear equation will be obtained

$$A = K(2\bar{F})^\alpha / \sigma_b \quad (\text{m/rev}) \quad (29)$$

Evidently, the above equation reveals the basic correlation among the material property, running condition and wear characteristic, i.e., the wear rate is increased with an increase in the frictional force, and is inversely proportional to the tensile strength. Therefore, the experimental observation that particulate fillers, notably carbon black, reduce the wear rate of amorphous elastomers to a remarkable degree at room temperature (Figure 7) (4,6), might be explained as resulting from an increase in the tensile strength of amorphous elastomers.

#### Characteristic Function of Unsteady State

There are two independent variables in the characteristic function of unsteady state, i.e., the number of revolutions and the tensile rupture ratio. The effect of the number of revolutions on unsteady-state rate of wear is obvious as seen by Figure 8 (5). However, the influence of the tensile rupture ratio on wear rate is still not established.

According to the results of numerical calculation of Equation (26) on condition that  $r = 1$ , two sets of function curve have been obtained (Figures 9 and 10). Obviously, the value of the characteristic function increases with an increase in the number of revolutions when  $\mathcal{E}_K$  is constant (Figure 9). It is in agreement with the experimental observation of the abrasion process in unsteady state (Figure 8).

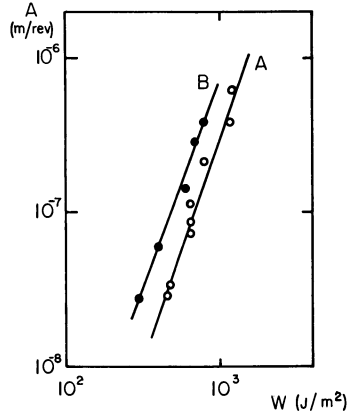


Figure 6. Wear rate of unfilled NR plotted against frictional work: (A) unsteady state (0-1000 rev); (B) steady state (data taken from Reference 4)(5).

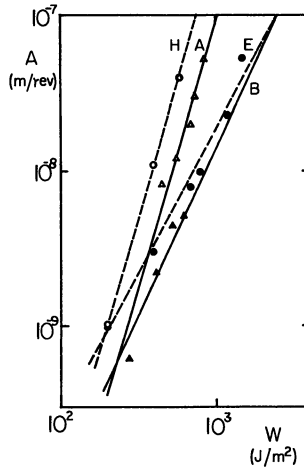


Figure 7. Steady-state rate of wear plotted against frictional work: (A) unfilled NBR; (B) filled MBP; (H) unfilled PB and (E) filled PB (data taken from Reference 4)(6).

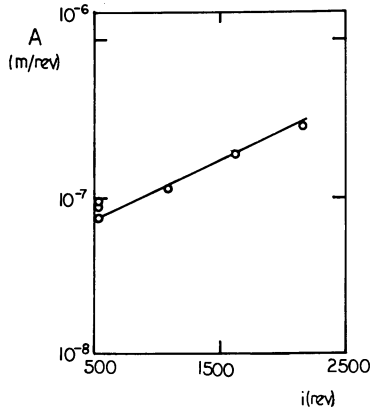


Figure 8. Unsteady-state rate of wear of unfilled NP plotted against the number of revolutions (5).

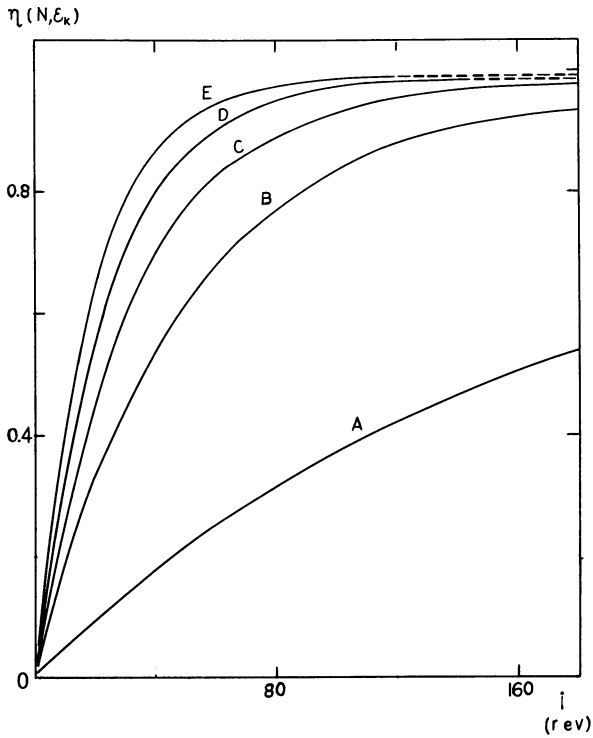


Figure 9. Characteristic function plotted against the number of revolutions: (A)  $\epsilon_K = 0.01$ ; (B)  $\epsilon_K = 0.02$ ; (C)  $\epsilon_K = 0.03$ ; (D)  $\epsilon_K = 0.04$ ; (E)  $\epsilon_K = 0.05$ .

As seen in Figure 10, the larger the tensile rupture ratio, the larger the value of the characteristic function is, and, the earlier the steady state is reached (Figure 9). It is also supported by the experimental observation that the larger the frictional force, the earlier the ridges appeared.

Besides, as shown in Figure 9, the slope of the curve is a steep rise along with an increase in the tensile rupture ratio. Hence, the fact that the unsteady-state rate of wear of unfilled NBR is much more sensitive to the number of revolutions than that of filled NBR would be ascribed to the difference in tensile strength or in tensile rupture ratio, i.e., the tensile strength of unfilled NBR is less than that of filled NBR, in other words, the tensile rupture ratio of unfilled NBR is much more than that of filled NBR.

### State Criterion of Rubber Abrasion

In general, the number of revolutions corresponding with the critical point to transform the wear state from unsteady to steady, is a constant under otherwise identical conditions. Hence, it can be considered as a state criterion of rubber abrasion, then

1.  $i < N$  unsteady state
2.  $i \geq N$  steady state

On the basis of the physical processes and mathematic description of rubber abrasion stated above, a theoretical relationship between  $N$  and  $\epsilon_K$  can be obtained through the use of numerical calculation under the condition of  $\Delta x_i = r$ , as shown in Figure 11. Moreover, it can be approximately represented as follows

$$N = 1.2\epsilon_K^{-0.9} \quad (30)$$

Evidently, the higher the tensile rupture ratio, the lower the value of the state criterion is. Thus, this state criterion can be applied to estimate the wear characteristics of different elastomers under similar running conditions.

### Conclusions

The physical process during dry abrasive wear is a gradual tearing leading to not only the crack growth but the rupture of tongue tip as well. It can be described mathematically through the medium of introducing a concept of tensile rupture ratio.

A wear curve can be used to describe the general process of rubber abrasion, in which it is divided into three regions: unsteady, steady and damage stage.

The wear equation of rubber abrasion in steady state reveals the basic correlation among the material property, running condition and wear characteristic. The wear rate increases with an increase in the frictional force, however, it is inversely proportional to the tensile strength.

The characteristic function,  $\eta(N, \epsilon_K)$ , is a characterizing factor of rubber abrasion in unsteady state. Its value increases with an increase in the number of revolutions and tensile rupture ratio. However, it approaches unity as a limit in the unsteady-state process of wear. Hence, a steady state is reached if once  $\eta(N, \epsilon_K) = 1$ .

Publication Date: September 12, 1985 | doi: 10.1021/bk-1985-0287.ch013

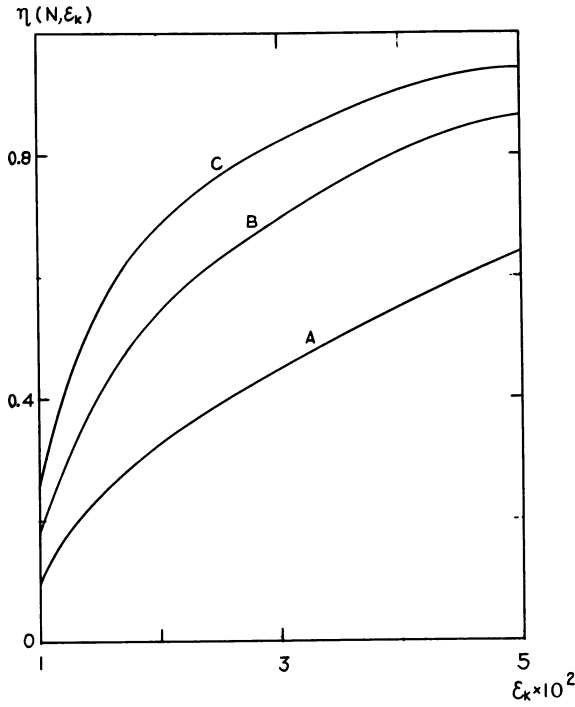


Figure 10. Characteristic function plotted against tensile rupture ratio: (A)  $i = 20$  rev; (B)  $i = 40$  rev; (C)  $i = 60$  rev.

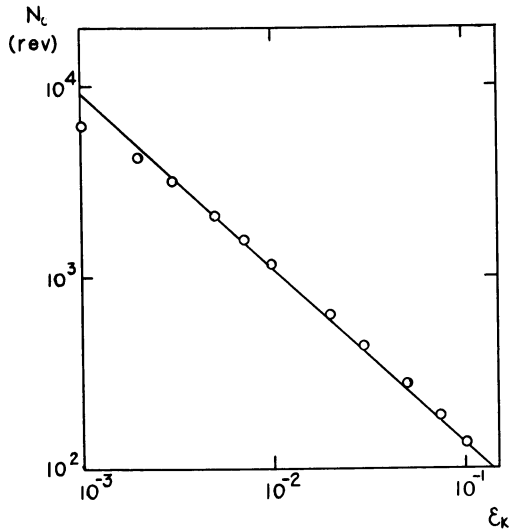


Figure 11. State criterion of rubber abrasion plotted against tensile rupture ratio ( $r = 1.0$ ).

The number of revolutions transformed the wear state from unsteady to steady can be regarded as a state criterion of rubber abrasion to estimate the wear characteristics of rubber under identical running conditions. It was found to be proportional to a negative exponent of the tensile rupture ratio.

It is concluded that the theory proposed can be applied to clarify the phenomena and processes of rubber abrasion in different stages of wear by a line contact.

### Acknowledgments

The author is indebted to Mr. J. A. Hartwell for experimental assistance, to Mr. H. F. Bai for computer assistance, and to Professor A. N. Gent for his encouragement and advice at the Institute of Polymer Science, The University of Akron. Also, the author is grateful to Professor K. C. Ludema for his much helpful comments on the draft manuscript at The University of Michigan.

### Legend of Symbols

A	linear wear rate
$\frac{B}{F}$	crack-growth constant
F	frictional force per width
K	coefficient
N	state criterion, the number of revolutions to transform the wear state from unsteady to steady
R	radius of testing rubber wheel
$\frac{S}{S}$	spacing of ridges
S	average spacing of ridges
$V_{\text{a}}$	sum of abraded volume of a tongue after N revolutions
W	frictional work
c	proportionality constant
h	width of tongue (testing rubber wheel)
i	number of revolutions (passes)
l	length of tongue
r	crack growth per revolution
t	time
$\Delta x$	rupture length of tongue
$\Delta y$	rupture thickness of tongue
$\alpha$	crack-growth constant
$\theta$	angle showing the direction of crack growth
$\sigma_b$	tensile stress at break
$\xi_K$	tensile rupture ratio
$\eta(N, \xi_K)$	characteristic function of unsteady state

### Literature Cited

1. Champ, D. H.; Southern, E.; Thomas, A. G. In "Advances in Polymer Friction and Wear"; Lieng-huang Lee, Ed.; Plenum: New York and London, 1974; p. 133
2. Southern, E.; Thomas, A. G. Rubber Chem. Technol. 1979, 52, 1008.
3. Gent, A. N.; Pulford, C. T. R. J. Mater. Sci. 1979, 14, 1301.
4. Gent, A. N.; Pulford, C. T. R. J. Appl. Polym. Sci. 1983, 28, 943.



5. Zhang, S. W. 'Mechanisms of rubber abrasion in unsteady state', Rubber Chem. Technol., to be published.
6. Zhang, S. W. 'Investigation of Abrasion of Nitrile Rubber', Rubber Chem. Technol., to be published.
7. Schallamach, A. J. Polymer Sci. 1952, 9, 385.
8. Schallamach, A. Proc. Phys. Soc. 1954, B67, 883.
9. Schallamach, A. Wear 1957/1958, 1 384.

RECEIVED January 23, 1985

## Molecular Features of Transfer Fragments When High-Density Polyethylene Rubbed Against Metals

V. A. Belyi and V. V. Nevzorov

Institute of Mechanics of Metal-Polymer Systems, Byelorussian S.S.R. Academy of Sciences, Gomel, U.S.S.R.

The method of thermal deposition of polymers is suggested for studying molecular weight distribution (MWD) of polyethylene transfer products. The method allows recording variations in the molecular characteristics of PE transfer products and evaluating the amount of the polymer taken from the metallic surface with a solvent using the light-scattering data. By analysing the variations in the integral and differential MWD-curves for the original PE and its transfer products, the peculiarities of wear and transfer for the polymer sliding against steel ( $R_a = 0.04 \mu\text{m}$ ) have been studied as influenced by loads and sliding velocities, chemical nature of the organic additives present in the polymer, and the counterface metal. The results obtained helped to substantiate the ways of wear control for polyethylene in terms of transfer.

Rubbing of polymers against metals is known to cause the changes in molecular weight of macromolecules. In the first place, and to a larger extent, changes take place in polymer fragments that transfer onto metals. Those fragments are the most changeable portion in a tribological system (1 - 3). Study of changes in molecular features of these fragments, on the one hand, leads to a better understanding of the orientation of physico-chemical processes within the metal-polymer rubbing zone during dry friction, and on the other hand, it allows the establishment of relations between the transfer process and the wear of polymers, which is of importance today.

Despite numerous investigations in the field of polymer wear, there is no unity of opinions on the wear process as related to the transfer of polymers onto metals because of inadequate knowledge of the structure and physical properties of the transfer fragments. In this paper the structure and

physical properties of transfer fragments mean the data accumulated on the distribution of polymers over metallic surfaces, weight of the transferred fragments, molecular weight distribution (MWD) and average molecular weights.

The data available on the degree of crystallinity, initiation of orientation in transfer fragments and mode of transfer, be it patch-like or film-like, do not give a proper idea of the structure and physical properties of the transferred particles; besides, they do not lead to the understanding of the features and orientation of physico-chemical processes resulting from rubbing and occurring at a molecular level in the transfer fragments. The establishment of the orientation in the dispersion process of the transfer fragments macromolecules would provide adequate knowledge of the transfer and wear mechanisms, it would also make it possible to find ways of improving friction characteristics of metal-polymer friction pairs.

### Experimental

Engineering thermoplastic polymers are usually polydispersed. Therefore changes in the molecular characteristics of the transfer and wear products have been studied by using integral curves of molecular weight distribution. The authors applied the procedure of polymer thermal deposition to studying MWD of HDPE transfer and wear products (4, 5). MWD characteristics of the transfer and wear products were analyzed according to the results of thermal deposition of highly diluted HDPE solutions (1 to  $5 \cdot 10^{-4}$  g/dl). Diphenyl oxide served as the  $\theta$  - solvent. Highly diluted polymer solutions were deposited using a device for polymer thermal oxidation (TOP-1, USSR) in the automatic regime when the solution was cooled at a rate of 1 deg./min. The intensity of the scattered light was measured at a  $20^\circ$ -angle with a green filter adjusted ( $\lambda = 0.550 \mu\text{m}$ ; absorption coefficient = 40%; and pass band  $\Delta \lambda = 0.013 \mu\text{m}$ ). Temperature curves of the light scattered by HDPE solutions were replotted to obtain MWD integral curves by using Flory - Huggins equation(5):

$$\frac{1}{T_i} \approx \frac{1}{\theta} \left( 1 + \frac{B}{\sqrt{M_i}} \right)$$

where  $M_i$  is the molecular weight of an i-polymer fraction,  $T_i$  and  $\theta$  are the deposition temperatures of an i-polymer molecular weight and of an infinitely large polymer molecular weight, and  $B$  is the constant for HDPE - diphenyl oxide system.

To estimate the amount of the polymer transferred onto the metal a master curve was drawn based on the light scattering results obtained for solutions of given HDPE concentrations.

Friction tests were performed on HDPE film specimens according to the schematic "shaft - partial bearing" under

the loads of up to 0.5 MPa at sliding velocities of up to 0.5 m/s. Steel rollers ( 40 mm in diameter ) served as a model shaft. The roller surfaces were polished with diamond paste to  $R_a = 0.04 \mu\text{m}$  and rinsed in benzene and acetone before tests.

### Results and Discussion

Effect of Rubbing Conditions. Study of the molecular characteristics of the fragments transferred at various loads and speeds showed considerable changes in HDPE molecular weight even during running-in ( test time was 1 h ) ( Fig. 1, Table I ).

It was found out that at the experimental conditions lower sliding velocities and higher loads caused greater shifts in the transfer product MWD curves to the lower molecular weight region ( Fig. 1 a, curves 1 to 3 ).

Analysis of the shape of  $q_w$ -MWD differential curves ( Fig. 1 b ) gave interesting results.  $q_w$  Curves were obtained by graphic differentiation of MWD integral curves.  $q_w$ -Curves for the original HDPE closely resembled unimodal ones ( Fig. 1 b, 1 ), while for the transfer products they may appear bimodal or trimodal depending on test conditions ( Fig. 1 b, 2 and 3 ). Changes in modality of  $q_w$ -curves are caused by dispersion, branching and increase in molecular weight of macromolecules in the transferred particles defined by the characteristics of mechanical and chemical processes in the course of rubbing.

Table I. Effect of Rubbing Conditions on Molecular Characteristics of HDPE Transfer Fragments

Parameters	Sliding Velocity, m/s						Original HDPE
	0.1		0.25		0.5		
	Load, MPa						
	0.1	0.5	0.1	0.5	0.1	0.5	
* $M_w \cdot 10^{-3}$	32	28	28	38	42	35	54
* $M_n \cdot 10^{-3}$	27	18	18	27	27	22	28
$M_w / M_n$	1.2	1.6	1.6	1.5	1.5	1.6	1.9
Weight of transfer fragments, $\text{mg} \cdot 10^3$	2.9	4.8	6	9.7	9.6	49.5	-
Coefficient of friction	0.4	0.35	0.4	0.4	0.4	0.4	-

\*  $M_w$  and  $M_n$  are the weight-average and number-average molecular weights

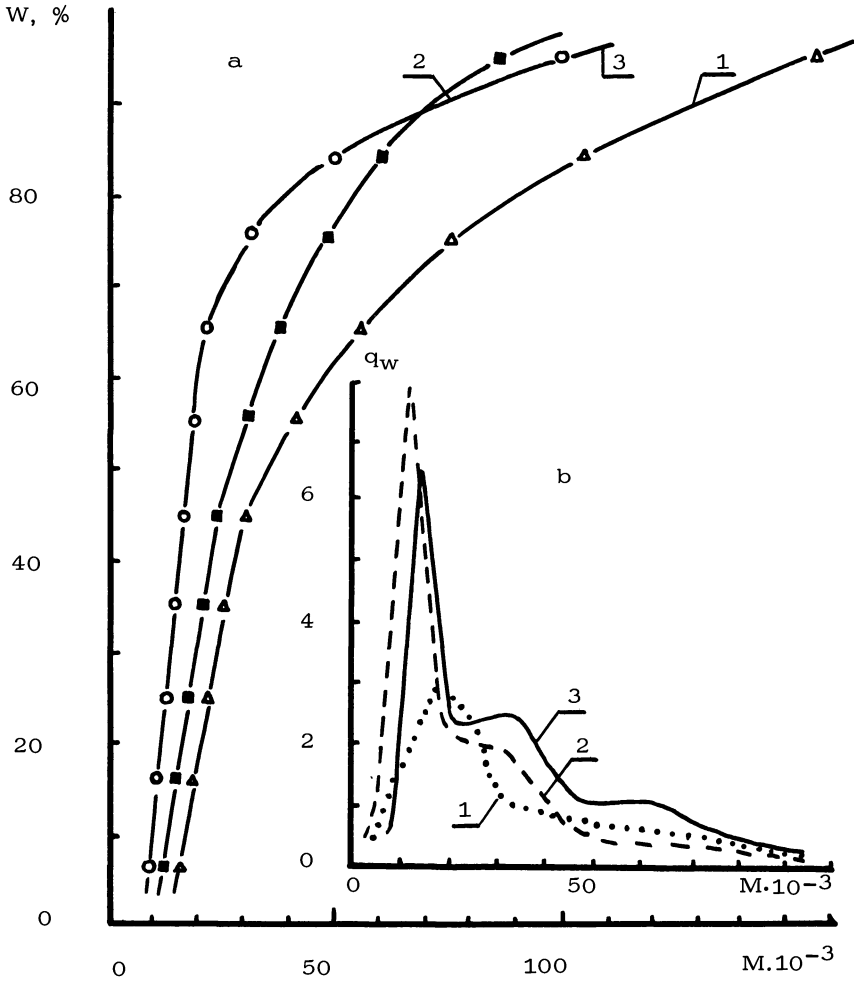


Figure 1. Molecular characteristics of HDPE (1) and fragments transferred onto steel at a sliding velocity of 0.1 m/s and loads of 0.1 MPa (2) and 0.5 MPa(3). a) MWD integral curves. b)  $q_w$ - MWD differential curves.

$q_w$ -Curves allow a qualitative estimation of the variations in weight fractions of macromolecules of various molecular weights with regard to rubbing conditions. The transferred particles demonstrated an increase in the weight fraction of macromolecules of  $1 \times 10^4$  to  $1.2 \times 10^4$  molecular weights as compared to the original HDPE ( Figs. 1 b, 2 and 3 ). The higher the load within the rubbing zone the greater the weight fraction ( peak intensity in the  $q_w$ -curve ). New peaks in  $q_w$ -curves for molecular weights of  $3 \times 10^4$  and  $5.5 \times 10^4$  indicate that besides macromolecular dispersion branching and molecular weight increase may take place on the rubbing surface resulting from macroradical recombination and chain breaking.

Variations in the HDPE molecular features such as  $M_w$  and  $M_n$  and MWD integral curves depend mainly on the mode of transfer.

At a sliding velocity of 0.1 m/s patch-like transfer was observed that roughened the metallic surfaces. The size of the polymer patches transferred onto metal increased with load which intensified macromolecular dispersion ( Figs. 1 to 3, Table I ).

Macromolecular dispersion in HDPE with patch-like transfer is defined by polymer-metal and polymer-polymer adhesive interactions. The major contribution to macromolecular dispersion is from the alternating areas of polymer-polymer and metal-polymer contacts. Macroradicals generated within polymer-polymer contact may recombine on the metallic surface to form chemisorption and coordination complexes with an oxide film<sup>6</sup>. Under the dynamic contact this process may increase the effect of mechanical actions on the macromolecular dispersion of polyolefine.

At a sliding velocity of 0.5 m/s under the environmental conditions film-like transfer took place which caused a decrease in macromolecular dispersion as compared to the patch-like mode of transfer ( Table I ). At a load of 0.5 MPa  $M_w$  and  $M_n$  dropped by 48 % and 37 % for patch-like transfer at a sliding velocity of 0.1 m/s, and by 35 % and 23 % for film-like transfer at a sliding velocity of 0.5 m/s.

It should be noted that the polydispersion ratio does not, in fact, depend upon rubbing conditions and in most cases it maintains the values of 1.5 to 1.6 ( Table I ).

The data given in the paper on HDPE macromolecular dispersion based on rubbing conditions allow a conclusion that the degree of dispersion depends mainly on load. Effect of velocity on this process is indirect and related to the transfer mode or to the ratio of the metal-polymer and polymer-polymer contact areas. If the metal-polymer contact area is predominant this leads to intensification of macromolecular dispersion.

The microscopy revealed large films of polymer particles attached to the transferred film surfaces. It was found out that these particles might have been resulted from the adhesive sticking between the transferred films and the polymer. In terms

of wear this process may increase HDPE wear rate when the attachment of particles is slight, otherwise wear rate decreases due to the retention of particles within the rubbing zone and increase in the transfer film thickness.

The steel surfaces with transfer fragments rinsed in boiling solvent (toluene and xylene) exhibited stable brown patches (up to 5  $\mu\text{m}$  in size) of the polymer. Strong attachment of the retained transfer fragments to the polished steel may be due to mechanical interaction and chemical bonding. The incomplete solution of the transfer fragments is also indicative of the possible crosslinkage of HDPE macromolecules at the initial stage of transfer.

### Active Additives

Mechano-chemical processes that are essential for HDPE macromolecular dispersion were defined by analyzing MWD of the transfer fragments of polyolefine-based composites doped with active additives (5 wt.%), such as antioxidant (Neozone D), aromatic compound (anthracene) and metal salt (zinc stearate). Effect of the active additives on molecular features and certain friction characteristics of HDPE (load = 0.5 MPa; sliding velocity = 0.25 m/s) is shown in Table II.

Table II. Effect of Active Additives on Molecular and Friction Characteristics of HDPE Transfer Fragments

	Original HDPE		HDPE +Zinc Stearate		HDPE + Neozone D		HDPE + Anthracene	
			R u b		b i n g			
	Before	After	Before	After	Before	After	Before	After
$M_w \cdot 10^{-3}$	54	41	62	35	76	68	56	45
Wear rate, mg/h	-	0.06	-	0.02	-	1.22	-	0.3
Coefficient of friction	0.4		0.2		0.4		0.4	

HDPE specimens doped with Neozone and anthracene exhibited higher wear rates ( by 20 and 5 times, respectively) than the original polyolefine ( Table II ). The microscopy found a great difference in the mode of transfer. With Neozone present within the rubbing zone, oriented polymeric film bands had been produced over the steel surface, while anthracene had given unoriented islands of large particles. In both cases the transferred particles were slightly attached to the metallic surfaces, which caused the high wear rates ( Table II ).

Slight attachment of the transferred particles to the metal allows a conclusion that inhibition of oxidation (Neozone) and relaxation (anthracene) of the HDPE transfer fragments macromolecules decrease the number of macroradicals capable of strong attachment to the steel surface. Transfer fragments undergo fewer deformation cycles and faster become wear debris. The molecular features of the above fragments have been found to correlate or to be superior to those of the original HDPE ( Fig. 2, curves 1, 3, and 4 ).

The incorporation of zinc stearate ( up to 5 wt.% ) into HDPE promoted the formation of the transferred films strongly attached to the steel surface, weakened the friction forces in the contact and led to a three-fold decrease in wear rates as compared to the original HDPE.  $M_w$  of the transfer fragments dropped by 45% (Table II). Low molecular weight fractions and zinc stearate of the rubbed surface caused weakening of the friction forces and decrease in the wear rate.

The experimental results obtained with the active additives promoted the following recommendations be derived about the substances that control the process of polymer transfer onto metals for optimizing unlubricated sliding regimes:

- The substance should not eliminate the adhesive interaction between the transfer fragments and the metal.
- The substance must be a lubricant for polymer-polymer contacts.
- The substance should provide intensive macromolecular dispersion in the transfer and wear products.

The molecular characteristics of the HDPE wear particles may be superior to or comparable with those of the transfer fragments. However, the test time ( from 2 to 8 h ) did not affect the values of  $M_w$  and  $M_n$  and MWD of the HDPE wear particles.

The origin of the metal influences undoubtedly the HDPE macromolecular dispersion. At a sliding velocity of 0.25 m/s and load of 0.5 MPa  $M_w$  of the transferred products decreased as compared to the original HDPE in the following way: in contact with steel - by 10%; with copper - by 12%; with aluminum alloy - by 30%. In contact with titanium a reverse process of the titanium oxide transfer onto the polymer was observed.

### Conclusions

Thus, the new method for studying the molecular characteristics of the thermoplastic polymer transfer and wear products makes it possible to establish the orientation of mechano-chemical processes in the rubbing zone and to find ways of dispersion and wear control. The method also enables the wear mechanisms of antifriction polymers to be studied in terms of the transfer phenomena.



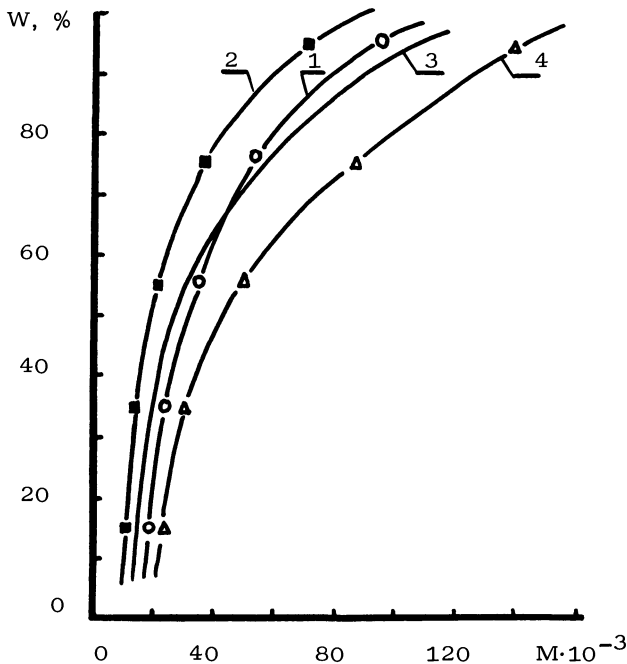


Figure 2. Molecular characteristics of the transfer products of the original HDPE (1) and composites thereof doped with : 5%-wt. zinc stearate (2); 5%-wt. anthracene (3); 5%-wt. Neozone D (4).

#### Literature Cited

1. Balakhanov, T. S., Babaev, A. G.; Guseinov, A. B.; Mustafaev, V. A., " On Solids Friction"; Nauka i Tekhnika: Minsk, 1971; pp. 407-414.
2. Kragelskii, I. V., Mekhanika Polimerov, 1972, No.5, pp.793-809.
3. Sviridyonok, A. I. ; Savkin V. G., Friction and Wear (Trenie i Iznos), 1981, 1, No. 1, pp. 150 - 167.
4. Belgovskii, I. M., Goldberg, V. M., ; Krasotkina, I. N.; Toptygin, D. Ya., Doklady AN SSSR (Reports of USSR Academy of Sciences), 1970, 192, No. 1, pp. 121 - 122.
5. Goldberg, V. M., Belgovskii, I. M.; Izyumnikov, A. L. , Vysokomolekul. Soedinenia (High Molecular Weight Compounds), 1971, 13A, No. 4, pp. 977 - 981.
6. Krylov, O. V.; Kiselev, V. F., "Adsorption and Catalysis on Transition Metals and Oxides Thereof"; Khimia: Moscow, 1981.

RECEIVED January 23, 1985

## Penetration of Metallic Femoral Components into Polymeric Tibial Components Observed in a Knee Joint Simulator

D. Dowson<sup>1</sup>, B. J. Gillis<sup>2</sup>, and J. R. Atkinson<sup>3</sup>

<sup>1</sup>Department of Mechanical Engineering, Institute of Tribology, The University of Leeds, Leeds LS2 9JT, United Kingdom

<sup>2</sup>Adelaide Brighton Cement Ltd., Birkenhead, South Australia

<sup>3</sup>Department of Metallurgy, The University of Leeds, Leeds LS2 9JT, United Kingdom

The major factors limiting the effective life of a total replacement synovial joint are loosening of one or more of the prosthetic components, a variety of medical problems (e.g. infection) and wear. Most internal prostheses now consist of metallic and polymeric components and it is the penetration of the former into the latter which is the subject of this paper.

A knee joint simulator designed to evaluate the mechanical and tribological characteristics of total replacement knee joints will be described. Measurements of penetrations of metallic femoral components into the polymeric tibial components by means of dual index holographic contouring will be presented and the findings compared with observations from detailed studies of wear in well-controlled laboratory machines and the limited evidence of in-vivo performance of replacement knee joints.

The development of satisfactory total replacement synovial joints is sometimes described as the major advance in orthopaedic surgery in recent times. The hip joint was the first major load bearing joint to respond to the efforts of surgeons, engineers and materials scientists in the past two decades to develop satisfactory replacements, but attention is now focussed upon the more complex knee joint.

Most total replacement joints consist of a metallic and a polymeric component, although alternative materials such as ceramics and carbon reinforced materials are currently being examined for this role. The life of a prosthesis is thus directly affected by the rate of penetration of the metallic component into the polymeric component and this has prompted considerable interest in the subject of wear of polymers in the hostile environment of the body.

When polytetrafluoroethylene (PTFE) was introduced in the early 1960's the life of total replacement hip joints was limited to about three years by the poor wear characteristics of the polymer. When ultra-high molecular weight polyethylene (UHMWPE) replaced PTFE, the rate of penetration of the metallic component into the polymeric component was reduced to such an extent that loosening emerged as a major aspect of prosthetic life. There is, nevertheless, a need to pursue studies of the wear of prosthetic materials to facilitate the development of satisfactory materials which can be used with confidence in long-life prostheses.

A knee joint simulator was designed and built in the bio-engineering laboratory at Leeds in the late 1970's to enable the mechanical and tribological characteristics of current and projected knee joint replacements to be assessed. The simulator has been described by Dowson et al<sup>(1)</sup> and it is shown in Figure 1. Realistic load and motion cycles are applied to the knee joints to simulate any desired activity, but usually walking, and the penetration of the metallic femoral components into the polymeric tibial components after a large number of cycles can then be used to assess the life of the joints. Furthermore, the penetrations recorded, which include both wear and creep, can be related to results of laboratory wear studies of the behaviour of UHMWPE and to the in-vivo performance of total replacement knee joints. The simulator is therefore an important machine in both the pragmatic and fundamental aspects of total replacement knee joint development.

Dual index holographic contouring has been used to record the nature and the extent of femoral penetration into worn polymeric tibial components tested on the knee joint simulator. The system is briefly described and results are presented for two different forms of prostheses.

Wear factors based upon at least  $10^6$  cycles have been derived from the overall penetrations recorded in the simulator and compared with laboratory wear studies and a single result from in-vivo conditions.

### Apparatus and Experimental Technique

The Morrison<sup>(2)</sup> load cycles were applied to selected prostheses in the simulator shown in Figure 1. Cyclic loading patterns were applied in the Tibial Axis and A-P directions, the hydraulic mechanisms being controlled by a waveform synthesiser supplied with some 200 bits of information. The primary joint motion in flexion-extension was achieved by means of a cam driven rack-and-pinion system, while a low-friction self-aligning bearing arrangement on the upper, femoral, specimen holder allowed rotation about the A-P axis.

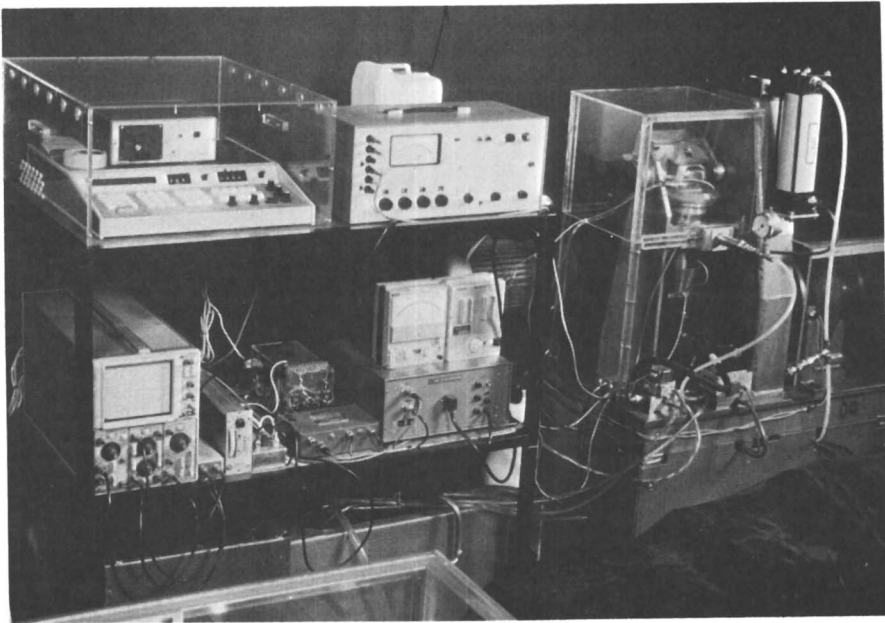
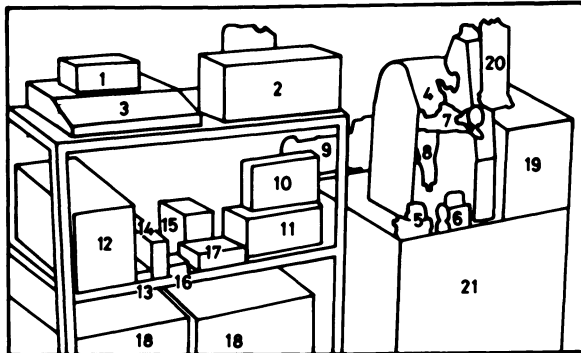


Figure 1a Knee Joint Simulator

b Key



- |    |                                  |    |   |
|----|----------------------------------|----|---|
| 1  | Tape Reader                      | 12 | Cathode Ray Oscilloscope                                |
| 2  | Peekel Strain measurement device | 13 | Filter  |
| 3  | Waveform Synthesiser             | 14 | Tibial Axis Carrier Frequency Amplifier                 |
| 4  | Joint Carriage and Holder        | 15 | Tibial Axis Power Amplifier and Power Pack              |
| 5  | Tibial Axis Servo Valve          | 16 | Tibial Axis Switching Box                               |
| 6  | A-P Axis Servo Valve             | 17 | A-P Axis Carrier Frequency Amplifier                    |
| 7  | A-P Axis Loading Cylinder        | 18 | 80L Oil Reservoir                                       |
| 8  | Tibial Axis Loading Cylinder     | 19 | Drive Shaft   |
| 9  | Drive Motor                      | 20 | Pressurised Oil Reservoir (A-P constant force cylinder) |
| 10 | Temperature Measurement Meters   | 21 | Pump Housing  |
| 11 | A-P Axis Power Amplifier         |    |   |

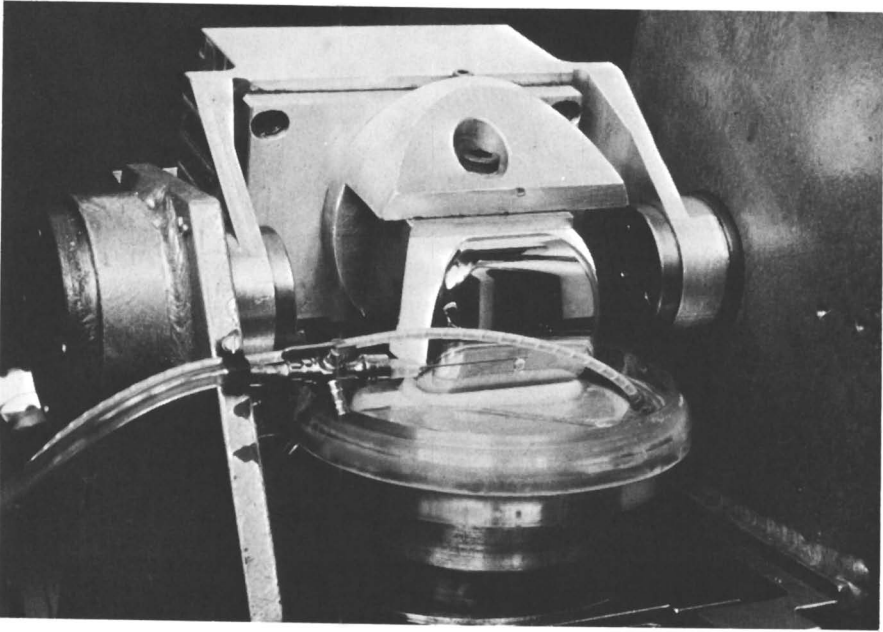


Figure 1(c) 'Freeman-Swanson' Prosthesis in Simulator.

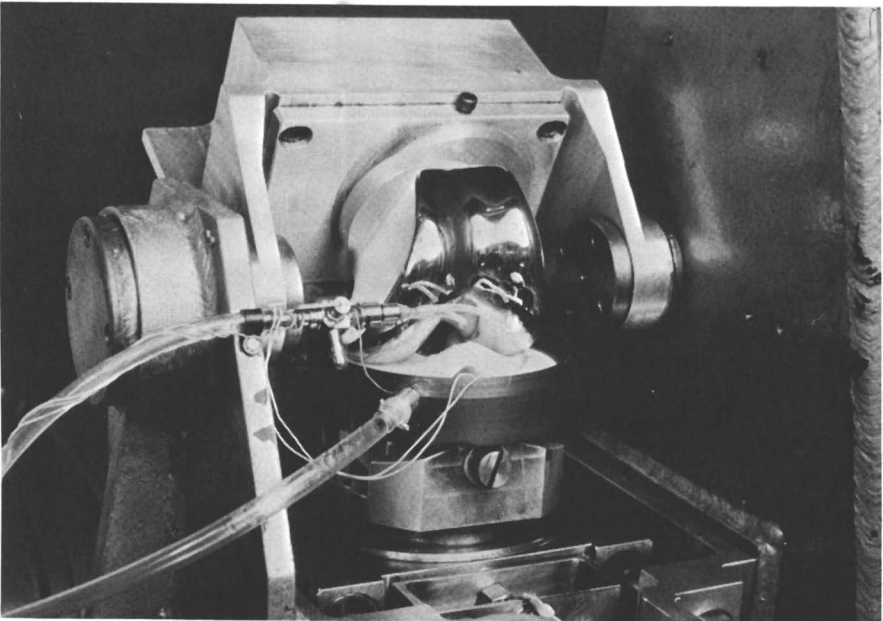


Figure 1(d) 'Leeds' Prosthesis in Simulator.

Reflective dual-index holography was used to measure the penetration of the metallic femoral component into the polymeric tibial component at the end of each test. The procedure produced contour maps of the images of the wear specimens before and after the wear process. The general arrangement of the measuring system is shown in Figure 2 and the authors gratefully acknowledge the advice and assistance made available by Dr. M.J. Lalor and Mr. J.T. Atkinson of Liverpool Polytechnic when the facility was established in Leeds. A 5-mW laser (L) and a rotational beam splitter (BS) were used, together with standard optical mirrors (M), spatial filters (S) and a convex collimating lens (C). The liquid cell (T) was fitted with an optical glass front and a peristaltic pump was used to change the immersion liquids. The two liquids used were ethanol or methanol or mixtures of both, depending upon the contour depth ( $\Delta h$ ) required. The contour depth is given by,

$$\Delta h = \frac{\lambda}{2|n_1 - n_2|}$$

where,

$\Delta h$  = contour depth increment

$\lambda$  = wavelength (laser beam)

$n_1, n_2$  = refractive indices of immersion liquids

The polymeric tibial components were coated with pure aluminium, some 100Å thick in a vacuum evaporation unit to improve the quality of the holographs. This film was removed in isopropyl alcohol before each wear test. Holographs of the 'unworn' and 'worn' tibial components were assessed and the volume of material removed (V) in a known period was estimated by simple geometrical procedures. The loading cycle enabled ( $\int PdX$ ) to be evaluated and an equivalent wear factor (k) was calculated from the relationship,

$$V = kN \int PdX$$

- where ( $\int PdX$ ) refers to one cycle and (N) is the number of cycles.

## Results

Experiments were carried out in the simulator on an early form of 'Freeman-Swanson' Knee Joint and on a 'Leeds' Knee Joint. Distilled water was allowed to drip onto the prosthesis to wet the interface, the flow rate being adjusted to maintain temperature of the tibial component at 37°C. Contour diagrams based upon holography are recorded for the initial and worn tibial components of each joint in Figures 3 and 4 and schematic representations of the wear scars are shown in Figures 5 and 6.

The operating conditions and the derived wear factors are recorded in Table I.

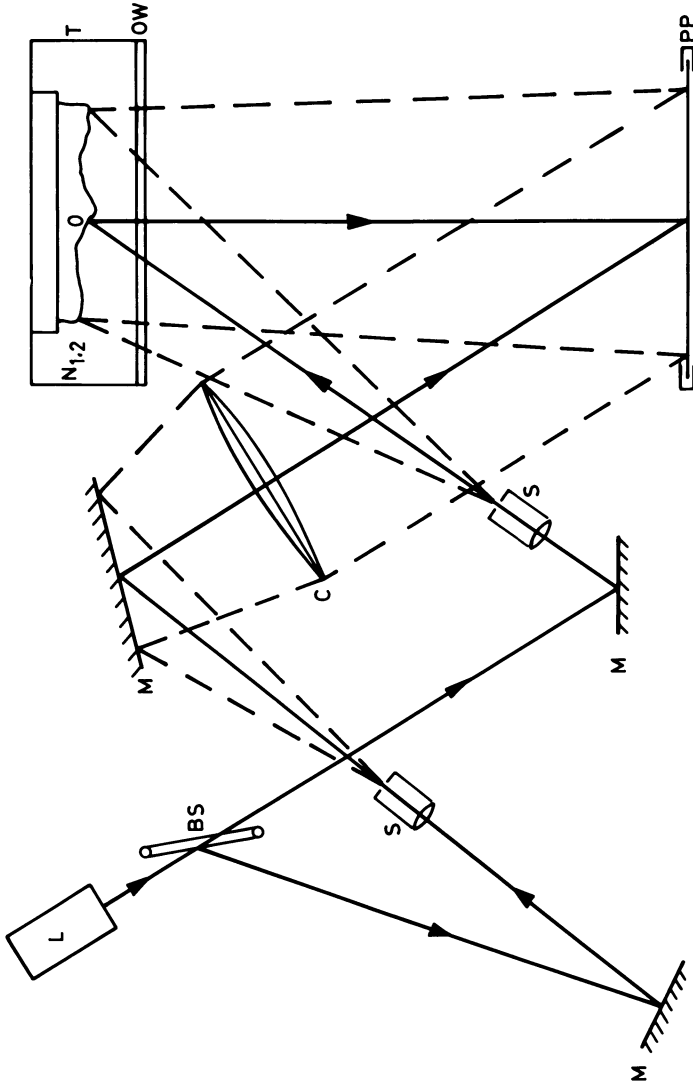
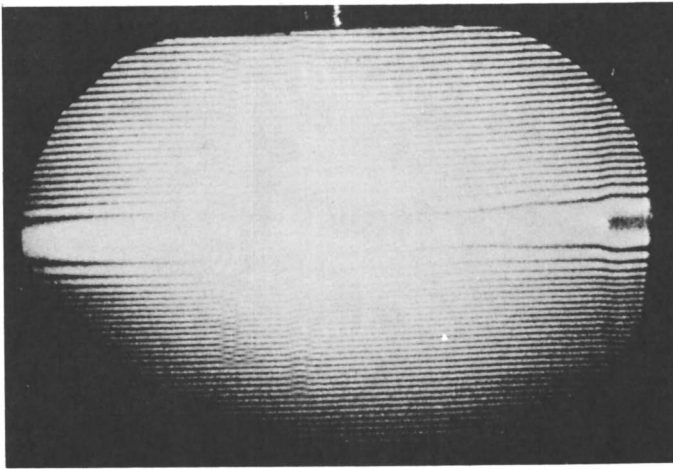
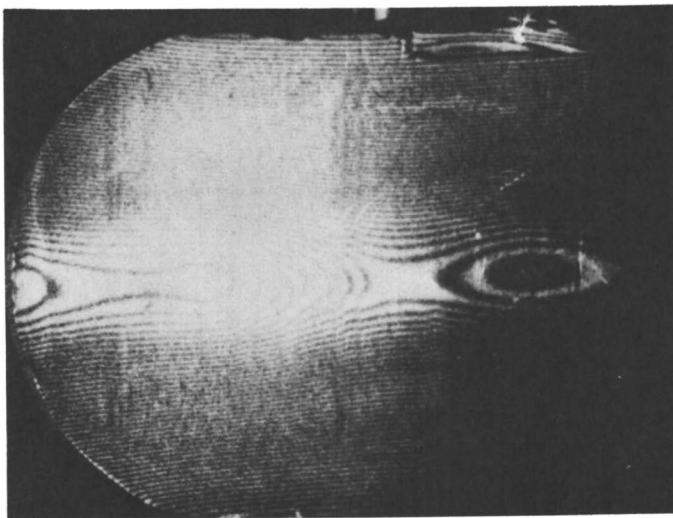


Figure 2 Dual Index Holographic Contouring System.



**Figure 3(a)** Contours of 'Freeman-Swanson' Knee Prosthesis Tibial Component (Initial Design). Prior to Test ( $\Delta h = 200 \mu\text{m}$ ).



**Figure 3(b)** Contours of 'Freeman-Swanson' Knee Prosthesis Tibial Component (Initial Design). After Test in Knee Joint Simulator ( $\Delta h = 140 \mu\text{m}$ ).



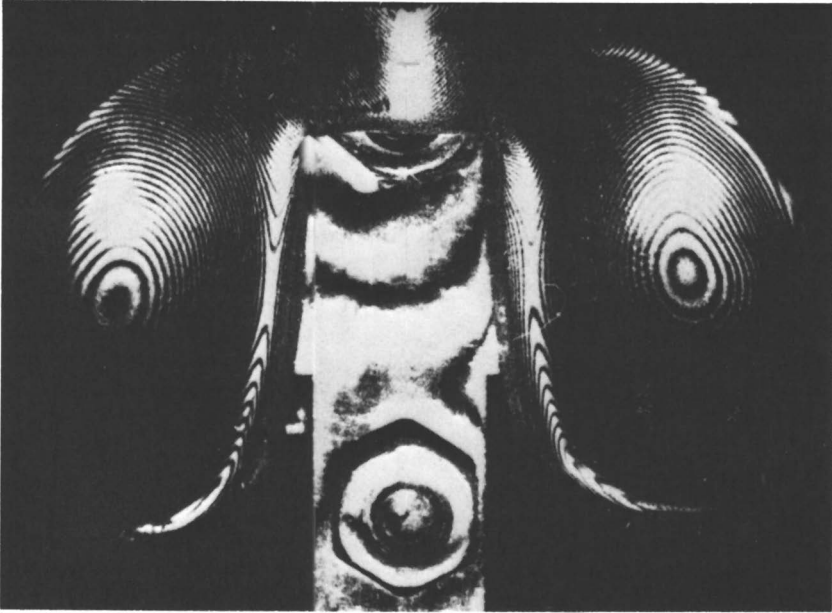


Figure 4a. Contours of 'Leeds' Knee Prosthesis Tibial Component prior to test in knee joint simulator ( $\Delta h = 1.75 \mu\text{m}$ ).

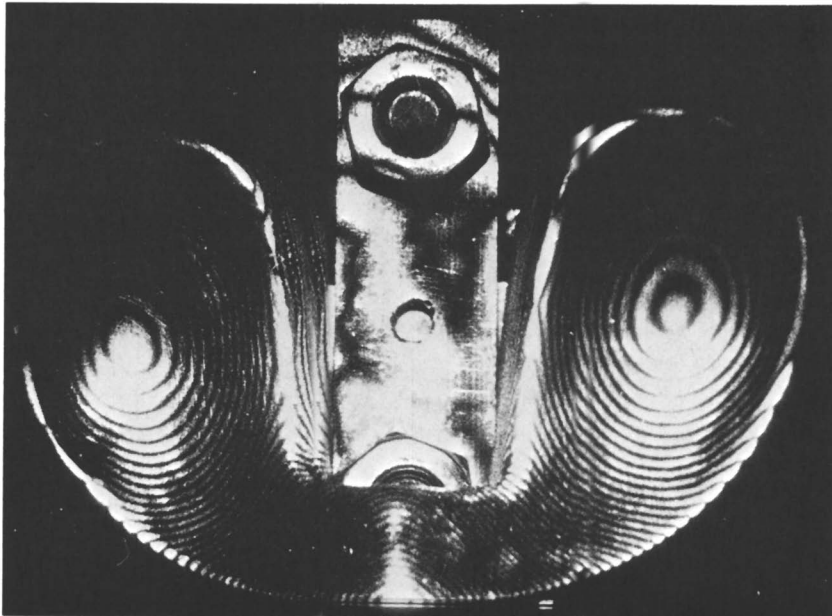


Figure 4b. Contours of 'Leeds' Knee Prosthesis Tibial Component after test in knee joint simulator ( $\Delta h = 350 \mu\text{m}$ ).

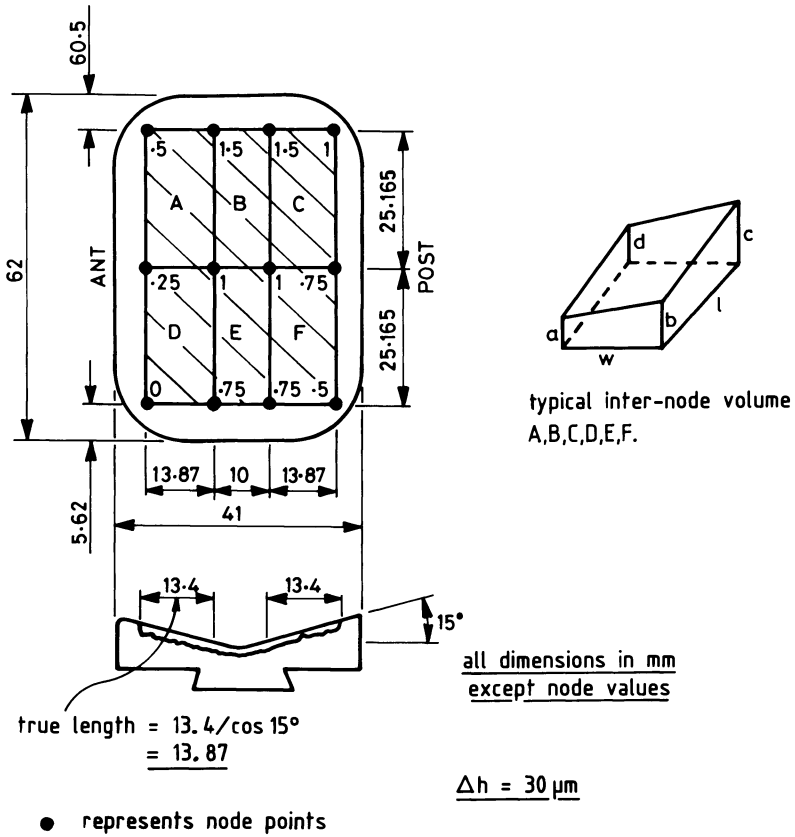
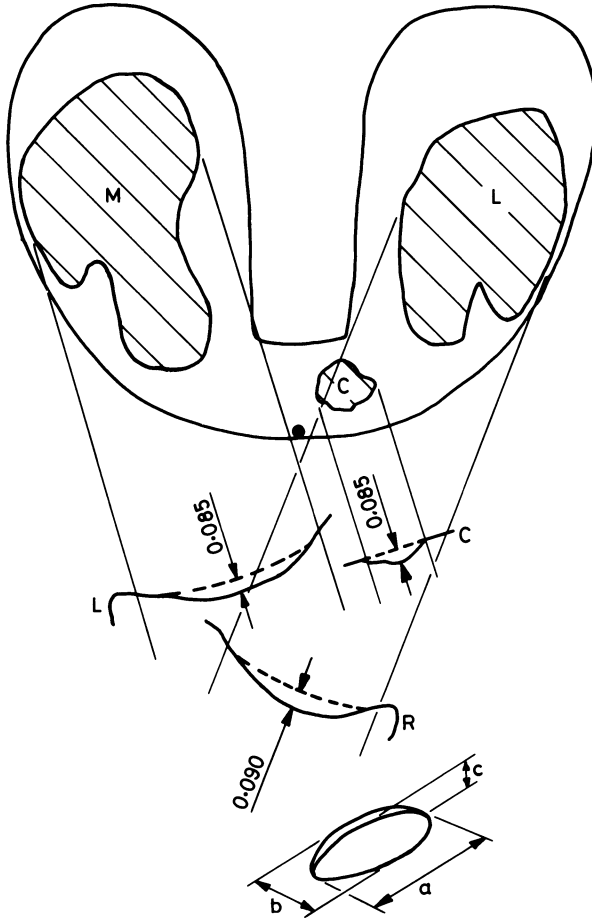


Figure 5 Representation of Wear Scar in 'Freeman-Swanson' Knee Joint. (Simulator test).



semi-ellipsoid representing volume lost to wear (and creep) each wear scar L,C,M.

● represents highest point on bridge

Figure 6 Representation of Wear Scar in 'Leeds' Knee Joint. (Simulator Test).

		KNEE PROSTHESIS		
		'FREEMAN-SWANSON' (initial design)	'LEEDS'	'FREEMAN-SWANSON' (in-vivo)
$\int WdX$ (Nm/cycle)		47.7	67.1	47.7
Number of Cycles		1,030,563	1,008,574	4,380,000 (estimated)
$V$ (mm <sup>3</sup> )		48.7	55.9	387
$R_a$ ( $\mu\text{m}$ )	FEMORAL	0.02	0.025	-
	TIBIAL	0.33	0.11	-
$k$ (mm <sup>3</sup> /Nm)		$0.99 \times 10^{-6}$	$0.83 \times 10^{-6}$	$1.86 \times 10^{-6}$

**TABLE I**      **KNEE JOINT OPERATING CONDITIONS AND DERIVED  
WEAR FACTORS**

### Discussion and Conclusions

The polymeric tibial components worn in the joint simulator exhibited the evidence of adhesive and abrasive wear found in reciprocating pin-on-plate experiments. However, there were also signs of abrasion associated with the particles of acrylic cement, some of which became embedded in the polyethylene. The femoral component exhibited fine scratching with deeper grooves superimposed. This was particularly evident in the case of the 'in-vivo' Freeman-Swanson prosthesis.

The derived wear factor ( $k$ ) for the 'Freeman-Swanson' and 'Leeds' knee joints tested in the simulator for about  $10^6$  cycles are both interesting and similar. The 'in-vivo' Freeman-Swanson joint was kindly made available by Professor S.A.V. Swanson and the conditions of service were not known with any certainty. The joint had functioned in an elderly patient for some four years, with a 'light to medium' level of walking activity. It was therefore assumed that  $\int PdX$  remained constant at 47.7 Nm/cycle and that the patient achieved 6000 strides or 3000 loading cycles per day. These assumptions are consistent with a subsequent study of the walking activity of patients fitted with total replacement joints reported by Wallbridge and Dowson<sup>(3)</sup>, but considerable scope for errors

remain in this part of such calculations. It can also be seen from Figure 7 that the wear scar on the 'in-vivo' joint was asymmetric. The overall wear factor of  $1.86 \times 10^{-6} \text{ mm}^3/\text{Nm}$  was slightly higher than those recorded in the simulator tests of  $0.99 \times 10^{-6} \text{ mm}^3/\text{Nm}$  and  $0.83 \times 10^{-6} \text{ mm}^3/\text{Nm}$  for the Freeman-Swanson and Leeds knee joints respectively.

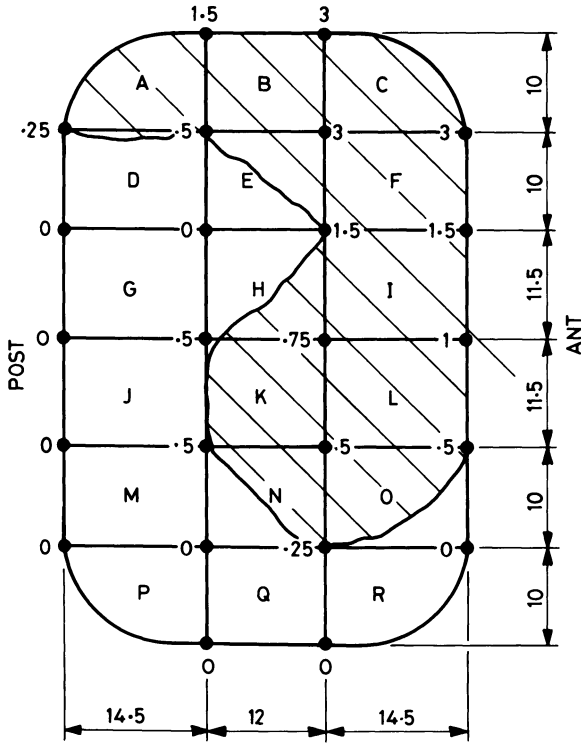
It is also of interest to estimate the 'effective' wear factor for a natural knee joint. If it is assumed that the joint is 'worn out' between the ages of 20 and 70 years and that the combined thickness of the layers of cartilage essentially worn away during this period is 4 mm, the volume of material removed can be estimated from measured areas of the condyles and is likely to be about  $10^4 \text{ mm}^3$ . If the average healthy person takes some 10,000 steps per day throughout this period, and the value of  $\int PdX$  is 47.7 Nm/loading cycle, then (k) is given by;

$$k = \frac{10^4}{5000 \times 47.7 \times 365 \times 50} = 2.3 \times 10^{-6} \text{ mm}^3/\text{Nm}$$

The derived wear factors can be compared directly with the results reported by Dowson et al.<sup>(4)</sup> elsewhere in this Conference for laboratory experiments based upon similar combinations of materials in a laboratory linear, reciprocating, wear testing machine. For counterfaces of similar roughness, in distilled water, the reciprocating machine results indicated wear factors of  $0.4 \times 10^{-6} \text{ mm}^3/\text{Nm}$  for the 'Freeman-Swanson' and 'Leeds' prostheses respectively, compared with the simulator results of  $0.99 \times 10^{-6} \text{ mm}^3/\text{Nm}$  and  $0.83 \times 10^{-6} \text{ mm}^3/\text{Nm}$ . These values are much closer than is commonly thought to be reasonable when simulator, and particularly 'in-vivo', results are compared with the findings from well controlled laboratory wear machines. This is particularly interesting when it is recalled that the simulator evaluations record 'wear and creep' and that there is considerable additional abrasive wear from acrylic cement particles in the simulator and in-vivo.

The experimental findings confirm the merit of joint simulators in furthering the development of total replacement joints. Dual-index holography has been shown to reveal the nature and extent of the wear scars on worn, polymeric tibial components in a satisfactory manner. The derived equivalent wear factors are reasonably consistent with, but somewhat greater than, the wear factors recorded on laboratory linear reciprocating wear machines. It is, however, most important to make the comparisons of simulator and in-vivo wear rates with findings from laboratory wear machine experiments in which the environment and counterface topography are adequately represented.

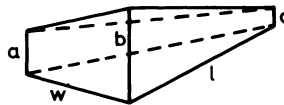
There is an urgent need for further careful analysis of the wear characteristics of total replacement joints after service in the body. Such studies would enhance the understanding of the long term performance of prostheses and would indicate the merit of versatile laboratory wear testing machines and joint simulators.



inter-node volumes are as previously defined,

except A,C,P,R

● represents node point.



inter-node volume bounded  
by 3 node points

$$\Delta h = 189\mu\text{m}$$

Figure 7 Representation of Wear Scar in 'Freeman-Swanson' Knee Joint. (in vivo).

Literature Cited

1. Dowson, D., Jobbins, B., O'Kelly, J. and Wright, V., 'A Knee Joint Simulator', Ch. 7, 'Evaluation of Artificial Hip Joints', Biological Engineering Society, U.K., 79-90, (1977).
2. Morrison, J.B., 'Bio-engineering Analysis of Force Actions Transmitted By The Knee Joint', Bio-Med. Eng., 3, No. 4, 164-170, (1968).
3. Wallbridge, N. and Dowson, D., 'The Walking Activity of Patients Fitted with Artificial Hip Joints', Engineering in Medicine, 11, 2, 95-96 (1982).
4. Dowson, D., Diab, El-Hady, Gillis, B.J. and Atkinson, J.R., 'The Influence of Counterface Topography Upon The Wear of Ultra-High Molecular Weight Polyethylene Under Wet or Dry Conditions', International Conference on Polymer Wear and Its Control, (1984).

RECEIVED January 23, 1985

## **Wear Characteristics of Articular Cartilage Effects of Time-Varying Loads and Intermittent Sliding**

**Harold Lipshitz<sup>1</sup>**

**Laboratory for Skeletal Disorders and Rehabilitation, Harvard Medical School  
and Children's Hospital Medical Center, Boston, MA 02115**

Bovine articular cartilage, worn under cyclic loading patterns against a highly polished characterized stainless steel surface, wore at significantly lower rates than would have been obtained under constant pressures equal to the time average of the oscillating pressures. The differences between the observed rates and those that would have been obtained under constant equivalent pressures were greater, the greater were the amplitudes of the cyclic pressures. These phenomena are interpreted as being due in large measure to the tissues greater ability to dissipate stress under these conditions.

Under time varying loads, gross surface fissures were evident during the wear experiments. This was not the case under constant loads.

When worn against articular cartilage that was slightly cross-linked with formaldehyde, interrupted sliding resulted in significantly greater wear rates than those obtained under constant sliding. During the interruptions the tissues underwent slow compression and reswelled on the resumption of sliding. The greater wear rates in this case are attributed to ploughing or large deformations on resumed sliding.

Articular Cartilage is a tissue that serves as a bearing material in diarthrodial joints (Fig. 1). Its wear properties have interested biomedical scientists for many years because of the belief that the tissue's wear is a factor in the etiology of osteoarthritis (1). Material and biological scientists have, on the other hand, sought an understanding of the mechanisms by which it is normally able to withstand the rather large stresses

<sup>1</sup>Current address: The Kendall Company, Lexington, MA 02173



during joint function without appreciable loss of mass; this, despite its poor biological reparative capability (2). Nevertheless, despite this interest, the tissue's wear characteristics have remained inadequately described and poorly understood. This has been due, in part, to the complexities of the phenomena - a result of its unique mechanical properties - and the experimental and theoretical difficulties of studying the problem. These have been, principally, the difficulties of isolating the variables that govern the tissue's wear (particularly under in vivo conditions).

Articular cartilage is a complex composite polymeric material that consists principally of a network of collagen (in various states of aggregation), protein-polysaccharides, living cells (chondrocytes) and inorganic ions. The latter are primarily counterions to the charged moieties of the polyelectrolytes of the matrix. The entire network is swollen with water, a major fraction of which is in regions between its fibrous elements. On compression this water is exuded. The tissue's network structure, composition, and equilibrium fluid contents vary with depth from the surface (3,4,5). Its structure and chemical composition have been extensively reviewed (6,7,8,9).

Mechanically, the tissue is anisotropic and inhomogenous, its moduli vary with direction and depth from the surface (10,11). Its principal mechanism for attaining stress relaxation, at strains above a critically small strain, is by exuding interstitial fluid (12). Its stress relaxation rates are therefore not only functions of the viscoelastic properties of its macromolecular network, but also the frictional resistances to fluid transport in and out of the tissue. Factors affecting fluid exudation and imbibition therefore necessarily affect the tissue's wear resistance.

In vivo, the tissue is subjected to pressures that vary with time. This occurs because of pressure variances during locomotion and the like and because articulation often results in regions of the tissue compressing opposite regions for intermittent periods during sliding. This is a consequence of joint incongruities. Sliding therefore results in regional contacts being broken or becoming effectively unloaded while other regions bear the loads (Fig. 2). During the unloaded periods, fluid from the media is reimbibed (13). Joint articulation therefore results in the tissue's interstitial fluid being alternately exuded and reimbibed. Dimensional recovery occurs during reimbibition (13). In vitro, it is found that cartilage that is not equilibrated with aqueous media does not completely recover dimensionally after compression. Dimensional recovery therefore results from a combination of the factors governing network "elasticity" and swelling.

The rates of dimensional recovery vary with the average compressive strain (14) and with certain characteristics of the solution with which the tissue is equilibrated (15). These include the concentration and type of ions dissolved in the water (15), its viscosity, temperature, and macromolecular content. The average compressive strain varies with load, loading frequency, and with the time a given region is subjected to

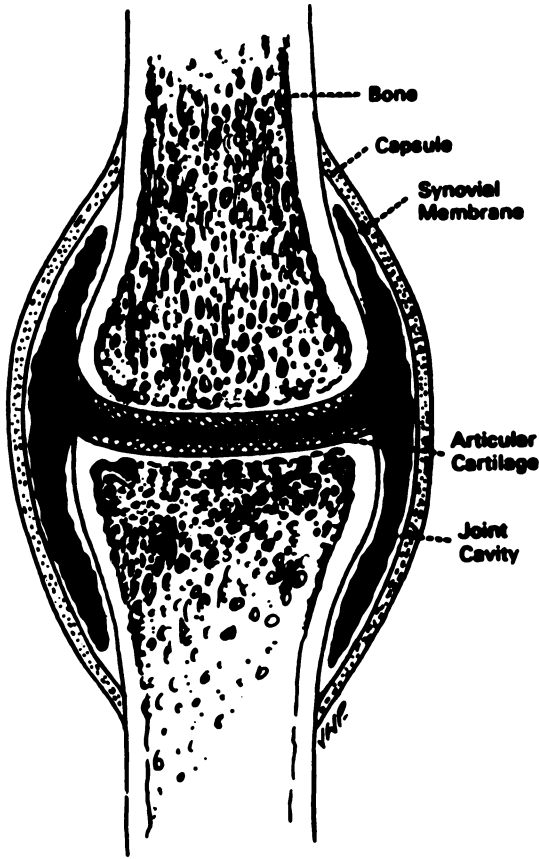


Figure 1. Schematic of Diarthrodial joint.

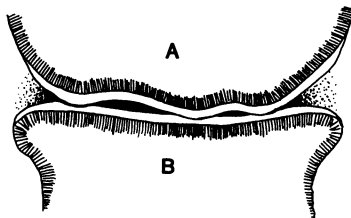


Figure 2. Schematic showing incongruities between the articular surfaces. As surface A rolls across surface B regions of the tissue undergo intermittent compression and relaxation.

load. Under time varying loads, this can become a function of sliding speed.

If sliding is interrupted, while a small region of the tissue under load is interfaced with a larger region, the tissues become progressively compressed. When sliding is resumed, the process is reversed and the tissues reswell. This results in greater deformation on the resumption of sliding with consequent effects on the wear of the tissue.

It is the purpose of this paper to describe the effects of time varying loads and interrupted sliding on the tissue's wear, under specified in vitro conditions and to compare its wear characteristics under these conditions with that under constant load and continuous sliding.

## EXPERIMENTAL PROCEDURES

### A. Source and Form of the Cartilage

The studies were carried out using circular cylindrical plugs of cartilage and bone that were cut from the medial femoral condyles of adult steers (approximately 2 years old). The techniques and tools used for their preparation have been described elsewhere (16). The condylar surfaces used were predominantly but not totally curved. The plugs obtained from them were prepared in such a manner that the surface of the tissue was both flat and perpendicular to the axis of the cylindrical shaft of underlying bone. They were used in these studies to assure that the geometric contact areas between wearing surfaces were reproducible under the same loads (17).

### B. The Wearing of the Tissue

#### 1. Apparatus

The tissue was worn in apparatus that is described in detail elsewhere (17). In essence, the instrument consists of a sturdily mounted stainless steel turntable (type 302) that is made to move back and forth, sinusoidally, by an attached rod, spring loaded against an off-center, motor-driven cam. The travel distance, for these studies, was 0.64 cm.

The tissues were worn either against a highly polished stainless steel surface designated previously as Surface A (see ref. 17) or against slightly cross-linked cartilage. The same apparatus was used for both types of experiments. The procedures for doing so are described below.

The surface of the metal was characterized by randomly oriented depressions, 0.2 to 0.3  $\mu\text{m}$  deep, 6 to 10  $\mu\text{m}$  long, spaced 4 to 8  $\mu\text{m}$  apart (17). These dimensions were determined using stereoscopic scanning electron microscopy at two angles of tilt and applying the equations described by Boyde (18).

The tissues were interfaced with the wearing surfaces as follows. The plugs were secured in stainless steel holders that were held by chucks attached to pneumatic actuators. The loads on the tissue were monitored by a load cell (BLH, Inc., Waltham, MA) positioned between the chuck and the piston of the actuators (Fig. 3). When loads were applied through the actuators, the

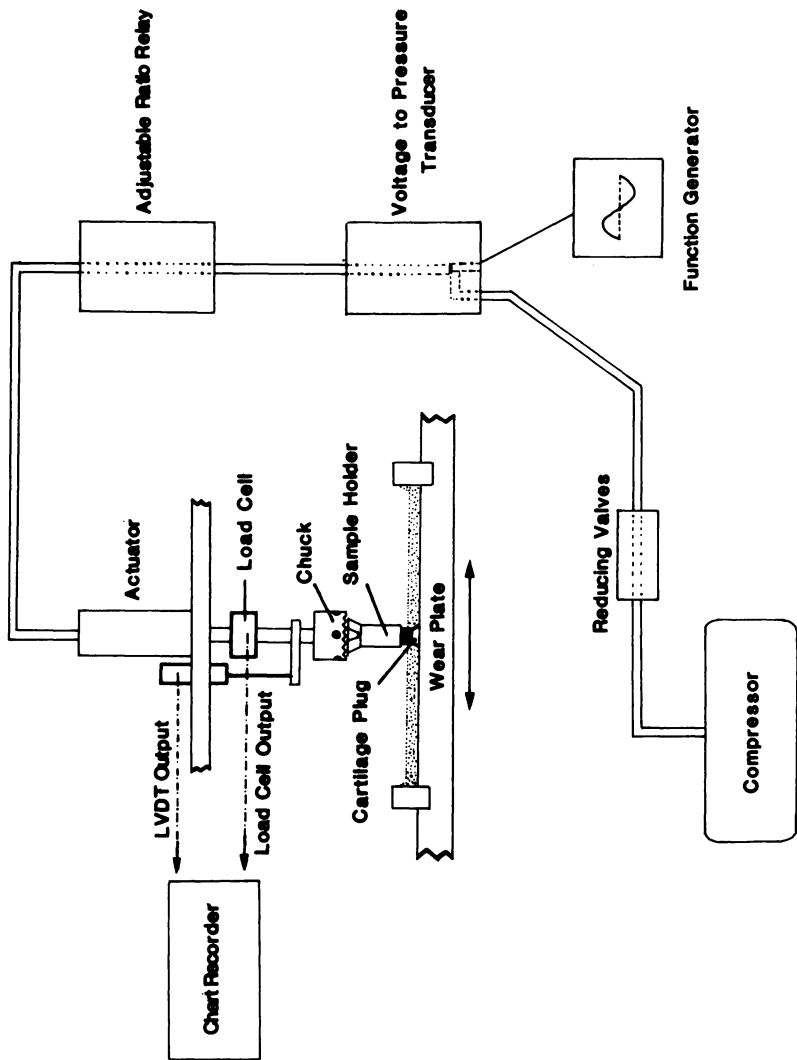


Figure 3. Schematic of the experimental arrangement used to obtain cyclic pressures. Air from the compressor flowed through the reducing valves through the voltage to pressure transducer, then through an adjustable ratio relay to the actuators. The air pressure out of the voltage-pressure transducer was controlled by the voltage input regulated by the function generator. The loads on the tissue and the tissue's displacement were monitored by a strip chart recorder.

tissue was compressed against the countersurface while the plate was made to move sinusoidally to effect its wear. The geometric contact areas between tissue and plate were previously determined as a function of load. As such the average pressures on the tissue were known for each load (17).

As stated, the tissue's mechanical properties are sensitive functions of its fluid content. The wear experiments therefore had to be carried out with the tissue bathed in aqueous media. This was accomplished as follows: A trough 0.64 cm deep, and 2.54 cm wide was accurately machined into the plate at its periphery. The trough was partitioned into compartments allowing duplicate experiments to be simultaneously run. Approximately 10 ml. of 0.03M tris(hydroxy)methylaminomethane buffer at pH 7.4 containing  $1 \times 10^{-4}$ M phenylmethylsulfonyl fluoride was placed in each compartment at the start of each experiment. The latter compound served to inhibit proteolytic enzymes within the tissue (17). The tissues were bathed in this solution throughout the experiments. The solutions served to both lubricate and hydrate the cartilage during the wear experiments.

## 2. Measurement of Wear

Wear was measured as follows: At selected times, the fluid from each compartment was quantitatively removed and rapidly replaced with fresh solution while oscillation of the plate was maintained. These procedures were previously shown to result in the quantitative removal of the wear debris and its dissolved constituents (4,17). In these experiments regular sliding patterns were maintained during sampling to assure that the tissue was not subjected to artifactual deformation. This was not a concern when the tissue was worn under constant pressure.

The extent of wear was determined by measuring the hydroxyproline content of the lubricant. Details of the procedure are described in reference 4. The assay used was that described by Grant (19). Hydroxyproline is an amino acid found almost exclusively in collagen. It was previously shown to have a constant relationship to the mass of organic material of this tissue throughout its thickness (4). This is so except for a thin surface region calculated to have been removed within the first few minutes of the experiments. Since the tissue's thickness varies with pressure, fluid content, etc., dimensional changes cannot be used to monitor the extent of wear.

While the constituents of the intact tissue are not extracted by this solvent, the wear debris' constituents are partially dissolved. Presumably, chain scission and/or network breakdown during wear results in the partial dissolution of the debris. It was therefore necessary to measure the hydroxyproline contents of the wear debris and its dissolved constituents.

Using these procedures, around 0.1  $\mu$ gm of hydroxyproline was detectable. Since the dry weight of this cartilage is, on average, 12.8 times the weight of its hydroxyproline content (4), as little as 1.3  $\mu$ gms of worn cartilage could be detected.

### 3. The Attainment of Varying Pressures on the Tissue

Time varying loads on the tissue were achieved as follows: Air, from a compressor, was forced through two reducing valves through a voltage-pressure transducer (model T-502, Fairchild Hiller, Inc., Winston Salem, NC). The air then flowed through an adjustable ratio relay to the pneumatic actuators through which loads on the tissue were applied. The load variations were controlled by voltage inputs to the voltage-pressure transducer through a function generator. A schematic of the flow pattern is seen in Figure 3. For the mechanical advantages in our system, between pressures on the actuators and pressures on the tissue, frequencies of up to 9 Hz could be obtained for pressure variations on the tissue of up to  $0.7 \text{ MN/m}^2$ . For pressure variations of  $7 \text{ MN/m}^2$  frequencies were limited to 3 Hz.

For the studies reported here, the form of the load changes with time were limited to modified "square" waves. The "square" waves were somewhat rounded because the system's response lagged somewhat behind the voltage changes to the voltage-pressure transducer. The actual form of the load variance obtained is seen in Figure 9.

The extents of tissue compression, during and following loading were monitored by a linear voltage displacement transducer (LVDT) positioned between the chuck and piston of the actuator (Fig. 3).

### 4. Interfacing Cartilage Against Cross-linked Cartilage

The interfacing of cartilage against lightly cross-linked cartilage was achieved as follows: Large diameter plugs (Diam. = 1.3 cm) were cut from the femoral condyles. These were prepared from selected condylar regions that had a flat area such that smaller flat plugs (Diam. = 0.57 cm) could slide over it a distance of 0.64 cm. The boney part of the larger plugs were ground to a thickness of around 0.6 cm. These were cross-linked (see below) and then press fit into holders that fit snugly into the troughs of the wear plate. The holders, made from poly-(methyl methacrylate) ("Lucite") were positioned within the compartments of the plate and secured to it with C clamps. Walls of "Lucite" were glued to the holders surrounding the larger plugs. These served to contain the lubricant. The arrangement is schematically illustrated in Figure 4.

The larger base plugs were reacted with formaldehyde prior to their use in the wear experiments. The extents of cross-linking were however small (see results section). This reaction was necessary because in this experimental arrangement, cartilage worn against unreacted cartilage resulted in significant tearing within a half to one hour after the start of the experiment. This rendered the data meaningless. Against cartilage that was cross-linked to a small extent, however, no tearing occurred and reproducible experiments were readily performed.

Reaction with formaldehyde was accomplished by equilibrating the plugs in aqueous solutions of 1% formaldehyde in 0.03M phosphate buffer at pH 7.4 for 16 hours at 37°C. The formaldehyde solutions were "spiked" with  $\text{C}^{14}\text{H}_2\text{O}$  to measure the

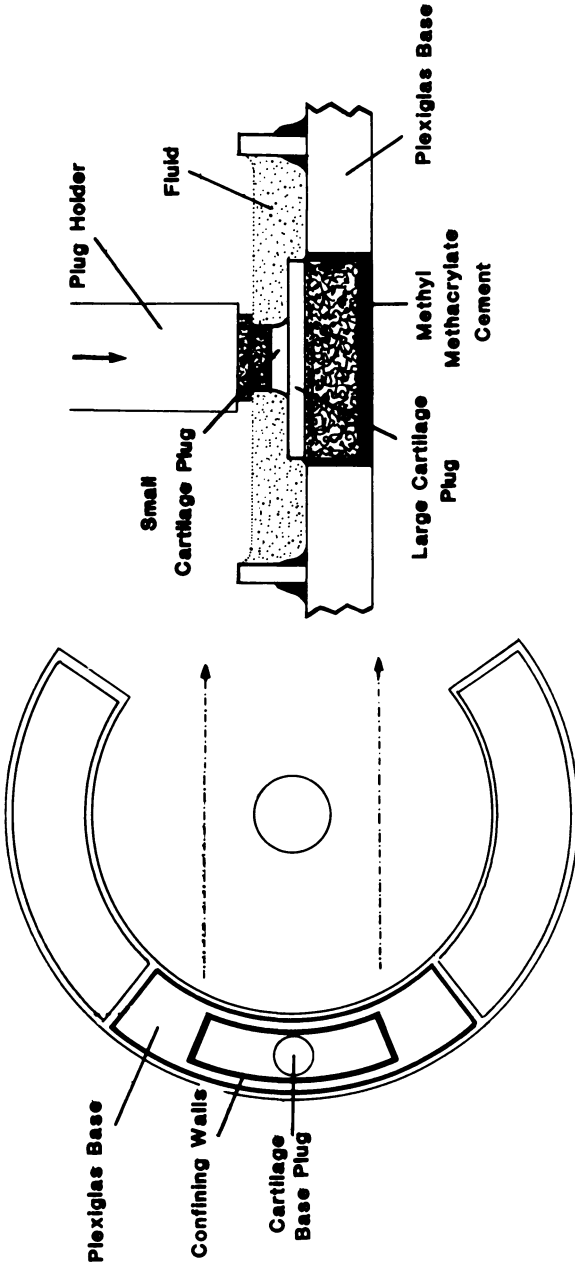


Figure 4. Schematic showing the experimental arrangement used to wear cartilage on cross-linked cartilage. The bottom plug fit into the holders. These were secured to the wearing plate with C clamps.

extents of reaction with the tissue. Radioactivity-formaldehyde content relationships were empirically established by colorimetric assay of the "hot" solutions for formaldehyde using the chromotropic acid assay acid and hexamethylene tetramine as primary standard (20). The methodology is described by Walker (20). Following equilibration, the plugs were washed extensively with phosphate buffer until no radioactivity was detectable in the wash solutions.

Formaldehyde remaining in the tissue, after washing, was assumed to have been reacted with the tissue. The extents of reaction were measured by determining the tissue's dry weight, then digesting the sample with "Protosol" (New England Nuclear Inc., Boston, MA) and measuring its radioactivity by liquid scintillation.

Different extents of reaction were obtained by equilibrating for shorter periods and/or lower temperatures. Under these conditions formaldehyde was shown to react with the tissue throughout its thickness (21).

#### 5. Surface Characteristics of the Tissue During Wear

To assess changes to the tissue's gross surface characteristics during the wear experiments, several plugs were each worn for different time periods (30, 60, 90, 310, 700, 1480, and 2100 minutes). These were then removed from the apparatus, equilibrated with phosphate buffer (pH 7.4) for 4 hours at 4°C. During this time the tissue's attained their equilibrium swelling characteristics. They were then stained with India ink using the procedure of Meachim (22). This procedure facilitates the visualization of surface fissures (22). The surfaces were then photographed through the lens of a dissecting microscope.

### RESULTS

The amount of cartilage worn as a function of time against the stainless steel surface is plotted in Figure 5 for the cyclic patterns: (1) 25 seconds at 0.69 MN/m<sup>2</sup> followed by 25 seconds at 6.9 MN/m<sup>2</sup> (Curve A) and 25 seconds at 0.69 MN/m<sup>2</sup> followed by 25 seconds at 4.14 MN/m<sup>2</sup> (Curve B). As was the case for all loading patterns, the tissue initially wore at higher rates that decreased with time during the first 180 to 200 minutes. After that the tissue wore at constant steady state rates. For the 0.69 to 6.9 MN/m<sup>2</sup> pattern these rates were sustained for the duration of the experiments. For the 0.69 to 4.14 MN/m<sup>2</sup> pattern, the tissue wore at an average steady state rate of 1.1 µgms. cart. worn/min. (all rates expressed on a dry weight basis) from about 200 to about 600 minutes and then at a higher rate of 1.6 µgms. cart. worn/min. for the remainder of the experiments.

When the pressure cycle was 47 seconds at 0.69 MN/m<sup>2</sup> and 3 seconds at 4.14 MN/m<sup>2</sup>, the tissue wore at a constant steady state rate of 0.4 µgm. cart. worn/min. after about 150 minutes. This was sustained to about 1100 minutes after which the rates increased to 0.7 µgm. cart. worn/min. In this cycle the higher pressure was imposed more pulse like.



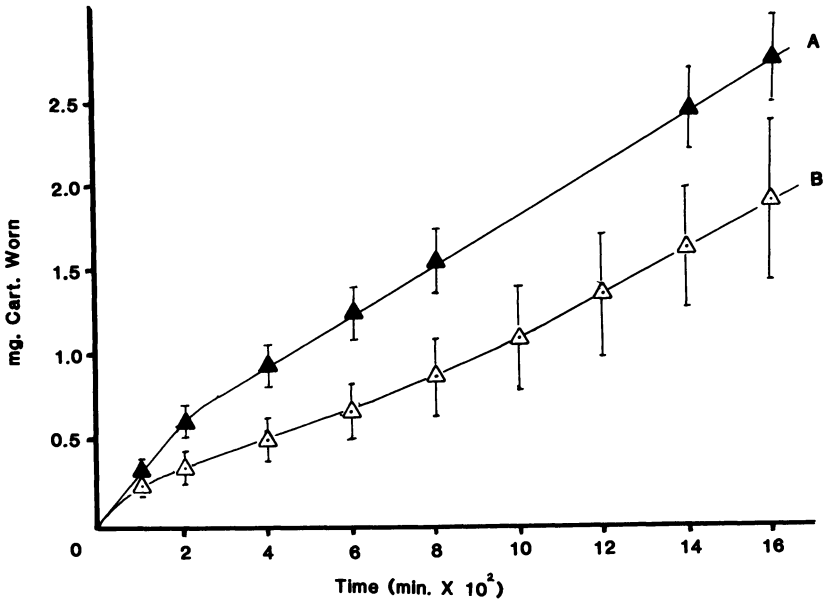


Figure 5. The wear of the tissue with time. (For all experiments the plate was made to oscillate at an average velocity of 0.52 M/min. The abscissas can therefore be converted to distance slid.) Curve A: pressure on the tissue alternated equally between 0.69 and 6.9 MN/m<sup>2</sup> at a frequency of 0.02 Hz. Curve B: the pressure was alternated equally between 0.69 and 4.14 MN/m<sup>2</sup> at a frequency of 0.02 Hz. Note the initial higher wear rates and the two steady state rates of Curve B. The mean values of 6 to 10 experiments  $\pm$  1 stdn. dev. are plotted. The same number of experiments were run for each of the figures.

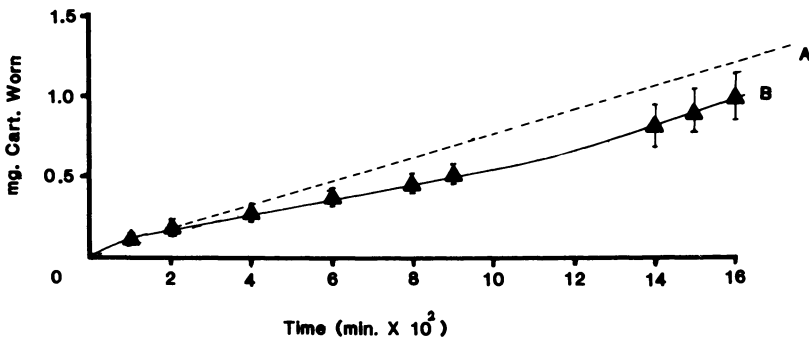


Figure 6. The wear of the tissue as a function of time when worn under pressures that were alternately 47 seconds at 0.69 MN/m<sup>2</sup> and 3 seconds at 4.14 MN/m<sup>2</sup>. The broken line is the wear that would be obtained were the tissue worn under a constant pressure equal to the time average of the two pressures.

In all cases, the tissue wore at considerably lower rates than would have been the case were it under a constant pressure equal to the time average of both pressures. (These are shown in Figures 7a and b). These rates were computed using an equation that was previously shown to describe empirically the steady state wear of the tissue under constant pressure against this surface (17). That is:

$$(1) \quad W = 1.13 VPt + 0.11$$

W is the micrograms of cartilage worn (on a dry weight basis); V is the average speed of the oscillating plate in meters/minute (in all experiments this was 0.52 m/min); P is the average pressure on the tissue in MN/m<sup>2</sup>; and t is the time in minutes. If the tissue was worn under constant pressure for a sustained period, this equation described its wear irrespective of its having been worn under other pressures (17).

The above equation is similar in form to the often used (23)

$$(2) \quad V = kLs$$

where V is the volume worn; L, the load; s, the sliding distance; and k, a wear factor. Since the tissue's average fluid content is around 81.1% (29) and its hydrated density around 1, equation 1 can be transformed to yield a wear factor, k, in the steady state region of  $5.35 \times 10^{-4} \mu$  liters/kgm-meter for this tissue against this highly polished surface. In this case V would be the volume of tissue worn if it were fully hydrated.

The effects of the frequency of changing pressure on the tissue's wear characteristics are seen in Figure 8. In these experiments the pressure was alternated equally between 0.69 and 4.14 MN/m<sup>2</sup> at frequencies of 0.02, 0.06, and 0.25 Hz (i.e. 25, 8.4, and 2 seconds at each pressure of the cycle). The tissue wore at its highest steady state rates at 0.06 Hz while at 0.02 and 0.25 Hz the rates were about equal.

Changes in cartilage thickness with time, when worn under cyclic pressures (0.69 - 4.14 MN/m<sup>2</sup> at 0.02 Hz) are seen in Figure 9. During the first 300 minutes, its thickness changed as follows. With the application of pressure it compressed instantaneously to a strain that depended on the pressure and particular cycle of the sequence. It then underwent slow further compression during the cycle such that its thickness changed linearly with time (Fig. 9). When pressure was relieved, it recovered rapidly (almost elastically) to a thickness (or hydration state) that was somewhat less than the starting point of the cycle. On repetition of the cycle the deformation pattern was repeated for about 300 minutes after which the tissue behaved almost elastically. The slow creep phase following the application of pressure did not occur and on the relief of pressure the tissue's thickness was the same as it was prior to the application of pressure. It should be noted that the tissue's thickness is generally proportional to its fluid content (14).

Changes to the tissue's surface features during the course of the wear experiments are shown in Figures 10 (a-f). Under constant time invariant loads, no evidence of gross surface fissures was seen at the end of the experiments (Fig. 10a and b). Essentially all the India ink used to visualize surface

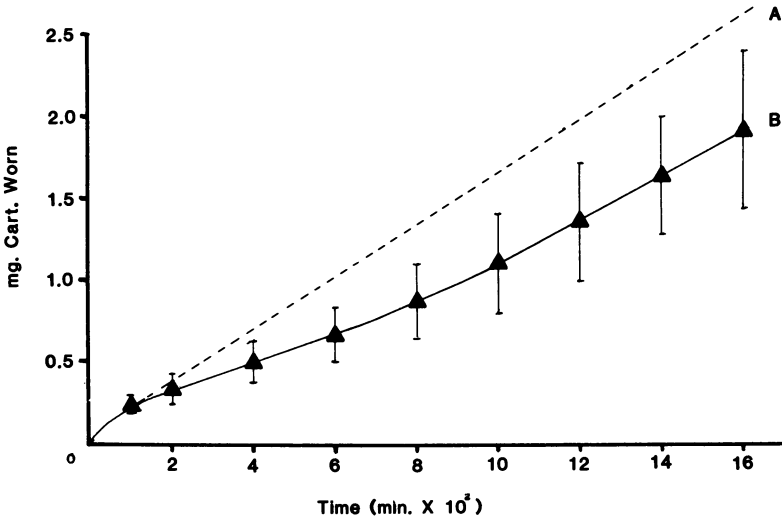


Figure 7a. Comparison of the wear of cartilage when worn under a pressure cycle of 0.69-6.9 MN/m<sup>2</sup> at 0.02 Hz. with that under a constant pressure equal to the time average of the two.

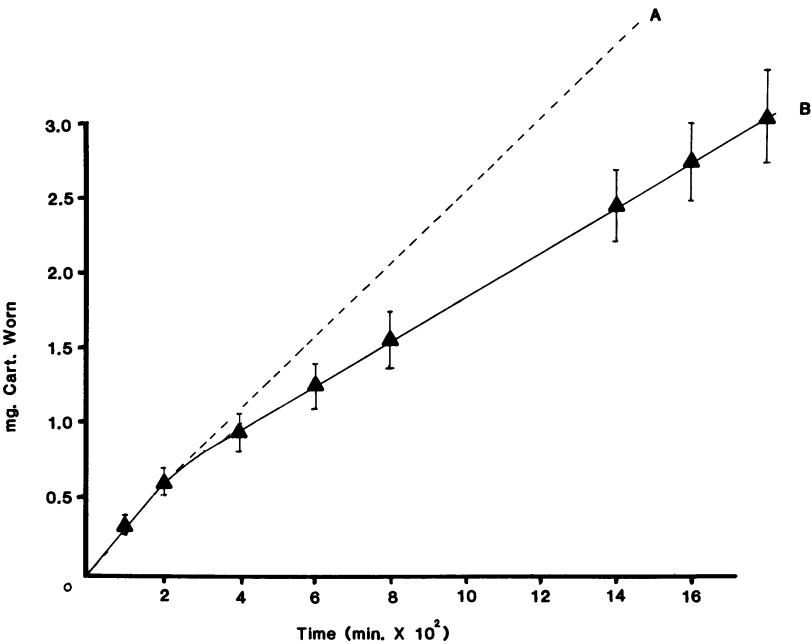


Figure 7b. Comparison between the wear under pressures that alternated between 0.69 and 4.14 MN/m<sup>2</sup> at 0.02 Hz with that under an equivalent constant pressure.

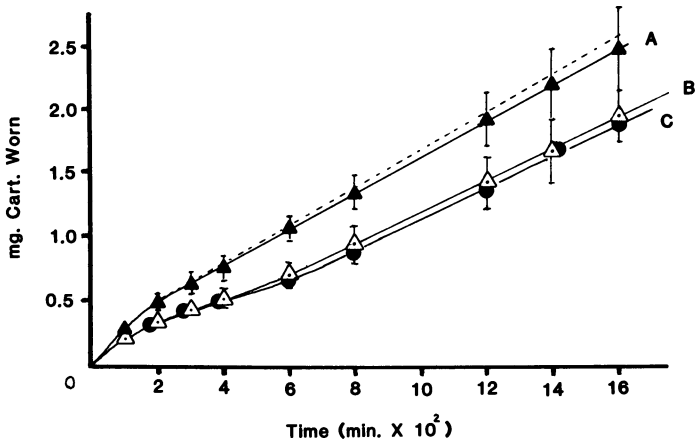


Figure 8. The effect of frequency on the wear of the tissue. Curve A = 0.06Hz; Curve B = 0.25Hz; and Curve C = 0.02Hz.

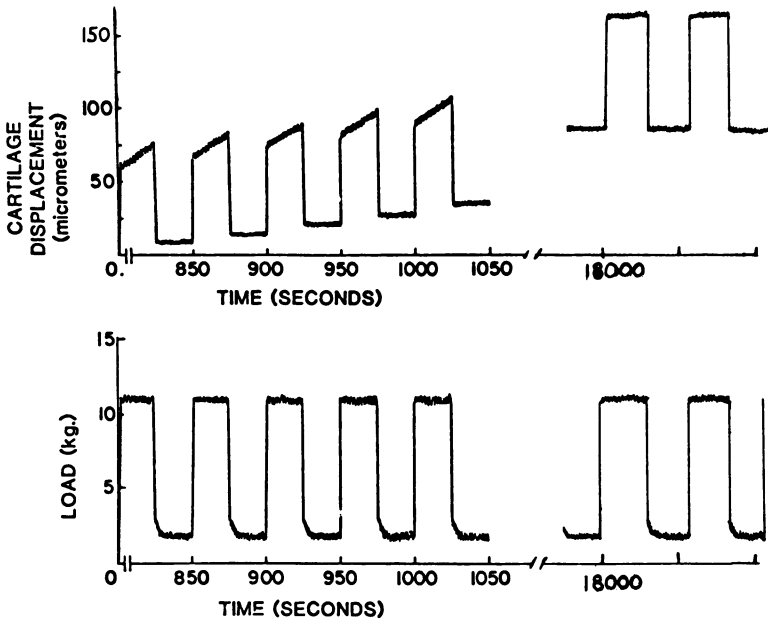


Figure 9. The displacements of cartilage while worn under cyclic alternating pressures. For the curves shown the pressure cycle was 0.69 to 4.14 MN/m<sup>2</sup> at 0.02 Hz. Note the dimensional changes of the tissue after pressure is applied that occurred during the first 300 minutes, and the lack of such changes after 300 minutes.

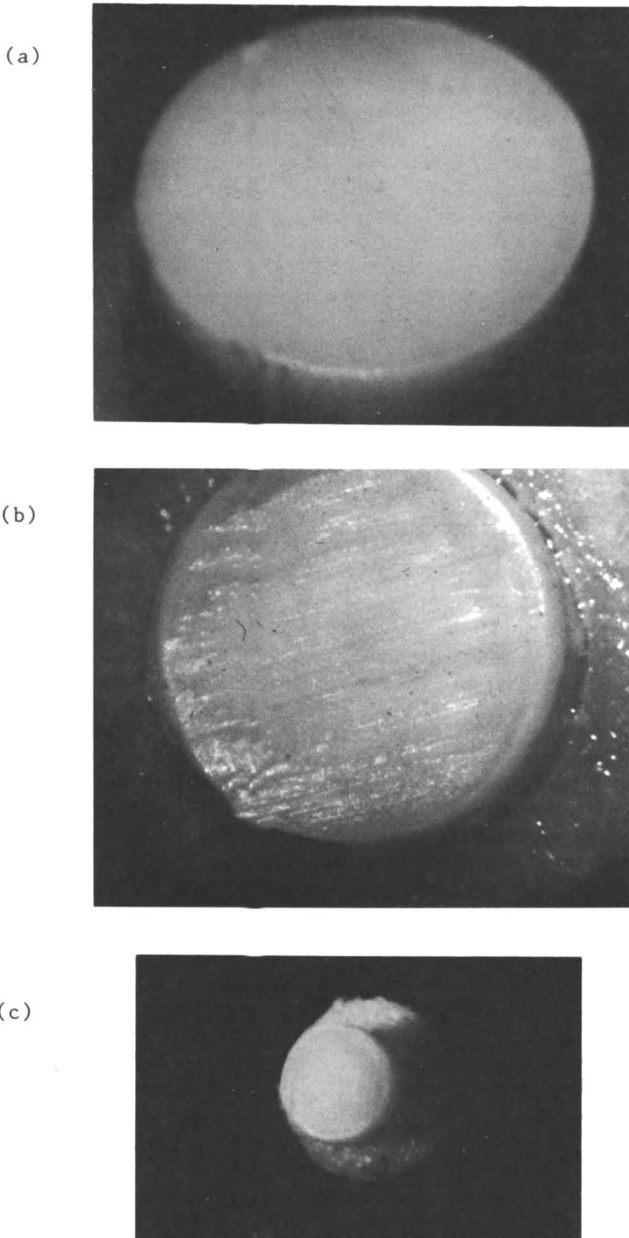
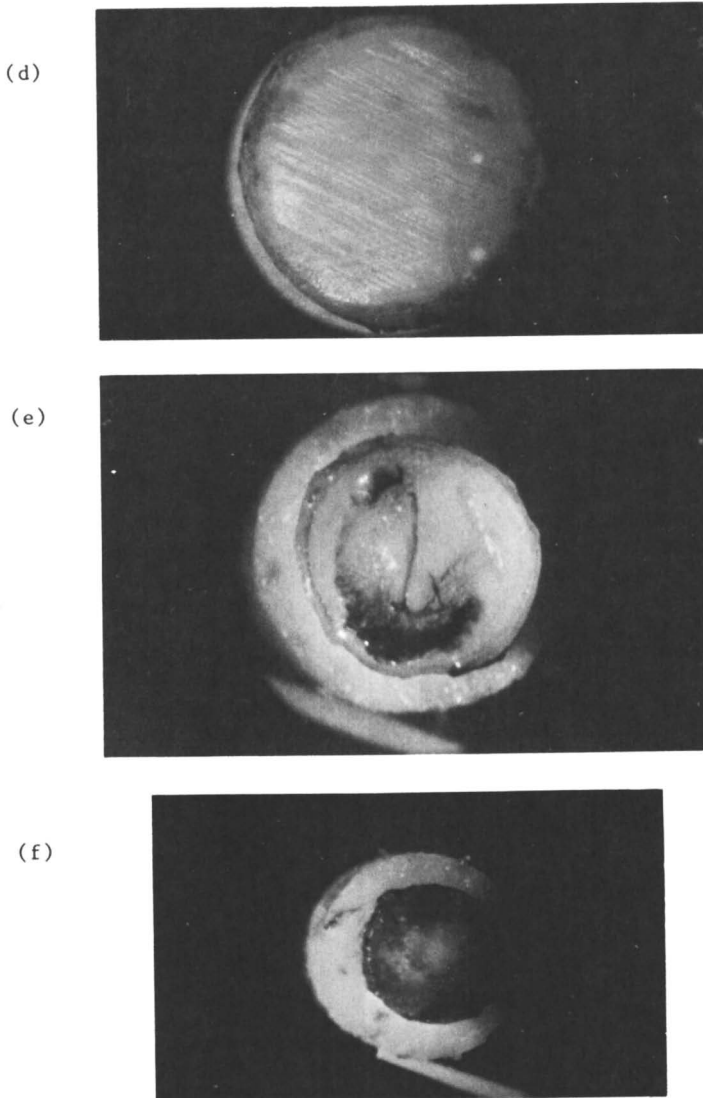


Figure 10. Surface features of the tissue at various times during the wear experiments after being re-swollen. The plugs were stained with India ink and washed.

- a) The surface of the tissue prior to its being worn
- b) After being worn for 1400 minutes under a constant pressure of  $2.07 \text{ MN/m}^2$ .
- c) After 180 minutes. Pressure cycles same as c.



**Figure 10. Surface features of the tissue at various times during the wear experiments after being reswollen. The plugs were stained with India ink and washed.**

- d) After 360 minutes. Pressure cycles same as c. Note appearance of fissures (dark regions).
- e) After 700 minutes. Pressure cycle same as C. Note split in the tissue. Not all specimens did this.
- f) After 1480 minutes. Pressure cycle same as c. The surfaces have many fissures.

fissures could be washed out. The tissue's surfaces had ridges on reswelling, that ran parallel to the wear direction. These were not, however, the result of different extents of wear. Rather, they were thought to be the result of macromolecular orientation within a surface region that caused the tissue to pucker on reswelling (17).

Under time varying loads, the tissue's surface characteristics were quite different. These are seen in Figures 10(c-f). In the cases shown the tissue was worn under a pressure pattern that alternated between 0.69 to 4.14 MN/m<sup>2</sup> at 0.02 Hz. In these experiments surface fissures appeared after around 300 minutes (Fig. 10). Their number increased with time until after around 20 hours the tissue's surfaces were almost totally black after being stained with India ink and washed. (This is taken as a qualitative measure of the extent of fissuring.) In many cases the tissues fractured or split to the bone after around 700 minutes of wear under this pattern. It's wear rates increased at about this time, but remained steady. When worn under constant pressure such splitting was never observed.

Under constant pressure, against stainless steel, interrupted sliding for different periods had no effect on the tissue's wear rates. This was not the case when the tissue was worn against slightly cross-linked cartilage. (In these experiments, the tissue was worn under a constant pressure of 2.07 MN/m<sup>2</sup>). Before describing the results of interrupted sliding, we should state first, that the extent of formaldehyde reaction of the bottom plug did not effect the tissues steady state wear rates (Fig. 11). We note further that while the amount of formaldehyde bound was easily assessed (by measuring the radioactivity) it was not possible to measure the degree of cross-linking. The reacted tissue was somewhat stiffer, but there was no detectable change in the tissue's swelling ratio in equilibrium with 0.03M phosphate buffer, at pH 7.4. The amount of formaldehyde bound was exceedingly small (Fig. 11) and the extents of cross-linking were likely only a small fraction of that (24).

When sliding was interrupted with the tissue under load, the tissues underwent steady compression (Fig. 12). The displacements measured by the LVDT were the sum of the compressions of both unreacted and formaldehyde reacted tissues. Visually, however, it was observed that both tissues were compressed. On the resumption of sliding reswelling occurred even though the tissues were under load (Fig. 12). The longer the stationary periods, the larger the compression. Likewise, the longer the oscillating period following interruption, the greater was the dimensional recovery until equilibrium swelling was attained.

The effect of interrupted sliding on the wear of the tissue is shown in Figure 13. When sliding was interrupted for 55 seconds, after being worn for 1 minute, the tissue wore at significantly higher rates than when sliding was interrupted for only 15 seconds.

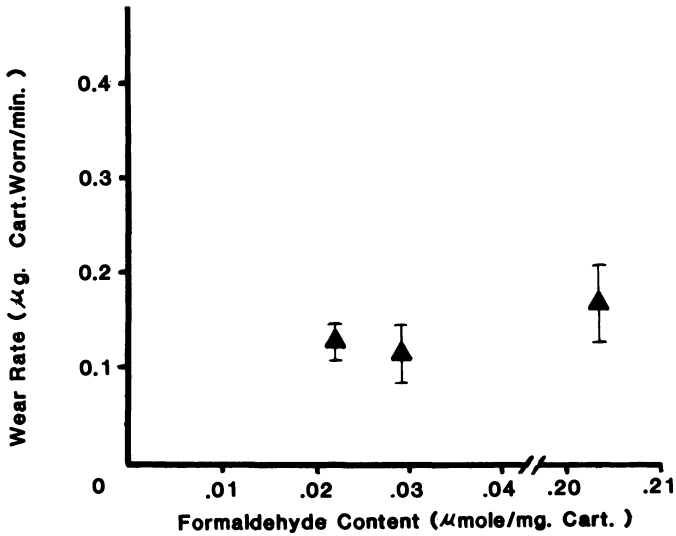


Figure 11. Steady state wear rates of cartilage when worn against cartilage that was reacted with formaldehyde to different extents. The tissues were worn under a constant pressure of  $2.07 \text{ MN/m}^2$  in these experiments. By comparison against Surface A of the stainless steel plate the tissue wore at a constant rate of  $1 \text{ μg cart./min.}$

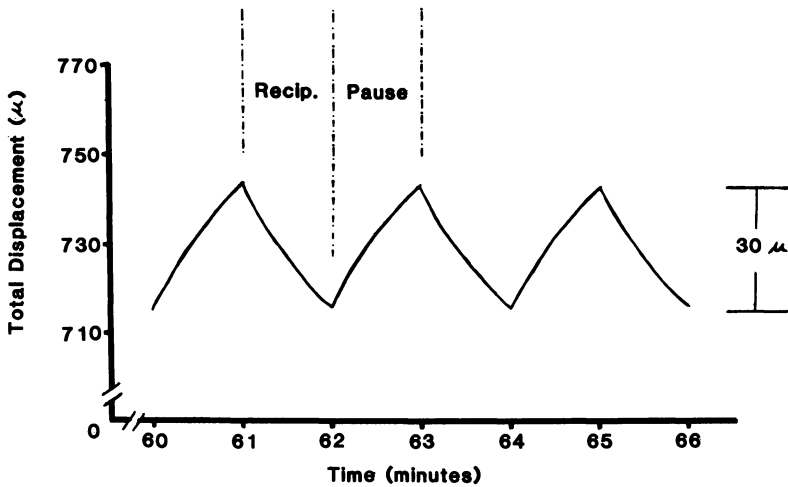


Figure 12. Displacement of both plugs during intermittent sliding under a constant pressure of  $2.07 \text{ MN/m}^2$ . Interrupting the oscillations for 55 seconds resulted in both tissues being compressed around  $30 \text{ μ}$ . When sliding was resumed the tissues recovered.



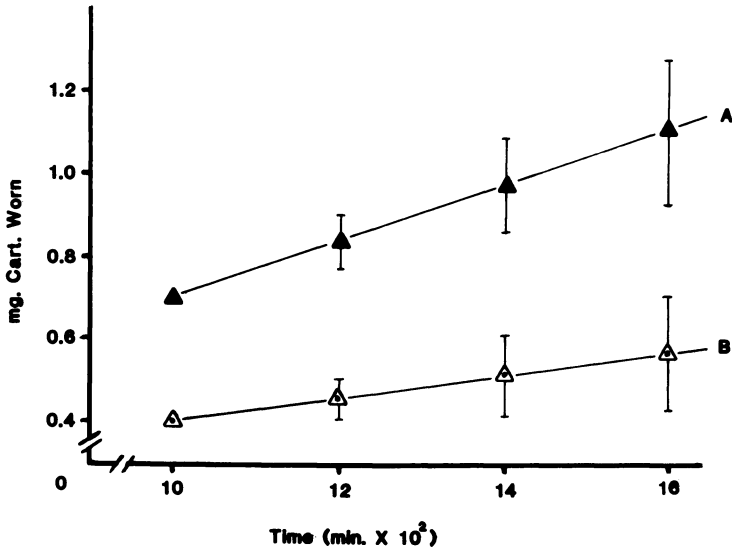


Figure 13. Steady state wear of the tissue under intermittent sliding. Curve A: oscillation stopped for 55 seconds, resumed for 1 min. Curve B: oscillation stopped for 15 seconds, resumed for 1 min. Pressure 2.07 MN/m<sup>2</sup>.

## DISCUSSION

The tissue's steady state wear rates, under cyclic pressures, were significantly lower than would have been obtained were it worn under a constant pressure equal to the time average of the two pressures. (In computing the equivalent pressure, account was taken of the fraction of each cycle spent at pressures between the two alternating pressures.) In the absence of detailed mechanical analyses, the explanations for this remain qualitative. Nevertheless, we would suggest that the lower wear rates are probably attributable, in large measure, to the tissues greater ability to dissipate stress under these conditions.

The reasoning is as follows: On the application of pressure, localized stresses are dissipated principally by fluid exudation and redistribution, the rates of which increase with the tissue's hydration state and the amounts of pressure applied (9,12,25,26). They likewise decrease with time (9,12,25,26). When pressure on the tissue is reduced, fluid is reimbibed and its thickness increases (Fig. 9). This is again reexuded on the reapplication of pressure. Since the tissues in these experiments were subjected to higher pressures for only relatively short periods, stress dissipation likely occurred at significantly higher rates throughout the experiment than would have been the case under constant equivalent pressures. This is so because the tissue's stress relaxation or stress dissipation rates decay exponentially with time (12,25,26). The net result is that the duration of localized stresses above that necessary to initiate failure would be less. Under constant pressure, imbibition and exudation could not occur to the same extent.

The reasoning is consistent with the greater differences in wear rates observed between the 0.69 - 6.9 MN/m<sup>2</sup> cycle and those that would have been attained under an equivalent constant pressure as opposed to the 0.69 - 4.14 MN/m<sup>2</sup> cycle and its equivalent counterpart. The relative rates of decay of localized stresses would be significantly greater under 6.9 MN/m<sup>2</sup> as compared with 4.14 MN/m<sup>2</sup> (9,12).

The higher rates during the initial 180 to 200 minutes are believed to be due to a combination of the following: (1) gradual orientation of segments of the tissue's macromolecules in a thin surface region that renders the tissue more wear resistant; and (2) gradual coating of tissue constituents or a transfer layer onto the steel plate in the region interfaced with the tissue. When worn under constant load against this surface, macromolecular orientation is believed to have occurred prior to its wearing at constant rates (17). After attaining constant rates, rotating the plugs 90° resulted in the tissue wearing briefly at higher rates before resuming the same rates it wore at prior to rotation (17). Such orientation could result from the contact stresses occurring during sliding.

With regard to the second factor, prior to the start of an experiment the plate was scrupulously cleaned with alkaline solutions until the wetting angle between buffer and plate was visually minimal (17). Failure to do this resulted in the tissue wearing at higher rates and the data not being reproducible. Nevertheless, during the first 200 minutes or so the wetting

angle between buffer and plate increased. This likely resulted from a hydrophobic, lipid-like material from the tissue coating the metal surface or a thin transfer layer of the tissue itself. This could have resulted in less friction between tissue and plate until steady state conditions were attained with consequent lower wear rates. Analogous phenomena have been reported for polytetrafluoroethylene sliding on metal (27).

The lower steady state wear rates, as compared with those under equivalent constant pressures were obtained for all frequencies tried (Fig. 8) and for the two loading patterns at the same frequency (Fig. 7). However, if the pressure differences in these experiments were much less or the frequencies considerably lower, the differences in wear rates would probably not be so evident. With lower frequencies the importance of stress dissipation on the tissue's overall wear rates would be smaller since the rates decay rapidly. Likewise, if the pressure differences were markedly less, the amounts of fluid reimpibition and the extents of stress dissipation would be smaller.

This suggests that, *in vivo*, the anatomical surface contours of the joints are of paramount importance in rendering the tissue wear resistant. If during articulation, tissue regions are periodically loaded and unloaded at sufficiently rapid frequencies, then localized stresses within the tissue are more likely to be kept below that needed to initiate failure than would be the case if the two hemi-joints were perfectly congruent such that fluid exudation was impeded.

The lower wear rates at 0.25 Hz as compared with those at 0.06 Hz are consistent with the above. However, we cannot explain why the rates at 0.02 Hz were lower than those at 0.06 Hz. Clearly stress dissipation and/or relaxation are not the only factors.

In the case of the 0.69 to 4.14 MN/m<sup>2</sup> cycle, the wear rates increased somewhat after around 700 minutes. This time coincided with the appearance of a large number of macroscopic fissures on the tissue's surfaces and in some cases splitting to the bone (Fig. 10c-f). Their number per unit area increased relatively rapidly with time. Nevertheless the wear-time curves remained linear. Such fissures were not observed when the tissue was worn under constant pressure. Apparently, under these conditions of periodic stress relief, cracks initiating near the tissue's surface do not necessarily propagate to form wear particles.

Weightman, et al. have concluded that fibrillation, the earliest changes in osteoarthritic cartilage visible to the naked eye, can result from fatigue failure (28). The phenomena observed here are consistent with their observations. It would seem that the extents of fissuring varies with the frequency, duration, and magnitudes of the pressure cycles. Clearly both fatigue and adhesive mechanisms were operative under these conditions.

The displacements of the tissues on cyclic loading, indicate that during the first 300 minutes the extents of fluid exudation were greater than reimpibition. The tissues did not completely recover dimensionally on reducing the pressure. The slow creep

after initial deformation likely resulted, in part, from network compaction which reduced the rates of fluid exudation. Its constancy with time may, however, be as much a function of the smooth surface it was interfaced with, as an inherent property of the tissue. A quantitative elucidation of the factors governing fluid exudation and reimbibition under prolonged cyclic loading with sliding would be most valuable in understanding the tissue's wear resistance.

After 300 minutes, steady state conditions were attained and fluid imbibition equalled fluid exudation. The tissues fluid contents were, however, lower than at the start of the experiments (17,29).

With cartilage interfaced with cross-linked cartilage, interrupted sliding resulted in both tissues being compressed (Fig. 12). When sliding was resumed the tissues reswelled even though they were under load. Evidently, the small intervals of time during oscillation that regions of the bottom plug were under reduced pressure and the changed stresses in both plugs during oscillation, resulted in their reswelling at significant rates. Interruptions for longer time periods resulted in significantly greater steady state wear rates (Fig. 13). It appears that the energy dissipated by the rather large deformations of the tissue on resumed sliding resulted in greater wear rates.

This points to an additional role of rapid fluid imbibition, other than its being able to effect internal stress dissipation and relaxation on applied pressure. It appears that rapid fluid imbibition reduces ploughing or large volume deformations during articulation.

The wear rates of cartilage under constant load were insensitive to the extents to which the bottom plugs were reacted with formaldehyde (Fig. 11). The wear rates were similar whether 0.2  $\mu$ moles of  $\text{CH}_2\text{O}/\text{gm}$ . cart. were reacted or 0.02  $\mu$ moles of  $\text{CH}_2\text{O}/\text{gm}$ . cart. Considering that only a small fraction of the bound formaldehyde participates in cross-links (24) it is astounding that this was sufficient to prevent the severe tearing that occurred with unreacted tissue. Further, the bottom plugs were hardly worn, if at all. No changes to its surface were evident at the end of the experiments. It would appear that its increased stiffness was important in increasing its wear resistance. This further illustrates the importance of minimizing large deformations in preventing excessive wear to the tissue.

There has been extensive investigative effort in trying to understand the mechanisms of the presumed low coefficients of friction between cartilage and cartilage (30). It has been thought that a breakdown of these mechanisms results in increased tissue wear. This work suggests that factors affecting fluid exudation and imbibition may be as significant in preventing tissue wear as low interfacial stresses.

Acknowledgments

This work was supported in part by funds from NIH grant AM15671, The New England Peabody Home for Crippled Children, and the Liberty Mutual Insurance Co. The author wishes to thank Mr. Robert Etheredge III for his invaluable help.

Literature Cited

1. Sololoff, L., "The Biology of Degenerative Joint Disease," Univ. of Chicago Press, Chicago, IL, 1969.
2. Stockwell, R.A.; Meachim, G., in "Adult Articular Cartilage" ed. Freeman, M.A.R., Grune and Stratton, N.Y., 1974, pp 83 - 84.
3. Lipshitz, H.; Etheredge, R., III; Glimcher, M.J., J. Bone and Jt. Surg., 58A: 1149 - 1156, 1976.
4. Lipshitz, H.; Etheredge, R., III; Glimcher, M.J., J. Bone and Jt. Surg., 57A, 527 - 534. 1975.
5. Balazs, E.A.; Bloom, G.D.; Swann, D.A., Fed. Proc., 25: 1813-1816, 1966.
6. Freeman, M.A.R. ed. "Adult Articular Cartilage", Grune and Stratton, N.Y., 1974.
7. Serafini-Fracassini, A.; Smith, J.W., "The Structure and Biochemistry of Cartilage", Churchill Livingstone, Edinburgh, 1974.
8. Barrett, A.J., in "Comprehensive Biochemistry", Florin, M., and Stolz, E.H., eds., Elsevier Publishing Company, Amsterdam, 1968, pp. 431-456.
9. Mow, V.C.; Lai, W.M., Ann. Rev. of Fluid Mech., 11, 247-288, 1979.
10. Kempson, G.E.; Freeman, M.A.R.; Swanson, S.A.V., Nature, 220, 1127, 1968.
11. Woo, S.L.Y.; Akeson, W.H.; Jemmott, C.F., J. Biomech., 9: 785-791, 1976.
12. Lipshitz, H., in "Water in Polymers," ed. S.P. Rowland, ACS symposium series 127, American Chemical Society, Wash., D.C. pp 403-430.
13. Mow, V.C., Mansour, J.M., J. Biomech. 10: 31-39, 1977.
14. Edwards, J., Proc. Inst. of Mech. Eng., 181, (Pt.3J), 16-24, 1967.

15. Sokoloff, L., Science, 141, 1055-1057, 1963.
16. Lipshitz, H.; Glimcher, M.J., J. Biomech., 7, 293-295, 1974.
17. Lipshitz, H.; Glimcher, M.J., Wear, 52, 297-339, 1979.
18. Boyde, A., J. Microsc., 98, 451-471, 1973.
19. Grant, R.A., J. Clin. Pathol, 17, 685-686, 1964.
20. Walker, J.F., Formaldehyde, ACS Monograph series, Reinhold Publishing Co., London, 1964, p. 469.
21. Lipshitz, H.; Etheredge, R., III; Glimcher, M.J., Trans. Orth. Res. Soc., 1: 92, 1976.
22. Meachim, G., Ann. Rheum. Dis., 31: 457, 1972.
23. Rabinowicz, E., Friction and Wear of Materials, John Wiley & Sons, Inc., N.Y., 1965, p. 137.
24. Cater, C.W., J. Soc. of Leather Trades Chem., 47: 259-274, 1963.
25. Lipshitz, H., Mow, V.C., Torzilli, P.A., Eisenfeld, J.; Glimcher, M.J., "Proc. VIII Int. Congress on Rheology," Klason, C., and Kubat, J., eds 1976, 198-199.
26. Grodzinsky, A.J., Lipshitz, H.; Glimcher, M.J., Nature, 275, 448-450, 1978.
27. Briscoe, B.J.; Tabor, D., in "Fundamentals of Tribology," Suh N.P. and Saka, N., eds. MIT Press, Cambridge, MA 1980.
28. Weightman, B.O., Freeman, M.A.R.; Swanson, S.A.V., Nature, 244, 303-304, 1973.
29. Lipshitz, H., Etheredge, R.; Glimcher, M.J., J. Biomech., 13: 423-436, 1980.
30. Malcom, L.L., Ph.D. Dissertation, Univ. of California, San Diego, CA, 1976.

## Discussion

Question: Professor D. Dowson (University of Leeds, Leeds, England)

I would like to congratulate the author on a very interesting investigation. The chemical approach to wear in biological material is most interesting. I wonder if the author has tried to relate his short-term wear results to the long-term performance of cartilage in the body- would the cartilage last for 50 or 70 years?

I would also like to know if the author has tried to relate his wear rates to the "wear factors (fr)" discussed throughout this Conference.

Answer: Dr. Lipshitz

With regard to the first question, it would be either difficult to relate this kind of data directly to the in vivo data.

With regard to the second question, I have tried to do it and have incorporated in the paper.

RECEIVED January 23, 1985

## Role of Fillers in the Friction and Wear Behavior of High-Density Polyethylene

S. Bahadur<sup>1</sup> and D. Tabor

Physics and Chemistry of Solids, Cavendish Laboratory, University of Cambridge, Cambridge, England

Sliding experiments between high density polyethylene filled with polar graphite, CuO, CuS, Pb<sub>3</sub>O<sub>4</sub>, 2-mercurobenzothiazole and S in different proportions and combinations and the steel surfaces were performed. The latter were finished by grinding, lapping, and abrasion against 600 grade Emery paper. In some of the experiments, in addition to the steel surfaces the glass and brass surfaces were also used. The steady-state wear rate of 5% CuO, 30% Pb<sub>3</sub>O<sub>4</sub>, 65% HDPE sliding against a ground steel surface was found excessive but it was very low while sliding occurred against an abraded steel surface. The steady-state wear rate of 30% CuS, 70% HDPE sliding against an abraded steel surface was practically zero. In this case a very thin transfer film of the filled polymeric material was formed on the steel surface. Electron diffraction studies indicated chemical bonding between the filler and steel surface.

The tribological behavior of high density polyethylene is of considerable interest due to its good mechanical properties, ease of processing and low material cost. When sliding against a metal surface under mild conditions, it exhibits low friction and low wear and forms a very thin highly oriented film on the metal counterface. Pooley and Tabor (1) associate this transfer behavior with the "smooth" molecular profile of high density polyethylene in contrast with the "rough" molecular profile of polymers which have either branching or the substitution of heavy atoms in their molecular chains. The thickness of the transferred film is greater and so is the coefficient of friction and wear rate for the latter class of polymers. However, under very severe sliding conditions, the wear rate of high density polyethylene is much higher and is accompanied by a considerable increase in thickness of the transfer film. This has been attributed to surface softening or melting

<sup>1</sup>Current address: Department of Mechanical Engineering, Iowa State University, Ames, IA 50011



under high speed sliding conditions (2, 3) and so accounting for a different mechanism of film formation as opposed to the interlamellar shear at low speeds (4). An alternative explanation offered for high wear rate is poor adhesion between the oriented polymer transfer film and the metal counterface (5). Thus, in the case of repetitive sliding, the transferred film is continuously removed and replenished resulting in a relatively high wear rate. If this is true, a filler material likely to increase adhesion between the transferred polymer film and the metal substrate, while retaining the smooth molecular profile of the polymer, would result in both low friction and low wear of the filled polymer. The mechanism of improved adhesion is still unresolved. Whereas the mechanical interlocking effects which depend upon the surface texture of counterface are obvious, the part played by chemical reaction in improving the adhesion of transfer films is obscure (6) Sviridyonok et al. (7) have indicated that for highly polar polymers, such as polyamides and polymethyl methacrylate, the transfer is controlled by the formation and interactions of free radicals generated during the sliding process.

Belyi et al. (8) have discussed various methods for decreasing wear and/or friction in polymer-metal sliding. These involve modification of the supramolecular structure of the polymer, structural transformations by gamma-irradiation, thermo-activation effects from the decomposition of filled materials under sliding conditions, and selective transfer by incorporating specific fillers in the polymeric material. The use of cuprous oxide as a filler in polytetrafluoroethylene (PTFE) has been shown to reduce the wear rate by a factor of 3. It is believed to be due to the selective transfer of copper to the steel surface because cuprous oxide is reduced to pure copper at the temperatures produced in sliding (9).

Pratt (10-12) studied the role of a large number of fillers in PTFE composites rubbing against steel and concluded that the active inorganic constituents in these composites were cupric oxide ( $\text{CuO}$ ) and lead monoxide ( $\text{PbO}$ ). By analogy with the case of PTFE, Briscoe et al. (5) experimented with  $\text{CuO}$  and  $\text{Pb}_3\text{O}_4$  (red lead) as fillers in high density polyethylene. Here  $\text{Pb}_3\text{O}_4$  was used because  $\text{PbO}$  degraded the polymer at the processing temperature. They found that 5%  $\text{CuO}$ , 35%  $\text{Pb}_3\text{O}_4$  and 60% high density polyethylene had practically zero wear rate after the initial few minutes of sliding.

The objective of this paper is to investigate the role of some potential fillers in modifying the friction and wear behavior of high density polyethylene. It has been studied in terms of the transfer film formation capability and its bonding to the counterface in view of the surface texture and chemical reaction possibilities.

### Experimental

The sliding experiments were performed on a pin-on-disc machine. The arrangement consisted of the circular end of a stationary cylindrical pin resting on the flat surface of a disc. The latter could be rotated at varying speeds. The friction force was measured using strain gauges and was continuously recorded. The wear data were obtained by weighing the polymer pin at suitable intervals. The sliding system was enclosed in a chamber. All the friction and wear experiments were performed at a sliding speed of 2.1 m/s and under ambient conditions.

The discs of the size, 100 mm-diameter and 6.5 mm-thick approximately, were made of mild steel, glass and brass. The sliding surfaces of the steel discs were finished by grinding, lapping, or abrasion against 600 grade Emery paper. These have been designated in the text as the ground, lapped and "abraded" surfaces. The last two finishing operations were performed on ground surfaces. The discs were then thoroughly cleaned in an ultrasonic bath and stored overnight for drying purposes. The pins were molded in the form of 13 mm-diameter cylinders. The base material was high density polyethylene (075-60 Rigidex Powder) supplied by the B.P. Chemicals International Co. A variety of filler materials, viz., graphite, CuO, CuS, Pb<sub>3</sub>O<sub>4</sub>, 2-mercurobenzothiazole and sulfur were used in different proportions and combinations. The graphite material was hydrophilic and polar in character. The samples were compression molded at a temperature of 150°C.

The surface roughness of the discs was measured using a profilometer. A detailed analysis of the steel disc surfaces, one of each of the ground, lapped and abraded types, was made in the first author's laboratory using a data acquisition system and an IBM 360 computer.

The transfer films were studied by optical and transmission electron microscopy.

### Results and Discussion

In order to detect the probable chemical reaction between the filler materials in the polymer and the disc surface, three counterface materials, viz., steel, brass and glass, were used. Of these materials, glass is the most inert while the constituents of brass are likely to react with sulfur in the free or combined form. In the event of a chemical reaction, the transfer film of the filled polymeric material would be more tenaciously bonded to the disc surface. Furthermore, the effect of surface texture on the transfer film formation and bonding capability was investigated using the ground, abraded and lapped surfaces for the steel discs and the flat and abraded surfaces for the glass discs. The effects of the finishing operations on the surface roughness parameters, based on our analysis of a typical steel surface of each kind, have already been described in our earlier paper (13). All the surfaces had nearly the same AA (0.176-0.251  $\mu\text{m}$ ) and rms (0.248-0.375  $\mu\text{m}$ ) roughness values. The asperity slopes of the abraded surfaces were found to be smaller than those for the ground and lapped surfaces. As for the asperity tips, the abraded surfaces had maximum rounding while the ground surfaces had maximum sharpness.

The results of the friction and wear tests for high density polyethylene sliding against the metallic disc surfaces are shown in Figures 1 and 2, respectively. The coefficients of sliding friction for the ground and lapped surfaces are about the same and are lower than that for the abraded steel surface. One probable reason for the latter is smaller slope and larger radius of curvature of asperities on the abraded surface resulting in increased area of contact. The wear rate of high density polyethylene sliding against the abraded and lapped surfaces is much smaller than that for the ground steel surface. It is believed to be due to the excessive

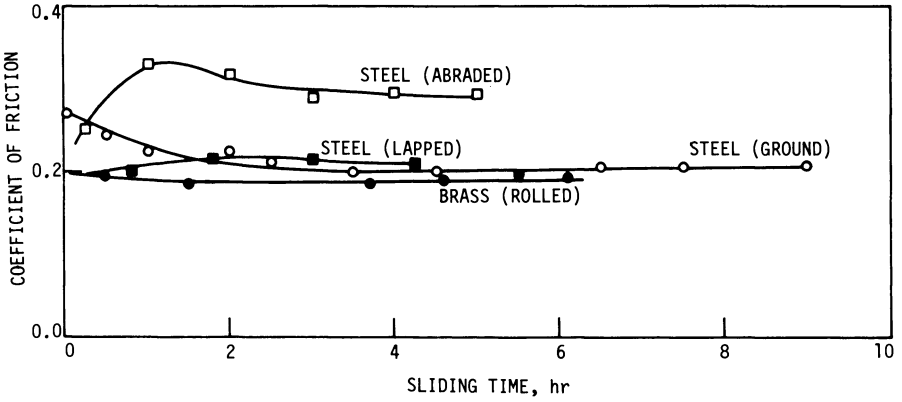


Figure 1. Coefficient of friction of high density polyethylene sliding against metal surfaces. Sliding conditions: 49 N load, 2.1 m/s speed.

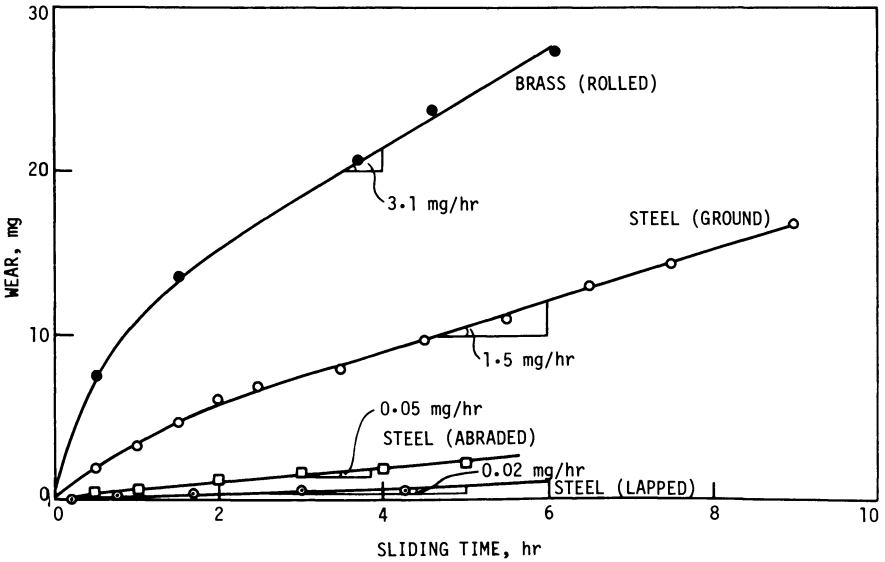


Figure 2. Wear of high density polyethylene sliding against metal surfaces. Sliding conditions: 49 N load, 2.1 m/s speed.

abrasion from sharp asperities on the ground surface, as evidenced on the worn surface of polyethylene pin in Figure 3. The transfer of polymer was minimal at best on the metal disc surfaces.

When sliding occurred between high density polyethylene pin and glass surfaces, there was no transfer of polymer on the smooth surface but there was some transfer on the abraded surface. The large fluctuations in the coefficient of friction in sliding against the smooth surface (Figure 4) indicate intermittent fracture of adhesive junctions at the interface. It was accompanied by a wear rate of 19.5 mg/hr which is considerably higher than the wear rate observed in the case of metallic surfaces (Figure 2). The wear rate jumped to about 44 mg/hr in the case of abraded glass surface due to the added effect of abrasion (Figure 4).

Since graphite as a filler is known to reduce drastically the wear rate of polytetrafluoroethylene, its effectiveness as a filler in high density polyethylene was investigated. From the results shown in Figures 5 and 6 for a ground steel surface, it is seen that 30% polar graphite in polyethylene doubles the coefficient of friction and increases the wear rate by about 30%. A similar trend was observed in the sliding of graphite-filled polyethylene against an abraded steel surface (Figures 7-8). It was, therefore, concluded that graphite is not a suitable filler in polyethylene for reduced wear.

As a next step, high density polyethylene was filled with 5% CuO and 30% Pb<sub>3</sub>O<sub>4</sub>. While sliding against a ground steel surface, the coefficient of friction was found to increase by about 25% and the wear rate increased by a factor of 15 (Figures 5-6). There was a considerable transfer of the filled polymeric material on the metal surface (Figure 9). It was an alarming observation because this particular filled composition has been reported to have a practically zero wear rate in sliding against an abraded steel surface (5). The experiments were, therefore, repeated against an abraded surface and the results are shown in Figures 7 and 8. There is not a significant change in the coefficient of friction but the wear rate is drastically reduced by a factor of 10<sup>3</sup> to about 0.019 mg/hr. There was again a transfer film of the filled material formed on the steel surface (Figure 10) but not as thick as in the case of the ground surface. The dramatic change in wear rate of the filled material brought about by a different finishing operation of the steel disc proves that the surface finish and texture have a lot to do with the stability of the transferred films and so the wear rate. The presence of abrasion marks on the filled polymer samples in both cases indicates that some abrasion does occur in the sliding process. The size of the detached wear fragment due to the abrasive action is governed by the shape, size, distribution and proportion of the filler material on one hand and the surface finish and texture of the hard counterface on the other. The latter being the case, the thickness of the transferred film on the ground surface was much larger than that on the abraded surface. Furthermore, a thick film of the transferred material is not necessary for reduced wear rate.

Since iron can react with sulfur and form sulfide films which can affect the tribological behavior significantly, CuS as a filler in high density polyethylene was next investigated. With 30% CuS, 70% HDPE sliding against the abraded steel surface, a steady-state wear rate of 0.01 mg/hr and a coefficient of friction of about 0.28

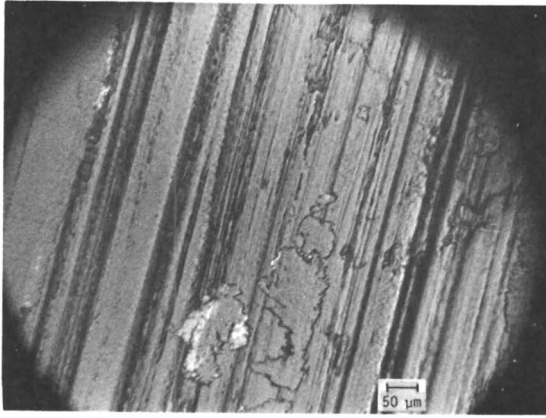


Figure 3. High density polyethylene pin worn against a ground steel disc.

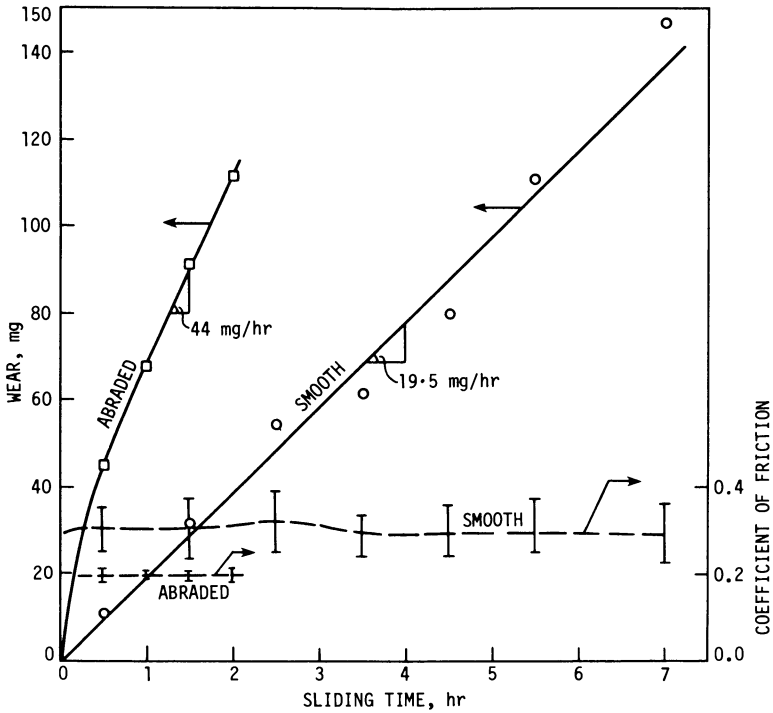


Figure 4. Coefficient of friction (--) and wear (—) of high density polyethylene sliding against smooth and abraded glass surfaces. Sliding conditions: 49 N load, 2.1 m/s speed.

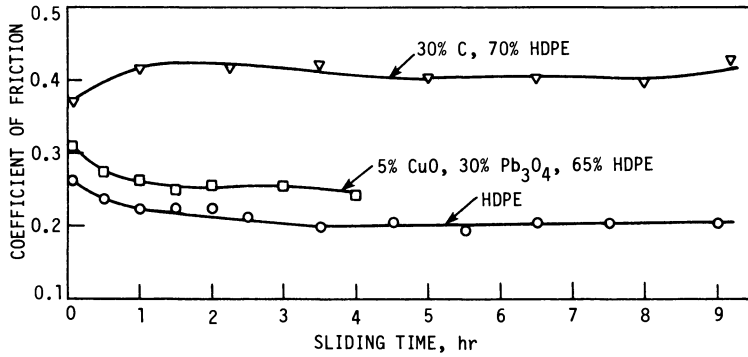


Figure 5. Coefficient of friction of filled and unfilled high density polyethylene sliding against a ground steel disc. Sliding conditions: 39 N load, 2.1 m/s speed.

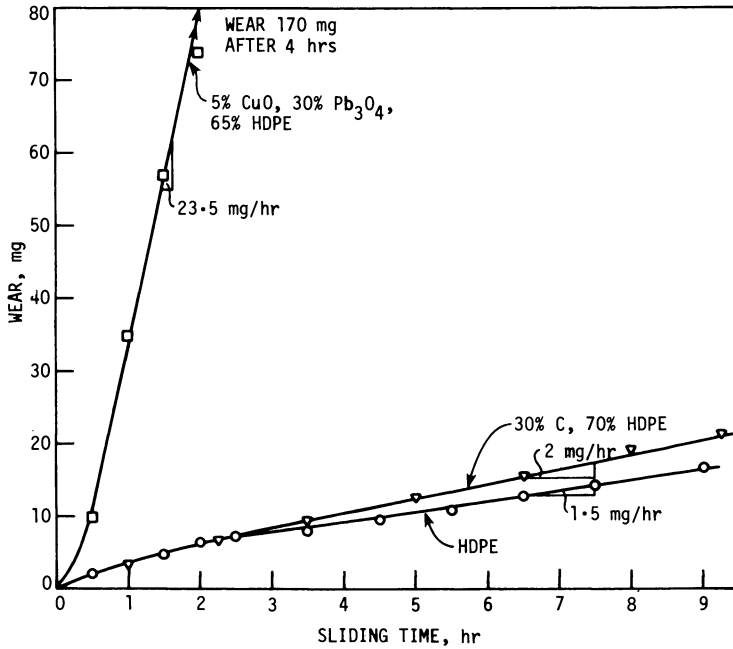


Figure 6. Wear of filled and unfilled high density polyethylene sliding against a ground steel disc. Sliding conditions: 39 N load, 2.1 m/s speed.

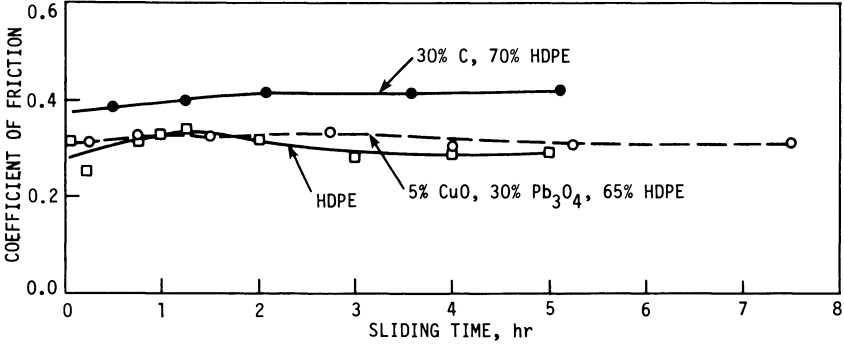


Figure 7. Coefficient of friction of filled and unfilled high density polyethylene sliding against an abraded steel disc. Sliding conditions: 49 N load, 2.1 m/s speed.

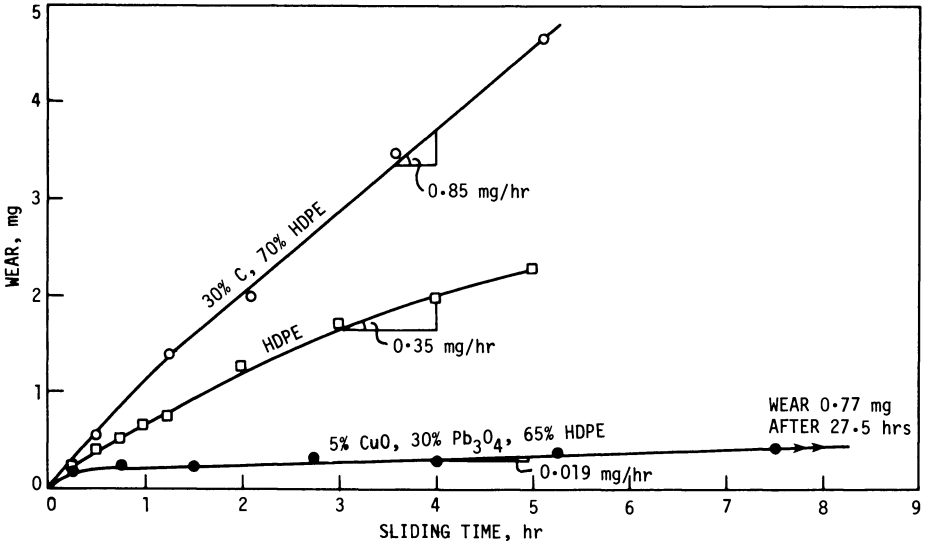


Figure 8. Wear of filled and unfilled high density polyethylene sliding against an abraded steel disc. Sliding conditions: 49 N load, 2.1 m/s speed.

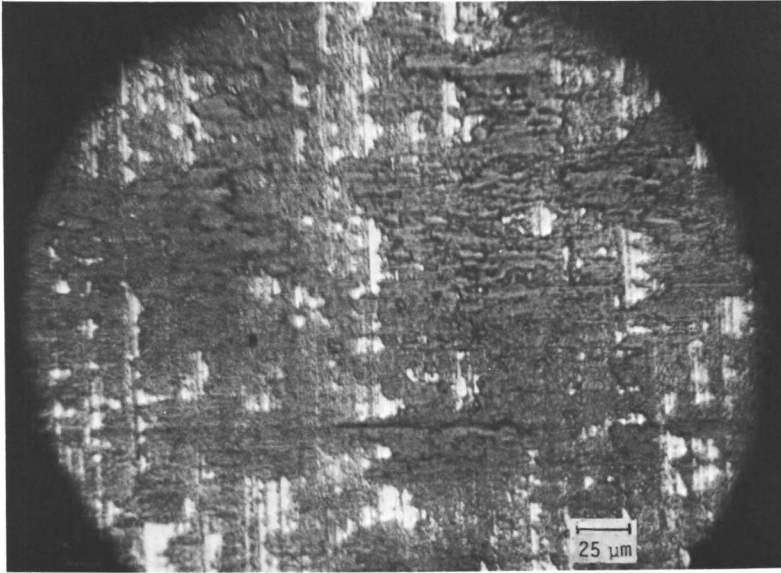


Figure 9. Transfer film of 5% CuO, 30% Pb<sub>3</sub>O<sub>4</sub>, 65% HDPE formed in sliding against a ground steel surface.

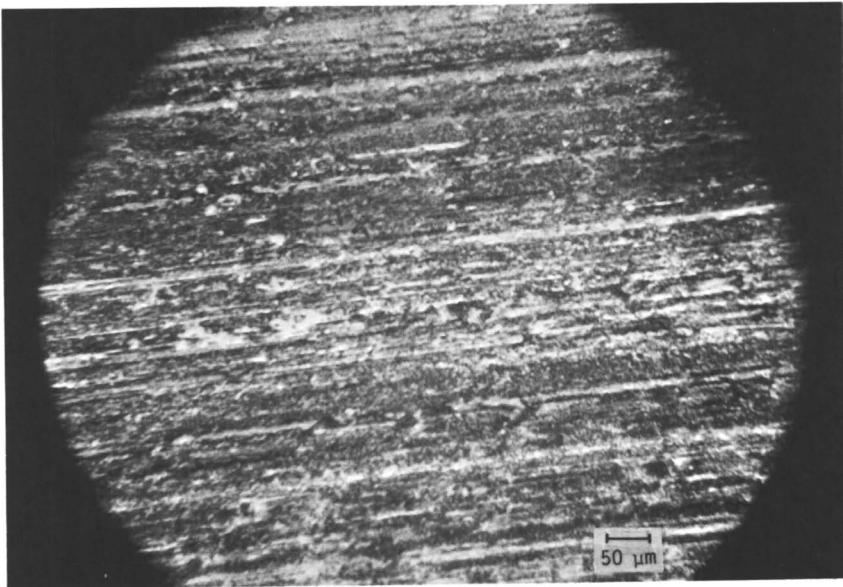


Figure 10. Transfer film of 5% CuO, 30% Pb<sub>3</sub>O<sub>4</sub>, 65% HDPE formed in sliding against an abraded steel surface.



was obtained (Figure 11). Thus, CuS as a filler produces a remarkable reduction in the wear rate of polyethylene without affecting the coefficient of friction. The same was true when sliding was performed between the filled material and the lapped steel surface. Here the wear in the initial 1 1/4 hr of sliding was 0.26 mg but then no wear could be detected in the subsequent sliding period of 16 hrs. As in the case of 5% CuO, 30% Pb<sub>3</sub>O<sub>4</sub>, 65% HDPE, the film formed in this case was also very thin (Figure 12). When 10% Pb<sub>3</sub>O<sub>4</sub> and 30% CuS were filled in the polymer, both the friction and the steady-state wear rate remained practically unchanged (Figure 11). Thus Pb<sub>3</sub>O<sub>4</sub> does not seem to play any significant role in modifying the friction and wear behavior of CuS-filled high density polyethylene.

In the sliding of 30% CuS, 70% HDPE against the rolled brass, the steady-state wear rate was 0.78 mg/hr (Figure 13) compared to 3.1 mg/hr for (unfilled) high density polyethylene (Figure 2) and the coefficient of friction was unaltered. Furthermore, the transfer film in sliding of the filled material was more pronounced. The brass surface had been badly abraded which must be from CuS in the filled material. It was probably this third body abrasion that prevented the wear rate of the filled material from being reduced considerably. While sliding against the smooth glass surface, the filled material had a steady-state wear rate of 0.67 mg/hr (Figure 13) compared to 19.5 mg/hr for the unfilled material (Figure 4) and the coefficient of friction was reduced from 0.3 to 0.2. There was no evidence of the transfer of polymeric film on glass surface in either case. The drastic reduction in the wear rate of the filled material sliding against glass considering that the latter is chemically inert leads to the conclusion that the lowering in wear rate which occurs here is due to the mechanical effects. Since glass offers the smoothest possible surface, the wear arises from adhesion due to the van der Waals' forces of attraction. The wear rate depends upon the rate at which junctions are formed and broken during sliding and the size of wear fragments which is governed by the size, shape and distribution of the filler particles. The transfer film is not formed because of the absence of asperities to lock in the worn particles as well as the absence of chemical bonding.

In order to investigate the effect of free sulfur in the wear process, high density polyethylene was filled with 2% S and 2% 2-mercurobenzothiazole. This composition provided almost the same wear rate as that of the unfilled material and the coefficient of friction was also the same. It proves that the strengthening of the polymer from the filler material is important for the reduction of wear.

Electron diffraction pattern analysis was performed on the wear fragments produced in the sliding of 30% CuS, 70% HDPE against the abraded steel surface. The indexing of the diffraction spots corresponded to diffraction from the planes (100), (210), (224), (300) and (308) of FeS, (210) of FeS<sub>2</sub>, (440) of Fe<sub>3</sub>S<sub>4</sub>, (024), (136) and (143) of CuFeS<sub>2</sub>, (006), (112), (113) and (208) of Cu<sub>5</sub>FeS<sub>6</sub> and (102) of Cu<sub>3.8</sub>Fe<sub>0.62</sub>S<sub>4</sub>. The d-spacings of some of the planes of these compounds are so close that it is not possible to conclude in a definite manner whether a few or all of these compounds are being

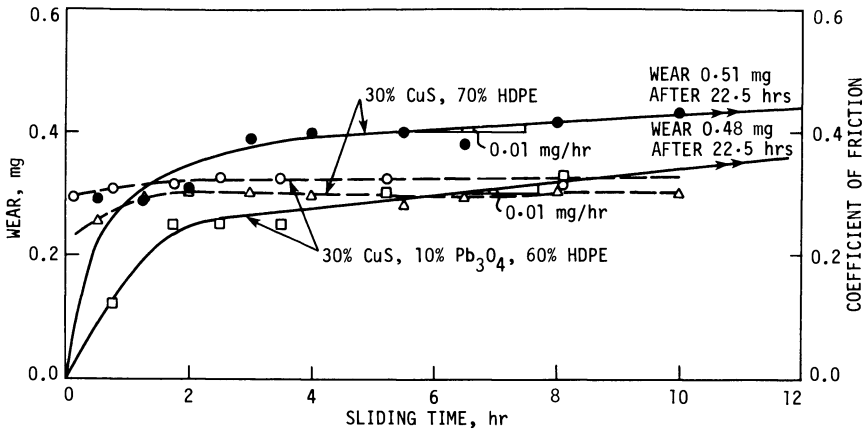


Figure 11. Wear (—) and coefficient of friction (---) of 30% CuS, 70% HDPE and 30% CuS, 10% Pb<sub>3</sub>O<sub>4</sub>, 60% HDPE sliding against an abraded steel disc. Sliding conditions: 49 N load, 2.1 m/s speed.

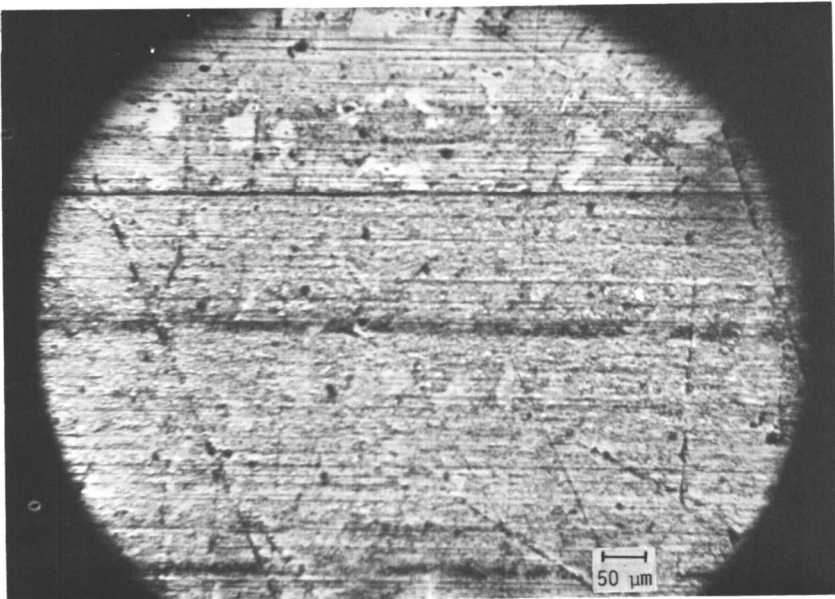


Figure 12. Transfer film of 30% CuS, 70% HDPE formed in sliding against an abraded steel surface.

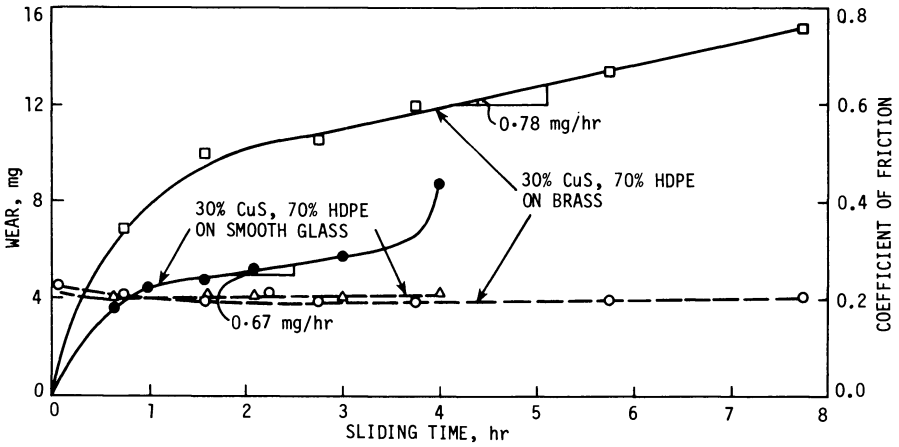


Figure 13. Wear (—) and coefficient of friction (---) of 30% CuS, 70% HDPE sliding against the smooth glass and brass surfaces. Sliding conditions: 49 N load, 2.1 m/s speed.

produced in the sliding process. However, it proves beyond any doubt that CuS particles do react chemically with the steel surface. Thus the transfer film of CuS-filled high density polyethylene is bonded both mechanically and chemically to the steel surface. The film is, therefore, not being easily scraped away during sliding which accounts for the negligible wear in this case.

It suggests that a careful selection of the filler materials that would strengthen the polymeric material and would also react chemically during sliding with the metallic surface to produce enhanced bonding is needed for reduced wear.

### Conclusions

1. For low wear in the case of polymer-metal sliding, a steel surface is better than a glass or brass surface. A ground surface produces too much abrasion due to sharp asperities. As such the surface should be finished smooth after grinding by abrasion.
2. The use of polar graphite as a filler in high density polyethylene results in both increased friction and wear.
3. In the sliding of 5% CuO, 30% Pb<sub>3</sub>O<sub>4</sub>, 65% HDPE against an abraded steel surface, a very low steady-state wear rate of 0.019 mg/hr is observed and the coefficient of friction is the same as that of the unfilled high density polyethylene. The wear rate of this composition is excessively high when sliding occurs against a ground steel surface.
4. Thirty percent CuS as a filler in high density polyethylene produces a dramatic reduction in the steady state wear rate to 0.01 mg/hr without affecting the coefficient of friction while sliding against an abraded steel surface.
5. In the case of 30% CuS, 70% HDPE sliding against an abraded steel surface, a thin film of the filled polymer is formed on the counterface. Electron diffraction analyses of the wear debris provided evidence of the presence of the compounds of Fe, S and Cu which implies that the transfer film is being bonded chemically to the steel surface.
6. The role of the filler in reducing the wear rate is threefold: strengthening of the polymeric material, enhanced bonding between the transfer film and the metal surface by chemical reaction, and reduction in the size of wear particles formed.
7. For reduced wear a very thin transfer film bonded strongly to the interface is needed.

### Literature Cited

1. Pooley, C. M.; Tabor, D., "Friction and Molecular Structure: the Behavior of some Thermoplastics," Proc. Roy. Soc. London, Ser. A329, 1972, pp. 251-274.
2. Kar, M. K.; Bahadur, S., "Micromechanism of Wear at Polymer-Metal Sliding Interface," Wear, Vol. 46, 1978, pp. 189-202.
3. Tanaka, K.; Uchiyama, Y., "Friction, Wear and Surface Melting of Crystalline Polymers," Advances in Polymer Friction and Wear, L. H. Lee, Ed., Polymer Sci. & Techn., Vol. 5B, Plenum Press, New York, 1974, pp. 499-531.

4. Kar, M. K.; Bahadur, S., "Mechanism of Film Formation in Polymer-Metal Sliding," Fundamentals of Tribology, N. P. Suh and N. Saka, Eds., Proc. Intl. Conf., M. I. T. Press, Cambridge, 1980, pp. 759-765.
5. Briscoe, B. J.; Pogolian, A. K.; Tabor, D., "The Friction and Wear of High Density Polythene: The Action of Lead Oxide and Copper Oxide Fillers," Wear, Vol. 27, 1974, pp. 19-34.
6. Pocock, G.; Cadman, P., "The Application of Scanning Calorimetry and Electron Spectroscopy to PTFE-Metal Reactions of Interest in Dry Bearing Technology," Wear, Vol. 37, 1976, pp. 129-141.
7. Sviridyonok, A. I.; Belyi, V. A.; Smurugov, V. A.; Savkin, V. G., "A Study of Transfer in Frictional Interaction of Polymers," Wear, Vol. 25, 1973, pp. 301-308.
8. Belyi, V. A.; Kragelskii, I. V.; Savkin, V. G.; Sviridyonok, A. I., "Methods of Decreasing Wear in Metal-Polymer Contacts," In Wear of Material 1977, W. A. Glaeser, K. C. Ludema and S. K. Rhee, Eds., ASME, New York, 1977, pp. 532-537.
9. Belyi, V. A.; Kupchinov, B. I.; Mikhnevich, A. S., "On the Problem of Mechanism of Friction for Filled Polymers," On the Nature of Solids Friction, Nauka i Tekhnika, Minsk, 1971, pp. 190-197.
10. Pratt, G. C., Plastic Bearings in Lubrication and Lubricants, E. R. Braithwaite, Ed., Elsevier, Amsterdam, 1965.
11. Pratt, G. C., "Plastics as Bearing Materials with Particular Reference to PTFE," Trans. J. Plastics Inst., London, Vol. 32, 1964, pp. 255-260.
12. Pratt, G. C., "Recent Developments in PTFE Based Dry Bearing Materials and Treatments," Proc. Conf. Lubrication and Wear, Paper 16, Instn. Mech. Engrs., London, 1967.
13. Bahadur, S.; Tabor, D., "The Wear of Filled Polytetrafluoroethylene," In Wear of Materials-1983, Ludema, K. C., Ed., ASME, New York, pp. 564-570.

#### Discussion

Question: M. P. Wolverton (LNP Corporation)

What steel and brass compositions and what surface roughness values were used for the discs?

Answer:

The steel disc was made of plain carbon steel with about 0.2% carbon in it. The composition of brass was about 70% Cu and 30% Zn. The arithmetic average surface roughness values for glass and brass disc surfaces were 0.006  $\mu\text{m}$  and 0.08  $\mu\text{m}$ , respectively. The roughness parameters for the steel disc surfaces are given in the table below.

Roughness Parameter	Ground		Abraded		Lapped	
	A*	P**	A	P	A	P
Arithmetic average (AA), $\mu\text{m}$	0.251	0.161	0.176	0.102	0.177	0.381
rms, $\mu\text{m}$	0.375	0.212	0.262	0.167	0.248	0.574
Asperity slope	0.015	0.035	0.013	0.014	0.028	0.039
Radius of curvature, $\mu\text{m}$	46.935	33.339	55.735	76.954	50.463	42.434

\*A - along the asperities.

\*\*P - perpendicular to the asperities.

Question: A. I. Medalia (Consultant, Newton, Massachusetts)

What is the mechanism whereby a thin transfer film causes a decrease in wear rate without causing a decrease in coefficient of friction?

Answer:

A polymer transfer film drapes over the asperities on the metal surface. This in effect suppresses the abrading action of metal asperities. If the transfer film is thin, it locks tenaciously into the metal surface by conforming better to the surface irregularities thereby reducing the likelihood of its being scraped away during sliding. When the film is finally worn away after repeated sliding, a new film of a small thickness is deposited again. The longer life of the film coupled with its smaller thickness result in lower wear. The coefficient of friction remains unaffected so long as sliding occurs between the polymer pin and the transferred film of polymer on metal surface. It is so because the adhesive forces which mostly contribute to frictional resistance are independent of the transfer film thickness.

Question: Donald H. Buckley (NASA, Lewis Research Center)

What was the technical basis for selecting the particular fillers used?

Answer:

The fillers graphite,  $\text{CuO}$  and  $\text{Pb}_3\text{O}_4$  which are known to reduce wear were used in this work to study the difference in the transfer films formed against surfaces of various textures and materials and thus investigating the role of these films in reducing wear.  $\text{CuS}$  was selected on the consideration that its low decomposition temperature of  $220^\circ\text{C}$  could promote, due to the heat generated at the interface during sliding, some sort of chemical bonding between  $\text{CuS}$  and the steel surface thereby rendering the transfer film removal from the counterface extremely difficult. This in effect would reduce wear. Sulfur and 2-mercurobenzothiazole were used as fillers to investigate the effect of free sulfur in the wear process.

Question: Donald H. Buckley (NASA, Lewis Research Center)

The high interface temperatures could promote the reactions between CuS and steel. If you reduce speed and/or load, will you eliminate the potential for reaction and accordingly the effectiveness of CuS as a filler?

Answer:

I think so. Unless experiments are carried out with varying sliding speed and load conditions, it is not possible to say when this change will occur.

Question: B. J. Briscoe (Imperial College of Science and Technology)

Early work suggests that the wear rate in these systems is quite sensitive to counterface temperature. Did you control counterface temperature in your experiments? Have you any data on wear in different environments which might reveal the influence of chemical processes?

Answer:

No. These are good suggestions for future work.

Question: N. S. Eiss, Jr. (VPI and S.U.)

The interface temperatures would be quite different for the glass and steel discs. Could your conclusions be modified by considering the effects of different interface temperatures?

Answer:

A considerably higher interface temperature during sliding of the polymer against glass surface could have produced thermal softening of the junctions and thereby contributed to a much greater wear rate. The large fluctuations in the coefficient of friction in Figure 4 support this explanation.

Question: G. Eisenbrand (Hughes Aircraft)

Did you make any measurements of particle size for the 5% CuO and 30% Pb<sub>3</sub>O<sub>4</sub> filler? Was the morphology of the polymer specimen identical before and after the experiment? Did either of the filler materials transfer preferentially to the counterfaces?

Answer:

The particles were extremely fine but specific measurements were not made. The morphology of the polymer before and after the wear experiment was not verified. The transfer seemed to depend more upon the disc material, surface roughness and texture than on the filler.

RECEIVED January 23, 1985

## Tribology of Fiber-Reinforced Polyimides Sliding Against Steel and Silicon Nitride

Paul Sutor

Midwest Research Institute, Kansas City, MO 64110

Graphite-polyimide composites, containing solid lubricant additives, were found to give low friction and wear when sliding against steel at 316°C. The same composites were found to give higher friction, with more wear and surface damage, when sliding against silicon nitride under identical conditions. High interfacial temperatures, graphite fiber abrasiveness, and adverse additive reactions contributed to the poor lubricant effectiveness of the composites sliding against silicon nitride. Composites which contained a MoS<sub>2</sub>-based solid lubricant additive were found to give substantially lower friction against silicon nitride than composites which contained a WSe<sub>2</sub>/GaIn-based additive. Composites which contained a coarse fiber weave, which produced a greater concentration of graphite fibers at the composite sliding surface, were found to give generally higher wear and friction against silicon nitride than composites which contained a fine fiber weave.

Graphite fiber-reinforced polyimides possess attractive properties as lubricating materials of construction, particularly for elevated temperature operation. Polyimides as a class are thermally stable and exhibit reasonably low friction and wear up to 300°-350°C. Graphite fiber reinforcement provides the strength and stiffness required in structural components, and can also improve the tribological properties of polyimides. Graphite-polyimide composites may be used as bearings, bearing separators, bushings, gears, and sliding seals.

Much of the recent work on the friction and wear behavior of polyimides, with and without graphite fiber reinforcement and/or solid lubricant additives, has been conducted by Fusaro (1), who has recently reviewed the field (2). Reduction of friction and wear of polyimides by inclusion of graphite fibers, particularly at elevated temperature, is illustrated in a study by Fusaro and Sliney (3). In



experiments in which stainless steel pins were slid against solid polyimide disks at 25°C, these authors found that addition of 50% graphite fibers to one polyimide markedly improved the friction coefficient (from 0.40 to 0.19) and wear rate (from  $35 \times 10^{-14}$  to  $0.6 \times 10^{-14}$  m<sup>3</sup>/m), compared to the base polyimide. At 300°C, the friction coefficient of the graphite fiber-reinforced polyimide was even lower (0.05), but the wear rate was nearly the same ( $0.7 \times 10^{-14}$  m<sup>3</sup>/m) as at 25°C.

Sliney and Johnson investigated graphite fiber-polyimide composites for spherical bearings to 340°C (4); Sliney and Jacobson investigated graphite fiber-polyimide composites in self-aligning plain bearings to 315°C (5). Gardos and McConnell subsequently initiated a long term program to develop graphite-polyimide composites suitable for use as self-lubricating separators for high speed ball bearings, operating at 316°C, in small, limited life gas turbine engines (6). The composite separators were to provide solid lubrication for bearings consisting of hot-pressed silicon nitride balls and M50 steel races. Inorganic solid lubricant additives were incorporated in these composites, with the aim of lowering friction and facilitating lubricant transfer to the bearing surfaces, while maintaining low wear.

Development and tribological evaluation of these self-lubricating composites over the past several years has recently been reviewed by Sutor and Gardos (7, 8). This work demonstrated that many of the composites which were excellent lubricants for steel were poor lubricants for silicon nitride. Thus, achieving effective solid lubrication of silicon nitride was of particular concern.

The work reported here was the culmination of our study of self-lubricating composites intended for use as lubricating separators in high speed ceramic and metal ball bearings. In this work, the friction, wear, and transfer behavior of four graphite-polyimide composites, containing solid lubricant additives, was evaluated in sliding versus M50 steel and hot-pressed silicon nitride, at 316°C in air. The effects on composite tribological properties of solid lubricant additive type, and of the manner in which the graphite fibers were woven, was examined.

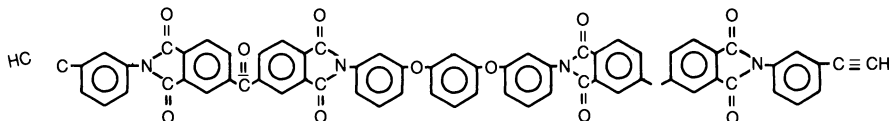
### Experimental

**Materials.** The composite lubricants contained four components: polyimide matrix resin, woven graphite fiber reinforcement, inorganic solid lubricant additives, and  $(\text{NH}_4)_2\text{HPO}_4$ . All composite formulations consisted of 40% graphite fiber, 45% polyimide, 13% inorganic lubricant pigment, and 2%  $(\text{NH}_4)_2\text{HPO}_4$ , based on the weight of each component before molding. Composition based on volume of each component after molding differed for each composite, as shown in Table I, due to the different densities of some components and to process variables which were not easily controlled.

Four composites were studied. Each contained the same polyimide matrix resin, graphite fiber, and  $(\text{NH}_4)_2\text{HPO}_4$ . The composites differed in the type of solid lubricant additive employed and in the manner in which the fibers were woven. Two types of inorganic solid lubricant additives, denoted L1 and L2, and two types of fiber weave, denoted W1 and W2, were employed. The materials to which

these designations refer are described in detail below. For brevity, the composites will be identified in this paper as L1W1, L1W2, L2W1, and L2W2, indicating the lubricant additive and fiber weave employed. Table I describes in detail the composite formulation to which each designation refers.

The polyimide matrix resin employed in all composites was THERMID 600, a thermosetting resin polymerized from acetylene-terminated oligomers. Its chemical structure is shown below (9).



THORNEL 50 graphite fibers were employed for reinforcement. These fibers, obtained by pyrolysis of polyacrylonitrile, have a tensile strength of 2.41 GPa and tensile modulus of 391 GPa. Tows containing several thousand THORNEL 50 filaments were woven into three dimensional, orthogonal preforms in one of two manners, illustrated in Figure 1. Weave 2 (W2) was relatively coarser than weave 1 (W1), although fiber volume in the preforms was similar (30.0% for W1 and 31.2% for W2).

One of two inorganic lubricant mixtures was employed. Lubricant 1 (L1), first reported by Boes (10), is formed by heating a compact of 80% WSe<sub>2</sub> and 20% Ga/In eutectic to 540°C. The resultant mixture contains WSe<sub>2</sub>, gallium and indium selenides, W, Ga, and In. The compact was ground to form a powder for inclusion in the composites. L1 resists oxidation at remarkably high temperatures due to formation of a passivating layer of gallium and indium oxides. Lubricant 2 (L2) was TURBOLUBE (ASU Composants), a mixture of layer lattice transition metal dichalcogenides. Elemental analysis is consistent with the approximate composition 75% MoS<sub>2</sub>, 20% MoSe<sub>2</sub>, and 5% WS<sub>2</sub> or WSe<sub>2</sub>, by weight. L2 was furnished as a powder.

Dibasic ammonium phosphate, (NH<sub>4</sub>)<sub>2</sub>HPO<sub>4</sub>, was included in all composites, acting both to improve fiber-matrix bonding and to reduce the friction and wear of the graphite fibers at elevated temperature, as reported by Lancaster (11).

The composites were fabricated by mixing the inorganic additives with the resin, infiltrating fiber preforms with this mixture, pressing in a hydraulic press, and curing. Test specimens were then machined from the composites. Although mechanical properties of the four new composites were not measured, similar previously fabricated materials had tensile strengths and moduli of approximately 200 MPa and 8 GPa, respectively.

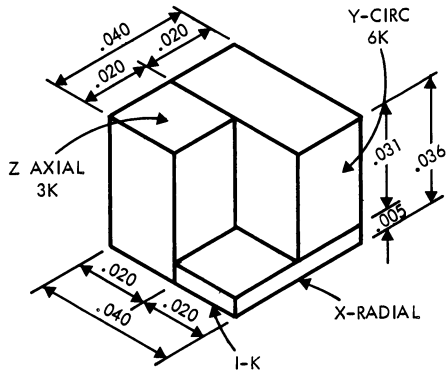
One sliding counterface was M50 steel (alloying elements: 4.0% Cr, 4.2% Mo, 1.0% V, 0.8% C, 0.2% Si, 0.2% Mn, by weight), hardened to Rockwell C 58-60, with an average surface roughness of 0.15-0.20 μm r.m.s. The other counterface was NC-132 hot-pressed silicon nitride (Norton Co.), which contains approximately 1% MgO as a sintering aid, of the same surface finish.

**Methods.** Sliding friction and wear experiments were conducted using a Hohman A-6 dual rub shoe machine. The sliding configuration

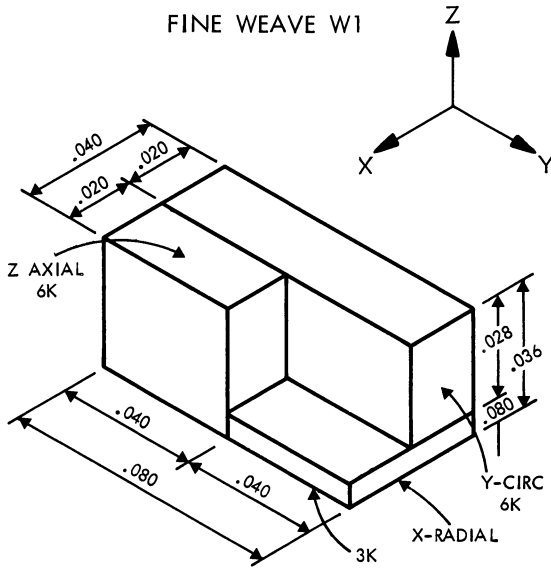
Table I. Composition of Self-Lubricating Composites

Composite	Lubricant Additive	Fiber Weave	Composition* (volume % after molding)				Density (g·cm <sup>3</sup> @ 25°C)	
			Fiber	Polyimide	Lubricant	(NH <sub>4</sub> ) <sub>2</sub> HPO <sub>4</sub>		Porosity
L1W1	WSe <sub>2</sub> /GaIn	Fine	49.4	44.6	2.4	1.6	2.0	1.65
L1W2	WSe <sub>2</sub> /GaIn	Coarse	54.0	40.0	2.2	1.4	2.4	1.65
L2W1	MoS <sub>2</sub> /MoSe <sub>2</sub>	Fine	42.4	46.1	3.4	1.6	6.5	1.58
L2W2	MoS <sub>2</sub> /MoSe <sub>2</sub>	Coarse	49.4	43.8	3.2	1.6	2.0	1.68

\* For all composites, formulation was based on weight % before molding = 40.0% fiber, 45.0% polyimide, 13.0% lubricant, and 2.0% (NH<sub>4</sub>)<sub>2</sub>HPO<sub>4</sub>.



FINE WEAVE W1



COARSE WEAVE W2

Figure 1. Unit cell comparison of fine weave (W1) and coarse weave (W2).

consists of two conforming rub shoes loaded against the outside diameter of a rotating disk. The rub shoes were made of composite laminates, adhesive bonded to stainless steel base blocks, and the disks were made of steel or silicon nitride. Relative humidity of the air in the laboratory was  $30 \pm 8\%$ . A 111 N (25 lb) load was applied to the rub shoes and the specimens were heated to  $316^\circ\text{C}$  by an oven which enclosed the test zone. Temperature was monitored and controlled by a thermocouple inserted in one of the rub shoe steel base blocks, 5.5 mm from the sliding interface. After temperature equilibration, the steel or ceramic counterface disk was rotated at a velocity of 1.10 m/s. Specimens were slid for 3.85 km, removed for wear measurement and optical microscopy, slid an additional 3.85 km against silicon nitride and 13.8 km against steel, and removed for wear and SEM/EDX analysis.

Frictional torque was recorded continuously. Wear was measured as weight loss, to the nearest mg, and converted to volume loss using the measured composite densities. The composites were hygroscopic. In order to obtain accurate and reproducible measurements of wear, in the absence of dehydration, by the method of weight loss, the following procedure was employed. Before each test, the composite rub shoes were heated to  $316^\circ\text{C}$  for 30 min and weighed immediately upon cooling to  $30^\circ\text{C}$ . After each test, they were also weighed immediately upon cooling to  $30^\circ\text{C}$ . Between tests, they were stored at  $25^\circ\text{C}$  in a desiccator.

## Results

Table II presents the specific wear rates (in  $\text{mm}^3/\text{Nm}$ , volume loss per unit load per unit sliding distance) and average kinetic friction coefficients of the composites sliding versus steel and silicon nitride, upon initial and continued sliding. Plots of friction coefficient versus sliding duration in kilocycles (1 kc = 107 m) are shown in Figures 2-5, for all experiments. All composites formed transfer films upon sliding against both steel and silicon nitride. The films were similar in appearance under optical microscopy, and covered approximately 30% of the contact region.

Steel Counterface. Wear and friction against steel, for all composites except L1W1, indicate excellent lubrication. Friction coefficients are near the minimum, and wear rates near the maximum, of the "low friction, low wear" regime delineated for a wide variety of polyimides by Fusaro (2).

The experiments in which composite L1W1 was sliding against steel were conducted at a reduced sliding velocity, 0.73 m/s, compared to the sliding velocity of 1.10 m/s employed in all other reported experiments. The sliding distance was the same, so that wear rates may be justifiably compared. The lower velocity was required for L1W1 because the composite soon began to glow red at the higher speed. Temperature measured by an optical pyrometer focused on the sliding interface quickly rose to  $510^\circ\text{C}$  at the higher speed, but the red glow indicates that interfacial temperatures may have been at or above  $650^\circ\text{C}$ . No gross thermal decomposition of the L1W1 composite

Table II. Wear Rates and Average Friction Coefficients ( $f_k$ ) at 316°C

Counterface	M50 Steel				NC-132 Silicon Nitride			
	Initial Sliding Wear Rate ( $\text{mm}^3/\text{Nm}$ )	$f_k$	Continued Sliding Wear Rate ( $\text{mm}^3/\text{Nm}$ )	$f_k$	Initial Sliding Wear Rate ( $\text{mm}^3/\text{Nm}$ )	$f_k$	Continued Sliding Wear Rate ( $\text{mm}^3/\text{Nm}$ )	$f_k$
L1W1	$21.8 \times 10^{-5}$	0.15			$12.0 \times 10^{-5}$	0.19	$13.8 \times 10^{-5}$	0.24
L1W2	2.69	0.14			12.1	0.34	17.9	0.53
L2W1	2.83	0.09	$1.85 \times 10^{-5}$	0.09	5.02	0.10	2.44	0.22
L2W2	3.40	0.05	2.51	0.16	11.8	0.08	9.44	0.29

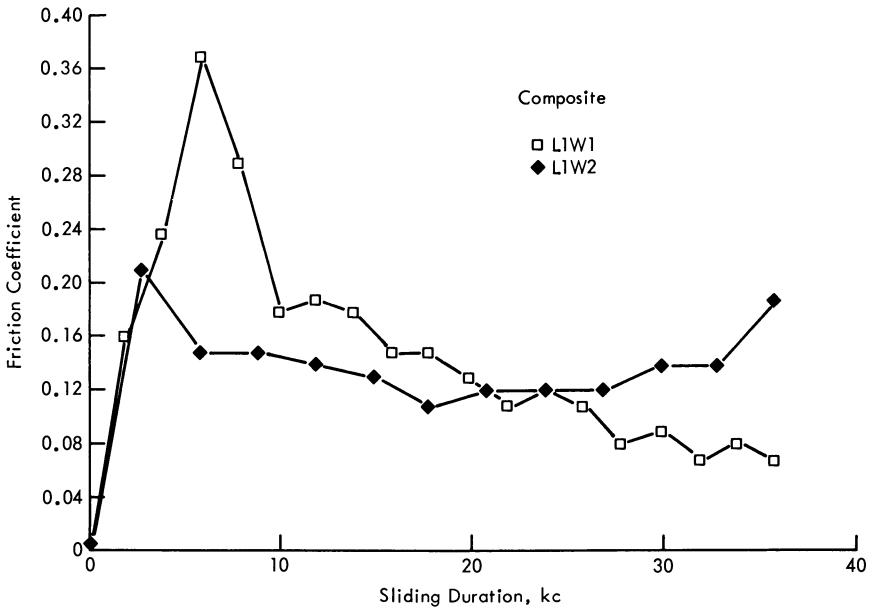


Figure 2. Friction coefficient as a function of sliding duration for L1 composites sliding against steel.

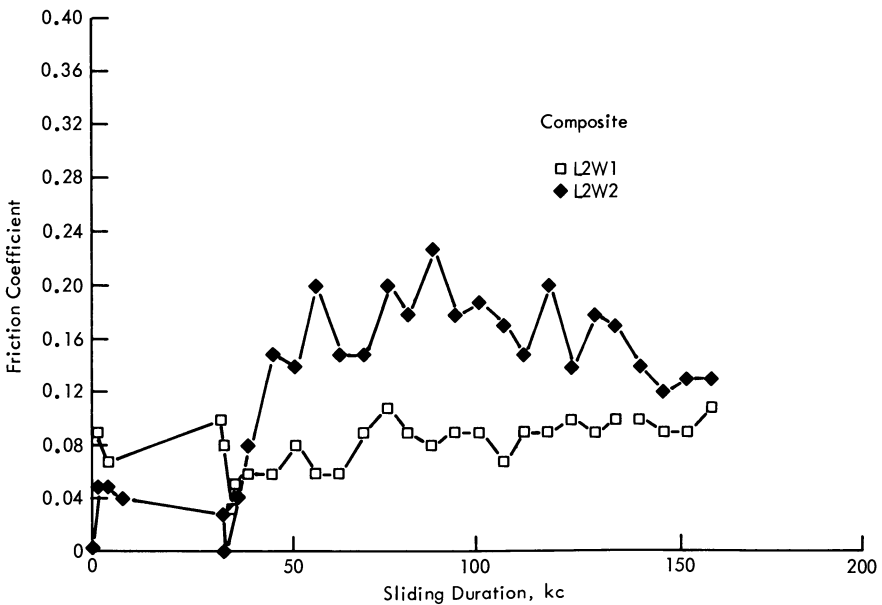


Figure 3. Friction coefficient as a function of sliding duration for L2 composites sliding against steel.

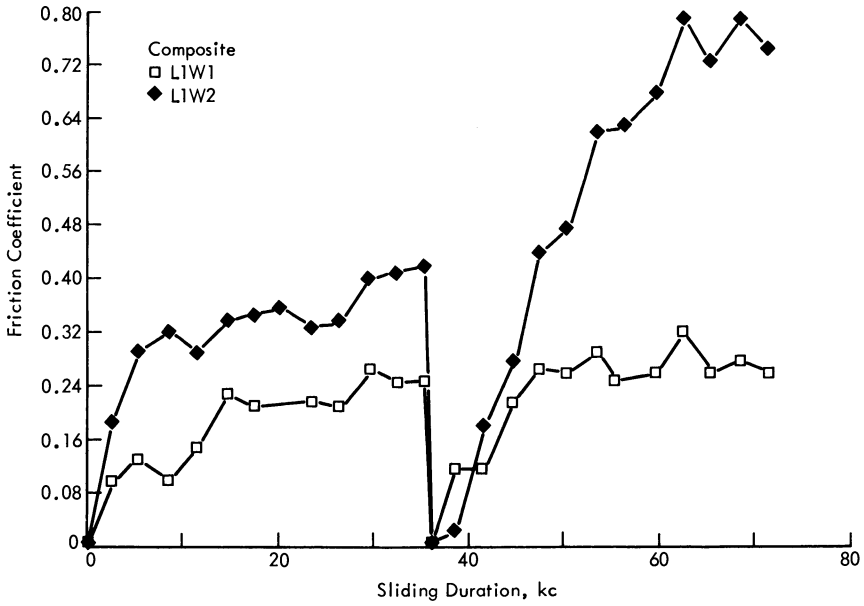


Figure 4. Friction coefficient as a function of sliding duration for L1 composites sliding against silicon nitride.

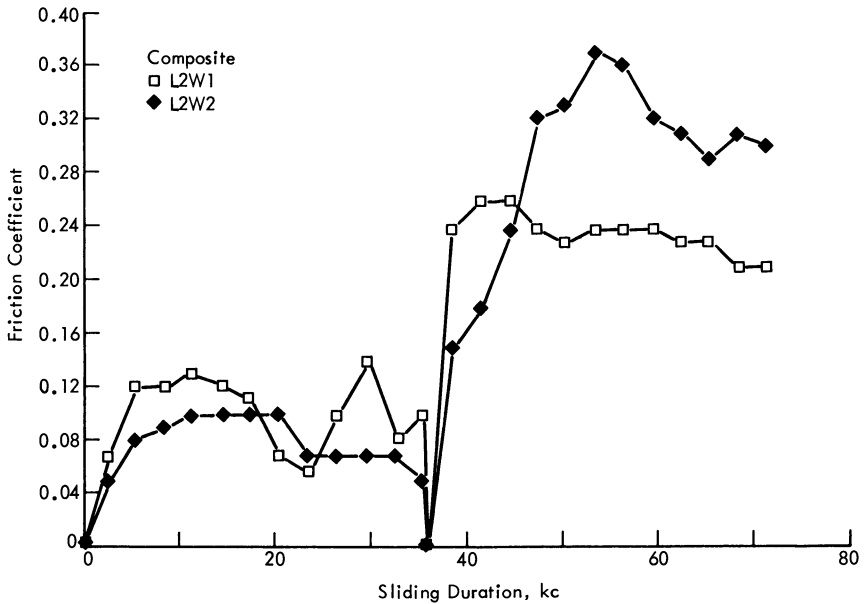


Figure 5. Friction coefficient as a function of sliding duration for L2 composites sliding against silicon nitride.



was observed during sliding at the reduced velocity, for which the wear and friction results are reported.

All composites, except L1W1, gave similar wear and friction when sliding against steel. The anomalously high wear of L1W1, even at reduced velocity, was due to complete spalling of the polyimide matrix from the region between the fibers, as shown in Figure 6. This extensive matrix spalling was not observed for the other composites, implying relatively weak fiber-matrix bonding in the L1W1 specimens. Weak bonding was possibly due to poor impregnation of the fibers by the matrix during fabrication, or a deficiency of the phosphate fiber-matrix binder in the near surface region of the composite.

Silicon Nitride Counterface. Increased wear, friction, and surface damage was apparent for every composite when sliding against silicon nitride, as compared to sliding against steel. Figure 6 compares the negligibly damaged, smooth surface of composite L1W1 after sliding against steel with the same composite after sliding against silicon nitride, in which gross breakage of fiber tows and chaotic mixing of fibers and matrix is apparent. Except for L1W1, wear of the composites was consistently greater against silicon nitride than against steel. More significantly, when sliding against silicon nitride, friction of the composites containing L1 was particularly high. In the case of L1W2, the friction coefficient increased monotonically to values approaching 1.0 with continued sliding. On continued sliding, friction of composites containing L2 also increased, although more modestly. It is clear that only L2W1 can be considered an effective lubricant for silicon nitride under the conditions investigated.

## Discussion

Comparison with Previous Work. Our previous work had shown that internally lubricated graphite-polyimide composites experienced more wear and gave much higher friction when sliding against silicon nitride, as compared to steel, at 316°C in air (8). We had also observed that composites containing inorganic lubricant additive L2 gave lower friction against silicon nitride than those containing additive L1. The present work confirms these effects for four new composites.

Previous composites contained a relatively tight weave of graphite fibers, corresponding to 46 volume-% fiber in the preforms. We hypothesized that the tribological properties of the composites might be improved if a relatively looser weave of graphite fibers was employed. This is because a looser weave would presumably allow better impregnation of the graphite fiber tows by the polyimide matrix and inorganic lubricant additives. Therefore, composites containing the looser W1 and W2 weaves (approximately 30 volume-% fiber in the preforms) were fabricated for this study.

Composites similar in all respects to those reported here, but reinforced with the tight graphite fiber weave, were previously evaluated in our laboratory, sliding against silicon nitride under conditions corresponding to those of the "initial sliding" results

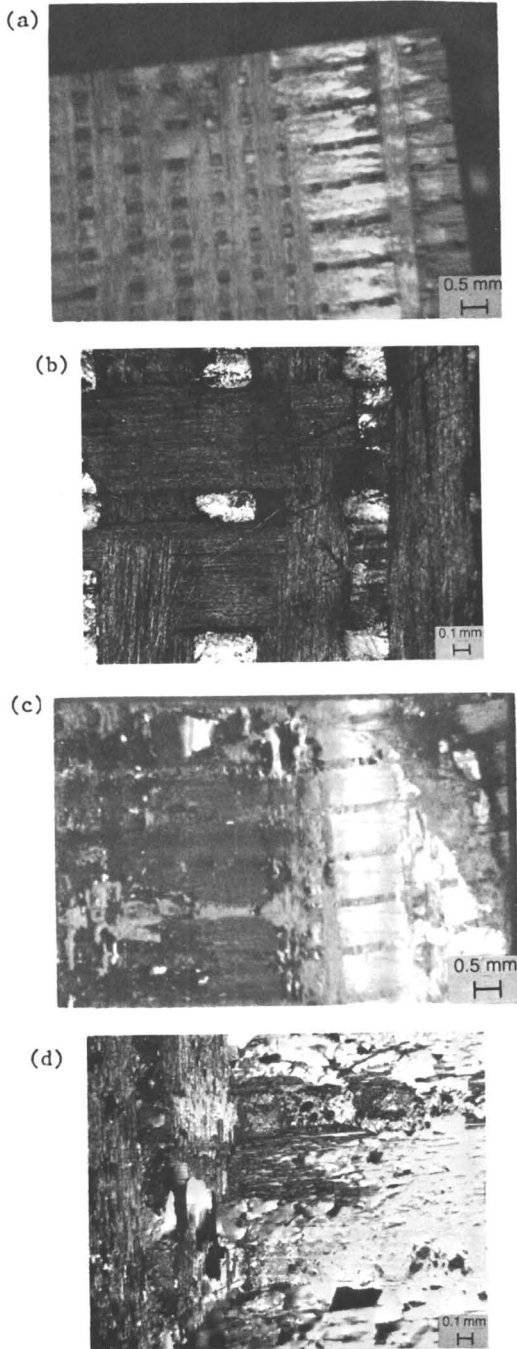


Figure 6. Surface of composite I1W1 after sliding against steel (a & b) and silicon nitride (c & d).

reported here. For these composites, the material containing lubricant additive L1 gave a wear rate of  $8.53 \times 10^{-5} \text{ mm}^3/\text{Nm}$  and average friction coefficient of 0.99; the material containing additive L2 gave a wear rate of  $6.79 \times 10^{-5} \text{ mm}^3/\text{Nm}$  and average friction coefficient of 0.08. Comparison with the results in Table II shows that no significant change in tribological properties of composites containing L2 occurs upon changing reinforcement from the former tight weave to the present loose weaves. For composites containing L1, on the other hand, considerable improvement in friction is associated with loose weave reinforcement, compared to tight weave reinforcement.

Effects of Counterface and Composite Variables. Some of the greater surface damage observed in composites sliding against silicon nitride, as compared to steel, is undoubtedly due to the lower thermal conductivity of silicon nitride. It is well known that interfacial temperatures between sliding surfaces are often much higher than the temperature of the test environment, and higher even than the temperatures which can be measured close to the interface (12). This is particularly true at higher sliding velocities. We have measured temperatures of  $100^\circ\text{C}$  as far as 5.5 mm from the interface for composites sliding against silicon nitride in  $26^\circ\text{C}$  air, at the load and velocity conditions reported here. The present results for L1W1 sliding against steel indicate that true interfacial temperatures during sliding may be double the  $316^\circ\text{C}$  temperature of the specimen enclosure. Since silicon nitride has a much lower thermal conductivity than steel, true surface temperatures during sliding are expected to be much higher.

As observed by Fusaro (2) and substantiated in our previous work (7), the properties of the graphite fibers tend to dominate the tribological performance of graphite-polyimide composites. Photomicrographs of composites reinforced with the W2 weave show that the composite surfaces are considerably enriched in fibers, compared to composites reinforced with the W1 weave. The generally higher wear and friction of composites reinforced with the W2 weave may be attributed to the higher concentration of graphite fibers at the surface.

At elevated temperature, graphite can be abrasive rather than lubricating, due to desorption of moisture, unless additives (such as dibasic ammonium phosphate) are incorporated. This abrasiveness appears to be more severe in the case of a silicon nitride counterface. Surface profilometry of the silicon nitride disks in the region of contact showed that the ceramics had been polished and, in some cases, grooves had been worn in the ceramic surfaces.

Wear of the silicon nitride counterface was substantiated by EDX detection of Si on the composite surfaces after sliding. This is shown most clearly in the EDX of Figure 7, for L2W2. A difficulty in detecting Si for the L1 composites is the presence of W in the additive; the major EDX peak for W overlaps that of Si. Sliding experiments with similar L1-containing composites have previously shown that Si-rich surface layers formed on the composites during sliding against silicon nitride may be from 0.6-3.0  $\mu\text{m}$  thick, and may completely prevent the inorganic lubricant additives from reaching the contact interface.

Since no N was found at the composite surface, Si was presumed to be in the form of silica,  $\text{SiO}_2$ . Two hypotheses have been advanced to explain the presence of silica in terms of ceramic oxidation. First, at interfacial temperatures above  $700^\circ\text{C}$ , oxidation of silicon nitride to silica can occur (13). The silica can then be abraded by the graphite fibers and wear particles may be imbedded in the composite surface. Second, the presence of locally reducing conditions (due to graphite) at the sliding interface can allow the so-called "active oxidation" of silicon nitride to take place, whereby volatile  $\text{SiO}$  is formed (14). Both hypotheses predict adverse affects due to a higher concentration of fibers at the surface, and the W2 composites do indeed give higher wear and friction than the comparable W1 composites.

Since the major component of lubricant 1 ( $\text{WSe}_2$ ) and all components of lubricant 2 are layer lattice transition metal dichalcogenides, it is at first difficult to explain the large differences in frictional behavior observed between L1 and L2 composites sliding against silicon nitride. We advance here a hypothesis for involvement of the phosphate additive in adverse reactions both with the ceramic counterface and with lubricant 1.

Dibasic ammonium phosphate melts with decomposition at  $155^\circ\text{C}$ . In fact, a large proportion of the porosity in the composites may be attributed to generation of volatile ammonia at the processing temperature. Globules of molten phosphate can be seen on the surface of composite L1W1 in Figure 8. EDX of all composite surfaces, except for the best performing L2W1, showed particularly high concentrations of P. Phosphates as a class are well known to be glass formers; phosphate glasses are expected to have high adhesion to hot-pressed silicon nitride, in which the nitride grains are bound together by magnesium silicate glasses. This high adhesion can cause high friction and promote counterface wear. We postulate that the free metals (W, Ga, and In) or metal oxides present in L1 may react preferentially with phosphate decomposition products to produce a glassy, brittle surface layer on the composites and hence decrease lubricant effectiveness. A more complete chemical and surface analysis than was possible in this work would be needed to confirm or deny this postulate.

### Conclusions

Internally lubricated, graphite-polyimide composites are excellent lubricants for steel at  $316^\circ\text{C}$ . They give very low friction and reasonably low wear, while maintaining exceptional strength and stiffness. When sliding against hot-pressed silicon nitride, however, both composite and counterface wear are higher, and friction can be very high. The adverse interfacial chemistry which may contribute to high friction against silicon nitride can be substantially mitigated when the concentration of graphite fibers at the sliding surface is decreased (as by fiber weave W1 discussed in the paper) and an inorganic lubricant pigment containing only molybdenum dichalcogenides (additive L2 discussed in the paper) is incorporated in the composites.

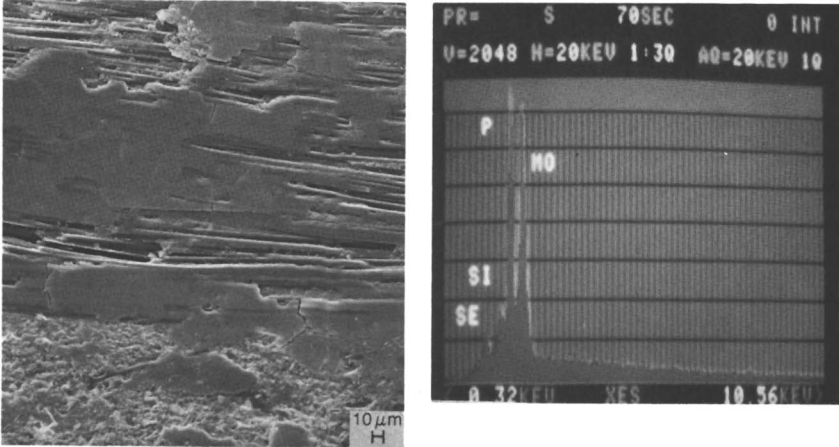


Figure 7. Silicon-containing layer on composite L2W2 after sliding against silicon nitride.

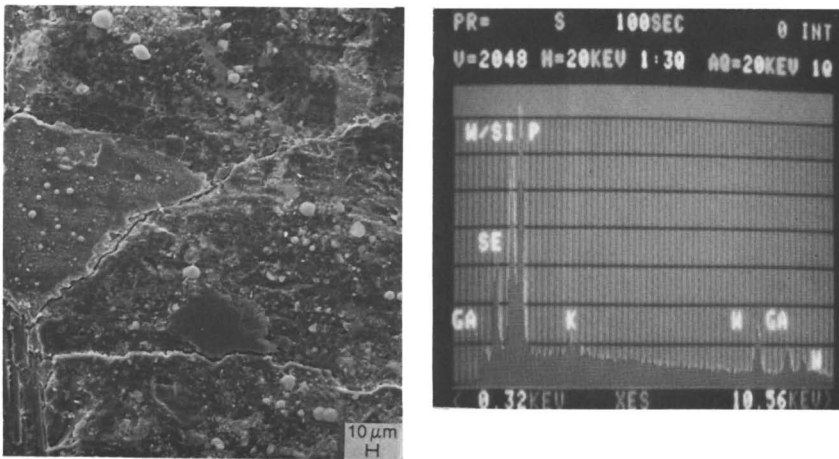


Figure 8. Phosphate globules on surface of composite L1W1 after sliding against silicon nitride.

### Acknowledgments

The author wishes to acknowledge the contributions of Messrs. Carl Windisch, Ed Harper, and Rick Bacon. This work was supported by the DARPA Solid Lubricated Rolling Element Bearing Program under Air Force Contract F33615-80C-5190; Mr. Karl R. Mecklenburg was project monitor.

### Literature Cited

1. Fusaro, R. L. ASLE Trans. 1984, 27(3), 189-96, and ref. 1-18 therein.
2. Fusaro, R. L. In "Polyimides"; Mittal, K. L., Ed.; Plenum: 1984; Vol 2, pp. 1053-80.
3. Fusaro, R. L.; Sliney, H. E. ASLE Trans. 1978, 21(4), 337-43.
4. Sliney, H. E.; Johnson, R. L. "Graphite Fiber-Polyimide Composites for Spherical Bearings to 340°C (650°F)," National Aeronautics and Space Administration TN D-7078, 1972.
5. Sliney, H. E.; Jacobson, T. P. Lubr. Eng. 1975, 31(12), 09-13.
6. Gardos, M. N.; McConnell, B. D. "Development of a High-Load, High-Temperature, Self-Lubricating Composite," American Society of Lubrication Engineers SP-9, 1982.
7. Sutor, P.; Gardos, M. N. Proc. 3rd Internat. Conf. on Solid Lubr., 1984, ASLE SP-14, pp. 258-65.
8. Gardos, M. N.; Sutor, P. ibid., pp. 266-74.
9. Hergenrother, P. M. Polymer Preprints 1984, 25(1), 97-9.
10. Boes, D. J. ASLE Trans. 1967, 10(1), 19-27.
11. Lancaster, J. K. Wear 1975, 34, 275-290.
12. Roberts, J. C.; Griffin, O. H., Jr. Proc. ASME/ASLE Lubr. Conf., 1982, Preprint 82-LC-2B-1.
13. Kiehle, A. J.; Heung, L. K.; Gielisse, P. J.; Rockett, T. J. J. Am. Ceram. Soc., 1975, 58(2), 17-21.
14. "Reliability of Ceramics for Heat Engine Applications," National Academy of Sciences NMAB-357, 1980.

RECEIVED January 23, 1985

## Characterization and Measurement of Polymer Wear

Donald H. Buckley and Paul R. Aron

National Aeronautics and Space Administration, Lewis Research Center, Cleveland, OH 44135

A host of analytical tools are available to assist the tribologist in understanding and characterizing the polymer wear process. They can be used in the study of polymer wear and the development of polymer transfer films to nonpolymer counterfaces. Some of the devices discussed include visual observation of polymer wear with SEM, quantifying it with surface profilometry and ellipsometry, studying chemistry with AES, XPS and SIMS, establishing interfacial polymer orientation and accordingly bonding with QUARTIR, polymer state with Raman spectroscopy and stresses that develop in polymer films using a X-ray double crystal camera technique.

When any two surfaces are brought into solid state contact and subsequently separated the nature of one or both surface frequently has changed as a result of the contact. It is even more likely to occur when mechanical forces are imposed on the contact. Polymeric materials are not different than other solids in this respect. The surface and near surface changes that have occurred in polymers may however be more difficult to characterize, in part because of the difficulty in identifying these materials with analytical tools.

Wear in a strict sense occurs whenever material is lost from a solid. The mechanism of loss can be abrasion, adhesion, erosion, cavitation, corrosion or fatigue. This loss can occur at the atomic level. At this level analytical tools such as the field ion microscope and the atom probe can be used to study wear loss of polymers. These tools have been used in the authors' laboratory for many years to study polymer adhesion and transfer to metal surfaces (1,2). They are capable of providing insight into the presence or absences of transfer (wear), the adhesive strength of polymer to metal, amount of transfer, bond scission, mechanical effects such as loading of surfaces together, chemical effects on bonding and surface energetics. The field ion microscope coupled with the atom probe is the ultimate tool for the study of polymer wear because it allows

the analysis both structural and chemical aspects of the wear process at the atomic level. While the field ion microscope with the atom probe may be the ultimate in polymer wear analysis in many instances such depth may not be required as the wear process may be a relatively gross event. In such cases much more conventional tools may be used to characterize polymer wear. Two such tools are the surface profilometer and the scanning electron microscope (SEM). These devices provide a macroscopic picture of the wear of polymers.

There are many other analytical tools that can assist the tribologist in the characterization of polymer wear. Many of these tools including those discussed herein are described fully in Reference 3 where their capabilities, sensitivities and limitations are given in detail. They can identify quantity of polymer transferred to a counterface surface (ellipsometer), amorphous versus crystalline state (Raman spectroscopy), stresses in transfer films and worn polymer surfaces (double crystal X-ray techniques), orientation of transferred molecules of polymer on the counterface (reflection-absorption infrared spectroscopy; RAIR), bonding mode (inelastic electron tunneling spectroscopy, IETS), elements present in polymer wear debris (Auger electron-spectroscopy, AES), mapping of polymer wear surface distribution (scanning Auger microscopy, SAM), distinguish between various homologs (low-damage secondary ion mass spectrometry, SIMS) and interfacial polymer to counterface chemical analysis (X-ray photoelectron spectroscopy, XPS).

The objective of this paper is to review the wear of polymers using the above tools in order to characterize the wear process. Wear analysis will include microscopy observation, profiling, thickness measurements and chemistry both structural and analytical.

### Visual Observation of the Wear Surface

The visual observation of the polymer wear surface is the simplest method for characterizing the wear process. Frequently a considerable amount of very useful information can be gained from the use of the light optical and scanning electron microscope studies of the polymer surface that has undergone wear.

An example of how visual observation can assist in wear studies has been demonstrated in the erosion behavior of thermoplastics (3). In the erosion of polymers the shape of the impinging particle on the polymer surface determines the mechanism by which wear occurs. If the particle is relatively smooth and spherical wear to the polymer surface occurs by the formation of deformation flakes, fracture and sub-surface fatigue. Where the particle have sharp edges the wear process is dominated by cutting analogous to an abrasive grit.

Figure 1 contains micrographs of polymethyl methacrylate (PMMA), polycarbonate (PC) and polytetrafluoroethylene (PTFE) surfaces which have undergone erosive wear by the impingement of glass beads. With all three polymers loss from the surface occurs by flake formation as indicated in each of the micrographs.

### Profiling Polymer Wear

In addition to seeing the wear surface it is often desirable to quantify the loss of polymer due to wear. One of the most straight-



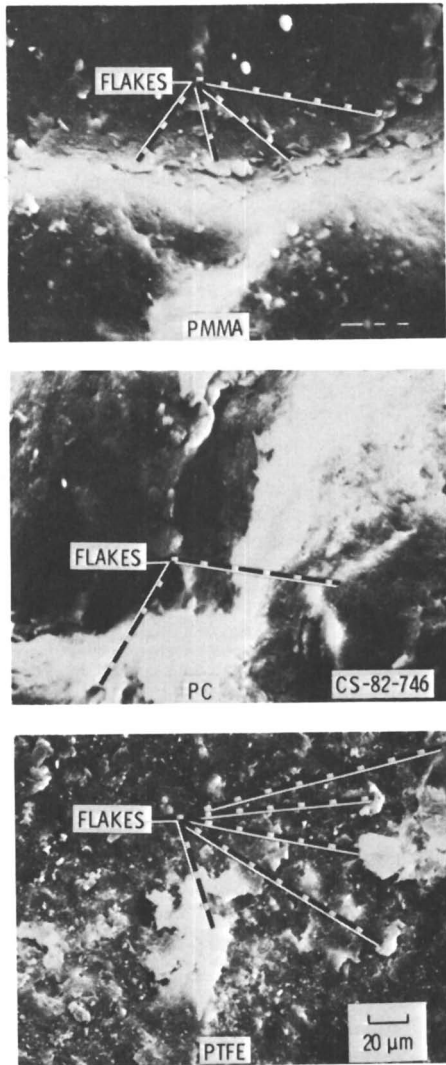


Figure 1. SEM micrographs (40 tilt) of eroded thermoplastic material surfaces. Exposure time, 10 min; gas pressure, 0.27 MPa; particle velocity, 72 m/s.

forward techniques for accomplishing this is to profile the wear area. This can be done with mechanical devices such as a stylus tracking of the profile or for extremely deformation prone surfaces with the use of optical or laser beam profiling.

An example of the use of the profilometer in following the erosive wear of polytetrafluoroethylene (PTFE) is presented in Figure 2. The profiles of the wear spot, which are circular in nature at the surface, are presented for various periods of exposure time to the erosive particles (4). With increasing time the depth of the pit continues to increase. It is important to note that magnification in the horizontal and vertical directions is not the same. Thus, in using the profiles and integrating the wear area to arrive at total loss, care must be taken to correct for the differences.

The profilometer can also be used to track polymer wear where one material in contact is a polymer and the other is, for example, a metal. If wear occurs by transfer of polymer to the metal, the surface of the metal can be profiled to identify the amount of polymer transferred.

#### Thin Film Identification

Where polymers transfer to counterface surfaces in extremely thin film forms, of the order of monolayers the surface profilometer becomes ineffective and other tools must be used. A device which can measure the thickness of such films is the ellipsometer. It can detect film thicknesses of polymers on the order of angstroms.

In Figure 3 the film thickness of a polymer is presented as a function of deposition time (5). It can be seen from the data of Figure 3 that polymer films of thicknesses of the order of 30 to 40 angstroms can be readily detected by ellipsometric techniques. This device, then, permits the transfer of extremely thin polymer films and allows for the identification of the onset of adhesion and transfer, providing the opportunity to identify when bonding occurs and some indication of bond strength. If the polymer is seen to transfer to a counterface surface, then it is reasonable to assume that the interfacial adhesive bond strength is greater than the cohesive strength of the polymer itself. This observation will only hold where the counterface surface is atomically smooth.

#### The Chemistry of Polymer Wear

Devices. The tools described thus far in this paper present a physical view of polymer wear. What about the chemistry of the polymer wear process. In studying chemistry it is desirable to have the analytical tool incorporated directly into the wear experiment. An example of such a device is presented in the schematic of Figure 4 from the authors laboratory (6).

Figure 4 presents what is commonly referred to as the pin-on-disk friction and wear device. A hemispherical rider mounted in a beam is loaded against a rotating disk. The disk is rotated unidirectionally. The beam containing the rider is mounted in a gimbal which is connected to a strain gage assembly for measuring friction force.

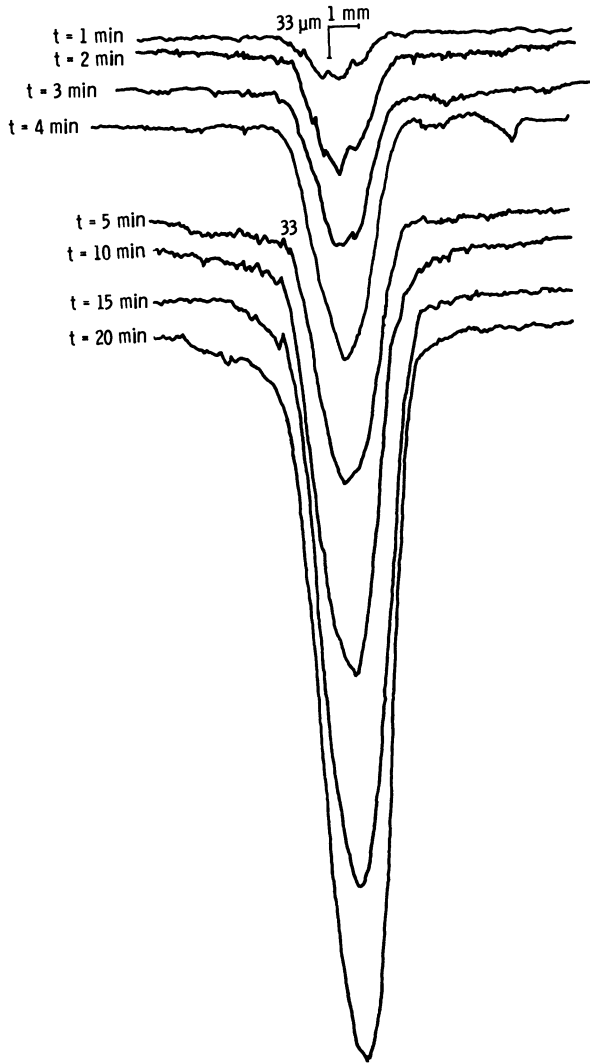


Fig. 2. - Surface traces on PTFE as a function of time.

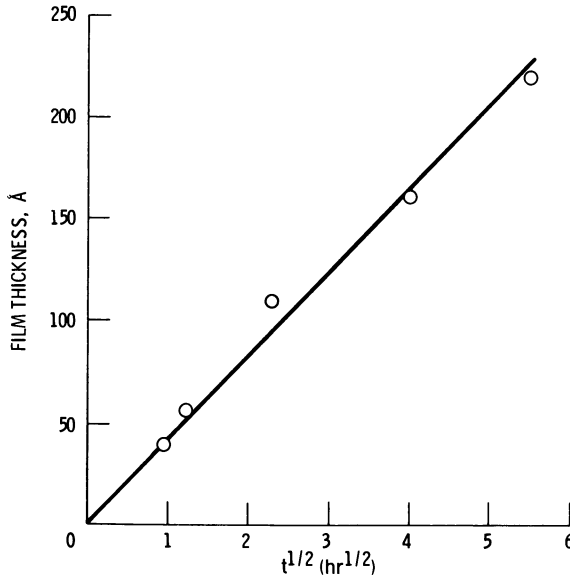


Fig. 3. - The thickness of a polymer film, as measured with the ellipsometer with deposition time (ref. 4).

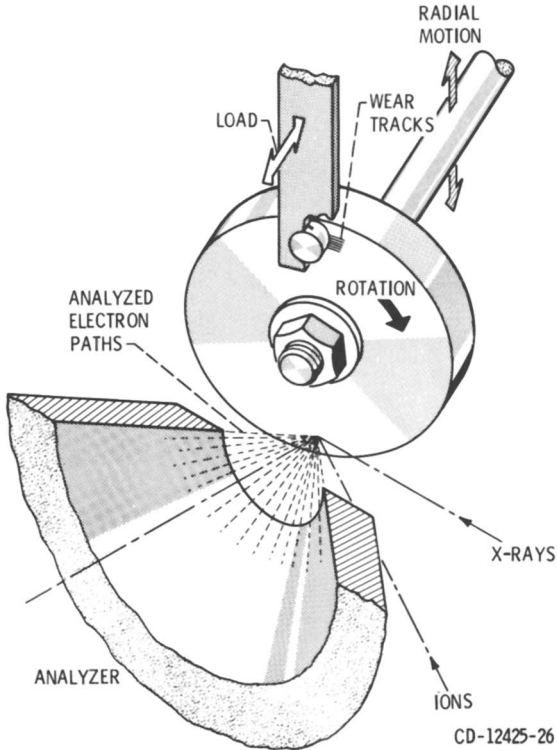


Fig. 4. - Schematic diagram of apparatus for XPS analysis of polymer transfer.

Wear to the rider and disk can be measured periodically or upon completion of an experiment. One or both specimens can be polymers or polymer compositions.

The system depicted in Figure 4 contains the components for XPS analysis of the disk and ion depth profiling for the removal of surface films and polymer layers. X-rays are the excitation for the emission of electrons from the surface whose binding energies are measured with the analyzer. A beam of argon ions are directed at the surface in the location of analysis for depth profiling.

The beam of X-rays strike the surface of the disk in Figure 4 at a location of  $180^\circ$  from where the rider contacts the disk. Thus, changes in surface chemistry in the wear track can be continuously monitored during the course of an experiment. A similar type of device is used for Auger analysis (AES) only the excitation source is a beam of electrons rather than X-rays as used for XPS. With AES an elemental analysis is obtained while with XPS compounds and changes in polymer chemistry can be followed.

Surfaces and Interfaces. Sliding friction and wear experiments were conducted with polytetrafluoroethylene (PTFE) sliding of nickel. An important question to be asked is does the polymer chemistry change when it undergoes wear? There is a considerable amount of energy dissipated at the sliding interface and this energy could conceivably degrade or alter the polymer from that observed for the bulk unworn polymer.

Figure 5 presents the fluorine KLL Auger spectra for both bulk PTFE and the wear transfer film (7). Feature 1 involves the 2s and 1s electrons, while feature 2 involves the 2p and 1s electrons and would be expected to change size with a change in chemical bond. Thus, a change in the ratio of feature 2 to feature 1 is indicative of a change in the chemical state of the film. Although the features are not sharp and feature 1 is particularly difficult to measure, there is no difference in the spectra beyond the limit of uncertainties. The transfer polymer wear film is therefore the same as the bulk PTFE.

The data of Figure 5 tell us that the surface of the transfer film has the same chemistry as the bulk polymer. Auger analysis is surface sensitive and probes only to a depth of four to five atomic layers. What about the chemistry at the interface between polymer and metal? Is there any chemical interaction resulting from the sliding process and contributing to polymer wear XPS with ion depth profile analysis can assist in answering these questions. First, XPS probes more deeply than AES and secondly ion depth profiling can assist in getting to the interface through removal of thick polymer wear transfer films and thereby arrive at the interface.

The XPS spectrum of Figure 6 for the F(1s) peak indicates that at the nickel to polymer interface some nickel fluoride ( $\text{NiF}_2$ ) forms. The amount is extremely small but is nonetheless present. Both peak heights and film thickness indicate that only an occasional fluorine has reacted with the nickel chemically. Since fluorine is monovalent, it is unlikely that it can function in the formation of a strong bond between the metal and the PTFE. The

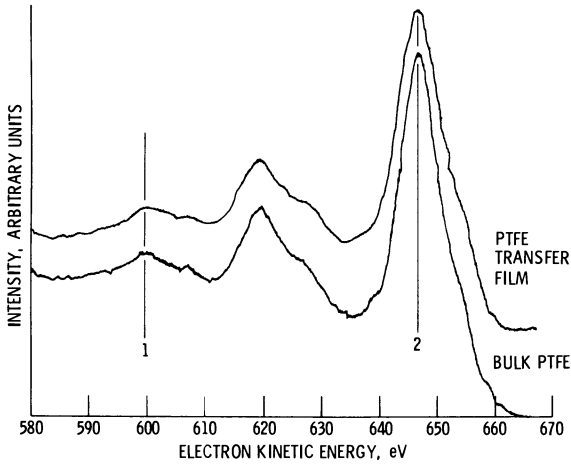


Fig. 5. - Fluorine auger electron spectra from PTFE transfer film (on clean nickel in vacuum) and from bulk PTFE. Load, 2 newtons; sliding speed, 0.94 millimeter per second. (To account for charging, the upper peak is shifted horizontally so that the spectra coincide.)

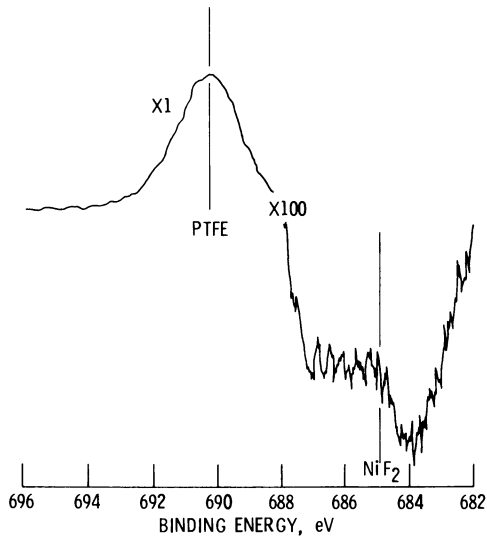


Fig. 6. - F(1s) XPS peak from PTFE transfer film on clean nickel in vacuum. Load, 2 newtons; sliding speed, 0.94 millimeter per second.

single fluorine bond must interact either with the metal when it forms nickel fluoride or with carbon of the polymer.

The presence of  $\text{NiF}_2$  at the polymer metal interface may be indirect evidence for the formation of a metal to carbon bonds. When the fluorine reacts with the nickel a carbon is available for bonding also to the metal.

Just as the ellipsometer can be used to measure polymer film thickness so can XPS. For example, with PTFE by the use of the ratio of intensities of the F(1s) and the C(1s) peaks and the attenuation of the nickel peak intensities it is possible to measure polymer film thickness and accordingly polymer wear (7).

Figure 7 indicates the amount of polymer transfer on wear that occurs as a function of a mechanical parameter, sliding speed. An examination of Figure 7 indicates that the higher the sliding speed for a polymer in contact with a metal the greater the film thickness and accordingly the amount of polymer wear.

Similarly AES can be used in two ways to probe the thickness of the transfer film. In Figure 8 is plotted the amplitude of the carbon Auger signal (derivative mode) as a function of the sputtering time (depth) for a sample of titanium on which a PTFE transfer film had been formed with a hemispherical rider 1 cm in diameter under a load of 2 Newtons. This depth profile contains information as to the thickness and composition of the film and can be used to gain an understanding as to the way in which these parameters vary as a function of the substrate condition. Films on three different substrates are shown. The film on the clean titanium is clearly thicker than the films on either the oxidized titanium or the iridium. The titanium was sputter cleaned just prior to forming the film which was done without exposure to atmosphere. The oxide is the native oxide which formed during the polishing, which was done in air. Both of the later substrates are expected to be less reactive than titanium.

The second way in which AES can be used to learn about the thickness is illustrated by Figure 9. This is an image of the film taken using the intensity of the 54 eV Auger line of iridium to modulate the brightness while the position of the electron beam is moved over the surface (scanning Auger microscopy, SAM). Since the inelastic mean free path of electrons of such a low energy is of the order of intermolecular distances it makes a sensitive probe of the thickness of these films. High brightness indicates low attenuation. A variation of the thickness over the surface is clearly indicated. This information can be quantified by taking data in the form of Figure 8 which is a single line scan through the center of the picture where the intensity of the line appears in the vertical direction and the position of the point sampled is on the horizontal axis.

While Auger electron spectroscopy and X-ray photoelectron spectroscopy can give elemental and organic structural information, respectively, they have limitations in the amount of material they can detect. For example, where polymers are in sliding, rolling or rubbing contact with metal or alloys wear to the metal as well as

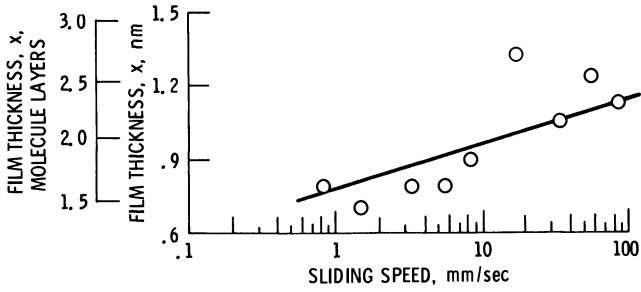


Fig. 7. - Average thickness of PTFE transfer film on nickel at various sliding speeds in vacuum. Load, 2 newtons; temperature, 24° to 27° C.

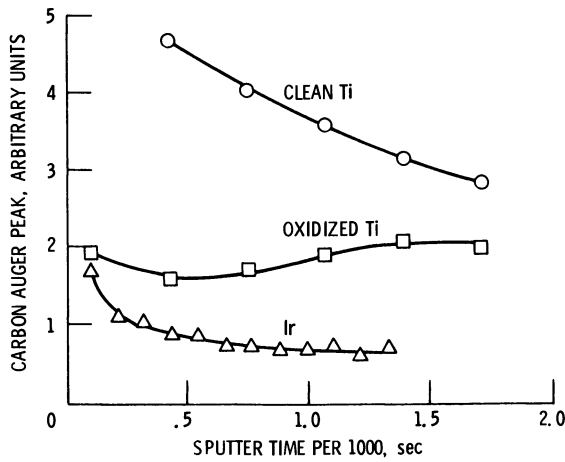
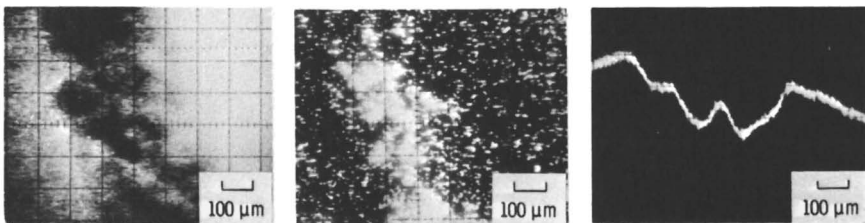


Fig. 8. - Depth profiling of a PTFE wear film on titanium and iridium substrates. Load, 2 N; temperature, 24° C; and sliding speed of 0.1 mm.



(a) Iridium map (53 eV)

(b) Fluorine map (651 eV)

(c) Iridium surface profile

Figure 9. Scanning auger microscopy (SAM) maps and surface profile trace for PTFE wear film on an Iridium substrate. Load, 2 newtons; temperature, 24 C; sliding speed, 0.1 mm per second.



wear to the polymer can occur. Metals have been observed to transfer to polymer surfaces (6). This transfer can be extremely discrete and difficult to detect in the polymer surface as well as polymer wear debris.

Static or low-damage secondary ion mass spectrometry (SIMS) can be used to characterize polymers and also detect very small amounts of metals transferred to polymers or in polymer wear debris. While SIMS uses an ion beam to sputter remove surface species and is therefore inherently destructive, damage can be minimized by using low ion beam fluxes ( $3 \times 10^{-9}$  A/cm<sup>2</sup>). This allows for monolayer analysis.

SIMS can be effectively utilized to distinguish, for example, among a series of polyalkyl methacrylate films deposited on a metal substrate.

Low-damage SIMS has distinguished thin transfer films of the homologous series of poly(methyl, ethyl, isobutyl, n-butyl and lauryl) methacrylates. Figure 10 is a SIMS spectrum from a poly-lauryl methacrylate films on a silver substrate (8).

The mass to charge ratios (m/Z) are detected in Figure 10 for the methyl (m/Z 15) ethyl (m/Z 29), propyl (m/Z 43) ions as well as that for  $[C_4H_7]^+$  ion (m/Z 55) associated with the breakup of the lauryl group. The  $[C_4H_7]^+$  has the greatest intensity. With the poly(methyl and ethyl) methacrylates, the methyl ion (m/Z 15) and the ethyl ion (m/Z 29) are respectively the most intense ion species present. In the case of the butyl isomers the ethyl ion (m/Z 29) is dominant over the propyl ion (m/Z 43) for the isobutyl isomer while with the n-butyl isomer the reverse is observed. With the lauryl isomer the (m/Z 55) is the most intense of the four ions and the other ion intensities decrease with decreasing m/Z. Silver is detected in the polymer from the silver substrate.

SIMS has proved to be a very useful tool in polymer film studied and accordingly wear analysis. Various polymers have been fingerprinted with SIMS including in addition to those already discussed, low density polyethylene, polypropylene, polystyrene, nylon-6 and polyethylene terephthalate (8,9).

Polymer to Counterface Bonding. Of extreme interest to the tribologist is the nature and structure of interfacial adhesion of polymers to substrate surfaces because it contributes heavily to the adhesive wear of polymers. A very useful tool for the study of this subject is quantitative absorption - reflection thickness infrared spectroscopy (QUARTIR). This device is uniquely suited for the study of preferential orientation of large molecules at interfaces. Thus, insight into the structural interfacial bonding of molecules can be had, adhesion and accordingly adhesive wear better understood.

Studies have been conducted with a surfactant, 4,5 dimethoxy-2-nitrobenzyl hexadecane sulfonate (PMS) cast on a copolymer-substrate. The structure of the surfactant is indicated in Figure 11(a). Films of thicknesses from 100 to 1000Å on an aluminum substrate were examined (10).

The use of QUARTIR (1) permitted the analysis from bulk film to near monolayer, (2) quantitatively established individual bond absorbances in the film, (3) allowed for the commutation of fractional changes in normalized absorbance between bulk and interface

values, (4) determined the transition moment direction of the modes producing each bond in terms of internal molecular coordinates, and (5) from (3) and (4) made possible the angles of the various transition moments and accordingly molecular coordinates of bonding to the solid surface.

Figure 11(b) presents the mechanism of bonding of the surfactant PMS to the oxidized aluminum surface. Certainly such information is extremely useful in predicting adhesive bond strengths at interfaces.

**Polymer Structure.** In addition to visualization, profiling, thickness measurements and chemistry of polymer wear it is frequently desirable to know whether the polymer is in the amorphous or crystalline state because other properties relate to state. Raman spectroscopy is very useful in studying very low frequency modes associated with vibrations of polymer chain backbones and the lattice modes of polymer crystals. It complements infrared spectroscopy.

The ability of Raman spectroscopy to distinguish between mylar in the crystalline and amorphous state is presented in Figure 12 taken from Reference 11. The figure reveals the distinct differences in peak shape with crystallization of the polymer.

Molecular relaxations, and molecular orientation of polymers can be related to tribological performance. Such studies have been conducted with polyimides (11).

**Stresses in Polymers.** During the sliding, rolling or rubbing process for polymers stresses are generated in the polymer. Where polymers are in contact with metals or alloys transfer films of the polymer generally develop on the counterface. These polymer wear films are generally highly stressed. Until recently there has been no good effective technique for the simple measurement of these stresses. A X-ray scheme has been demonstrated as being capable of providing such measurements. It has been used for the measurement of stresses generated in polyimide films (12).

Figure 13 presents a schematic of a double crystal camera arrangement with a) unstrained crystals, and b) a strained crystal. The polymer films have been deposited on single crystal silicon substrates. In Figure 13(a) an unstrained crystal is in position two, with each crystal aligned to obtain Bragg diffraction in transmission from a set of planes. Translation of the two crystals produces no change in the double-diffracted X-ray intensity because the Bragg angle remains constant across the crystal. The crystal in position two of Figure 13(b) has a curvature due to the stresses generated in the polymer. Translation of the two crystals of Figure 13(b) results in a sharp decrease in the double-diffracted X-ray intensity due to lattice curvature. Details of the technique can be found in Reference 13.

With the X-ray technique described stresses in polymer wear films can be measured. One could incorporate a pin-on-disk friction device within the opening of the X-ray camera and conduct *in situ* measurements. The stresses developed in the film with repeated passes, increasing load, varied sliding speeds and polymer compositions can be measured. This could lead to a better understanding of the role of stresses in polymers on their wear behavior.

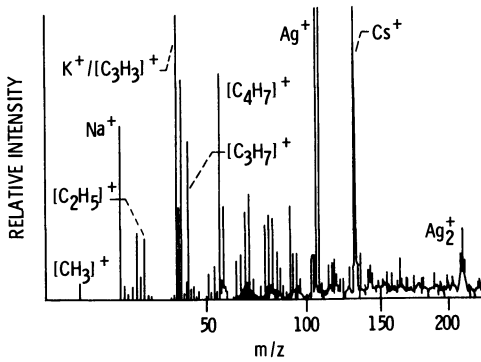
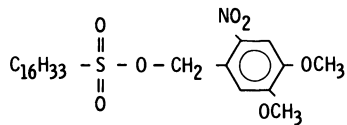
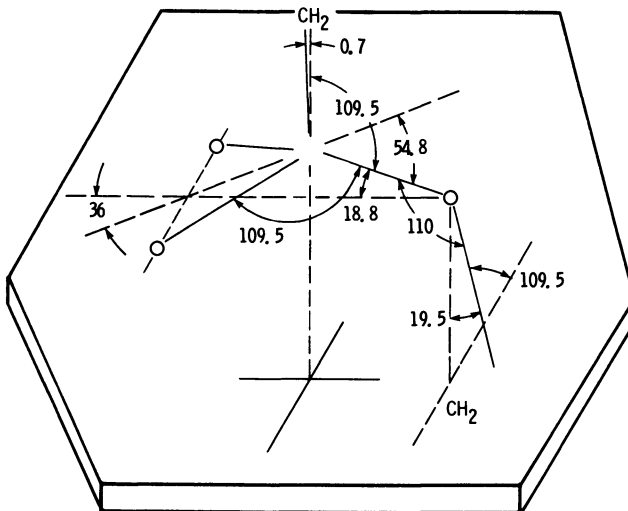


Fig. 10. - Static SIMS spectrum of polylaurylmethacrylate (ref. 9).



(a) Surfactant (PMS), 4, 5 dimethoxy-2-nitrobenzylhexadecanesulfonate.



(b) Bonding of the surfactant (PMS) to a oxidized aluminum surface.

Fig. 11. - The use of quartir for the determination of molecular coordination of a surfactant (PMS) with a oxidized aluminum surface (ref. 10).

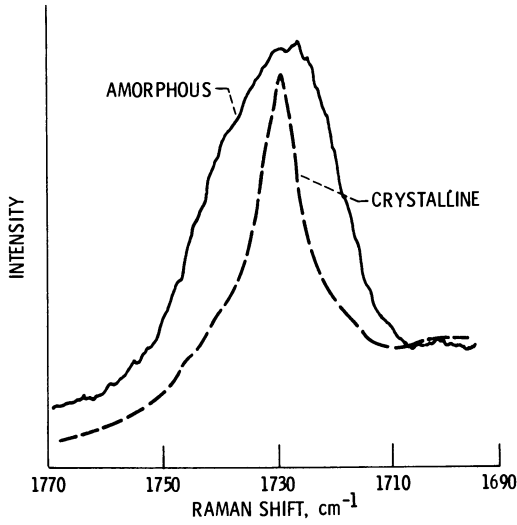
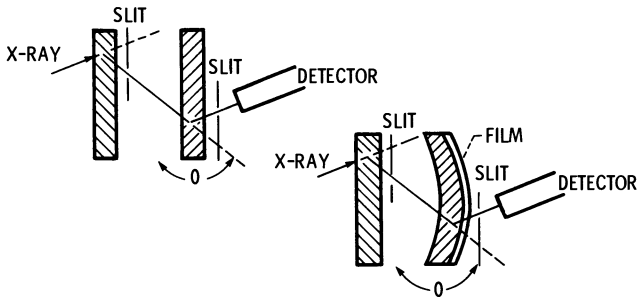


Fig. 12. - Raman spectrum of Mylar - appearance of the carbonyl stretching band of quenched and crystallized polyethelene terephthalate (ref. 11).



(a) With unstrained crystals. (b) With a strained crystal.

Fig. 13. - Schematic of double crystal camera arrangement.

The effect of temperature on polymer stresses can also be measured. Again, this could be done in situ. Figure 14 presents a plot of stress as a function of temperature (13). The data for a polyimide in Figure 14 indicates that interfacial stress decreases with an increase in temperature. This could be effectively utilized to determine the effect of frictional heating on polymer stress as well as wear.

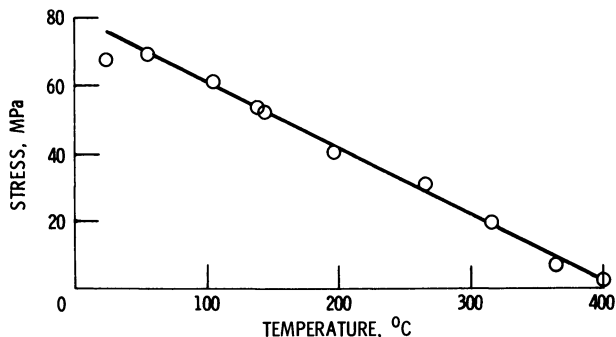


Fig. 14. - Plot of stress versus temperature for a polyimide film (ref. 13).

### Concluding Remarks

A host of analytical tools are available to the tribologist for the study of the wear of polymers and polymer films. Much can be learned about the wear behavior of polymer with visual observation of the wear surfaces with the scanning electron microscope while surface profilometer can assist in quantifying polymer wear.

The thickness of polymer transfer films to counterface surfaces can be measured with sensitivities into the angstrom range with the ellipsometer. The device can be arranged for in situ thin film measurements.

The chemistry of polymer surfaces and their wear can be measured in situ with Auger electron spectroscopy, X-ray photoelectron spectroscopy and secondary ion mass spectrometry. These tools provide elemental, compound analysis and distinguish among a series of homologs respectively.

Orientation at the interface between polymers and metals where the polymer transfer to the metal can be determined with quantitative absorption-reflection thickness infrared spectroscopy. With an understanding of polymer interfacial orientation, bonding mechanisms can be identified and accordingly adhesion of polymers to metals better understood.

Raman spectroscopy can be used to identify the polymer state and double camera X-ray techniques to determine the amount of stresses developed in films of transferred polymers.

Literature Cited

1. Buckley, D.H.; Brainard, W.A.: "The Atomic Nature of Polymer-Metal Interactions in Adhesion, Friction and Wear," *Advance in Polymer Friction and Wear*, edited by Lee, L.H. Polymer Science and Technology, Volume 5A, Plenum Press, New York (1974).
2. Buckley, D.H.: "Surface Effects in Adhesion, Friction, Wear and Lubrication," Elsevier, Scientific Publishing Company, Amsterdam, (1981).
3. Kane, P.F. and Larrabee, G.B., Editor: *Characterization of Solid Surfaces*, by Plenum Press, New York 2nd Printing (1976).
4. Rao, P.V.; Buckley, D.H.: "Spherical Microglass Particle Impingement Studies of Thermoplastic Materials at Normal Incidence," NASA TM-83410, (1983).
5. Baba, M.; Gottesfeld, S.: "Ellipsometric Study of the Polymeric Surface Films Formed on Platinum Electrodes by the Electrooxidation of Phenolic Compounds", Surf. Sci., 96, pp. 461-475, (1980).
6. Brainard, W.A.; Buckley, D.H.: "Adhesion and Friction of PTFE in Contact With Metals as Studied by Auger Spectroscopy, Field Ion and Scanning Electron Microscopy," WEAR, 26, pp. 75-93, (1973).
7. Wheeler, D.R.: "Polytetrafluoroethylene Transfer Film Studied With X-Ray Photoelectron Spectroscopy," NASA TP-1728, November (1980).
8. Campana, J.E.; DeCorpo, J.J.; Colton, R.J.: "Characterization of Polymeric Thin Films by Low-Damage Secondary Ion Mass Spectrometry," Appli. Surf. Sci., 8, pp. 337-342, (1981).
9. Briggs, D.; Wooton, A.B.: "Analysis of Polymer Surfaces by SIMS: 1 - An Investigation of Practical Problems," Sur. and Inter. Ana., 4, 3, pp. 109-115, (1982); Briggs, D.: "Analysis of Polymer Surfaces by SIMS: 2 - Fingerprint Spectra from Simple Polymer Films," Surf. and Inter. Anal., 4, 4, pp. 151-155, (1982).
10. Debe, M.K.: "Organic/Metal Interface Studies with Reflection-Adsorption Infrared Spectroscopy: Photomarked Surfactants and Organic Photoconductors on Aluminum", Appli. of Surf. Sci., 14, 1-40, (1982-83).
11. Andrews, R.D.; Hart, T.R.: "Use of Laser Raman Technique in the Study of Polymers," "Characterization of Metal and Polymer Surfaces," Vol. 2, "Polymer Surfaces" editor Lee, L.-H. Academic Press, pp. 207-241, (1977).
12. Fusaro, R.L.: "Molecular Relaxations, Molecular Orientation and the Friction Characteristics of Polyimide Films," ASLE Trans., 20, 1, pp. 1-14, (1975).
13. Goldsmith, C., Geldermans, P., Bedetti, F. and Walker, G.A.: "Measurement of Stresses Generated in Cured Polyimide Films," J. Vac. Sci. & Techn., A1 (2), pp. 407-409, (1983).

## Wear of Polymers in the Pin-on-Disk Configuration

B. J. Briscoe<sup>1</sup> and T. A. Stolarski<sup>2</sup>

<sup>1</sup>Department of Chemical Engineering and Chemical Technology, Imperial College, London SW7, England

<sup>2</sup>Department of Mechanical Engineering, Brunel University, Uxbridge, Middlesex, England

A common simulation technique which is used to evaluate the wear of polymers is to slide the polymer, usually in the form of a pin, over the surface of a rotating disc. The pin may be loaded along its major axis, either in a direction normal to or parallel with the axis of rotation. Hence the contact area is produced on the edge or the face of the disc.

We will show that the rate of wear produced in these two cases may be different for certain polymers and further when the pin is slid over the disc face the rate of wear is also a function of the radius which the pin describes on the disc surface.

Organic polymers wear by a variety of mechanisms (1-5) but in general there are two distinct classes of behaviour. Certain polymers such as polytetrafluoroethylene (PTFE) and the linear polyethenes have a characteristic mode of wear which involves the formation and removal of highly orientated thin transferred films. Some polymers form rather thick unorientated transferred films as for example low-density polyethylene (LDPE) and others do not apparently form these films without gross surface melting. Polymethylmethacrylate (PMMA) is an example of the latter. The special thin film transfer of PTFE and high-density polyethylene (HDPE) and the associated low friction, while not fully understood, does seem to correspond with the vague notion of a "smooth molecular profile" (3). This connotation is not causal but it is apparently comprehensive. These polymers (PTFE, HDPE) also showed an unusual load axis spin sensitivity in their friction and transfer behaviour. This aspect is dealt with later in more detail. The present paper concentrates upon the influence of contact geometry on the wear of range of polymers when they are studied in a pin-on-disc configuration. Rather unusual wear characteristics are seen in the polymers which wear by the creation and loss of highly orientated transferred films. In essence, the adhesive or transfer wear process involves the formation of adhesive junctions between the polymer and the counterface followed by bulk failure in the surface layers of

the polymer in response to the applied shear stress. Polymer is consequently transferred to the counterface, and repeated traversals of the polymer specimen over this layer detach the film which is then ultimately displaced from the contact zone. A further layer is transferred, the process is repeated and the polymer gradually wears away. Accordingly, the wear of a polymer like PTFE and HDPE should be a function of the number of traversals over the same wear path. With an increasing number of traversals the wear should increase. This is not observed in practice in the experiments described in this paper.

To assess the wear properties of polymers a number of relatively simple wear testing machines have been developed (6-7). These tests attempt, as far as possible, to reproduce the sliding conditions encountered in practice. A common simulation technique which is widely used to evaluate the wear of polymers is to slide the polymer, usually in the form of a pin, over the surface of a rotating disc. There are two basic configurations; the pin may be loaded, along its major axis, either in a direction normal to or parallel with the axis of rotation. Hence the contact area is produced on the edge or the face of the disc. It will be shown that the rate of wear produced in these two configurations may be different for certain polymers and furthermore, when the polymer pin is slid over the disc face, the rate of wear is also a function of the radius of a circular path which the pin describes on the disc surface. By changing the radius of this path while maintaining the sliding velocity constant, it is possible to test whether the wear of the polymer is a function of the number of traversals. A very simple model suggests that the rate of wear should be a linear function of the number of traversals.

#### Experimental method

The wear experiments were carried out on two types of pin-on-disc machine. The first type, called "vertical" configuration is shown schematically in Figure 1.

The polymer pin (A) was clamped into a special specimen holder (B), which in turn was attached to a shaft (C) supported in a linear bearing (D). With the special specimen holder (B), it was possible to impose a rotation of the pin around its load axis, independent from rotation of a disc, as well as to change the radius of the wear path prescribed by the pin on the counterface (J).

Rotation of the disc resulted in a torque on the shaft which was monitored by means of strain gauges (G).

Loading of the specimen was achieved by placing weights on the loading platform (H). The load range was 25 to 150 N and the sliding velocity could be continuously varied from 50 to 1500 rpm. The bulk temperature of the counterface was controlled by passing cooling water through a series of seals into the hollow counterface via the hollow drive shaft (M). This arrangement allowed the bulk temperature of the counterface to be kept within  $20^{\circ} \pm 2^{\circ}\text{C}$  during experiments.



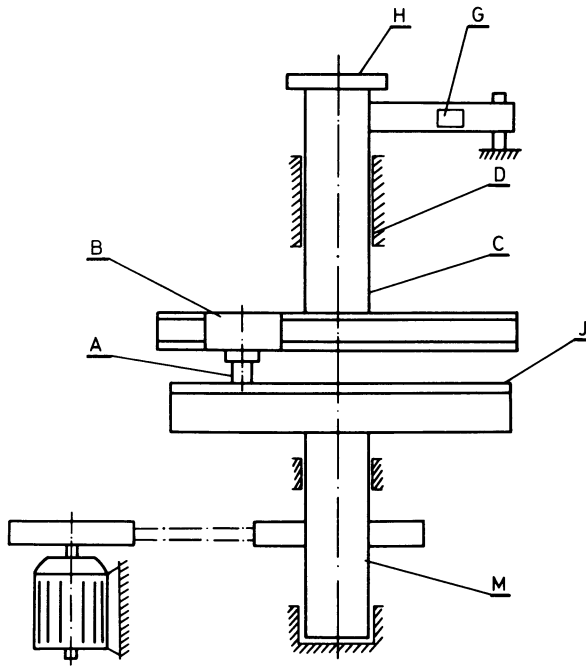


Fig.1. Schematic representation of the "vertical" in-on-disc machine.

The second type of pin-on-disc machine, called "horizontal" configuration, is schematically shown in Figure 2.

The polymer pin (A) was mounted in the specimen holder which in turn was supported by two strain-gauge beams fixed to the loading arm (H) in such a way that the measurement of the tangential force was possible during the application of the normal load. The polymer pin was loaded against a disc (B) of fixed diameter (100 mm) which was rotated on the shaft (C) horizontally supported by two tapered ball bearings (D). The shaft was driven by an AC motor (E) which, together with a variable speed gear box (F) and belt drive (G), was capable of continuous variation in speed over the range 120 to 1280 rpm. Loading of the polymer pin by means of a dead load could be changed from 10 to 150 N. The bulk temperature of the disc was controlled by blowing air upon it by means of a fan with variable speed. This arrangement allowed to keep the bulk temperature of the counterface within  $20^{\circ} \pm 30^{\circ}\text{C}$  during wear tests.

To create a random texture on the counterface a special grinding and polishing procedure was adopted. The mild steel counterfaces used in both types of pin-on-disc machine were finished to 0.2-0.3  $\mu\text{m}$  c.l.a., as revealed by Talysurf examination. Before the beginning of the wear test, the counterface was cleaned with "Analar" acetone.

The wear behaviour of polytetrafluoroethylene (PTFE), carbon-filled PTFE, high density polyethylene (HDPE), ultrahigh molecular weight polyethylene (UHMPE), low density polyethylene (LDPE) and polymethyl methacrylate (PMMA) was studied. To ensure consistent and controlled properties of the samples, many of the materials were processed in the authors' laboratory. The details of sample preparation and processing techniques are reported elsewhere (8).

In the majority of cases, the diameter of the polymer pin was 13 mm, the linear sliding,  $V = 0.5 \text{ ms}^{-1}$  and the specific contact pressure,  $P = 6 \times 10^5 \text{ Nm}^{-2}$ . These parameters were maintained at a constant value for each wear path radius and the specimen. In the case of the "vertical" pin-on-disc configuration, five different values of the radius,  $R$ , of the path described by the pin on the disc were chosen: 6.5 mm; 10 mm; 25 mm; 40 mm; and 65 mm. In all wear experiments, flat-ended pins were used. Polymer specimens were pre-weighed on an analytical balance before being positioned in the test machine. Test parameters (load, sliding velocity) were determined before the initiation of testing. The test was continued for 10 hours in all cases and the sample was removed and weighed after 2 hourly intervals at an accuracy of  $\pm 0.0001 \text{ g}$ . Prior to weighing any loose debris was carefully brushed from the pin and its holder. The wear debris was collected for further examination and the wear path was cleaned with "Analar" acetone to remove loosely attached debris.

The wear rate was considered to be steady after an initial running-in period of 15-20 minutes. This relatively short running-in period was attributed to the fact that it was possible to align carefully the polymer surface and counterface on initiation of testing. Duplicate experiments were carried out to ensure the consistency of the wear data. Generally, wear tests on similar samples under similar conditions were reproducible to within 10%.

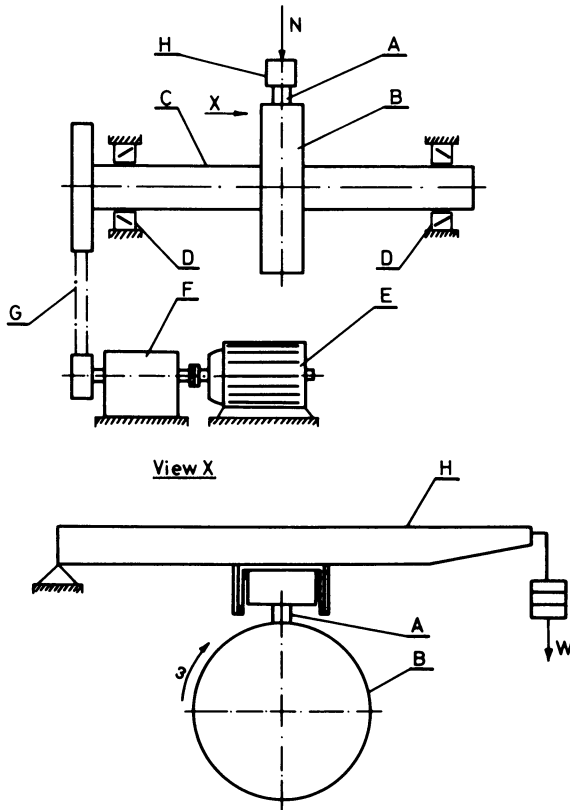


Fig.2. Schematic representation of the "horizontal" pin-on-disc machine.

## Results

Typical data for wear of the polymers studied, expressed as a total loss of materials, as a function of sliding distance at a value of wear path,  $R = \infty$  are shown in Figure 3. The immediate observation to note is that, the wear is proportional to the sliding distance. This is consistent with the findings of other workers. Figure 4 shows the data for the wear, expressed as the mass loss per unit sliding distance,  $K$ , as a function of  $R$ . It is clear that  $K$  is a marked function of  $R$  for PTFE and, to a lesser extent, for HDPE and UHMPE but not for LDPE and PMMA. In addition, there is a rather surprising result that  $K$  decreases as  $R$  decreases. Thus,  $K$  actually decreases as the number of traversals over the transferred film increases. Figure 5 shows the same data and also the data for 20% polar graphite-filled PTFE. Here, the wear data have been normalised by dividing the value of  $K(R)$ , obtained at a particular value of  $R$ , by the value for  $K(\infty)$ , which was obtained by extrapolating  $K(R)$  against  $1/R$  curves to  $1/R = 0$ . The extrapolated value  $K(\infty)$  corresponds to the wear rate for "pure" linear sliding which exists in the "horizontal" configuration (see Figure 3). In Figure 5 the data are presented as the ratio of  $K(R)/K(\infty)$  against  $1/R$  which has the virtue of superimposing the sets of data for PTFE, linear polythenes and PMMA on three master curves. Two polymers, namely PMMA and LDPE, show no radius effect until  $R$  approaches the radius of the pin. For PTFE and to a lesser extent for HDPE and UHMPE the wear decreases as  $R$  is reduced.

Simultaneous measurements of the coefficient of friction have also been made, and these data indicate that where the wear decreases the friction increases (9).

An optical microscope was used to carry out a study of the large quantities of wear debris collected during the course of wear experiments on PTFE. The wear debris was placed between two glass microscope slides which in turn were clamped together with a pressure sensitive tape. Characteristic features of the wear debris were recorded at low magnification (X13) in transmitted light. A series of photographs were taken at higher magnification (X60) between cross polarisers in order to obtain more detailed information about features of the wear debris. The wear debris for PTFE obtained in "horizontal" pin-on-disc configuration (pure linear sliding) is highly fibrillar in form (Figure 6a). Clearly, under these wear conditions the transfer of the polymer to the counterface could be compared with the process of drawing out the molecular chains or morphological units. On the other hand, this structure was lost and was replaced by material which forms relatively regular plates (Figure 6b) when PTFE was tested in "vertical" pin-on-disc configuration. There are also differences in the appearance of the transferred PTFE films formed on the counterface during tests carried out in "vertical" and "horizontal" configurations (8). One of the important observations is that the thickness of the transferred film increases with decreasing radius of the wear path,  $R$ . At the smallest value of  $R$  (6.5 mm), relatively large lumps of polymer are seen on the wear track.

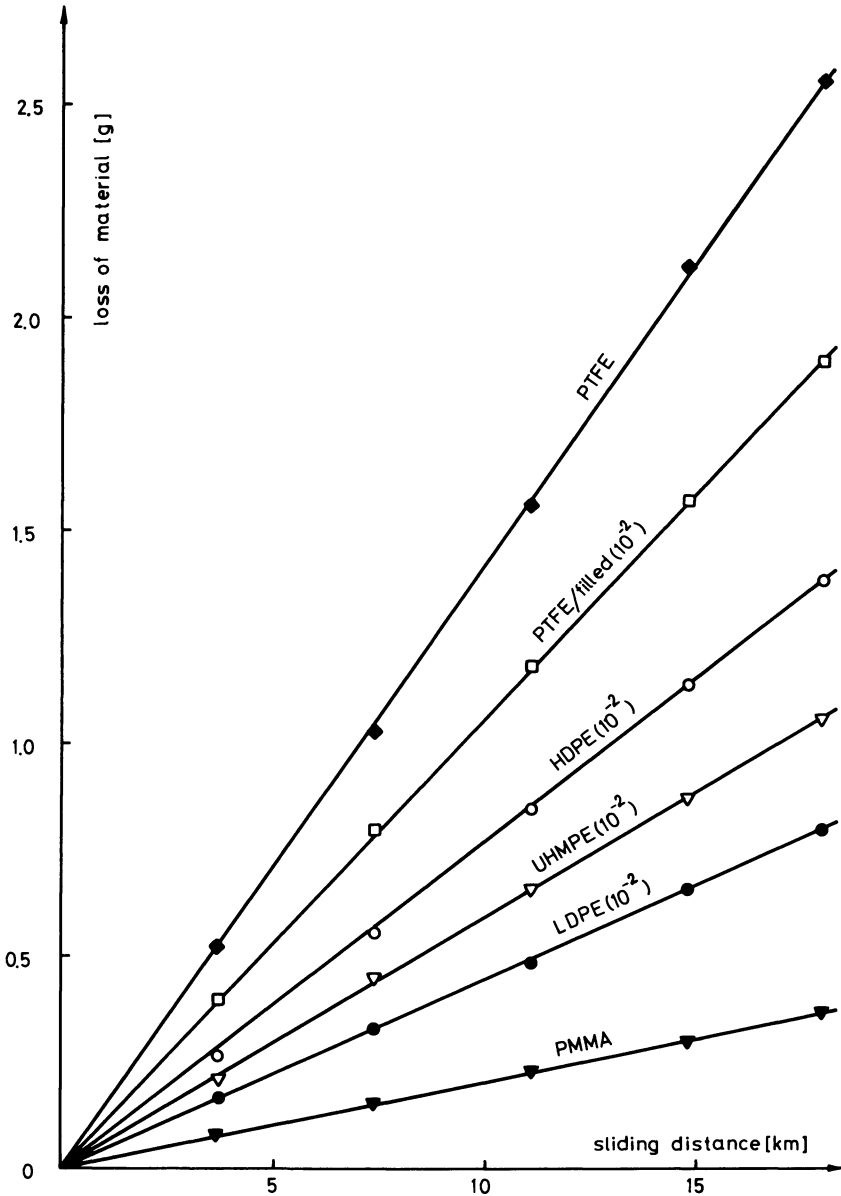


Fig.3. Wear as a weight loss of material against sliding distance. Sliding velocity - 0.5 m/s; Load -  $6 \times 10^5$  N/m<sup>2</sup>; Pin diameter - 13 mm; Wear path diameter -  $\infty$ ; Counterface roughness - 0.2-0.3  $\mu$ m c.l.a.; Counterface temperature -  $20 \pm 3^\circ$ C.

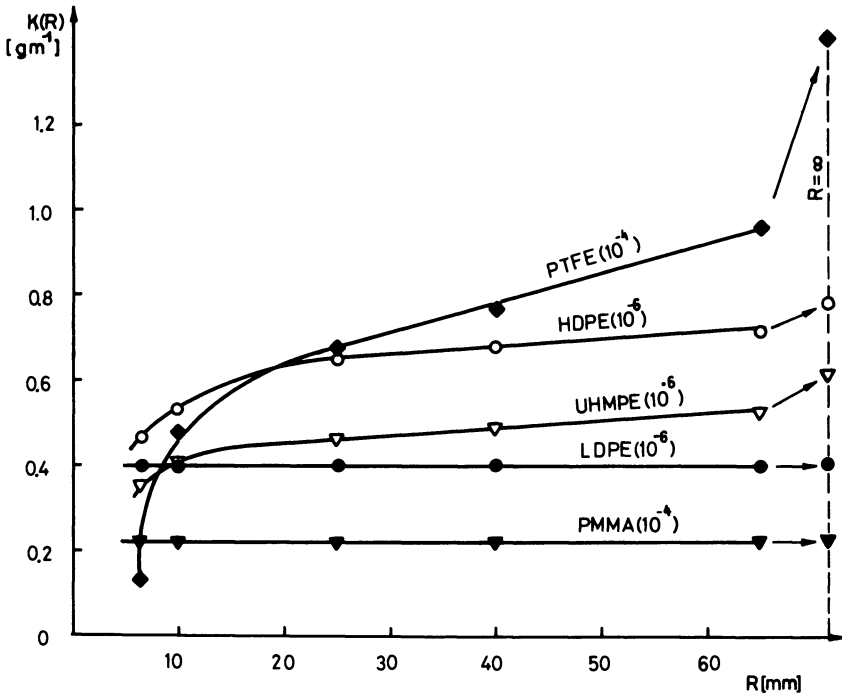


Fig.4. Rate of wear,  $K(R)$ , expressed as a mass loss per unit sliding distance as a function of  $R$ , the radius of the wear path.

Sliding velocity - 0.5 m/s; Load -  $6 \times 10^5 \text{ N/m}^2$ ; Pin diameter - 13 mm;

Counterface roughness -  $0.2-0.3 \mu\text{m c.l.a.}$ ; Counterface temperature -  $20 \pm 2^\circ\text{C}$ .

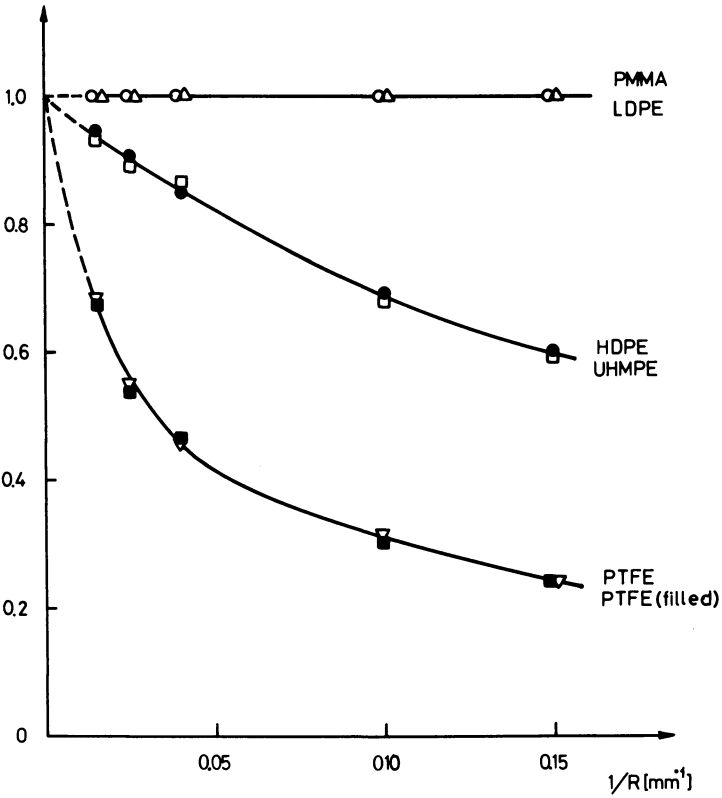


Fig.5. Normalised wear rate, expressed as  $K(R)/K(\infty)$ , against  $1/R$  where  $K(\infty)$  is the wear rate obtained in "horizontal" configuration.  
 Sliding velocity - 0.5 m/s; Load -  $6 \times 10^5 \text{ N/m}^2$ ; Pin diameter - 13 mm;  
 Counterface roughness - 0.2-0.3  $\mu\text{m}$  c.l.a.

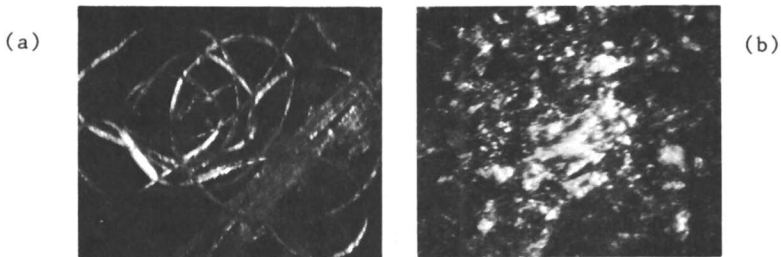


Fig.6. Optical micrographs of wear debris showing the changes in their appearance resulting from the rotation of the contact area in the pin-on-disc machine.  
 a) "horizontal" configuration - 0° rotation  
 b) "vertical" configuration - 90° rotation

### Discussion

Experimental data presented here indicate that the wear behaviour of PTFE, as well as linear polythenes, is quite different from that expected on the basis of the simple thin film transfer mechanism described earlier. The results are unambiguous but at first sight difficult to explain. In the search for an explanation of the unusual wear behaviour shown by PTFE and linear polythenes, an analysis of the relative motions in "vertical" pin-to-disc configuration was carried out. There was a strong indication that this unusual wear behaviour of PTFE, HDPE and UHMPE arises from a peculiarity in the pin-on-disc method (10). Since the fixed pin describes a circular path, the motion is complex. To a good approximation it may be considered to be comprised of a linear vector  $V$ , combined with a pin effectively rotating about its axis with an angular velocity,  $\omega$ , equal to that of the disc,  $\omega_d$ . As  $R$  decreases while  $V$  is maintained constant,  $\omega_d$  increases as  $1/R$ . This angular component produces a complex strain history in the contact which is believed to be responsible for the unusual friction and wear behaviour shown by PTFE and linear polythenes.

LDPE and PMMA show no such radius effect. The wear of these polymers is constant regardless of the value of the wear path radius,  $R$ , save for the regions where the value of  $R$  becomes less than that of the pin radius. Similarly, the friction of these polymers is insensitive to the changes in the value of  $R$ . The common reduction in wear as  $R$  approaches the pin radius is almost certainly due to the fact that while the polymer surface is damaged, the comparatively small relative displacement of the contacting surfaces facilitates the confinement of the wear debris in the contact zone.

The precise mechanism of this radius effect is not entirely clear, but the following rationale accounts for the experimental results. PTFE and HDPE have unusual friction and transfer behaviour, although this is more pronounced with PTFE (11-12). If a PTFE pin is slid linearly at low speeds against a clean, hard, smooth surface, the static frictional force is initially high and a relatively thick transferred layer is deposited. Further sliding produces a thinner and more highly oriented film and a lower dynamic frictional force. If sliding is arrested and the polymer pin is then rotated about its load axis by  $90^\circ$ , the initial behaviour is repeated (8), (11). The frictional force in the direction of linear motion significantly increases with the introduction of rotation in the contact area for polymers like PTFE and to a lesser extent HDPE and UHMPE but not for LDPE and PMMA. These friction data are consistent with wear data for PTFE which is at its lowest for smallest radius of the wear path,  $R$ . Under such test conditions, the thin film transfer process of PTFE and linear polythenes is apparently non-existing and the thicker film transfer process characteristic for LDPE takes place. Thus, introducing the various amount of rotation of the contact area by changing the radius of the wear path in "vertical" pin-on-disc machine, it is possible to change the mode of the transfer process of PTFE and linear polythenes from thin, orientated film to thicker, less orientated film. The special wear behaviour seems to be restricted to the genetic class



of "smooth molecular profile" polymers. To explain the reduction in wear of these polymers with small additions of angular velocity, it is necessary to assume that the thick unorientated layers adhere more strongly to the substrate than the thinner, more orientated films. The comparatively low wear of LDPE compared with PTFE in comparable conditions is consistent with this hypothesis.

### Conclusions

In the "vertical" pin-on-disc configuration, the motion is complex and results in an intrinsic rotation of the contact area. This intrinsic rotation appears to be responsible for the special wear behaviour of PTFE and linear polythenes which are observed to be sensitive to the orientation of their molecular chains in the contact region.

LDPE and PMMA either do not transfer or if the transfer occurs it is not highly orientated. Hence the wear process is not spin sensitive. There is therefore need for caution when measuring the wear of PTFE and linear polythenes using the "vertical" pin-on-disc configuration. Thus, in addition to specifying the usual variables of the wear test, it is also desirable to state both the radius of the pin and the radius of the wear path. The radius of the wear path seems to be a new and interesting variable for probing the friction and wear mechanism of organic polymers. It provides a clear indication of the presence of interface molecular or morphological reordering.

### Literature Cited

1. Briscoe, B.J.; Tabor, D. Proc. Int. Conf. on Fundamentals of Tribology, 1978, p.103.
2. Lancaster, J.K. In "Polymer Science"; Jenkins, A.D., Ed.; North Holland Publ.Co., London 1972, Chap.14.
3. Briscoe, B.J., Tabor, D. In "Polymer Surfaces"; Clark, D.; Feast, J., Eds.; J.Wiley & Sons, 1978.
4. Evans, D.C.; Lancaster, J.K. "The Wear of Polymers"; RAE, Materials Dept., Farnborough, 1978.
5. Lee, L.H., Ed.; "Advances in Polymer Friction and Wear"; Plenum Press, New York, 1975.
6. Brown, R.D. in "Appraisal of World Literature"; Ling, F.F., Klaus, E.F., Fein, R.S., Eds.; ASME, 1963.
7. Bayer, R., Ed.; "Wear Tests for Plastics: Selection and Use"; STP 701, ASTM, 1980.
8. Stolarski, T.A. DIC Thesis, Imperial College of Science and Technology, London, 1978.
9. Briscoe, B.J.; Stolarski, T.A. Trans. ASME, J. Lub. Techn. 1981, 103,503.
10. Briscoe, B.J.; Stolarski, T.A. Nature. 1979, 281, 206.
11. Pooley, C.M.; Tabor, D. Proc. R. Soc. London, 1972, A329, 251.
12. Briscoe, B.J.; Tabor, D. In "Colloques Internationaux du CNRS 1974, 233.

RECEIVED January 23, 1985

## Relating Laboratory Wear Testing to the In-Service Wear of Polymers

J. C. Anderson<sup>1</sup> and P. K. Williamson<sup>2</sup>

<sup>1</sup>National Centre of Tribology, Risley, Warrington WA3 6AT, United Kingdom

<sup>2</sup>Lubrication and Wear Unit, Railway Technical Centre, Derby DE2 8UP, United Kingdom

A large quantity of wear data for polymers and polymer composites is now available from laboratory tests. Except in special circumstances, much of the in-service wear data is incomplete and cannot readily be compared with laboratory data. This paper draws together some laboratory and selected in-service wear data in an attempt to relate the two.

The uncertainties in calculating specific wear rates from in-service data are discussed, as well as the data from laboratory tests which attempt to simulate particular modes of wear (eg abrasion, fretting).

From the information presented, conclusions are drawn on the capability of predicting in-service wear from laboratory tests.

Over 70 different types of polymer-based materials are sold in the UK alone as dry bearing materials. Whilst the number of basic polymers used in these materials is limited to about 6 - viz polyacetal, nylon, polyethylene, PTFE, polyimide and phenolic - it is the incorporation of a great variety of fillers into these polymers, and the different methods of fabrication employed, that gives rise to the large number of commercially available materials. The number of polymer bearing materials has grown steadily over the last twenty years, and this growth is bound to continue as newer polymers, polymer blends and polymer/filler combinations reach the stage of commercial production.

Polymers and composites can be used as bearing materials in a wide range of applications. They are particularly appropriate for bearings in which a film of lubricant cannot be maintained between the working surfaces at all times.

The selection of an appropriate material, and the estimation of its likely performance in a particular application, can become complicated because of the combined effects of bearing pressure, temperature, counterface roughness, sliding speed, and other parameters, on the wear rate of the material. Guidance on the selection of polymer materials for bearings is available, for example

in the Engineering Sciences Data Unit Item No 76029 (1), the Wear Control Handbook (2) and in the recently published Polymer Materials for Bearing Surfaces (3). All contain useful information and in ref 3 comprehensive data is given for a large number of commercially available polymers and composites. This data was obtained from thrust bearings and other tests at the National Centre of Tribology. However considerable differences can exist between the test conditions from such sources and those pertaining to the wide variety of possible service applications. The theme of this paper therefore is the importance of relating laboratory test to in-service wear data and the problems involved.

#### Laboratory Wear Assessment

Considerable research efforts have been made in recent years into the study and measurement of the wear of a range of polymer-based materials in the laboratory. This has resulted in the publication of numerous stimulating papers which describe in detail the wear mechanisms pertaining to restricted test conditions and specific materials. Useful and general references on polymer tribology are given in refs. 4, 5, 6. A designer could be forgiven for being somewhat confused by this wealth of data, with perhaps little of it applicable to his particular problem. In service applications, particularly when exposed to a changing environment, bearings may be subjected to a complex interaction of wear processes and conditions, and no laboratory test can perfectly simulate these. Also, by their very nature, mixed wear processes involve a significant degree of statistical variation in wear rates and this makes an accurate prediction of in-service life from laboratory tests even more difficult (see ref 6).

Therefore in laboratory tests it is common to choose specific combinations of load, speed, contact geometry (point, line or area), motion (continuous rotation, oscillation, reciprocation or fretting), counterface material and surface finish, ambient temperature and the presence or absence of lubricant or abrasive. The number of possible test combinations is therefore vast, and yet it is vitally important for the correct choice to be made if the results are to be of value in predicting in-service bearing life.

In the British Rail laboratories at Derby a number of small-scale tests are carried out and the results given in this paper are from tests which simulate the following; 3-body abrasion, low frequency fretting, continuous rotation and wear in long stroke reciprocating motion. The 3-body abrasion test is carried out on a rotating lapping machine using finely divided silica in a light oil as the abrasive slurry. The fretting test uses a displacement of 5 degrees and a frequency of 5 Hz, which is typical of the major vibrational frequencies of bogie-mounted equipment induced by track forces. The continuous rotation test has a standard pin-on-ring configuration and the reciprocating test comprises a block of polymer loaded onto a steel plate which reciprocates over a 127mm stroke at 0.5 Hz. In the NCT laboratories a variety of wear test methods are used including thrust washer, pin-on-disc and reciprocating tests.

From the large number of polymers that have been tested, two observations are worthy of note here. Firstly, the presence of a fine abrasive slurry can increase the wear rate of many polymers by about 2

orders of magnitude. Figure 1 indicates the range of wear rates of seven polymers of different types under different wear test conditions and the marked increase in wear under abrasive conditions is shown for four out of the seven polymers. The increase was less pronounced for the filled nylon. However both the polyurethane elastomers and ultra-high molecular weight polyethylene did not give higher wear rates under 3-body abrasion compared with other wear processes, and this is associated with their high fracture toughness. Figure 1 also illustrates the second observation, namely that the wear rates of the materials are ranked differently in each type of wear test. A filled polyimide, for example, gave a very low wear rate under clean reciprocating conditions where a transfer film can form, but under abrasive conditions wore very rapidly.

In order to produce data in a form which can be analysed directly when generated under different test conditions, a "specific wear rate" (swr) is commonly used. Specific wear rate is defined as the volume of wear per unit applied load per unit sliding distance and is proportional to the slope of the wear depth-sliding distance curve. It is sometimes also referred to as a "wear factor". Following a running-in period, the volume of wear tends to be proportional to the applied load and sliding distance unless the mechanism of wear changes. As an example of the latter, work on ultra-high molecular weight polyethylene has indicated that a transition in wear rate can occur and this is thought to be associated with the onset of surface fatigue on the polymer, after a certain sliding distance (7) and therefore care would be needed when using the swr for this material.

When attempting to extrapolate laboratory wear data to predict the life of a service bearing, one further limitation is that of scaling. This is normally carried for two reasons; firstly to reproduce service bearing pressures on a small scale laboratory rig and secondly to accelerate the wear process. In laboratory tests the frictional heat generation and dissipation will be different from service and the wear rates of many polymers are sensitive to temperature. Also, the wear debris generated in small scale laboratory tests can escape more readily than in larger conformal bearings and the retention of wear debris is known to affect wear rate adversely in some cases (8). Other factors to be considered are the ratio of contact area to parameters such as surface finish, polymer and filler particle size and metal grain size.

Finally, with regard to laboratory testing all the important service conditions must be incorporated if the results are to be of value to the designer. For example the effect of abrasives has already been mentioned, but in aircraft applications the leakage of fuel or other fluids onto polymer bearings can be a major factor in their performance. In the nuclear industry candidate bearing materials for exposed applications must have been tested under suitably irradiated conditions.

However, because of these difficulties, candidate materials for an application should not be selected by an arbitrary method if a laboratory test is not feasible. The published data should be consulted taking into account the parameters of the application with a critical appraisal of the environmental conditions. An in-service trial can be undertaken and the problems associated with this approach are considered next.

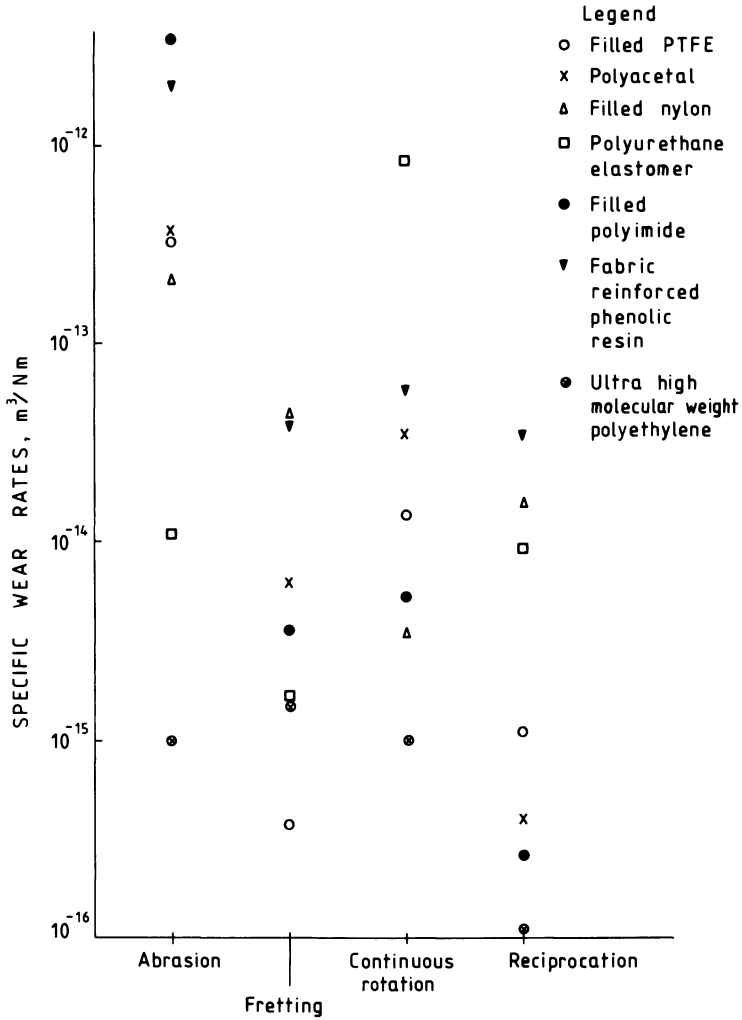


Figure 1. Comparison of laboratory wear of 7 polymer composites under different laboratory wear tests.

## In Service Wear Assessment

Once a prototype bearing is installed in a service application it is often difficult, by virtue of the service duty requirements, for the tribologist to gain access to it or to have sufficient time to make adequate measurements. Disassembly can be difficult or impossible, and the accuracy of the wear measurement may well be inferior to that of a laboratory test. To take an extreme example, artificial hip joints cannot be removed from the body for routine wear measurement, and wear is assessed from periodic X-ray photographs of the joint from which the thickness of the polymer lining can be estimated. A similar problem exists in many engineering examples where bearings are not accessible (the nuclear, offshore oil and aerospace industries) or where they cannot be dismantled during normal service.

Since wear and friction are system-based properties, it is also important to measure other factors such as bearing temperature, although this generally only carried out in critical applications. Service wear can comprise a complex mixture of wear processes and the effect of machine variables such as vibration, ingress of dirt and corrosion products needs to be taken into account for each application, although a quantitative assessment of the effect of each is virtually impossible.

All the above makes the comparison of the relative in-service performance of different materials far from accurate. The calculation of specific wear rate for a given application may require estimates to be made of the average load if it is dynamic, but this would not take account of the possible effect of the few high load conditions. Moreover estimating the relative distance of sliding between the surfaces may be very imprecise.

For a continuously rotating shaft the estimate of sliding distance may be more acceptable. However, for an intermittently operating support shaft bearing for, say, a railway vehicle braking system, the estimate includes not only the number of brake applications within the trial period, but also the amount of relative pin/bush movement that occurs as a result of the "rattling" of the brakegear during the period when it is hanging freely. Obviously considerable errors could arise in such an estimate since it is based on "average values" for train speed, bogie vibrational frequency and angular displacement, and frequency of application, dynamic forces from bogie oscillation and certain component weights. Moreover, a calculation must be made of the worn volume based on the measured increase in bushing diameter, which normally occurs essentially at one position around the circumference as a result of a unidirectional load. In other instances, the bushes are "belled out" at their ends. Calculations and estimations have to be made for each of these wear volumes where necessary.

In the case of a service trial of polymer bushing for a railcar brake linkage the estimated total relative pin/bush sliding distance as a result of occasional brake applications was only 0.3% of that arising from the fretting of the surfaces during free movement of the brakegear over the trial period. Using the estimated volume wear of the bushing for each material together with the distance of sliding and the bushing load, the specific wear rate in service for each of the four materials could be calculated. The average values are plotted in Figure 2 together with the values obtained from each of the

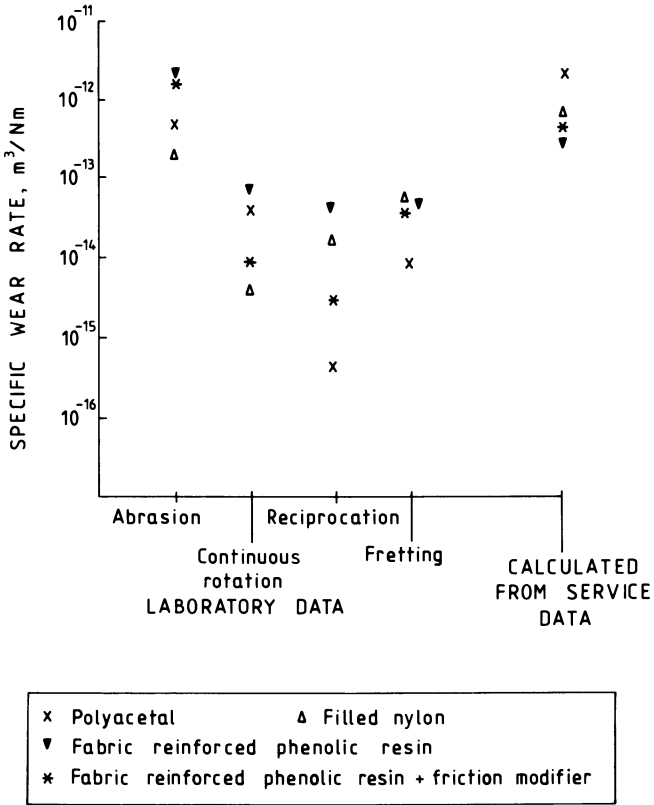


Figure 2. Railcar and brakegear bushes comparison of service and laboratory data.

laboratory tests. It is evident that the band of service values lies close to that for the abrasion test. In practice, the large initial clearances in this equipment allowed the entry of large volumes of airborne dust (originating from the brakes and the track ballast) and it can be assumed that the main cause of the wear is the free movement of the linkage especially when in the presence of abrasive dust.

#### Comparison Of Laboratory And In-Service Assessments

In certain fairly rare circumstances a sufficient number of materials are tested in a single service application to allow a direct in-service comparison to be carried out although a comparison with the laboratory data requires considerable estimation. Nevertheless this can be a useful exercise.

It cannot be denied that data taken from a service trial compares bearing materials in their true working environment, although a good performance in one application will not necessarily ensure the same in another, unless the mixture of wear mechanisms is identical. However, duty requirements and economic considerations do not always allow full in-service trials to be undertaken.

An alternative approach is to assess a service application in terms of the relative importance of basic wear mechanisms (abrasion, fatigue, adhesion, impact/slide, erosion etc) and the geometry and motion. Small scale tests are then carried out in the laboratory to simulate these mechanisms and parameters in order to produce relevant wear data. The performance data for each material with reference to each of these tests will therefore grade the suitability of that material to the proposed application.

In many laboratories (BR and NCT) further tests at either full or reduced scale are carried out on rigs designed to simulate specific applications. Candidate materials with suitable properties chosen from the small scale mechanism tests are then run on these rigs under realistic or scaled loads, speeds, geometries, types of motion and surface finishes. Sometimes the actual service component can be operated in the laboratory to avoid the necessity to manufacture a special rig. In either instance it is still not possible to simulate all factors which affect wear such as vibration, shock loads, abrasion from airborne dust and corrosion.

In the following paragraphs data from service and laboratory are compared for seven case histories, four from the railway industry, and three from other areas. The relationship between performance in the component and on a laboratory rig is demonstrated on a correlation graph such as in Figure 3 comparing the specific wear rates from the two sources on logarithmic coordinates. A perfect correlation would be shown by points lying along the line at 45° to the x-axis and all points below this line indicate a higher wear rate in the laboratory test than in service, that is a conservative or safe life prediction. Above this line the value obtained in service is higher than would be expected from laboratory tests and, on the figure, the dotted lines indicate the deviation from exact correlation.

In the case of human hip and knee prostheses, some data is available (9) which compares wear test results from joint simulators, and other laboratory tests with "in-vivo" wear rates. In joint simulators the amplitude and frequency of motion and the cyclic loads related to walking are simulated as closely as possible. The



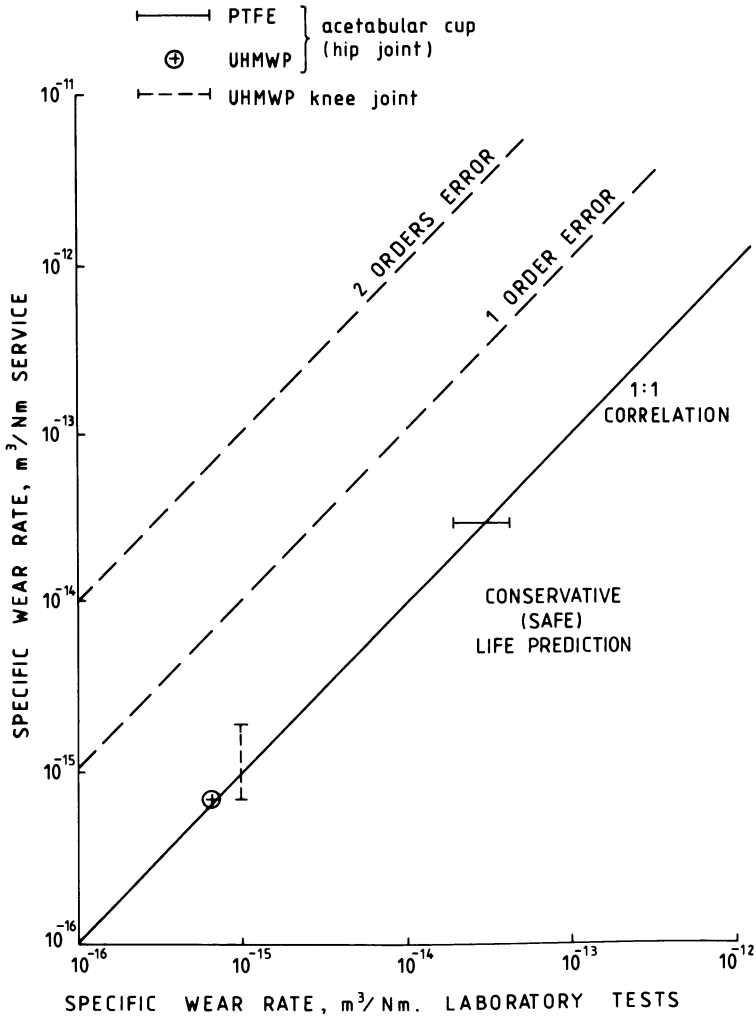


Figure 3. Correlation of laboratory and service wear data.

estimation of an "in-vivo" specific wear rate is again difficult since assumptions have to be made concerning patient activity. In Figure 3 "in-vivo" and laboratory test wear rates are compared for unfilled PTFE and for ultra-high molecular weight polyethylene. For both materials the laboratory wear test data were obtained from pin-on-plate reciprocating tests in which the environment and counterface topography in a hip joint were simulated as closely as possible. Also in the same figure are data for knee joints tested in a simulator compared with estimated wear rates from "in-vivo" measurements. In all cases the agreement of laboratory and "in-vivo" wear rates is within a factor of three which demonstrates the care taken in their calculation and in close laboratory simulation of the important wear parameters.

A comparison between the laboratory and in-service wear assessment of two large marine bearings is shown in Figure 4. In service, the load on, and motion of, these bearings is dictated by wind and sea conditions. In order to calculate a specific wear rate for the in-service bearings, an average load and amplitude of motion was derived. From measurements of the diameters of bearings after 2.5 years of use, average wear depths were calculated. The laboratory wear data was obtained from thrust washer tests on identical material combinations at the mean in-service load and amplitude of oscillation. The agreement for bearing 1 is remarkably good considering the assumptions made, and the fact that the actual (journal) bearings were an order of magnitude larger than the test (thrust) bearings. In the case of bearing 2 the in-service wear rate was lower than the laboratory rate by a factor of 6-7. The reason for this is that the axis of motion of this bearing was believed to be further removed from the prevailing wind and sea conditions compared with bearing 1.

Also in fig 4 is the comparison of in-service and laboratory wear data for small bearings for an electrical charge conveyor. The reason for the higher than predicted in-service wear of these bearings was that, in the presence of, high voltages, an electrical discharge occurred through the thin polymer layer between the steel backing and the bearing pin. Consequently, some of the bronze filler in the polymer was deposited on the counterface, causing a significant increase in the roughness of the pin and hence in the wear rate of the polymer. Following this finding, steps were taken to eliminate this discharge, and the wear rates of replacement bearings appear to be similar to those obtained in the laboratory.

Within the BR laboratories both small-scale wear process simulation and large-scale service simulation rigs are used but the data regarding the following railway applications originate only from the small-scale tests. Therefore for each material a set of four laboratory wear values are plotted on the correlation graphs relating to; three-body abrasion, low frequency fretting, continuous rotation and reciprocating sliding. Figure 5, for instance, shows the four laboratory values plotted against the calculated wear rate from service for each of the three materials used in a trial on a railcar anti-roll suspension system. The wear in service was similar for the three materials and the 1:1 correlation line indicates that the abrasion tests in the laboratory greatly over-estimate the observed service wear whereas the correlation with the other results is

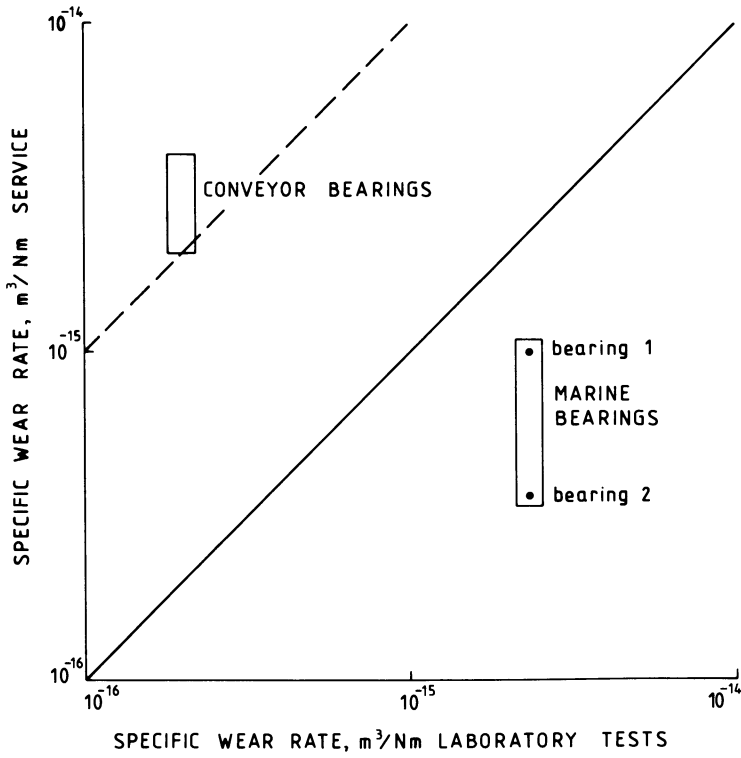


Figure 4. Correlation of laboratory and service wear data.

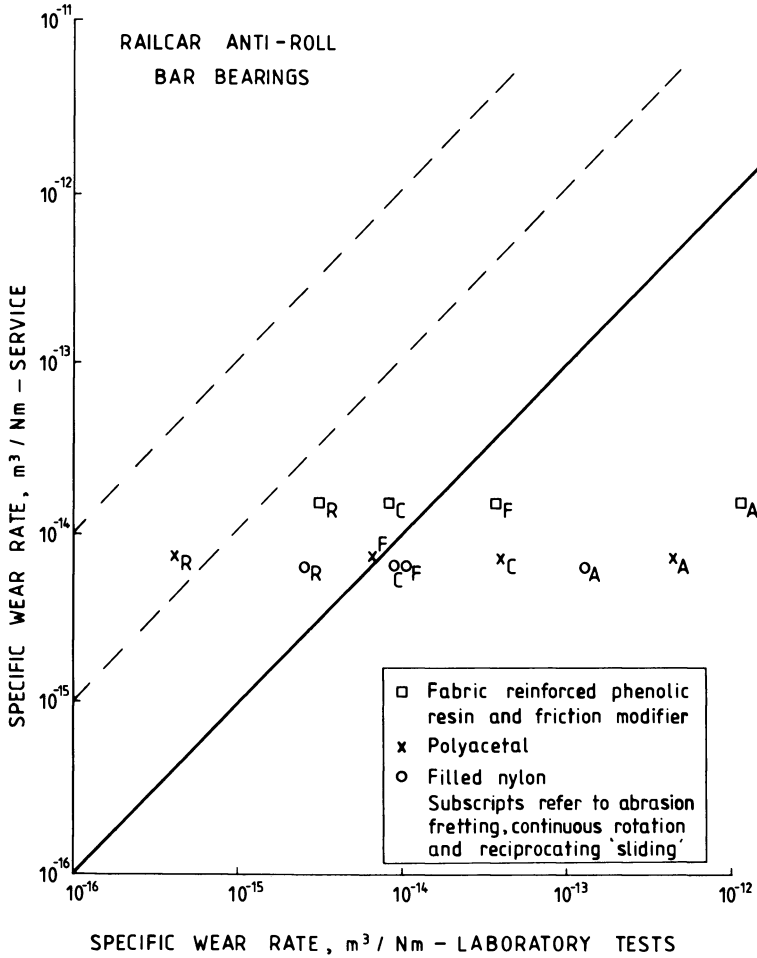


Figure 5. Correlation of laboratory and service data.

reasonable. A short discussion of the relationship of this data to the known service environment for the four railway applications is given later.

Figure 6 shows the data for the railcar brakegear application discussed earlier but here the service wear rates are calculated to be higher than for the anti-roll bar bearings although the vehicle is similar. The 1:1 line correlation here passes through the laboratory abrasive wear values and corresponds to the service observation of large deposits of abrasive dust in these bushings.

Two further trials have been carried out on the treadbrake system of the Advanced Passenger Train (APT) and the High Speed Train (HST) using polymer bushes in the linkage, and the correlation graph on Figure 7 again shows a spread of laboratory values for each service wear calculation. It should be pointed out that the polyacetal bush on the HST trial was run against a low-temperature-nitrided steel pin as opposed to a case hardened steel for the other applications. To date only the continuous rotational wear test has been carried out on this combination of materials and the laboratory data on Figure 7 is therefore restricted. The 1:1 correlation line passes between the abrasion and the other laboratory test results, indicating a mixed wear process, with only a small abrasive wear component.

The data from the above four railway applications can be further analysed since one material, polyacetal, was used in all of the trials and Figure 8 shows the variation of the calculated service wear rates. The highest wear was in the railcar application and is associated with high initial clearances and a fairly long service life resulting in considerable rattling of the brakegear and the entry of a high proportion of airborne dust. The APT treadbrake trial, in contrast, was very much shorter and the initial clearances were very small resulting in a large reduction in abrasive dust contamination. However, the brakegear support pins on the APT were axle mounted which resulted in high track impact forces being transmitted through the pin/bush assembly which would produce an increase in wear rate.

The HST treadbrake support bushes are mounted on the bogie at a greater distance from the track than the railcar and APT bushes, and, therefore, the volume of abrasive dust entering the bearings was much reduced. The wear rates calculated from these three service applications are therefore in line with the severity of the bearing environment and, in particular, the amount of abrasive airborne dust entering the bearing.

The final service result shown in figure 8 refers to the bushes in the anti-roll system of railcars designed by British Rail for operation in Taiwan, where the initial clearances were small and the operation allegedly smooth. However some evidence of abrasive wear was seen on the surfaces of these bushes resulting in a fairly high wear rate with respect to time in service. The calculated swr is therefore rather less than might have been expected from the observations of the worn bearings and the only possible reasons are that the values for the angular displacement, frequency or load are overestimated, or other unusual environmental considerations have not been taken into account.

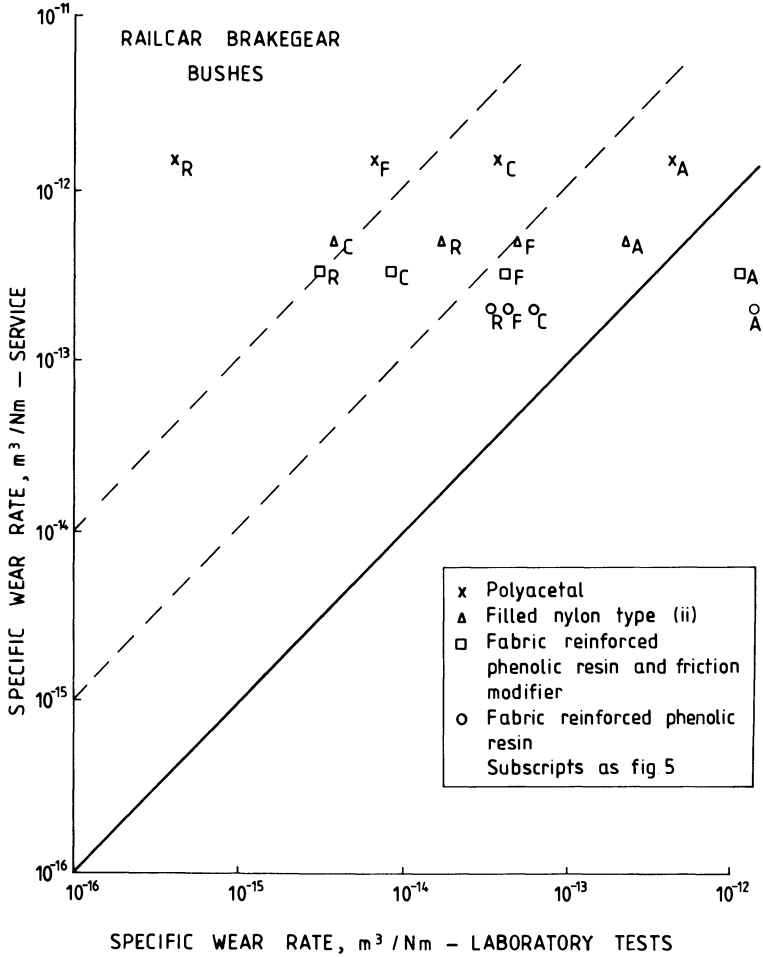


Figure 6. Correlation of laboratory and service data.



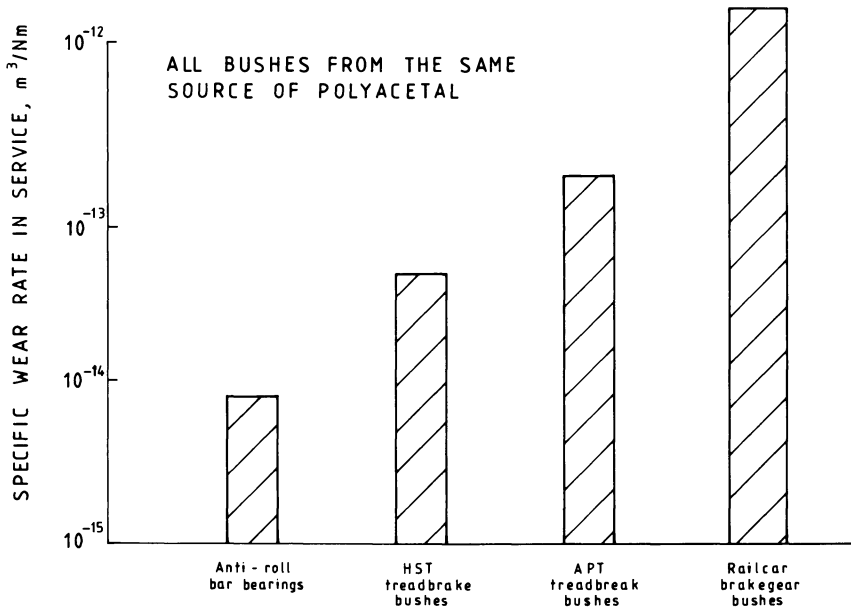


Figure 8. Relationship between service and specific wear rate and application.



### Recommendations

The paper has outlined the problems which can arise when using wear data from laboratory tests or from service trials. The examples illustrate the potential error of wear rates and hence life predictions. It would be inappropriate to conclude this paper without some positive recommendations which may help to reduce this error.

Firstly, it is clear that if laboratory tests are to be carried out then they must simulate the service environment if they are to give a reasonable prediction of expected life. A good simulation is necessary for a good correlation.

If the wear data supplied by a polymer bearing supplier has to be relied upon, full details of the test conditions should be obtained. In addition, the application must be assessed in terms of the likely wear processes. Where possible, an independent assessment of a material's performance should be sought.

Where in-service tests are used to select materials the designer should be cautious about using the data from one trial to predict performance in another. Even if the load, motion and speed are similar, unforeseen environmental changes can markedly alter the wear performance of polymer bearings.

The wear data on materials obtained from published literature may not be relevant to the service conditions proposed and advice from an independent source should be sought in such cases.

### Conclusions

- (a) Obtaining an accurate prediction of the life of a bearing from specific wear rates generated in a laboratory test is not an easy task. Not only do the important wear parameters of the application have to be identified and simulated but environmental factors can have a significant effect on in-service wear rates.
- (b) Not only do specific wear rates of materials vary with the type of laboratory test; the ranking of materials also changes with test type.
- (c) Where service conditions can be defined and simulated in the laboratory, then the correlation between in-service and laboratory test wear rates can be close; that is in agreement to within a factor of 2 or less.
- (d) Conversely where service conditions are variable and cannot be closely simulated, or if wear rate data is used to predict life without consideration of the appropriate factors, then the predicted life could be in error (ie optimistic) by an order of magnitude or more.

### Acknowledgments

The authors wish to thank Dr T N Marsham, Managing Director, Northern Division, UKAEA and Dr A H Wickens, Director of Engineering Development and Research, British Rail, for their permission to publish this paper.

Literature Cited

1. "A Guide to the Design and Selection of Dry Rubbing Bearings." Engineering Data Unit Data Item 76029, 1976.
2. "The Wear Control Handbook". Ed. M B Peterson ; W O Winer, ASME, N.Y, 1980.
3. "Polymer Materials for Bearing Surfaces; Selection and Performance Guide". 1983, National Centre of Tribology. United Kingdom.
4. Briscoe, B. "Wear of Polymers : an Essay on Fundamental Aspects", in "Wear of Materials" 7-16, ASME, 1981.
5. Tabor, D. "The Wear of Non-Metallic Materials - a Brief Review", and other papers, Proc. 3rd Leeds - Lyon Symposium on Tribology, 3-8, Leeds 1976.
6. Lancaster, J K. "Dry Bearings; A survey of materials and factors affecting their performance". Trib. Int. 1973 6, 219.
7. Anderson, J C. "High Density and Ultra-High Molecular Weight Polyethenes", Trib. Int. Vol 15 No 1, 43-47, 1982.
8. Anderson. J C ; Robbins. E J. "The Role of Wear Debris in the Wear of some Polymer Composites at High Loads" in Wear of Materials 1981, ASME NY 1981, 539-544.
9. Dowson. D ; Gillis. B J. "The Penetration of Metallic Femoral Components Into Polymeric Tibial Components Observed in a Knee Joint Simulator". International Symposium on Polymer Wear and its Control, ACS April 1984.

RECEIVED March 26, 1985

## Standardization of Laboratory Methods to Evaluate Friction Behavior of Polymer-Based Materials

A. I. Sviridyonok and Yu. E. Kirpichenko

Institute of Mechanics of Metal-Polymer Systems, Byelorussian S.S.R. Academy of Sciences, Gomel, U.S.S.R.

The paper deals with the problem of standardization of friction and wear test methods for polymer-based materials. A review is presented of the test methods available in the developed countries. Their classification is given with the consideration of friction process modelling. The reasons of data discrepancies are discussed between different sources. It is concluded that procedures for comparative tests should include tests for generalized regimes. A procedure is described for evaluation of the tribological properties of polymer-based materials as suggested in IMMS AS BSSR which is reviewed in ISO as a draft of International Standard. Friction test data are arranged as a map on the material and used to compile a bank of standardized reference information on the tribological properties of polymeric materials.

In recent years a variety of novel antifriction polymer-based materials have been developed and the known improved at different research centers and laboratories of the world. However, even a very learned expert in the field of friction is in a difficulty to evaluate truly the publicity and literary data when making comparative analysis or selecting proper materials for particular friction applications. The reasons lie in the unavailability of common methods for friction testing of materials as well as evaluating criteria on the friction characteristics of materials. Explanation and selection of evaluating criteria largely depend upon the factors that influence the friction characteristics of polymers, and capabilities of the testing equipment.

### Factors Influencing the Friction in Metal-Polymer Pairs

The factors that influence the friction and wear processes can be combined into three groups: i) structural ( geometrical dimensions, shape of the parts, geometry of contact, etc. ); ii) physical ( presence of vibrations, thermal conditions, duration of continuous operation, presence of radiation, electric or magnetic fields, etc.); and iii) chemical ones ( working environments and their activity towards the materials rubbed ). Each factor in turn has its own features. For instance, physical factors may be constant or varied in the direction or values; great is the variety of the contact geometry, i. e., it may be a sphere, a plane or a cylinder, or any combination thereof, to give point, line or plane contacts ( 1 ).

In view of the above, of interest are the data reported by the Organization for Economic Cooperation and Development ( OECD ) with the headquarters in Paris resulted from a Program of Comparative Wear Tests conducted on the same materials (copper, brass, bronze and steel) in different laboratories of different countries on different testing equipment ( 2 ). The analysis of the test results showed that the values of wear resistance obtained from different laboratories differed almost 20-fold. Similar pictures are now observed with polymeric materials. This lack of correlation between the test results underlines the losses owing to the unavailability of common testing procedures and explanation of the main factors that influence greatly the friction characteristics of materials.

Specific physical and mechanical behavior of polymeric materials allows to identify the main factors that influence the friction process:

- \* temperature in the contact zone
- \* viscoelastic behavior of polymers under load (creep)
- \* dimensions
- \* chemical activity of the environments in the contact zone
- \* overlapping ratio for thrust bearings or encompassing angle between the testing shaft and polymeric bearing or bushing tested
- \* the processes of polymer transfer onto rubbed metallic surfaces.

It is clear that the influence of these factors upon friction and wear should be studied in combination with friction parameters such as load, sliding velocity, and surface roughness.

The conventional methods of friction testing provide measurement of the main tribometrical characteristics that specify the material applicability for dry operation at given loads and sliding velocities. The main tribometrical characteristics for polymers are as follows:

- \* load-carrying capacity with minimum deformation
- \* wear rate
- \* coefficient of friction
- \* service life of bearings in terms of P, V, and T.

All these factors are interrelated to a certain degree, and to obtain true and useful data for designing friction units, testing methods are required that are capable of establishing the influence of the main friction factors and conditions on the interrelation of the characteristics mentioned.

### Methods of Friction Investigation

The methods available for evaluating the tribometric characteristics can be classified by the mode of modelling the friction processes. These are tribometric schematics modelling the following:

- \* simple acts of frictional interaction
- \* performance of particular friction units and parts
- \* service conditions.

The methods of the first group are mostly intended for research laboratories and developing most dynamically. Of these are the methods designed for studying the structure-and-friction properties of materials (1), (3-6), and those modelling simple acts of friction interaction on a certain structure level (7-9). Several procedures and instruments of this group are unique, however, one meets officially approved and universal ones for tackling urgent problems such as selection of constituents for self-lubricated compositions, studying adhesion and deformation processes at rubbing (10), (11).

The second group is for laboratory estimation of the performance of actual friction units such as plain bearings, gear or chain drives, or other standard friction units on special stands. The purpose of these tests is to obtain data for predicting performance of actual friction assemblies.

The third group of methods for friction testing is at present most important in studying the effect of friction parameters and main factors upon the values of tribometrical characteristics. The variety of techniques for friction testing and devices for their realization (12), (13) indicate a wide search for "universal" procedures for testing materials. However, the standards available (14-16) describe in most instances the way of estimation of certain tribometrical characteristics (coefficient of friction, wear rate) for particular conditions of material applications. The data obtained during these tests find limited usage, fail to give complete understanding of the effect of friction parameters and main factors upon the characteristics mentioned, and do not allow comparison of the materials.

The search for complete understanding of friction properties led to the methods (17), (18) accounting for the combined effects of the main factors. From Ref. (17) relations are found for the friction coefficient, temperature, wear rate versus sliding velocities and loads. Then by the data obtained, a set of curves is drawn in  $P - V$  coordinates, having the same values of the friction coefficient, temperature, and wear rate. It is clear that great difficulties arise in obtaining and using this volume of information. Crease (18) finds only

relations for the friction coefficient versus loads and temperatures ( $K = f(P)$ ,  $K = f(T)$ ), and maximum tolerable pressure versus temperature ( $P_{\max} = f(T)$ ). This provides a prediction of the wear resistance for friction units with the relation  $K = f(T)$  using equation

$$T_{fr} = T_{env} + c \cdot f \cdot P \cdot V$$

where  $T_{fr}$  is the temperature in the friction zone;  $T_{env}$  is the temperature of the environment;  $c$  is a coefficient dependent on the assembly design;  $f$  is the coefficient of friction;  $P$  is the unit load on the bearing, and  $V$  is the sliding velocity.

#### Novel Methods for Accelerated Evaluation of Friction Characteristics

In the Institute of Mechanics of Metal-Polymer Systems, Byelorussian SSR Academy of Sciences, USSR a method MR 74-82 (20) for evaluating the tribotechnical properties of polymer-based materials had been developed based on the generalization of techniques and taking into consideration the friction behavior of polymers and polymer-based composites (19).

With polymeric materials in friction pairs the working capacity of the assembly is lost for three reasons: i) temperature rise in the friction zone above the limiting value, ii) wear exceeding the tolerable limit, and iii) loads over the yield point of the polymeric material.

In view of this and other works (19, 21 - 23), the following criteria of accelerated prediction of friction properties for polymeric materials were selected when developing the method mentioned:

\* A complex of loads and velocities at which the wear rate of the polymeric material is below  $0.25 \mu\text{m/h}$  [ $PV_{25}$ ].

\* A complex of loads and velocities at which the temperature in the friction zone increases significantly along with the friction moment, i. e. [ $PV$ ] regimes are reached corresponding to the loss of working capacity by the polymeric material.

\* Coefficient of friction  $f$  and wear  $K = \frac{\Delta h}{SP}$ ,

where  $\Delta h$  is linear wear of the polymeric specimen;  $S$  is the rubbed distance, and  $P$  is the load on the specimen.

The selection of friction parameters in order to determine the above criteria for evaluating the friction properties was based on the analysis and statistical treatment of the data on the regimes of friction units operation where it is beneficial to use self-lubricated polymeric materials. The characteristic operation regimes were found to be in the range of sliding velocities from 0.01 up to 5.0 m/s and loads from

0.1 up to 20 MPa. 90% of the units examined showed a surface-to-surface contact; 80% of these were cylinders with inside contacts and 20% were bearings with butt-end contacts. Thus, the schematic "shaft-partial bearing" is most suitable for a generalized model of the friction contact.

The procedure suggested is realized as follows: the complex of loads and velocities corresponding to the loss of working capacity by the polymeric material is found automatically with friction machines UMT, SMT-1 and computer system SM-1, Figure 1. A minimum load from Table I is applied to a cleaned run-in specimen with a block of load selection. The block of velocity selection provides a minimum sliding velocity from Table I as well. Signals from the devices that measure the temperature, friction moment and wear go to the register where they are recorded ( Figure 2 ) and to the block showing the extreme values. After the temperature and the friction moment become steady, the block showing the extreme values, forms a signal being recorded by a bridge device which forces the velocity-selection-block to give another value from Table I. After the whole set of velocities were taken or a limiting load reached for a given material, the signal from the pulse counter goes to the coincidence circuit which switches on the loading device that provides a next load level. For this load level the same algorithm gives a limiting sliding velocity.

After the results of a group of tests have been treated mathematically, a curve is constructed in the coordinates of load (P) and velocity (V) covering the set of limiting loads and velocities [PV] .

The set of loads and velocities at which the wear rate reaches  $0.25 \mu\text{m/h}$  for the polymeric material is determined from the curve of the [PV] limiting values. From Table I a minimum velocity is selected and a load applied that provides pressure on the friction unit of  $0.5 [PV]$  . After 100 h operation the wear is measured. Should its value be over  $25 \mu\text{m}$ , another testing is conducted at a lower loading level. Should the wear be below  $25 \mu\text{m}$ , the load is increased up to a next level.

Similar tests are conducted for all the rest ranges of sliding velocities. The test results are presented as curves from which a complex of loads and velocities is selected that corresponds to wear rate of  $25 \mu\text{m}$  after 100 h operation (Figure 3).

Tribotechnical properties of 30 polymer-based materials widely used in engineering have been specified according to the USSR Testing Method MR-74-82. The high degree of reproducibility allows a successful application of the data obtained in designing practice.

The wear ratio of the materials tested that corresponds to the wear rate of  $0.25 \mu\text{m/h}$  is characterized by a wide range of values from 0.2 up to 2.1, which depend to a large extent on the temperature in the friction zone. Thus by using the dependence of the wear ratio on the temperature it is possible to forecast the performance of a true friction unit as it had been similarly done elsewhere (18, 21).



Figure 1. Center where tribotechnical properties of materials are tested. Tests are carried out on standard machines SMT-1, UMT and computer system SM-1.

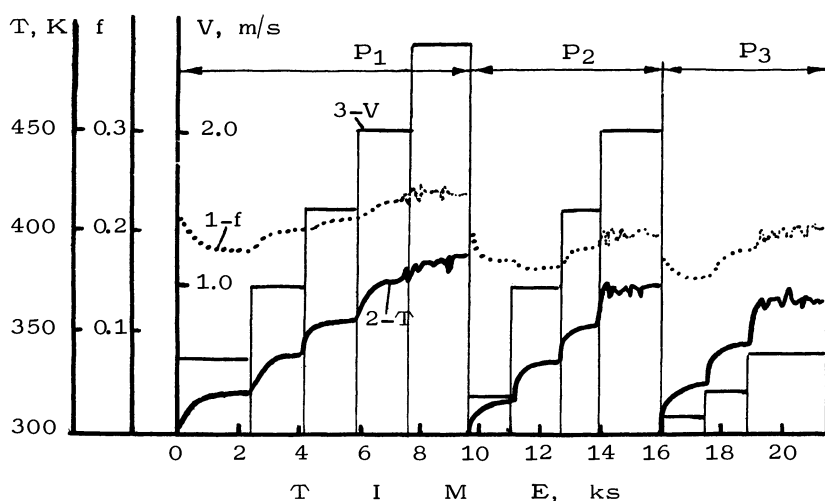


Figure 2. Dependence of friction zone temperature ( $T$ ) (curve 2) and the coefficient of friction ( $f$ ) (curve 1) upon  $PV$ .

For load values from  $P_{min}$  up to  $P_{max}$  with stepwise velocity increase, a limiting value for sliding velocity ( $V_{max}$ ) is found at which the material suffers frictional failure. In the course of testing the coefficient of friction (curve 1) and temperature in the subsurface layer of the polymeric specimen (curve 2) are recorded.



Publication Date: September 12, 1985 | doi: 10.1021/bk-1985-0287.ch022

Table I. Values of Loads (P) and Velocities (V) for Finding [PV] and  $PV_{25}$

$V, m \cdot s^{-1}$	0.01	0.05	0.1	0.25	0.5	1.0	2.5	3.5	5.0
P, MPa	0.1	0.25	0.5	1.25	2.5	5.0	10.0	20.0	50.0

To systematize the data obtained, keypunched cards are used with two rows. The free field of the one card-side (Figure 4) is filled with the necessary information on the tribotechnical properties of the material (testing schematic, equipment, materials in contact, procedure of specimen preparation, and surface conditions, test results, etc.). The edge punching of the cards allows coding the necessary data and efficient searching of the required information. The data is coded with a universal key by using outer punching. In the sections of load, velocity, and temperature both outer and inner punchings are used. The inner punching is for operation regimes; the outer punching is for the tolerable limiting values of  $[P]$ ,  $[V]$ ,  $[T]$ . The other side of the card carries the main physical-and-mechanical, thermophysical and technological properties of the materials tested.

The procedure described had been passed to ISO as a draft of an international method for accelerated testing of polymer-based materials for bearings.

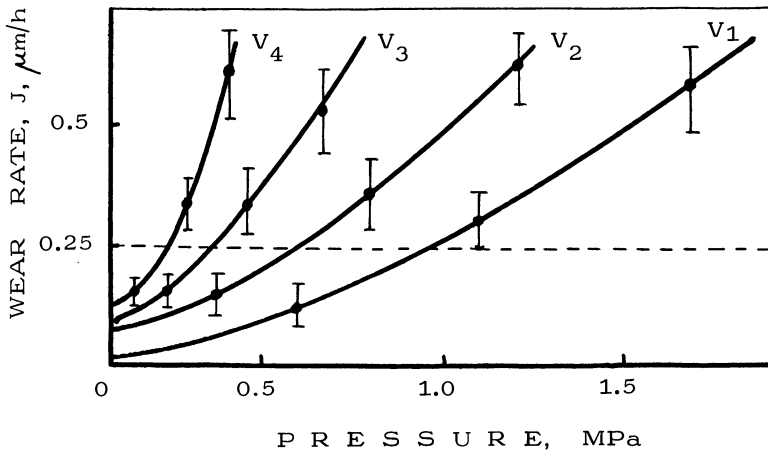


Figure 3. Wear rate dependence on load and sliding velocity.

For sliding velocities from  $V_{\min}$  to  $V_{\max}$  loads are found at which after 100 h operation wear reaches 15 to 35  $\mu\text{m}$ . Interception of  $V_1, V_2, V_3, \dots$  curves with a line at 25  $\mu\text{m}$  gives load values that correspond to wear rate of 0.25  $\mu\text{m/h}$  for given sliding velocities.

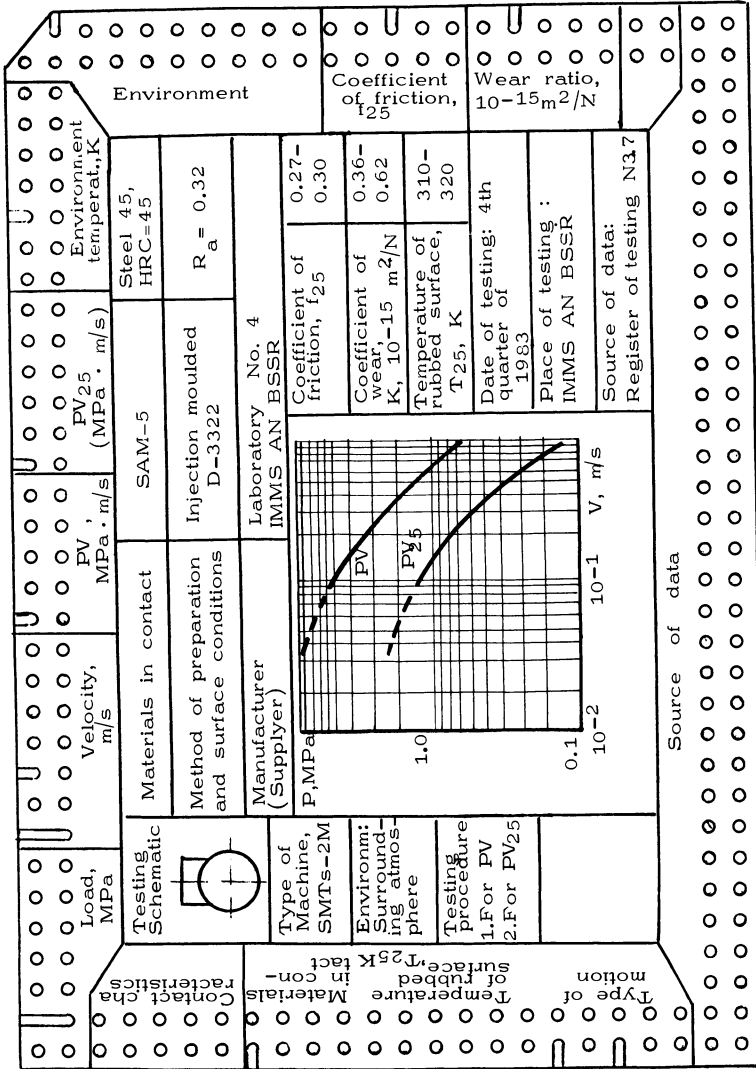


Figure 4. Card for friction characteristics of materials. The conditions and friction test results from Figures 2 and 3 are filled into cards. [PV] and PV25 curves in P - V coordinates are a complex of loads and velocities at which limiting operation regime [PV] and wear rate 0.25 μm/h (PV25) are reached.

### Conclusions

The described method MR-74-82 allows in a short time an estimation of the performance limits for polymer-based materials depending on the friction parameters ( $P - V$ ). The method considers the temperature, environment, variations of the loading regime, etc. The bank of data compiled as the result of testing the tribotechnical properties allows the comparative analysis to be done when selecting materials for friction assemblies.

### Literature Cited

1. Kragelskii I. V. , "Friction and Wear", Mashinostroenie, Moscow, 1968.
2. Begelinger, A.; Gee, A. W. L., Lubrication Engineering 1970, 2, 56-63.
3. Buckley, D. H.; Brainard, W. A., " The Atomic Nature of Polymer-Metal Interaction in Adhesion, Friction and Wear", In " Advances in Polymer Friction and Wear", N. Y., 1974. Editor Lee, L. H, Plenum Press.
4. Bely, V. A.; Sviridyonok, A. I., "Role of Structure in the Friction Mechanism of Polymer Materials"; In "Advances in Polymer Friction and Wear", N. Y., 1974. Editor Lee, L. H., Plenum Press.
5. Kostetskii, B. I., "Friction, Lubrication and Wear in Machines"; Tekhnika, Kiev, 1970.
6. Richardson, M. O. W. "Chemical Aspects of Wear Process in Polymers", Wear , 1971, 17, p. 89.
7. Shchukin, E. D. et al., "On the Initiation of Simple Plastic Deformations within Single Crystals of Fluorous Lithium at Boundary Friction", DAN SSSR, 1971, N 6, p. 200.
8. Barquins, M., Kennel, M. ;Courtel, R., "Compartement de monocristaux hemispherique", Wear, 1968, 11, p. 87.
9. Belyi, V. A., Petrokovets, M. I., Savkin, V. G.; Sviridyonok, A. I., "A New Method of Investigation of Supermolecular Deformation at External Friction", Mekhanika Polimerov, 1969, N 5.
10. USSR GOST 23.203-78 , "Method of Measuring Strength of Adhesive Bonds for Rubbed Solids", Standards Publishers, Moscow, 1978.
11. US Standard ANSI/A TM 1894-78 , "Plastic Films. Method for Estimation the Friction Coefficient".
12. Reshetov, D. N., Editor , "Machines and Stands for Testing Parts". Mashinostroenie: Moscow, 1979, 343 ps.
13. "A Catalog of Friction and Wear Devices", ASLE, 1973.
14. Norme Francaise NF T 51-107-77 , "Matiere Plastiques. Essai d'Usure et de Frottement de Cylindre sur Plan".
15. Norme Francaise NF T 51-110-75 , "Matiere Plastiques, Essai d'Usure et de Frottement".
16. USSR GOST 23.210-80 , "Method for Estimation of Friction Heat Resistance of Materials", Standards Publishers, Moscow, 1980.

17. "Problems of Performance Estimation of Polymeric Materials," In "Methods of Testing and Evaluation of Performance Properties of Plain-Bearing Materials", Nauka: Moscow, 1972, pp. 140-144.
18. Crease, A. B., "The Wear Performance of Rubbing Bearing-Improved Data for Design", in "The Wear of Non-Metallic Materials, Proceedings of the 3rd Leeds-Lyon Symposium", 1976, pp. 245-251.
19. Belyi, V. A., Sviridyonok, A. I., Petrokovets, M. I.; Savkin, V. G., "Friction and Wear of Polymer-Based Materials," Nauka i Tekhnika: Minsk, 1976, 432 ps.
20. Recommendations MR 74-82. "Method for Estimation of Tribological Properties of Polymer-Based Materials", Moscow, 1982.
21. "A Guide to the Design and Selection of Dry Rubbing Bearing", Eng. Sciences Data, Item Number 76029, London: Inst. of Mech. Eng., 1976, 43 ps.
22. Kragelskii, I. V., Kombalov, B. S.; Loginov, A. R. et al., "On Single Wear Criteria". In "The Estimated and Experimental Methods of Friction and Wear Evaluation". Nauka: Moscow, 1980.
23. Sviridyonok, A. I.; Alexeev N. M., Kenko, V. M. "Estimation of Tribotechnical Characteristics of Polymer-Based Materials," in "The Effect of Surface Quality on Performance Characteristics of Machine Moving Units", Synopses. Rybinsk, USSR, 1979.

RECEIVED January 23, 1985

# Deterioration Processes of Polymeric Materials and Their Influence on the Durability of Reinforced Concrete

Toshio Fukushima and Kenji Motohashi

Building Research Institute, Ministry of Construction, The Japanese Government, 1-Tatehara, Oho-machi, Tukuba-gun, Ibaraki Prefecture 305, Japan

From the viewpoint of prediction of service lives, the photochemical deterioration processes of polymers used as paints and finishes are theoretically analyzed based upon unsteady state dynamics. Theoretical results are compared with experimental data under natural and accelerated exposure. Infrared spectra and scanning micrographs show that the deterioration proceeds continuously inwards from the surface, but differently with the exposure conditions. Parabolic ( $\sqrt{t}$ ) law was derived approximately for the increase in the depth of the deteriorated layer of polymers with time. Paying attention to the influence of the deterioration of polymeric finishes, the parabolic law involving a constant term was also derived for the progress of carbonation of concrete. These parabolic laws well predict the progress of deterioration and explain the protective function of finishes on reinforced concrete.

The development of the petrochemical industry has enabled the mass supply of various types of polymers with attractive properties. Although many polymers are widely used in various fields (e.g. as paints, adhesives, coatings and finishes in housing), they are subject to gradual deterioration under natural exposure.

With the enlargement of recent social needs for the conservation of natural resources and energy, and for the high functions of in-service materials, the importance of the concept of durability as performance with time and the prediction of service lives of materials has been increasingly appreciated among many researchers and engineers in various fields. In pursuit of rational criteria for evaluating the progress of deterioration and for identifying deterioration mechanisms of materials, a lot of phenomenological data have been accumulated for the deterioration processes. However there still remain major difficulties to be solved for analytical methods of the deterioration processes.

On the other hand, in housing under ordinary atmospheric enviro-

0097-6156/85/0287-0347\$06.00/0  
© 1985 American Chemical Society

American Chemical Society  
Library

1155 16th St., N.W.  
Washington, D.C. 20036

onment, the carbonation of concrete is very important from the point of view of the durability of reinforced concrete component, because it causes the neutralization of concrete, resulting in the reduction of corrosion protective function against reinforcing bars. Many efforts have been done to delay or suppress the progress of neutralization of concrete effectively, e.g. by using paints and finishes.

This report deals with dynamic processes of the deterioration of polymers often used as paints and finishes in housing, and also refers to their influence as the reduction in protective performance on the durability of reinforced concrete. The deterioration processes of polymers by the simultaneous action of ultraviolet (UV) light and diffusive oxygen is explained theoretically based upon unsteady state dynamics. The parabolic law ( $\sqrt{t}$  law) is derived for a typical path for the progress of the deterioration of polymers inwards from the surface (1), and compared with some experimental data. The same parabolic law involving a constant term was also derived for the carbonation of concrete, which well explains the retardation effects of finishes on the carbonation (2).

#### Dynamic Analysis of Deterioration Processes of Polymeric Materials

Outline of the Theoretical Model. The main assumptions for the unsteady state dynamics are as follows: 1) Only polymer molecules which are raised into excited state by absorbing UV light (photon flux,  $n_0$ ; wavelength,  $\lambda$ ) near the absorption band characteristic of polymers can participate in photochemical reactions (efficiency,  $\eta$ ; molar concentration,  $C^*$ ). (2) Photochemical reactions are: i) depolymerization of activated polymer molecules (first order reaction,  $R_1 = k_1 C^*$ ), ii) photo-oxidation by the collision of diffusive oxygen (initial and time-dependent molar concentration,  $C_{A0}$  and  $C_A$ ; effective diffusion coefficient,  $D_A$ ) and activated polymer molecules (second order reaction,  $R_2 = k_2 C^* C_A$ ). We can consider this reaction to be quasi-first order reaction ( $R_2 = k_1' C_A$ ) (3) Deteriorated polymer molecules (molar concentration,  $C_B$ ) do not diffuse and remain in the original positions. (4) The influence of temperature on photochemical reactions is included in material property constants ( $k_1$ ,  $k_2$ ) and diffusive coefficient ( $D_A$ ) according to the Arrhenius law. (5) Deterioration proceeds inwards from the surface and the degree of deterioration varies with exposure time ( $t$ ) and the depth from the surface ( $x$ ). As the deterioration advances, deteriorated polymer molecules having infrared (IR) active functional groups as carbonyl ( $-CO$ ) are created, and the degree of deterioration is reflected in IR spectra and in the morphological change of the surface. The deteriorated surface layer results in the reduction in the flexural strength and in protective performance of polymers. (6) Compared with the thickness of the plate of polymer, the deteriorated depth ( $\delta$ ) can be considered to be small enough for the thickness of the plate to be regarded as infinitely large.

Basic differential equations for the dynamic analysis, together with the initial and boundary conditions, are summarized as follows:

$$\frac{\partial C_A}{\partial t} = D_A \frac{\partial^2 C_A}{\partial x^2} - k_1' C_A \quad (1)$$

$$\frac{\partial C^*}{\partial t} = \left( \eta n_0 / N_0 \right) C_0 \epsilon_\lambda \exp(-C_0 \epsilon_\lambda x) - k_1' C^* - k_1 C_A \quad (2)$$

$$\frac{\partial C_B}{\partial t} = k_1 C^* + k_1' C_A \quad (3)$$

Here,  $N_0$  is Avogadro's constant;  $C_0$ , initial molar concentration of undeteriorated polymer molecules;  $\epsilon_\lambda$ , molar absorption coefficient.

[Initial Conditions];  $t \leq 0$ :  $C^* = C_A = C_B = 0$

[Boundary Conditions]; [I]  $t > 0$ ,  $x = 0$ :  $C_A = C_{A0}$

[II]  $t > 0$ ,  $x \rightarrow \infty$ :  $C_A = 0$

[III]  $t > 0$ ,  $x = \delta$ :  $\partial C_B / \partial x = 0$

Results of Dynamic Analysis. Solving the simultaneous differential equations 1.-3. under the given initial and boundary conditions by the Laplace transformation method, analytical solutions 4.-8. are obtained in the form of dimensionless concentrations:

$$\phi_A \equiv C_A(x,t)/C_A = (1/2)[\exp(-x\sqrt{k_1/D_A}) \operatorname{erfc}(x/2\sqrt{D_A t} - \sqrt{k_1 t}) + \exp(x\sqrt{k_1/D_A}) \operatorname{erfc}(x/2\sqrt{D_A t} + \sqrt{k_1 t})] \quad (4)$$

$$\phi^* \equiv C^*(x,t)/C_0^* = [1 - \exp(-k_1 t)] \exp(-C_0 \epsilon_\lambda x) - (C_{A0}/C_0^*) k_1 t \phi_A \quad (5)$$

$$\phi_B \equiv C_B(x,t)/C_0^* = \{k_1 t - [1 - \exp(k_1 t)]\} [\exp(-C_0 \epsilon_\lambda x / k_1)] + (k_1' - k_1) (C_{A0}/C_0^*) \int_0^t \phi_A dt + [1 - \exp(-k_1 t)] (C_{A0}/C_0^*) \phi_A \quad (6)$$

Here,  $C_0^* = C_0 n_0 \epsilon_\lambda / N_0$

On the other hand, using the boundary condition [III], we can obtain approximately the parabolic law for the progress of the depth of the deteriorated layer as follows:

$$\delta = \sqrt{\beta t} \quad (7)$$

$$\beta = D_A (5k_1 + 2k_1') (7k_1 - 2k_1') / (k_1 - 2k_1') (3k_1 - 2k_1') \quad (8)$$

#### Dynamic Analysis of the Progress of Carbonation of Concrete

The neutralization of concrete leads to reduction of the corrosion protective function of concrete against reinforcing steel, and has an important influence on the durability of reinforced concrete structures. The neutralization is influenced by various factors (concentration of  $\text{CO}_2$  gas, type of concrete, water-to-cement ratio ( $W/C$ ), water content, type of finishes and their thickness and permeability, temperature and humidity conditions, etc.). From the physico-chemical point of view, this process can be considered to be the diffusion of  $\text{CO}_2$  inwards into concrete from the surface, accompanied by the conversion of  $\text{Ca}(\text{OH})_2$  into  $\text{CaCO}_3$ . In this context, unsteady state dynamics has been done for the progress of neutralization of concrete in order to rationally understand the process and the influence of finishes on the process (3, 4).

The main assumptions are as follows:

(1) In the initial state,  $\text{Ca}(\text{OH})_2$  exists homogeneously in semi-infinite concrete (initial molar concentration,  $C_{b0}$ ), and the carbonation process begins when  $\text{CO}_2$  in gas phase (initial molar concentration,  $C_{ag}$ ) comes into contact with the surface of concrete (take  $x = 0$  at the surface). (2) Diffusive  $\text{CO}_2$  (molar concentration,  $C_{a2}$ ; diffusion coefficient,  $D_{a2}$  in concrete) feels the mass transfer resistance at the surface of concrete (surface mass transfer coefficient,  $K_{ag}$ ), unless the equilibrium  $C_{a2} = mC_{a1}$  is satisfied ( $k_{ag} \rightarrow +\infty$ ). The retardation effects of finishes on the diffusion of  $\text{CO}_2$  (thickness,  $L$ ; diffusion coefficient,  $D$  in a finish) are incorporated into the



total mass transfer coefficient ( $K_{ag}$ ) defined as follows:

$$1/k_{ag} = 1/k_{ag} + L/D \quad (9)$$

(3)  $\text{Ca}(\text{OH})_2$  diffuses slowly backwards (molar concentration,  $C_{b2}$ ; diffusion coefficient,  $D_{b2}$  in concrete) from the inner layer of concrete, and converts instantaneously into  $\text{CaCO}_3$  with  $\text{CO}_2$  which diffuses forwards from the surface.

Based upon the above assumptions, fundamental differential equations are obtained. Laplace transformation method was also used to solve the simultaneous differential equations under the given initial and boundary conditions. Analytical solutions are obtained in the form of dimensionless concentrations which involve error functions concerning time and the depth from the surface. For the progress of neutralization, the parabolic law involving constant terms was derived as follows ( $X$ , neutralization depth of concrete):

$$X = k_e \sqrt{t} - l \quad (10)$$

$$k_e = m \sqrt{D_{a1}/D_{a2}} \{ (C_{ag}/2C_{b0}) - D_{b2}/D_{a1} \} \quad (11)$$

$$l = D_{a2}/k_{ag} \quad (12)$$

### Experimental

SEM Observation of Masonry Coating Materials. For samples of the masonry coating materials listed in Table I., the surface morphological changes due to outdoor exposure and sunshine carbon arc irradiation were investigated by scanning electron microscopy (SEM) by Hitachi Model S-450 after metallizing with platinum by sputter coating. The cross sections of the specimens were exposed by fracture after freezing in liquid nitrogen.

Masonry coating materials, which are the mixture of organic polymer, filler and fine aggregates, often applied some 0.3 to 15mm thick by spraying or rolling on the various types of external surface such as concrete, cement mortar, asbestos cement sheets and other boards, are objects in this investigation.

The coated layers of masonry coating materials (excluding substrates) were exposed on the acrylic resin sheet mounted on the exposure racks at an angle of  $30^\circ$  facing south in the Building Research Institute for one year. Sunshine carbon arc acceleration test based on JIS A 1415 (black panel temperature  $63 \pm 3^\circ\text{C}$ , ion-exchanged water spray 18 minutes in every two hours) was conducted using specimens of the same samples used in the outdoor exposure test above up to 1000 hours (5).

Results. Examples of the SEM micrographs obtained are shown in Figures 1 to 8. It can be found that the surface morphology of the outdoor exposed specimens is evidently different from that of specimens exposed to sunshine carbon arc irradiation in the laboratory.

surface of the specimens exposed outdoor is uniformly weathered (Figure 1). On the contrary, the surface of the specimens exposed to the accelerated aging test is not uniformly deteriorated depending upon the surface textures, but shows further the deterioration in concave parts probably due to longer remaining of sprayed water (Figure 2).

The difference in the surface morphology of masonry coating ma-

Table I. Description of Masonry Coating Materials

type of specimen	average thickness (mm)
A under coat (acrylic rubber emulsion) + top coat	1.5
B single layer (acrylic resin emulsion)	1.4
C single layer (acrylic resin emulsion)	1.5
D under coat (acrylic resin emulsion) + top coat	1.6
E under coat (acrylic resin emulsion) + top coat	1.6

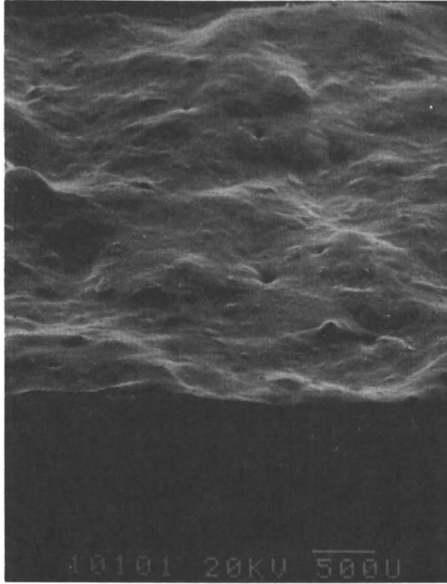


Figure 1. Micrograph of A in Table I. outdoor exposure; 1 year, magnification bar; 500 $\mu$ .

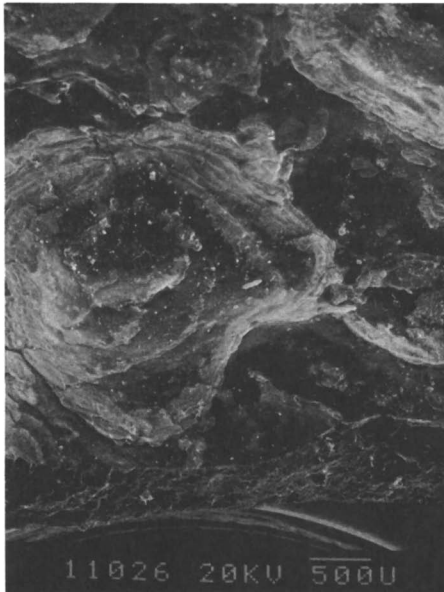


Figure 2. Micrograph of A in Table I. acceleration test; 1,000 hrs., magnification bar; 500 $\mu$ .

materials is more clearly observed in micrographs at rather high magnification. The surface organic polymer exposed outdoors might be gradually degraded and inorganic filler in the coated layers became explicitly observable (Figures 3 to 5). The degree of this deterioration, namely chalking behaviour, differs depending upon types of organic polymer, and reasonably corresponds to the result of practical chalking test based on JIS K 5516. On the other hand, microcracks (Figures 6 and 7) and microflaking (Figure 8) can be observed on the surface of every specimen after the acceleration test.

### Discussion

Degradation of Polymers. From the results of dynamic analysis, the degree of the deterioration of polymers varies with time and the depth from the surface, and is influenced by the photochemical reaction constants ( $k_1$ ,  $k_2$ ) and diffusion coefficient ( $D_A$ ). Figure 9 shows the theoretical result of the influence of photo-oxidation on the distribution of oxygen in polymers. Deriving the time dependence of surface deterioration, we obtain equation 13.

$$\phi_B(0,t) = C_B(x,t)/C_0^* \approx k_1 \sqrt{t} (C_{A0}/C_0^*) = k_1 C_{A0} \sqrt{t} \quad (13)$$

This shows that the surface deterioration advances approximately in proportion to exposure time, and that the progress of deterioration depends upon the surface oxygen concentration and the rate constant of photo-oxidation, though it depends, of course, linearly on the intensity of incident light. The surface deterioration can be observed in IR absorption spectra and in the morphological change in SEM, and further in the change of material properties.

Watanabe et al. (4) have measured IR absorption spectra of sliced samples of outdoor exposed plates of polystyrene (PS) and other polymers. Their experimental data are shown in Figure 10. The absorption near  $1730 \text{ cm}^{-1}$ , due to the carbonyl functional group, is seen to increase in intensity with time. This may show that the photo-oxidation proceeds rather in the surface layers of polymers.

Figures 1 to 8 show the morphological change of masonry coating materials under outdoor and accelerated aging exposure. For outdoor-exposed samples, it was observed that acrylic rubber emulsion type polymer is gradually lost and that filler becomes explicitly disclosed after one-year exposure (chalking phenomena) (Figures 1, 4 and 5). For accelerated-aged samples, however, the flaking was observed. The difference in the surface morphology between the outdoor exposure test and laboratory test can be due to many complex factors which have not been completely revealed.

On the basis of unsteady state dynamics, the degree of the surface deterioration of polymers becomes heavier in linear proportion as the irradiation level of incident light becomes higher, but the progress of deterioration inwards from the surface depends mainly upon the diffusion of oxygen (or water). In the case of accelerated-aged samples under rather strong and short-term irradiation by sunshine carbon arc in the laboratory, the surface of polymers becomes strongly deteriorated as the result of rapid photochemical reactions. However, the deterioration of polymers is considered not to extend to the deep inner layers. On the other hand, for outdoor-exposed samples under rather mild and long-term irradiation

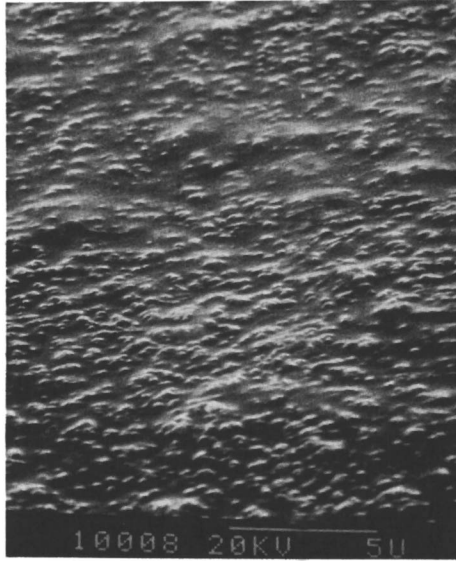


Figure 3. Micrograph of A in Table I. initial specimen, magnification bar;  $5\mu$ .

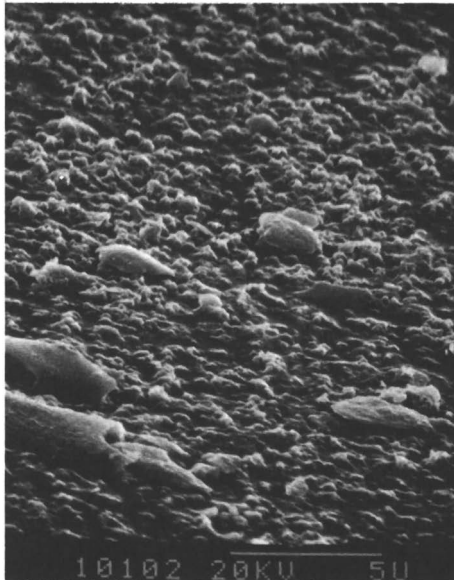


Figure 4. Micrograph of A in Table I. outdoor exposure; 1 year, magnification bar;  $5\mu$ .

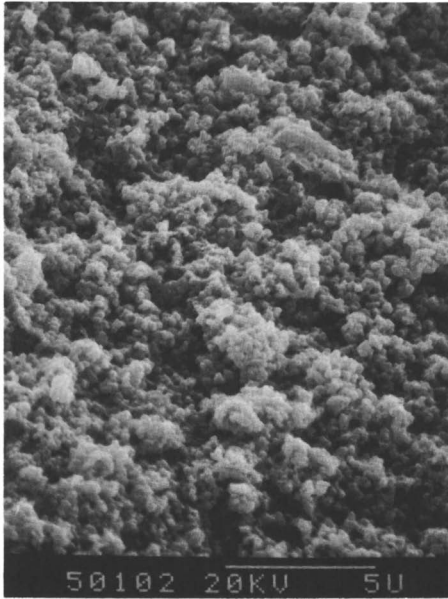


Figure 5. Micrograph of E in Table I. outdoor exposure; 1 year, magnification bar;  $5\mu$ .



Figure 6. Micrograph of B in Table I. acceleration test; 700 hrs., magnification bar;  $5\mu$ .

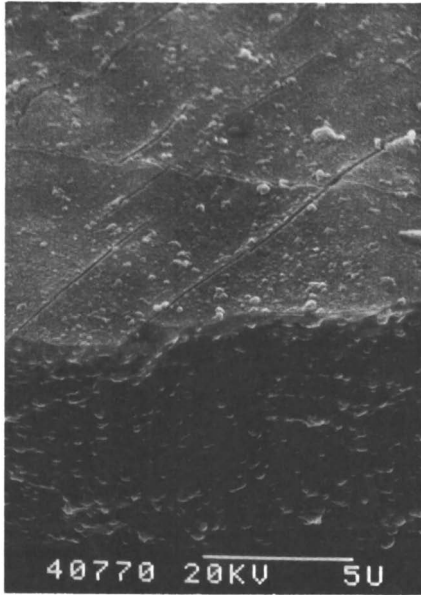


Figure 7. Micrograph of D in Table I. acceleration test; 700 hrs., magnification bar;  $5\mu$ .

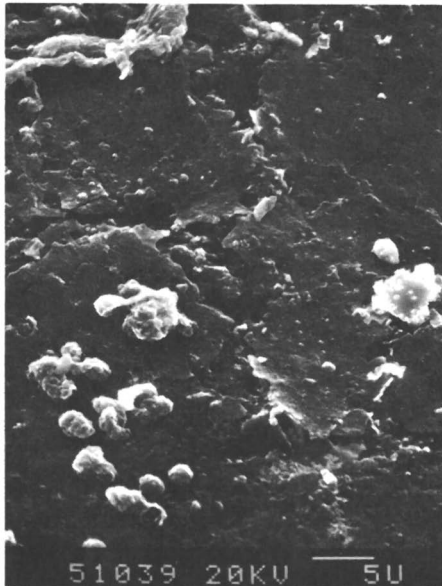


Figure 8. Micrograph of E in Table I. acceleration test; 1000 hrs., magnification bar;  $5\mu$ .

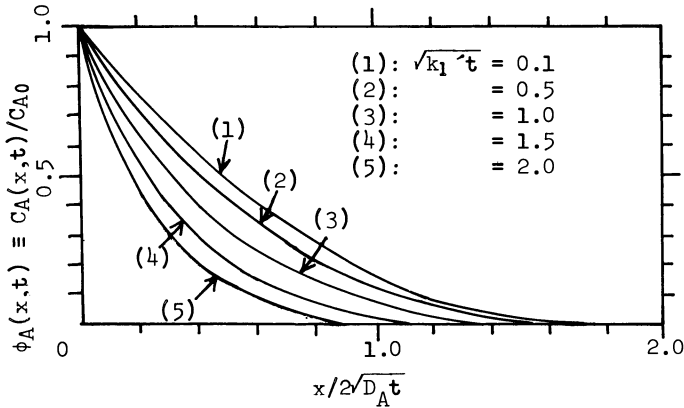


Figure 9 Influence of photo-oxidation on the distribution of oxygen in polymeric materials (result of theoretical calculation).

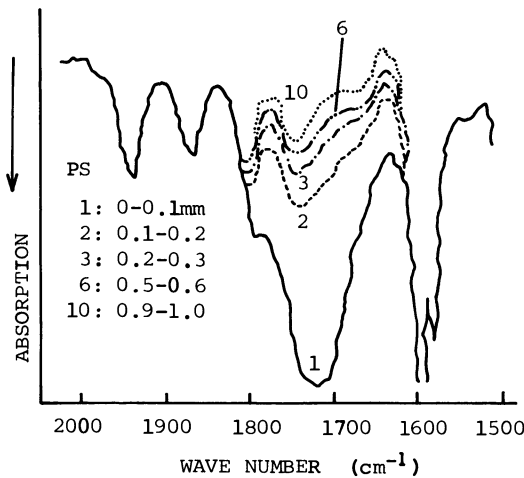


Figure 10. Change of infrared absorption with distance below the surface of polystyrene (PS) polymer exposed outdoors (at Chosi) for three years (Reproduced with permission from Ref. XI Copyright 1979, Japan Ind. Tech. Assoc.).



by natural sun-light, the surface deterioration is considered to be not so strong, and the deterioration is mainly ruled by the diffusion. The deterioration is considered to proceed slowly but deeper into the inner layers. This conceptual diagram is illustrated in Figure 11, which seems to be one of the reasons why the different morphology was caused on the surface layers.

The depth of the deteriorated layer was to be a few microns at most for both specimens exposed outdoors for one year and those exposed to sunshine carbon arc irradiation for 1000 hours by observing their cross sections. Of course, the depth is only based on the morphological changes; therefore, molecular structure changes, such as formation of carbonyl functional groups, cross-linking reaction, rupture of molecular chains etc. are supposed to be directly invisible.

The deterioration progresses continuously from the surface, and the depth of the deteriorated layer increases in proportion to the square root of exposure time as shown in equations 7. and 8. This parabolic ( $\sqrt{t}$ ) law was obtained as the natural derivation based upon unsteady state dynamics, assuming the simultaneous action of UV-light and diffusive oxygen. Figure 12 is the least-square plot based on experimental data from Kubota et al. (5). It can be seen that many polymers show the deterioration by the power law of exposure time ( $t^n$ ;  $n = 0.5 - 1.0$ ). The difference between theory and experiment is considered to be due to the complex mechanisms not explicitly treated in this theory.

Retardation Effects of Polymeric Finishes on Carbonation. The retardation effects of polymeric finishes can be well explained, using equations 9. and 12., where  $l$  is the constant term which includes total surface mass transfer constant, and describes the retardation of carbonation or induction period before the carbonation begins to proceed. From equation 9. it can be seen that the effects depend on the thickness and diffusion coefficients of finishes (Figure 13).

If the functional thickness of finish decreases, or the diffusion-resistance of finish reduces by the deterioration processes, it is considered that the protective function of polymeric finishes against the carbonation of concrete gradually degrades. After a given long time the neutralization depth is seen to be reduced in proportion to the thickness of a given finishing material. Though these retardation effects have not been, so far, well established, Figure 14 shows the retardation effects of inorganic finishes in the field research for indoor vertical walls in an existing reinforced building aged 17 ( $X_0$  indicates the neutralization depth of concrete without finishes). The results represent the evidence for the considerations described above, and the importance of the thickness as well as the permeability of finishes in the retardation of carbonation.

### Conclusions

The photochemical deterioration processes of polymeric materials often used as paints and finishes are studied both theoretically and experimentally. Theoretical models for the deterioration processes are developed based upon unsteady state dynamics. The results were compared with experimental data under outdoor and accelerated aging

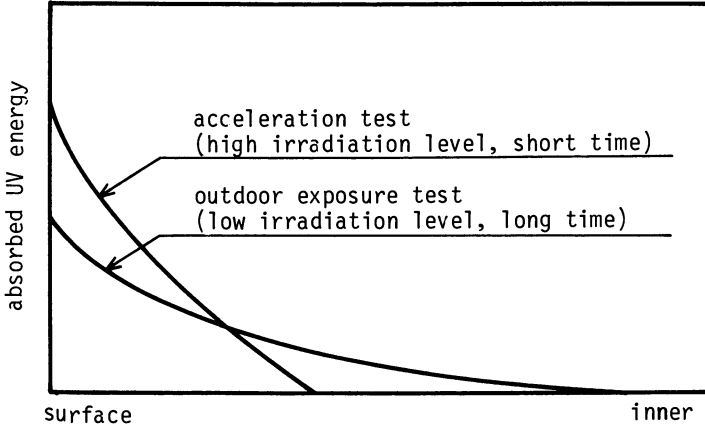


Figure 11. Schematic model of absorbed UV energy distribution in thickness for the outdoor exposure test and the sunshine carbon arcs type acceleration test.

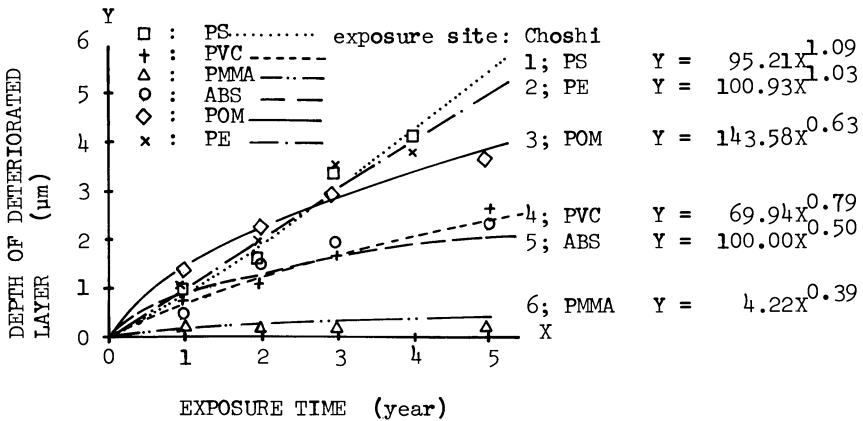


Figure 12. Least-squares plot using the power law for the depth of the deteriorated layer of various polymers after various periods of outdoor exposure (at Choshi). Experimental data are from Kubota et al. Ref. 12.

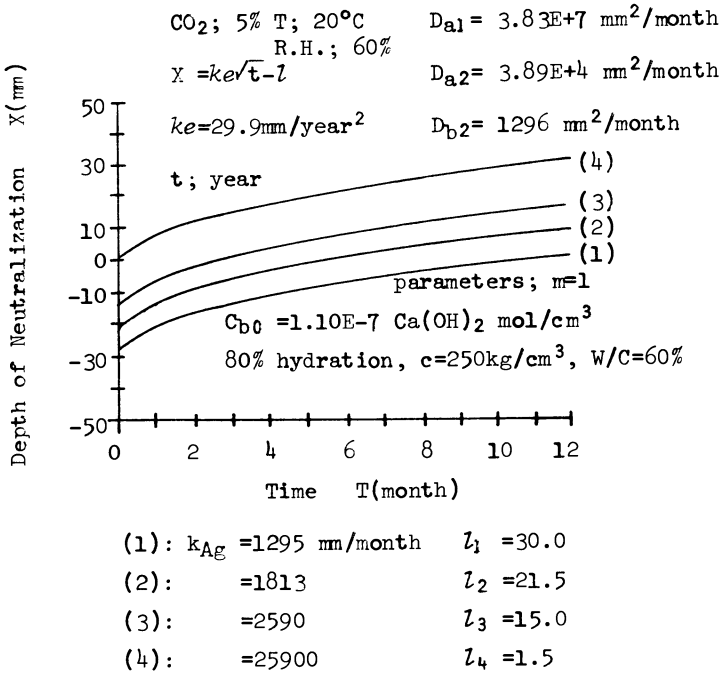


Figure 13. Influence of the surface mass transfer resistance on the progress of carbonation under accelerated condition.

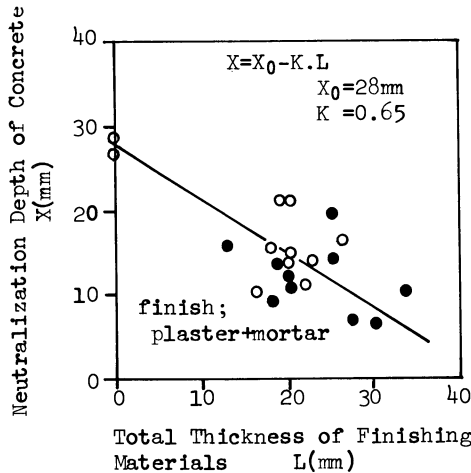


Figure 14. Relationship between the carbonation (neutralization) depth of indoor concrete and the total thickness of finishes (Result of field Research for external vertical walls in an existing reinforced concrete aged 17).

exposures. Infrared spectra and scanning electron micrographs show that the deterioration proceeds continuously inwards from the surface of polymeric materials, but the behaviour of deterioration are different with the exposed conditions. Parabolic ( $\sqrt{t}$ ) law was derived approximately for the increase in the depth of the deteriorated layer with time.

Paying attention to the influence of the deterioration of polymeric finishes, the parabolic law involving a constant term was also derived for the progress of carbonation of concrete. These parabolic laws combined predict the progress of the deterioration under natural weathering and explain well the protective performance of finishing materials on reinforced concrete.

#### Acknowledgments

The authors would like to express thanks to Mr. T. Nireki, Head of the Durability Division, and Dr. F. Tomosawa, Head of the Inorganic Materials Division, Materials Department of the Building Research Institute for their kind discussions. Thanks are expressed to Dr. H. Kubota and their co-workers for their supplying valuable experimental data in considering the deterioration from the surface of polymeric materials. They would like to express thanks also to editors of the literature cited here for their kind permissions for the copyright transfer in order for them to use the part of the figures and articles to constitute this paper.

#### Literature Cited

1. Fukushima, T. Durability of Building Materials 1983, 1. 327-343
2. Fukushima, T.; Kawase, K.; Tomosawa, F.; Akashi, H. Proc. Annual Symp. Archit. Inst. Japan, Tokyo, 1982, p. 253 (in Japanese).
3. Fukushima, T. Proc. Annual Symp. Archit. Inst. Japan, Hokuriku, 1983, p. 199 (in Japanese).
4. Fukushima, T. Proc. 27th Japan Cong. Materials Res., Kyoto, Japan Sept. 1983, p.225
5. Motohashi, K.; Nireki, T. Proc. 3rd Internat. Conf. Durability of Building Materials and Components, Espoo, Finland, Aug. 1984
6. Watanabe, Y.; Kitajima, F.; Hattori, S. Proc. 15th Symp. Polymer Res. Works Japan Ind. Tech. Assoc., Tokyo, 1979, p. 177 (in Japanese).
7. Kubota, H.; Suzuki, S.; Nishihara, O.; Yoshikawa, K; Shiota, T. inbid, p. 147 (in Japanese).

RECEIVED January 23, 1985

## Effect of the Degree of Crystallinity on Friction and Wear of Poly(ethylene terephthalate)

Yoshinori Yamada and Kyuichiro Tanaka

Department of Precision Engineering, Faculty of Engineering, Kanazawa University, Kanazawa 920, Japan

Measurements of friction and wear were made on poly(ethylene-terephthalate) (PET) sliding against a smooth steel disk. The friction was little dependent upon crystallinity, while the wear rate increased with increase in crystallinity, especially remarkable in the range above about 40%. It was found that the reciprocal of wear rate was closely related to the Vickers hardness in PET of different crystallinity. The wear of PET with a low crystallinity as small as 8% was mainly due to transfer. On the other hand, wear of high crystallinity PET is different from that of the low crystallinity PET and seemed to be mainly due to a surface fatigue during sliding. The difference between the mechanisms in PET of low and high crystallinity was essentially due to the difference in morphological structures.

It is well known that the morphological and molecular structures of polymers play an important role in their wear behavior. It seems that the degree of crystallinity is also a structural factor of semi-crystalline polymers important to their wear. Lontz et al. (1) reported that the wear of poly(tetrafluoroethylene), (PTFE) decreased with the increase in crystallinity. Tanaka et al. (2) studied the wear of heat-treated PTFE specimens and concluded that the wear rate was affected by the width of the band in the fine structure rather than crystallinity. Recently, Hu et al. (3) have studied the effect of crystallinity on wear of PTFE using various heat-treated specimens. They have shown that the wear decreases with the increase in crystallinity, when molecular weight is constant. Eiss et al. (4) reported that poly(chlorotrifluoroethylene) of a crystallinity of 65% exhibited higher wear than that of 45%. The results obtained by the authors mentioned above indicate that the effect of crystallinity on the wear of polymers is somewhat complicated and further investigation is needed to clarify the effect of crystallinity on polymer wear.

It is known that poly(ethylene-terephthalate), (PET) has a peculiar property that its crystallinity varies in a very wide range

after heat treatment. In the present work, therefore, the effect of crystallinity on friction and wear of PET sliding against a smooth steel surface at a relatively low speed was studied within a crystallinity range of 8% to 75%. In addition, the friction experiment using a steel sphere sliding on a flat PET surface was also carried out at a low speed under various load in order to study the fundamental frictional properties of the PET specimens with various crystallinity.

### Experimental

#### Procedures for Studying the Fundamental Frictional Properties of PET

To study the fundamental frictional properties of PET specimens of various crystallinity, a steel sphere of 2.38 mm in radius was slid on the PET specimens mounted on the glass plate at a speed of 0.25 mm/s under loads in a range from 0.5 to 8.0 N. After a constant load was applied for 30 seconds, sliding was started and the frictional force was measured using strain gauges attached to the spring plates, where the steel sphere was mounted at one end, while the other end was connected to the steel arm supported by a ball bearing. A steel ball for ball bearing was used as the steel sphere in the experiments. The PET specimen surfaces were abraded with 1500-grade abrasive cloth in water and made as clean as possible using ethylalcohol.

Wear-Testing Apparatus and Experimental Procedure. To study the effect of crystallinity on wear of PET specimens with different degrees of crystallinity, the pin-on-disk type wear-testing apparatus used in our previous work (5) was again employed. With this apparatus, measurements of frictional force and wear depth can be made continuously during the wear process. When the wear-testing apparatus was used, experiments were carried out at a sliding speed 0.1 m/s under a load 10 N. The PET specimens of 3 mm in diameter were bonded on the flat ends of polypropylene pins of the same diameter in order to mount the specimens to the pin holder and were rubbed against the disks made of a stainless steel (SUS 304). Finally, the frictional surface of the disk was abraded with a 1500-grade waterproof abrasive cloth in water and it had about 0.02 m c.l.a. roughness. The diameter of the frictional tracks on the disks was 5 cm. After the specimen was mounted to the holder, the specimen was initially rubbed against a 6/0 grade Emery paper placed on the disk. This pre-rubbing was useful for allowing a uniform contact between the specimen surface and the disk. After the pre-rubbing, the specimen and disk surfaces were made as clean as possible by rubbing with a soft cloth wetted with ethylalcohol. All experiments in this work were carried out in the room air of  $20 \pm 2$  C and of  $55 \pm 10$  % relative humidity.

PET Specimen. The PET plate of 2-mm thick and of very low crystallinity was supplied by the Teijin Ltd.. By annealing the plate, the PET specimens of two different crystallinity ( 39 % and 55 % ) were obtained. On the other hand, the PET film of very high crystallinity ( 75 % ) was also used as the specimen which was obtained by annealing a film of 0.5-mm thick and of 60 % crystallinity. The original film was produced by Toray Industries, Inc. The crystallinity of

specimens was determined by measuring their density and using the values of  $1.328 \text{ g/cm}^3$  and  $1.450 \text{ g/cm}^3$  as the values of the density of amorphous and crystalline phases, respectively. The crystallinity, density and annealing condition for the specimens are listed Table I.

Table I. Condition of Annealing and Crystallinity

Specimen	Condition of Annealing	Density ( $\text{g/m}^3$ )	Degree of Crystallinity (%)
1-0	none	1.337	8
1-L	Original, 1-0, Annealed; 120 C, 20 min	1.373	39
1-H	Original, 1-0, Annealed; 210 C, 60 min	1.392	55
2-H	Original, Density 1.399, D.C. 60 % Annealed; 200 C, 90 min	1.417	75

**Morphology of the Specimens.** In order to examine the morphology of specimens, the sections perpendicular to the surfaces used as the frictional surface were cut from the plate and film specimens and were observed by a polarizing microscope with crossed-Polaroid. Figures 1(a) and (b) show the polarizing micrographs of the sections of various specimens at a certain position under a polarizing microscope and those at the position turned 45 degrees from the micrograph (a), respectively. The structure of the specimen 1-0 is almost amorphous and very different from that of the other specimens, because any morphological structure cannot be observed in the micrographs of the specimen 1-0. The bright bands seen in the micrograph of the specimen 1-0 must be due to the local drawing during the sectioning process. The specimen 1-H has a spherulite structure and the spherulites are very small. With the specimen 1-L; however, the micrograph in Figure 1 (a) shows a maze-like pattern and that in Figure 1 (b) shows a mesh-like pattern. Thus, the specimen 1-L may have a structure somewhat different from the spherulite structure of the other semicrystalline polymers such as polyethylene and nylon. On the other hand, micrograph (b) of the specimen 2-H shows a fiber-like pattern and this may be due to a strong drawing during a fabrication process of the film.

### Experimental Results and Discussion

**Sliding of the Steel Sphere on Flat PET Surfaces.** Figure 2 shows typical friction traces in the sliding of a steel sphere at a speed  $0.25 \text{ mm/s}$  under a load  $8 \text{ N}$ . It is seen that the static friction is considerably higher than the kinetic friction and there is no stick-slip phenomenon. Comparing the friction of PET with that of other polymers obtained in the sliding experiment (6) similar to that in the present work, it was found that PET exhibited relatively lower

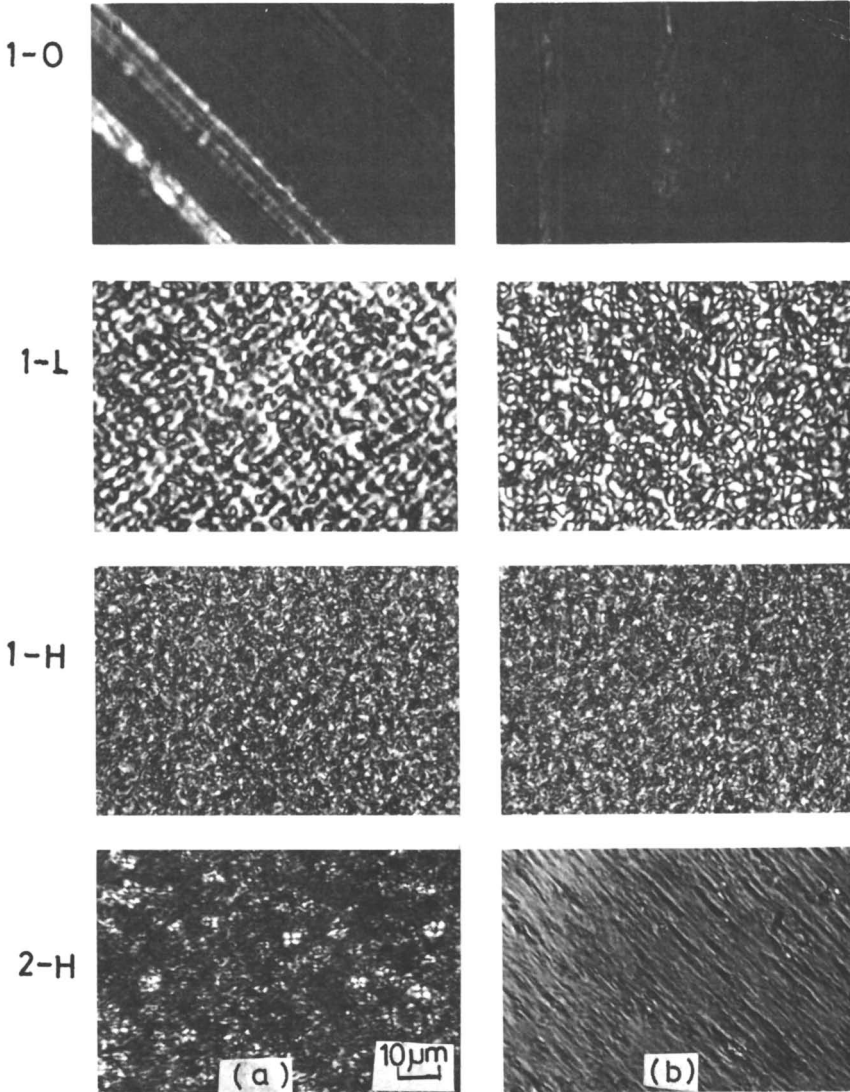


Figure 1. Polarizing micrographs of the sections of various PET specimens. The sections in the micrograph (b) are turned 45 degrees from the position in the micrograph (a).



friction. The coefficient of static friction,  $\mu_s$  obtained from the friction traces measured under various loads. As shown in Figure 3,  $\mu_s$  decreases with the increase in load and is represented by the relation  $\mu_s \propto W^{-n}$ , where  $W$  is the load. The index  $n$  was estimated to be respectively 0.14, 0.12, 0.14 and 0.25 for specimens 2-H, 1-H, 1-L and 1-O. The difference of kinetic friction,  $\mu_k$  was also proportional to  $W^{-n}$  and the index  $n$  was estimated to be in the range 0.10 to 0.16. The values obtained show that the deformation at the contact is partially elastic in the load range studied, because the index  $n$  should be 1/3 and 0 for perfectly elastic and plastic deformations respectively. Figure 4 shows the dependence of the width of frictional track,  $d$  on the load  $W$ . the width of frictional track was measured after sliding experiments. The values measured,  $d$  may be underestimated, because of the recovery of elastic deformation at the contact. It is seen that  $d$  is proportional to  $d^m$  in the load range studied. However, the data for low crystallinity specimen 1-L showed some disagreement with the line drawn in Figure 4. The data for the specimen 1-O were not included in Figure 4, because it was difficult to observe the frictional track clearly. As shown in Figure 4, the index  $m$  was estimated to be 2.4 for all PET specimens. According to the approach by Tabor (7) the coefficient of friction should be proportional to  $W^{2/m-1}$ , assuming that the friction force is due to the shearing of adhesive junction at the contact and that the true area of contact is given by  $\pi d^2/4$ . If the value, 2.4 estimated above are used, it should be expected that  $\mu$  is proportional to  $W^{-0.17}$ . The value of 0.17 calculated from the frictional track is in relatively good agreement with the index  $n$  measured. Moreover, shear strength for various PET specimens is calculated to be approximately 15 MN/cm<sup>2</sup>. Figure 5 shows the relationship between the coefficients of friction measured at a load 8 N and crystallinity. It was found that the coefficients of static and kinetic friction are little dependent upon crystallinity.

Friction of PET Pins Sliding Against Stainless Steel Disk. Figure 6 shows the variations with sliding distance in the coefficient of friction and wear depth of various specimens rubbing against stainless steel disk. It was found that the steady state of friction appeared after the sliding distance reached several kilometers. Friction of the initial stage of sliding is generally somewhat higher than that during steady state of sliding. The coefficient of friction as described in the following was obtained during the steady state of friction. The coefficient of friction is plotted against the crystallinity in Figure 7. It seems that friction is little dependent upon crystallinity, although it tends to take a minimum value at a certain crystallinity. It is noted that PET exhibits much lower friction than nylon and polyacetal under similar sliding condition (5). The magnitude of the coefficient of friction and its dependence upon crystallinity shown in Figure 7 are different from those observed in the case of the sliding of a steel sphere. This must be due to the difference in experimental conditions.

Wear of PET Pins Sliding Against Stainless Steel Disk. In Figure 6, it is seen that the steady state of wear following a transient state generally appears. The specific wear rate,  $K$  for various PET

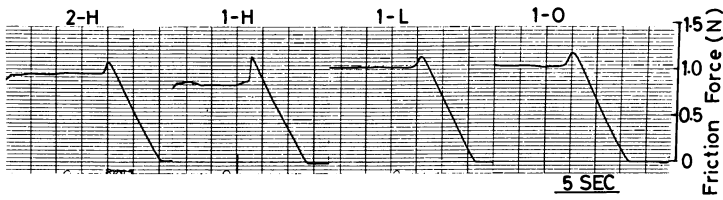


Figure 2. Typical friction traces in the sliding of a steel sphere on various PET specimens.

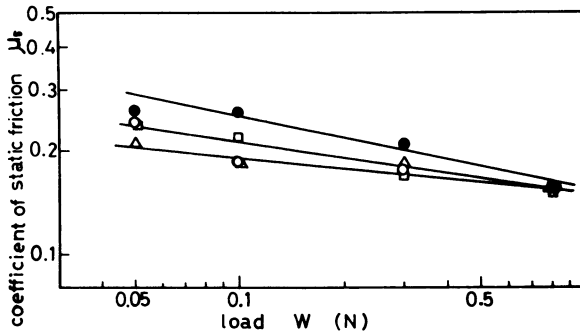


Figure 3. Variations of coefficient of static friction,  $\mu_s$  in the sliding of steel sphere with load: ●, 1-0; ○, 1-L; △, 1-H; □, 2-H.

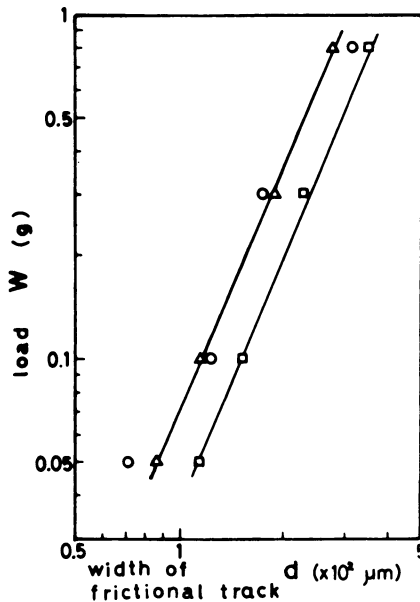


Figure 4. Relation between the width of frictional track and load : ○, 1-L; △, 1-H; □, 2-H.

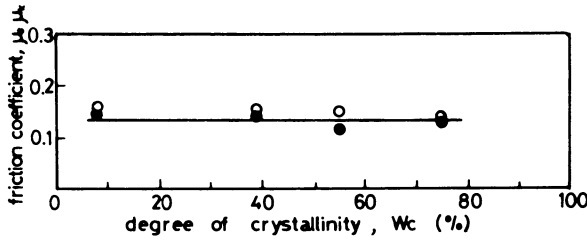


Figure 5. Relation between the coefficient of static and kinetic friction,  $\mu_s$  and  $\mu_k$  in the sliding of steel sphere and crystallinity: ○,  $\mu_s$ ; ●,  $\mu_k$ .

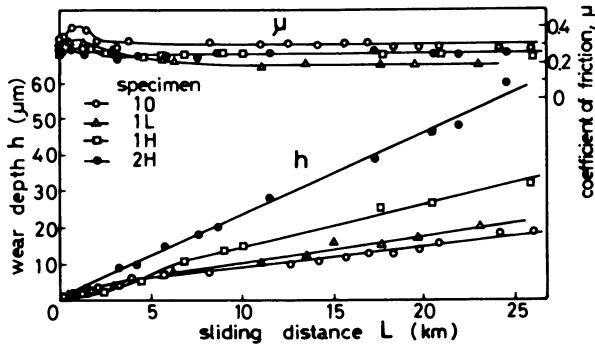


Figure 6. Variations with sliding distance in the coefficient of friction  $\mu$  and wear depth  $h$  of various PET specimens sliding against stainless steel disk: ○, 1-0; △, 1-L; □, 1-H; ●, 2-H.

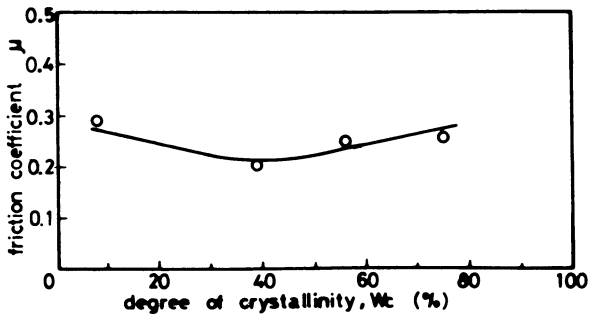


Figure 7. Relation between the coefficient of friction  $\mu$  of PET specimens sliding against stainless steel disk and crystallinity.

specimens was obtained during the steady state of wear and is plotted against crystallinity  $W_c$  in Figure 8 (a) and (b), where normal and logarithmic scales are used in the Figure (a) and (b), respectively. It is seen that the wear rate of PET increases with the increase in crystallinity, especially remarkable in the crystallinity range above about 40%. The fact that the relationship between  $\log K$  and  $\log W_c$  is represented by a steep straight line for higher crystallinity range suggests that the predominant mechanism in the wear of the higher crystallinity PET is very different from that of the low crystallinity PET. It is also noted that the specific wear rate of PET is generally much lower than those of nylon and polyacetal (5). It was found that there is a good correlation between the reciprocal of specific wear rate  $1/K$  and Vickers hardness  $H$ . The Vickers hardness, which was measured under the condition of 1.0 N load and a loading time of 20 s, increased with the increase in crystallinity. The reciprocal will be called the wear resistance. Figure 9 shows the relationship between the wear resistance and Vickers hardness. Considering that the definite relationship between wear resistance and hardness for wear of polymers, it should be remarkable that the wear resistance decreases with the increase in hardness.

#### Optical and Electronmicroscopic Examinations of Frictional Surfaces.

In order to obtain the information on the wear mechanism, microscopic observations of the frictional tracks and worn surfaces of pins were made by optical and electron microscopes. It was found that the specimen of the lowest crystallinity was much smaller than those in the specimens of higher crystallinity. Figures 10(a) and (b) show the optical micrographs of the wear particles of the specimen 1-0 and of the specimen 1-L, respectively. It appears that the increase in crystallinity by a factor of about 5 causes the size of wear particles to increase by a factor of 5 or more. Figures 11(a) and (b) show the optical micrographs of worn surfaces of the specimen 1-0 and 1-L, respectively. With the specimen 1-0, many scratches parallel to the sliding direction can be seen on the worn surface and the feature of the worn surfaces is somewhat similar to that of other semicrystalline polymers rubbing against smooth steel surface (8). On the other hand, the feature of worn surface of the specimen 1-L is relatively rough and very different from that of the specimen 1-0.

The friction tracks on the disks and the worn surfaces of pins were observed by means of a transmission electron microscope (TEM). Figure 12 (a) and (b) show TEM micrographs of the worn surface of specimen 1-0 and 1-H, respectively. There are many long striations parallel to the sliding direction on the worn surface of the specimen 1-0 and the feature is also similar to that of other semicrystalline polymers rubbed against smooth steel surface (5). On the other hand, in the case of specimen 1-H, the pitted feature surrounded by a boundary shown in the micrograph Figure 12(b) were frequently observed on the worn surface. The feature shown in Figure 12(b) seems to be caused by the separation of flake-like wear debris from the frictional surface. Figures 13(a), (b) and (c) show TEM micrographs of frictional track on the disks rubbing against the specimens 1-0, 1-H, and 2-H, respectively. It is seen that with the specimen 1-0, relatively coherent transferred film is produced on the disk. The feature of the transferred film is very similar to that of the other

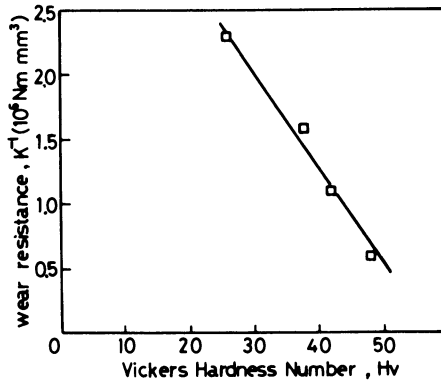


Figure 8. Variation of specific wear rate  $K$  of PET specimens with crystallinity.

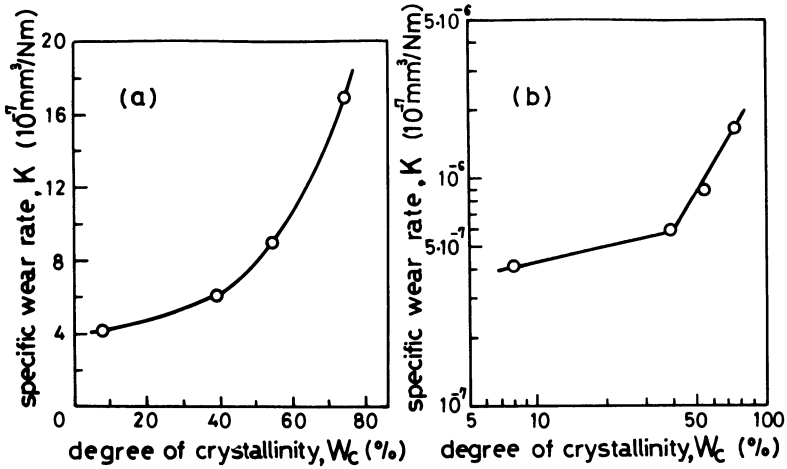


Figure 9. Variation of wear resistance  $1/K$  of PET specimens with Vickers hardness  $H_V$ .

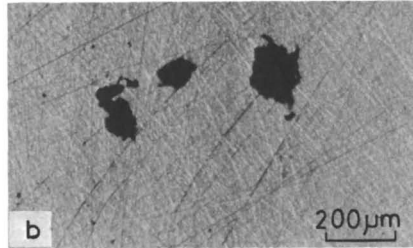
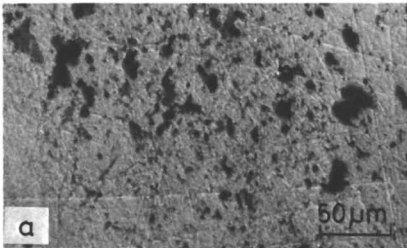


Figure 10. Optical micrographs of wear particles : (a), 1-0; (b), 1-L.

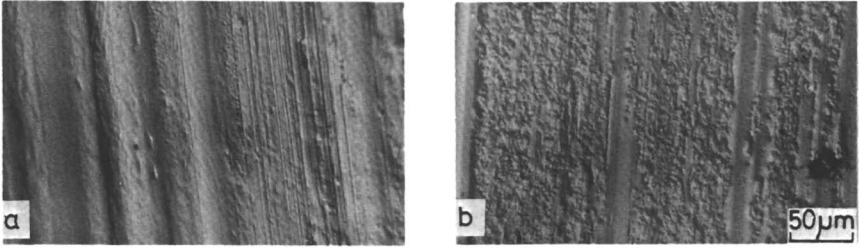


Figure 11. Optical micrographs of the worn surfaces : (a),1-0;  
(b),1-H .

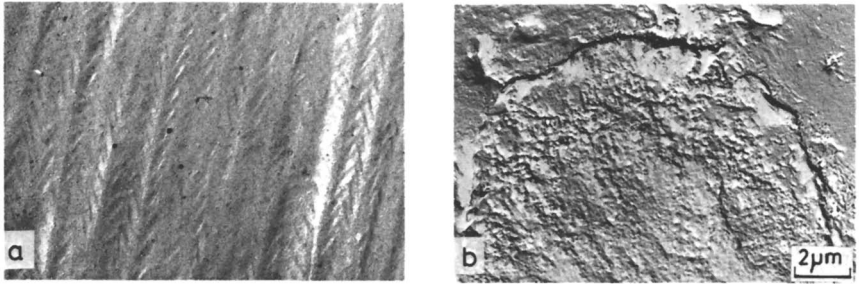


Figure 12. Electron micrographs of the worn surfaces : (a),1-0;  
(b), 1-H .

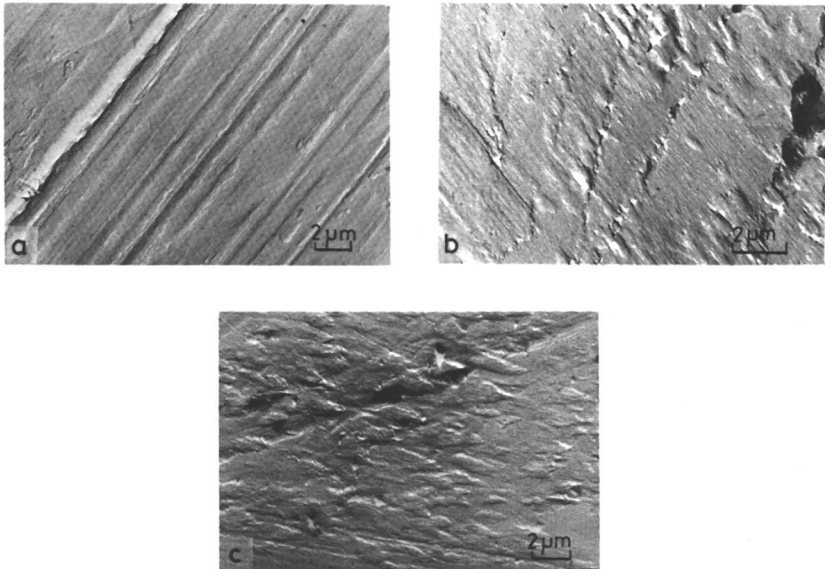


Figure 13. Electron micrographs of frictional tackscrubbing against  
PET specimens: (a) ,1-0; (b),1-H; (c),2-H .

semicrystalline polymers (9). On the other hand, the surfaces of the transferred materials are very irregularly rough in the case of the specimens of higher crystallinity and seems to be the roughest in the case of the specimen with highest crystallinity, 2-H.

The differences of the surface features of frictional tracks and worn surfaces between the lowest and higher crystallinity specimens, which were observed by optical and electron microscopes suggest that the predominant wear mechanism in the specimens of the lowest crystallinity is very different from that in those of higher crystallinity. On the basis of microscopic observations, we believe that the wear mechanism of the lowest and higher crystallinity specimens may be considered as follows: in the case of the specimen 1-0, the wear may be mainly due to the transfer which is the predominant wear mechanism in other semicrystalline polymers sliding against a smooth steel surfaces (8,9). On the other hand, in the case of PET of higher crystallinity, the wear seems to be predominantly caused by the fatigue of the surface layer during sliding. As described above, the morphological structure of the specimens is different one another. However, the wear mechanism in three specimens of higher crystallinity is similar as seen in crystallinity dependence of their wear rate shown in Figure 9 (b) and in the microscopic observations of the worn surfaces and frictional tracks. Therefore, the difference in the morphological structures of three specimens of higher crystallinity seems not to play an important role in the wear mechanism

### Conclusions

In order to study the effect of the degree of crystallinity on friction and wear of PET, the friction measurements in which the steel sphere was slid on flat PET surfaces were carried out. Measurements of the friction and wear rate were also made on the PET pins sliding against a smooth steel surface at a speed 0.1 m/s under a load 10 N by means of a pin-on-disk type apparatus. The PET specimens of four different crystallinity (8, 39, 55 and 75 %) were used in the present work. The specimen of the lowest crystallinity had a structure similar to an amorphous polymer, while two specimens of crystallinity, 39 % and 55 % had a spherulite-like structure. The highest crystallinity had a fiber-like structure. Conclusions obtained are as follows:

- (1) The friction was little dependent upon crystallinity.
- (2) The wear rate increased with the increase in crystallinity and especially remarkable in the crystallinity range above about 40%.
- (3) The relationship between the reciprocal of specific wear rate and Vickers hardness for various PET specimens was expressed by a straight line and the reciprocal decreased with the increase in hardness.
- (4) The wear in PET of low crystallinity as small as 8 % was mainly due to transfer of PET to the counterface, while the wear of PET with higher crystallinity is different from that of PET with the lowest crystallinity and seemed to be mainly caused by fatigue during sliding.
- (5) The difference in wear mechanisms for PET specimens of the lowest and higher crystallinity is essentially due to the difference in morphological structures.

Acknowledgments

The authors thank Mr. Ueda S. for his assistance throughout this work.

Literature Cited

1. Lontz, L.F.; Kumnick, M.C. ASME Trans. 1963, 6, 276.
2. Tanaka, K.; Uchiyama, Y.; Toyooka, S. Wear 1973, 23, 153.
3. Hu, T.Y.; Eiss, N.S., Jr. In "Wear of Materials-1983"; Ludema, K. C., Ed.; ASME: New York, 1983, p. 636.
4. Eiss, N.S., Jr.; Warren, J.H. In "The Wear of Non-Metallic Materials"; Dowson, D.; Godet, M.; Taylor, C.M., Ed.; Mechanical Engineering Publications Ltd. : Leeds, 1978, p. 18.
5. Tanaka, K.; Uchiyama, Y. In "Advances in Polymer Friction and Wear"; Lee, L.H., Ed.; Plenum Publishing Corp.: New York, 1974, p. 499.
6. Tanaka, K. J. Phys. Soc. Jpn. 1961, 6, 2003.
7. Tabor D. "The Friction and Lubrication of Solids"; Oxford University Press: London, 1964, p. 214.
8. Tanaka, K.; Yamada, Y. In "Wear of Materials-1983"; Ludema, K.C., Ed.; ASME: New York, 1983, p. 617.
9. Tanaka, K. In "Wear of Materials-1981"; Rhee, S.K.; Ruff, A.W.; Ludema, K.C., Ed.; ASME: New York, 1981, p. 98.

RECEIVED January 23, 1985



## Wear of Poly(ethylene terephthalate) Monofilaments

B. J. Briscoe<sup>1</sup>, T. K. Wee<sup>1</sup>, A. Winkler<sup>1</sup>, and M. J. Adams<sup>2</sup>

<sup>1</sup>Department of Chemical Engineering and Chemical Technology, Imperial College, London, England

<sup>2</sup>Unilever Research, Port Sunlight Laboratory, Port Sunlight, Merseyside, England

The frictional force between poly(ethyleneterephthalate) monofilaments (PET) and between PET sliding over glass or human hair fibres has been found to depend on the sliding distance. This non-stationarity can be described using linear or exponential functions of time and provides a sensitive means of detecting very low levels of wear which occur at normal loads considerably less than that required to produce plastic deformation. There is a close relationship between the extent of damage and the magnitude of the microslip which precedes a slip phase during the intermittent sliding. Microslip is probably the result of a sequence of adhesive junction ruptures prior to the catastrophic slip and effectively increases the sliding distance and hence the interfibre wear. At comparable normal loads, both the microslip and damage increases with the imposed sliding velocity.

The wear of fine monofilaments when they slide over one another has important practical consequences in the deformation behaviour and the durability of fibrous assemblies. The frictional forces at the internal micro-contacts provide the local restraints which generate the cohesive response of the assembly. The flexibility of ropes and the tactile properties of fabrics are in many respects governed by these local forces. The frictional work produces surface damage and wear; hence the macroscopic response of an assembly is modified by deformation. Ultimately the damage is sufficient to undermine the strength of the fibres and the assembly strength is weakened.

The measurement of surface damage at monofilament contacts is problematical. Usually such filaments are small (ca. 15  $\mu\text{m}$  in diameter) and the contact areas are in the submicron range. Direct measurement of mass loss is impracticable and electron microscopy is particularly subjective. We have found that the measurement on the frictional force provides an indication of the damage produced during the sliding of one fibre over another. The procedures for monitoring the change in friction are described in this paper. It has not proved practicable to make comparisons between the trend in

the frictional force and the damage detected in a scanning electron microscope; invariably the surface damage produced during sliding is so small that no worthwhile quantitative assessment can be made.

Actually, the data to be described in this paper are not primarily designed to monitor surface damage directly rather the influence that this damage has on the static friction of monofilament contacts. The acquisition of these data are an intrinsic part of an attempt to model the mechanical properties of non-woven monofilament assemblies. An assembly of this type accommodates a macroscopic strain by two means which involve internal motion in an element of monofilament which is strained locally by at least two contacts with adjacent monofilaments. The element may distort between fixed contact points. At high strains, however, the stresses on the contact points induce relative motion between monofilaments; the critical stress is produced by the friction at the point contact.

In practice the frictional characteristics of monofilament contacts is complex. The magnitude of the force is governed by stochastic processes and is not single valued. In addition there is a slow creep of the contact prior to failure. The most probable value of the frictional force does, however, follow the trends seen in larger contacts; it varies with load and surface topography in a predictable manner. A particularly important feature of these contacts, in the context of assembly modelling, is that the most probable value of the frictional force changes with the extent of the relative displacement of the contact. It is the analysis of these changes which is the subject of the present paper.

### Experimental Techniques

A full account of the experimental method and general data analysis has been reported elsewhere (1-4). A brief summary of the features relevant to the present work is useful.

Poly(ethyleneterephthate), PET, fibres were supplied by Imperial Chemical Industries Limited, Harrogate with various titania contents although the work described will be restricted to systems with nominally zero titania contents. Typical fibre radii ranged from 15-20  $\mu\text{m}$ . They were cleaned by Soxhlet extraction with petroleum ether. The precise diameter of the fibres was measured optically and the bending modulus of each fibre was computed by measuring its deflection under a series of bending moments (2); (see Figure 1a). Simple beam theory gives the deflection  $\Delta h$  under a load  $W$  imposed at a distance  $l$  from the fixed end as:

$$\Delta h = Wl^3 / (3EI) \quad (\text{for small deflections}) \quad (1)$$

where  $E$  is a composite longitudinal modulus and  $I$  is the second moment of area normal to the fibre axis. Since  $I$  is given by  $\pi r^4 / 4$ , where  $r$  is the radius, the deflection is a sensitive function of  $r$  and hence the need for individual characterisation. In the present work the small deflection approximation is accurate.

The calibration procedure provides the basis for the construction of the friction experiment. Figure 1b is a schematic diagram of the apparatus. One fibre is incarcerated under a slight tension at both ends (fibre 1). The second fibre (fibre 2) is held rigidly

at one end only and positioned orthogonally over fibre 1. Both fibres are mounted in a series of instrumented manipulation stages beneath an optical microscope (magnification  $\times 100$ ). Figure 2 is pressed against fibre 1 and the normal load computed using Equation 1. A complication in small contacts is that the autoadhesive load, which may be accurately measured by reversing the normal load and imposing a tensile force on the contact, is comparable with the applied load imposed by the bending moment. We will not discuss this point further and only state that the loads reported here are the sums of the applied load and the magnitude of the measured autoadhesive force (2). Relative motion of the contact point is achieved by moving fibre 1 in a direction coincident with its axis. Various imposed velocities were studied but the data given here are mainly for an imposed velocity of  $29 \mu\text{ms}^{-1}$ . The frictional force produces a discontinuous motion of the contact point.

The frictional force as a function of time was determined from the tangential bending of the fibre using elastic beam theory. An optical microscope, to which was attached a photodiode array, was used to sense the position of the contact and hence the flexural displacement. The array used was of the IPL M series of linear photodiodes manufactured by Integrated Photomatrix Limited. It had integrated scanning circuitry with variable scan rate and 512 diodes with a pitch of  $2.58 \times 10^{-3}$  cm. The array was interfaced to an 8-bit microprocessor which reduced the effective number of diodes to 256 (full resolution required a 16-bit microprocessor). The scan rate was set at 5 Hz which meant that a diode was scanned every  $384.6 \mu\text{s}$ . The same scan rate was used when the velocity was  $3.6 \mu\text{ms}^{-1}$  except that only every seventh point was retrieved to reduce the number of data points to an acceptable level; a typical experiment at this velocity had a duration of about 3 hours. The primary data were recovered directly by a microcomputer and stored on diskette. It was then transferred to a main frame computer for subsequent processing. The digital output of the array was calibrated using a stage micrometer; it was found that each diode corresponded to  $5.79 \mu\text{m}$  in real space.

### Data Analysis

A schematic representation of the contact motion is shown in Figure 2. The motion is a sequence of the apparent stick events, where there is no pronounced relative motion, followed by a brief period of rapid sliding of the order of one meter per second; the slip event. In this work we have discovered that some relative motion of the contact also occurs in the stick event although the average velocity is small; perhaps a few microns, although it is not the classical microslip which involves relative motion of distances which are a fraction of the contact diameter (5). In the present work, the contact often moves through many contact diameters before gross slip occurs at the critical junction rupture stress.

Our analytical techniques provide several results. In summary they define:

(i) The statistical representations of various characteristic points in the data, particularly the statistical distributions of the static frictional force.

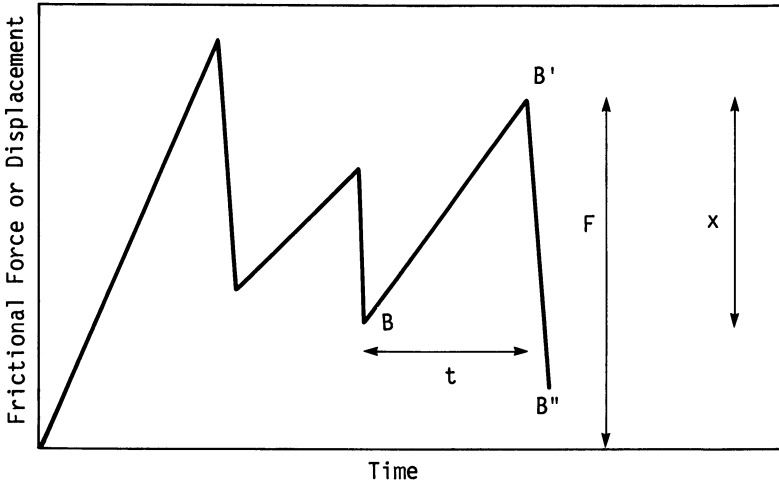
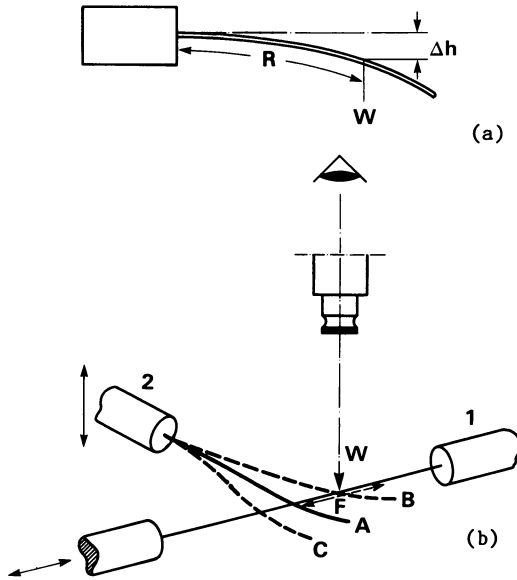


Figure 2. A schematic trace of the stick-slip movement detected in regions A and B (Figure 1b) shown as frictional force or displacement against lapsed time. The point A (Figure 1b) is the origin of this trace and the region  $BB'$  is normally the stick phase and  $B'B''$  the slip phase. The quantities  $F$  and  $t$  respectively the static friction and period.

(ii) The extent of microslip in the stick phase.

(iii) The variation of the mean or most probable value of the static friction as a function of time.

The details of the first two of these analytical methods and their application to similar data are depicted in another publication (4).

### Experimental Results

Figure 3 shows a histogram of the measured static friction of a monofilament contact. Also included in this figure is the best statistical fit which is a gamma distribution. Most PET contacts are best described by gamma distributions. This particular example is for a case where rather little damage to the contact is observed; that is the most probable value of the friction at the stick-slip transition is not a strong function of time or displacement. When a strong trend of this type is present the quality of comparison between experiment and a best gamma fit is significantly reduced and higher confidence levels are required. This aspect of data fitting will be discussed later when the reason for this loss of fitting capability will be apparent; it does however arise because the frictional force is slowly changing with time. This point will now be examined further.

A set of static friction data which contain a trend are shown in Figure 4. These data are said to be non-stationary. The existence of these trends may be demonstrated using either serial correlation analysis or a periodic data averaging technique known as the 'run-test'. Serial correlation involves calculation of the autocorrelation coefficient  $r_k$  at a lag  $k$ , which is a measure of the correlation between events at a distance  $k$  apart, and is given by:

$$r_k = \frac{\sum_{t=1}^{N-k} (x_t - \bar{x})(x_{t+k} - \bar{x})}{\sum_{t=1}^N (x_t - \bar{x})^2} \quad (2)$$

where  $\bar{x}$  is the mean:  $\frac{\sum_{t=1}^N x_t}{N}$  and  $N$  is the number of events.

If a time series is approximately random, then for large  $N$ ,  $r_k \approx 0$ ; the coefficients of such a series would be expected to lie between  $\pm 1.96/\sqrt{N-1}$ . Correlograms of non-stationary data are characterised by relatively large values of  $r_k$  that slowly converge to zero as  $k$  increases. Although this technique is strictly only valid for events occurring at fixed intervals (e.g. in time), it can be used to a first approximation for events occurring randomly in time (6) such as the static frictional force values generated in the present experiments.

Figure 5 shows two examples of such an analysis; non-stationary behaviour is clearly evident. Little, other than a trend exists can be inferred from this analysis (7) although an autocorrelation

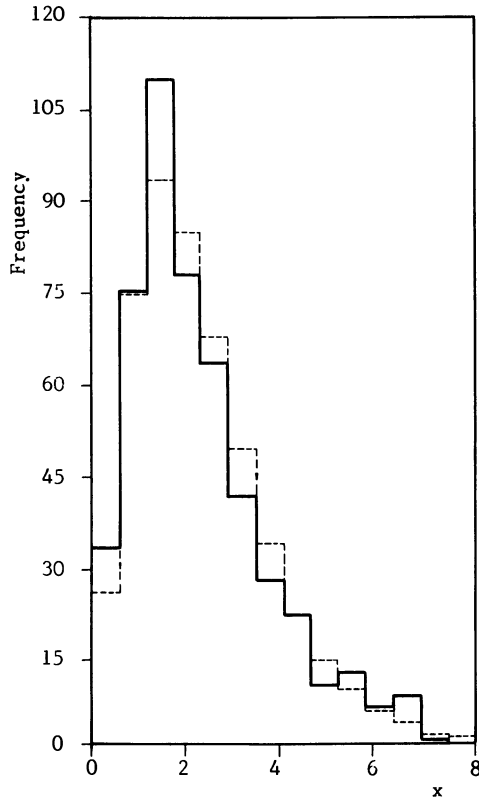


Figure 3 A typical experimental frequency distribution for PET contacts (continuous line). The abscissa is in displacement units which are proportional to the static friction  $F$  (Figure 2). The ordinate is the frequency for a sample of 500 measurements of  $F$ . A calculated gamma frequency distribution (95% confidence  $\chi^2$  test) is shown as a broken line.

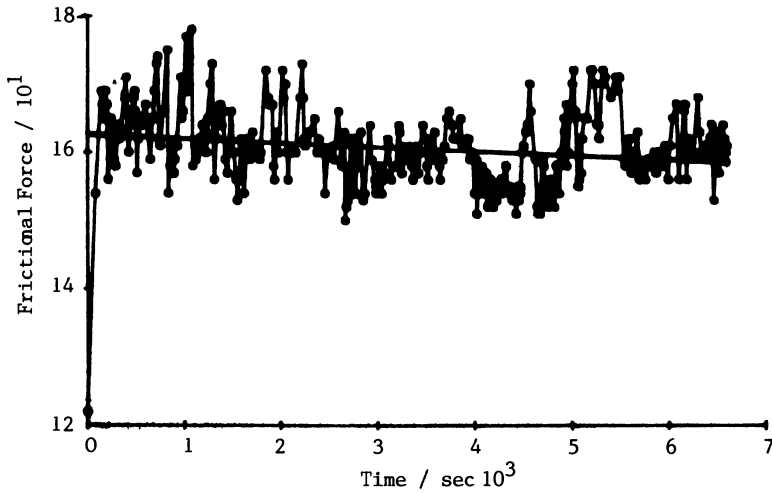


Figure 4 Static frictional force, in arbitrary units, against lapsed time. Each point represents one value of static friction. The trend obtained by least mean squares is shown.

length (a value of  $r_k$  for an arbitrary value of  $k$ ) may be readily computed. A number of  $r_k$  ( $k = 20$ ) values are listed in Table I and a trend is noted (see later).

A more useful approach is the run test which is a simple non-parametric test that is equally valid for point processes and time series. The data are divided into a number of equal domains and for each region a statistic, e.g. the mean, variance or mean square value, is calculated. The median of these values is calculated and the number of times the statistic lies above or below the median determines the stationarity of the data. The test can be used as a criterion for independence using tables of the run distribution (8).

In principle it is possible to account for this non-stationarity by fitting a bivariate distribution in  $F$  and  $t_c$  where  $t_c$  is the duration of sliding. A much simpler alternative, however, was used in practice. This involved fitting a regression model to the data and correcting these data to make them independent of time. Linear and exponential regression were adequate for this purpose, viz: some of the data could be regressed with one or another of the following equations:

$$F(t_c) = a + b t_c \quad (3)$$

$$F(t_c) = a' \exp(b' t_c) \quad (4)$$

Thence the modified detrended data  $F_m(t_c)$  are given by:

$$F_m(t_c) = F(t_c) - b t_c \quad (5)$$

$$\ln F_m(t_c) = \ln F(t_c) - b' t_c \quad (6)$$

There is no theoretical basis for these equations but it was found that much of the detrended data could then be fitted to particular distributions. One of the values of these empirical relationships is that they allow a point-wise correction of data in time. Essentially the data may be normalised to zero time. Data treated in this manner are found to show better comparisons with calculated gamma distributions. In the context of this paper these fitting equations provide a means of quantifying the rate of damage induced in the contact. Table I shows a set of  $b$  values generated using Equation 5. The data are for a fixed relative velocity ( $29 \mu\text{ms}^{-1}$ ) and it is seen that  $b$  is an increasing function of the normal load. These parameters are plotted in Figure 6.

Microslip can be quantified by any one of the equivalent bases relating to the stick phase: time, displacement or velocity by calculating the difference between the real and theoretical values of that property. The most convenient equation is based on displacement in which case microslip is defined as:

$$\epsilon = \frac{V_m \bar{t} - \bar{x}}{V_m \bar{t}} = 1 - \frac{1}{V_m} \frac{\bar{x}}{\bar{t}} \quad (7)$$

$V_m$  is the imposed sliding velocity and  $\bar{x}$  and  $\bar{t}$  are the mean values



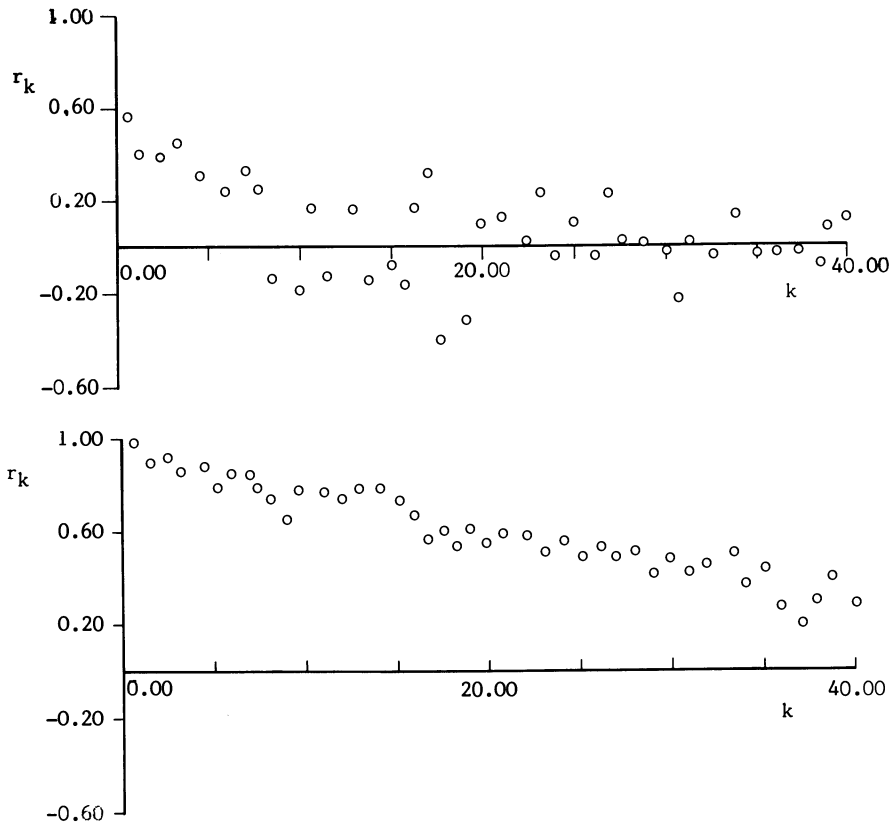


Figure 5 Correlograms of almost stationary random data (a) and random data which are non-stationary (b). Non-stationary data are characterised by finite values of the autocorrelation coefficient  $r_k$  even at large value of the lag,  $k$ .

Table I. Data for Cleaned PET-PET Contacts

Load/ $\mu\text{N}$	Microslip $\epsilon$	$b \cdot 10^4$ $\mu\text{N}\cdot\text{s}^{-1}$ *	$r_k(k=20)$ AutoCorrelation Coefficient
0.38	0.28	0.16	0.16
0.48	0.22	0.64	0.28
0.66	0.18	1.35	0.20
0.98	0.16	2.10	0.16
1.13	0.15		0.01
1.61	0.10	6.70	0.18
2.46	0.08	9.60	0.25

\*  $F(t) = F(0) - bt$

The parameters  $\epsilon$  and  $r_k(k=20)$  are defined in the text.

of the displacement and period respectively (Figure 2). For  $\epsilon=0$  there is unambiguous stick-slip and  $\epsilon=1$  represents continuous motion.

Table I gives the values of  $\epsilon$  for the PET fibre pairs and shows that the microslip decreases with increasing normal load (cf. Figure 7). Figure 6 also displays the computed values of the microslip for this particular system.

A comparison between the microslip observed for PET-PET contacts at sliding velocities of 29 and  $145 \mu\text{s}^{-1}$  is made in Table II. The  $b$  value at  $145 \mu\text{s}^{-1}$  is considerably greater than that at  $29 \mu\text{s}^{-1}$  despite the much higher normal force at the lower velocity which, as indicated above, would tend to produce greater non-stationarity. The  $\epsilon$  values for sliding at  $145 \mu\text{s}^{-1}$  were also greater than those at  $29 \mu\text{s}^{-1}$  at comparable loads except at very small loads when the microslip was similar (4).

At  $3.6 \mu\text{s}^{-1}$  the microslip was found to be zero at all normal loads investigated. The tentative conclusion is therefore that both the microslip and non-stationarity increase with increasing imposed sliding velocity.

Table II also lists some examples of non-stationarity corrections for other fibre combination where the fibre which is fixed at one end only is PET. These data show that the  $b$  values depend on the fibre type, as might be expected, but insufficient data has thus far been obtained to make any general observations.

### Discussion

Damage is detectable in terms of non-stationarity at all loads but is particularly pronounced when the normal load exceeds ca.  $2 \mu\text{N}$ . In a previous study (2) we have computed that gross plastic deformation occurs in this type of system at about  $30 \mu\text{N}$  in purely normal loading and the frictional data was also consistent with this calculation; above a  $30 \mu\text{N}$  load, the friction coefficient is not very sensitive to the normal load which is associated with the onset of gross plastic deformation in sliding. The interesting point is that we are detecting appreciable damage at a load of less than one tenth of this value.

There are precedents for time-dependent frictional behaviour in large contacts. In particular the sliding of rubber on glass has been studied in some detail. At low sliding velocities, the friction decreases with sliding distance (9) while at higher velocities the converse was observed (10). The origin of these effects, however, is related to the deposition of lubricant material from the rubber to the counter-surface (10) and are therefore not close analogies to the present fibre system.

Wear is a complex phenomenon involving a wide range of possible processes (11) but invariably two of the most important governing factors are the normal load and sliding distance. At a constant normal load we have observed that both the non-stationarity and microslip increase with velocity. In terms of the adhesion model of friction, which provides a quantitative description of the frictional behaviour of PET fibres (2-3) a 'frictional event' is the formation and subsequent rupture of an adhesive junction. It is reasonable to suppose that these events are the underlying cause of wear. Micro-

Publication Date: September 12, 1985 | doi: 10.1021/bk-1985-0287.ch025

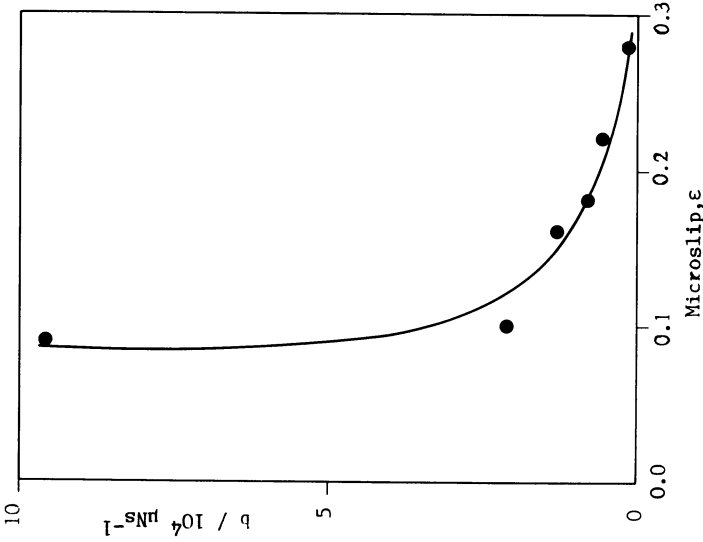


Figure 7. The cross correlation of the extents of microslip and non-stationarity from Figure 6.

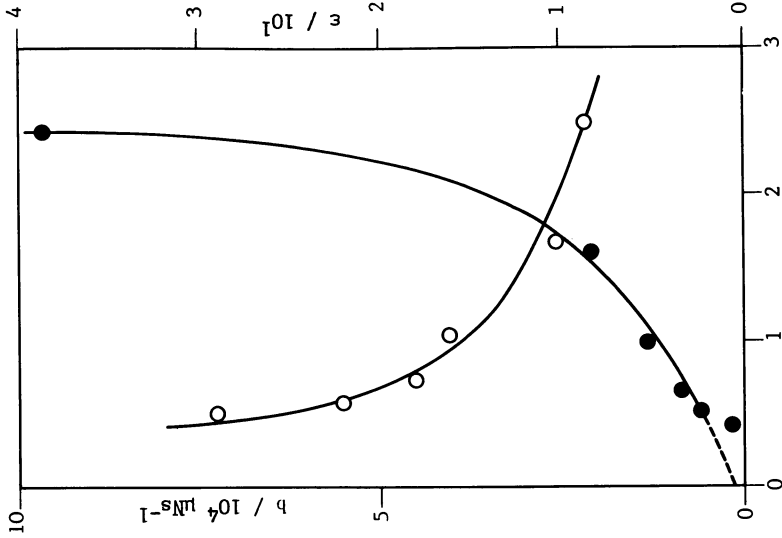


Figure 6. The linear non-stationary parameter  $b$  as a function of normal load. The value of  $b$ , which describes the extent of non-stationarity, increases rapidly above  $1 \mu\text{N}$ . Also shown is the microslip parameter  $\epsilon$ ; large values of  $\epsilon$  indicate significant microslip.

Table II. Various  $b$  and  $b'$  Coefficients for Contacts where a PET Monofilament is the Cantilever

Contacting Fibre	Imposed Velocity $\mu\text{m}\cdot\text{s}^{-1}$	F/ $\mu\text{N}$	W/ $\mu\text{N}$	$b \cdot 10^5$ $\mu\text{N}\cdot\text{s}^{-1}$	$b' \cdot 10^4$ $\text{s}^{-1}$
PET	29	2.50	2.34	9.60	6.00
Glass	29	0.09	0.49	1.83	-
Glass	29	0.42	0.77	-	1.52
Human Hair	29	0.12	0.09	4.00	-
PET	145	0.19	0.15	37.12	-

slip results from secondary junction formation following a peak frictional force in the stick phase. On this basis we may ascribe microslip to an effective increase in sliding distance.

The measurements as a function of increasing normal load demonstrate that there is not a simple relationship between microslip and non-stationarity. Greater damage is produced during junction breakdown at high loads but the microslip decreases with normal load. It is believed that this reduction in microslip with load is related to the corresponding increase in the frictional force with load (4). This produces high bending moments and hence a relatively greater acceleration of the fibre after junction failure. The opportunity for the secondary junction formation is then reduced since the kinetic frictional force will decrease rapidly with velocity. There is some analogy to the dwell time effect in autoadhesion.

### Conclusions

Small amounts of surface damage are found to produce a marked change in the most probable value of the static friction of monofilament contacts. This frictional force or critical junction rupture stress decreases with time often in a linear manner. The rate of change is a function of the normal load and becomes pronounced above a critical load which is about one tenth of the calculated plastic flow stress in normal loading. There is an empirical correlation between this rate of friction change and the extent of microslip detected in the contact prior to the initiation of the rapid slip phase. At a constant normal load the observed rate increases with velocity. It is not yet possible to identify the processes responsible for the type of damage produced in these fibre systems but it has been demonstrated that frictional measurements can provide a very sensitive means of detecting low levels of wear which may ultimately lead to a severe deterioration in physical properties.

### Literature Cited

1. Pascoe, M.W.; Tabor, D. Proc.R.Soc. 1956, A235, 210.
2. Briscoe, B.J.; Kremintzer, S.L. J.Phys.D:Appl.Phys. 1979, 12, 505.
3. Adams, M.J.; Briscoe, B.J.; Kremintzer, S.L. in "Physicochemical Aspects of Polymer Surfaces"; K.L. Mittal, Ed.; Plenum Press : New York, 1983; p.425.
4. Briscoe, B.J.; Winkler, A.; Adams, M.J.; To be published in J.Phys.D:Appl.Phys.
5. Courtney; Pratt; Proc.R.Soc. 1957, A238, 529.
6. Cox, D.R.; Lewis, P.A.W. "The Statistical Analysis of Series Events"; Academic Press: London, 1978.
7. Chatfield, C.; "The Analysis of Time Series; An Introduction; Chapman and Hall, London, 1980.
8. Bendat, J.S.; Piersol, A.G. "Random Data: Analysis and Measurement Procedures"; Wiley-Interscience, London 1971.
9. Roth, F.L.; Driscoll, R.L.; and Holt, W.L. J.Res.Natl.Bur.Std. 1942, 28, 439.
10. Cooper, R.P.; Ellis, B. J.Appl.Polym.Sci. 1982, 27, 4735.
11. Archard, J.F. J.Appl.Phys. 24, 981, 1953.

RECEIVED January 23, 1985

## Quantitation of Nonvolatile Components from the Photochemical Decomposition of Poly(ethylene terephthalate)

S. Krishnan<sup>1</sup>, S. B. Mitra, P. M. Russell, and G. Benz

Central Research Process Technologies Laboratory, 3M Center, 3M Company,  
St. Paul, MN 55144

The photochemical degradation of poly(ethyleneterephthalate) was studied using an analytical spectroscopic procedure to quantitate the water soluble non-volatile products. Irradiations of film samples were carried out in air, under ambient humidity using light in the range of wavelengths from 280 to 400 nm. Under these conditions only chain scissions occur leading to the formation of water extractable phthalate residues. The extent of photodegradation was measured as the amount of water extractable phthalate residues. This information was used to study the efficiency of an additive used to retard photodegradation of poly(ethyleneterephthalate).

Photochemical degradation of poly(ethyleneterephthalate) (abbr. PET) has been exhaustively described by researchers at the National Research Council of Canada (1-5). These reports describe the effect of various light wavelength regions on the polymer, the variations in the yield of volatile decomposition products and chemical changes in both the surface and bulk resulting from the variations in the pressure and the composition of the gaseous environment around the sample being irradiated. It has also been pointed out that irradiations in the presence of air or oxygen do not induce cross linking in the polymer (4,6-8). In this study we observe that the photochemical chain scission in irradiated PET can be monitored by a procedure involving aqueous extraction of a sample followed by ultraviolet spectral analysis of the extract. Conventional ultraviolet light absorbers incorporated in PET films do not interfere in the analysis. We observe that the amount of water extractable material increases with the time of exposure to radiation.

<sup>1</sup> Author to whom correspondence should be directed.

### Experimental

**Materials.** Film samples of PET were obtained from the Specialty Films Division of 3M Company, St. Paul, Minnesota 55144, U.S.A. Two samples of thicknesses 6.3  $\mu$  and 12.5  $\mu$  contained no additives. All of the other samples contained varying amounts of a substituted 2,4-dihydroxybenzophenone type (9,10) ultraviolet light absorber. The densities of the film samples were in the range 1.31 to 1.32 g/ml. Relative viscosities of 1:1 phenol:tetrachloroethylene solutions of PET were determined using a Ubbelohde viscometer at  $25 \pm 0.1^\circ\text{C}$ . Intrinsic viscosities were calculated using the equation of Solomon (11). Average molecular weights were calculated using the Mark-Houwink-Sakurada relationship (12).

**Irradiations.** A QUV-accelerated weathering tester (Q-Panel Co., Cleveland, Ohio) was used in the experiments. This chamber was provided with a total of eight QFS-40 lamps set in two arrays. The film samples were mounted on aluminum panels (30 cm X 10 cm) and arranged in the chamber so that the surface of the samples were 2.5 cm away from the surface of the lamps. Figure 1 depicts the range of wavelengths and the relative energy outputs for the lamp measured at 2.5 cm away from the surface of the lamp. A constant temperature of  $60^\circ\text{C}$  was set in the chamber. All irradiations were done at ambient humidity and the lamps were switched off only for brief periods while a sample was being withdrawn for analyses. Successive samples were taken out of the same location in the chamber and the remaining samples moved in a queue to advance through each of the possible exposure positions to eventually take up the exit slot for the last aliquot of exposure. This scheme enabled the samples to navigate through all possible local differences in the radiation dosage within the chamber.

The 50  $\mu$  samples were cut into 2.5 cm X 20 cm strips and two strips of different films were mounted on the same panel side by side. Each panel contained a strip of film #6 (Table I) and one of another 50  $\mu$  sample. After irradiation for a specific period of

Table I. Characteristics of PET Films

Film #	Film Thickness	UV-Absorber Content (a) (w/w %)	Density (g/ml)	Molecular Weight
1	6.3 $\mu$	0.0	1.318	19,500
2	12.4 $\mu$	0.0	1.320	22,100
3	25.0 $\mu$	2.5	1.315	21,204
4	50.0 $\mu$	2.0	-	-
5	50.0 $\mu$	3.0	-	-
6	50.0 $\mu$	4.0	-	-

(a) 2-hydroxybenzophenone derivative (ref.9, 10).

time, samples for analysis were cut out of the same panel-latitude on both films (Figure 2). This procedure assured the same irradiation temperature and dosage for a direct comparison as well as enabled the comparison of all films normalized with respect to film #6.

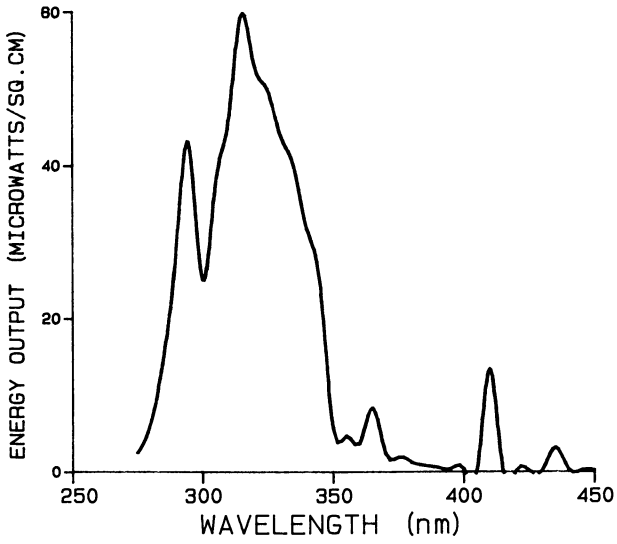


Figure 1. Irradiation Source: QFS-40 Lamp.

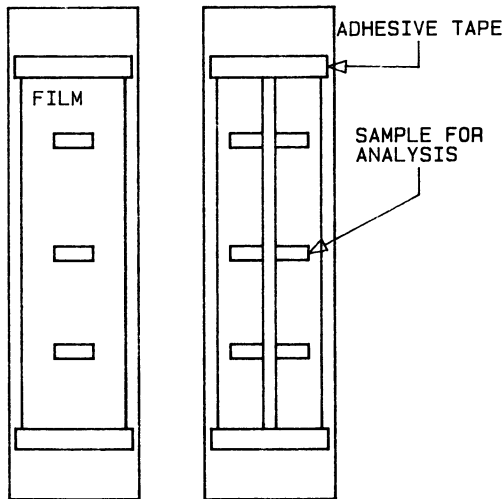


Figure 2. Mounting Film Samples.



Spectra. A Perkin-Elmer Hitachi model 200 spectrophotometer was used to record all ultraviolet spectra. The infrared spectra of the films were obtained using a Nicolet FTIR-7199. The transmission spectra of films were obtained from samples moistened in tetrachloroethylene (2) and mounted between NaCl plates. Attenuated total reflection (ATR) spectra were taken by placing the exposed side of the film in contact with a germanium crystal at a 45° angle of incidence. Fluorescence from film surfaces were measured using a Perkin-Elmer MPF-44B fluorescence spectrometer. The excitation beam (340 nm, slit, 4nm) was incident on the film at 45° and the emission (400-500 nm) was measured at 90° to the excitation beam.

Extraction of Non-volatile Decomposition Products. A sample of PET film (5-10 mg) was weighed using a Cahn 25 Automatic electrobalance and placed in a 10 ml volumetric flask. Deionized water was added to the sample and made up to the volumetric mark. The flask was then loosely stoppered and placed in a support frame immersed in the water bath of a Bronson B321 ultrasonicator. The water bath temperature was between 55 and 60°C. After half an hour of sonication, the volumetric flask was removed and equilibrated to room temperature. More deionized water was added (usually a few drops, if needed) to the volumetric flask to make up for any loss of solvent due to evaporation. The absorbance of the aqueous extract was measured at 242 nm by taking 2 ml of the solution in a quartz cuvette (path length, 1 cm). The sample from the cuvette was transferred back to the volumetric flask and the sonication was repeated for another half hour period followed by a measurement of absorbance of the solution at 242 nm. The extraction was deemed complete and exhaustive when the absorbance of the extract at 242 nm reached a maximum constant value. At least 3 samples were cut from different panel-latitudes and an average value of the absorbance of the extracts was used in calculations of the amount of soluble components extracted from the sample. A preparatory extraction was performed by using 20 g of 12.5 u PET that had been irradiated to brittleness (circa 80 hours).

Chromatography. The material extracted from irradiated PET (12.5 u) was used in the chromatographic analyses. Liquid chromatography was performed using a Hewlett-Packard 10848 instrument with a variable wavelength detector. The sample solution concentration was 1 mg/ml in methanol. The chromatogram was obtained by injecting 50 ul of the solution via a loop injector on to a 10 u ES Chromegabond MC-18 (30 cm, 4.6 cm, i.d.) column. The solvent system (MeOH-water, both containing 0.2% (v/v) HOAc) was programmed from 10% MeOH to 100% MeOH in 30 minutes. The elution of peaks were recorded by continuously monitoring the absorbance at 240 nm. The flow of solvent was stopped at the maxima of peaks and a continuous spectral scan of the solution in the detector cell was recorded in the range 200-350 nm.

Non-volatile material (ca. 5 mg) from irradiated PET was derivatized using borontrifluoride-methanol (13) reagent. The

product was dissolved in 0.5 ml of ether and used for gas chromatographic analysis. A OV-101 (5% on Chrom-GP, 2m X 2mm i.d.) column installed in a Hewlett-Packard 5840 gas chromatograph interfaced through a glass jet separator to a duPont 21-491B mass spectrometer was used for the analysis. A 2 ul sample was used for each injection and helium carrier gas flow was 20 ml/min. The elution was temperature programmed from 100 to 330°C at 20°C/min. and the effluent was split in two parts and channeled to both a flame ionization detector and the mass spectrometer. The mass spectrometer was operated in the electron impact mode.

## Results

The viscosity average molecular weights of the PET samples used in this study are presented in Table I. The ultraviolet spectra of the unstabilized film samples were similar to those reported in the literature (2,8). The samples that contain the ultraviolet light absorber show an absorbance of  $> 2$  for wavelengths under 365 nm. Unstabilized films became brittle after about 80 hours of irradiation.

The ultraviolet spectrum of the aqueous extract from irradiated PET showed peaks at 195, 242 and 290 nm. In the exhaustive extraction procedure, the absorbance of the extract measured at 242 nm reached a maximum value in about 3 hours (Figure 3) of sonication. The time required for the complete extraction of water soluble decomposition products from irradiated PET films was found to be the same for all film thicknesses used in this study. The amount of water soluble decomposition products that absorb light at 242 nm was formed at a greater rate in the unstabilized films than in the films containing the ultraviolet light absorber. Extraction of control samples, oven aged in the dark for the same duration as the irradiated films yielded solutions that have negligible absorbance at 242 nm.

Fluorescence from the irradiated surface of 12.5 u PET films increased with exposure time. The emission spectrum contained a single peak at 460 nm (14). For the unstabilized 12.5 u PET film a number of broad bands in the 3600-2500  $\text{cm}^{-1}$  region were observed in both transmission and ATR infrared spectra. Figures 4,5, and 6 depict the trends with increasing exposure periods. The viscosity average molecular weights decreased rapidly in the initial stages of irradiation (Figure 7).

Liquid chromatography of the MeOH solution of the material isolated from irradiated PET required the solvent system be spiked with acid (HOAc) to get close to ideal peak shapes on the elution profile. There were four major components in the extracted mixture. The ultraviolet spectra of all these compounds obtained through the "stop-scan" procedure contained peaks around 240 and 290 nm (Figure 8). Gas chromatographic mass spectral analysis of the methyl esters showed three major compounds. Table II lists the retention times, mass spectra of compounds and the structures assigned to the parent compound or the largest fragment observed on the mass spectrum. Compounds eluting from the column at temperatures above 300°C yielded poor mass spectra as the transfer lines including the jet

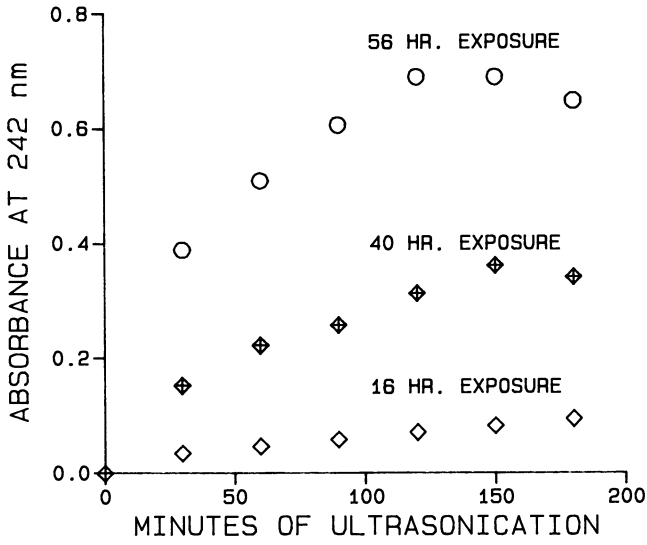


Figure 3. Exhaustive Ultrasonic Extraction.

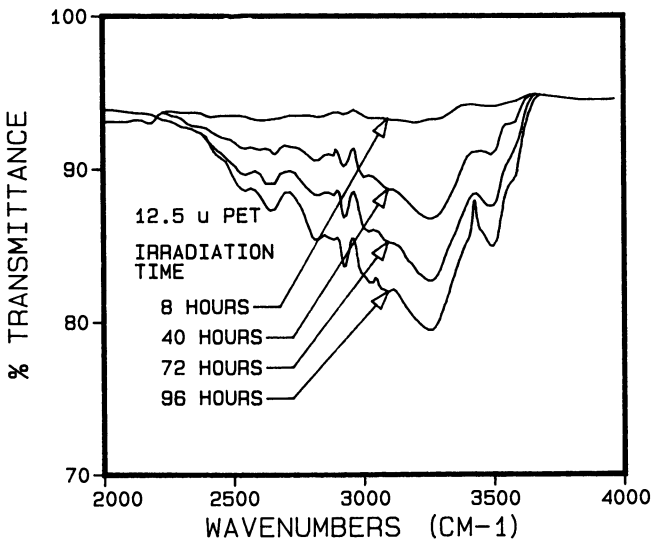


Figure 4. FT-IR Subtraction Spectra.

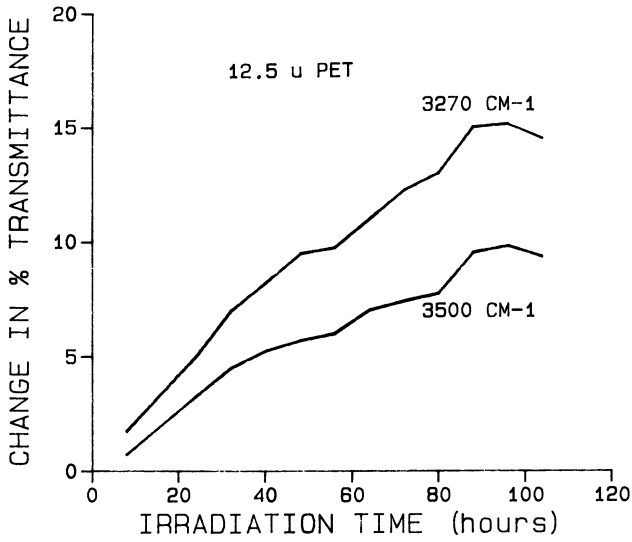


Figure 5. Changes in Infrared Transmission.

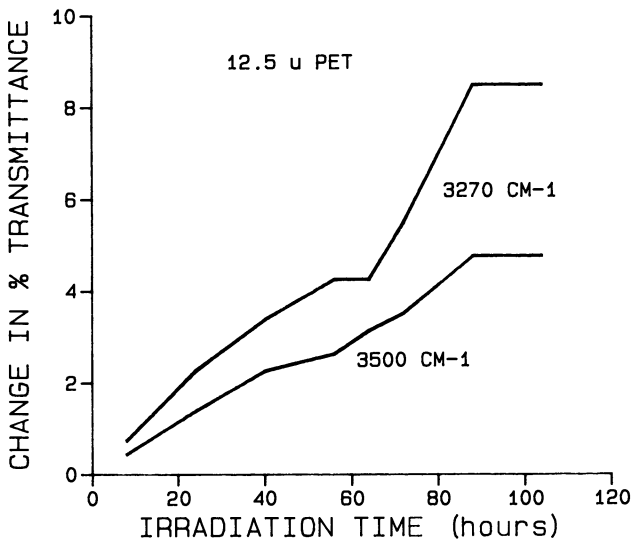


Figure 6. Changes in Attenuated Total Reflection (Infrared).

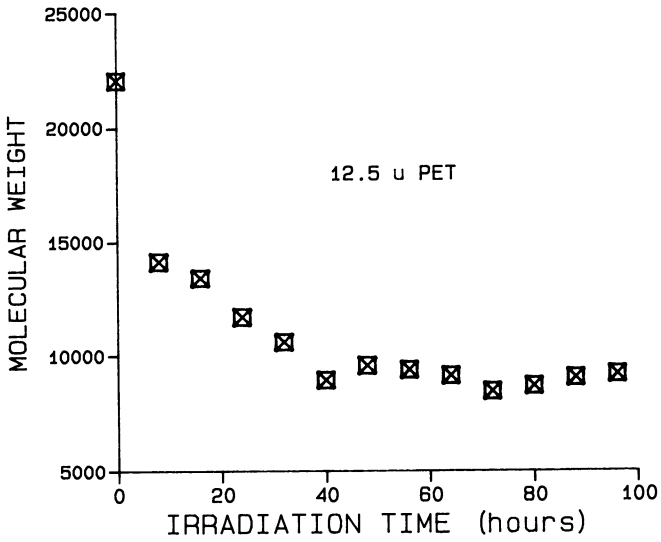


Figure 7. Molecular Weight vs. Time.

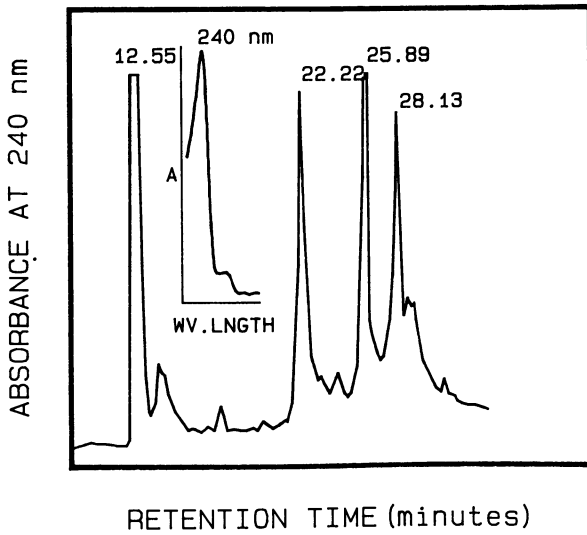


Figure 8. Liquid Chromatographic Analysis.

separator had been maintained at 300°C. The highest mass fragment observed on the mass spectrum of the last major peak on the chromatogram had an m/e value of 577.

### Discussion

The major non-volatile materials isolated from photooxidized PET are acidic compounds. This necessitated the use of acid spiked solvent system for the liquid chromatographic separation of the mixture. All the major compounds separated on the liquid chromatogram showed typical phthalate ultraviolet absorption spectra with peaks at 240 and 290 nm (inset, figure 8). Three major compounds are observed on the GC-MS chromatogram (Table II). The largest mass spectral fragment (m/e=577) can be accounted for on the basis of a parent

Table II. Gas Chromatographic Mass Spectrometry

Retention Time (minutes)	Mass Spectrum m/e (rel.int.)	Structure (Compound or Fragment)
5.92	194(17)	$\text{H}_3\text{COOC}-\text{C}_6\text{H}_4-\text{COOCH}_3$
	163(100)	
	135(19)	
	103(12)	
	76(7)	
8.24	252(3)	$\text{H}_3\text{COOC}-\text{C}_6\text{H}_4-\text{COOCH}_2\text{COOCH}_3$
	221(2)	
	163(100)	
	149(10)	
13.40	577(1.5)	$\text{H}_3\text{C}(\text{OOC}-\text{C}_6\text{H}_4-\text{COOCH}_2\text{CH}_2)_2\text{COO}-\text{C}_6\text{H}_4-\text{COO}$
	385(3)	
	359(3.5)	
	341(26)	
	221(25)	
	193(100)	

compound with at least three aromatic nuclei. This is a direct evidence for Blais' calculated value of 3 repeat units per polymer chain on the irradiated (555 hours, Xenon arc) surface of PET (5). The structures deduced for the methyl esters (Table II) show that photooxidation of PET results in both aromatic and aliphatic carboxylic acid groups.

The procedure used to quantitate the amount of extracted phthalate involved an estimate of a gravimetric extinction coefficient for the phthalate peak around 240 nm in the absorption spectra (Table III). An average extinction coefficient of 106.8 ml/mg.cm was used to convert the absorbance values into amounts of phthalate residues extracted from 1 mg of irradiated film (soluble fraction).

Table III. Extinction Coefficients of Phthalates

Compound	Abs.Max. (nm)	$M^{-1}cm^{-1}$	$mlmg^{-1}cm^{-1}$
Terephthalic acid	241	17,500	105.4
Dimethylterephthalate	241	20,630	106.3
PET(a)	244	23,880	108.6

(a) Cheung, P-S.R.; Roberts, C.W. *J. Appl. Polym. Sci.* 1979, 24, 1809.

Plots of this soluble fraction from irradiated PET versus exposure periods are shown in Figures 9 and 10. The amounts of extractable non-volatile products initially showed a linear increase with irradiation time and then decreased to almost a constant value at longer exposure times. The y-values at these plateaux (Figures 9 and 10) can be recognized as inversely proportional to the film thicknesses. When the densities of the samples are not significantly different from one another, the same weight of 6.3 u film has about four times the surface area exposed to radiation as the 25 u film and twice as the 12.5 u film. The 25 u film containing the stabilizer undergoes degradation at a much slower rate and takes a much longer period of exposure to produce the same amount of photodegradation products from the same unit surface.

Fluorescence from the surface of irradiated PET has been ascribed to the product from the hydroxylation of the aromatic ring in the polymer (14). The increase in the fluorescent emission (460 nm) from the irradiated surface of the 12.5 u film (Figure 11) is similar to the data available from the literature(3). Hydroxylation of the aromatic ring during the photooxidation of PET introduces a continually increasing surface concentration of the 2-hydroxyphthalate function. The 2-hydroxyphthalate group can act as a ultraviolet screen by filtering light at the surface. This group may also act as a ultraviolet light absorber through mechanisms involving the dissipation of energy in Keto-Enol interconversion (15). These factors operate to produce a steep, linear increase in fluorescence at first and then a decrease in emission at longer exposures (Figure 11).

Comparative FT-IR spectroscopy of the 12.5 u samples is in agreement with the results of the extraction study on photoxidised PET. Representative subtraction spectra of control PET films from irradiated ones are shown in Figure 4. A number of broad bands in the  $3600-2500\text{ cm}^{-1}$  region are typical hydroxyl and carboxy O-H stretching vibrations (16). Similar bands have been reported in the literature for PET films irradiated with Xenon and carbon arc radiation(2). The progressive increase in hydroxyl and carboxyl groups upon exposure is qualitatively evident from Figure 4. The band centered at  $3270\text{ cm}^{-1}$  was assigned to carboxyl O-H stretching mode(16) and its increase was plotted against irradiation time in Figure 5. The band centered around  $3500\text{ cm}^{-1}$  was assigned (17) to hydroxyl group and was also similarly plotted (Figure 5). Both curves show profiles analogous to that observed for the increase in

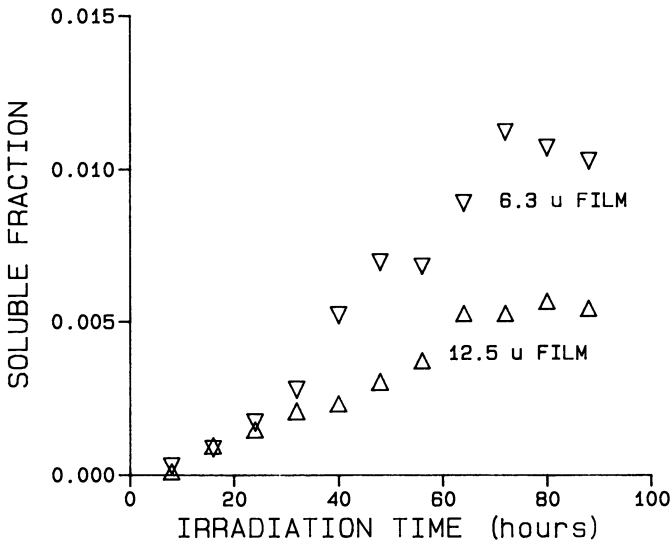


Figure 9. Soluble Fraction vs. Time.

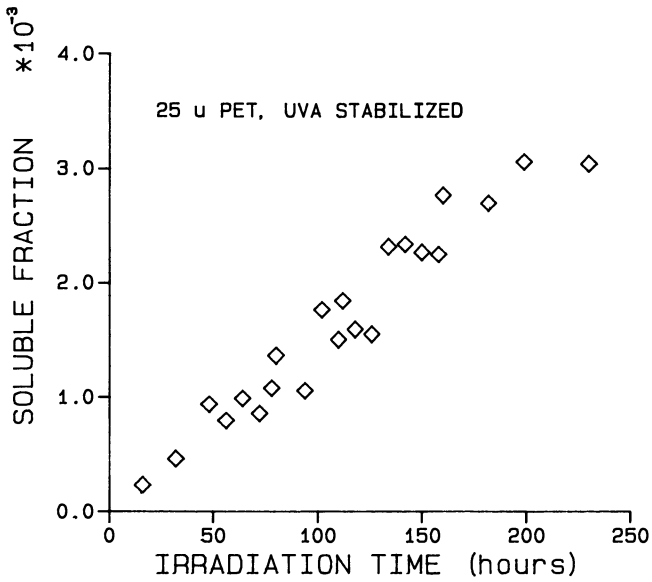


Figure 10. Soluble Fraction vs. Time.



fluorescence and the amount of extractable material. The results of the ATR subtraction spectra (Figure 6) also show comparable plots. The decrease in molecular weight (Figure 7) indicates the absence of cross-linking.

The procedure of exhaustive extraction followed by analytical spectroscopy of the aqueous extract was applied to determine the increase in photostability when the ultraviolet light absorber content in the 50  $\mu$  PET film is increased from 2 to 4 % (w/w). Figure 12 shows the variation of the soluble fraction with the

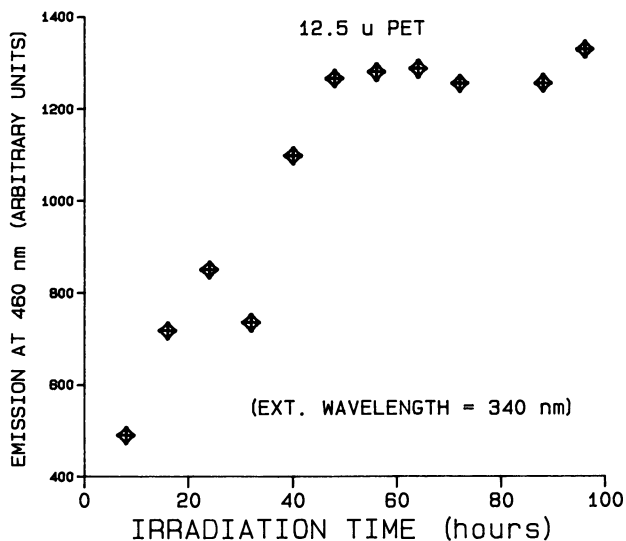


Figure 11. Fluorescence from Exposed Surface.

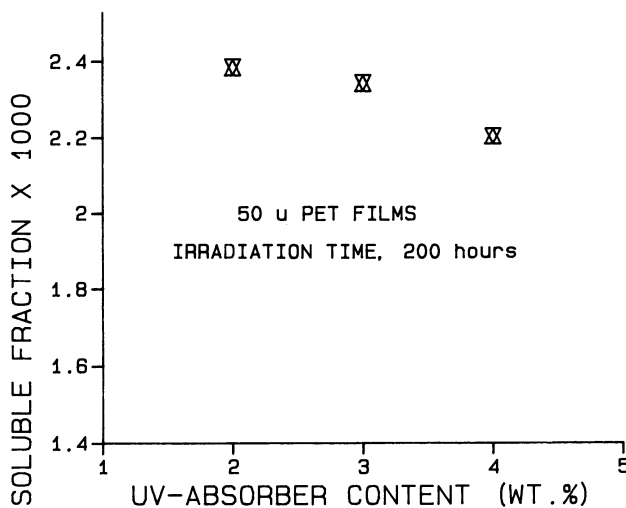


Figure 12. Soluble Fraction vs. UV-Absorber Content.

increasing amounts of UV absorber content in the film. As expected there is a decrease in the extractable material (and hence an increase in photooxidative stability) as the UV absorber content is increased. The slope of the regression line is a determinant of the efficiency of the additive.

### Conclusion

Under photooxidative conditions where no cross-linking occurs, the water extractable non-volatile residues provide a facile quantitative means of studying the photodegradation of PET. This method could conceivably be adapted for fibers as well. The relative efficiency of photostabilisers and/or their combinations included in PET can be determined from the rates of formation of extractable non-volatile products after a short duration of exposure to radiation.

### Acknowledgments

The authors thank Joseph N.Schroepfer and Craig G.Markell for their skilled assistance in chromatographic analyses.

### Literature Cited

1. Carlsson, D.J.; Wiles, D.M. In "Ultraviolet Light Induced Reactions in Polymers"; Labana, S.S., Ed.; ACS Symposium Series No. 25, American Chemical Society: Washington, D.C., 1976; p 321.
2. Day, M.; Wiles, D.M. J. Appl. Polym. Sci. 1972, 16, 175.
3. Day, M.; Wiles, D.M. J. Appl. Polym. Sci. 1972, 16, 191.
4. Day, M.; Wiles, D.M. J. Appl. Polym. Sci. 1972, 16, 203.
5. Blais, P.; Day, M.; Wiles, D.M. J. Appl. Polym. Sci. 1973, 17, 1895.
6. Stephenson, C.V.; Moses, B.C.; Burks, R.E.; Coburn, W.C.; Wilcox, W.S. J. Polym. Sci. 1961, 55, 465.
7. Stephenson, C.V.; Wilcox, W.S. J. Polym. Sci. 1963, A1, 2741.
8. Marcotte, F.B.; Campbell, D.; Cleaveland, J.A.; Turner, D.T. J. Polym. Sci. 1967, A1, 5, 481.
9. Wear, R.L. U.S. Patent 3 580 927, 1971.
10. Wear, R.L. U.S. Patent 3 666 713, 1972.
11. Solomon, O.F.; Gotesman, B.S. Makromol. Chem. 1967, 104, 177.
12. Rudin, A. "Elements of Polymer Science and Engineering", Academic Press, New York, 1982; p 98.
13. Hallas, G. J. Chem. Soc. 1965, 5770.
14. Pacifici, J.G.; Straley, J.M. J. Polym. Sci. 1969, B7, 7.
15. Valk, G.; Kehren, M.L.; Daamen, I. Die Angew. Makromol. Chemie 1970, 13, 97.
16. Conley, R.T. "Infrared Spectroscopy", Allyn & Bacon, Inc., Boston, 1972; p 129, 160.
17. Patterson, D.; Ward, I.M. Trans. Faraday Soc. 1957, 53, 291.

RECEIVED January 23, 1985

## Author Index

- Adams, M. J., 375  
 Anderson, J. C., 315  
 Aron, Paul R., 287  
 Atkinson, J. R., 171,215  
 Bahadur, S., 253  
 Belyi, V. A., 205  
 Benz, G., 389  
 Boundy, R. R., 129  
 Briscoe, B. J., 151,303,375  
 Buckley, Donald H., 287  
 Chow, T. S., 67  
 Czichos, Horst, 3  
 Dowson, D., 171,215  
 Eiss, Jr., N. S., 59,135  
 El-Hady Diab, M. M., 171  
 Fukushima, Toshio, 347  
 Gillis, B. J., 171,215  
 Good, Robert J., 39  
 Jones, J. W., 135  
 Kimball, D. J., 129  
 Kirpichenko, Yu. E., 333  
 Krishnan, S., 389  
 Lee, Lieng-Huang, 27,77  
 Lipshitz, Harold, 229  
 Mitra, S. B., 339  
 Motohashi, Kenji, 347  
 Nevzorov, V. V., 205  
 Potter, III, J. R., 59  
 Russell, P. M., 389  
 Shoraka, Fereydoun, 39  
 Stolarski, T. A., 303  
 Sutor, Paul, 269  
 Sviridyonok, A. I., 333  
 Tabor, D., 253  
 Tanaka, Kyuichiro, 103,363  
 Vincent, H. L., 129  
 Wee, T. K., 375  
 Williamson, P. K., 315  
 Winkler, A., 375  
 Yamada, Yoshinori, 103,363  
 Yasuda, H. K., 89  
 Zhang, S. W., 189

## Subject Index

- A
- Abraded metal surfaces, effect on wear rate of HDPE, 255
- Abrasion  
 rubber, by a line contact, 189-202  
 test parameter, predicting in-service bearing life, 316
- Abrasion-resistant coatings for plastic substrates, 129-34
- Abrasive cutting, mechanisms of polymer wear, 59
- Abrasive slurry, effect on wear rate of polymers, 316
- Abrasive-transfer modes, transition between, PTFE, 159
- Abrasive wear  
 $\gamma$ -irradiated PTFE, 158f
- Abrasive wear--Continued  
 multiple asperity contacts, PTFE, 153  
 polymer wear mechanisms, 31-32  
 polymeric tibial components, 225  
 PTFE, 152
- Absorption-reflection thickness IR spectroscopy (QUARTIR), quantitative, polymer wear analysis, 297
- Acrylic cement, particles, wear of polymeric tibial components, 225
- Active additives, effect of, HDPE-metal transfer fragments, 210
- Adhesion  
 effect on polymer wear, 3-26  
 fibril-craze model, 43  
 initial frictional behavior, polymer-polymer pairs, 21

## Author Index

- Adams, M. J., 375  
 Anderson, J. C., 315  
 Aron, Paul R., 287  
 Atkinson, J. R., 171,215  
 Bahadur, S., 253  
 Belyi, V. A., 205  
 Benz, G., 389  
 Boundy, R. R., 129  
 Briscoe, B. J., 151,303,375  
 Buckley, Donald H., 287  
 Chow, T. S., 67  
 Czichos, Horst, 3  
 Dowson, D., 171,215  
 Eiss, Jr., N. S., 59,135  
 El-Hady Diab, M. M., 171  
 Fukushima, Toshio, 347  
 Gillis, B. J., 171,215  
 Good, Robert J., 39  
 Jones, J. W., 135  
 Kimball, D. J., 129  
 Kirpichenko, Yu. E., 333  
 Krishnan, S., 389  
 Lee, Lieng-Huang, 27,77  
 Lipshitz, Harold, 229  
 Mitra, S. B., 339  
 Motohashi, Kenji, 347  
 Nevzorov, V. V., 205  
 Potter, III, J. R., 59  
 Russell, P. M., 389  
 Shoraka, Fereydoun, 39  
 Stolarski, T. A., 303  
 Sutor, Paul, 269  
 Sviridyonok, A. I., 333  
 Tabor, D., 253  
 Tanaka, Kyuichiro, 103,363  
 Vincent, H. L., 129  
 Wee, T. K., 375  
 Williamson, P. K., 315  
 Winkler, A., 375  
 Yamada, Yoshinori, 103,363  
 Yasuda, H. K., 89  
 Zhang, S. W., 189

## Subject Index

- A
- Abraded metal surfaces, effect on wear rate of HDPE, 255
- Abrasion  
 rubber, by a line contact, 189-202  
 test parameter, predicting in-service bearing life, 316
- Abrasion-resistant coatings for plastic substrates, 129-34
- Abrasive cutting, mechanisms of polymer wear, 59
- Abrasive slurry, effect on wear rate of polymers, 316
- Abrasive-transfer modes, transition between, PTFE, 159
- Abrasive wear  
 $\gamma$ -irradiated PTFE, 158f
- Abrasive wear--Continued  
 multiple asperity contacts, PTFE, 153  
 polymer wear mechanisms, 31-32  
 polymeric tibial components, 225  
 PTFE, 152
- Absorption-reflection thickness IR spectroscopy (QUARTIR), quantitative, polymer wear analysis, 297
- Acrylic cement, particles, wear of polymeric tibial components, 225
- Active additives, effect of, HDPE-metal transfer fragments, 210
- Adhesion  
 effect on polymer wear, 3-26  
 fibril-craze model, 43  
 initial frictional behavior, polymer-polymer pairs, 21

## Adhesion--Continued

- interfacial forces and viscoelastic effects, 39-56
- PI friction, 145
- pin-on-disk wear method, 313
- plasma polymers to substrate polymers, 95
- polysiloxane-silica hybrid resins to plastic substrates, 131
- PTFE transfer film, 162
- various polymers, contact deformation studies, 22f
- Adhesive interactions, polymer-polymer and polymer-metal transfer products, 209
- Adhesive transfer, mechanisms of polymer wear, 59
- Adhesive wear
  - PI, 141
  - polymer wear mechanisms, 28
- Adiabatic systems, heat effects in the failure of a bulk polymer, 40
- AES--See Auger electron spectroscopy
- Aluminum surface, oxidized, QUARTIR determination of molecular coordination of a surfactant, 299f
- Amorphous elastomers, tensile strength, effect of particulate fillers, 197
- Amorphous polymer, wear of pins sliding against steel disk, 124
- Analysis of adhesion separation process, 45-50
- Analytical methods, standardization, friction behavior of polymer-based materials, 333
- Anatomical surface contours, joints, effects on wear rates of articular cartilage, 248
- Annealing, PET, 365
- Articular cartilage
  - description, 230
  - measurement of wear, 234
  - steady-state wear, 239
  - surface features during wear, 242f
  - surface incongruities, 231f
  - wear properties, 229
  - wear with pressure, 240f
  - wear with time, 238f
- Assessment, in-service wear
  - comparison with laboratory, 321
  - related to lab wear data, 319
- Atomic polymerization, chemical structure of monomer, 90
- Auger electron spectroscopy (AES)
  - fluorine, PTFE transfer film, 294f
  - polymer wear, discussion, 293
  - wear analysis, 288

## B

- Backbone structure, main chain, control of polymer wear, 78
- Barrier characteristics, plasma polymers, 97
- Bearing materials, polymers and composites, 315
- Bicyclic step-growth mechanism, plasma polymerization, 96f
- Biomaterials, wear, 215-82
- Bonding
  - analytical tools, 297
  - transfer film of CuS-filled HDPE to metal surface, 265
- Bovine articular cartilage, wear, 229
- Brakegear and railcar bushes, comparison of service and lab data, 320f
- Branches and short segments, networks, plasma polymers, 91
- Brittle polymers
  - abrasive wear, 31
  - crack propagation, 41
- Brittle separation
  - adhering system, under loading, 43
  - craze mechanism, 53
- Burger model, deformation behavior, 12f

## C

- Carbon arc acceleration test, sunshine, masonry coating materials, 350
- Carbon black, effect on rubber abrasion, 197
- Carbon fibers, enhancement of wear resistance, 84
- Carbon-filled PTFE composites
  - influence of environment on wear, 167f
  - wear rate as a function of initial counterface roughness, 160f
- Carbonation, concrete
  - dynamic analysis of the progress, 349
  - related to depth of concrete and finish thickness, 360f
  - retardation effects of polymeric finishes, 358
- Carbonyl groups, effect on wear rate, PI films, 145

- Cartilage
- articular
    - measurement of wear, 234
    - steady-state wear, 239
    - surface features during wear, 242f
    - wear properties, 229
    - wear with pressure, 240f
    - wear with time, 238f
  - displacement under cyclic
    - alternating pressures, 241f
  - under constant load, wear rates, 249
  - wear as a function of time, 237
- Cartilage-cartilage systems
- cross-linked with formaldehyde
    - displacement during intermittent sliding, 245f
    - steady-state wear rates, 245f
    - frictional coefficients, 249
- Cartilage-cross-linked cartilage
- interfacing, wear of articular cartilage, 235
  - schematic, 236f
- Catalysis, synthesis of polysiloxane-silica hybrid resins, 130
- CH<sub>2</sub> linkage, effect on fatigue wear, 63
- Chain entanglement, control of polymer wear, 78
- Chain flexibility, effect on wear rate, PI films, 143
- Chain length, effect on wear rate, PI films, 145
- Chain scission, rupture of a fibril, 41
- Chalking, degradation of masonry coating materials, 353
- Characterization of polymer wear, 287-343
- Chemical characteristics, factors affecting friction, polymer-metal pairs, 334
- Chemical resistance, plastics coated with polysiloxane-silica hybrid resins, 133
- Chemical structure, PI thin films, effect on friction and wear, 135-48
- Chemistry of polymer wear, analytical tools, 290-301
- Coatings
- masonry, surface morphological changes due to outdoor exposure, 350
  - polysiloxane-silica hybrid resins to plastic substrates, 131
  - ultrathin layer of plasma polymer, 95
- Cohesive energy density, dependence of diffusion constant, solubility constant, and permeability constant, 94f
- Composites
- comparison of various lab wear tests, 318f
  - interlaminar toughness, 84
  - self-lubricating graphite-PI, 280
- Compressive strain, articular cartilage, 230
- Concrete carbonation
- dynamic analysis of the progress, 349
  - reinforced, effect of deterioration processes of polymeric materials, 347
  - retardation effects of polymeric finishes, 358
- Conformal polymer-polymer pairs, effect on static friction at the onset of motion, 21
- Contact deformation behavior
- effect of loading and unloading modes, 15
  - main influences, 9
  - polymer pin specimen and steel disk, 123
  - polymers, 3-26
- Contact deformation displacement
- curves, 8f
  - simplified formulas, 16f
  - variation as function of time, 12f
  - various polymers,
    - curves, 16f,17f,19f
- Contact diameter, displacement curves, 8f
- Contact geometry
- effect on polymer wear, pin-on-disk configuration, 303-313
  - fatigue-abrasive wear mechanism, 69f
  - test parameter, effect on predicting in-service bearing life, 316
- Contact stress, total, determination of wear, 70
- Copolymerization, modification through, LCPs, 81
- Copper oxide, as filler, effect on HDPE wear rate, 257
- Copper sulfide, as filler, effect on HDPE wear rate, 257
- Counterface material, effect on predicting in-service bearing life, 316
- Counterface-polymer bonding, analytical tools, 297
- Counterface roughness, UHMWPE, wear factor related to, 181

- Counterface topography, effect on wear of UHMWPE, 171-87
- Counterface variables, effects, self-lubricating graphite-PI composites, 280
- Counterformal polymer-glass contacts, effect on contact deformation behavior, 21
- Covalent bonds, effect on separation of adhesive systems, 53
- Crack formation and crack propagation, fatigue wear, 34
- Crack growth  
per revolution, wear equation of rubber abrasion, 196  
theory of rubber abrasion, 192  
wear of articular cartilage, 248
- Craze fibrils, polymer residue related to drawing, 50
- Craze mechanism  
brittle separation, 53  
separation of an adhering system at or near an interface, 44
- Crazing and failure, polymer, review, 40-43
- Cross-linking  
cartilage-cartilage  
interfacing, wear of articular cartilage, 235  
schematic, 236f  
effect on polymer surface wear, 82  
HDPE-metal transfer fragments, 210  
plasma polymers, 91
- Crystallinity  
condition, PET, 365  
effect on friction and wear, PET, 363-74  
effect on wear rate, PI films, 143  
wear of pins sliding against steel disk, 124
- Cure conditions, polysiloxane-silica hybrid resins to plastic substrates, 131
- Curved thermoplastic polymeric materials, estimation of the contact deformation behavior, 15
- Cyclic pressure, steady-state wear rates, articular cartilage, 247
- D
- Deformation behavior  
analysis of adhesion separation process, 45-50  
contact  
effect of loading and unloading modes, 15
- Deformation behavior--Continued  
main influences, 9  
model, 9  
polymer pin specimen and steel disk, 123  
recovery curves after, 14f  
thermoplastic polymers, 6  
various effects, discussion, 21  
four-parameter or Burger model, 12f  
wear of articular cartilage, 249  
wear of PTFE, 154f
- Deformation component, PI  
friction, 145
- Deformation displacement, contact  
simplified formulas, 16f  
variation as function of time, 12f  
various polymers,  
curves, 16f,17f,19f
- Deformation losses, fatigue wear, 64
- Density, polymer, effect on static friction, 25
- Deterioration of polymers, masonry coating materials, 353
- Diarthrodial joints  
bearing material, wear  
properties, 229  
schematic, 231f
- Diffusion, surface deterioration of exposed polymeric materials, 358
- Diffusion constant, dependence on the cohesive energy density, 94f
- Dimensional recovery, articular cartilage, 230
- Displacement  
cartilage, under cyclic alternating pressures, 241f  
during intermittent sliding, cartilage-cartilage cross-linked with formaldehyde, 245f
- Displacement curves  
contact deformation, 8f  
contact diameter, 8f  
polymer-glass contacts, 10f
- Dissipation mechanism, brittle separation, 43
- Double bond, effect on wear rate, PI films, 143
- Drawing and rupture, fibril, bounds of prediction, 55
- Dry abrasive wear, physical process, 200
- Dry wear factors, UHMWPE on steel, 181
- Dual-index holographic contouring system, prosthetic knee-joint component, 220
- Ductile fracture energies of various polymers, 33f
- Ductile polymers, abrasive wear, 31

- Dyes, permeabilities, effect of plasma polymer coating, 97
- Dynamic analysis, carbonation of concrete, 349
- Dynamic processes, deterioration of polymers, 348
- Epoxies, siloxane-modified, wear rates, 62
- ESCA--See Electron spectroscopy for chemical analysis
- Extended Hertzian formula, contact deformation displacement in loading-unloading cycles, 21

## E

- Elastic deformation processes, effect on contact deformation behavior, 9
- Elastic energy, release, rupture of a fibril, 41
- Elastic modulus  
related to wear rate  
discussion, 64  
PI thin films, 141  
various polymers, 62
- Elastomers  
abrasive wear, 32  
amorphous, tensile strength, effect of particulate fillers, 197
- Electrical charge conveyor, comparison of in-service and laboratory wear, 323
- Electron diffraction pattern analysis, HDPE wear fragments, 262
- Electron microscopy, PET-metal contact, effect of crystallinity, 370
- Electron spectroscopy for chemical analysis (ESCA)  
plasma polymers  
effect of substrate temperature, 91  
spectra, 92f  
surfaces treated with plasma polymers, 99
- Elemental structural analysis, polymer transfer films, 295
- Ellipsometer, thickness of a polymer film, 292f
- Ellipsometric techniques, characterization and measurement of polymer wear, 290
- Energetics, polymer wear, 27-36
- Energy dissipation, separation of adhesive systems, 49
- Engineering thermoplastic polymers, characteristics of transfer and wear products, 206
- Entanglement density, control of polymer wear, 78
- Environmental changes, effect on fatigue failure, 66

## F

- Failure and crazing, polymer, review, 40-43
- Fatigue, mechanisms of polymer wear, 59
- Fatigue-abrasion wear mechanism, polymeric surfaces, 67-74
- Fatigue crack propagation behavior of various polymers, 35f
- Fatigue resistance coefficients of various polymers, 34t
- Fatigue wear  
PIs, 141  
polymer wear mechanisms, 32,34-35  
polymers, 59-66
- Femoral metallic components, penetration into polymeric tibial components 215-27
- Fiber  
glass, temperature dependence of friction and wear of some heat-resistant polymers, 127  
graphite, effect on tribological performance of graphite-PI composites, 280  
various types, comparison of properties, 80
- Fiber-reinforced PIs sliding against steel and silicon nitride, tribology, 269-83
- Fibril(s)  
attached to a solid, 46f  
craze, polymer residue related to drawing, 50  
drawing, separation of adhesive systems, 47  
drawing and rupture, bounds of prediction, 55  
formation and rupture, 41  
rupture  
plastic necking down, 43  
pressure-sensitive tapes, 52  
structure, peeling a pressure-sensitive tape, 42f
- Fibril-craze model, adhering and wearing systems, 43



Fibrillation, wear of articular cartilage, 248

Fibrous or particulate reinforcement, control of polymer wear, 83

Filaments  
 polymeric, degradation and wear, 347-400  
 stretched, mechanisms of instability, 42f

Fillers, role in friction and wear behavior of HDPE, 253-66

Film, polymeric, degradation and wear, 347-400

Film mechanical properties, PIs, 137

Film thickness  
 polymer, XPS measurement, 295  
 variation with deposition time, 292f

Flake formation, PMMA, PC, PTFE wear, 288

Flexibility  
 backbone, effect on polymer wear, 78  
 designed backbone, PIs, 79f  
 related to wear rate, PI thin films, 141

Fluid exudation and reimpibition, wear of articular cartilage, 249

Fluorine auger electron spectra (AES), PTFE transfer film, 294f

Fluorine X-ray photoelectron spectroscopy (XPS), PTFE transfer film, 294f

Foam modulus and particle properties, wear, 72f

Formaldehyde cross-linking, effect on wear of articular cartilage, 229-50

Four-parameter model, deformation behavior, 12f

Fracture energetics, polymer wear, 27-36

Fracture energy, related to fatigue resistance, 83

Freeman-Swanson prosthesis, in knee-joint simulator, 218

Frequency, effect on wear of articular cartilage, 241f

Friction  
 effect of chemical structure, PI thin films, 135-48  
 factors influencing metal-polymer pairs, 334  
 HDPE, role of fillers, 253-66  
 heat-resistant polymers, effect of temperature, 103-127  
 initial static, definition, 25  
 initiation processes, 3  
 investigational methods, 335  
 PET pins sliding against stainless steel disk, effect of crystallinity, 367

Friction-Continued  
 polymer-polymer pairs, various, 19f  
 sliding, and wear experiments, PTFE on nickel, 293  
 standardization of test methods, 333  
 static  
 effect of adhesion component, 21  
 polymer-polymer pairs, 15  
 steel sphere on various PET specimens, 368f  
 various polymers, contact deformation studies, 22f  
 wear  
 HDPE against metallic disk surfaces, 255  
 PET, effect, crystallinity, 363-74  
 self-lubricating graphite-PI composites against steel, 274  
 surface damage, graphite-PI composites against silicon nitride, 278

Friction-zone temperature, dependence on load and velocity, 338f

Frictional coefficient  
 as function of sliding distance, various polymer-polymer pairs, 18  
 cartilage-cartilage, 249  
 dependence on load and velocity, 338f  
 during wear track initiation, PIs, 138f  
 effect of structure, PIs, 139f  
 effective, versus wear, 74f  
 friction and wear tests, PI thin films, 137  
 function of sliding, self-lubricating graphite-PI composites, 276f  
 HDPE against an abraded steel disk, 260f  
 HDPE against ground steel disk, 259f  
 HDPE sliding against smooth glass and brass surfaces, 264f  
 HDPE-glass surfaces, 258f  
 HDPE-metal surfaces, 256f,263f  
 measurement, pin-on-disk configuration, 308  
 PIs, effect of structure, 140  
 static, PET, 367  
 variations  
 sliding of steel sphere on various polymers, 107f  
 various polymers with disk temperature, 125f  
 various polymers, variations with load, 106

Frictional properties  
 novel methods for accelerated evaluation, 336

Frictional properties--Continued

- PET, procedures for studying, 364
- various polymers, pin-on-disk method, 312
- Frictional surfaces, microscopic examinations after wear, 112
- Frictional track, width, related to load, PET, 368f
- Frictional work and work of adhesion, correlation, 22f

## G

- Gamma radiation, effect on transfer wear of PTFE, 163
- Gases and vapors, permeability, conventional polymers and plasma polymers, 93
- Geometry of polymeric wear pin, UHMWPE, 174f
- Glass, smooth, and brass surfaces, HDPE wear, 264f
- Glass fibers
  - enhancement of wear resistance, 84
  - temperature dependence of friction and wear of some heat-resistant polymers, 127
- Glow discharge polymers, plasma polymerization and plasma polymers, 90
- Graphite
  - fibers
    - effect on tribological performance of graphite-PI composites, 280
    - enhancement of wear resistance, 84
    - filler, effect on HDPE wear rate, 25f
    - fine weave and coarse weave, unit cell comparison, 273f
  - Graphite-polyimide composites, self-lubricating, wear and friction against steel and silicon nitride, 269-83
- Growth mechanism, plasma polymerization, 95

## H

- Hardness
  - modulus of polymeric substrates versus wear, 73f
  - polymer, effects in the failure of a bulk polymer, 40

Hardness--Continued

- variation of wear resistance, PET, 371f
- HDPE--See High density polyethylene
- Heat-resistant polymers, effect of temperature on friction and wear, 103-127
- Hertzian formula, extended, contact deformation displacement in loading-unloading cycles, 21
- High-density polyethylene (HDPE)
  - role of fillers in friction and wear behavior, 253-66
  - wear behavior, pin-on-disk method, 312
- High-density polyethylene (HDPE)-metal systems, molecular features of transfer fragments, 205-211
- Hip and knee prostheses, human, comparison of wear data from service and laboratory, 321
- Holography, reflexive dual-index, penetration of the metallic femoral component into the polymeric tibial component, 219
- Horizontal pin-on-disk configuration, schematic representation, 305f
- Hybrid resins, polysiloxane-silica, abrasion-resistant coatings for plastic substrates, 129-34
- Hydrophilic surfaces, enhancement by plasma polymers, 99
- Hydrophobic surfaces, enhancement by plasma polymers, 99
- p-Hydroxybenzoic acid (PHB), copolymerization, 81

## I

- IETS--See Inelastic electron tunneling spectroscopy
- Imide bond formation, synthetic processes of PI and PAI, 126f
- In-service wear assessment, related to lab wear data, 319,321
- Inelastic electron tunneling spectroscopy (IETS), wear analysis, 288
- Inert gas plasma treatment, polymer surface modification, 82
- Inherent viscosity, wear of PI films, 147
- Interface analysis, analytical tools, 293
- Interfacial adhesion
  - analytical tools, 297

Interfacial adhesion--Continued

- effect on contact deformation behavior, 9
- effect on static friction at the onset of motion, 21
- Interfacial craze formation, separation of an adhering system at or near an interface, 44
  - Interfacial forces and viscoelastic effects, joint role in polymer adhesion and wear, 39-56
- Interfacial peeling at fibril base, separation of adhesive systems, 47
- Interfacial properties
  - effect on adhesive wear, 28
  - tribological effects, 30t
- Interfacial separation, pressure-sensitive tapes, 52
- Interfacial shear stresses, effect, surfaces PTFE, 166
- Interfacial temperatures, effect on HDPE wear rate for various surfaces, 268
- Interfacial voids, separation of an adhering system at or near an interface, 4
- Interfacing of cartilage against cross-linked cartilage, wear of articular cartilage, 235
- Interlaminar toughness of composites, 84
- Interpenetrating networks (IPN), control of polymer wear, 84
- Ion-depth profiling, polymer wear, discussion, 293
- IPN--See Interpenetrating networks
- IR absorption spectra, degradation of masonry coating materials, 353
- Iridium and titanium, PTFE wear film, depth profiling, 296f
- Iridium substrate, PTFE wear film, SAM, 296f
- Irradiation
  - PTFE
    - abrasive wear, 158f
    - wear rate, 164f
    - sunshine carbon arc, masonry coating materials, 350
- Isothermal systems, heat effects in the failure of a bulk polymer, 40

## J

- Joints, total replacement, discussion, 216

## K

- Kevlar, properties, 80
- Kevlar fibers, enhancement of wear resistance, 84
- Kinetic and static friction, relation between the coefficient, 369f
- Knee and hip prostheses, human, comparison of wear data from service and laboratory, 321
- Knee-joint simulator, penetration of metallic femoral components into polymeric tibial components observed, 215-27

## L

- Lapped metal surfaces, effect on wear rate of HDPE, 255
- LCP--See Liquid crystalline polymers
- LDPE--See Low-density polyethylene
- Lead oxide, as filler, effect on HDPE wear rate, 257
- Leeds prosthesis, in knee-joint simulator, 218
- Linear polyethenes, wear behavior, pin-on-disk method, 312
- Liquid crystalline polymers (LCP)
  - lyotropic, properties, 80
  - modification through copolymerization, 81
  - thermotropic, 81
- Liquid crystalline structure, control of polymer wear, 79
- Loading
  - constant, wear rates of cartilage under, 249
  - dependence of friction-zone temperature and frictional coefficient, 338f
  - effect on contact deformation, 15
  - effect on fatigue wear, 63
  - plot with sliding velocity, wear rate dependence, 340f
  - test parameter, effect on predicting in-service bearing life, 316
- Low-damage secondary ion mass spectrometry (SIMS), wear analysis, 288
- Low-density polyethylene (LDPE), wear behavior, pin-on-disk method, 312
- Lubricant, test parameter, effect on predicting in-service bearing life, 316

Lubricant entrapment, deformation studies, 24  
 Lubrication  
   effect on contact deformation behavior, 9  
   PTFE, and wear, 163  
 Lyotropic liquid crystalline polymers, properties, 80

M

Macroscopic peeling separation, mechanism, 48  
 Marine bearings, comparison between the laboratory and in-service wear, 323  
 Masonry coating materials, surface morphological changes due to outdoor exposure, 350  
 Material parameters, various polymers, contact deformation studies, 14f  
 Mathematical description of the processes of rubber abrasion, 190  
 Mechanical properties  
   tensile stresses, various polymers, 62  
   tribological effects, 30t  
 Metal-polymer pairs, factors influencing friction, 334  
 Metal surfaces, various, effect on wear rate of HDPE, 255  
 Metallic femoral components, penetration into polymeric tibial components, knee-joint simulator, 215-27  
 Microflaking, degradation of masonry coating materials, 353  
 Microscopic examinations, polymer-metal contact surfaces, 112  
 Microstructure  
   contact deformation mechanisms, various polymers, 13  
   control of polymer wear, 79  
   tribological effects, 30t  
 Model  
   contact deformation of polymers, 9  
   deterioration processes of polymeric materials, 348  
   fatigue wear, 60  
   neutralization of concrete, 349  
   physical, theory of rubber abrasion, 194f  
   rubber abrasion, 190  
   scratch hardness, PTFE, 155  
   tribometric schematics, 335  
 Modulus and hardness of polymeric substrates versus wear, 73f

Moisture, effect on static friction, 25  
 Molecular weight  
   and distribution, control of polymer wear, 78  
   effect on wear rate, PI films, 145  
 Morphological change, degradation of masonry coating materials, 353  
 Motion, test parameter, effect on predicting in-service bearing life, 316  
 Mylar, Raman spectrum, 300f

N

Networks of short segments and branches, plasma polymers, 91  
 Neutralization of concrete, main assumptions, 349  
 Nonlinear viscoelastic parameters, critical to adhesion, 54  
 Nylon 6 film, permeability, effect of plasma polymer coating, 97  
 Nylon 66, microstructure, 8f

O

Optical microscopy  
   disk surfaces rubbed against  
     PAI, 119f  
     PEEK, 120f  
     PES, 122f  
     PI, 118f  
     PPS, 121f  
   PET wear particles, 371f  
   PET-metal contact, effect of crystallinity, 370  
   pin-on-disk configuration, 311f  
   PTFE wear debris, 308  
 Organic fibers, enhancement of wear resistance, 84  
 Organic structural analysis, polymer transfer films, 295  
 Organic surface, conversion into a ceramic surface, 83  
 Osteoarthritic cartilage, fibrillation, 248  
 Outdoor exposure, masonry coating materials, 350  
 Oxygen concentration, surface, degradation of masonry coating materials, 353  
 Oxygen linkage  
   effect on fatigue wear, 63

## Oxygen linkage--Continued

- effect on wear rate, PI films, 143
- Oxygen permeability, various polymers, 93

## p

- PAI--See Polyamide-imide
- Particle properties and foam modulus, wear, 72f
- Particulate fillers, effect on rubber abrasion, 197
- Particulate or fibrous reinforcement, control of polymer wear, 83
- PC--See Polycarbonate
- PEEK--See Polyether-ether-ketone
- Performance limits, estimation based on friction parameters, 340
- Permeability
  - dyes, effect of plasma polymer coating, 97
  - gases and vapors, conventional polymers and plasma polymers, 93
- PES--See Poly(ether sulfone)
- PET--See Poly(ethylene terephthalate)
- PHB--See *p*-Hydroxybenzoic acid
- Phosphate globules, worn surface of self-lubricating graphite-PI composites after sliding against silicon nitride, 282f
- Photochemical deterioration processes, polymeric coating materials, 358
- Photooxidation
  - degradation of masonry coating materials, 353
  - influence on the distribution of oxygen, polymeric materials, 357f
- Photopolymerization, surface, surface modification techniques, control of polymer wear, 83
- Physical model, rubber abrasion, theory, 194f
- Physical parameters, factors affecting friction, polymer-metal pairs, 334
- Physical processes, rubber abrasion, 189
- Physical properties, tribological effects, 30t
- PI--See Polyimide
- Pin-on-disk configuration
  - wear of polymers, 303-313
  - wear test methods, 316
- Pin-on-disk configuration, friction and wear device, 290
- Plasma treatment
  - plasma polymerization, modification of polymer surfaces, 89-102
  - surface modification techniques, control of polymer wear, 82
- Plastic deformation of a compressed particle, 71
- Plastic substrates, abrasion-resistant coatings, 129-34
- PMMA--See Poly(methyl methacrylate)
- Poisson's ratio, various polymers, 62
- Polar side groups, effect on wear rate, PI films, 143
- Polarizing micrographs, various PET specimens, 366f
- Polyacetyl material, in-service wear related to lab data, 326
- Poly(alkyl methacrylate) films, SIMS, 297
- Polyamide 66, microstructure, 8f
- Polyamide-imide (PAI)
  - SEM and TEM analysis of wear surfaces, 112
  - synthetic processes, imide bond formation, 126f
  - variations in coefficient of friction and wear depth, 106
  - various temperatures, polymer-metal wear, 123
  - wear of pins sliding against steel disk, 124
- Polycarbonate (PC)
  - micrographs, 288
  - wear material and process parameters, 72
  - wear surface, 71
- Polyether-ether-ketone (PEEK)
  - SEM and TEM analysis of wear surfaces, 112
  - variations in coefficient of friction and wear depth, 106
  - various temperatures, polymer-metal wear, 123
  - wear of pins sliding against steel disk, 124
- Poly(ether sulfone) (PES)
  - SEM and TEM analysis of wear surfaces, 112
  - variations in coefficient of friction and wear depth, 106
  - various temperatures, polymer-metal wear, 123
  - wear of pins sliding against steel disk, 124
- Polyethylene
  - high-density, role of fillers in friction and wear behavior, 253-66

- Polyethylene--Continued**  
 ultra-high molecular weight, influence of counterface topography, 171-87
- Poly(ethylene terephthalate) (PET)**  
 copolymer with PHB, mechanical properties, 81  
 copolymerization, 81  
 effect of the degree of crystallinity on friction and wear, 363  
 flat surfaces sliding against steel sphere, effect of crystallinity, 365  
 frictional properties, procedures for studying, 364  
 pins sliding against stainless steel disk  
 friction, effect of crystallinity, 367  
 wear, effect of crystallinity, 367  
 variation of wear resistance with hardness, 371f  
 wear particles, optical micrographs, 371f
- Polyimide (PI)**  
 fiber-reinforced, sliding against steel and silicon nitride, tribology, 269-83  
 film, plot of stress versus temperatures, 301f  
 SEM and TEM analysis of wear surfaces, 112  
 synthetic processes, imide bond formation, 126f  
 thin films, effect of chemical structure on friction and wear, 135-48  
 variations in coefficient of friction and wear depth, 106  
 various temperatures, polymer-metal wear, 123  
 wear of pins sliding against steel disk, 124  
 wear rates, 63  
 with designed backbone flexibility, 79f
- Poly(lauryl methacrylate), static SIMS spectrum, 299f**
- Polymer-based materials, used as dry bearing materials, 315**
- Polymer composites**  
 comparison of laboratory wear, various wear tests, 318f  
 various, correlation of lab and service wear data, 322f, 324f, 325f, 327f, 328f  
 wear, 215-82
- Polymer-counterface bonding, analytical tools, 297**
- Polymer deposition, separation of an adhering system, 44**
- Polymer-glass contact, counterformal, effect on contact deformation behavior, 21**
- Polymer-metal contact**  
 coefficient of friction and wear depth, 106  
 effect of the degree of crystallinity on friction and wear, 363  
 factors influencing friction, 334  
 molecular features, transfer products, 205-211
- Polymer-polymer contact**  
 dominant mechanism of polymer friction, 28  
 friction, various polymers, 19f
- Polymer residue, related to drawing of craze fibrils, 50**
- Polymer-solid contact**  
 analysis of adhesion separation process, 45-50  
 separation of adhesion, 43
- Polymer structure, analytical tools, 298**
- Polymer transfer film, mechanism of wear rate reduction, 267**
- Polymer wear**  
 control, 77  
 mechanisms, 3-74  
 profiling, analytical tools, 288
- Polymeric finishes, effect on retardation of concrete carbonation, 358**
- Polymeric materials, influence of photooxidation on the distribution of oxygen, 357f**
- Polymeric surfaces, fatigue-abrasive wear mechanism, 67-74**
- Polymeric tibial components, penetration of metallic femoral components, 216**
- Polymerization, plasma, and plasma treatment, modification of polymer surfaces, 89-102**
- Poly(methyl methacrylate) (PMMA)**  
 micrographs, 288  
 wear behavior, pin-on-disk method, 312
- Polyoxymethylene, microstructure, 7f**
- Poly(phenylene sulfide) (PPS)**  
 SEM and TEM analysis of wear surfaces, 112  
 variations in coefficient of friction and wear depth, 106  
 various temperatures, polymer-metal wear, 123  
 wear of pins sliding against steel disk, 124

Polysiloxane-silica hybrid resins, abrasion-resistant coatings for plastic substrates, 129-34

Polystyrene (PS), outdoor exposure, change in IR absorption, 357

Poly(tetrafluoroethylene) (PTFE) effect of crystallinity on wear, 363 micrographs, 288 total replacement hip joints, 216 transfer film average thickness on nickel at various sliding speeds in vacuum, 296f fluorine AES, 294f fluorine XPS, 294f wear, 151-67 wear behavior, pin-on-disk method, 312 wear film, titanium and iridium, depth profiling, SAM, 296f

Polythenes, linear, wear behavior, pin-on-disk method, 312

PPS--See Poly(phenylene sulfide)

Pressure changing, effect on wear rate, articular cartilage, 239 cyclic, steady-state wear rates under, articular cartilage, 247

Pressure-sensitive tape, peeling, fibrillar structure, 42f

Profiling polymer wear, analytical tools, 288

Profilometer, quantification of polymer wear, 290

Prosthesis Freeman-Swanson, in knee-joint simulator, 218 human hip and knee, comparison of wear data from service and laboratory, 321 Leeds, in knee-joint simulator, 218

PS--See Polystyrene

PTFE--See Poly(tetrafluoroethylene)

## Q

Quantitative absorption-reflection thickness IR spectroscopy (QUARTIR), polymer wear analysis, 297

## R

Radiation effect on wear, PTFE, 157 gamma, effect on transfer wear of PTFE, 163

Radius effect, wear behavior, pin-on-disk method, 312

Railcar and brakegear bushes, comparison of service and lab data, 320f

Railway industry, comparison of wear data from service and laboratory, 321

RAIR--See Reflection-absorption IR spectroscopy

Raman spectroscopy analysis of polymer wear, 298 Mylar, 300f

Ratner-Lancaster plot, wear of PTFE, 156f

Reciprocating tests, wear test methods, 316

Recovery curves after contact deformation, 14f

Reflection-absorption IR spectroscopy (RAIR), wear analysis, 288

Reflexive dual-index holography, penetration of the metallic femoral component into the polymeric tibial component, 219

Relaxation times, possible irreversible viscoplastic contact deformation, 13

Retardation effects of polymeric finishes, carbonation of concrete, 358

Ridge formation, theory of rubber abrasion, 191f

Rigidity, effect of flexible oxygen linkage, PIs, 144f

Roughness, effect on separation of adhesive systems, 53

Rubber abrasion by a line contact, theory, 189-202

Rubbing conditions, effect of, molecular characteristics of HDPE transfer products, 207

Rupture and drawing, fibril, bounds of prediction, 55

Rupture process, theory of rubber abrasion, 192,194f

## S

SAM--See Scanning auger microscopy

Scanning auger microscopy (SAM) PTFE wear film on an iridium substrate, 296f wear analysis, 288

Scanning electron microscopy (SEM) degradation of masonry coating materials, 350,352f,354f,355f,356f

- Scanning electron microscopy (SEM)--  
Continued  
 eroded thermoplastic material  
 surfaces, 289f  
 wear surface  
 PEEK, 114f  
 PPS, 115f  
 wear tracks, PI thin films, 140  
 Scratch hardness, abrasive wear of  
 PTFE, 152  
 Secondary ion mass spectrometry  
 (SIMS), poly(lauryl methacrylate),  
 static, 299f  
 Segments, short, and branches,  
 networks, plasma polymers, 91  
 Self-lubricating composites,  
 composition, 272t  
 SEM--See Scanning electron microscopy  
 Semicrystalline thermoplastic  
 polymers, characteristic  
 appearances, 6  
 Separation, within a bulk polymer,  
 compared to at or near an  
 interface, 44  
 Separation criterion for a flat  
 surface, separation of adhesive  
 systems, 49  
 Separation process, adhesion,  
 analysis, 45-50  
 Service and specific wear rate and  
 application, relationship  
 between, 329f  
 Shear, effect of contact  
 deformation, 25  
 Shear strengths, variations of various  
 polymers with temperature, 108f  
 Shear stress to shear strength, ratio,  
 effect on fatigue wear, 63  
 Shear-thinning, effect on adhesion, 54  
 Silanols, control of spontaneous  
 condensation, 130  
 Silica, surface of graphite-PI com-  
 posites after sliding against  
 silicon nitride, 281  
 Silicon nitride  
 counterface, self-lubricating  
 graphite-PI composites, 278  
 frictional coefficient as a function  
 of sliding graphite-PI  
 duration, 276f  
 Silicon-containing layer, surface of  
 self-lubricating graphite-PI com-  
 posites after sliding against  
 silicon nitride, 282f  
 Silicone modifications, surface  
 modification techniques, control  
 of polymer wear, 83  
 Siloxane-modified epoxies, wear  
 rates, 62
- SIMS--See Secondary ion mass  
 spectrometry  
 Sliding  
 articular cartilage, 230  
 distance related to wear, pin-on-  
 disk configuration, 308  
 friction and wear experiments, PTFE  
 on nickel, 293  
 HDPE-glass surfaces, 257  
 intermittent, effect on wear of  
 articular cartilage, 229-50  
 load velocity, wear rate  
 dependence, 340f  
 speed variation of the wear peak of  
 PI, 126f  
 steel sphere on flat PET surfaces,  
 effect of crystallinity, 365  
 Solid, polymer, surface properties,  
 variation, 98  
 Solid lubrication, graphite-PI  
 composites, 270  
 Solubility constant, dependence on the  
 cohesive energy density, 94f  
 Speed, test parameter, effect on  
 predicting in-service bearing  
 life, 316  
 Stainless steel disk, PET sliding  
 wear, effect of crystallinity, 367  
 State criterion of rubber abrasion,  
 steady to unsteady, 200  
 Static friction  
 coefficient related to kinetic  
 coefficient, 369f  
 effect of adhesion component, 21  
 initial, definition, 25  
 polymer-polymer pairs, 15  
 polymers, 3-26  
 Static secondary ion mass spectrometry  
 (SIMS)  
 poly(lauryl methacrylate), 299f  
 polymer wear analysis, 297  
 Steady-state friction, various  
 polymer-metal contacts, 123  
 Steady-state wear  
 articular cartilage, 239  
 cartilage under intermittent  
 sliding, 246f  
 cartilage-cartilage cross-linked  
 with formaldehyde, 245f  
 equation of rubber abrasion, 196  
 fatigue wear, 59  
 friction and wear tests, PI thin  
 films, 137  
 HDPE against various surfaces, 262  
 PIs, 141  
 under cyclic pressures, articular  
 cartilage, 247



- Steel, frictional coefficient as a function of duration of sliding, self-lubricating graphite-PI composites, 276f
- Steel counterface, self-lubricating graphite-PI composites, 274
- Steel sphere on flat PET surfaces, sliding, effect of crystallinity, 365
- Steel surface, effect on HDPE wear, 265
- Step-growth mechanism, bicyclic, plasma polymerization, 96f
- Strain hardening-softening effects, effect on contact deformation behavior, 9
- Strength polymer, effects in the failure of a bulk polymer, 40
- Stress  
plot vs. temperature for a PI film, 301f  
polymers, analytical tools, 298
- Stress concentration, isolated, abrasive wear of PTFE, 152
- Stress relaxation, articular cartilage, 230
- Structural design features, control of polymer wear, 78
- Structure  
chemical, PI thin films, effect on friction and wear, 135-48  
factors affecting friction, polymer-metal pairs, 334  
polymer, analytical tools, 298
- Stylus tracking, polymer wear, 290
- Substrate polymers, adhesion of plasma polymers, 95
- Substrate-transfer film interface, 162
- Sulfur, free, effect on HDPE wear rate, 262
- Sunshine carbon arc acceleration test, masonry coating materials, 350
- Surface characteristics  
anatomical, joints, effects on wear rates of articular cartilage, 248  
articular cartilage during wear, 237,242f  
PET-metal contact, effect of crystallinity, 373  
unperturbable, plasma polymers, 98-102  
wear of articular cartilage, 239
- Surface damage, wear of PTFE, 156f
- Surface drawing mechanism  
analysis of adhesion separation process, 45-50  
rupture of a fibril, 41
- Surface energetics, polymer wear, 27-36
- Surface finish  
effect on HDPE wear rate, 257  
test parameter, effect on predicting in-service bearing life, 316
- Surface mass transfer resistance, influence, progress of carbonation, 360f
- Surface modifications  
control of polymer wear, 82-83  
plasma treatment and plasma polymerization, 89-102
- Surface morphology, degradation of masonry coating materials, 350
- Surface oxygen concentration, degradation of masonry coating materials, 353
- Surface properties  
plastics coated with polysiloxane-silica hybrid resins, 132  
polymer solid, variation, 98  
tribological effects, 30t
- Surface roughness parameter, HDPE wear, 267
- Surface texture  
effect on HDPE transfer film formation and bonding capability, 255  
effect on HDPE wear rate, 257
- Surface wear  
analytical tools, 293  
friction damage, graphite-PI composites against silicon nitride, 278  
PTFE as a function of time, 291f  
self-lubricating graphite-PI after sliding against steel and silicon nitride, 279f
- Synovial joints, total replacement, 216
- Synthesis, polysiloxane-silica hybrid resins, 130
- System dependent aspect, plasma polymerization, 90

## T

- Taylor instability mechanism, formation of fibrils, 44
- TEM--See Transmission electron microscopy
- Temperature  
ambient, test parameter, effect on predicting in-service bearing life, 316

- Temperature--Continued  
 effect on friction and wear, 103-127  
 effect on tribological performance of graphite-PI composites, 280  
 friction zone, dependence on load and velocity, 338f  
 measurement of effect on polymer stresses, 301  
 plot vs. stress for a PI film, 301f  
 substrate, effect on plasma polymerization, 91
- Temperature dependence, yield strength of fibrils, 51
- Temperature rise, peeling separation, pressure-sensitive tape, 43
- Tensile rupture ratio  
 plot vs. state criterion of rubber abrasion, 201f  
 related to rubber abrasion, 200  
 theory of rubber abrasion, 192
- Tensile strength  
 amorphous elastomers, effect of particulate fillers, 197  
 related to wear rate, PI thin films, 141
- Tensile stress  
 maximum, sphere sliding on a plane, 61  
 mechanical properties, various polymers, 62
- Tensile stress-yield strength ratio, effect on fatigue wear, 63
- Test parameters, correlation of laboratory data to in-service data, 317
- Thermal deposition, study of molecular features of HDPE transfer products, 205
- Thermoplastic material surfaces, eroded, SEM micrographs, 289f
- Thermoplastic polymers  
 contact deformation, 6  
 curved, estimation of the contact deformation behavior, 15  
 engineering, characteristics of transfer and wear products, 206  
 semi-crystalline, characteristic appearances, 6
- Thermotropic liquid crystalline polymers, 81
- Thin film identification, characterization and measurement of polymer wear, 290
- Thrust washer, wear test methods, 316
- Time varying loads, effect on wear of articular cartilage, 229-50
- Titanium and iridium, PTFE wear film, depth profiling, 296f
- Toughness and abrasive wear, correlation, PTFE, 155
- Transfer and abrasive modes, transition between, PTFE, 159
- Transfer film  
 characterization and measurement of polymer wear, 290  
 effect of water on formation, UHMWPE on steel, 186  
 HDPE-metal surfaces, 263f  
 PTFE  
 average thickness on nickel at various sliding speeds in vacuum, 296f  
 fluorine AES and XPS, 294f  
 sliding, HDPE-metal surfaces, 261f  
 UHMWPE on steel, wear ratio, 181
- Transfer film-substrate interface, 162
- Transfer mode, general classification, PTFE, 161
- Transfer process, various polymers, pin-on-disk method, 312
- Transfer products, polymer-metal systems, molecular features, 205-211
- Transfer wear  
 PTFE, 159,161  
 rates, PTFE composites, 165f
- Transition between abrasive and transfer modes, PTFE, 159
- Transmission electron microscopy (TEM)  
 disk surfaces rubbed against PI, 116f  
 PET-metal contact, effect of crystallinity, 370  
 worn PI surfaces, 113f
- Tribochemical wear, polymer wear mechanisms, 36
- Tribological behavior  
 fiber-reinforced PIs sliding against steel and silicon nitride, 269-83  
 graphite-PI composites, effect of graphite fibers and temperature, 280  
 HDPE, 253  
 methods available for evaluating, 335  
 PIs, 136  
 polymers, 29f,151-211  
 total replacement knee joints, 215
- Tribological processes, definition, 3
- Tribological properties, polymers, 30t
- Tribometer  
 block diagram, 7f  
 photograph, 5f
- Tribotechnical properties  
 evaluation, polymer-based materials, 336  
 testing center, 338f

## U

- Ultra-high molecular weight polyethylene (UHMWPE)
  - influence of counterface topography, 171-87
  - total replacement hip joints, 216
  - wear behavior, pin-on-disk method, 312
- Unloading mode, effect on contact deformation, 15,21
- Unperturbable surface characteristics, from plasma polymers, 102
- Unsteady state, abrasion process, 197
- Unsteady state dynamics, main assumptions, 348
- UV energy distribution, absorbed, outdoor exposure test, 359f

## V

- Vapors and gases, permeability, conventional polymers and plasma polymers, 93
- Velocity, dependence of friction zone temperature and frictional coefficient, 338f
- Vertical pin-on-disk apparatus, schematic representation, 305f
- Viscoelastic deformation processes, effect on contact deformation behavior, 9
- Viscoelastic effects and interfacial forces, polymer adhesion and wear, 39-56
- Viscoelasticity
  - contact deformation, effect of loading and unloading modes, 15
  - effect on contact deformation behavior, 21
  - effect on polymer wear, 3-26
  - influence on contact deformation behavior, 11
  - nonlinear, critical to adhesion, 54
- Viscoplastic deformation processes, effect on contact deformation behavior, 9

## W

- Water, effect on influence of counterface topography on wear rate of UHMWPE, 171-87

- Water vapor permeability, various polymers, 93

## Wear

- effect of chemical structure, PI thin films, 135-48
- fibril-craze model, 43
- foam modulus and particle properties, 72f
- friction
  - and surface damage, graphite-PI composites against silicon nitride, 278
  - HDPE against metallic disk surfaces, 255
  - PET, effect of crystallinity, 363-74
  - PTFE on nickel, 293
  - self-lubricating graphite-PI composites against steel, 274
- HDPE
  - against an abraded steel disk, 260f
  - against ground steel disk, 259f
  - against metal surfaces, 256f
  - against smooth glass and brass surfaces, 264f
  - role of fillers, 253-66
- heat-resistant polymers, effect of temperature, 103-127
- in-service assessment
  - comparison with laboratory data, 321
  - related to lab wear data, 319
- measurement, articular cartilage, 234
- plot vs. effective frictional coefficient, 74f
- plot vs. modulus and hardness of polymeric substrates, 73f
- polycarbonate surface, 71
- PTFE, 151-67
  - related to sliding distance, pin-on-disk configuration, 308
- standardization of test methods, 333
- total contact stress, 70
- weight loss of material, pin-on-disk configuration, 309f
- Wear curve, general processes of rubber abrasion, 193,195f
- Wear debris, PTFE, pin-on-disk configuration, 308
- Wear equation
  - general processes of rubber abrasion, 193
  - rubber abrasion in steady state, 200
- Wear factors
  - knee prosthesis, 225
  - related to counterface roughness, UHMWPE, 181

- Wear groove, formation, effect on friction coefficient, 64
- Wear machine, six-head linear reciprocating, UHMWPE films on steel, 173f
- Wear particle  
 loose, three stages in formation, 31  
 PET, optical micrographs, 371f
- Wear processes, initiation, 3
- Wear rate  
 cartilage under constant load, 249  
 dependence on load and sliding velocity, 340f  
 equation, abrasion of rubbers and their vulcanizates, 21  
 PET pins sliding against stainless steel disk, effect of crystallinity, 367  
 pin-on-disk configuration, 310f,311f  
 PIs, 63  
 plot vs. frictional work, 198f  
 reduction mechanism, polymer transfer film, 267  
 siloxane-modified epoxies, 62  
 specific and service and application, relationship between, 329f  
 steady state, under cyclic pressures, articular cartilage, 247
- Wear resistance, variation with hardness, PET, 371f
- Wear scar, knee-joint prosthetic components, 223f,224f,227f
- Wear surface, visual observation, analytical tools, 288
- Wear testing  
 frictional properties of PET, 364  
 laboratory, related to in-service wear, 315-330
- Wear track initiation data, various polymers, 61
- Wear volume, brittle polymers, simple expression, 31
- Wet wear factors, UHMWPE on steel, 181
- Work of friction and adhesion, various polymers, contact deformation studies, 22f
- Working capacity, loss, polymeric materials in friction pairs, 336
- X
- X-ray analysis  
 polymer wear, schematic of double crystal camera arrangement, 300f  
 stresses in polymer wear, 298
- X-ray photoelectron spectroscopy (XPS)  
 fluorine, PTFE transfer film, 294f  
 polymer transfer, schematic diagram of apparatus, 292f  
 polymer wear, discussion, 293  
 wear analysis, 288
- Y
- Yield pressures, variations of various polymers with temperature, 108f
- Yield strength  
 effect on adhesional wear, 54  
 pressure-sensitive tapes, 52  
 various polymers, 62
- Yield strength-tensile stress ratio, effect on fatigue wear, 63

*Production by Hilary Kanter  
 Indexing by Deborah H. Steiner  
 Jacket design by Pamela Lewis*

*Elements typeset by Hot Type Ltd., Washington, D.C.  
 Printed and bound by Maple Press Co., York, Pa.*